

From normal to abnormal coordination:
Macrocyclic and open-chain transition metal NHC complexes in
epoxidation catalysis and beyond

Greta Gundis Zámbo

Vollständiger Abdruck der von der TUM School of Natural Sciences der Technischen
Universität München zur Erlangung einer

Doktorin der Naturwissenschaften (Dr. rer. nat.)

genehmigten Dissertation.

Vorsitz: Prof. Dr. Lukas Hintermann

Prüfende der Dissertation:

1. Prof. Dr. Fritz E. Kühn
2. Prof. Dr. Klaus Köhler

Die Dissertation wurde am 20.12.2024 bei der Technischen Universität München eingereicht
und durch die TUM School of Natural Sciences am 12.02.2025 angenommen.

„Teufelschlag!“

Aladár András Zámbo

Die vorliegende Arbeit wurde im Fachgebiet Molekulare Katalyse der Technischen Universität München angefertigt.

Mein ganz besonderer Dank gilt meinem Doktorvater

Herrn Prof. Dr. Fritz E. Kühn

für die Aufnahme in seinen Arbeitskreis, sowie das mir entgegengebrachte Vertrauen. Vielen Dank für die Unterstützung und Sicherheit, die mir im Rahmen der gesamten Arbeit gewährt wurde. Ihre Expertise und Ihr Rat haben wesentlich zu meiner Arbeit beigetragen, und ich bin dankbar für die anregenden Diskussionen, die mir neue Perspektiven sowohl in der Wissenschaft als auch darüber hinaus eröffnet haben.

Danksagung

Ohne die Unterstützung und Hilfe zahlreicher Personen wäre die Realisierung dieser Arbeit nicht möglich gewesen. An dieser Stelle möchte ich mich von Herzen bei all jenen bedanken, die mich auf meinem Weg begleitet, unterstützt und mir wertvolle Anleitung gegeben haben, auch bei denen, die möglicherweise unbeabsichtigt unerwähnt geblieben sind.

In erster Linie möchte ich mich bei **Robert Reich** bedanken, für seine Unterstützung in jeglicher Hinsicht. Vielen Dank für die tägliche Organisation unseres Arbeitskreises und deine Expertise, sogar auch noch über die Zeit beim AK Kühn hinaus. Vieles wäre ohne deine Erfahrung wesentlich schwieriger gewesen. Außerdem kann man sich von den kreativen „Meme-Fähigkeiten“ und vielen Wortwitzen noch einiges abschauen. Ich glaube, dass nach einigen Jahren unser Humor daran gewachsen ist.

Ein besonderer Dank gilt Frau **Ulla Hifinger**, die eine Bereicherung für Jeden ist und mit viel Engagement und Herz die alltägliche anstehende Arbeit und Organisationen erledigt. Ich wünsche Ihnen viel Erfolg und Freude auf Ihrem neuen Weg. In diesem Sinne wünsche ich einen guten Start und viel Glück an **Renate Schuhbauer-Gerl**.

Für jegliche Aufgaben als Vorlesungsassistentin zur Durchführung der Lehre möchte ich mich besonders für die Unterstützung von **Tobias Kubo** bedanken. Ebenso danke ich **Markus Drees**, der auf meine zahlreichen Fragen zu Themen wie Prüfungsvorbereitungen für Studierende oder organisatorischen Anliegen zur TUM Graduate School stets mit einer Prise Humor reagiert hat. Ein Dankeschön geht auch an das Praktikums Team, unter anderem an **Oksana Storcheva**, **Thomas Miller** und vielen weiteren Technikern für die labortechnische Unterstützung während der jährlich wiederkehrenden AC-Praktikumsbetreuung.

Für die Anleitung zu den Feinheiten der Gaschromatographie, sowie die Unterstützung bei der Kalibrierung, Methodenentwicklung und Problembehebung bedanke ich mich bei **Jürgen Kundermann**. Mein Dank gilt auch **Ulrike Ammari**, **Petra Ankenbauer** und **Bircan Dilki**, ebenfalls aus der zentralen Analytikabteilung, für die Durchführung zahlreicher Elementaranalysen.

Weiterer Dank gilt **Isabelle Rüter** und **Serhiy Demeshko** für die analytischen Messungen einiger Eisenkomplexe. Natürlich möchte ich an dieser Stelle auch ihrem Arbeitsgruppenleiter Prof. **Franc Meyer** für die unkomplizierte Kooperation danken.

Vieles wäre nicht ohne die Hilfe fleißiger Studenten und Auszubildenden möglich gewesen. Hier möchte ich mich bei **Vanessa Ramm, Carla Esslinger, Jeff Offorjindu, Tommy Andrijanic** und **Johannes Mayr** für ihre super Arbeit und Engagement bedanken. Es hat mir Spaß gemacht mit euch zusammen zu arbeiten und hoffe, dass ihr ein wenig daraus mitnehmen konntet, so wie auch ich.

Für die Einführung in die Thematik und Arbeitsgruppe möchte ich mich herzlich bei **Jonas Schlagintweit** bedanken, der mich bereits in meinen frühen Anfängen beim AK Kühn betreut hatte und mir alle nötigen synthetischen Tricks gezeigt hat. Auch meinem Mentor **Benjamin Hofmann** gilt ein herzlicher Dank, vor allem für zahlreiche Abende der Überlegung und Entwicklung von neuen Katalysemethoden. Vielen herzlichen Dank an **Markus**, der sowohl bei jeglichen fachlichen Fragen, auch außerhalb der Chemie geholfen hat, als auch eine sehr große Unterstützung in den letzten Jahren war.

Besonders möchte ich mich bei all meinen Kollegen bedanken, die meine Promotion zu einer tollen Zeit gemacht haben und für eine schöne und äußerst lustige Gruppenatmosphäre gesorgt haben. Danke, dass die „ehemaligen“ Doktoranden bestehend aus **Flo, Marco, Ben, Christian** und **Jonas** mich so unkompliziert in die Gruppe aufgenommen haben und für die vielen mehr oder weniger konstruktiven Abende im Seminarraum. Mit eurer Begeisterung für gutes bzw. vor allem viel Essen, Trinken und Kaffee habt ihr stets für eine gute Zeit, auch außerhalb des Labors gesorgt. Vielen Dank Flo, dass du mir die Epox, als wesentlichen Bestandteil der vorliegenden Arbeit gezeigt hast. Auch **Eva** und **Nici** möchte ich herzlich danken. Ihr habt das Herz am rechten Fleck und habt wesentlich zu unvergessenen Momenten beigetragen. Grade solche Momente, wenn Eva wieder vom Stuhl fällt oder wir im VT-NMR Raum ans Telefon gehen werde ich nicht vergessen. Nici, ich bin außerdem beeindruckt von deinem künstlerischen Talent, sei es, wenn du Pokémon oder Gudrun das Truthuhn zeichnest. Danke, dass du für den nötigen Zusammenhalt in der Gruppe gesorgt hast. Vielen Dank an **Tim** für die großartige und reibungslose Zusammenarbeit und die daraus resultierenden Publikationen. Und falls alle Stricke reißen, sehe ich dich definitiv als zukünftigen Profi-Surfer. Danken möchte ich hier auch allen des oberen Labors mit **Alex I.**, unserem AK-Daddy und

Tüftler und **Melanie**, mit denen ich vor einigen Jahren hier an der TUM gestartet bin. Melli, du warst mir schon in den ersten Minuten der allerersten Vorlesung bekannt, gut, dass du dich damals nicht für die LMU sondern die TUM entschieden hast. Wer hätte gedacht, dass wir am Ende doch noch gemeinsam am gleichen AK landen würden? Es war eine ereignisreiche Zeit, die mit den Freundschaften mit **Anna**, **Laura** und **Jojo**, die auch seit Tag 1 dabei sind umso schöner wurde. Ein weiterer Dank geht an **Carla**, ein halbes Ca, der grade ihr ci fehlt. Vielen Dank für die zahlreichen Backkünste und Kuchen, auch wenn ich mit vollem Genuss nur 1/8 Stück schaffe. Und an **Stefan**, der als einziger, der Kollegen meine Begeisterung für Fußball geteilt hat. Vielen Dank an **Leon**, der mit seinem Charakter für jede Menge gute Stimmung sorgt und sich um die wesentlichen Dinge, wie den 3D-Druck kümmert. Ich hoffe, dass dir zukünftig weitere Fußverletzungen, z.B. beim Säulen erspart bleiben. Danke an **Yogi** für die tollen Gespräche, die Unterstützung und die manchmal dringend notwendigen Kaffeepausen. Deine Expertise in NHC-Makrozyklen, Mensa-Nachtisch und Kuchen ist unübertroffen und niemand isst Chickenwings so stilvoll wie du.

Besonders dem unteren Labor bestehend aus **Alex** „Böthi-Boy“, **Michi** und **Johannes** möchte ich für den lustigen Alltag danken. Ihr habt die Arbeit stets mit Spaß gefüllt, immer ein offenes Ohr gehabt und zu einer wirklich tollen Atmosphäre beigetragen. Auch wenn wir teilweise komplett unterschiedliche Themengebiete hatten konnte ich mich auf einen konstruktiven Rat von euch verlassen und somit einige Probleme in Synthese und Katalyse lösen. Alex und Michi, ihr habt mit eurer positiven Art andere mitreisen können und für den nötigen Zusammenhalt gesorgt. Alex, du warst immer zur Stelle, wenn irgendwo ein „Brand“ gelöscht werden musste, es sei denn, du warst grade auf der Toilette. Michi, vielen Dank für die Messungen meiner Kristalle und die Zeit, die du darin investiert hast. Für deine künftigen Abenteuer wünsche ich dir immer eine griffbereite Bärenglocke und, besonders bei deinen langen Fahrradtouren im Winter, warme Kleidung. Joehainis, auch wenn es im unteren Labor ziemlich leer geworden ist freu ich mich sehr, dass deine Reise beim AK Kühn weitergegangen ist, da du eine Bereicherung für die Gruppe bist, auch durch deine Einsatzbereitschaft. Ich hoffe in baldiger Zukunft wird dich stets ein Cola trinkendes Huhn namens Leon begleiten.

Weiterhin wünsche ich **Simon** und **Björn**, die in nächster Zeit anfangen werden einen guten Start und viel Glück und Erfolg.

Von Herzen bedanke ich mich bei meiner **Familie** und besonders bei meiner Mama **Gundis** und meinen Großeltern **Gundis** und **Aladár**, die mir die entscheidenden Werte und Fähigkeiten vermittelt haben und immer für mich da sind. Eure bedingungslose Unterstützung und die Sicherheit, die ihr mir gegeben habt, haben es mir ermöglicht, Herausforderungen zu meistern und meinen Weg zu gehen, dafür bin ich unendlich dankbar. Mama, vielen Dank, dass du mich so hast werden lassen, wie ich bin, mir stets Halt gegeben und mich in so vieles mit einbezogen hast. Du hast mir von Anfang an die Welt gezeigt und mir ermöglicht, sie mit offenen Augen zu entdecken. Omama und Opapa, ich danke euch für all das Wissen, das ihr mit mir vermittelt habt, und dafür, wie sehr ihr meine handwerklichen und sportlichen Fähigkeiten von klein auf gefördert habt. Natürlich gehört hier auch **Maya** dazu, die zwar nicht so gerne Hüte trägt, es aber dennoch tapfer versucht.



Ein großer Dank geht an meine **Freunde**, an meine **Gäng**, die seit der Schulzeit zusammenhält, was unfassbar schön ist und an mein **Team** vom TBM. Jede einzelne Freundschaft und jeden unvergessenen Moment miteinander weiß ich sehr zu schätzen.

Abschließend danke ich dir **Michi**, dass du nun schon seit so vielen Jahren an meiner Seite bist und mein Leben bereicherst. Ich bin unendlich froh dich zu haben und dass du so ein positiver Mensch bist. Danke, dass du mich immer wieder unterstützt und aufmunterst, das macht mich unendlich froh und glücklich. Ich freu mich auf die gemeinsame Zukunft und alles, was sie mit sich bringt.

*„Lebe lustig, lebe froh,
wie der Flo, im Haferstroh“*

Abstract

Over the past decades, transition metal *N*-heterocyclic carbene (NHC) complexes have emerged as a significant area of research within organometallic chemistry. The expanding range of their applications has garnered considerable attention, primarily due to their excellent adaptability in terms of steric and electronic properties. Consequently, NHC chemistry has established as a crucial component of modern homogeneous catalysis, organometallic materials and medicinal chemistry. In particular, abnormally coordinating NHCs (aNHCs) exhibit generally enhanced electronic properties compared to normal NHCs, such as stronger σ -donor and π -acceptor capabilities, which can improve the stability and reactivity of metal complexes in their corresponding oxidation states.

In this thesis, a macrocyclic tetra-aNHC ligand system, consisting of four methyl-bridged and methyl-substituted 1,2,3-triazoles was designed as a mimic of its imidazole counterpart, known for efficiently in stabilizing and supporting a variety of transition metals. Specifically iron stands out for its advantages in oxidation catalysis due to its abundance, cost-effectiveness, and environmental compatibility, making it a sustainable alternative to heavier, toxic metals. Inspired by biological systems, numerous iron oxidation catalysts have been studied over the last years. As part of this work, the synthesis and characterization of iron(II) and iron(III) NHC complexes have furthered the understanding of catalytic oxidation, by emphasizing the pivotal role of electronic properties and ligand design in catalysis. The first macrocyclic iron aNHC complexes were synthesized and characterized, displaying strong σ -donor properties and achieving selective olefin epoxidation with H_2O_2 , yielding turnover frequencies (TOFs) of up to $60,000 \text{ h}^{-1}$. Additionally, a comparative study of four open-chain iron(II) NHC complexes reveals that ligand electronic variations influence catalytic activity and stability. The addition of Lewis acids significantly enhances the performance of all the catalysts studied.

Beyond iron, the macrocyclic aNHC ligand was also employed to synthesize and characterize silver(I), gold(I), nickel(II), palladium(II), and platinum(II) complexes. The silver and gold complexes adopt a molecular box-like structure containing four metal ions, while the nickel, palladium, and platinum complexes exhibit ideal square planar geometries.

Kurzzusammenfassung

In den letzten Jahrzehnten haben sich Übergangsmetall *N*-heterocyclische Carben (NHC) Komplexe als ein bedeutender Forschungsbereich innerhalb der organometallischen Chemie etabliert. Das wachsende Spektrum ihrer Anwendungen hat aufgrund ihrer hervorragenden Anpassungsfähigkeit in Bezug auf sterische und elektronische Eigenschaften beträchtliche Aufmerksamkeit erregt. Folglich hat sich die NHC Chemie als wesentlicher Bestandteil der modernen homogenen Katalyse, der organometallischen Materialien und der medizinischen Chemie etabliert. Insbesondere abnormal koordinierende NHCs (aNHCs) weisen im Vergleich zu normalen NHCs allgemein verbesserte elektronische Eigenschaften auf, wie stärkere σ -Donor- und π -Akzeptorfähigkeiten, die die Stabilität und Reaktivität von Metallkomplexen in ihren jeweiligen Oxidationszuständen verbessern können.

In dieser Arbeit wurde ein makrocyclisches tetra-aNHC-Ligandensystem entwickelt, das aus vier methylverbrückten und methylsubstituierten 1,2,3-Triazolen besteht und als Nachbildung seines Imidazol-Gegenstücks dient, das dafür bekannt ist, eine Vielzahl von Übergangsmetallen effizient zu stabilisieren und zu unterstützen. Besonders Eisen sticht durch seine Vorteile in der Oxidationskatalyse hervor, da es reichlich verfügbar, kostengünstig und umweltfreundlich ist, was es zu einer nachhaltigen Alternative zu schwereren, toxischen Metallen macht. Inspiriert von biologischen Systemen wurden in den letzten Jahren zahlreiche Eisenoxidationskatalysatoren untersucht. Im Rahmen dieser Arbeit haben die Synthese und Charakterisierung von Eisen(II)- und Eisen(III)-NHC-Komplexen das Verständnis der katalytischen Oxidation vorangetrieben, indem sie die zentrale Rolle der elektronischen Eigenschaften und des Ligandendesigns in der Katalyse hervorheben. Die ersten makrocyclischen Eisen-aNHC-Komplexe wurden synthetisiert und charakterisiert, die starke σ -Donoreigenschaften aufweisen und eine selektive Olefinepoxidierung mit H_2O_2 erreichen, was zu Umsatzzahlen (TOFs) von bis zu 60.000 h^{-1} führt. Zusätzlich zeigt eine vergleichende Studie von vier offenkettigen Eisen(II)-NHC-Komplexen, dass elektronische Variationen der Liganden die katalytische Aktivität und Stabilität beeinflussen. Die Zugabe von Lewis-Säuren steigert die Leistung aller untersuchten Katalysatoren erheblich.

Über Eisen hinaus wurde der makrocyclische aNHC-Ligand auch für die Synthese und Charakterisierung von Silber(I)-, Gold(I)-, Nickel(II)-, Palladium(II)- und Platin(II)-Komplexen

verwendet. Die Silber- und Goldkomplexe bilden eine molekulare, box-type Struktur mit vier Metallionen, während die Nickel-, Palladium- und Platinkomplexe ideale quadratisch-planare Geometrien aufweisen.

Abbreviations

$^{13}\text{C}_{\text{NHC}}$	^{13}C carbene carbon signal
aNHC	abnormal <i>N</i> -heterocyclic carbene
BPMCN	<i>N,N</i> -bis(2-pyridylmethyl)- <i>N,N</i> -dimethyl-trans-1,2-diamino-cyclohexane
BPMEN	<i>N,N</i> -dimethyl- <i>N,N</i> -bis(2-pyridylmethyl)-1,2-diaminoethane
btsa	bis(trimethylsilyl)amide
<i>ca.</i>	<i>circa</i>
CAAC	cyclic (alkyl)(amino) carbene
CAArC	cyclic (aryl)(amino) carbene
CuAAC	Cu ^I catalysed azide-alkyne cycloaddition
CYP	cytochrome P450
CV	cyclic voltammetry
DFT	density functional theory
EPR	electron paramagnetic resonance
ESI	electrospray ionization
<i>et al.</i>	<i>et alia</i>
eq.	equivalents
HOMO	highest occupied molecular orbital
HR	high-resolution
+/-I	+/-inductive
LUMO	lowest occupied molecular orbital
+M	mesomeric
max	maximum
MIC	mesoionic carbene
MS	mass spectrometry
MTO	methyltrioxorhenium
NHC	<i>N</i> -heterocyclic carbene
nNHC	normal <i>N</i> -heterocyclic carbene
OTf	triflate
PDP	2-((<i>S</i> -2-[<i>S</i> -1-(pyridine-2-ylmethyl)pyrrolidin-2-yl]pyrrolidin-1-yl)-methyl)pyridine
PyTACN	1-(2-pyridylmethyl)-4,7-dimethyl-1,4,7-triazacyclononane
ref.	reference

rds	rate-determining step
rNHC	remote <i>N</i> -heterocyclic carbene
r.t.	room temperature
SC-XRD	single-crystal X-ray diffraction
sMMO	soluble methane monooxygenases
Th	thianthrene
TIPS	triisopropylsilyl
TMC	tetramethylcyclam
TPA	tris(2-pyridylmethyl)amine
TOF	turnover frequency
TON	turnover number
UV/Vis	UV-Visible
<i>vs.</i>	<i>versus</i>
VT-MS	variable-temperature mass spectrometry
wap	water-assisted pathway

Table of contents

I	Introduction	1
1	Carbenes as ligands for transition metal complexes	1
1.1	Fischer and Schrock carbenes.....	1
1.2	<i>N</i> -heterocyclic carbenes (NHCs)	2
1.2.1	Structural features of NHCs.....	4
1.2.2	Abnormal or mesoionic <i>N</i> -heterocyclic carbenes (aNHCs).....	7
1.2.3	Synthetic access to imidazole precursors.....	9
1.2.4	Copper(I)-catalyzed alkyne-azide “click” reaction.....	9
1.2.5	Macrocyclic tetra-NHC ligand precursors.....	11
2	Carbon feedstock for chemical industry	12
3	Homogenous epoxidation catalysis	14
3.1	Ti, Mn, Re and Mo olefin epoxidation catalysts.....	16
3.2	Bio-inspired iron complexes in epoxidation catalysis.....	17
3.2.1	Non-heme iron catalysts with <i>N</i> -donor ligands.....	19
3.2.2	Iron NHC catalysts	22
4	Macrocyclic late transition metal NHC complexes.....	28
II	Objective.....	32
III	Results and discussion – publication summaries.....	33
1	The effect of <i>trans</i> axial isocyanide ligands on iron(II) tetra-NHC complexes and their reactivity in olefin epoxidation	33
2	Organometallic 3d transition metal NHC complexes in oxidation catalysis.....	35
3	The first macrocyclic abnormally coordinating tetra-1,2,3-triazole-5-ylidene iron complex: A promising candidate for olefin epoxidation.....	37
4	Tailoring activity and stability: Effects of electronic variations on iron-NHC epoxidation catalysts	39
5	Exploring the impact of abnormal coordination in macrocyclic <i>N</i> -heterocyclic carbene ligands on bio-inspired iron epoxidation catalysis.....	42
6	Impact of ligand design on an iron NHC epoxidation catalyst	44
7	Unpublished results	46
7.1	Silver(I) <i>bis</i> -calix[4]3-methyl-1,2,3-triazol-5-ylidene triflate.....	46
7.2	Silver(I) <i>bis</i> -calix[4]3-methyl-1,2,3-triazol-5-ylidene hexafluoro-phosphate.....	47
7.3	Nickel(II) calix[4]3-methyl-1,2,3-triazol-5-ylidene triflate	49
7.4	Palladium(II) calix[4]3-methyl-1,2,3-triazol-5-ylidene triflate	51
7.5	Platinum(II) calix[4]3-methyl-1,2,3-triazol-5-ylidene triflate.....	53
7.6	Gold(I) <i>bis</i> -calix[4]3-methyl-1,2,3-triazol-5-ylidene triflate.....	55

IV	Conclusion and outlook	56
V	Reprint permissions and licenses.....	59
1	Wiley-VCH Journals.....	59
2	Royal Society of Chemistry Journals	61
3	Elsevier Journals.....	64
VI	Complete List of Publications and Contributions.....	67
VII	References	69

I Introduction

1 Carbenes as ligands for transition metal complexes

Carbenes are electron-deficient carbon compounds characterized by a divalent carbon atom with two non-bonding electrons. These electrons can exist either in the same orbital with antiparallel spins (singlet state) or in separate orbitals with parallel spins (triplet state), resulting in an incomplete octet with a six-electron valence shell (Figure 1).^{1,2}

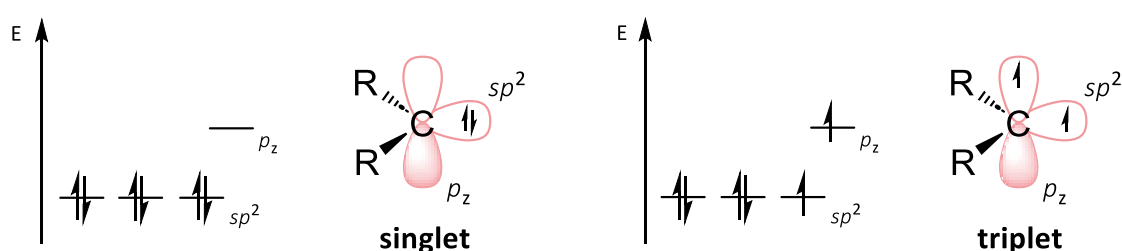


Figure 1 Schematic representation of electronic carbene singlet and triplet ground states.¹⁻³

1.1 Fischer and Schrock carbenes

In 1964, E. O. Fischer⁴ considerably advanced the applications of carbenes by demonstrating their ability to act as ligands in stable transition metal complexes, known as Fischer carbenes. Fischer carbene complexes are characterized as singlet state carbenes due to their significant energy gap between their singlet and triplet ground states. They typically feature a π -donating substituent at the α -position, such as an amino or alkoxy group. The metal-carbene bond is formed *via* the interaction of two closed-shell singlet fragments, involving σ -donation from the carbene to the metal and generally weak π -back donation from the metal to the carbene (Figure 2). The resulting electron polarization towards the metal renders the carbene electrophilic. The carbon-metal bond exhibits partial double bond character due to the metal π -back bonding. In general, Fischer carbenes coordinate to late transition metals in a low oxidation state.^{1,2,5,6}

One decade after Fischer's discovery, R. R. Schrock⁷ introduced a novel class of carbene complexes that differ significantly from Fischer carbenes in both structure and reactivity. Schrock's carbenes are characterized *via* a small energy gap between their singlet and triplet states, which leads to a preference for the triplet state due to the poor stabilization provided by neighboring alkyl or alkylidene groups. This results in a highly covalent metal-carbene bond,

where the bonding electrons are nearly equally distributed between the carbon and the metal, forming what is effectively a true double bond (Figure 2). These complexes are typically found with early transition metals in high oxidation states, displaying nucleophilic characteristics at the carbon-metal bond, contrasting with Fischer carbenes.^{2,8,9} Schrock carbenes are particularly notable for their reactivity with electrophiles and their significant role in industrial catalysis, such as in olefin metathesis, a process that was awarded the 2005 Nobel Prize in Chemistry.^{7,10-12}

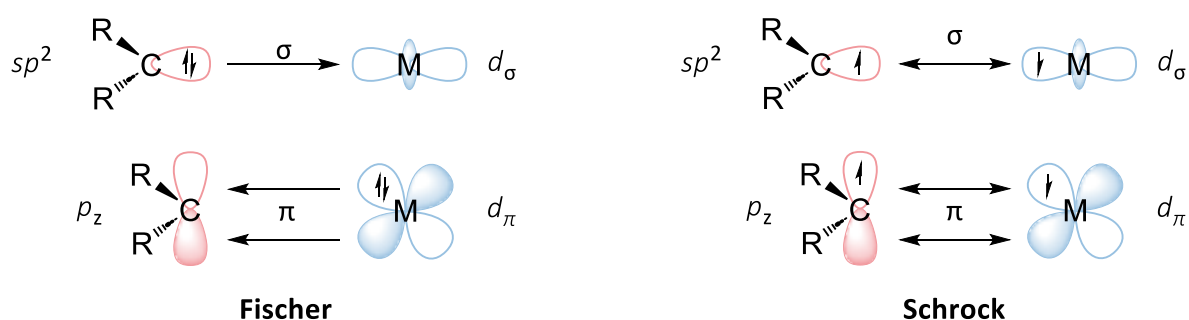


Figure 2 Schematic representation of the important orbital interactions in Fischer-type carbenes^{5,6} (left) and Schrock-type carbenes^{2,8,9} (right) with transition metals (M).

1.2 N-heterocyclic carbenes (NHCs)

N-heterocyclic carbenes (NHCs) as a subclass of Fischer-type carbenes are classified as organic compounds characterized by a heterocyclic framework containing a divalent carbon atom with only six electrons in its valence shell – a defining feature of carbenes (*vide supra*) – and at least one nitrogen atom. Carbenes are typically highly reactive and unstable due to their incomplete electron octet and the presence of unpaired electrons.^{13,14} The initial research on the synthesis of NHC complexes already began in the 1960s with Wanzlick, Schönherr¹⁵ and Öfele¹⁶, who identified NHCs as ligands for mercury(II) and chromium(0) (Figure 3). In 1988, Bertrand¹⁷ and coworkers were the first to discover that introducing heteroatoms, such as phosphorus or silicon, next to the carbon center significantly increase the stability of the carbene species (Figure 3). Despite Bertrand's discovery it took until 1991 for Arduengo *et al.*¹⁸ to isolate the first stable free NHC in the solid state, which was achieved by the incorporation of bulky substituents into a nitrogen containing heterocycle (Figure 3).^{13,14} The incorporation of adamantyl groups at the amino positions proved to be an innovative feature, as they provide steric protection to the resulting carbene, preventing dimerization *via* the Wanzlick equilibrium.^{2,19} Since this pioneering discovery, the field has rapidly advanced, deepening the

understanding of NHC behavior and expanding their fundamental applications in natural sciences.^{13,14}

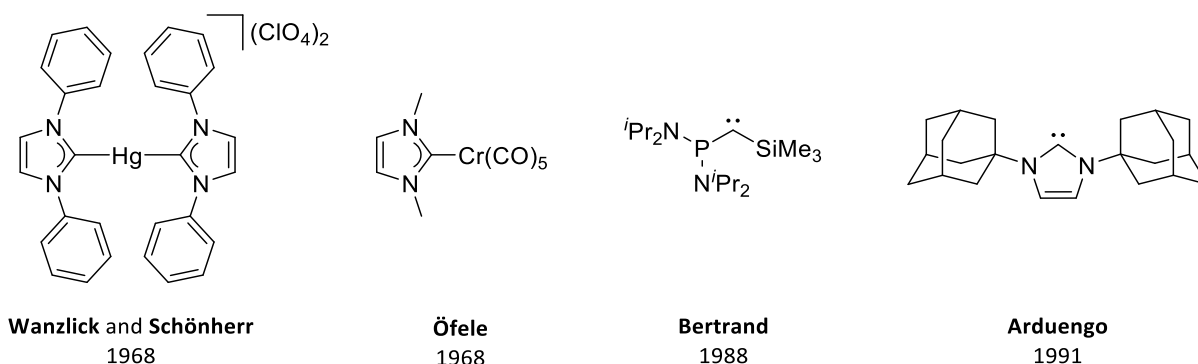


Figure 3 First NHC metal complexes reported by Wanzlick, Schönherr¹⁵ and Öfele¹⁶, the first isolable carbene by Bertrand and coworkers and the first isolable NHC published by Arduengo *et al.*¹⁸ (adapted from ref. ²⁰).

Traditional carbenes typically have a triplet electronic ground state (Figure 1), which is energetically favored according to Hund's rule, particularly in linear carbenes.²¹ In contrast, NHCs exhibit a singlet ground state (Figure 1), stabilized by two key effects (Figure 4, left): π -electron donation from adjacent nitrogen atoms into the empty p_z -orbital of the carbene carbon (LUMO), and σ -electron withdrawal from the non-bonding lone pair on the carbene (HOMO) due to the high electronegativity of the neighboring nitrogen atoms. These mesomeric (+M) and inductive (-I) effects create a push-pull stabilization, further supported by the bent geometry of NHCs, which reinforces the singlet state.^{13,22}

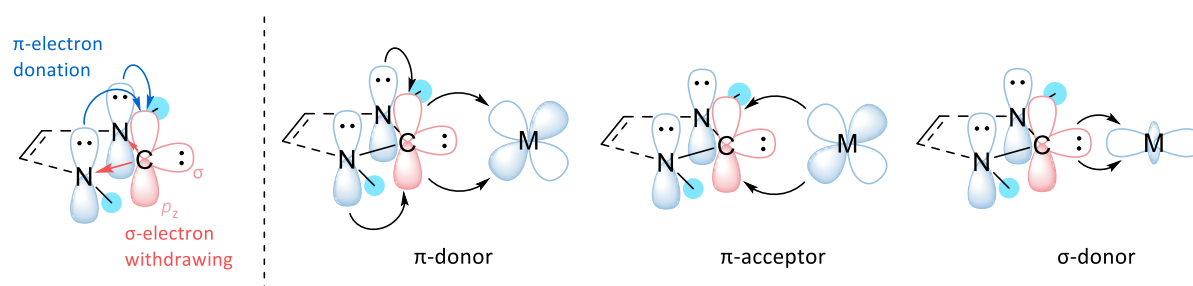


Figure 4 Representation of the electronic stabilization of the singlet carbene by adjacent heteroatoms (left)¹³ and the three dominant orbital interactions between a NHC and a transition metal (M) forming a carbene-metal bond (right).^{23,24}

NHC ligands offer three orbital interactions with transition metals (Figure 4): π -donor, π -acceptor (π^* -backbonding into the vacant p_z -orbital) and σ -donor abilities, depending on the electronic nature of both, the metal and the coordinating NHC. The unique details of NHC bonding interactions with transition metals clearly distinguish them from Fischer and Schrock carbenes. The predominant σ -donating character over π -acidity making them capable of

stabilizing metal ions, even in high oxidation states, which is particularly valuable for catalytic applications.^{13,24} Often compared with phosphines, NHCs overall show even stronger σ -donation, which is reflected *inter alia* by their ability to bind metal centers incapable of π -backdonation, like main group elements²⁵ or rare earth metals²⁶. The strong donor capability and kinetic stability prevent rapid ligand dissociation and association processes, replacing established phosphine ligands in studied areas.^{13,27}

1.2.1 Structural features of NHCs

The kinetic and thermodynamic stability of NHCs, along with their specific reactivity and binding behaviors, are influenced by several structural features. In general, four key aspects contribute to these characteristics (Figure 5, top, left): ① the presence and arrangement of heteroatoms; ② the placement of substituents in nearby positions (“wingtip” positions); ③ the structure of the backbone, such as unsaturation and substituents; and ④ the size of the ring.^{13,14}

Building on Arduengo's pioneering work, the field of different NHC classes has expanded significantly. As a result, an extensive library of NHCs with diverse structures and properties has been developed. A selection of some of the most important classes of NHCs is shown in Figure 5. The classical Arduengo-type carbenes feature either saturated or unsaturated backbones with varying nitrogen and backbone substituents. In this context, imidazol-2-ylidenes, along with their saturated (imidazolin-2-ylidenes) and benzo-fused (benzimidazol-2-ylidenes) derivatives, have been the most extensively studied.¹³ NHCs with saturated backbones concentrate more electron density on the C2 carbene carbon atom, as there are no π interactions, leading to increased basicity and thus tend to be slightly stronger σ -donors. In contrast, an unsaturated backbone provides enhanced thermodynamic stability to the NHC, due to partial aromaticity, which reduces the need for bulky substituents to stabilize the carbene.^{13,28} Altering the *N*-substituents enables control over both the electronic and steric characteristics of the carbene, which in turn affects the properties of the coordinated metal. Introducing electron-withdrawing groups at this position reduces the electron donation from the nitrogen atoms to the carbene's vacant p_z -orbital, thereby diminishing its donation ability to the metal center. Conversely, the opposite effect occurs when electron-donating groups are added. Incorporating bulky substituents leads to carbenes that are less prone to dimerization within the Wanzlick equilibrium. Additionally, the steric hindrance can provide

protection to the coordinated metal.^{1,2,29} Modifying the backbone position primarily affects the electronic properties of the carbene, since these substituents typically do not cause steric hindrance to the metal center. Introducing electron-withdrawing groups (like benzene) reduce electron density and can also extend the aromatic structure. *Vice versa*, electron-donating groups (like methyl, due to its +I-effect) at the backbone raises the electron density at the carbene, enhancing the carbene's σ -donor strength.^{1,30,31}

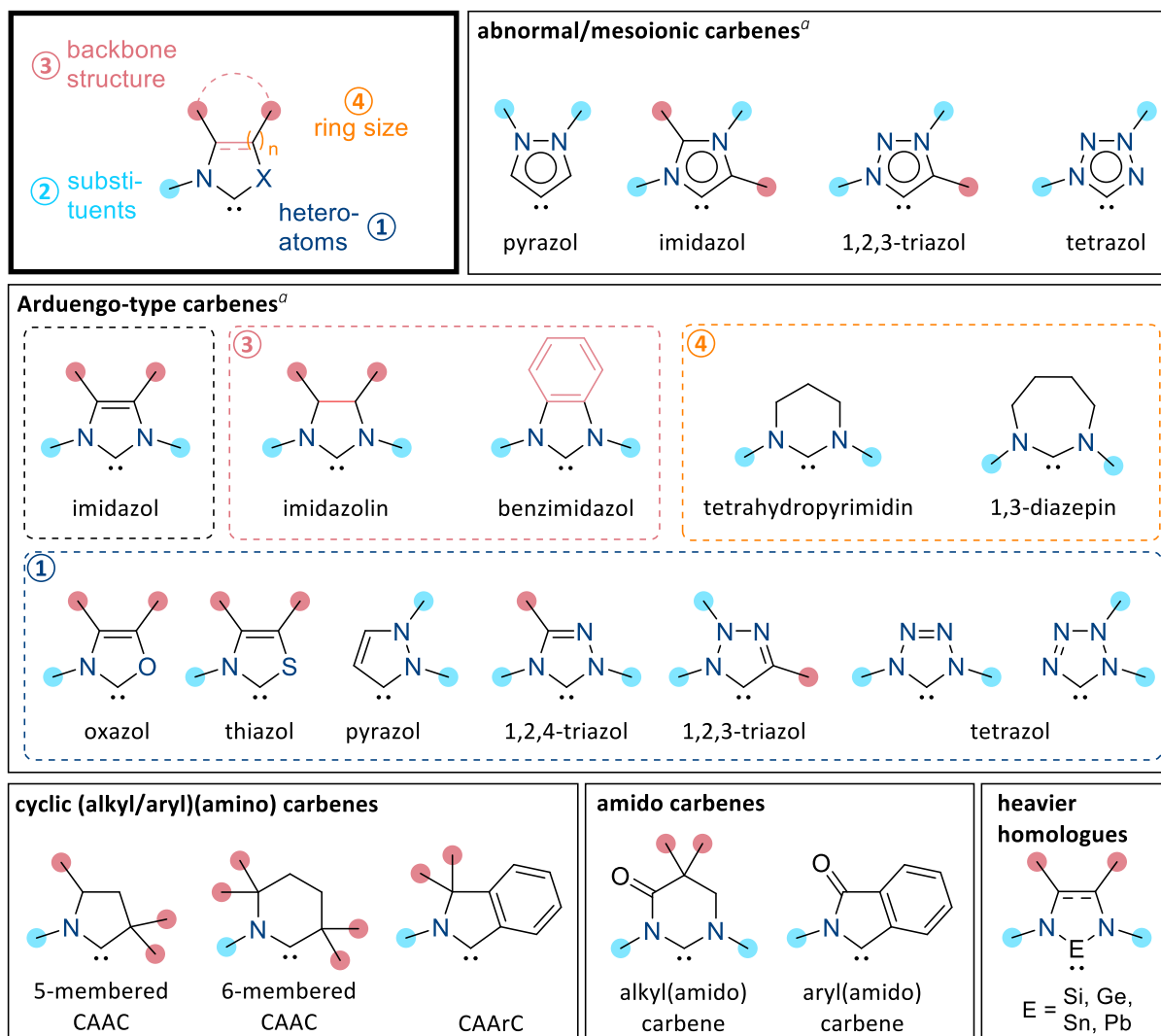


Figure 5 General structural features of NHCs with X = CR', NR', O, PR', S (top, left) and selected classes of relevant NHCs and selected NHC-homologues. ^aThe carbene position followed by the suffix "ylidene" should be added to obtain the generic name of each NHC subclass.^{13,14,32-35}

The majority of NHCs consist of a five-membered ring at their core, although several ring-expanded variants have been reported, incorporating structures such as tetrahydropyrimidine and diazepine frameworks.³⁶ These ring-expanded NHCs demonstrate increased basicity and stronger σ -donating abilities compared to traditional five-membered imidazole-type NHCs.

This is attributed to the wider N-C-N bond angle, which enhances the p_z -character of the lone pair orbital. For instance, this angle in a typical five-membered carbene is 101.4° vs. 114.6° in a six-membered analogue. The higher energy of the HOMO results in stronger electron donation. Additionally, the presence of methylene groups in the ring backbone contributes to a positive inductive effect, further enhancing the electron-donating properties. Steric effects also differentiate ring-expanded NHCs from their five-membered counterparts. Due to the larger N-C-N angle and more flexible backbone, ring-expanded NHCs exhibit greater steric demand. The larger ring size directs *N*-substituents towards the metal center, promoting stronger interactions within the catalytic pocket and enhanced metal stabilization by blocking two coordination sites.³⁷

Notably, two nitrogen atoms adjacent to the carbene carbon are not required for stability,³⁸ allowing for the development of NHCs with other heteroatoms, such as sulfur in thiazol-2-ylidenes or oxygen in oxazol-2-ylidenes. While these variants exhibit weaker σ -donating abilities than imidazol-2-ylidenes – with oxazol-2-ylidenes being slightly weaker than thiazol-2-ylidenes – they are superior π -acceptors, due to reduced π -donation from the heteroatoms into the carbene carbon's p_z -orbital.³⁹⁻⁴¹ Further NHC fine-tuning can be achieved by modifying the heterocyclic cores to change the number and arrangement of heteroatoms, allowing for tailored electronic and steric properties. This facilitates the introduction of pyrazol, triazole and tetrazol NHC scaffolds. In their normal forms, these carbenes feature nitrogen in their backbone, which results in diminished σ -donor strength, but enhanced π -acceptor capabilities compared to imidazol-2-ylidenes. Carbenes can also be generated in configurations where a neutral, non-zwitterionic resonance structure cannot be formally depicted. In such cases, the species is referred to as an abnormal or mesoionic carbene (*vide infra*). When the carbene center is located at a position that is not adjacent to a nitrogen atom, the species is called remote carbene (rNHC).¹³

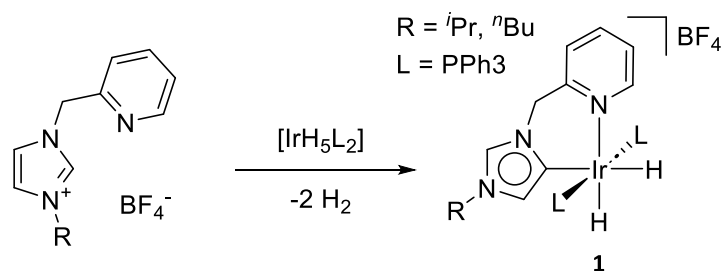
Another group of stable NHCs exhibit only one nitrogen atom next to the carbene, with the other neighboring atom being carbon. Cyclic (alkyl)(amino)carbenes (CAACs), developed by the group of Bertrand in 2005, feature a nitrogen atom replaced by a carbon atom with alkyl groups.⁴² This substitution increases the electron density at the carbene carbon due to the reduced electronegativity of carbon and the inductive effect of alkyl groups. As a result, CAACs are stronger σ -donors than Arduengo-type NHCs.^{13,43} However, the absence of π -donation

from the nitrogen makes CAACs more electrophilic, enhancing their π -accepting properties.^{13,44} Substituting alkyl with aryl groups forms cyclic (amino)(aryl)carbenes (CAACs), which maintain strong σ -donating and better π -accepting abilities. Amido carbenes, similar to CAACs, can be categorized into alkyl(amido)carbenes, diamidocarbenes, and aryl(amido)carbenes. The presence of an electron-withdrawing carbonyl group increases their electrophilicity, making them even stronger π -acceptors than CAACs or CAACs. However, this enhanced π -accepting ability comes at the expense of σ -donor strength, rendering amido carbenes weak σ -donors, much weaker than Arduengo-type NHCs.^{13,45}

Furthermore, NHCs have expanded beyond carbon-based systems to include heavier group 14 analogs, where the central carbene atom is replaced by silicon, germanium, tin, or lead. These systems exhibit unique reactivity and coordination properties, broadening the scope of NHC chemistry and are listed here for completeness.⁴⁶⁻⁴⁹

1.2.2 Abnormal or mesoionic *N*-heterocyclic carbenes (aNHCs)

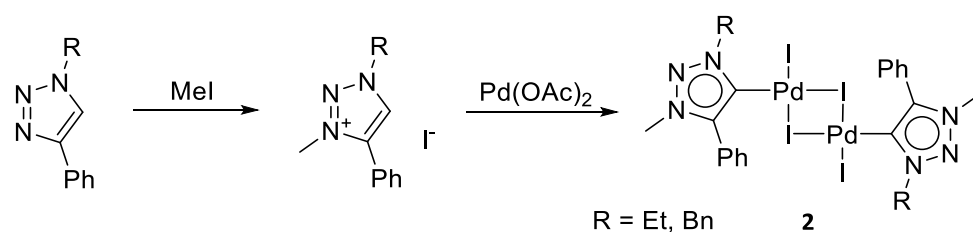
As described in chapter 1.2.1, Arduengo-type NHCs coordinate to the metal center *via* the C2 carbon due to the significant lower acidity of the backbone, with a pK_a value for the C2-bound hydrogen in imidazolium salts between 16 to 23 vs. for the C5-H of 33.0.^{31,50} Nevertheless, the carbene carbon can be shifted to the C4 or C5 position, forming a distinct subclass known as abnormally coordinating NHCs (aNHCs), or more generally classified as mesoionic carbenes (MICs).^{51,52} MICs generally feature less heteroatom stabilization of the carbenic carbon and hence impart specific donor properties and reactivity schemes when coordinated to a transition metal.⁵² The concept of abnormal coordination was first introduced by Crabtree⁵³ and coworkers in 2001, when they reported the cationic iridium complex **1** converted from pyridyl-substituted imidazolium (Scheme 1).



Scheme 1 Synthetic route of the first reported aNHC complex by Crabtree and coworkers.⁵³

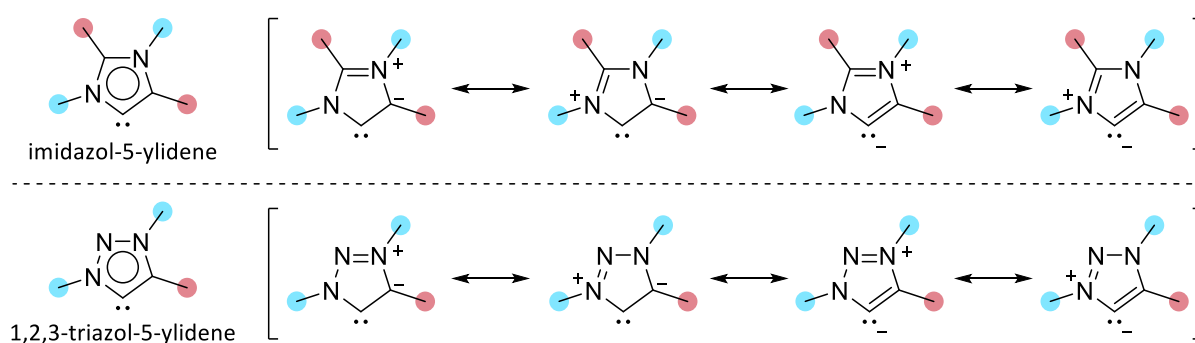
The unexpected metal coordination *via* the C5 carbon within the backbone of the imidazolylidene ring, rather than between the nitrogen atoms is forced by steric factors, particularly the substitution on the carbon adjacent to the metal-bound carbon. Hence, abnormal coordination tends to be favored when bulky substituents, such as mesityl or isopropyl groups, are attached to the nitrogen atom.⁵⁴

In 2008, Albrecht⁵⁵ and colleagues developed a novel class of aNHCs based on a 1,2,3-triazole scaffold. These 1,3,4-substituted 1,2,3-triazol-5-ylidenes are synthesized *via* copper(I)-catalyzed azide-alkyne cycloaddition (CuAAC, *vide infra*), followed by an alkylation step at the N3 position (Scheme 2). Direct metalation of the triazolium salt *via* thermally induced C–H bond activation with Pd(OAc)₂ affords the dinuclear aNHC complex **2**.^{32,55}



Scheme 2 Synthetic route of the first reported triazole based aNHC complex by Albrecht and coworkers.⁵⁵

A key feature of these aNHC complexes is their dipolar structure, forming 5- or 6-membered heterocycles with partial charge delocalization. Such characteristics are consistent with the IUPAC definition of MICs⁵¹, wherein no feasible resonance structure can be depicted for the free carbene without introducing additional charges (Scheme 3, exemplified for imidazole and triazole aNHCs).^{52,56}



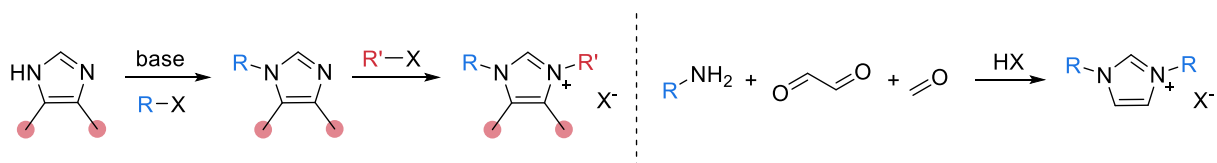
Scheme 3 Resonance structures of imidazole-5-ylidene⁵⁷ and 1,4-disubstituted 1,2,3-triazol-5-ylidene⁵⁸.

Positioning the carbene center at the C5 position renders abnormal aNHCs less thermodynamically stable but more strongly donating compared to their normal NHC (nNHC)

counterparts. Energy decomposition analysis has demonstrated that the energy gap between the parent nNHC and aNHC is approximately 19 kcal/mol.^{50,59,60} Experimental approaches aimed at investigating the electronic properties of C5-carbenes consistently show that aNHCs exhibit stronger electron-donating characteristics than their nNHC analogs. Consequently, aNHCs present promising candidates for stabilizing high-valent metal species in catalytically active complexes.⁵⁰

1.2.3 Synthetic access to imidazole precursors

A straightforward strategy to synthesize NHC precursors involves the quaternization of the nitrogen atom on a pre-existing neutral *N*-substituted imidazole, oxazole, or thiazole, efficiently yielding the desired compounds.⁶¹ Notably, the most common method for preparing imidazole-based NHCs involves deprotonation of imidazole, followed by stepwise alkylation, allowing for the formation of both symmetric and asymmetric motifs (Scheme 4, left).⁶² Another method is the multicomponent reaction building up the heterocycle with the appropriate substituents in a one-pot reaction. In this process, two equivalents of primary amines are reacted with glyoxal and paraformaldehyde in the presence of an acid, such as hydrochloric acid. Initially, the formaldehyde forms an *N,N'*-disubstituted aminal, which then undergoes condensation with glyoxal to yield the corresponding symmetric imidazolium salt (Scheme 4, right).^{61,63}



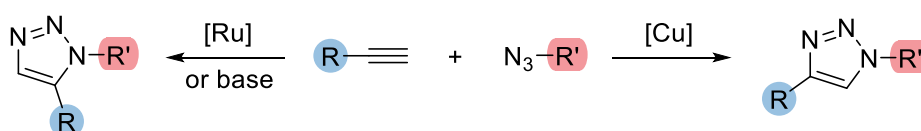
Scheme 4 The two most common synthetic strategies towards imidazole NHC precursors.

The NHC framework can be expanded by linking multiple NHC units *via* carbon bridges, resulting in the formation of poly-NHC ligands. This extension enables the creation of multidentate ligand systems with enhanced coordination capabilities and diverse applications in catalysis and coordination chemistry.⁶⁴

1.2.4 Copper(I)-catalyzed alkyne-azide “click” reaction

In 2001, a revolution in synthetic chemistry occurred when Kolb, Finn and Sharpless introduced the concept of “click” chemistry.⁶⁵ Independently, Sharpless and Fokin *et al.*⁶⁶ and

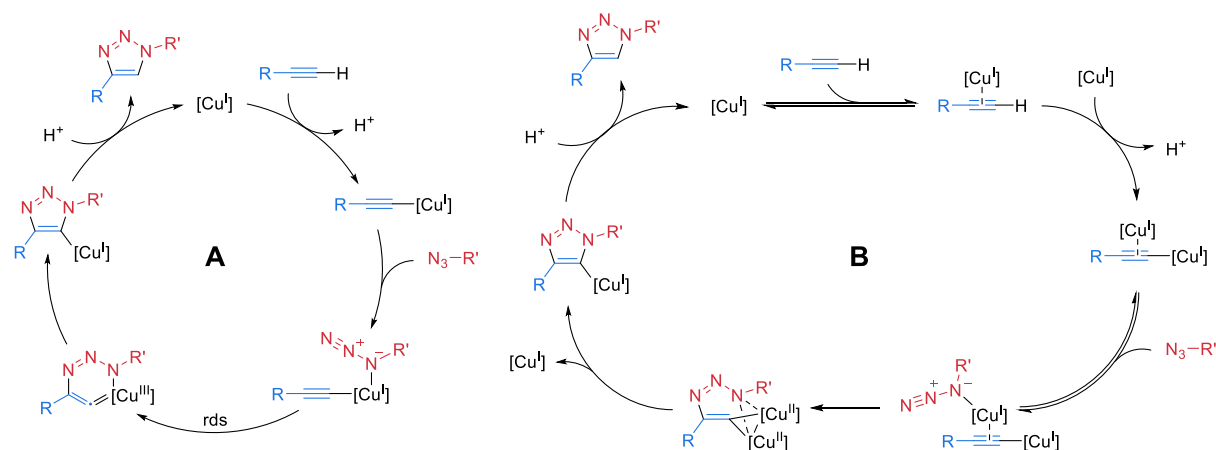
Meldal *et al.*⁶⁷ facilitated the accessibility of synthesizing 1,4-disubstituted 1,2,3-triazoles selectively under mild water-tolerant conditions, fulfilling the criteria of “click” reactions (Scheme 5). Generally, this so-called Cu^I catalysed azide-alkyne cycloaddition (CuAAC) yields the desired triazoles from terminal alkynes with little or no by-product formation.⁶⁸⁻⁷⁰ The non-catalyzed azide-alkyne reaction dates back to 1893, when 1,2,3-triazole was first synthesized from diethyl acetylenedicarboxylate and phenyl azide. This type of 1,3-dipolar cycloaddition reaction, known as the Huisgen reaction⁷¹, produces, in contrast to the CuAAC, a non-selective mixture of 1,4- and 1,5-disubstituted products and generally requires high temperatures.⁶⁸ The selective formation of the 1,5-regioisomere is achieved applying base or ruthenium catalyzed conditions (Scheme 5).^{69,72}



Scheme 5 General ruthenium or base (left) and copper (right) catalyzed azide-alkyne cycloaddition.⁷⁰

The general mechanism of the CuAAC has not yet been clarified. The 1,4-disubstituted 1,2,3-triazole is obtained by reacting a terminal alkyne with an azide using a Cu^I catalyst. Various copper catalysts are applicable for the CuAAC, providing a Cu^I species is generated. Conventionally, in a solvent mixture of water and an alcohol (*t*BuOH, MeOH or EtOH) 0.20 eq. CuSO₄ is applied as Cu^{II} pre-catalyst together with 0.40 eq. sodium ascorbate as reducing agent, which additionally enables aerobic conditions due to oxidation prevention.⁶⁸ In a first proposed mechanism, following a mononuclear reaction, the catalytically active copper(I) generated *in situ* reacts with the terminal alkyne under the formation of a σ -bond to a Cu^I-acetylide intermediate (Scheme 6, **A**). Subsequently, the alkylated Lewis-basic nitrogen of the azide coordinates to Cu^I, followed by a transformation into a 6-membered metallocycle with copper being oxidized to Cu^{III}, considered as rate-determining step. Contracting the ring to a cuprous triazolide, with copper being reduced and substituting the transition metal by a proton completes the catalytic cycle.^{73,74} However, recent advances propose a bimetallic mechanism (Scheme 6, **B**). The high activation energy required for the formation of the constrained six-membered metallocycle contradicts the mononuclear mechanism. Density functional theory (DFT) calculations reveal that the activation barrier for the alkyne is significantly lowered when two copper ions are involved in the complexation, possibly *via* an

σ - and π -bimetallic intermediate. Moreover, kinetic studies support the involvement of two copper centers in the CuAAC mechanism. Consequently, mechanisms incorporating more than one copper ion have been proposed and are widely referenced in literature, although several intermediates remain uncertain and are still being studied.^{74,75}



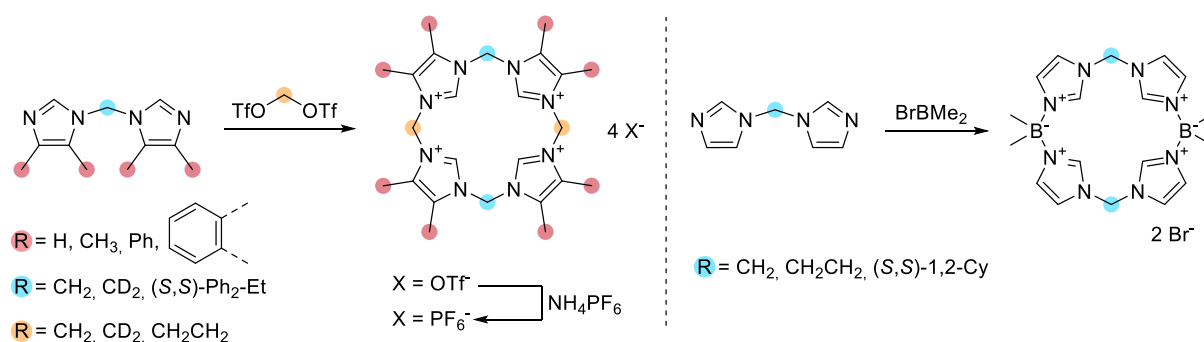
Scheme 6 Proposed catalytic mechanism following a mononuclear reaction (**A**) and a bimetallic reaction (**B**). For simplification [Cu] represents a copper-ion with an unspecific environment.

1.2.5 Macrocyclic tetra-NHC ligand precursors

Macrocyclic ligands, which form a continuous ring around a metal center and include at least nine ring atoms (three of which are potential donor atoms) are known for their ability to form highly stable metal complexes. The macrocyclic effect, which enhances both kinetic and thermodynamic stabilization, is crucial in the design of ligand frameworks in coordination chemistry and leads to the formation of metal complexes that exhibit significantly greater stability compared to their acyclic counterparts.^{31,76} When combined with NHC chemistry, such NHC metal complexes demonstrate potential as effective catalysts in various reactions, including oxidation and hydrogenation processes. Particularly, macrocyclic tetra-NHC ligands show the capacity to chelate metal ions with coordination numbers of four or higher.^{77,78} Since the report of a macrocyclic tetracarbene Pt^{II} complex formed *via* template controlled reaction by Hahn *et al.*⁷⁹ in 2007 these ligand subclass has received considerable attention.⁸⁰ Shortly after, a more convenient route for obtaining macrocyclic tetra-NHC metal complexes was developed by deprotonating imidazolium salts *in situ*.⁸¹

Apart from template synthesis, where the ligand system assembles around the metal center^{78,81}, the conventional synthesis of macrocyclic tetra-NHCs typically starts with the preparation of a bis-imidazole unit. This is achieved through a bimolecular nucleophilic

substitution reaction between the corresponding imidazole and a dihalogenated alkyl compound. The resulting bis-imidazole unit is then connected *via* a strong dielectrophilic coupling agent with efficient leaving groups, such as triflate (OTf^-), to form the macrocyclic structure (Scheme 7, left).³¹ A similar reaction employing dihaloalkanes for tetracarbene ring formation often results in the partial formation of larger cycles.⁸² The group of Jenkins concentrated on the synthesis of macrocyclic tetraimidazole diborates, which exhibit an increased σ -donor strength compared to alkyl-bridged tetra-NHCs. The ring formation proceeds *via* the reaction of the corresponding bis-imidazole with bromodimethylborane (Scheme 7, right).⁸³⁻⁸⁵ To minimize the risk of intermolecular coupling, the reactions are often conducted under dilute conditions.³¹



Scheme 7 General synthetic routes of macrocyclic tetraimidazoles.³¹

2 Carbon feedstock for chemical industry

The synthesis of various of bulk and fine chemicals is fundamentally reliant on the availability of carbon feedstocks, predominantly derived from the refining of mineral oil and natural gas.⁸⁶⁻⁸⁸ These carbon-based building blocks play a crucial role in the production of polymers, pharmaceuticals, flavors, fragrances, and coatings, among other industrial and consumer products.⁸⁶⁻⁹¹ Crude oil, primarily composed of alkanes with varying chain lengths and minor quantities of olefins, aromatics, and acetylene, undergoes a refining process that includes desalting and fractional distillation into various products such as gaseous fuels, naphtha, kerosene, and diesel.^{88,92} Notably, thermal steam cracking of naphtha (Figure 6, right), which consists mainly of lighter alkanes, produces significant quantities of ethylene and propylene (approximately 225 million tons⁹³ and 150 million tons annually⁹⁴, respectively) through the breaking of carbon-carbon bonds at elevated temperatures (450 to 900 °C) and pressures (up to 70 bar).^{87,88,92,95} Importantly, the production of ethylene and propylene has been increasing

over the years (Figure 6, left), reflecting the growing demand for these key intermediates in the chemical industry.^{93,94} The reaction temperature critically influences the product distribution, with higher temperatures favoring ethylene production.⁹⁵

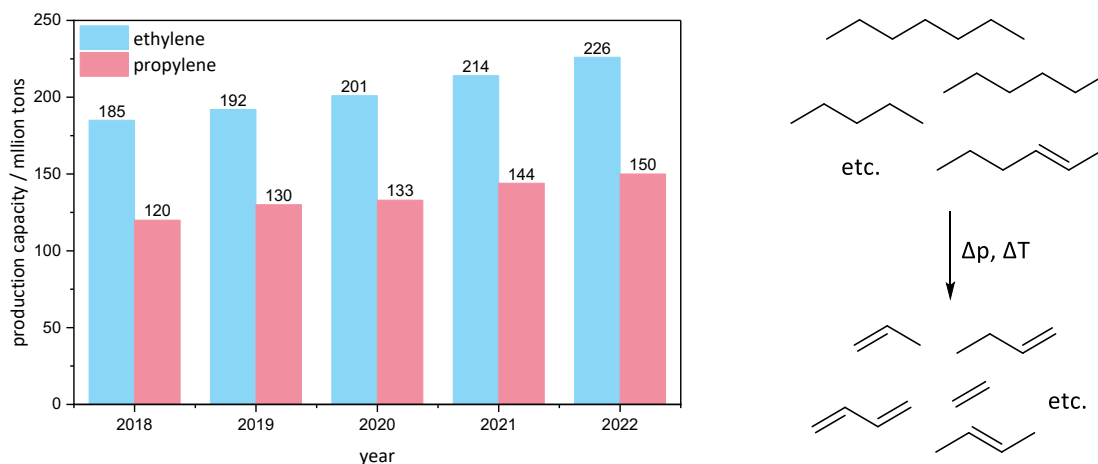
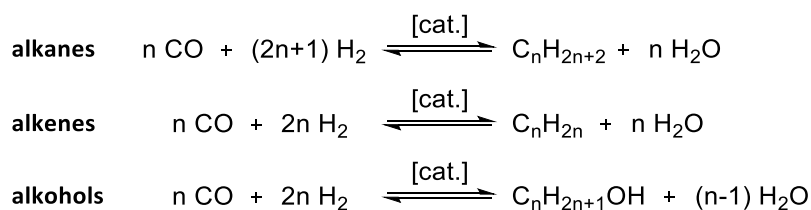


Figure 6 Production capacity of ethylene and propylene worldwide from 2018 to 2022 (left)^{93,94} and simplified representation of thermal steam cracking (right)^{86,96}.

Syngas, or synthesis gas, is a mixture of carbon monoxide and hydrogen produced from the gasification of carbon-containing materials, such as coal, natural gas, or biomass. This versatile intermediate can be used in various applications, including the production of chemicals and fuels. A key process for converting syngas into liquid hydrocarbons is the Fischer-Tropsch synthesis, which catalyzes the reaction of CO and H₂ to form liquid hydrocarbons, primarily synthetic fuels and lubricants, applying Co/Mn or Fe/Mn on a partially reduced oxide support as catalyst (Scheme 8).^{88,97}



Scheme 8 Reaction equations of the Fischer-Tropsch synthesis of alkanes, alkenes and alcohols.⁹⁷

The water-gas shift reaction is crucial for adjusting the CO to CO₂ ratio in the Fischer-Tropsch process. Water and carbon monoxide are converted into hydrogen and carbon dioxide using iron or copper-based catalysts. This reaction not only facilitates the regulation of the CO₂ ratio but also serves the additional benefit of transforming toxic carbon monoxide into less harmful

carbon dioxide, thereby improving the overall safety and environmental impact of the synthesis process.^{88,98,99}

These processes not only highlight the evolution of organic chemistry, which previously relied on coal-derived feedstocks, but also addresses the limitations associated with coal, such as toxic waste generation and safety hazards. The transition to using mineral oil fractions in the chemical industry has enhanced the ability to convert simpler hydrocarbons into more complex, valuable molecules through advanced techniques like catalytic and thermal steam cracking/reforming, thereby supporting the growing demand in various industrial applications.^{86,96}

3 Homogenous epoxidation catalysis

Parts of the following chapter are based on a previously published perspective³⁰, that was developed as part of this doctoral thesis. These sections have been integrated into this dissertation to expand upon the original insights and provide additional context to the overall research. In accordance with the citation guidelines outlined in the university's regulations on good scientific practice, these portions are correctly cited where necessary to ensure transparency and proper attribution.

Catalytic alkene epoxidation has received significant interest in both the chemical industry and academia due to the importance of epoxides in the production of bulk and fine chemicals.^{30,100,101} Ethylene oxide and propylene oxide are particularly notable as key intermediates, ranking among the most produced chemicals in industry, especially for polymer synthesis.^{30,102} For example, in 2022, global production of ethylene oxide reached approximately 31.6 million tons,¹⁰³ with the majority being utilized for the synthesis of ethylene glycol.¹⁰⁴ Furthermore, the epoxide functionality is presented in highly specific organic molecules, representing key compounds in polymer production, fragrances, detergents, flavors and pharmaceutical products (Figure 7). Among the latter, many are classified as anticancer agents.^{102,105-110}

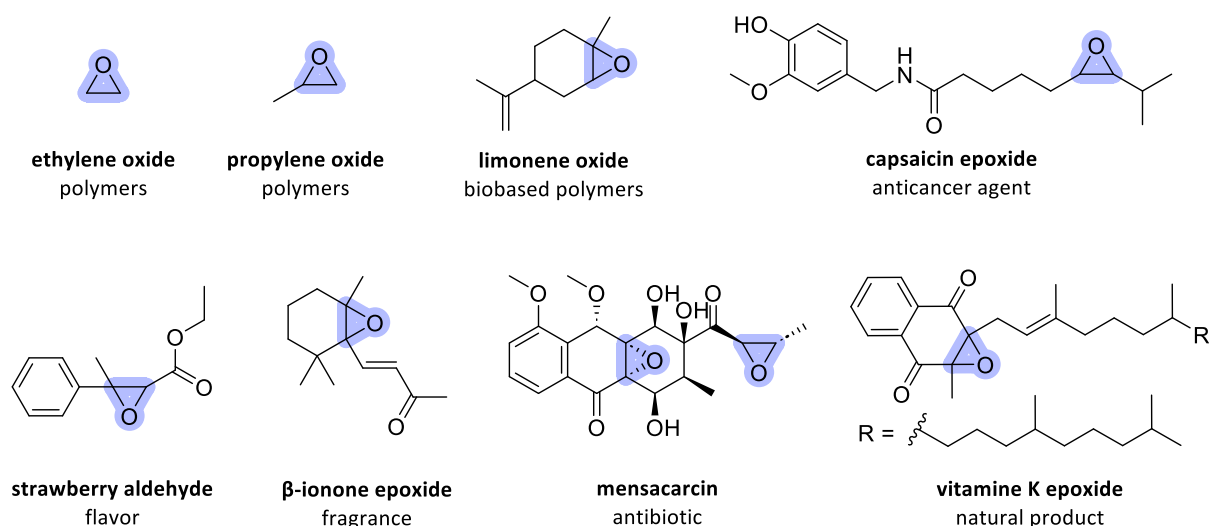


Figure 7 Selection of relevant fine chemicals with epoxide functionalities (highlighted), including pharmaceuticals, flavors and fragrances.^{102,105-110}

While the importance of epoxides in various industrial applications is undeniable, traditional methods for their production have faced several challenges. Historically, epoxidation reactions have been studied without the use of catalysts, often employing peroxocarbonic acids as stoichiometric oxidizing agents. However, these reagents tend to be unselective and relatively aggressive.^{30,111,112} In industrial applications, heterogeneous epoxidation catalysts, particularly silver- or gold-based systems, are commonly used for the conversion of simple bulk alkenes, such as the epoxidation of ethylene. While effective, these systems are typically very substrate-specific and exhibit little to no tolerance for functional groups.^{30,113} To address these limitations, homogeneous catalysts are frequently utilized in the production of specialized chemicals, offering enhanced selectivity and activity.^{30,114-116} However, many of these homogeneous epoxidation catalysts rely on scarce and often toxic transition metals, such as rhenium, tungsten and molybdenum, particularly noted for their use in processes like the *Arco-Halcon* process for propene epoxidation.^{30,117} Consequently, there is an ongoing effort to develop more suitable catalysts based on cheaper, more abundant, and non-toxic metals for selective epoxidation reactions. Iron, as the most abundant transition metal in earth's crust,^{118,119} has shown significant potential in various catalytic applications, including alkene epoxidation.^{30,100,117,120} Inspired by biological systems, catalysts have been designed with iron-stabilizing ligands.^{30,121,122} These catalysts often involve octahedral iron(II) complexes coordinated by tetradentate nitrogen donor ligands such as amines, pyridines, and pyrroles. Two labile ligands are typically coordinated to the metal center, oriented either *cis* or *trans*, mimicking the active sites of oxidation-catalyzing enzymes.^{30,122-125} Oxidants such as

hypochlorites¹²⁶, periodates¹²⁷, molecular oxygen¹²⁸, and peroxides^{117,120,122} are used for these reactions, with hydrogen peroxide being the most common due to its atom efficiency.^{30,122,129} *Cis*-cyclooctene is widely used as a model substrate for epoxidation in scientific literature.³⁰

3.1 Ti, Mn, Re and Mo olefin epoxidation catalysts

Significant advancements in homogeneous epoxidation catalysis have been made by pioneers such as Sharpless^{130,131}, Kochi¹³², Jacobsen^{133,134}, Katsuki^{135,136}, Espenson^{137,138} and Herrmann^{139,140}, who studied the performance and mechanism of titanium, manganese and rhenium complexes (Figure 8).^{88,117} Sharpless, in particular, made notable contributions to the field of asymmetric homogeneous epoxidation, for which he was awarded the 2001 Nobel Prize in Chemistry¹⁴¹. His work focused on the epoxidation of allyl alcohols, achieving over 90% enantiomeric excess. This method utilizes an *in situ* generated dinuclear titanium(IV) complex containing diethyl tartrate and alkoxy ligands, where the enantiomer of the product is determined by the tartrate configuration.^{88,130,131} For a broader substrate range, including olefins with aromatic and aliphatic substituents, manganese(III) salen catalysts have proven to be effective for highly stereoselective epoxidation reactions.^{88,132-136}

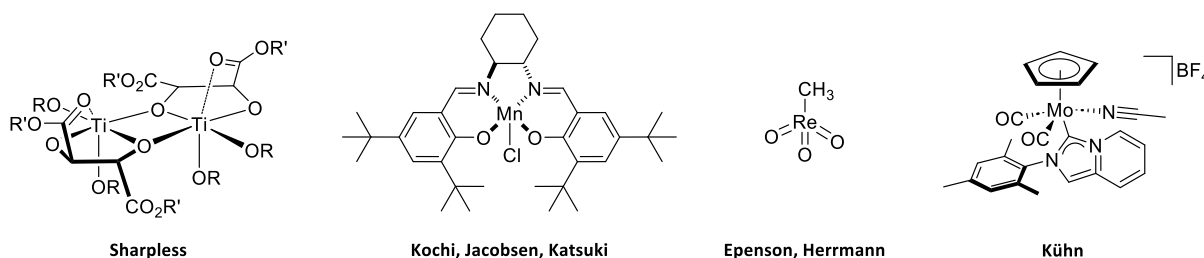
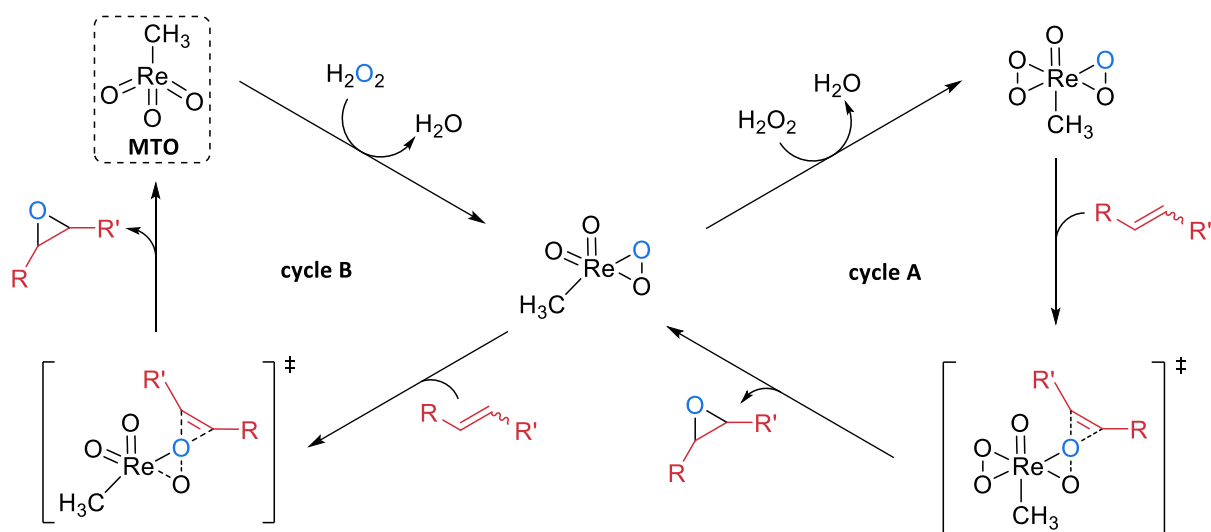


Figure 8 Relevant homogenous epoxidation catalysts studied by Sharpless^{130,131}, Kochi¹³², Jacobsen^{133,134}, Katsuki^{135,136}, Espenson^{137,138}, Herrmann^{139,140} and Kühn¹⁴² (adapted from ref. ⁸⁸).

Methyltrioxorhenium (MTO) stands out as a highly effective homogeneous epoxidation catalyst, overcoming many limitations of earlier systems, by facilitating the oxidation of various substrates under mild conditions. Initially discovered by Beattie and Jones in 1979¹⁴³, MTO was later applied for epoxidation by Espenson and Herrmann. Two key intermediates have been identified as the active species in these reactions (Scheme 9): the mono-peroxo complex¹³⁷, detected *via* spectroscopic methods, and the bis-peroxo complex¹³⁹, characterized by single-crystal X-ray diffraction (SC-XRD). Both species are formed upon reaction with one or two hydrogen peroxide molecules under elimination of water, respectively. These intermediates facilitate the epoxidation process *via* a concerted attack of

the peroxy moiety on the olefin, forming the epoxide product.^{117,144} The epoxidation of *cis*-cyclooctene with MTO achieves turnover frequencies (TOFs) up to 40,000 h⁻¹. However, the high cost of rhenium has driven interest in cheaper alternatives, such as molybdenum-based catalysts.¹¹⁷ In 2014, our group reported a Mo^{II}-NHC complex, which can achieve even higher TOFs in the epoxidation of *cis*-cyclooctene (up to 53,000 h⁻¹) but with a more limited substrate scope (Figure 8).^{117,142}



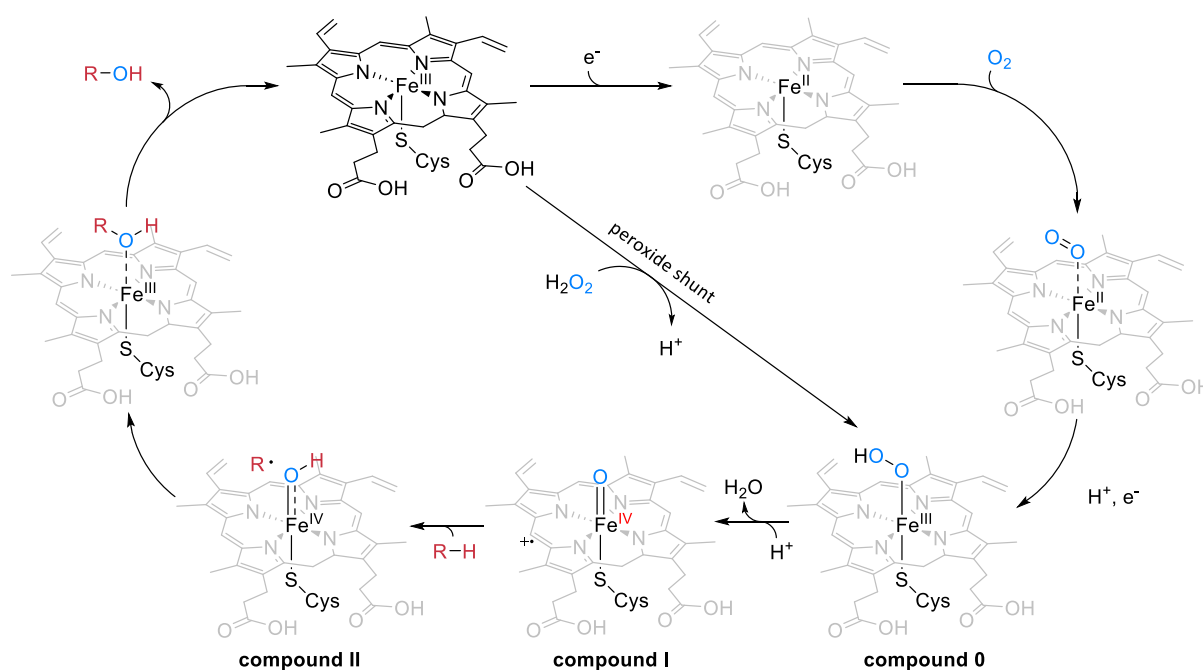
Scheme 9 Mechanism of the catalytic epoxidation of olefins with MTO with aqueous hydrogen peroxide as the oxidant.^{117,144}

3.2 Bio-inspired iron complexes in epoxidation catalysis

Nature overcomes the challenge of selective oxofunctionalization of diverse substrates under mild conditions by utilizing metalloenzymes, which facilitate these reactions with exceptional chemo-, regio-, and stereoselectivity.^{145,146} These enzymes contain active sites within hydrophobic pockets, enabling lipophilic substrates to access the catalytic center while promoting the release of more hydrophilic oxidation products. This arrangement helps to prevent undesired reactions, such as overoxidation.^{146,147} Notable examples of enzymes that catalyze the oxidation of C–H bonds in challenging substrates include heme-containing monooxygenases from the cytochrome P450 (CYP) family^{148,149} (*vide infra*), soluble methane monooxygenases (sMMO)¹⁵⁰, Rieske dioxygenases¹⁴⁵, and aromatic amino acid hydroxylases¹⁵¹. A common feature among these enzymes is their iron-containing active sites.¹⁴⁸⁻¹⁵¹ For example sMMO catalyzes the conversion of methane to methanol,¹⁵⁰ while CYP enzymes oxidize alkanes, alkenes, and aromatic compounds^{148,149}. They all utilize molecular oxygen as the terminal oxidant, forming a peroxy intermediate that is further converted into

a highly reactive iron-oxo species. Electrons required for the oxidation process are typically provided by a NAD(P)H cofactor.^{146,148-151}

Cytochrome P450 enzymes are essential for the oxidative transformation of both endogenous and exogenous compounds across a wide range of organisms, including plants, bacteria, and mammals. This extensive family of heme enzymes comprises over 2,000 members.^{148,149} Each enzyme features an active site that contains an iron(III) porphyrin cofactor, which is axially coordinated by a cysteine residue (Scheme 10).



Scheme 10 Proposed C–H activation mechanism of hydrocarbons on the active site of cytochrome P450 monooxygenase including key intermediate compounds 0, I and II.^{122,149}

This unique structural arrangement is critical for the enzyme's catalytic function, facilitating the oxidation of various substrates. The oxidation mechanism of CYP enzymes initiates with the low-spin Fe^{III} resting state, which transitions to a high-spin Fe^{II} center upon the coordination of an oxygen molecule (Scheme 10). This interaction leads to the formation of an iron(III) hydroperoxy intermediate (compound 0). The subsequent proton assisted heterolytic O–O bond cleavage generates a formal iron(IV) oxo species (compound I), as active species, featuring a porphyrin π -cation radical. This high-valent intermediate acts as the primary oxidant, facilitating the epoxidation of hydrocarbons *via* radical abstraction by forming an iron(IV) hydroxo complex (compound II). Additionally, the stabilization of compound I *via* the delocalization of the positive charge within the porphyrin ligand enhances its reactivity. The cycle concludes with the regeneration of the initial Fe^{III} heme complex. If

hydrogen peroxide is utilized as the terminal oxidant, the catalytic pathway diverges, leading to the direct formation of the $\text{Fe}^{\text{III}}\text{-OOH}$ intermediate through the peroxide shunt pathway.^{122,148,149,152,153}

Advances in biological research and the growing understanding of enzyme structure and active site motifs have provided valuable insights for catalyst development over the past decades. As a result, there has been increasing interest in designing biomimetic catalysts, particularly those based on more affordable, abundant, and environmentally friendly metals like manganese and iron. These metals offer a promising alternative for mimicking the function of natural enzymes while maintaining sustainability and reducing toxicity.^{121,122}

3.2.1 Non-heme iron catalysts with *N*-donor ligands

Bio-inspired iron catalysts can generally be categorized into two main classes: heme and non-heme complexes. Heme catalysts are characterized by their porphyrin ligands, mimicking the natural iron-porphyrin systems. In contrast, non-heme iron catalysts are more structurally diverse and typically incorporate tetradentate *N*-donor ligands (Figure 9). These complexes often feature two labile ligands, such as triflate (OTf) or acetonitrile (MeCN), which play a key role in their catalytic activity by enabling substrate coordination and activation.^{88,117,154} Heme complexes exhibit *trans* orientated labile ligands, whereas non-heme iron complexes mostly feature *cis* labile coordination sites.^{88,129,154,155}

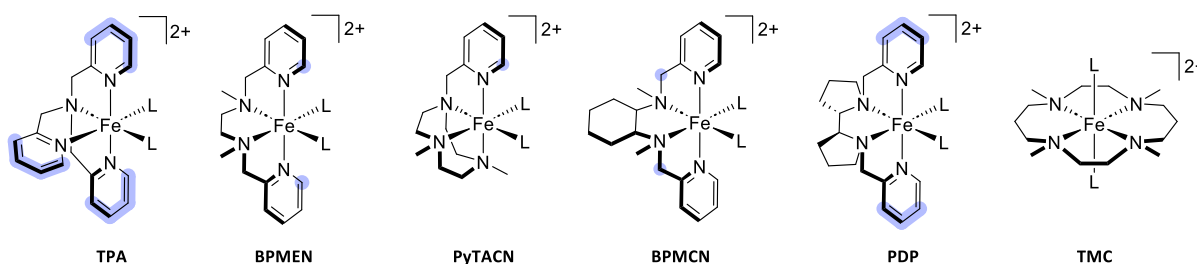
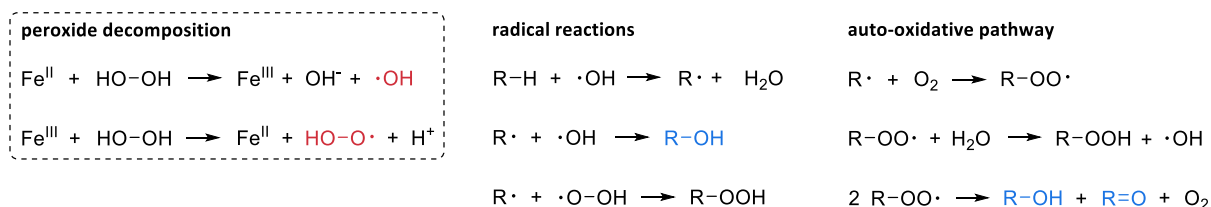


Figure 9 Structures of selected non-heme iron (ep)oxidation catalysts with their ligand abbreviations below. L = labile solvent ligand (generally MeCN or OTf). Known functional positions in literature are highlighted.^{117,154}

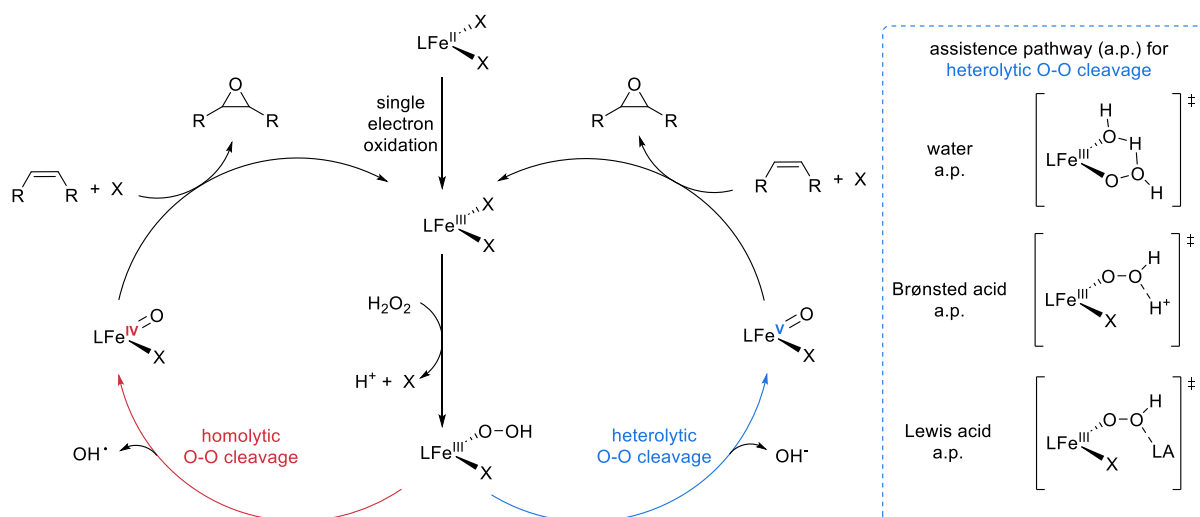
Two primary catalytic pathways are described for oxidation reactions involving synthetically generated non-heme iron catalysts. The mechanism involving high-valent iron-oxo species compete with undesired radical-based Fenton-type pathway. The Fenton-type¹⁵⁶ mechanism proceeds *via* the formation of long-lived radicals (Scheme 11). In this mechanism, the peroxide species decomposes in the presence of Fe^{II} or Fe^{III} , generating powerful, but highly unselective (hydroxyl) radicals. These radicals rapidly engage in various radical-based reactions with

organic substrates. When dioxygen is present, the reaction can lead to a termination step, known as the auto-oxidative pathway. This step results in the formation of equal amounts of alcohol and ketone as the final oxidation products, reflecting the non-selective nature of this mechanism.^{30,157,158}



Scheme 11 Fenton-type mechanism of irons catalyzed oxidation reactions with H_2O_2 as oxidant and following radical reactions.^{157,158}

The second, and desirable, pathway for the oxidation mechanism of alkenes involves a metal-centered process mediated by high-valent Fe^{IV} - or Fe^{V} -oxo intermediates. This pathway is largely accepted as the operative mechanism, though certain aspects remain to be fully elucidated. It draws parallels with the catalytic cycle observed at the active site of CYP enzymes. The preferred oxidation state of this species is influenced by the electronic and steric characteristics of the tetradentate spectator ligand and the associated orientation of labile ligands. Notably, extensive research conducted by the groups of Que¹⁵⁴, Costas¹⁵⁹ and Nam^{160,161} has significantly advanced the mechanistic understanding of non-heme iron complex catalysis. The reaction begins with a single electron oxidation of the Fe^{II} catalyst precursor, typically by oxidants such as hydrogen peroxide, leading to the formation of a Fe^{III} -hydroperoxo intermediate.^{30,122,125} The formation of $\text{Fe}^{\text{III}}\text{-OOH}$ is supported by various spectroscopic techniques. UV-visible (UV/Vis) spectroscopy reveals a characteristic absorption band, often associated with the intense purple color of these species.^{30,122} This intermediate, formed *in situ* upon deprotonation of H_2O_2 and coordination to the Fe^{III} center, undergoes either homolytic or heterolytic cleavage of the O–O bond, as the rate-determining step (rds) due to the poor leaving ability of the hydroxide, generating the catalytically active species (Scheme 12). Importantly, Que, Mück, Nam¹⁶² and co-workers have provided direct experimental confirmation of the homolytic bond cleavage through SC-XRD analysis, identifying the $[\text{Fe}^{\text{IV}}(\text{O})(\text{TMC})(\text{MeCN})]^{2+}$ species as a key intermediate for iron complexes with *trans* labile ligands. Additionally, variable-temperature mass spectrometry (VT-MS) has been employed to detect the formation of iron(V) species, further corroborating the mechanistic pathway.^{30,163}

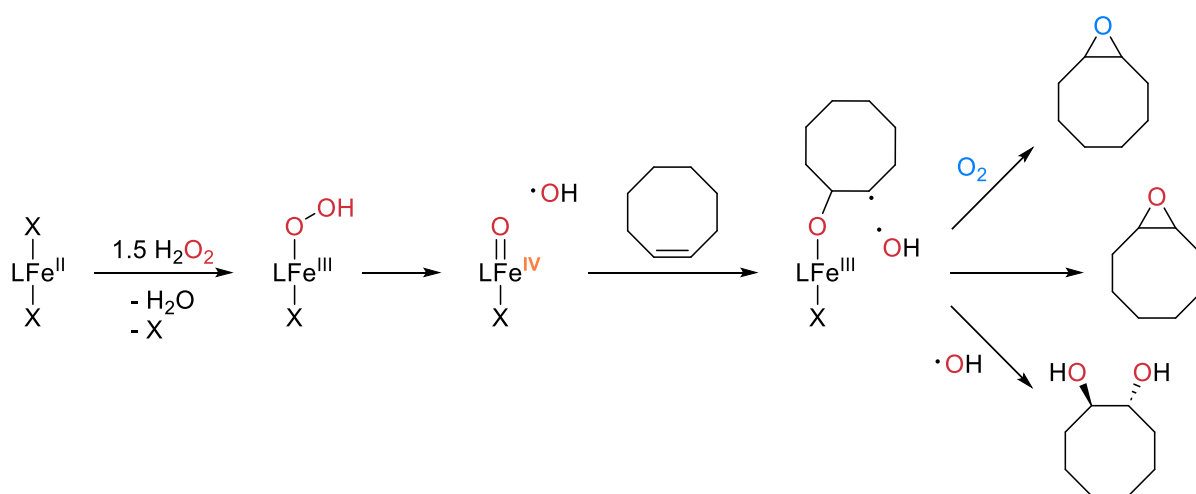


Scheme 12 Catalytic mechanism for epoxidation of alkenes by non-heme iron(II) complexes with tetradentate *N*-donor ligands (L) affording *cis*-labile coordination sites and transition states for assistance pathways (X = labile solvent ligand). Acceleration of the rds heterolytic O–O bond cleavage is possible by water, Brønsted acid or Lewis acid (LA) assistance (adapted from ref. ³⁰).

The heterolytic cleavage of the O–O bond, which results in the formation of a high-valent Fe^V-oxo species, can be facilitated by the presence of water. The water-assisted pathway (wap) operates exclusively with *cis*-labile coordination sites.^{30,124,164} Here, water coordinates near the hydroperoxo intermediate *via* hydrogen bonds, accelerating the heterolytic O–O cleavage and Fe^V-oxo formation.^{30,124} Subsequent electrophilic attack on the alkene substrate yields the product epoxides. During this process, the oxygen atom involved in the epoxide cycle can originate from either the coordinated water molecule or the hydrogen peroxide used initially. This occurs due to rapid oxo-hydroxo tautomerization within the iron complex.^{30,122,125,129} Alternatively, the presence of *cis*-oriented labile ligands within the wap may drive the reaction towards *cis*-dihydroxylation, where the high-valent iron-hydroxo intermediate attacks the alkene to form *cis*-diols.^{30,122-124} This dihydroxylation mechanism, however, is not observed when *trans*-labile ligands are present, especially in tetradentate non-heme iron complexes.^{30,160}

The addition of Brønsted or Lewis acids, making OH⁻ to a better leaving group by protonation or coordination further enhance the catalysts performance. When acetate binds to the Fe^{III}-OOH intermediate in a manner similar to water, it facilitates the formation of the catalytically active Fe^V(O)(OAc) intermediate by suppressing H₂O coordination. This intermediate is both highly electrophilic and selective for epoxide formation.^{30,165}

Research into the epoxidation mechanisms of tetradentate non-heme iron complexes with *trans*-labile coordination sites remains relatively limited. Complexes utilizing H_2O_2 as an oxidant have often been overlooked due to lower turnover numbers and modest yields compared to *cis*-configured systems, leading to assumptions about their limited efficiency in epoxidation processes.^{122,166,167} However, recent findings reveal that *trans*-labile iron complexes exhibit distinct mechanistic pathways and key intermediates, offering unique selectivity advantages.^{122,166} The proposed mechanism is primarily characterized by the formation of a Fe^{IV} -oxo species, rather than a Fe^{V} -oxo intermediate.^{122,168} Upon reaction with H_2O_2 , the formed Fe^{III} -OOH intermediate undergoes O–O bond cleavage (Scheme 13). The epoxide is either formed *via* direct oxygen transfer to the C=C bond or a radical mechanism involving molecular oxygen. The electrophilic nature of the Fe^{IV} -oxo species is key to the selective epoxidation of alkenes, without promoting dihydroxylation (as observed with Fe^{V} -oxo complexes) Additionally, the *trans*-labile configuration restricts water coordination near the hydroperoxo ligand, making a water-assisted heterolytic O–O bond cleavage unfeasible.^{122,166,169}



Scheme 13 Schematic representation of the catalytic mechanism for epoxidation of *cis*-cyclooctene with H_2O_2 by non-heme iron(II) complexes with tetradentate *N*-donor ligands (L) affording *trans*-labile coordination sites; X = labile solvent ligand (adapted from ref. ¹²²).¹⁶⁹

3.2.2 Iron NHC catalysts

Unfortunately, most non-heme iron catalysts perform rather poorly compared to the enzymes they are meant to mimic or to metal-based complexes containing titanium, manganese, molybdenum and rhenium. The group of Que¹⁷⁰ reported the highest TOF of 25,200 h^{-1} , achieving a 50% yield of cyclooctene oxide with a 0.5 mol% catalyst loading in just 14 s, using

the non-heme iron epoxidation catalyst $[\text{Fe}(\text{BPMEN})(\text{MeCN})_2]^{2+}$. However, this result required acetic acid as additive. In additive-free conditions, the maximum reported TOF was around $4,100 \text{ h}^{-1}$, yielding 17% after 30 seconds. Although a few studies report TOFs exceeding $1,000 \text{ h}^{-1}$ with additives,¹⁷¹ most systems typically reach maximum TOFs^{123,172} in the range of $100\text{-}1,000 \text{ h}^{-1}$.¹⁷³

In 2014 our group were the first who described the application of an active iron NHC complex in epoxidation catalysis.¹⁷³ The complex coordinates an acyclic tetradentate di(*o*-imidazol-2-ylidenepyridine)methane ligand *via* its two carbene carbon atoms and two pyridine *N*-donors (Figure 10, **3**). The ligand adopts an equatorial geometry around the metal center, leaving the axial positions available for additional coordination.^{30,174} While iron carbon bonds are generally more thermodynamically unstable than iron oxo bonds, complex **3** remains air- and water-stable due to the ligands chelating and stabilizing nature. **3** demonstrates impressive selectivity (> 99%) for producing cyclooctene oxide using H_2O_2 as oxidant and the benchmark substrate *cis*-cyclooctene. At room temperature (r.t.) **3** achieves a 99% conversion within just 5 minutes at a catalyst loading of 5 mol%, operating effectively without additional additives. TOFs reach *ca.* $2,600 \text{ h}^{-1}$ (1 min, 2 mol% of **3**, 25 °C) with high selectivity across various alkenes. However, under oxidative conditions, the catalyst experiences deactivation, and increased concentrations of the oxidant reduce alkene conversion, indicating partial catalyst deactivation. At lower concentrations, hydrogen peroxide limits the reaction by providing insufficient oxidizing agents. Two opposing effects were noted with decreasing temperatures: reaction rates decrease, but catalyst stability significantly improves.^{30,173}

One year later our group reported the catalytic activity of a more heme like iron NHC system.¹²⁰ The iron complexes studied here feature a macrocyclic imidazole based tetracarbene ligand that coordinates in an equatorial plane around the iron center, creating a near-perfect octahedral geometry, with two acetonitrile molecules occupying the axial positions (Figure 10, **4**).¹⁷⁵ Since single electron oxidation to iron(III) is considered to be part of the catalytic mechanism in non-heme iron complexes with tetradentate *N*-donor ligands (*vide supra*) both Fe^{II} and Fe^{III} oxidation states are investigated. Excellent catalytic performance is obtained using complexes **4** as catalyst in the epoxidation of *cis*-cyclooctene with H_2O_2 . At r.t. and a catalyst concentration of 0.5 mol% full conversion is reached within 5 min and an epoxide selectivity of > 99%, highlighting the remarkable catalytic potential of

this framework. **4a** reaches a TOF of *ca.* 50,400 h⁻¹ (10 s, 0.10 mol% of **4a**, 25 °C)¹²⁰ and a TON of 480 (5 min, 0.05 mol% of **4a**, 20 °C)¹⁷⁶. Applying Fe^{III} catalyst **4b** pushes the TOF significantly to *ca.* 183,600 h⁻¹ (10 s, 0.10 mol% of **4b**, 25 °C). The improved activity may indicate a reduced decomposition of H₂O₂, due to Fenton-type radical pathways suppression (*vide supra*). Furthermore, the oxidation of complex **4a** to its Fe^{III} counterpart likely initiates the reaction mechanism, evidenced by an induction period observed in **4a** that is absent in **4b**. Although detailed mechanistic studies specific to iron NHC complexes are lacking, insights from similar *N*-ligated iron complexes suggest that an Fe^{III}-OOH intermediate forms as the next step. This intermediate may then undergo either a homolytic or heterolytic cleavage, producing a catalytically active high-valent Fe^{IV}-oxo or Fe^V-oxo species, respectively.^{31,120}

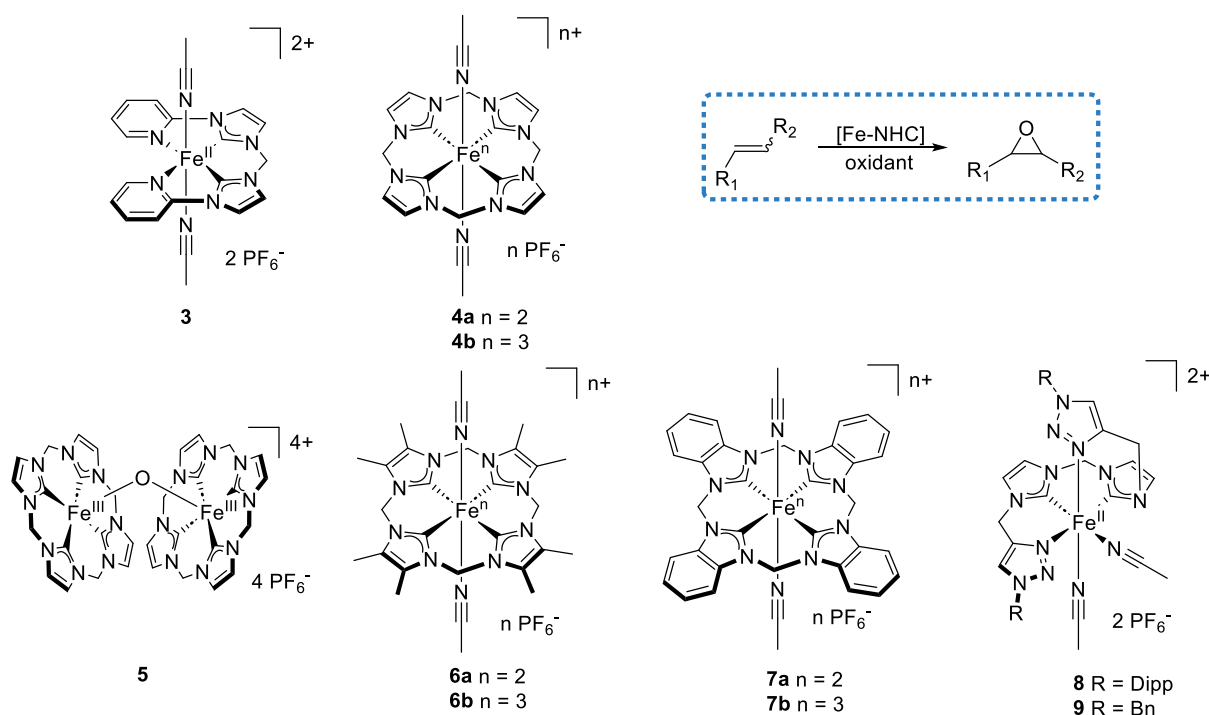
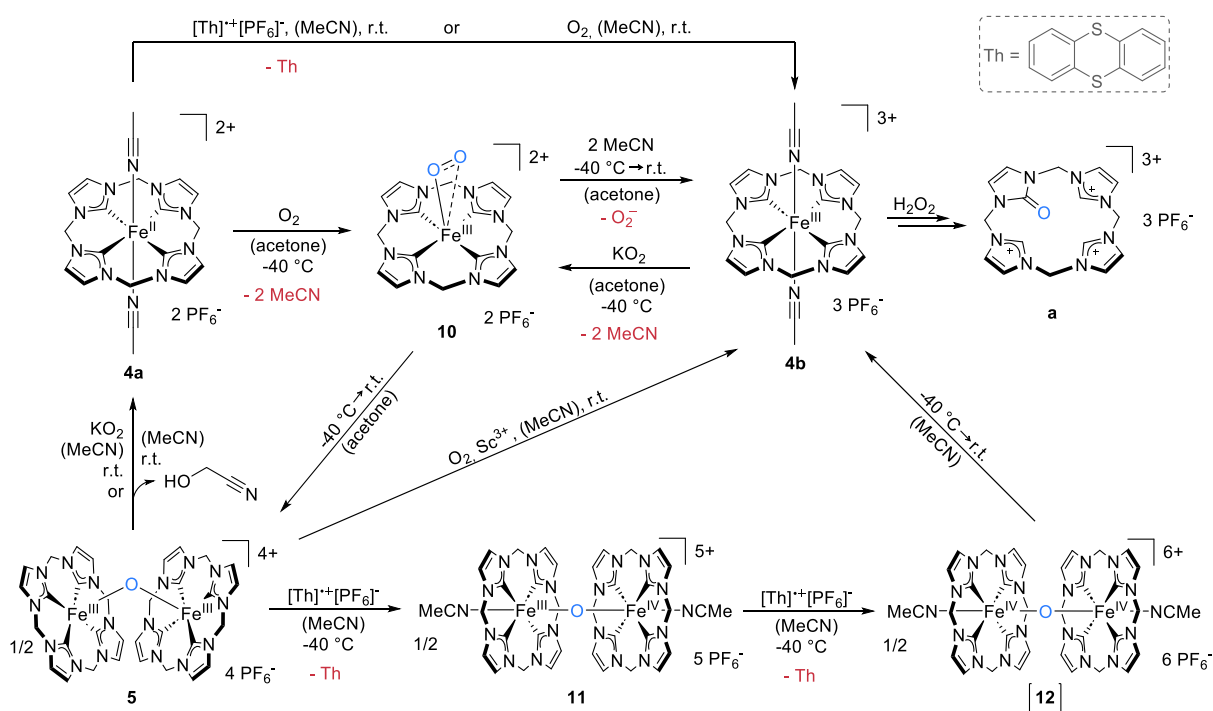


Figure 10 Iron NHC epoxidation catalysts (adapted from ref. ³⁰).

Compound **4b** maintains high activity and selectivity even at low temperatures, with complete conversions at temperatures as low as -10 °C. Decreasing temperatures again slow reaction rates but enhance the catalyst stability. Optimal epoxidation yields are achieved with moderate H₂O₂ concentrations, particularly between 150-300 mol%. Higher levels of H₂O₂ slightly lower catalytic yields, as excess oxidant reduces the catalyst's stability over time. Interestingly, the addition of water, often beneficial in other non-heme Fe catalysts with *cis*-labile coordination sites, does not enhance the activity of the iron tetracarbene complexes

and can even reduce epoxide yields. This confirms that macrocyclic Fe tetra-NHCs operate *via* a non-wap (like *trans*-labile non-heme iron catalysts with *N*-donor ligands).¹²⁰

Oxidative conditions in iron complex catalysis often lead to the formation of stable diiron(III)- μ_2 -oxo complexes, which are typically catalytically inactive and reduce reaction efficiency. Specifically, diiron(III)- μ_2 -oxo complex **5** has been observed to form under oxidative conditions from complexes **4a** and **4b** (Scheme 14), showing limited catalytic activity with a TOF of *ca.* 23,000 h⁻¹ and a turnover number (TON) of 140 ($t_{\text{TOF}} = 10$ s, $t_{\text{TON}} = 5$ min, 0.05 mol% based on iron, 20 °C).^{31,176,177} The addition of Lewis acids reactivates complex **5** by preventing the formation of Fe–O–Fe compounds and promoting the consistent formation of the active iron(III) complex **4b**.^{31,176} Furthermore, Lewis acids are believed to assist in the cleavage of the O–O bond in the Fe^{III}–OOH species, shifting the rds towards more efficient olefin oxidation.³¹ Adding Lewis acids such as Sc³⁺, Ce⁴⁺, and Fe³⁺ salt significantly enhance the performance of complexes **4a**, **4b** and **5**, achieving similar results for all three catalysts, with TOFs of *ca.* 410,000 h⁻¹ and TONs of *ca.* 1,200 ($t_{\text{TOF}} = 10$ s, $t_{\text{TON}} = 5$ min, 0.05 mol% based on iron, 20 °C).^{31,176}



Scheme 14 Overview of detected and/or isolated species formed upon oxidative reaction of **4a**.³¹

Under ambient conditions in MeCN, complex **4a** is suggested to react stoichiometrically with O₂, leading to the formation of the iron(III) complex **4b**. This process likely involves an oxygen-

axial ligand exchange. No iron-oxo intermediates or oxygenated species are observed under these conditions, likely due to MeCN oxidation. However, using solvents with less reactive C-H bonds, like acetone, results in the formation of a μ_2 -oxo bridged diiron(III) complex **5**. On the path to forming **5**, a stable intermediate **10** can be isolated at $-40\text{ }^\circ\text{C}$ in acetone, remaining stable for days in solution or in solid state (Scheme 14). The superoxide identity of **10** is confirmed *via* EPR spectroscopy, where an oxygen-centered radical is shown to be coordinated to the iron center, establishing **10** as an iron(III)-superoxo complex. Alternatively, **10** can also be formed by reacting complex **4b** with KO_2 at $-40\text{ }^\circ\text{C}$ in acetone, which converts to **5** upon warming. The reduction of complex **5** with KO_2 or dissolving in MeCN at r.t. (with MeCN undergoing oxidation to form glycolonitrile) regenerates complex **4a**. Addition of MeCN to **10** yields iron(III) complex **4b**, mirroring the reactivity of **4a** with O_2 .^{31,177} Further oxidation of **5** with ThPF_6 in MeCN at $-40\text{ }^\circ\text{C}$ yields diiron(III,IV)- μ_2 -oxo complex **11**, which is stable for several months at $-37\text{ }^\circ\text{C}$. The Fe–O–Fe bond angle in **11** shifts to nearly linear, from 162.7° for **5** to 176.3° . The increased Lewis acidity at the iron center is proposed to allow the coordination of two axial MeCN ligands. Cyclic voltammetry (CV) suggests that **11** can be oxidized further to a diiron(IV)- μ_2 -oxo complex **12**, evidenced by a color change upon adding one equivalent ThPF_6 at $-40\text{ }^\circ\text{C}$ to **11**. This transient species quickly reverts to **4b** upon warming to r.t. (studied *via* UV/Vis spectroscopy).^{31,178}

While the found deactivation pathway, where **4a** and **4b** convert into the μ_2 -oxo-bridged complex **5** during catalysis, can be suppressed, the stability remains insufficient for practical applications. Typical decomposition in non-heme iron oxidation catalysts with *N*-donor ligands additionally involves C–H oxidation of methylene bridges.^{31,179,180} Investigations into the deactivation of active catalyst **4b**, C–H oxidation was ruled out, as catalytic tests with deuterated **4b-*d*₈**, in which all proton atoms of the methylene bridges are replaced by deuterium, showed no kinetic isotope effect. NMR analysis revealed a main decomposition product, identified as a mono-oxidized, threefold-protonated ligand species **a** (Scheme 14). It is suggested that oxidation occurs before carbene protonation, as mass spectrometry detected only this partially oxidized ligand and not a fully protonated version. Additionally, a species with a mono-oxidized ligand still bound to iron was detected.^{31,181}

A comprehensive overview of the characteristic and reactivity of macrocyclic tetra NHC iron complexes is provided in ref. ³¹.

The electronic properties of iron complexes can be adjusted by modifying their ligand frameworks, which directly impacts their catalytic efficiency. In this context, two series of iron(II) and iron(III) complexes, each with distinct modifications in their NHC backbone, are developed (Figure 10, **6** and **7**).¹⁸² Complexes **7a** and **7b** incorporate benzimidazole units in their tetracarbene ligands, reducing σ -donation compared to complexes **4a** and **4b** and creating a less electron-rich iron center. This decreased electron density is expected to influence catalytic activity since a more electron-rich iron center is supposed to favor the formation of electrophilic iron(IV/V)-oxo species. Complexes **7a** and **7b** display moderate activity at 20 °C, achieving a TOF of *ca.* 11,000 h⁻¹ for **7b** (with addition of Sc(OTf)₃, 10 s, 1 mol% of **7b**). However, complex **7b** stands out for its stability, showing a TON of 1,000 (with addition of Sc(OTf)₃, 0.10 mol% of **7b**, 20 °C) and demonstrating tolerance for higher temperatures, reaching a TOF of 95,000 h⁻¹ at 80 °C (with addition of Sc(OTf)₃, 10 s). Additionally, complex **7b** exhibits superior performance over **4b** in processing more challenging alkenes under similar conditions.^{31,182,183}

In contrast, iron complexes **6a** and **6b** are based on a methyl-substituted tetracarbene ligand backbone, which is supposed to increase the electron density at the iron center. This greater electron richness, provided by the positive +I-effect of the methyl groups, is expected to enhance σ -donor properties and could theoretically support higher catalytic activity. Indeed, **6a** and **6b** display greater initial catalytic activity than **7a** and **7b**, but show less stability than complexes **4a** and **4b**, even at ambient temperatures. The best conversion for *cis*-cyclooctene with complex **6a** is achieved at 20 °C with the addition of Sc(OTf)₃ (yielding 82% with 49% selectivity), while at 20 °C without the addition of Sc(OTf)₃, both **6a** and **6b** maintain similar conversions of 40% and 46%, respectively. This performance is likely due to a rapid initial oxidation from Fe^{II} to Fe^{III}, as suggested by the absence of an induction period, which is seen in **7a**. Although complexes **6a** and **6b** exhibit lower stability, DFT calculations reveal significant π -backbonding, which appears to counterbalance the electron-donating influence of the methyl groups. This balance between σ -donation and π -backbonding could explain their comparatively lower catalytic activity in relation to complexes **4a** and **4b**, despite their higher inherent electron-donating properties.^{31,182,183}

In 2020, the first iron NHC complexes, featuring exclusively *cis* labile coordination sites, were introduced and applied in olefine epoxidation (Figure 10, **8** and **9**).¹⁸⁴ These complexes feature

acyclic mixed tetradentate NHC/1,2,3-triazole ligands. In acetonitrile, they exhibit an equilibrium between a "sawhorse-type" coordination with *cis*- α acetonitrile ligands and a C_2 -symmetric configuration with *cis*- β oriented labile acetonitrile ligands, which can be observed *via* NMR spectroscopy. An equatorial arrangement of the ligand framework could not be confirmed, likely due to the steric hindrance posed by substituents (Dipp in **8** or Bn in **9**) on the triazole units acting as nitrogen donors. Non-heme systems with *cis* labile coordination sites often show higher oxidation activity, achieved by water or Brønsted acid involvement in the catalytic cycle (*vide supra*). Initial studies of the catalytic performance of **8** and **9** showed only minimal activity without additives. However, introducing acidic additives such as acetic acid significantly enhanced both selectivity (97%) and catalytic activity, achieving a TOF of *ca.* 76,000 h⁻¹ and a TON of *ca.* 200 with **9** ($t_{\text{TOF}} = 10$ s, $t_{\text{TON}} = 3$ h, 0.1 mol%, 20 °C). In contrast, when HOAc was applied to related complexes, **4a** and **4b**, which feature *trans* labile coordination sites, no improvement in activity was observed, supporting the proposed catalytic pathway favoring *cis*-oriented sites. **8** and **9** exhibit strong tolerance to functional groups with high selectivity.^{183,184}

4 Macrocyclic late transition metal NHC complexes

The coordination chemistry of late transition metals such as nickel, palladium, platinum, copper, silver and gold, has gained significant interest due to their unique electronic properties and diverse applications in catalysis, photoluminescence and biological activity. Among the diverse ligands available, NHCs have emerged as particularly versatile and robust options, offering high σ -donating and tunable electronic characteristics. These properties enable stabilization of metals in multiple oxidation states and varied coordination geometries, thereby broadening their applicability.¹⁸⁵⁻¹⁸⁷

Silver NHC complexes are notable for their stability and controlled ion release, which underlines their exceptional antimicrobial and anticancer properties. These complexes surpass traditional silver compounds in efficacy, disrupting bacterial, fungal, and cancer cell functions with precision, making them invaluable in bioorganometallic chemistry. Silver NHC complexes are often used as transmetalation agents, enabling the synthesis of other transition metal complexes. Similarly, gold NHC complexes exhibit exceptional stability and unique biological activity, including anticancer, antimicrobial, and antiplasmodial effects. Their robust

metal-ligand bonds and structural adaptability, typically achieved *via* transmetalation methods of corresponding silver NHC complexes, have established them as leading candidates in drug development, with particular promise in targeting cancer and bacterial infections.¹⁸⁵

In the field of catalysis, nickel NHC complexes play a crucial role, leveraging the electronic and steric properties of NHC ligands to stabilize nickel in various oxidation states and geometries. Their contributions to green chemistry are profound, particularly in facilitating C–C and C–heteroatom coupling reactions, small molecule activation, and sustainable catalytic processes.¹⁸⁶ Palladium NHC complexes, on the other hand, have revolutionized organic synthesis through their impact on cross-coupling and hydrogenation reactions, while also exhibiting significant biological activity in anticancer therapies. Their structural diversity and stability have allowed for precise tuning, enabling advances in both catalysis and medicinal chemistry.¹⁸⁵

Platinum NHC complexes have redefined the potential of organometallic compounds in oncology, addressing limitations of traditional platinum-based drugs like cisplatin. Their robust metal-ligand bonds and enhanced stability reduce toxicity while improving therapeutic effectiveness. The ability to modify these complexes post-synthetically has opened new pathways for targeted drug delivery, imaging, and broader medicinal applications.¹⁸⁷ The integration of NHCs into macrocyclic frameworks has been especially transformative, providing ligands with enhanced stability due to the macrocyclic effect.¹⁸⁷

In 2016, our group explored the coordination modes of silver(I), gold(I), nickel(II), palladium(II) and platinum(II) complexes **13-17** supported by the methylene-bridged macrocyclic imidazole based tetracarbene ligand (Figure 11),⁷⁷ which has been described in the catalytic iron alkene epoxidation (*vide supra*). Ag^I ions typically form linear coordination with two NHC ligands. Macrocyclic Ag(I) complexes can be categorized into three distinct types: (a) structures where silver ions are exclusively coordinated within the cavity of the NHC ligand,^{77,81,188} (b) box-type complexes formed by two ligands and four silver ions, with two ions occupying the ligand cavities and the other two serving as bridges between the ligands,^{77,189,190} and (c) box-type complexes where all Ag^I ions are positioned exclusively as bridges between two ligand frameworks. Silver(I) complex **13** exhibits a distinctive molecular box-type structure, characterized by close silver–silver contacts within a tetranuclear core. The compound serves as an effective transmetalation reagent for synthesizing analogous gold(I) and group 10 metal

complexes. The gold(I) derivative **14** mirrors the molecular box geometry, demonstrating shorter gold–gold distances indicative of aurophilic interactions. The group 10 metal complexes of nickel(II) (**15**), palladium(II) (**16**) and platinum(II) (**17**) adopt a square planar coordination geometry within the macrocyclic cavity. The study reveals subtle structural differences influenced by the ionic radii of the central metals, affecting both ligand distortion and vibrational dynamics.⁷⁷

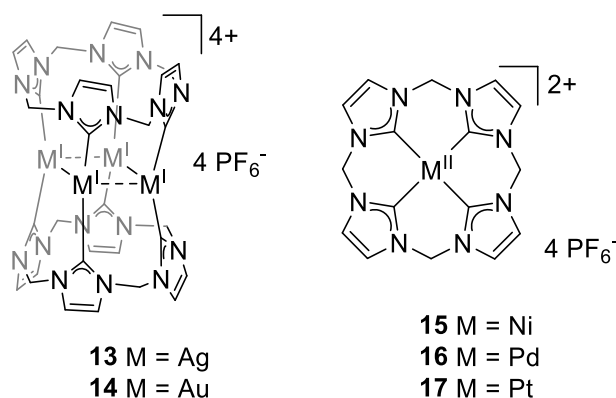


Figure 11 Silver(I), gold(I), nickel(II), palladium(II) and platinum(II) complexes supported by methylene-bridged macrocyclic imidazole based tetracarbene ligand.⁷⁷

Replacing the macrocyclic ligand system with a modified one, consisting of benzimidazole units leads to the isolation of complexes **18-22** (Figure 12).^{191,192} Silver(I) complex **18** exhibits a rigid box-type coordination geometry, comparable to its imidazole counterpart **13**. The corresponding gold(I) complex **19**, displays a markedly different mixed coordination geometry, where two gold atoms are linearly coordinated within the macrocyclic cavity of each ligand, forming internal C–Au–C units. These gold atoms exhibit Au–C bond lengths around 2.03 Å, slightly longer than those of the external gold centers. The other two gold atoms are positioned externally, connecting the two ligands in a bridging arrangement through additional linear C–Au–C interactions. The internal gold atoms are involved in aurophilic interactions, with Au–Au distances of approximately 3.20 Å and 3.33 Å.¹⁹¹ Ni^{II}, Pd^{II}, and Pt^{II} compounds **20-22** exhibit less distortion from square planar geometry compared to compounds **15-17** as the benzimidazole-based ligand provides a more optimal coordination environment, reducing angular deviations and structural deformation.¹⁹²

II Objective

The notable activity of non-heme iron complexes **4a** and **4b** in epoxidation catalysis, offers an excellent basis for advancing the study of macrocyclic tetra-NHC iron complexes. Enhancing the catalytic system could be achieved by fine-tuning the NHC ligand framework. Specifically, modulating the level of electron donation to the iron center can influence the catalytic properties in a controlled manner. Adjustments to the ligand design could improve catalytic activity enhance system stability, enable reactions at elevated temperatures, or facilitate the conversion of more challenging substrates.

The impact of axial ligands' occupation on the catalytic epoxidation activity of **4a** and **4b** is a focus of this thesis, providing insights into how ligand coordination affects catalytic performance.

For example, reducing the σ -donation of the macrocyclic NHC system to create a less electron-rich iron center can be accomplished by incorporating benzimidazole units. While this modification did not enhance catalytic activity, it significantly improved thermal stability. Conversely, introducing methyl substituents into the NHC backbone influenced the ligands' σ -donor properties and introduced substantial π -backbonding, partially offsetting the electron-donating effect of the methyl groups. Abnormally coordinating NHCs are considered stronger σ -donors than their normally coordinating NHC counterparts, making them a powerful tool for tuning the electronic properties of the central metal. These aNHCs are also believed to enhance the stabilization of higher iron oxidation states, which is crucial for epoxidation and CH activation catalysis.

This thesis primarily focuses on the development and characterization of macrocyclic iron aNHC complexes and their performance in (ep)oxidation reactions, compared to normally coordinated macrocyclic iron NHC complexes. Additionally, the catalytic activity and stability of iron(II) open-chain NHC complex **3** and its complexes with modified backbones are investigated, particularly in relation to macrocyclic complexes **4a** and **4b**. Finally, transition metal complexes of group 10 and 11 with macrocyclic aNHC frameworks are synthesized, characterized, and compared to their imidazole-based counterparts with normal NHC coordination.

III Results and discussion – publication summaries

This chapter provides a summary of the publications that originated from this thesis. The articles are arranged chronologically according to their publication dates. A complete list of publications and the individual contributions to the publications are given in chapter VI. The full text of the publications is attached to this thesis, reprint permissions and bibliographic data are given in chapter V.

1 The effect of *trans* axial isocyanide ligands on iron(II) tetra-NHC complexes and their reactivity in olefin epoxidation

Eva-Maria H. J. Esslinger, Jonas F. Schlagintweit, **Greta G. Zámbo**, Alexander M. Imhof, Dr. Robert M. Reich, Prof. Dr. Fritz E. Kühn*

*corresponding author

published in *Asian J. Org. Chem.*, **2021**, *10*, 2654-2662.¹⁹³

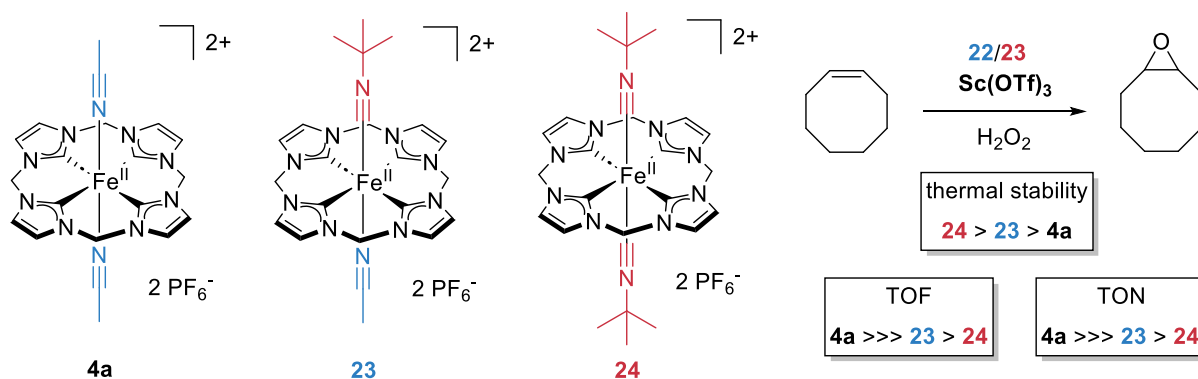


Figure 13 Structures of iron-NHC complexes **4a**, **23** and **24** employed in the epoxidation of *cis*-cyclooctene.

This study investigates the effect of *trans* axial isocyanide ligands on macrocyclic iron(II) tetra-NHC complexes and their catalytic performance in olefin epoxidation reactions. Two complexes mono-(*tert*-butylisocyanide) **23** and bis(*tert*-butylisocyanide) **24** were evaluated using H₂O₂ as the oxidant and *cis*-cyclooctene as substrate (Figure 13). Notably, the addition of Sc(OTf)₃ as a Lewis acid additive was crucial, as no significant catalytic performance was observed in the absence of this additive. The thermal stability of both complexes is impressive, with **24** displaying a higher decomposition temperature compared to **23**. The maximum TOF of **23** reaches *ca.* 25,900 h⁻¹ (0.25 mol% of **23**, 60 °C) and TON of *ca.* 330 (0.10 mol% of **23**,

20 °C), while **24** exhibits a TOF of *ca.* 4,300 h⁻¹ (0.25 mol% of **24**, 60 °C) and a TON of *ca.* 150 (0.10 mol% of **24**, 20 °C). The study underscores the essential role of Sc(OTf)₃, which is supposed to facilitated the cleavage of the O–O bond in the iron(III) hydroperoxo intermediate, thereby promoting the formation of active species (*vide supra*). Thermogravimetric analysis (TGA) was used to assess the thermal stability of the complexes, with **23** and **24** decomposing at higher temperatures than the parent compound **4a**, while **24** displaying a higher decomposition temperature compared to **23**. The findings suggest that while these new complexes offer high thermal stability, they are limited by low catalytic activity, prompting further research into catalyst modification to improve both stability and activity.

2 Organometallic 3d transition metal NHC complexes in oxidation catalysis

Greta G. Zámbo, Jonas F. Schlagintweit, Robert M. Reich and Fritz E. Kühn*

*corresponding author

published in *Catal. Sci. Technol.*, **2022**, *12*, 4949-4961.³⁰

This article provides an overview about the field of 3d transition metal NHC complexes in oxidation catalysis (especially Cr, Mn, Fe, Co, Ni and Cu), focusing on the advances towards the conversion of the most important substrates namely alkenes, alkanes, aromatics, alcohols and amines until the end of 2021. These metals are explored as affordable and eco-friendly alternatives to expensive, toxic noble metals traditionally used in catalytic processes. The strong σ -donor characteristics of NHCs, which stabilize metals in high oxidation states, essential for oxidation reactions is emphasized. Additionally, the role of molecular oxygen as an environmentally friendly oxidant is investigated.

Research into the aziridination and epoxidation of alkenes reveals the promising catalytic activity, selectivity, and stability of chromium and iron NHC complexes. Notably, iron-based NHC catalysts demonstrate high efficiency in alkene epoxidation, achieving TOFs that exceed those of catalysts such as MTO. The selective hydroxylation of C–H bonds in alkanes and aromatic compounds with iron, nickel cobalt and copper NHC complexes is discussed, addressing the difficulty of activating these stable bonds. Again, iron NHC complexes demonstrate high selectivity in hydroxylation reactions with compounds such as benzene and toluene. Cobalt NHC complexes, with *cis*-oriented reactive sites, exhibit enhanced selectivity toward alcohol formation in cyclohexane oxidation, while nickel NHC complexes demonstrate variable selectivity based on the structure of their ligands, effectively oxidizing substrates like cyclohexane and n-octane. Copper NHC complexes, though unstable, can catalyze the oxidation of alkanes through in situ formation, with a likely radical-based mechanism for C–H bond activation. The NHC complexes of iron, copper, cobalt, and manganese are effective catalysts for the oxidation of alcohols to carbonyl compounds and amines to imines or nitroso compounds. Iron exhibits remarkable activity and selectivity across these transformations. Copper is especially efficient for the selective oxidation of alcohols to aldehydes. Cobalt, with

its *cis*-oriented active sites, is well-suited for more challenging substrates. Manganese is ideal for the selective oxidation of both alcohols and amines under milder conditions, effectively minimizing over-oxidation and reducing byproduct formation.

Mechanistic insights provided in the review include pathways involving high-valent metal-oxo species and Fenton-type reactions, contrasting the stability and activity of various metal NHC complexes. Also, the study addresses challenges in oxidation catalysis, such as maintaining catalyst stability and preventing undesired side reactions.

3 The first macrocyclic abnormally coordinating tetra-1,2,3-triazole-5-ylidene iron complex: A promising candidate for olefin epoxidation

Greta G. Zámbo, Johannes Mayr, Michael J. Sauer, Tim P. Schlachta, Robert M. Reich and Fritz E. Kühn*

*corresponding author

published in *Dalton Trans.*, **2022**, 51, 13591-13595.¹⁹⁴

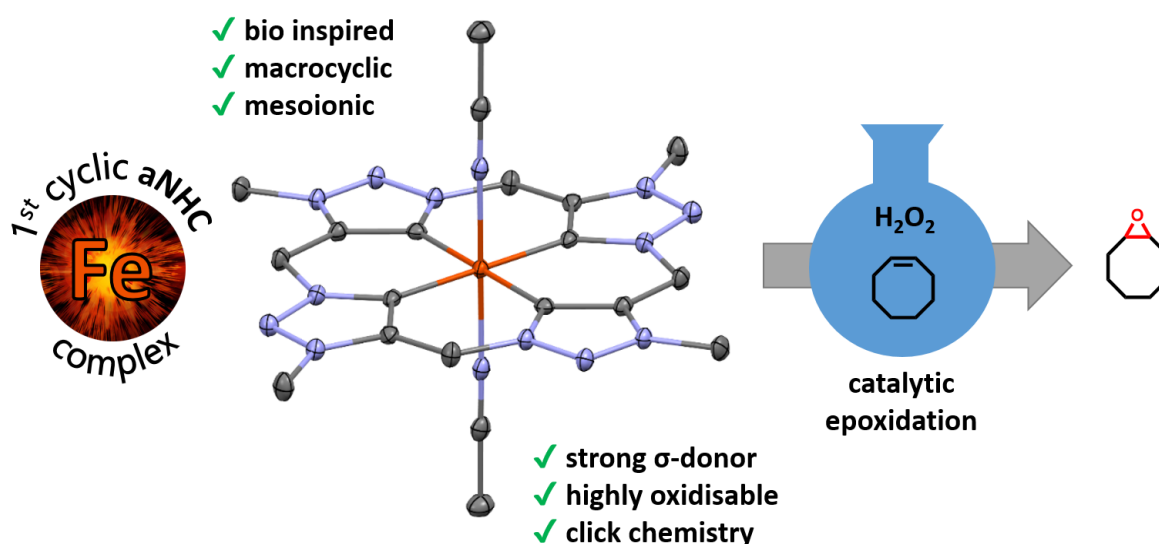
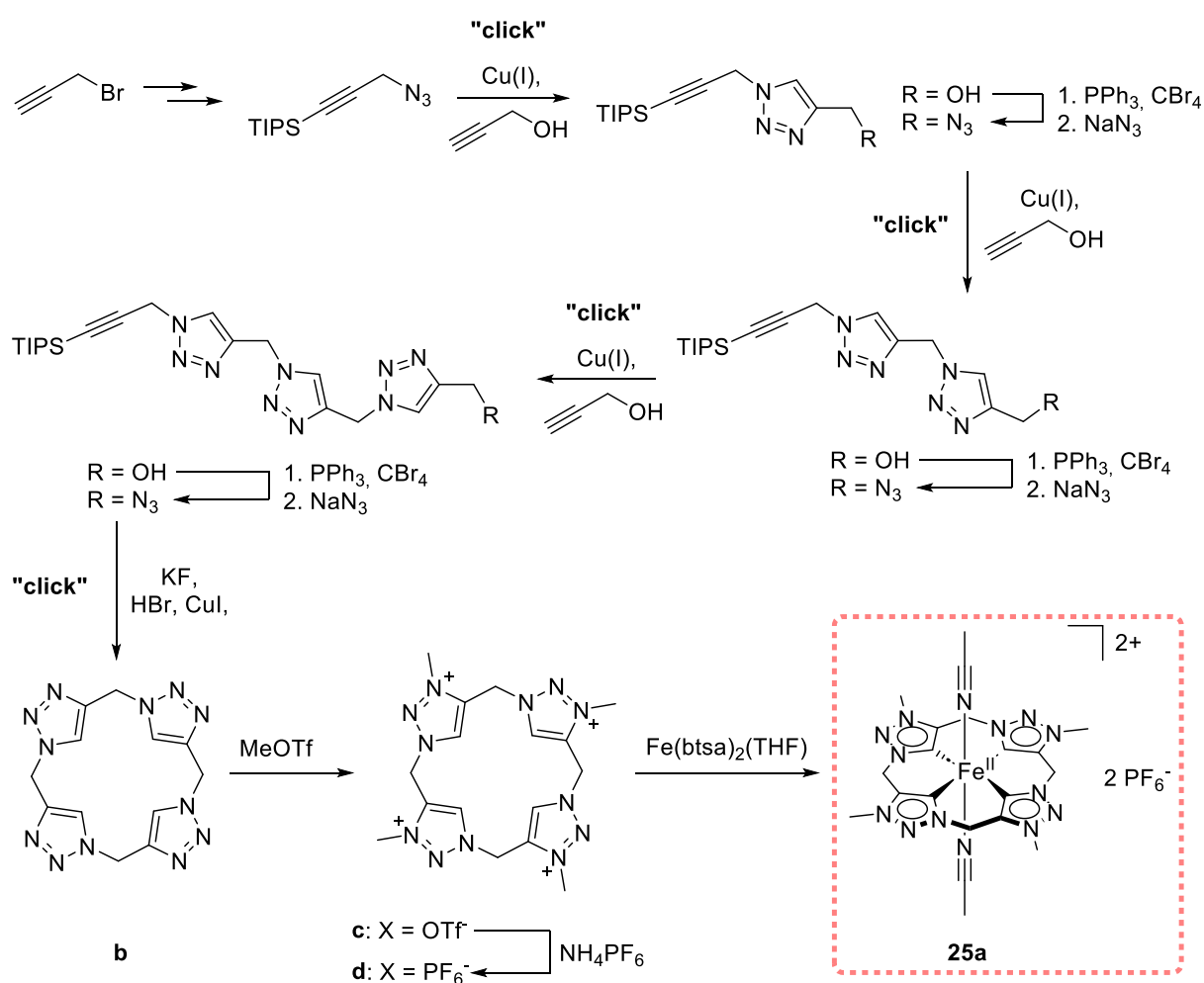


Figure 14 Graphical abstract of ref. ¹⁹⁴.

As described in the introduction aNHCs show significantly stronger σ -donor properties compared to normal coordinating Arduengo-type NHCs, while having negligible π -acceptor properties. All macrocyclic tetracarbene iron complexes synthesized so far, however, contain normally coordinating imidazole-2-ylidene NHC moieties. This article describes the synthesis of the first macrocyclic aNHC tetracarbene iron complex consisting of four 1,2,3-triazole-5-ylidene units (Scheme 15). The modified synthesis of the methylene-bridged calix[4]1,2,3-triazole **b** proceeds *via* repeated “click” reactions. Methylation of the N3 positions with methyltriflate and subsequent salt metathesis of **c** with NH_4PF_6 quantitatively yields the ligand precursor **d**. Complexation of **d** with $\text{Fe}(\text{btsa})_2(\text{THF})$ forms the desired compound **25a**. The complex exhibits a distorted octahedral coordination sphere around the iron with the aNHC ligand in ideal square-planar fashion, shown by SC-XRD measurements (Figure 14). The new

aNHC tetracarbene ligand demonstrates strong electron-donating properties, as indicated by the upfield shift of the $^{13}\text{C}_{\text{NHC}}$ signal (190.35 ppm vs. 205.05 ppm) and a more negative redox potential (-0.34 V vs. 0.15 V) compared to its imidazole counterpart **4a** $\text{Fe}^{\text{II}}[\text{cCCCC}]_{\text{im}}$. In initial catalytic epoxidation tests, using 0.5 mol% of **25a** with $\text{Sc}(\text{OTf})_3$ at 20 °C results in an initial turnover frequency (TOF) of 41,000 h^{-1} for the epoxidation of *cis*-cyclooctene, achieving a 97% conversion after 30 minutes. Without $\text{Sc}(\text{OTf})_3$, the catalyst's activity diminishes rapidly, completing the reaction in just 30 seconds with a 37% conversion. Lower temperatures improve the catalyst's stability, with an increased conversion ($X = 89\%$) observed at -10 °C in the absence of $\text{Sc}(\text{OTf})_3$.



Scheme 15 Simplified synthesis of the calix[4]1,2,3-triazolium salts **c** and **d** subsequent complexation to iron(II) complex **25a** (adapted from ref. ¹⁹⁴).

4 Tailoring activity and stability: Effects of electronic variations on iron-NHC epoxidation catalysts

Tim P. Schlachta, **Greta G. Zámbo**, Michael J. Sauer, Isabelle Rüter, Carla A. Hoefler, Serhiy Demeshko, Franc Meyer, Fritz E. Kühn*

*corresponding author

published in *J. Catal.*, **2023**, 426, 234-246.¹⁹⁵

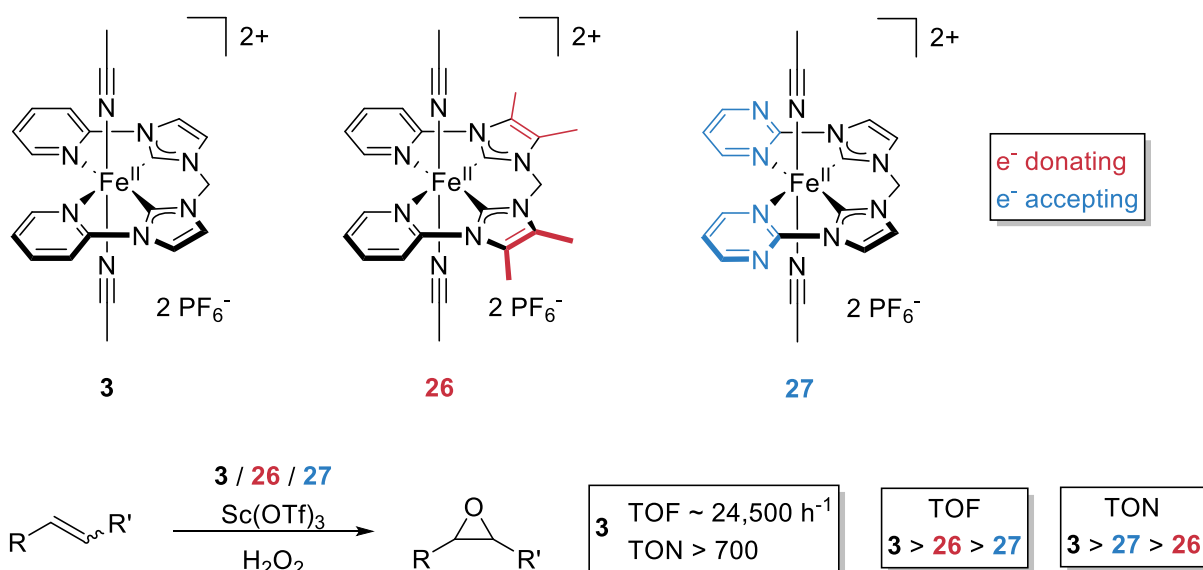


Figure 15 Modified iron NHC complexes employed in epoxidation catalysis (adapted from ref. ¹⁹⁵).

A series of three iron(II) open-chain NHC complexes in the epoxidation of olefins are investigated, focusing on how variations in electronic properties influence catalytic activity and stability (Figure 15). These complexes differ in the electron-donating or -withdrawing nature of their ligands, affecting the electron density at the iron center. As described in the introduction electronically modifications of the macrocyclic tetracarbene ligands in complexes, yielding **6** and **7**, did not enhance catalytic efficiency over the performance of **4**. However, this study provides information on whether the influence the ligand modification can also be transferred to other NHC systems.

The equatorial NHC ligand was modified to create a more electron-donating (complex **26**) and a more electron-accepting ligand (complex **27**), which is confirmed *via* NMR, CV and Mössbauer spectroscopy. Detailed characterizations of the complexes, including SC-XRD, SQUID and DFT calculations, provide more insights into the structural and electronic effects.

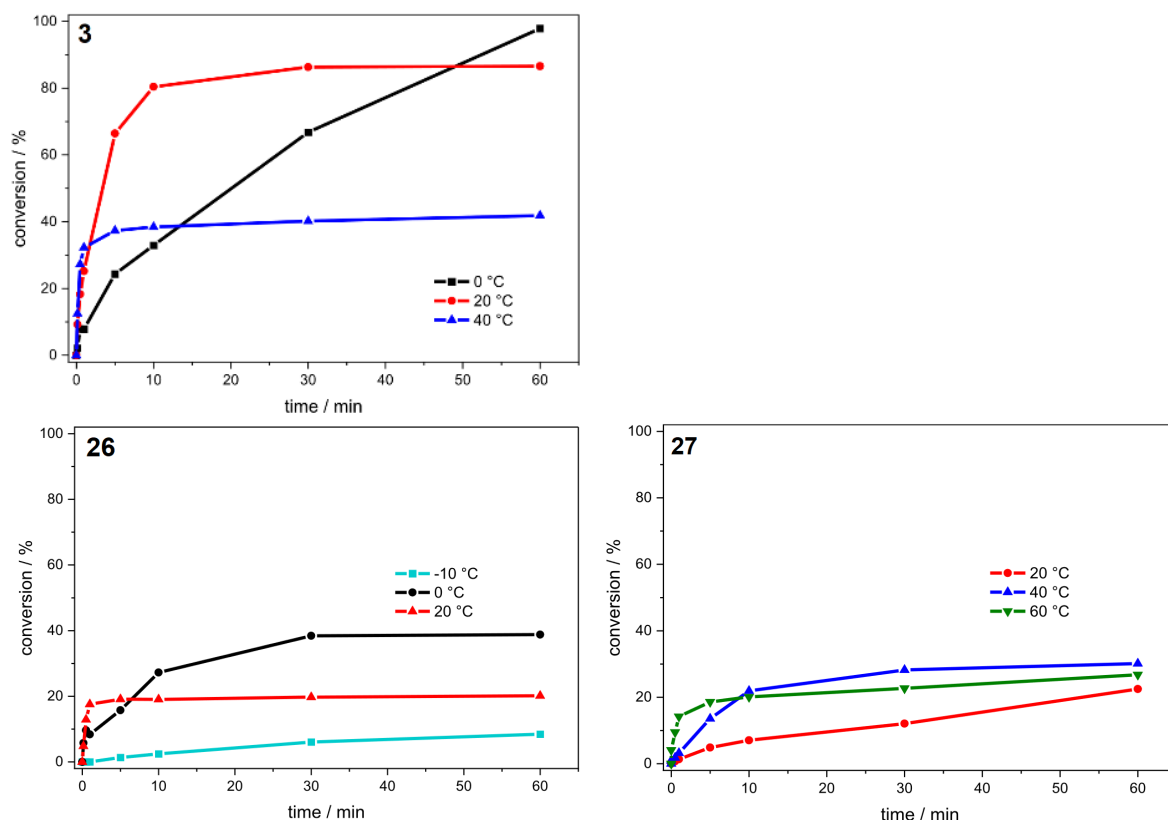


Figure 16 Time-dependent epoxidation of *cis*-cyclooctene (67.3 $\mu\text{mol/mL}$, 1.00 eq.) in MeCN using **3**, **26** and **27** (1.35 $\mu\text{mol/mL}$, 0.02 eq.) as catalyst and H_2O_2 (50% aq., 101 $\mu\text{mol/mL}$, 1.50 eq.) as oxidant at different temperatures. Conversions are determined by GC-FID.

The complexes were tested in the epoxidation of *cis*-cyclooctene. Different from expectations, a higher electron density does not necessarily improve catalytic activity but can impact catalyst stability. Testing Lewis acid additives, such as $\text{Sc}(\text{OTf})_3$, shows that activity and stability were again enhanced, indicating that these additives can counteract deactivation pathways. Consequently, the TOF and TON of the unmodified complex **3** can be pushed to *ca.* 24,500 h^{-1} and *ca.* 700 (0.10 mol%, 20 °C; vs. previously published values, described in the introduction), which is the highest achieved in this complex series. Complex **26** shows the next highest TOF of *ca.* 7,600 h^{-1} (10 s, 2 mol%, 20 °C), while complex **27** had the second-highest TON of 49 (1 h, 2 mol%, 20 °C) due to its stability under oxidative conditions. All complexes exhibit high selectivity. Temperature variation influences the catalytic stability and activity in distinct ways. For complex **3**, lowering the temperature to 0 °C enhanced its stability, achieving a higher TON compared to runs at 20 °C; however, raising the temperature to 40 °C increased initial activity but led to faster deactivation, reducing overall conversion. Complex **26** also demonstrated improved stability at lower temperatures, with a significant increase in TON at 0 °C compared to 20 °C. Conversely, complex **27** shows greater tolerance to elevated temperatures, with

increased catalytic activity observed at 40°C and optimal activity at 60°C, reflecting its resilience under higher thermal conditions.

5 Exploring the impact of abnormal coordination in macrocyclic *N*-heterocyclic carbene ligands on bio-inspired iron epoxidation catalysis

Greta G. Zámbo, Carla A. Esslinger, Michael J. Sauer, Isabelle Rüter, Robert M. Reich, Serhiy Demeshko, Franc Meyer, Fritz E. Kühn*

*corresponding author

published in *Catal. Sci. Technol.*, **2024**, *14*, 6259-6269.¹⁸³

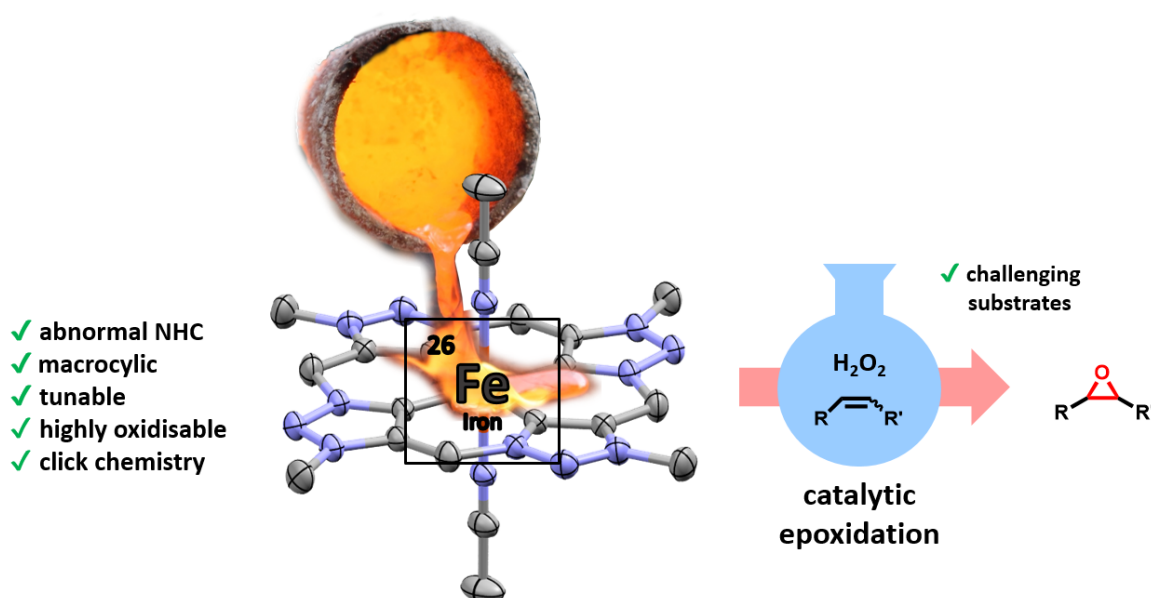


Figure 17 Graphical abstract of ref. ¹⁸³.

The influence of abnormal coordination in macrocyclic *N*-heterocyclic carbene ligands on bio-inspired iron epoxidation catalysis is explored. The synthesis, characterization, and catalytic performance of the first macrocyclic aNHC iron(III) complex **25b** using a calix[4]3-methyl-1,2,3-triazole-5-ylidene ligand system is described. Analytical methods, including Mössbauer spectroscopy, SQUID and DFT calculations are employed for **25b** and for its previously published iron(II) counterpart **25a**, to understand the structural and electronic properties of the complexes. The study highlights the differences in the behavior of iron(II) and iron(III) aNHC complexes to the epoxidation complexes **4a** and **4b** with normal NHC coordination. The aNHC Fe complexes demonstrated significant catalytic activity, with *cis*-cyclooctene serving as a model substrate (Figure 18). Key findings suggest that aNHC ligands, due to their stronger σ -

donor properties, enhance catalytic activity by stabilizing high oxidation states of iron. However, the stability of the complexes remains a challenge, with degradation of the Fe-aNHC bond under oxidative conditions, identified *via* NMR and mass spectrometry. Decomposition studies further revealed the formation of mono-oxidized ligands and an iron-oxo species. Moreover, the addition of Lewis acids such as $\text{Sc}(\text{OTf})_3$ improved the catalytic efficiency, enhancing both TOFs and TONs (up to almost $60,000 \text{ h}^{-1}$ and 250). Adding 0.10 equivalents of $\text{Sc}(\text{OTf})_3$ to a reaction with 0.50 mol% of **25a** at 20°C significantly extends the catalyst's lifetime and improves its performance. This modification speeds up the reaction, achieving 97% conversion in 30 min (TOF of *ca.* $40,900 \text{ h}^{-1}$). When **25b** is used under the same conditions, the reaction completes even faster, within 10 min, reaching 99% conversion, with a TOF of $51,800 \text{ h}^{-1}$ (Figure 18). This suggests a slower *in situ* oxidation process for **25a** to **25b** compared to other systems, such as **4a** to **4b**. The introduction of Lewis acids in the reaction appears to enhance activity and stability by potentially regenerating degraded species, similar to the mechanism seen in systems **4a** to **4b**.

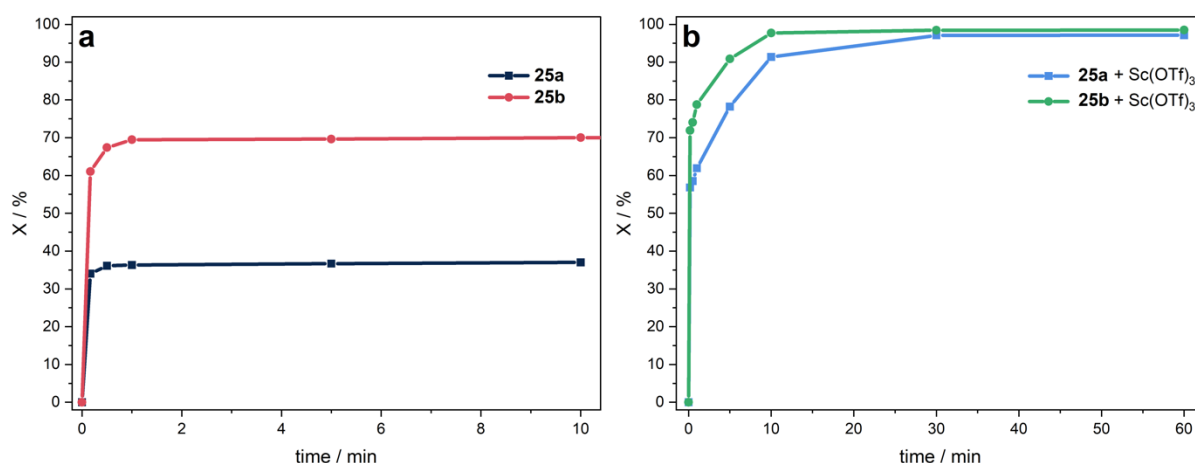


Figure 18 Time-dependent epoxidation of *cis*-cyclooctene ($67.3 \mu\text{mol/mL}$, 1.00 eq.) in MeCN at 20°C using **25a** or **25b** ($0.34 \mu\text{mol/mL}$, 0.005 eq.) as catalyst and H_2O_2 ($101 \mu\text{mol/mL}$, 1.50 eq.) as oxidant, (a) without additive and (b) with the addition of $\text{Sc}(\text{OTf})_3$ ($6.73 \mu\text{mol/mL}$, 0.10 eq.). Conversions are determined by GC-FID.

The study and underscores the necessity of balancing electronic properties with stability for practical industrial applications. Although the performance of the aNHC iron complexes did not surpass the existing benchmark catalysts, their novel coordination mode offers promising directions for future ligand design and catalytic optimization. The findings contribute to the limited understanding of iron aNHC complexes and create opportunities for further investigations into their catalytic mechanisms and potential applications.

6 Impact of ligand design on an iron NHC epoxidation catalyst

Tim P. Schlachta[§], Greta G. Zámbo[§], Michael J. Sauer, Isabelle Rüter, Fritz E. Kühn*

*corresponding author

[§]equally contributing authors

published in *ChemistryOpen*, **2024**, *13*, e202400071.¹⁹⁶

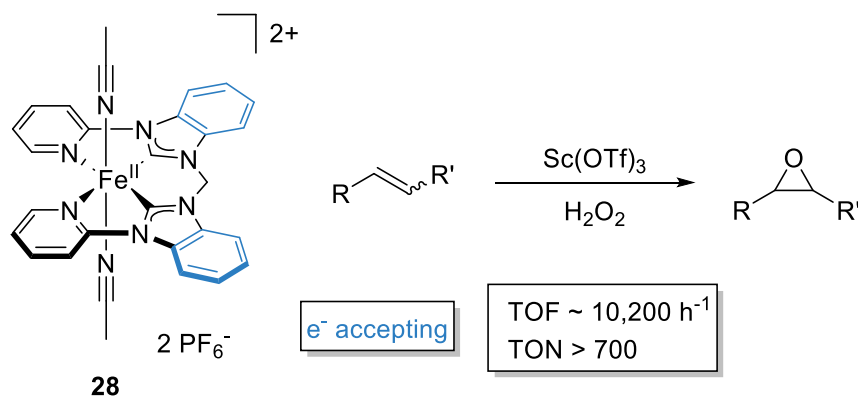


Figure 19 Graphical abstract of ref. ¹⁹⁶.

The design and performance of an open chain iron(II) pyridine-NHC framework, applied as epoxidation catalyst is explored. Benzimidazole units are introduced in the NHC backbones (Figure 19), aiming to understand how electronic modifications affect the catalyst's stability and effectiveness. Analyzation of electronic and structural properties involves *inter alia* SC-XRD and Mössbauer spectroscopy. CV measurements indicate complex **28** as the most positive in the series of the NCCN complexes **3**, **26** and **27**. The positive redox potential and the strong downfield shift of the $^{13}\text{C}_{\text{NHC}}$ signal reveal a lower electron density around the iron center, attributed to the benzimidazole's electron-withdrawing characteristics.

This modified complex, demonstrates thermal stability and reaches a moderate TOF of *ca.* 10,000 h^{-1} (determined at the highest slope of X, 0.10 mol%, 60 °C) and TON of *ca.* 700 (1 h, 0.10 mol%, 60 °C) in the epoxidation of *cis*-cyclooctene, particularly in the presence of the Lewis acid $\text{Sc}(\text{OTf})_3$, which suppresses degradation pathways and increases reactivity. Although the complex shows lower catalytic activity at r.t., it performs significantly better at higher temperatures, achieving the second-highest TOF among similar iron NHC complexes. Furthermore, tests with different substrates indicate that complex **28** favors nucleophilic alkenes.

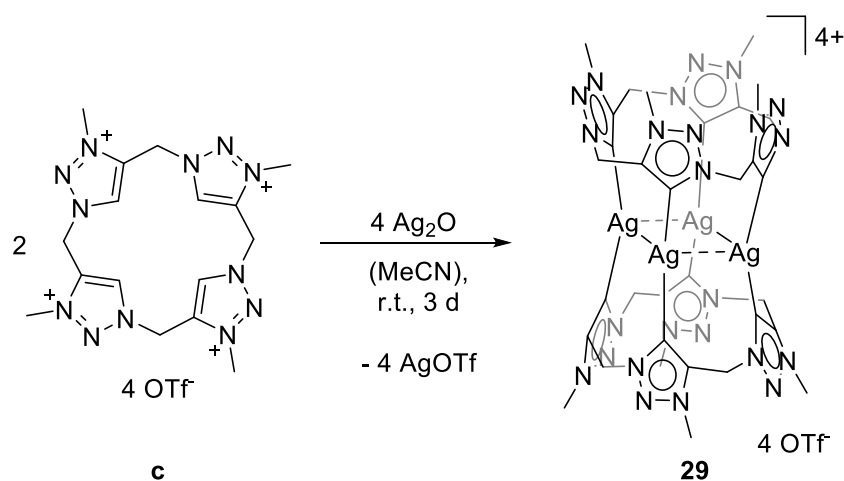
This work contributes to understanding how ligand design in iron-based epoxidation catalysts can impact stability and reactivity, suggesting that modifications like benzimidazole integration could facilitate the development of more robust catalysts for industrial applications.

7 Unpublished results

This chapter summarizes the unpublished results of this doctoral thesis.

7.1 Silver(I) *bis*-calix[4]3-methyl-1,2,3-triazol-5-ylidene triflate

Silver(I) complex **29** is synthesized by reacting the ligand precursor with a slight excess of Ag_2O , according to known literature procedures for similar complexes^{77,191} (Scheme 16). Under atmospheric conditions 220 mg of the ligand precursor calix[4]3-methyl-1,2,3-triazolium triflate **c** (224 μmol , 1.00 eq.) are dissolved in 10 mL acetonitrile. 125 mg Ag_2O (538 μmol , 2.40 eq.) are added to the solution. The suspension is stirred for 3 d at r.t. under the exclusion of light. The mixture is filtered through a plug of Celite resulting in a clear, slightly yellowish solution. Fractional precipitation with Et_2O results in the formation of a colorless solid. After drying in vacuum, 101 mg of **29** (56.5 μmol , 50%) are obtained as colorless solid, which is stored at 2 °C under the exclusion of light. However, after 24 h and dissolved in MeCN **29** remains stable even at 40 °C.



Scheme 16 Synthesis of the macrocyclic silver(I) *bis*-aNHC complex **29**.

The ^1H -NMR spectrum of compound **29** in CD_3CN displays a single sharp peak at 4.24 ppm for the methyl substituent protons on the triazoles, along with a pair of doublets at 6.10 and 5.88 ppm corresponding to the protons in the bridging methylene groups. These doublets have a coupling constant of 15.5 Hz, which is in the range of geminal coupling between two magnetically inequivalent protons. This pattern indicates a non-square planar and rigid binding arrangement for the ligand, consistent with the preference of Ag^{I} for linear coordination. In the ^{13}C -NMR spectrum, four groups of signals are observed. The resonance

for the carbene carbon appears at 169.59 ppm, splitting into two distinct doublets due to strong coupling with the two silver isotopes⁷⁷. The peak is significantly upfield shifted, compared to its imidazole counterparts **13** and **18** ($^{13}\text{C}_{\text{NHC}} = 183.2$ and 194.27 ppm)^{77,191}, which indicates a high σ -donor strength of the aNHCs. Due to the relatively strong Ag–C coupling, this interaction is detectable across up to three bonds.⁷⁷ Consequently, the signal for the carbon atom next to the carbene carbon at 145.17 ppm is also spitted into two doublets. The signal at 50.09 ppm, appears as a single sharp peak, corresponding to the methylene bridges and the methyl substituent signal appears at 38.28 ppm. ESI-MS and elemental analysis confirm these results.

¹H-NMR (400 MHz, CD₃CN): δ [ppm] = 6.10 (d, $^2J = 15.46$ Hz, 8 H, CH₂), 5.88 (d, $^2J = 15.46$ Hz, 8 H, CH₂), 4.24 (s, 24 H, CH₃).

¹³C-NMR (101 MHz, CD₃CN): δ [ppm] = 169.59 (C_{carbene}), 145.17 (C_{trz}CH₂N), 50.09 (CH₂), 38.28 (CH₃).

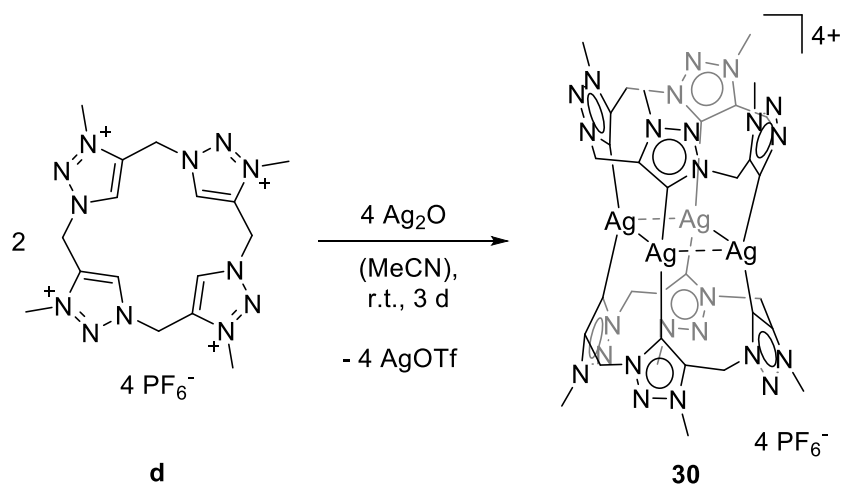
¹⁹F-NMR (376 MHz, CD₃CN): δ [ppm] = -79.27 (s, 12 F).

ESI-MS (*m/z*): calcd [M]⁴⁺: 298.00; found: 298.14; calcd [M⁴⁺OTf]³⁺: 446.99; found: 446.98; calcd [M⁴⁺2(OTf)]²⁺: 744.95; found: 745.09; calcd [M⁴⁺3(OTf)]⁺: 1638.86; found: 1638.57.

Analytical calculation (%) for C₃₆H₄₀Ag₄F₁₂N₂₄O₁₂S₄: C 24.18; H 2.25; N 18.80; S 7.17. Found: C 24.50; H 2.35; N 18.72; S 6.90.

7.2 Silver(I) *bis*-calix[4]3-methyl-1,2,3-triazol-5-ylidene hexafluoro-phosphate

Silver(I) complex **30** is synthesized similar to compound **29** (Scheme 17). Under atmospheric conditions 25.0 mg of the ligand precursor calix[4]3-methyl-1,2,3-triazolium hexafluorophosphate **d** (25.9 μmol , 1.00 eq.) are dissolved in 1 mL acetonitrile. 14.4 mg Ag₂O (62.2 μmol , 2.40 eq.) are added to the solution. The suspension is stirred for 3 d at r.t. under the exclusion of light. The mixture is filtered through a plug of Celite resulting in a clear, colourless solution. Precipitation with Et₂O results in the formation of a colorless solid. After drying in vacuum, 22.0 mg of **30** (12.4 μmol , 96%) are obtained as colorless solid, which is stored at 2 °C under the exclusion of light.



Scheme 17 Synthesis of the macrocyclic silver(I) *bis*-aNHC complex **30**.

The NMR spectroscopic results and elemental analysis confirm the formation of the same structural pattern as observed in complex **29**. Single crystals of **30** suitable for SC-XRD are obtained by the slow diffusion of diethyl ether into a solution of **30** in acetonitrile under the exclusion of light. The molecular structure in the solid state is consistent with the analytical data obtained in solution. The complex exhibits a similar box-type coordination pattern (Figure 20), as seen in the previously studied macrocyclic silver(I) NHC complexes.^{77,191} All four Ag^I ions are positioned between the two ligands and each metal is coordinated *via* two carbene carbons. The average Ag–C bond length is 2.09 Å, which is comparable of that of **13**⁷⁷, but slightly than that of **18** (2.11 Å)¹⁹¹. The Ag–Ag distances are in the range of 3.21 to 3.31 Å. The C–Ag–C angles are determined to be 164.74, 166.28, 166.33, and 169.39°.

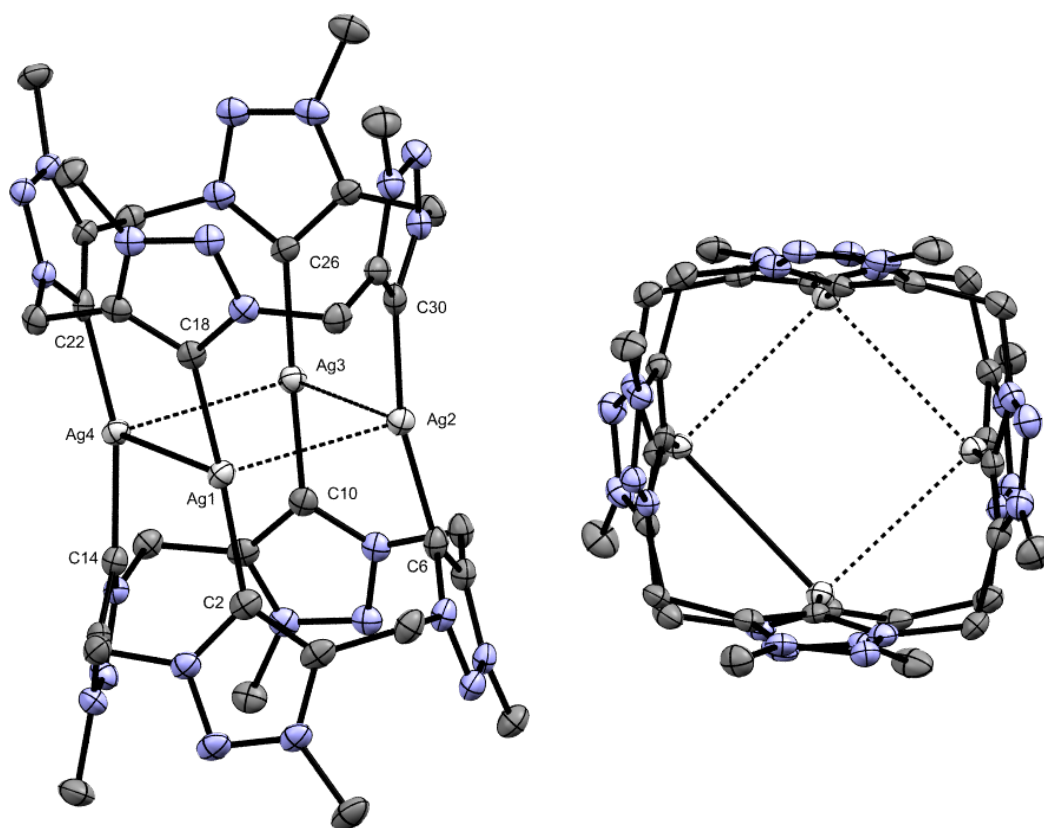


Figure 20 ORTEP style representation of the cationic fragment of **30** with ellipsoids shown at 50% probability level. Hydrogen atoms and PF_6^- anions, as well as two co-crystallized MeCN molecules are omitted for clarity. Front view (left) and view from above (right).

$^1\text{H-NMR}$ (400 MHz, CD_3CN): δ [ppm] = 6.06 (d, $^2J = 15.53$ Hz, 8 H, CH_2), 5.87 (d, $^2J = 15.46$ Hz, 8 H, CH_2), 4.24 (s, 24 H, CH_3).

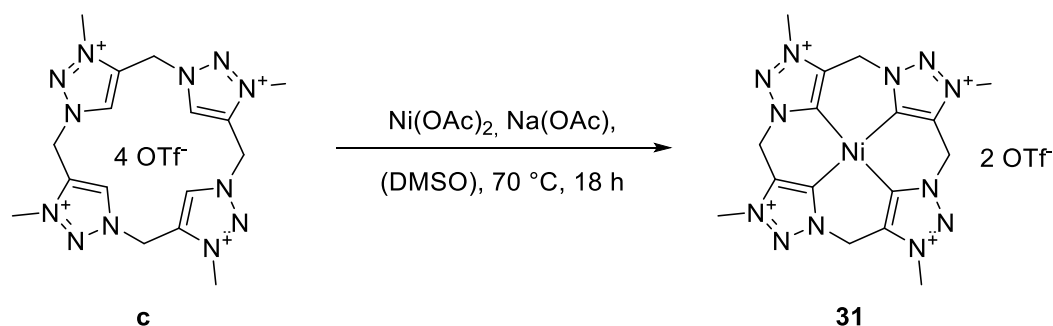
$^{13}\text{C-NMR}$ (101 MHz, CD_3CN): δ [ppm] = 169.61 ($\text{C}_{\text{carbene}}$), 145.21 ($\text{C}_{\text{trzCH}_2\text{N}}$), 50.18 (CH_2), 38.36 (CH_3).

Analytical calculation (%) for $\text{C}_{32}\text{H}_{40}\text{Ag}_4\text{F}_{24}\text{N}_{24}\text{P}_4$: C 21.69; H 2.28; N 18.97. Found: C 21.45; H 2.40; N 17.20.

7.3 Nickel(II) calix[4]3-methyl-1,2,3-triazol-5-ylidene triflate

Nickel(II) complex **31** is synthesized *via* direct metalation by reacting the ligand precursor with a slight excess of $\text{Ni}(\text{OAc})_2$ in combination with an excess of $\text{Na}(\text{OAc})$ as mild base, according to known literature procedures for similar complexes¹⁹² (Scheme 18). Under *Schlenk*-conditions 100 mg of the ligand precursor calix[4]3-methyl-1,2,3-triazolium triflate **c** (102 μmol , 1.00 eq.), 19.8 mg $\text{Ni}(\text{OAc})_2$ (112 μmol , 1.10 eq.) and 41.8 mg $\text{Na}(\text{OAc})$ (510 μmol , 5.00 eq.) are dissolved in 4 mL dry and degassed DMSO, resulting in a yellow suspension. The

mixture is stirred at 70 °C for 5 d, which turns the suspension orange. Subsequently, DMSO is removed at 70 °C under vacuum. The purification is carried out under atmospheric conditions. After cooling to room temperature, the residue is washed with 4 mL methanol and the yellow solid is separated *via* centrifugation. This step is repeated by washing the residue with 1 mL methanol prior to its separation. After drying in vacuum, 44.8 mg of **31** (61.2 μmol , 60%) are obtained as yellow solid.



Scheme 18 Synthesis of the macrocyclic nickel(II) aNHC complex **31**.

The ¹H-NMR spectrum displays two singlets at 6.23 ppm assigned to the methylene bridges and at 4.31 ppm originate from the methyl substituents. ¹³C-NMR reveal the carbene carbon signal at 150.60 ppm, which is again significantly upfield shifted, compared to its imidazole counterparts **13** and **18** (¹³C_{NHC} = 166.6 and 175.38 ppm)^{77,191}. The other three signals at 138.67, 47.26 and 37.12 ppm can be assigned to the remaining triazole carbon atom, the methylene bridge and the methyl substituent, respectively. Elemental analysis confirm these results. Single crystals of **31** suitable for SC-XRD are obtained by the slow diffusion of diethyl ether into a solution of **31** in acetonitrile under an argon atmosphere. The complex exhibits a highly symmetric framework (Figure 21). The metal ions are coordinated in an ideal square-planar fashion with C–Ni–C angles of exact 180°. The average Ni–C bond length with 1.90 Å is slightly longer than that of **13** and **18** (1.87 Å for both)^{77,191}.

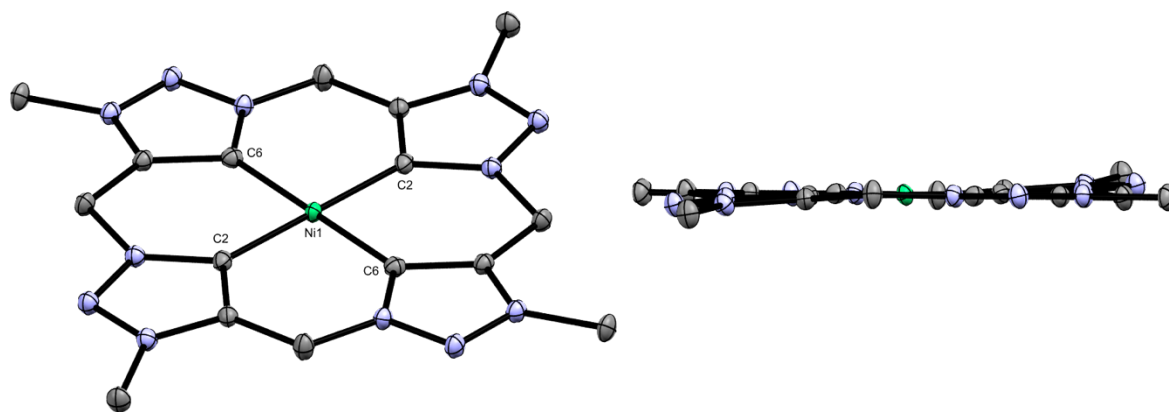


Figure 21 ORTEP style representation of the cationic fragment of **31** with ellipsoids shown at 50% probability level. Hydrogen atoms and an OTf anion, are omitted for clarity. View from above (left) and front view (right).

$^1\text{H-NMR}$ (400 MHz, DMSO- d_6): δ [ppm] = 6.23 (s, 8 H, CH_2), 4.31 (s, 12 H, CH_3).

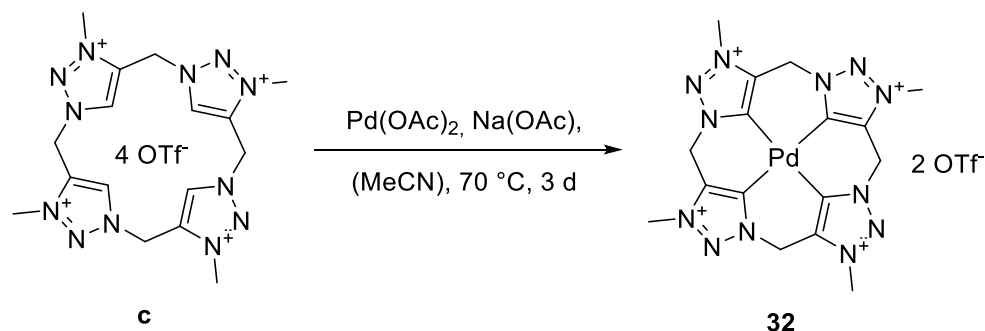
$^{13}\text{C-NMR}$ (101 MHz, DMSO- d_6): δ [ppm] = 150.60 ($\text{C}_{\text{carbene}}$), 138.67 ($\text{C}_{\text{trzCH}_2\text{N}}$), 47.26 (CH_2), 37.12 (CH_3).

$^{19}\text{F-NMR}$ (376 MHz, DMSO- d_6): δ [ppm] = -77.76 (s, 4 F).

Analytical calculation (%) for $\text{C}_{18}\text{H}_{20}\text{F}_6\text{N}_{12}\text{NiO}_6\text{S}_{22}$: C 29.33; H 2.73; N 22.80; S 8.70. Found: C 29.71; H 2.66; N 22.29; S 8.84.

7.4 Palladium(II) calix[4]3-methyl-1,2,3-triazol-5-ylidene triflate

Palladium(II) complex **32** is synthesized similar to compound **31** (Scheme 19). Under *Schlenk*-conditions 100 mg of the ligand precursor calix[4]3-methyl-1,2,3-triazolium triflate **c** (102 μmol , 1.00 eq.), 25.2 mg $\text{Pd}(\text{OAc})_2$ (112 μmol , 1.10 eq.) and 41.8 mg $\text{Na}(\text{OAc})$ (510 μmol , 5.00 eq.) are dissolved in 7 mL dry and degassed MeCN, resulting in a yellow-brown suspension. The mixture is stirred at 70 $^\circ\text{C}$ for 3 d, which turns the solution yellow. The purification is carried out under atmospheric conditions. The solvent is removed under reduced pressure. The yellow-brown residue is washed with methanol (3 x 3 mL) and the grey solid is separated respectively *via* centrifugation. The solid is suspended in 15 mL MeCN and heated up to 70 $^\circ\text{C}$. The hot suspension is filtered through a short plug of basic alumina, which is flushed with another 20 mL of hot MeCN. The solution is reduced under reduced pressure. Et_2O is added to the clear solution resulting in the precipitation of a colorless solid. The solid is separated *via* centrifugation and dried in vacuum. 29.6 mg of **32** (37.7 μmol , 37 %) are obtained as colorless solid.



Scheme 19 Synthesis of the macrocyclic palladium(II) aNHC complex **32**.

^1H - and ^{13}C -NMR spectroscopy are performed in $\text{DMSO-}d_6$ and in CD_3CN , revealing the same signal pattern as observed for complex **31** (*vide supra*). The carbene carbon signal appears at 151.38 ppm in $\text{DMSO-}d_6$ and at 153.40 ppm in CD_3CN . These findings are further supported by ESI-MS and elemental analysis. Single crystals of **32** suitable for SC-XRD are obtained by the slow diffusion of diethyl ether into a solution of **32** in acetonitrile under an argon atmosphere. Comparable to **31**, the complex features a highly symmetrical structure (Figure 22), where the metal ions are arranged in a perfect square-planar geometry with C–Pd–C bond angles precisely at 180° . The average Pd–C bond length of 1.98 Å is in the range of the bond lengths observed in compounds **13**⁷⁷ and **18**¹⁹¹.

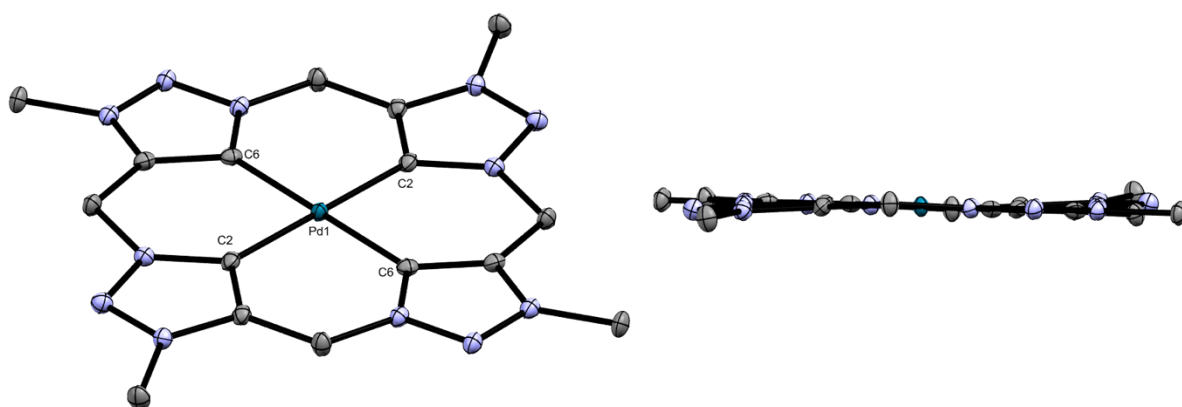


Figure 22 ORTEP style representation of the cationic fragment of **32** with ellipsoids shown at 50% probability level. Hydrogen atoms and an OTf⁻ anion, are omitted for clarity. View from above (left) and front view (right).

$^1\text{H-NMR}$ (400 MHz, $\text{DMSO-}d_6$): δ [ppm] = 6.43 (s, 8 H, CH_2), 4.33 (s, 12 H, CH_3).

$^1\text{H-NMR}$ (400 MHz, CD_3CN): δ [ppm] = 6.11 (s, 8 H, CH_2), 4.23 (s, 12 H, CH_3).

$^{13}\text{C-NMR}$ (101 MHz, $\text{DMSO-}d_6$): δ [ppm] = 151.38 ($\text{C}_{\text{carbene}}$), 137.47 ($\text{C}_{\text{trzCH}_2\text{N}}$), 49.71 (CH_2), 37.28 (CH_3).

¹³C-NMR (101 MHz, CD₃CN): δ [ppm] = 153.40 (C_{carbene}), 138.15 (C_{trz}CH₂N), 50.91 (CH₂), 38.18 (CH₃).

¹⁹F-NMR (376 MHz, DMSO-*d*₆): δ [ppm] = -79.36 (s, 4 F).

ESI-MS (*m/z*): calcd [M]²⁺: 243.05; found: 243.19; calcd [M]: 486.10; found: 485.13; calcd [M²⁺(OTf)]⁺: 635.05; found: 634.85.

Analytical calculation (%) for C₁₈H₂₀F₆N₁₂PdO₆S₂₂: C 27.54; H 2.57; N 21.42; S 8.17. Found: C 27.51; H 2.51; N 21.10; S 8.12.

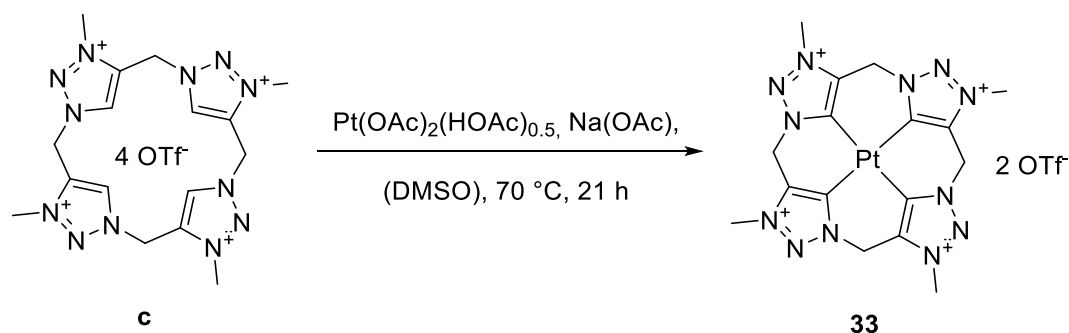
7.5 Platinum(II) calix[4]3-methyl-1,2,3-triazol-5-ylidene triflate

The metal precursor Pt(OAc)₂(HOAc)_{0.5} is synthesized according to a modified literature method.¹⁹⁷ 206 mg PtCl₂ (774 μ mol, 1.00 eq.) and 271 mg Ag(OAc) (1.63 mmol, 2.10 eq.) are suspended in 12 mL glacial acetic acid under the exclusion of light, The brown suspension is refluxed at 130 °C for 45 min, turning into a dark brown suspension. After cooling to r.t. the mixture is filtered through a short plug of Celite, which is flushed with another 2 mL of glacial acetic acid, resulting in a dark blue solution. The solvent is removed under reduced pressure. The dark blue solid is solved in 10 mL dichloromethane and again filtered through a short plug of Celite, which is flushed with another 10 mL of dichloromethane. The solvent is removed under reduced pressure. The solid is suspended in 10 mL Et₂O, separated *via* centrifugation and dried in vacuum. 102 mg of Pt(OAc)₂(HOAc)_{0.5} (294 μ mol, 38%) are obtained as dark blue solid.

Analytical calculation (%) for C₁₀H₁₆F₆O₁₀Pt₂: C 17.50; H 2.35. Found: C 17.49; H 2.15.

Platinum(II) complex **33** is synthesized similar to compound **31** (Scheme 20). Under *Schlenk*-conditions 150 mg of the ligand precursor calix[4]3-methyl-1,2,3-triazolium triflate **c** (153 μ mol, 1.00 eq.), 57.7 mg Pt(OAc)₂(HOAc)_{0.5} (168 μ mol, 1.10 eq.) and 62.4 mg Na(OAc) (765 μ mol, 5.00 eq.) are dissolved in 5 mL dry and degassed DMSO and under the exclusion of light, resulting in a dark purple suspension. The mixture is stirred at 70 °C for 21 h, which turns the solution brownish. The suspension is stored for 48 h at -37 °C. The purification is carried out under atmospheric conditions. The suspension is filtered through a short plug of basic alumina, which is flushed with another 3 mL of DMSO and subsequently diluted with 8 mL

MeCN. Fractional participation with Et₂O results 30.7 mg of **33** (35.2 μmol, 23%) as colourless solid.



Scheme 20 Synthesis of the macrocyclic platinum(II) aNHC complex **33**.

¹H- and ¹³C-NMR spectroscopy are performed in CD₃CN, revealing the same signal pattern as observed for complex **31** and **32** (*vide supra*). The carbene carbon signal appears at 147.57 ppm in CD₃CN. Single crystals of **33** suitable for SC-XRD are obtained by the slow diffusion of diethyl ether into a solution of **33** in acetonitrile under an argon atmosphere. Comparable to **31** and **32**, the complex features a highly symmetrical structure (Figure 23), where the metal ions are arranged in a perfect square-planar geometry with C–Pt–C bond angles precisely at 180°. The average Pt–C bond length of 1.96 Å is slightly shorter as observed in compounds **13** and **18** (1.98 Å for both)^{77,191}.

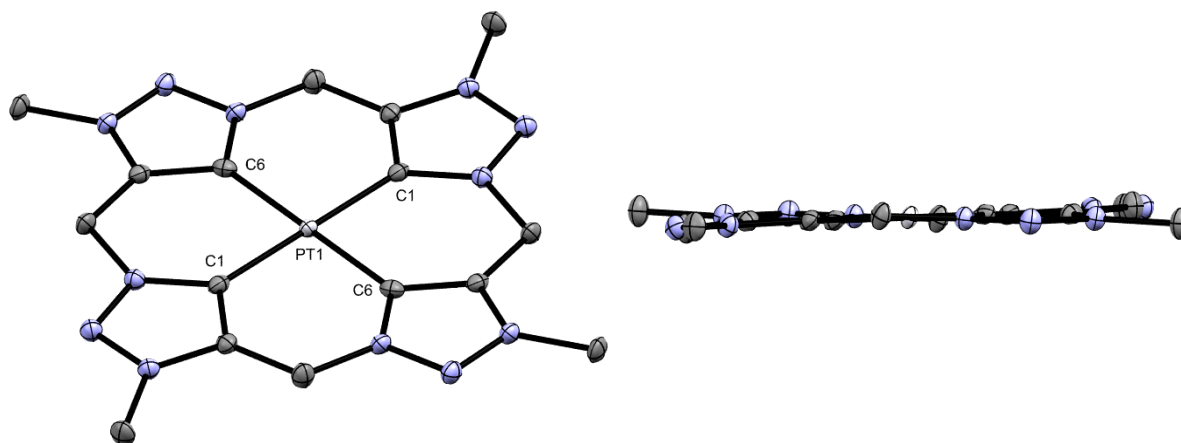


Figure 23 ORTEP style representation of the cationic fragment of **33** with ellipsoids shown at 50% probability level. Hydrogen atoms and an OTf anion, are omitted for clarity. View from above (left) and front view (right).

¹H-NMR (400 MHz, CD₃CN): δ [ppm] = 6.27 (m, 8 H, CH₂), 4.21 (s, 12 H, CH₃).

¹³C-NMR (101 MHz, CD₃CN): δ [ppm] = 147.57 (C_{carbene}), 137.51 (C_{tr2}CH₂N), 50.99 (CH₂), 38.13 (CH₃).

7.6 Gold(I) *bis*-calix[4]3-methyl-1,2,3-triazol-5-ylidene triflate

Under the exclusion of light, 50.0 mg of silver complex **29** (28.2 μmol , 1.00 eq.) and 36.6 mg Au(THT)Cl (114 μmol , 4.04 eq.) are suspended in 2 mL MeCN. The slightly pink suspension is stirred for 24 h at room temperature. The suspension is centrifuged and the supernatant is separated. Precipitation of the supernatant with Et₂O forms a white solid, which is washed with Et₂O (2 x 3 mL). After drying *in vacuo*, the product is obtained as white solid in a yield of 57.0 mg (26.6 μmol , 95%). The NMR spectra show increased signal splitting than for the corresponding silver(I) complexes due to a loss symmetry in comparison to **29** and **30**. The assumption that four Au^I atoms are boxe-type coordinated *via* two ligands with two metal atoms occupying the ligand cavities and the other two serving as bridges between the ligands is in accordance with the results obtained for the macrocyclic benzimidazole complex **19**¹⁹¹ (*vide supra*). The ¹³C_{NHC} signals, presented at 172.51 and 161.17 ppm, are significantly upfield shifted compared to **19**¹⁹¹. These findings are further supported by ESI-MS and elemental analysis.

¹H-NMR (400 MHz, CD₃CN): δ [ppm] = 6.35 (ddd, ²J = 49.69, ²J = 15.70 Hz, ²J = 5.13 Hz, 8 H, CH₂), 5.91 (t, ²J = 16.39 Hz, 8 H, CH₂), 4.24 (dd, ²J = 46.96 Hz, ²J = 1.68 Hz, 24 H, CH₃).

¹H-NMR (400 MHz, D₂O): δ [ppm] = 6.42 (ddd, ²J = 52.15, ²J = 15.64 Hz, ²J = 6.10 Hz, 8 H, CH₂), 6.11 (dd, ²J = 21.42 Hz, ²J = 15.66 Hz, 8 H, CH₂), 4.30 (d, ²J = 32.64 Hz, 24 H, CH₃).

¹³C-NMR (101 MHz, CD₃CN): δ [ppm] = 172.51 (C_{carbene}), 161.17 (C_{carbene}), 149.44 (C_{trz}CH₂N), 145.66 (C_{trz}CH₂N), 48.78 (CH₂), 39.01 (CH₃).

¹⁹F-NMR (376 MHz, CD₃CN): δ [ppm] = -79.27 (s, 4 F).

ESI-MS (*m/z*): calcd [M⁴⁺OTf]³⁺: 565.74; found: 565.74; calcd [M⁴⁺]: 387.42; found: 387.06.

Analytical calculation (%) for C₃₆H₄₀Au₄F₁₂N₂₄O₁₂S₄ x 1.2 AgCl: C 18.65; H 1.74; N 14.51; S 5.53. Found: C 18.66; H 1.66; N 14.59; S 5.49.

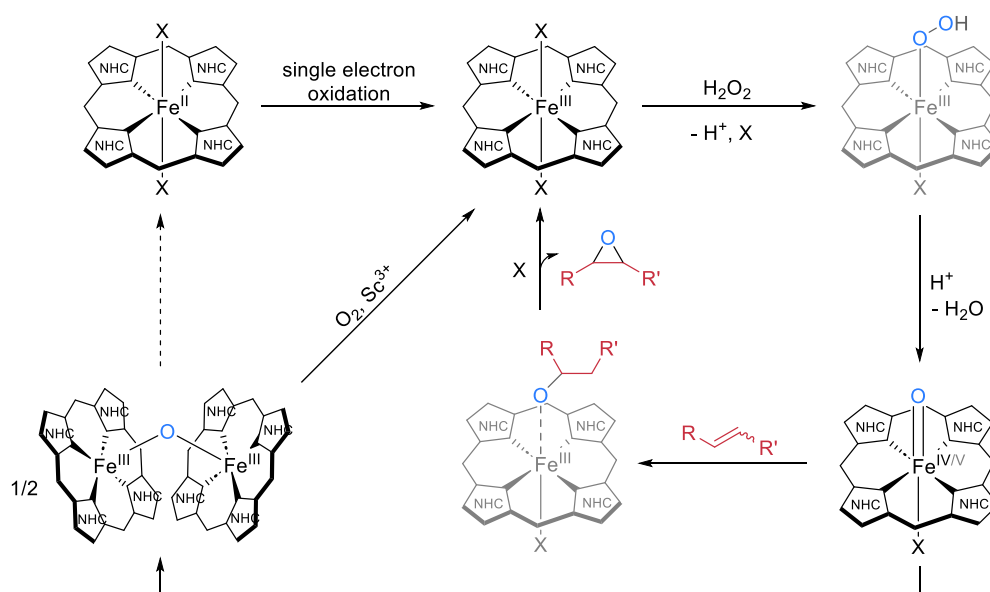
IV Conclusion and outlook

In conclusion, this doctoral thesis advances the understanding and development of macrocyclic tetracarbene and open chain tetradentate NHC iron complexes, particularly in their application as catalysts for epoxidation reactions. Investigations into catalytic epoxidation have revealed that the occupation of *trans* axial coordination sites in the macrocyclic benchmark imidazolium-based iron catalyst with non-labile isocyanide ligands exhibits exceptional stability at elevated temperatures. However, these mono- and *bis*(*tert*-butylisocyanide)-substituted iron(II) complexes require the addition of Sc(OTf)₃ and exhibit significantly lower catalytic activity compared to their counterparts featuring exclusively labile MeCN ligands.

The major focus has been on the development of an abnormally coordinating macrocyclic tetra-NHC ligand system with high electron-donation properties and its Fe^{II} and Fe^{III} complexes **25a** and **25b**. These complexes have been investigated for their applicability as catalysts in epoxidation reaction in comparison to the benchmark imidazolium-based complexes **4a** and **4b**. Notably, the synthesis and characterization of the first macrocyclic iron aNHC complexes – featuring 1,2,3-triazol-5-ylidene units – demonstrate enhanced σ -donating ability, underscoring their catalytic potential. Even though the performance of the original iron NHC catalyst could not be surpassed, it is reasonable to assume that increased σ -donation stabilizes iron in its higher oxidation states. Therefore, it is possible that the isolation and study of key species involved in oxidative reactions, such as epoxidation or C–H activation, could be achieved using such frameworks.

As described in the introduction, regarding the reaction mechanism in the catalytic epoxidation of *cis*-cyclooctene with H₂O₂, it is assumed to resemble the mechanism observed for non-heme iron complexes with *N*-donor ligands. Even though the studies conducted here primarily focus on catalysts with *cis*-labile coordination sites, a water-assistant pathway can be ruled out for complexes featuring *trans*-labile coordination sites. Based on the reactivity of macrocyclic tetra-NHC complexes, described in the introduction and in the results, Scheme 21 proposes a simplified reaction mechanism for the epoxidation of olefins using macrocyclic tetra-NHC iron complexes. The involvement of a Fe^{III}–OOH species is assumed. However, such an intermediate has not been described in the context of iron NHC catalysts.

Stoichiometrically controlled experiments under specific conditions (*inter alia* solvent and environment choice) using iron NHC complexes **4**, **7** or **25**, exhibiting different electron donation properties, with H_2O_2 and under reduced temperatures could provide insights in the formation of key compounds, like the hydroperoxo species. As described by the group of Que (*J. Am. Chem. Soc.* **2002**, *124*, 3026-3035) ESI-MS has demonstrated to be an excellent tool in determining the molecular compositions of transient species involved in iron-catalyzed oxidation processes. Additionally, HR-ESI-MS, UV/Vis and EPR spectroscopic measurements offer valuable complementary insights. Isotope labeling experiments with labeled oxidants can trace the oxygen atom's origin in specific intermediates or products by providing insights into whether O_2 is incorporated from air due to potential autoxidation and may give insights if the formation of a superoxide like **10** is formed. The isolation of a macrocyclic tetra-NHC oxoiron(IV) complex by the group of Meyer (*Angew. Chem. Int. Ed.* **2013**, *52*, 901-905) upon reaction of the iron(II) precursor with an oxo transfer reagent at $-40\text{ }^\circ\text{C}$ supports the possible mechanism *via* an active $\text{Fe}^{\text{IV}}=\text{O}$ compound. In both cases, reactions of complexes **4** and **25** with H_2O_2 form a mono-oxidized and threefold protonated ligand.



Scheme 21 Proposed and simplified reaction mechanism for the epoxidation of olefins using macrocyclic tetra-NHC iron complexes featuring *trans*-labile coordination sites with X = labile ligand. Species not yet characterized are grayed out.

The modification of an open-chain NHC ligand led to the development of various iron NHC complexes with differing electronic properties. These complexes have been utilized in epoxidation catalysis to assess how ligand modifications influence the catalytic efficiency of iron NHC complexes. Interestingly, the unmodified iron NHC complexes demonstrated the

highest catalytic efficiency in terms of both activity and stability. Through systematic investigation of electronic modifications, it was found that achieving an optimal balance between the electron density at the metal center and the stability of the complex is crucial. While electron-donating ligands enhance catalytic activity, they often reduce stability, whereas electron-accepting ligands improve stability but diminish activity. No clear relationship was observed between the electron density at the iron center, which is influenced by the electron-donating or electron-accepting nature of the ligands, and the catalytic performance in epoxidation. Other factors, such as the oxidative stability of the ligand or its structural rigidity, might have a considerable impact.

Finally, the macrocyclic tetra-aNHC ligand was successfully employed to synthesize late transition metal complexes of Ag^I, Au^I, Ni^{II}, Pd^{II} and Pt^{II}. These complexes have been generally characterized by means of ¹H- and ¹³C-NMR spectroscopy, ESI-MS, SC-XRD and elemental analysis and compared to their imidazole counterparts described in the introduction. Their potential in medicinal chemistry opens promising opportunities for future research, particularly in exploring their biological and pharmacological applications. Recent studies have highlighted the potential of aNHCs, particularly through a series of gold(I) bis-1,2,3-triazole-5-ylidene complexes (*J. Med. Chem.* **2021**, *64*, 15747–15757). These compounds exhibit remarkable anticancer activity, comparable to the most potent gold-based agents, against a range of solid tumor cell lines and blood cancer cells. Furthermore, the macrocyclic imidazole tetracarbene ligand proved to form copper(I) complexes in a molecular box-type structure, and square planar copper(III) (*Chem. Sci.* **2018**, *9*, 8307-8314), gold(III) (*Dalton Trans.* **2019**, *48*, 16615-16625) and cobalt(II) complexes (*Chem. Eur. J.* **2021**, *27*, 1311-1315) with potential in medicinal chemistry and molecular oxygen reactions. The tetra-NHC ligand could be replaced by the macrocyclic tetra-aNHC ligand, which has been developed with this thesis.

V Reprint permissions and licenses

1 Wiley-VCH Journals

“The Effect of *trans* Axial Isocyanide Ligands on Iron(II) Tetra-NHC Complexes and their Reactivity in Olefin Epoxidation”

E.-M. H. J. Esslinger, J. F. Schlagintweit, **G. G. Zámbo**, A. M. Imhof, R. M. Reich, F. E. Kühn

Asian Journal of Organic Chemistry, **2021**, *10*, 2654-2662.

DOI: [10.1002/ajoc.202100487](https://doi.org/10.1002/ajoc.202100487)

Reproduced from ref. ¹⁹³ with permission of Wiley-VCH.

“This article is available under the Creative Commons CC-BY-NC-ND license and permits non-commercial use of the work as published, without adaptation or alteration provided the work is fully attributed.”

CCC RightsLink GZ ⓘ 🔍

The Effect of *trans* Axial Isocyanide Ligands on Iron(II) Tetra-NHC Complexes and their Reactivity in Olefin Epoxidation

Author: Greta G. Zámbo, Alexander M. Imhof, Robert M. Reich, et al
 Publication: Asian Journal of Organic Chemistry
 Publisher: John Wiley and Sons
 Date: Sep 2, 2021

© 2021 The Authors. Asian Journal of Organic Chemistry published by Wiley-VCH GmbH

Order Completed

Thank you for your order.

This Agreement between Greta Zámbo ("You") and John Wiley and Sons ("John Wiley and Sons") consists of your license details and the terms and conditions provided by John Wiley and Sons and Copyright Clearance Center.

Your confirmation email will contain your order number for future reference.

License Number	5903670171466	Printable Details
License date	Nov 07, 2024	

Licensed Content	Order Details	
Licensed Content Publisher	John Wiley and Sons	
Licensed Content Publication	Asian Journal of Organic Chemistry	
Licensed Content Title	The Effect of <i>trans</i> Axial isocyanide Ligands on Iron(II) Tetra-NHC Complexes and their Reactivity in Olefin Epoxidation	
Licensed Content Author	Greta G. Zámbo, Alexander M. Imhof, Robert M. Reich, et al	
Licensed Content Date	Sep 2, 2021	
Licensed Content Volume	10	
Licensed Content Issue	10	
Licensed Content Pages	9	
	Type of use	Dissertation/Thesis
	Requestor type	Author of this Wiley article
	Format	Print and electronic
	Portion	Full article
	Will you be translating?	No

“Impact of Ligand Design on an Iron NHC Epoxidation Catalyst”

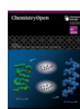
T. P. Schlachta, G. G. Zámbo, M. J. Sauer, I. Rüter and F. E. Kühn

ChemistryOpen, **2024**, *13*, e202400071.

DOI: [10.1002/open.202400071](https://doi.org/10.1002/open.202400071)

Reproduced from ref. ¹⁹⁶ with permission of Wiley-VHC.

“This is an open access article distributed under the terms of the Creative Commons CC BY license, which permits unrestricted use, distribution, and reproduction in any medium, provided the original work is properly cited.”



Impact of Ligand Design on an Iron NHC Epoxidation Catalyst

Author: Tim P. Schlachta, Greta G. Zámbo, Michael J. Sauer, et al

Publication: ChemistryOpen

Publisher: John Wiley and Sons

Date: Sep 24, 2024

© 2024 The Authors. ChemistryOpen published by Wiley-VCH GmbH

Open Access Article

This is an open access article distributed under the terms of the [Creative Commons CC BY](#) license, which permits unrestricted use, distribution, and reproduction in any medium, provided the original work is properly cited.

You are not required to obtain permission to reuse this article.

For an understanding of what is meant by the terms of the Creative Commons License, please refer to [Wiley's Open Access Terms and Conditions](#).

Permission is not required for this type of reuse.

2 Royal Society of Chemistry Journals

“Organometallic 3d transition metal NHC complexes in oxidation catalysis”

G. G. Zámbo, J. F. Schlagintweit, R. M. Reich, F. E. Kühn

Catalysis Science & Technology, **2022**, *12*, 4949-4961.

DOI: [10.1039/D2CY00127F](https://doi.org/10.1039/D2CY00127F)

Reproduced from ref. ³⁰ with permission of Royal Society of Chemistry.

“If you are an author contributing to an RSC publication, you do not need to request permission provided correct acknowledgement is given. If you are the author of this article, you do not need to request permission to reproduce figures and diagrams provided correct acknowledgement is given. If you want to reproduce the whole article in a third-party publication (excluding your thesis/dissertation for which permission is not required) please go to the Copyright Clearance Center request page.”

Issue 16, 2022 Previous Article | Next Article



From the journal:
Catalysis Science & Technology

Organometallic 3d transition metal NHC complexes in oxidation catalysis

 Check for updates

Greta G. Zámbo,  Jonas F. Schlagintweit,  Robert M. Reich^a and Fritz E. Kühn ^a

 Author affiliations

Abstract

The development of processes for the selective oxidation of hydrocarbons is a major focus in catalysis research. Making this process simultaneously environmentally friendly is still challenging. 3d transition metals are highly promising candidates to replace expensive and/or toxic heavier metals in their applications as oxidation catalysts. Optimizing such catalytic systems is closely connected to the improvement of stabilizing ligands. In this context, *N*-heterocyclic carbenes (NHCs) have attracted particular attention. Their strong σ -donor properties, compared to nitrogen or oxygen-donor ligands, allow the stabilisation of transition metals in high oxidation states, known to be key intermediates in oxidation catalysis. This review provides an overview of recent applications of 3d transition metal NHC complexes in oxidation catalysis, by summarising the advances towards the catalytic oxidation of the most important substrates namely alkenes, alkanes, aromatics, alcohols and amines until the end of 2021. Additionally the activation of molecular oxygen, representing a green and abundantly available oxidant, is described with first row transition metal NHC complexes.

About	Cited by	Related
<div style="text-align: right; border: 1px solid #ccc; width: 20px; height: 20px; margin-bottom: 5px; display: flex; align-items: center; justify-content: center;">×</div> <p>Organometallic 3d transition metal NHC complexes in oxidation catalysis</p> <p>G. G. Zámbo, J. F. Schlagintweit, R. M. Reich and F. E. Kühn, <i>Catal. Sci. Technol.</i>, 2022, 12, 4940 DOI: 10.1039/D2CY00127F</p> <p>To request permission to reproduce material from this article, please go to the Copyright Clearance Center request page.</p> <p>If you are an author contributing to an RSC publication, you do not need to request permission provided correct acknowledgement is given.</p> <p>If you are the author of this article, you do not need to request permission to reproduce figures and diagrams provided correct acknowledgement is given. If you want to reproduce the whole article in a third-party publication (excluding your thesis/dissertation for which permission is not required) please go to the Copyright Clearance Center request page.</p> <p>Read more about how to correctly acknowledge RSC content.</p> <div style="text-align: right; border: 1px solid #ccc; width: 20px; height: 20px; margin-top: 10px; display: flex; align-items: center; justify-content: center;">×</div>		

“The first macrocyclic abnormally coordinating tetra-1,2,3-triazole-5-ylidene iron complex: a promising candidate for olefin epoxidation”

G. G. Zámbo, J. Mayr, M. J. Sauer, T. P. Schlachta, R. M. Reich, F. E. Kühn

Dalton Transactions, **2022**, *51*, 13591-13595.

DOI: [10.1039/D2DT02561B](https://doi.org/10.1039/D2DT02561B)

Reproduced from ref. ¹⁹⁴ with permission of Royal Society of Chemistry.

“If you are an author contributing to an RSC publication, you do not need to request permission provided correct acknowledgement is given. If you are the author of this article, you do not need to request permission to reproduce figures and diagrams provided correct acknowledgement is given. If you want to reproduce the whole article in a third-party publication (excluding your thesis/dissertation for which permission is not required) please go to the Copyright Clearance Center request page.”

The screenshot shows the article page for "The first macrocyclic abnormally coordinating tetra-1,2,3-triazole-5-ylidene iron complex: a promising candidate for olefin epoxidation" in Dalton Transactions, 2022, 51, 13591-13595. The page includes the journal logo, issue information (Issue 36, 2022), and navigation links for "Previous Article" and "Next Article". The article title is prominently displayed, along with a "Check for updates" button. The authors listed are Greta G. Zámbo, Johannes Mayr, Michael J. Sauer, Tim P. Schlachta, Robert M. Reich, and Fritz E. Kühn. Below the authors, there is a link for "Author affiliations". The abstract section begins with the text: "The first macrocyclic and abnormally coordinating, mesoionic N-heterocyclic carbene iron complex has been synthesised and characterised via ESI-MS, EA, SC-XRD, CV, NMR and UV/Vis spectroscopy. ¹³C-NMR spectroscopy and CV measurements indicate a strong σ -donor ability of the carbene moieties, suggesting an efficient catalytic activity of the iron complex in oxidation reactions. Initial tests in the epoxidation of *cis*-cyclooctene as a model substrate confirm this assumption." On the right side of the page, there is a sidebar with tabs for "About", "Cited by", and "Related". The "About" tab is active, showing the article title, authors, journal information, and a section for requesting permission to reproduce material, which includes a link to the Copyright Clearance Center request page and instructions for authors and third-party publishers.

“Exploring the impact of abnormal coordination in macrocyclic *N*-heterocyclic carbene ligands on bio-inspired iron epoxidation catalysis”

G. G. Zámbo, C. A. Esslinger, M. J. Sauer, I. Rüter, R. M. Reich, S. Demeshko, F. Meyer, F. E. Kühn

Catalysis Science & Technology, 2024, 14, 6259-6269.

DOI: [10.1039/D4CY00992D](https://doi.org/10.1039/D4CY00992D)

Reproduced from ref. ¹⁸³ with permission of Royal Society of Chemistry.

“This article is open Access. This article is licensed under a Creative Commons Attribution 3.0 Unported Licence. You can use material from this article in other publications without requesting further permissions from the RSC, provided that the correct acknowledgement is given.”

The screenshot displays the article page for "Exploring the impact of abnormal coordination in macrocyclic *N*-heterocyclic carbene ligands on bio-inspired iron epoxidation catalysis" in the journal *Catalysis Science & Technology*. The page includes the journal logo, issue information (Issue 21, 2024), and navigation links for "Previous Article" and "Next Article". The article title is prominently displayed, followed by the authors: Greta G. Zámbo, Carla A. Esslinger, Michael J. Sauer, Isabelle Rüter, Robert M. Reich, Serhiy Demeshko, Franc Meyer, and Fritz E. Kühn. A "Check for updates" button is visible next to the title. The abstract section begins with: "The first macrocyclic abnormal *N*-heterocyclic carbene (aNHC) Fe^{III} complex, featuring a calix[4]3-methyl-1,2,3-triazole-5-ylidene ligand system is synthesised and characterised *inter alia* via EA, SC-XRD, NMR and UV/vis spectroscopy. Including Mössbauer spectroscopy, SQUID and DFT calculations, the impact of the aNHC on the Fe^{III} complex and its corresponding Fe^{II} derivative is investigated. A comprehensive study of the aNHC Fe complexes in their performance in homogenous epoxidation reactions is reported and compared to the established benchmark catalysts. The complexes demonstrate efficient and selective catalytic activity in the epoxidation of *cis*-cyclooctene with H₂O₂, with TOFs up to almost 60 000 h⁻¹. Additionally, the epoxidation of more challenging olefinic substrates is possible. The reactivity under oxidative conditions of both complexes is investigated. NMR measurements reveal the formation of a mono-oxidised triazole ligand as degradation product. HR-ESI-MS measurements, supported by DFT calculations indicate the formation of an oxoiron species." A Creative Commons Attribution 3.0 Unported Licence notice is present, stating: "This article is licensed under a Creative Commons Attribution 3.0 Unported Licence. You can use material from this article in other publications without requesting further permissions from the RSC, provided that the correct acknowledgement is given." A link to "Read more about how to correctly acknowledge RSC content" is also provided.

3 Elsevier Journals

“Tailoring activity and stability: Effects of electronic variations on iron-NHC epoxidation catalysts”

T. P. Schlachta, **G. G. Zámbo**, M. J. Sauer, I. Rüter, C. A. Hoefler, S. Demeshko, F. Meyer, F. E. Kühn

Journal of Catalysis, **2023**, 426, 234-246.

DOI: [10.1016/j.jcat.2023.07.018](https://doi.org/10.1016/j.jcat.2023.07.018)

Reproduced from ref. ¹⁹⁵ with permission of Elsevier.

“Please note that, as the author of this Elsevier article, you retain the right to include it in a thesis or dissertation, provided it is not published commercially. Permission is not required, but please ensure that you reference the journal as the original source.”



Tailoring activity and stability: Effects of electronic variations on iron-NHC epoxidation catalysts

Author: Tim P. Schlachta, Greta G. Zámbo, Michael J. Sauer, Isabelle Rüter, Carla A. Hoefler, Serhiy Demeshko, Franc Meyer, Fritz E. Kühn

Publication: Journal of Catalysis

Publisher: Elsevier

Date: October 2023

© 2023 Elsevier Inc. All rights reserved.

Journal Author Rights

Please note that, as the author of this Elsevier article, you retain the right to include it in a thesis or dissertation, provided it is not published commercially. Permission is not required, but please ensure that you reference the journal as the original source. For more information on this and on your other retained rights, please visit: <https://www.elsevier.com/about/our-business/policies/copyright#Author-rights>

“Unraveling the potential of backbone modifications in iron(II) NHC complexes for olefin aziridination and imination”

C. A. Hoefler, N. K. Dietl, **G. G. Zámbo**, T. P. Schlachta, R. M. Reich, F. E. Kühn

Journal of Organometallic Chemistry, **2024**, 1006, 123018.

DOI: [10.1016/j.jorganchem.2024.123018](https://doi.org/10.1016/j.jorganchem.2024.123018)

Reproduced from ref. ¹⁹⁸ with permission of Elsevier.

“Please note that, as the author of this Elsevier article, you retain the right to include it in a thesis or dissertation, provided it is not published commercially. Permission is not required, but please ensure that you reference the journal as the original source.”



Unraveling the potential of backbone modifications in iron(II) NHC complexes for olefin aziridination and imination

Author: Carla A. Hoefler, Nicole K. Dietl, Greta G. Zámbo, Tim P. Schlachta, Robert M. Reich, Fritz E. Kühn

Publication: Journal of Organometallic Chemistry

Publisher: Elsevier

Date: 15 February 2024

© 2024 The Authors. Published by Elsevier B.V.

Journal Author Rights

Please note that, as the author of this Elsevier article, you retain the right to include it in a thesis or dissertation, provided it is not published commercially. Permission is not required, but please ensure that you reference the journal as the original source. For more information on this and on your other retained rights, please visit: <https://www.elsevier.com/about/our-business/policies/copyright#Author-rights>

“Homobimetallic *bis*-NHC(Ptdvtms)₂ Complexes for the Hydrosilylation of Alkenes”

M. J. Sauer, J. Offorjindu, **G. G. Zámbo**, R. M. Reich, F. E. Kühn

Journal of Organometallic Chemistry, **2024**, 1007, 123030.

DOI: [10.1016/j.jorganchem.2024.123030](https://doi.org/10.1016/j.jorganchem.2024.123030)

Reproduced from ref. ¹⁹⁹ with permission of Elsevier.

“Please note that, as the author of this Elsevier article, you retain the right to include it in a thesis or dissertation, provided it is not published commercially. Permission is not required, but please ensure that you reference the journal as the original source.”



Homobimetallic bis-NHC(Ptdvtms)₂ Complexes for the Hydrosilylation of Alkenes

Author: Michael J. Sauer, Jeff Offorjindu, Greta G. Zámbo, Robert M. Reich, Fritz E. Kühn

Publication: Journal of Organometallic Chemistry

Publisher: Elsevier

Date: 1 March 2024

© 2024 The Author(s). Published by Elsevier B.V.

Journal Author Rights

Please note that, as the author of this Elsevier article, you retain the right to include it in a thesis or dissertation, provided it is not published commercially. Permission is not required, but please ensure that you reference the journal as the original source. For more information on this and on your other retained rights, please visit: <https://www.elsevier.com/about/our-business/policies/copyright#Author-rights>

VI Complete List of Publications and Contributions

- [8] T. P. Schlachta[§], **G. G. Zámbo**[§], M. J. Sauer, I. Rüter and F. E. Kühn*, “Impact of Ligand Design on an Iron NHC Epoxidation Catalyst”, *ChemistryOpen*, **2024**, *13*, e202400071, DOI: 10.1002/open.202400071.
- [7] **G. G. Zámbo**, C. A. Esslinger, M. J. Sauer, I. Rüter, R. M. Reich, S. Demeshko, F. Meyer, F. E. Kühn*, “Exploring the impact of abnormal coordination in macrocyclic *N*-heterocyclic carbene ligands on bio-inspired iron epoxidation catalysis”, *Catal. Sci. Technol.*, **2024**, *14*, 6259-6269, DOI: 10.1039/D4CY00992D.
- [6] M. J. Sauer, J. Offorjindu, **G. G. Zámbo**, R. M. Reich, F. E. Kühn*, “Homobimetallic bis-NHC(Ptdvtms)₂ Complexes for the Hydrosilylation of Alkenes”, *J. Organomet. Chem.*, **2024**, *1007*, 123030, DOI: 10.1016/j.jorganchem.2024.123030.
- [5] C. A. Hofer[§], N. K. Dietl[§], **G. G. Zámbo**, T. P. Schlachta, R. M. Reich, F. E. Kühn*, “Unraveling the potential of backbone modifications in iron(II) NHC complexes for olefin aziridination and imination”, *J. Organomet. Chem.*, **2024**, *1006*, 123018, DOI: 10.1016/j.jorganchem.2024.123018.
- [4] T. P. Schlachta, **G. G. Zámbo**, M. J. Sauer, I. Rüter, C. A. Hofer, S. Demeshko, F. Meyer, F. E. Kühn*, “Tailoring activity and stability: Effects of electronic variations on iron-NHC epoxidation catalysts”, *J. Catal.*, **2023**, *426*, 234-246, DOI: 10.1016/j.jcat.2023.07.018.
- [3] **G. G. Zámbo**, J. Mayr, M. J. Sauer, T. P. Schlachta, R. M. Reich, F. E. Kühn*, “The first macrocyclic abnormally coordinating tetra-1,2,3-triazole-5-ylidene iron complex: a promising candidate for olefin epoxidation”, *Dalton Trans.*, **2022**, *51*, 13591-13595, DOI: 10.1039/D2DT02561B.
- [2] **G. G. Zámbo**, J. F. Schlagintweit, R. M. Reich, F. E. Kühn*, “Organometallic 3d transition metal NHC complexes in oxidation catalysis”, *Catal. Sci. Technol.*, **2022**, *12*, 4949-4961, DOI: 10.1039/D2CY00127F.
- [1] E.-M. H. J. Esslinger, J. F. Schlagintweit, **G. G. Zámbo**, A. M. Imhof, R. M. Reich, F. E. Kühn*, “The Effect of *trans* Axial Isocyanide Ligands on Iron(II) Tetra-NHC Complexes and their Reactivity in Olefin Epoxidation”, *Asian J. Org. Chem.*, **2021**, *10*, 2654-2662, DOI: 10.1002/ajoc.202100487.

[§] equally contributing authors

* corresponding author

VI Complete List of Publications

no.	data	ref.	author	contribution, CRediT roles
[8]	<i>ChemistryOpen</i> , 2024 , <i>13</i> , e202400071	196	2 nd §	catalysis: conceptual approach, experimental work and related data interpretation, project administration, conception and writing – review & editing, data curation, formal analysis, investigation, methodology, visualization
[7]	<i>Catal. Sci. Technol.</i> , 2024 , <i>14</i> , 6259-6269	183	1 st	conceptual approach, experimental work and related data interpretation, project administration, conception and writing – original draft, writing – review & editing, data curation, formal analysis, investigation, methodology, visualization
[6]	<i>J. Organomet. Chem.</i> , 2024 , <i>1007</i> , 123030	199	3 rd	experimental work, writing – review & editing
[5]	<i>J. Organomet. Chem.</i> , 2024 , <i>1006</i> , 123018	198	3 rd	supervision, writing – review & editing
[4]	<i>J. Catal.</i> , 2023 , <i>426</i> , 234-246	195	2 nd	catalysis: conceptual approach, experimental work and related data interpretation, project administration, conception and writing – review & editing, data curation, formal analysis, investigation, methodology, visualization
[3]	<i>Dalton Trans.</i> , 2022 , <i>51</i> , 13591-13595	194	1 st	conceptual approach, experimental work and related data interpretation, project administration, conception and writing – original draft, writing – review & editing, data curation, formal analysis, investigation, methodology, visualization
[2]	<i>Catal. Sci. Technol.</i> , 2022 , <i>12</i> , 4949-4961	30	1 st	conceptualization, data curation, formal analysis, investigation, methodology, visualization, writing – original draft, writing – review & editing
[1]	<i>Asian J. Org. Chem.</i> , 2021 , <i>10</i> , 2654-2662	193	3 rd	experimental work and related data interpretation, conception, writing – review & editing, data curation, formal analysis, investigation, methodology, visualization

§ equally contributing first authors

CRediT: <https://credit.niso.org/contributor-roles-defined/>

VII References

1. S. Díez-González and S. P. Nolan, *Coord. Chem. Rev.*, **2007**, *251*, 874-883.
2. P. De Fremont, N. Marion and S. P. Nolan, *Coord. Chem. Rev.*, **2009**, *253*, 862-892.
3. K. A. Savin, *Writing reaction mechanisms in organic chemistry*, Academic Press, **2014**.
4. E. Fischer and A. Maasböl, *Angew. Chem., Int. Ed. Engl.*, **1964**, *3*, 580-581.
5. S. F. Vyboishchikov and G. Frenking, *Chem. Eur. J.*, **1998**, *4*, 1428-1438.
6. G. Frenking, M. Solà and S. F. Vyboishchikov, *J. Organomet. Chem.*, **2005**, *690*, 6178-6204.
7. R. R. Schrock, *J. Am. Chem. Soc.*, **1974**, *96*, 6796-6797.
8. J. Won, H. Jung, M. V. Mane, J. Heo, S. Kwon and M.-H. Baik, in *Advances in Inorganic Chemistry*, Elsevier, 2019, vol. 73, pp. 385-443.
9. D. Bourissou, O. Guerret, F. P. Gabbaï and G. Bertrand, *Chem. Rev.*, **2000**, *100*, 39-92.
10. R. H. Grubbs, *Angew. Chem., Int. Ed.*, **2006**, *45*, 3760-3765.
11. Y. Chauvin, *Angew. Chem., Int. Ed.*, **2006**, *45*, 3740-3747.
12. C. P. Casey, *Journal*, **2006**.
13. P. Bellotti, M. Koy, M. N. Hopkinson and F. Glorius, *Nat. Rev. Chem.*, **2021**, *5*, 711-725.
14. M. N. Hopkinson, C. Richter, M. Schedler and F. Glorius, *Nature*, **2014**, *510*, 485-496.
15. H. W. Wanzlick and H. J. Schönherr, *Angew. Chem., Int. Ed. Engl.*, **1968**, *7*, 141-142.
16. K. Öfele, *J. Organomet. Chem.*, **1968**, *12*, P42-P43.
17. A. Igau, H. Grutzmacher, A. Baceiredo and G. Bertrand, *J. Am. Chem. Soc.*, **1988**, *110*, 6463-6466.
18. A. J. Arduengo III, R. L. Harlow and M. Kline, *J. Am. Chem. Soc.*, **1991**, *113*, 361-363.
19. H. W. Wanzlick, *Angew. Chem., Int. Ed. Engl.*, **1962**, *1*, 75-80.
20. T. P. Schlachta, Dissertation, *The reactivity of iron NHC complexes, their application in epoxidation catalysis and the development of new NHC ligand systems*, Technische Universität München, Garching, Germany, **2024**.
21. E. Riedel, *Allgemeine und anorganische Chemie*, de Gruyter, **2010**.
22. T. Dröge and F. Glorius, *Angew. Chem., Int. Ed.*, **2010**, *49*, 6940-6952.
23. U. Radius and F. M. Bickelhaupt, *Coord. Chem. Rev.*, **2009**, *253*, 678-686.
24. H. Jacobsen, A. Correa, A. Poater, C. Costabile and L. Cavallo, *Coord. Chem. Rev.*, **2009**, *253*, 687-703.
25. V. Nesterov, D. Reiter, P. Bag, P. Frisch, R. Holzner, A. Porzelt and S. Inoue, *Chem. Rev.*, **2018**, *118*, 9678-9842.
26. Y. Pan, X. Jiang, Y.-M. So, C. T. To and G. He, *Catalysts*, **2020**, *10*, 71.
27. R. H. Crabtree, *J. Organomet. Chem.*, **2005**, *690*, 5451-5457.
28. M. Scholl, S. Ding, C. W. Lee and R. H. Grubbs, *Org. Lett.*, **1999**, *1*, 953-956.
29. F. E. Hahn and M. C. Jahnke, *Angew. Chem., Int. Ed.*, **2008**, *47*, 3122-3172.
30. G. G. Zámbo, J. F. Schlagintweit, R. M. Reich and F. E. Kühn, *Catal. Sci. Technol.*, **2022**, *12*, 4949-4961.
31. T. P. Schlachta and F. E. Kühn, *Chem. Soc. Rev.*, **2023**.
32. O. Schuster, L. Yang, H. G. Raubenheimer and M. Albrecht, *Chem. Rev.*, **2009**, *109*, 3445-3478.
33. S. Diez-Gonzalez, N. Marion and S. P. Nolan, *Chem. Rev.*, **2009**, *109*, 3612-3676.
34. F. Nahra, D. J. Nelson and S. P. Nolan, *Trends Chem.*, **2020**, *2*, 1096-1113.
35. R. Jothibasu and H. V. Huynh, *Organometallics*, **2009**, *28*, 2505-2511.

36. D. J. Nelson and S. P. Nolan, *Chem. Soc. Rev.*, **2013**, *42*, 6723-6753.
37. T. Zhou, G. Utecht-Jarzyńska and M. Szostak, *Coord. Chem. Rev.*, **2024**, *512*, 215867.
38. M. Melaimi, M. Soleilhavoup and G. Bertrand, *Angew. Chem., Int. Ed.*, **2010**, *49*, 8810-8849.
39. J. Zhang, T. Li, X. Li, A. Lv, X. Li, Z. Wang, R. Wang, Y. Ma, R. Fang and R. Szostak, *Commun. Chem.*, **2022**, *5*, 60.
40. M. Joost, M. Nieger, M. Lutz, A. W. Ehlers, J. C. Slootweg and K. Lammertsma, *Organometallics*, **2020**, *39*, 1762-1771.
41. D. M. Andrada, N. Holzmann, T. Hamadi and G. Frenking, *Beilstein J. Org. Chem.*, **2015**, *11*, 2727-2736.
42. V. Lavallo, Y. Canac, C. Präsang, B. Donnadieu and G. Bertrand, *Angew. Chem., Int. Ed.*, **2005**, *44*, 5705.
43. F. E. Hahn, *Angew. Chem., Int. Ed.*, **2006**, *45*, 1348-1352.
44. R. Jassar, M. Soleilhavoup and G. Bertrand, *Chem. Rev.*, **2020**, *120*, 4141-4168.
45. B. Rao, H. Tang, X. Zeng, L. L. Liu, M. Melaimi and G. Bertrand, *Angew. Chem., Int. Ed.*, **2015**, *54*, 14915-14919.
46. N. Mohebi and M. Z. Kassaei, *Struct. Chem.*, **2021**, *32*, 731-757.
47. O. Kühn, *Coord. Chem. Rev.*, **2004**, *248*, 411-427.
48. S. Raoufmoghaddam, Y.-P. Zhou, Y. Wang and M. Driess, *J. Organomet. Chem.*, **2017**, *829*, 2-10.
49. R. Dasgupta and S. Khan, in *Advances in Organometallic Chemistry*, Elsevier, 2020, vol. 74, pp. 105-152.
50. S. C. Sau, P. K. Hota, S. K. Mandal, M. Soleilhavoup and G. Bertrand, *Chem. Soc. Rev.*, **2020**, *49*, 1233-1252.
51. A. D. McNaught and A. Wilkinson, *Compendium of chemical terminology*, Blackwell Science Oxford, **1997**.
52. A. Vivancos, C. Segarra and M. Albrecht, *Chem. Rev.*, **2018**, *118*, 9493-9586.
53. S. Gründemann, A. Kovacevic, M. Albrecht, J. W. F. Robert and H. Crabtree, *Chem. Commun.*, **2001**, 2274-2275.
54. A. R. Chianese, A. Kovacevic, B. M. Zeglis, J. Faller and R. H. Crabtree, *Organometallics*, **2004**, *23*, 2461-2468.
55. P. Mathew, A. Neels and M. Albrecht, *J. Am. Chem. Soc.*, **2008**, *130*, 13534-13535.
56. G. Guisado-Barrios, J. Bouffard, B. Donnadieu and G. Bertrand, *Angew. Chem., Int. Ed.*, **2010**, *49*, 4759.
57. G. Guisado-Barrios, M. Soleilhavoup and G. Bertrand, *Acc. Chem. Res.*, **2018**, *51*, 3236-3244.
58. J. M. Aizpurua, M. Sagartzazu-Aizpurua and Z. Monasterio, *Chemistry of 1, 2, 3-triazoles*, **2015**, 211-267.
59. G. Sini, O. Eisenstein and R. H. Crabtree, *Inorg. Chem.*, **2002**, *41*, 602-604.
60. R. Tonner, G. Heydenrych and G. Frenking, *Chem. Asian J.*, **2007**, *2*, 1555-1567.
61. L. Benhamou, E. Chardon, G. Lavigne, S. Bellemin-Lapponnaz and V. César, *Chem. Rev.*, **2011**, *111*, 2705-2733.
62. W. Hermann, T. Weskamp and V. P. Bohm, *Advances in organometallic chemistry*, **2001**, *48*, 1-71.
63. M. C. Jahnke and F. E. Hahn, **2016**.
64. K. Riener, S. Haslinger, A. Raba, M. P. Högerl, M. Cokoja, W. A. Herrmann and F. E. Kühn, *Chem. Rev.*, **2014**, *114*, 5215-5272.
65. H. C. Kolb, M. Finn and K. B. Sharpless, *Angew. Chem., Int. Ed.*, **2001**, *40*, 2004-2021.

66. V. V. Rostovtsev, L. G. Green, V. V. Fokin and K. B. Sharpless, *Angew. Chem.*, **2002**, *114*, 2708-2711.
67. C. W. Tornøe, C. Christensen and M. Meldal, *J. Org. Chem.*, **2002**, *67*, 3057-3064.
68. L. Liang and D. Astruc, *Coord. Chem. Rev.*, **2011**, *255*, 2933-2945.
69. C. Wang, D. Ikhlef, S. Kahlal, J.-Y. Saillard and D. Astruc, *Coord. Chem. Rev.*, **2016**, *316*, 1-20.
70. D. Schweinfurth, L. Hettmanczyk, L. Suntrup and B. Sarkar, *Z. Anorg. Allg. Chem.*, **2017**, *643*, 554-584.
71. R. Huisgen, *Angew. Chem., Int. Ed. Engl.*, **1963**, *2*, 565-598.
72. L. Zhang, X. Chen, P. Xue, H. H. Sun, I. D. Williams, K. B. Sharpless, V. V. Fokin and G. Jia, *J. Am. Chem. Soc.*, **2005**, *127*, 15998-15999.
73. F. Himo, T. Lovell, R. Hilgraf, V. V. Rostovtsev, L. Noodleman, K. B. Sharpless and V. V. Fokin, *J. Am. Chem. Soc.*, **2005**, *127*, 210-216.
74. B. T. Worrell, J. Malik and V. V. Fokin, *Science*, **2013**, *340*, 457-460.
75. V. O. Rodionov, V. V. Fokin and M. Finn, *Angew. Chem., Int. Ed.*, **2005**, *44*, 2210-2215.
76. C. Wang, X. Yang, C. Dong, K. Chai, J. Ruan and S. Shi, *Coord. Chem. Rev.*, **2023**, *487*, 215156.
77. P. J. Altmann, D. T. Weiss, C. Jandl and F. E. Kühn, *Chem. Asian J.*, **2016**, *11*, 1597-1605.
78. P. G. Edwards and F. E. Hahn, *Dalton Trans.*, **2011**, *40*, 10278-10288.
79. F. E. Hahn, V. Langenhahn, T. Lügger, T. Pape and D. Le Van, *Angew. Chem., Int. Ed.*, **2005**, *44*, 3759-3763.
80. A. H. Mageed, *J. Organomet. Chem.*, **2019**, *902*, 120965.
81. R. McKie, J. A. Murphy, S. R. Park, M. D. Spicer and S.-z. Zhou, *Angew. Chem., Int. Ed.*, **2007**, *46*, 6525-6528.
82. H. M. Bass, S. A. Cramer, J. L. Price and D. M. Jenkins, *Organometallics*, **2010**, *29*, 3235-3238.
83. J. F. DeJesus and D. M. Jenkins, *Chem. Eur. J.*, **2020**, *26*, 1429-1435.
84. H. M. Bass, S. A. Cramer, A. S. McCullough, K. J. Bernstein, C. R. Murdock and D. M. Jenkins, *Organometallics*, **2013**, *32*, 2160-2167.
85. M. R. Anneser, G. R. Elpitiya, X. B. Powers and D. M. Jenkins, *Organometallics*, **2019**, *38*, 981-987.
86. M. Baerns, *Technische chemie*, John Wiley & Sons, **2013**.
87. H.-J. Arpe, *Industrielle Organische Chemie: Bedeutende Vor-und Zwischenprodukte*, John Wiley & Sons, **2007**.
88. J. F. Schlagintweit, Dissertation, *Transition Metal NHC Complexes in Oxidation Catalysis and Medicinal Chemistry*, Technische Universität München, Garching, Germany, **2021**.
89. A. Schuhmacher, M. Hinder and O. Gassmann.
90. R. Teranishi, E. L. Wick and I. Hornstein, *Flavor Chemistry: Thirty Years of Progress*, **1999**, 1-8.
91. G. Fráter, J. A. Bajgrowicz and P. Kraft, *Tetrahedron*, **1998**, *54*, 7633-7703.
92. M. Bajus, *Petrochemistry: Petrochemical Processing, Hydrocarbon Technology and Green Engineering*, John Wiley & Sons, **2020**.
93. GlobalData, Production capacity of ethylene worldwide from 2018 to 2022 (in million metric tons), *Statista*, **2023**, <https://www.statista.com/statistics/1067372/global-ethylene-production-capacity/>, (accessed October 17, 2024).
94. GlobalData, Production capacity of propylene worldwide in 2018 and 2022, with a forecast to 2030 (in million metric tons), *Statista*, **2023**,

- <https://www.statista.com/statistics/1065879/global-propylene-production-capacity/>, (accessed October 17, 2024).
95. T. Ren, M. Patel and K. Blok, *Energy*, **2006**, *31*, 425-451.
 96. W. Posch, in *Applied Plastics Engineering Handbook*, Elsevier, 2011, pp. 23-48.
 97. L. Yang and X. Ge, in *Advances in bioenergy*, Elsevier, 2016, vol. 1, pp. 125-188.
 98. E. Rebrov, *Advances in Clean Hydrocarbon Fuel Processing*, **2011**, 387-412.
 99. J. G. Speight, in *Fuel flexible energy generation*, Elsevier, 2016, pp. 145-174.
 100. F. Cavani and J. H. Teles, *ChemSusChem: Chemistry & Sustainability Energy & Materials*, **2009**, *2*, 508-534.
 101. S. A. Hauser, M. Cokoja and F. E. Kühn, *Catal. Sci. Technol.*, **2013**, *3*, 552-561.
 102. V. Russo, R. Tesser, E. Santacesaria and M. Di Serio, *Ind. Eng. Chem. Res.*, **2013**, *52*, 1168-1178.
 103. AgileIntel Research, (ChemIntel360), Market volume of ethylene oxide worldwide from 2015 to 2022, with a forecast for 2023 to 2030 (in million metric tons), *Statista*, **2023**, <https://www.statista.com/statistics/1245260/ethylene-oxide-market-volume-worldwide/>, (accessed October 22, 2024).
 104. S. T. Oyama, in *Mechanisms in homogeneous and heterogeneous epoxidation catalysis*, Elsevier, 2008, pp. 3-99.
 105. E. Louisy, V. Khodyrieva, S. Olivero, V. Michelet and A. Mija, *ChemPlusChem*, **2022**, *87*, e202200190.
 106. M. Zviely, *Chemistry and Technology of Flavors and Fragrances*, **2005**, 85.
 107. V. Lu, M. Bastaki, A. M. Api, M. Aubanel, M. Bauter, T. Cachet, J. Demyttenaere, M. M. Diop, C. L. Harman and S.-m. Hayashi, *Curr. Res. Toxicol.*, **2021**, *2*, 192-201.
 108. A. Lewinska, P. Chochrek, K. Smolag, E. Rawska and M. Wnuk, *Redox Report*, **2015**, *20*, 116-125.
 109. J. K. Tie and D. W. Stafford, *Vitamins & Hormones*, **2008**, *78*, 103-130.
 110. L. F. Tietze, C. Güntner, K. M. Gericke, I. Schuberth and G. Bunkoczi, *Journal*, **2005**.
 111. K. A. Jørgensen, *Chem. Rev.*, **1989**, *89*, 431-458.
 112. D. I. Metelitsa, *Russian Chemical Reviews*, **1972**, *41*, 807.
 113. T. A. Nijhuis, M. Makkee, J. A. Moulijn and B. M. Weckhuysen, *Ind. Eng. Chem. Res.*, **2006**, *45*, 3447-3459.
 114. Q.-H. Xia, H.-Q. Ge, C.-P. Ye, Z.-M. Liu and K.-X. Su, *Chem. Rev.*, **2005**, *105*, 1603-1662.
 115. G. Parshall, *J. Mol. Catal.*, **1978**, *4*, 243-270.
 116. B. Cornils, W. A. Herrmann, J.-H. Xu and H.-W. Zanthoff, *Catalysis from A to Z: a concise encyclopedia*, John Wiley & Sons, **2020**.
 117. J. W. Kück, R. M. Reich and F. E. Kühn, *Chem. Rec.*, **2016**, *16*, 349-364.
 118. S. Enthaler, K. Junge and M. Beller, *Angew. Chem., Int. Ed.*, **2008**, *47*, 3317-3321.
 119. E. Wiberg, *Lehrbuch der anorganischen Chemie*, Walter de Gruyter GmbH & Co KG, **2019**.
 120. J. W. Kück, M. R. Anneser, B. Hofmann, A. Pöthig, M. Cokoja and F. E. Kühn, *ChemSusChem*, **2015**, *8*, 4056-4063.
 121. L. Que Jr and W. B. Tolman, *Nature*, **2008**, *455*, 333-340.
 122. S. M. Hölzl, P. J. Altmann, J. W. Kück and F. E. Kühn, *Coord. Chem. Rev.*, **2017**, *352*, 517-536.
 123. Y. Feng, J. England and L. Que Jr, *ACS Catal.*, **2011**, *1*, 1035-1042.
 124. K. Chen, M. Costas, J. Kim, A. K. Tipton and L. Que, *J. Am. Chem. Soc.*, **2002**, *124*, 3026-3035.
 125. A. R. McDonald and L. Que Jr, *Coord. Chem. Rev.*, **2013**, *257*, 414-428.

126. D. Y. Kim, Y. J. Choi, H. Y. Park, C. U. Joung, K. O. Koh, J. Y. Mang and K.-Y. Jung, *Synth. Commun.*, **2003**, *33*, 435-443.
127. B. Bahramian, V. Mirkhani, M. Moghadam and S. Tangestaninejad, *Catal. Commun.*, **2006**, *7*, 289-296.
128. L. Hadian-Dehkordi and H. Hosseini-Monfared, *Green Chemistry*, **2016**, *18*, 497-507.
129. A. Lindhorst, S. Haslinger and F. E. Kühn, *Chem. Commun.*, **2015**, *51*, 17193-17212.
130. M. Finn and K. B. Sharpless, *J. Am. Chem. Soc.*, **1991**, *113*, 113-126.
131. T. Katsuki and K. B. Sharpless, *J. Am. Chem. Soc.*, **1980**, *102*, 5974-5976.
132. K. Srinivasan, P. Michaud and J. K. Kochi, *J. Am. Chem. Soc.*, **1986**, *108*, 2309-2320.
133. E. N. Jacobsen, W. Zhang, A. R. Muci, J. R. Ecker and L. Deng, *J. Am. Chem. Soc.*, **1991**, *113*, 7063-7064.
134. W. Zhang, J. L. Loebach, S. R. Wilson and E. N. Jacobsen, *J. Am. Chem. Soc.*, **1990**, *112*, 2801-2803.
135. T. Linker, *Angew. Chem., Int. Ed. Engl.*, **1997**, *36*, 2060-2062.
136. R. Irie, K. Noda, Y. Ito, N. Matsumoto and T. Katsuki, *Tetrahedron: Asymmetry*, **1991**, *2*, 481-494.
137. A. M. Al-Ajlouni and J. H. Espenson, *J. Org. Chem.*, **1996**, *61*, 3969-3976.
138. A. M. Al-Ajlouni and J. H. Espenson, *J. Am. Chem. Soc.*, **1995**, *117*, 9243-9250.
139. W. A. Herrmann, R. W. Fischer, W. Scherer and M. U. Rauch, *Angew. Chem., Int. Ed. Engl.*, **1993**, *32*, 1157-1160.
140. W. A. Herrmann, R. W. Fischer and D. W. Marz, *Angew. Chem.*, **1991**, *103*, 1706-1709.
141. A. Ault, *J. Chem. Educ.*, **2002**, *79*, 572.
142. A. Schmidt, N. Grover, T. K. Zimmermann, L. Graser, M. Cokoja, A. Pöthig and F. E. Kühn, *J. Catal.*, **2014**, *319*, 119-126.
143. I. R. Beattie and P. J. Jones, *Inorg. Chem.*, **1979**, *18*, 2318-2319.
144. F. E. Kühn, A. Scherbaum and W. A. Herrmann, *J. Organomet. Chem.*, **2004**, *689*, 4149-4164.
145. M. Costas, M. P. Mehn, M. P. Jensen and L. Que, *Chem. Rev.*, **2004**, *104*, 939-986.
146. A. C. Lindhorst, Dissertation, *Towards Real-Life Applications: Reactivity of Biomimetic Iron N-Heterocyclic Carbene Complexes in Homogeneous Catalysis*, Technische Universität München, Garching, Germany, **2017**.
147. J. Mortier, *Arene chemistry: reaction mechanisms and methods for aromatic compounds*, John Wiley & Sons, **2015**.
148. I. G. Denisov, T. M. Makris, S. G. Sligar and I. Schlichting, *Chem. Rev.*, **2005**, *105*, 2253-2278.
149. K. P. Bryliakov and E. P. Talsi, *Coord. Chem. Rev.*, **2014**, *276*, 73-96.
150. M.-H. Baik, M. Newcomb, R. A. Friesner and S. J. Lippard, *Chem. Rev.*, **2003**, *103*, 2385-2420.
151. J. A. Pavon and P. F. Fitzpatrick, *Biochemistry*, **2006**, *45*, 11030-11037.
152. B. Meunier, S. P. De Visser and S. Shaik, *Chem. Rev.*, **2004**, *104*, 3947-3980.
153. P. R. Ortiz de Montellano, *Chem. Rev.*, **2010**, *110*, 932-948.
154. S. Kal, S. Xu and L. Que Jr, *Angew. Chem., Int. Ed.*, **2020**, *59*, 7332-7349.
155. I. Prat, D. Font, A. Company, K. Junge, X. Ribas, M. Beller and M. Costas, *Adv. Synth. Catal.*, **2013**, *355*, 947-956.
156. H. J. H. Fenton, *Journal of the Chemical Society, Transactions*, **1894**, *65*, 899-910.
157. M. Costas, K. Chen and L. Que Jr, *Coord. Chem. Rev.*, **2000**, *200*, 517-544.
158. F. Gozzo, *Journal of molecular catalysis A: Chemical*, **2001**, *171*, 1-22.
159. G. Olivo, O. Cussó, M. Borrell and M. Costas, *J. Biol. Inorg. Chem.*, **2017**, *22*, 425-452.

160. W. Nam, *Acc. Chem. Res.*, **2007**, *40*, 522-531.
161. J. Cho, S. Jeon, S. A. Wilson, L. V. Liu, E. A. Kang, J. J. Braymer, M. H. Lim, B. Hedman, K. O. Hodgson and J. S. Valentine, *Nature*, **2011**, *478*, 502-505.
162. J.-U. Rohde, J.-H. In, M. H. Lim, W. W. Brennessel, M. R. Bukowski, A. Stubna, E. Münck, W. Nam and L. Que, *Science*, **2003**, *299*, 1037-1039.
163. I. Prat, J. S. Mathieson, M. Güell, X. Ribas, J. M. Luis, L. Cronin and M. Costas, *Nat. Chem.*, **2011**, *3*, 788.
164. W. N. Oloo, A. J. Fielding and L. Que Jr, *J. Am. Chem. Soc.*, **2013**, *135*, 6438-6441.
165. S. R. Iyer, M. M. Javadi, Y. Feng, M. Y. Hyun, W. N. Oloo, C. Kim and L. Que, *Chem. Commun.*, **2014**, *50*, 13777-13780.
166. R. Mas-Ballesté, M. Costas, T. Van Den Berg and L. Que Jr, *Chem. Eur. J.*, **2006**, *12*, 7489-7500.
167. L. V. Liu, S. Hong, J. Cho, W. Nam and E. I. Solomon, *J. Am. Chem. Soc.*, **2013**, *135*, 3286-3299.
168. J. Park, Y.-M. Lee, K. Ohkubo, W. Nam and S. Fukuzumi, *Inorg. Chem.*, **2015**, *54*, 5806-5812.
169. M. R. Bukowski, P. Comba, A. Lienke, C. Limberg, C. Lopez de Laorden, R. Mas-Ballesté, M. Merz and L. Que Jr, *Angew. Chem., Int. Ed.*, **2006**, *45*, 3446-3449.
170. R. Mas-Ballesté and L. Que, *J. Am. Chem. Soc.*, **2007**, *129*, 15964-15972.
171. E. A. Mikhalyova, O. V. Makhlynets, T. D. Palluccio, A. S. Filatov and E. V. Rybak-Akimova, *Chem. Commun.*, **2012**, *48*, 687-689.
172. S. Taktak, W. Ye, A. M. Herrera and E. V. Rybak-Akimova, *Inorg. Chem.*, **2007**, *46*, 2929-2942.
173. J. W. Kück, A. Raba, I. I. Markovits, M. Cokoja and F. E. Kühn, *ChemCatChem*, **2014**, *6*, 1882-1886.
174. A. Raba, M. Cokoja, S. Ewald, K. Riener, E. Herdtweck, A. Pöthig, W. A. Herrmann and F. E. Kühn, *Organometallics*, **2012**, *31*, 2793-2800.
175. M. R. Anneser, S. Haslinger, A. Pöthig, M. Cokoja, J.-M. Basset and F. E. Kühn, *Inorg. Chem.*, **2015**, *54*, 3797-3804.
176. F. Dyckhoff, J. F. Schlagintweit, R. M. Reich and F. E. Kühn, *Catal. Sci. Technol.*, **2020**, *10*, 3532-3536.
177. M. R. Anneser, S. Haslinger, A. Pöthig, M. Cokoja, V. D'Elia, M. P. Högerl, J.-M. Basset and F. E. Kühn, *Dalton Trans.*, **2016**, *45*, 6449-6455.
178. T. P. Schlachta, M. R. Anneser, J. F. Schlagintweit, C. H. Jakob, C. Hintermeier, A. D. Böth, S. Haslinger, R. M. Reich and F. E. Kühn, *Chem. Commun.*, **2021**, *57*, 6644-6647.
179. M. Costas, *Coord. Chem. Rev.*, **2011**, *255*, 2912-2932.
180. M. R. Bukowski, S. Zhu, K. D. Koehntop, W. W. Brennessel and L. Que, *J. Biol. Inorg. Chem.*, **2004**, *9*, 39-48.
181. F. Dyckhoff, J. F. Schlagintweit, M. A. Bernd, C. H. Jakob, T. P. Schlachta, B. J. Hofmann, R. M. Reich and F. E. Kühn, *Catal. Sci. Technol.*, **2021**, *11*, 795-799.
182. M. A. Bernd, F. Dyckhoff, B. J. Hofmann, A. D. Böth, J. F. Schlagintweit, J. Oberkofler, R. M. Reich and F. E. Kühn, *J. Catal.*, **2020**, *391*, 548-561.
183. G. G. Zámbo, C. A. Esslinger, M. J. Sauer, I. Rüter, R. M. Reich, S. Demeshko, F. Meyer and F. E. Kühn, *Catal. Sci. Technol.*, **2024**, *14*, 6259-6269.
184. J. F. Schlagintweit, F. Dyckhoff, L. Nguyen, C. H. Jakob, R. M. Reich and F. E. Kühn, *J. Catal.*, **2020**, *383*, 144-152.
185. S. Y. Hussaini, R. A. Haque and M. R. Razali, *J. Organomet. Chem.*, **2019**, *882*, 96-111.
186. A. A. Danopoulos, T. Simler and P. Braunstein, *Chem. Rev.*, **2019**, *119*, 3730-3961.

187. S. Bellemin-Laponnaz, *Eur. J. Inorg. Chem.*, **2020**, 2020, 10-20.
188. F. E. Hahn, C. Radloff, T. Pape and A. Hepp, *Chem. Eur. J.*, **2008**, *14*, 10900-10904.
189. Z. Lu, S. A. Cramer and D. M. Jenkins, *Chem. Sci.*, **2012**, *3*, 3081-3087.
190. T. Pape and F. E. Hahn, *Dalton Trans.*, **2013**, *42*, 7330-7337.
191. E. B. Bauer, M. A. Bernd, M. Schütz, J. Oberkofler, A. Pöthig, R. M. Reich and F. E. Kühn, *Dalton Trans.*, **2019**, *48*, 16615-16625.
192. M. A. Bernd, E. B. Bauer, J. Oberkofler, A. Bauer, R. M. Reich and F. E. Kühn, *Dalton Trans.*, **2020**, *49*, 14106-14114.
193. E.-M. H. J. Esslinger, J. F. Schlagintweit, G. G. Zámbo, A. M. Imhof, R. M. Reich and F. E. Kühn, *Asian J. Org. Chem.*, **2021**, *10*, 2654-2662.
194. G. G. Zámbo, J. Mayr, M. J. Sauer, T. P. Schlachta, R. M. Reich and F. E. Kühn, *Dalton Trans.*, **2022**, *51*, 13591-13595.
195. T. P. Schlachta, G. G. Zámbo, M. J. Sauer, I. Rüter, C. A. Hoefler, S. Demeshko, F. Meyer and F. E. Kühn, *J. Catal.*, **2023**, *426*, 234-246.
196. T. P. Schlachta, G. G. Zámbo, M. J. Sauer, I. Rüter and F. E. Kühn, *ChemistryOpen*, **2024**, *13*, e202400071.
197. M. Basato, A. Biffis, G. Martinati, C. Tubaro, A. Venzo, P. Ganis and F. Benetollo, *Inorg. Chim. Acta*, **2003**, *355*, 399-403.
198. C. A. Hoefler, N. K. Dietl, G. G. Zámbo, T. P. Schlachta, R. M. Reich and F. E. Kühn, *J. Organomet. Chem.*, **2024**, *1006*, 123018.
199. M. J. Sauer, J. Offorjindu, G. G. Zámbo, R. M. Reich and F. E. Kühn, *J. Organomet. Chem.*, **2024**, *1007*, 123030.

The Effect of *trans* Axial Isocyanide Ligands on Iron(II) Tetra-NHC Complexes and their Reactivity in Olefin Epoxidation

Eva-Maria H. J. Esslinger, Jonas F. Schlagintweit, Greta G. Zámbo, Alexander M. Imhof, Robert M. Reich, and Fritz E. Kühn^{*,[a]}

Abstract: The performance of *trans* axially substituted mono- (**2a**) and bis(*tert*-butylisocyanide) (**2b**) complexes derived from the highly active bio-inspired iron(II) (pre-)catalyst **2** containing an equatorial macrocyclic tetra *N*-heterocyclic carbene in homogenous olefin epoxidation catalysis is reported. H₂O₂ is used as oxidant in combination with the Lewis acid Sc(OTf)₃ as additive resulting in a considerable

improvement of catalytic activity. In contrast to other iron epoxidation catalysts, the introduction of π -accepting isocyanide ligands does not improve the catalytic performance of **2a** and **2b** posed by cyclic voltammetry. However, besides their lower activity, a high temperature tolerance of both compounds is found as a unique feature for iron NHC epoxidation catalysts.

Introduction

Oxidation catalysis, especially the oxidation of olefins to epoxides as wide-ranging intermediates plays a pivotal role in polymer industry as well as in the production of fine chemicals, food additives, and drug intermediates.^[1]

As electronic and catalytic properties are mainly influenced by the choice of the central metal and the surrounding ligand sphere, a variety of catalysts have been designed and tested over time. Among them, many homogeneous catalysts based on expensive noble metals such as palladium, rhodium, molybdenum, rhenium, and ruthenium are characterized by high efficiency in several applications.^[2] With regards to economic costs and the rising interest in sustainable catalysis,^[3] the use of earth-abundant and non-toxic transition metals came more into focus.^[4] Iron is the most common transition metal in the earth's crust (4.7 wt%) and in living organisms with iron cofactors that are capable to catalyze manifold oxidation reactions from demanding C–H activation to *cis*-dihydroxylation and epoxidation with high selectivity and activity at mild conditions.^[2b,4–5] Thus, using nature as a role model led to the mimicking of heme and non-heme iron complexes^[6] and their application in the oxidation of organic molecules.^[7] Cytochrome P450 (CYP), one of the most intensively studied oxygen-activating superfamily of heme-containing enzymes, enables

the controlled hydroxylation of aliphatic C–H bonds and the epoxidation of C=C double bonds with high regio- and stereoselectivity.^[6,8] These natural systems have an iron-porphyrin core^[9] as a key structural motive in common, based on a Fe(II/III) center and coordinating polydentate, mostly tetradentate *N*-donor ligands.^[6] Due to the mentioned structure-activity insights, the synthesis and application of *N*-heterocyclic carbene (NHC) ligands with easy-to-modify steric and electronic properties have become increasingly interesting for transition-metal centers in oxidation catalysis.^[10] A wide range of these artificial bio-inspired iron catalysts exhibit an octahedral structure of iron(II) complexes with two labile ligands (e.g. solvent molecules) in *cis* or *trans* position to each other, determined by the coordination mode of the NHC ligand, containing amine, pyridine, pyrrolidine, and pyrrole units.^[5a,11]

Since reaction performance under aerobic conditions (activation of dioxygen in nature often involving cofactors like NADPH/H⁺ as reducing agent)^[8b] is often difficult to control, hydrogen peroxide has become an established alternative as an oxidant in catalytic reactions. Besides its relatively high atom efficiency (47%), water is generated as the only by-product making it an environmentally friendly oxidant^[5a,12] in contrast to other sources such as Peroxysulfates,^[13] Hypochlorites,^[14] or Periodates.^[15] First of all, the reaction of the Fe-complex with hydrogen peroxide initiates the formation of an iron(III) hydroperoxo intermediate by a ligand exchange reaction after an essential one electron step (Fenton).^[11b,16] According to mechanistic studies, either a high valent iron(V)-oxo compound or an iron(IV)-oxo species with an oxyl radical can be formed in the following step depending on a homolytic or heterolytic cleavage pathway. The latter is less preferred as electron-deficient oxidants like H₂O₂ do not have stabilizing ability for the resulting radical, rendering it incapable to attack the oxygen source and the catalyst.^[11b,16] Furthermore, the interplay of the ligand arrangement (*cis/trans*) at the central atom and selectivity emphasize the competing character between dihydroxylation and epoxidation.^[17] Complexes with *cis*-oriented ligands tend more to dihydroxylation, whereas epoxidation takes rather

[a] E.-M. H. J. Esslinger, J. F. Schlagintweit, G. G. Zámbo, A. M. Imhof, Dr. R. M. Reich, Prof. Dr. F. E. Kühn
Molecular Catalysis, Catalysis Research Center and Department of Chemistry
Technische Universität München
Lichtenbergstrasse 4, D-85748 Garching bei München (Germany)
E-mail: fritz.kuehn@ch.tum.de

Supporting information for this article is available on the WWW under <https://doi.org/10.1002/ajoc.202100487>

© 2021 The Authors. Asian Journal of Organic Chemistry published by Wiley-VCH GmbH. This is an open access article under the terms of the Creative Commons Attribution Non-Commercial NoDerivs License, which permits use and distribution in any medium, provided the original work is properly cited, the use is non-commercial and no modifications or adaptations are made.

place when the labile sites are in *trans* position.^[11a] It has been observed, that the activity of the catalysts of the type described in this work can be noticeably improved by additives, such as Lewis (*e.g.* scandium(III)-triflate) or Brønsted (*e.g.* perchloric, acetic acid) acids.^[18] The presence of additives is supposed to facilitate the O–O bond heterolysis towards the formation of a highly electrophilic active species.^[18a,19] The suppressing effect of Sc³⁺ on the deactivation pathway leading to an oxo-bridged Fe^{III}–O–Fe^{III} species of a non-heme iron-NHC-complex epoxidation reaction is also another essential point with regard to a significant increase of the turnover number.^[20]

Well-studied prototypes of successful artificial catalytic models are primarily represented by bio-inspired iron-complexes **1** and **2** bearing tetradentate NHC ligands (Figure 1).^[10,21a]

Their applicability as catalyst precursors includes a variety of transformations such as the oxidation of unreactive alkanes, aromatic hydroxylation, and olefin epoxidation.^[10a,21a]

Complex **1**, bearing a bis(pyridyl-NHC) ligand NCCN was the first organometallic iron complex (with a Fe–C bond) used for epoxidation reactions enabling high activity and selectivity.^[22] Compared to **1**, complex **2** and its Fe(III) derivative, bearing a tetradentate macrocyclic NHC ligand cCCCC has been standing out with particularly high activity (turnover frequencies up to 183,000 h⁻¹) and in comparison to other iron catalysts high turnover numbers (TON up to 4,300). Here again, the activity-rising-effect of additives (largely doubling TOFs to values up to 410,000 h⁻¹) by applying Sc(OTf)₃, Ce(OTf)₄, or Fe(ClO₄)₃·H₂O on complex **2** is of high relevance in epoxidation catalysis.^[20] These reference points showcase again the competitive potential of iron complexes over more expensive metal catalysts.^[4]

Specific electronic and hence associated catalytic characteristics (activity, selectivity, stability) of the complexes can be obtained by variation of the polydentate scaffold or the introduction of ligands with individual electron pulling or pushing properties.^[21a] Concerning this matter, the influence of axial ligands on catalytic properties through axial ligand exchange at accessible coordination sites has been thoroughly investigated by cyclic voltammetry (CV) experiments concerning the Fe–NCCN complex **1**.^[21a] The result is a better catalyst

performance, recognizable by an increase in selectivity and turnover number in the precious C–H-oxidation of alkanes^[23] by introduction of a *tert*-butyl isocyanide ligand (**1a**) with π -acceptor and σ -donor features at one coordinating site of the complex.^[21] On account of the easily modifying functionality, isocyanides were synthetically favored instead of their isolobal CO counterpart.^[10a,21a] Increasing the substitution grade from 1 to 3 π -accepting isocyanide ligands at complex **1** (**1e–h**) (two-isocyanide substituted complexes could not be isolated) has resulted in an increase of the half-cell potential ($E_{1/2}$ = 0.57 V–1.092 V).^[21a] With respect to this observed tendency, all iron NHC complexes in olefin epoxidation display a typical correlation pattern between the redox potential and the resulting catalytic activity. Thus, a lower half-cell potential of the reversible Fe(II)/Fe(III) redox couple indicates a higher activity and vice versa.^[4,22,24]

This concept of isocyanide ligand substitution was transferred to the notably more active Fe–cCCCC complex **2** to create novel complexes with mixed catalytic properties released by axial π -acceptor ligands.^[4,21b] Accordingly, the mono- (**2a**) and bis(*tert*-butylisocyanide) derivatives (**2b**) were already synthesized and characterized by NMR-spectroscopy, elemental analysis, ESI-MS, and single crystal X-ray diffraction (SC-XRD) before.^[21b] Preceding cyclic voltammetry studies of both new compounds reveal the same redox potential trend, rising from mono- to bis(*tert*-butylisocyanide) ligand substitution. In comparison to **2** ($E_{1/2}$ = 0.15 V) and **2a** ($E_{1/2}$ = 0.35 V), **2b** displays the highest half-cell potential ($E_{1/2}$ = 0.44 V) corresponding to the reversible Fe(II)/Fe(III) redox process.^[21b] Another derivative **3** with a tetradentate macrocyclic NHC ligand cCCCC (Figure 2) showing similar electrochemical properties ($E_{1/2}$ = 0.44 V) is also examined and serves as an interpretation basis for the obtained catalytic results of **2a** and **2b**. Compared to **2a** and **2b**, complex **3** is bearing a backbone-modified imidazole structure without any modification at the axial positions.^[25]

The characteristic macrocyclic benzimidazolylidene ligand is inducing lower electron-donating properties because of the enlarged aromatic ring system and provokes analogously a decreased electron density at the iron center, but through

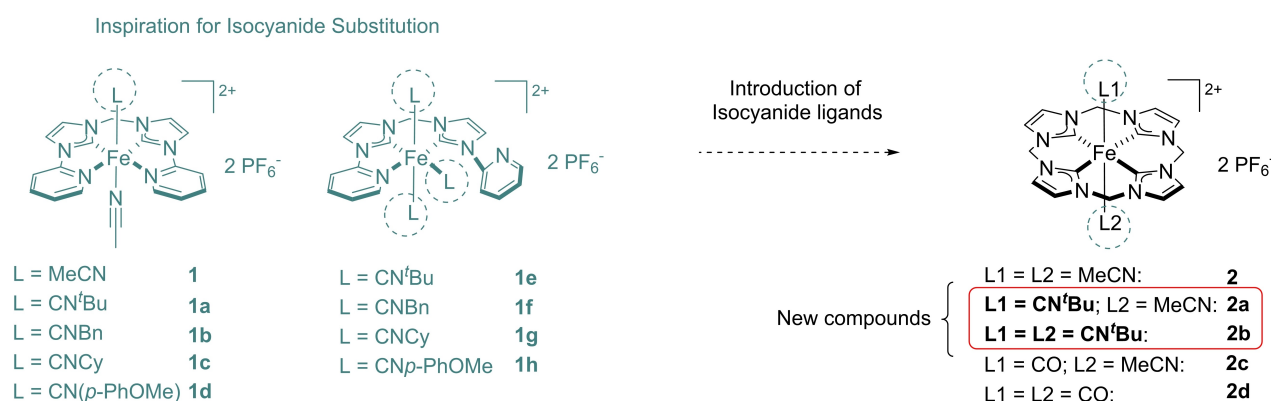


Figure 1. Structures of iron(II) complexes **1a–1d** containing tetradentate bis(pyridyl-NHC) ligand NCCN and one isocyanide ligand and **1e–1h** containing tridentate NCCN and three isocyanide ligands (left).^[21] Structures of complex **1** as an example for the application of one or two isocyanide ligands at complex **2** leading to mono- and bis(*tert*-butylisocyanide) substituted derivatives **2a** and **2b**. Their isolobal carbonyl analogs **2c** and **2d** containing tetradentate macrocyclic NHC ligand cCCCC are also depicted (right).^[10a,21b]

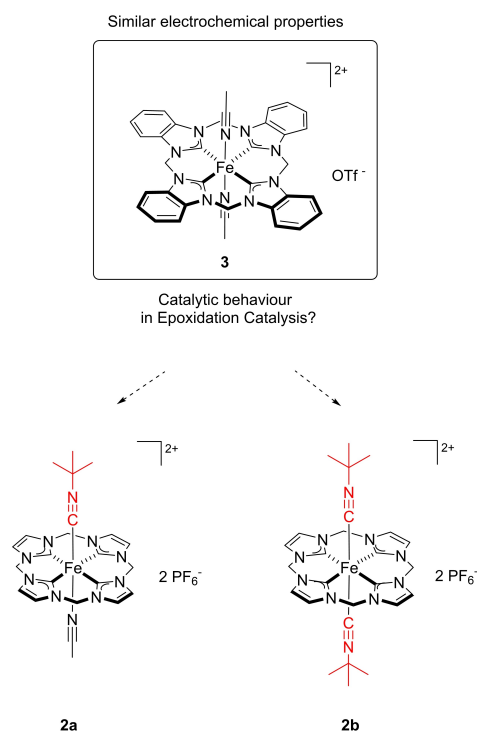


Figure 2. Comparison of the mono- and bis(*tert*-butylisocyanide) substituted derivatives **2a** and **2b** with an already existing and in epoxidation catalysis tested system **3**.^[25]

equatorial modification.^[25] These electronic features are reflected in an overall lower activity, high turnover numbers and especially in a light increase in stability towards higher temperatures in epoxidation catalysis.^[25] In this work, compounds **2a** and **2b** are applied in olefin epoxidation catalysis as a means of confirming the described redox behavior and its degree of influence on higher TONs as for complex **3**. Looking at the diversity of chemical features including compounds **1**, **2**, their derivatives, and compound **3**, the novel compounds **2a** and **2b** are expected to be unique in their catalytic performance. Furthermore, UV/Vis spectroscopy and thermogravimetric analysis of compounds **2a** and **2b** should reinforce the catalytic results and are also reported in this work.

Results and Discussion

Catalytic Olefin Epoxidation

Complexes **2a** and **2b** are studied in terms of their applicability as catalysts in olefin epoxidation reactions. Their performance is compared to the most active literature known non-heme iron complexes **1** and **2** as well as to complex **3** which possess similar electrochemical features (room temperature). Under standard conditions, H₂O₂ is applied as oxidant, acetonitrile as solvent, and *cis*-cyclooctene as a model substrate.

GC-FID analytic method is applied for the model substrate, particularly for the quantification of the formed epoxide and the respective *cis*-diol as a common byproduct. The catalytic

performance of both new compounds related to other substrates is conducted *via* ¹H-NMR spectroscopy.

When evaluating the curve progression, specifically the curve slope of (pre-)catalysts **2a** and **2b** in view of conversion [%] and yield [%] at 20 °C, it is obvious, that the mono-(*tert*-butylisocyanide) substituted derivative **2a** reveals a higher catalyst activity compared to the bis-(*tert*-butylisocyanide) substituted derivative **2b** (Figure 3). Hence, the activity estimation with the aid of half-cell potentials of each compound still remain a solid comparative basis. This is underlined by considering the reaction time (~12 h) of **2a**, which is about twice as high as for **2b** (~6 h). Moreover, this finding in terms of the catalytic reaction rate is supported by specific turnover numbers of **2a** (TON=84) and **2b** (TON=72) at a catalyst concentration of 1.0 mol%. However, the combination of a high catalyst concentration (1.0 mol%) and the necessary usage of scandium(III)-triflate as an additive demonstrates an overall low activity, but appropriate higher stability for both catalysts in the epoxidation reaction. These findings can be explained through the different substitution grades with *trans* axial *tert*-butylisocyanide ligands at the iron center. First, accessible coordination sites must be present for the attack of the oxidant in order to form the active species.^[11b] Accordingly to the examined reversibility of the redox process in cyclic voltammetry for compound **2b**, no isocyanide ligand dissociation after the oxidation step is expected, so that ligand exchange reactions at the beginning are hampered.^[21b]

Even the reduced π -backbonding at the iron center because of two competing axial isocyanide ligands with π -acceptor character leads only to weak dissociation of the ligands in acetonitrile, determined by ¹H-NMR spectroscopy.^[21b] Contrarily, the more active (pre-)catalyst **2a** exhibits one accessible coordination site with a weakly coordinating acetonitrile ligand which can be easily exchanged. Nevertheless, the π -backbonding from the iron center is reinforced by the stronger electron donating cCCCC-scaffold compared to NCCN and shortens the Fe–C_{isocyanide} bond so that the dissociation of the isocyanide ligand is impeded. This could explain the limited catalyst activity of **2a** despite the freely accessible coordination site.^[21a] As can be observed in both cases, the reaction needs a strong additive as first initiator, otherwise barely low or rather no conversion can be noticed if only H₂O₂ interacts with the catalyst (Figure 3). This indicates that Sc(OTf)₃ does not only accelerate the O–O-cleavage of the formed iron(III) hydroperoxo intermediate,^[18a] but also accelerates the formation of a free coordination position at the iron center, which is also confirmed by UV/Vis spectroscopy (see SI for further information). A closer look at conversion and yield of both catalysts reveals that no high selectivities are achieved. *Via* GC-FID analysis, many unidentifiable side-products besides small amount of *cis*-diol, explaining the gap between the conversion and yield graphs can be detected with help of the respective chromatograms.

Reducing the temperature provides further insights into existing induction periods of both compounds. In terms of the extremely low catalyst activities, a temperature of 0 °C instead of –10 °C or –20 °C as for other known high performance catalysts is chosen (Figure 4).^[4,24]

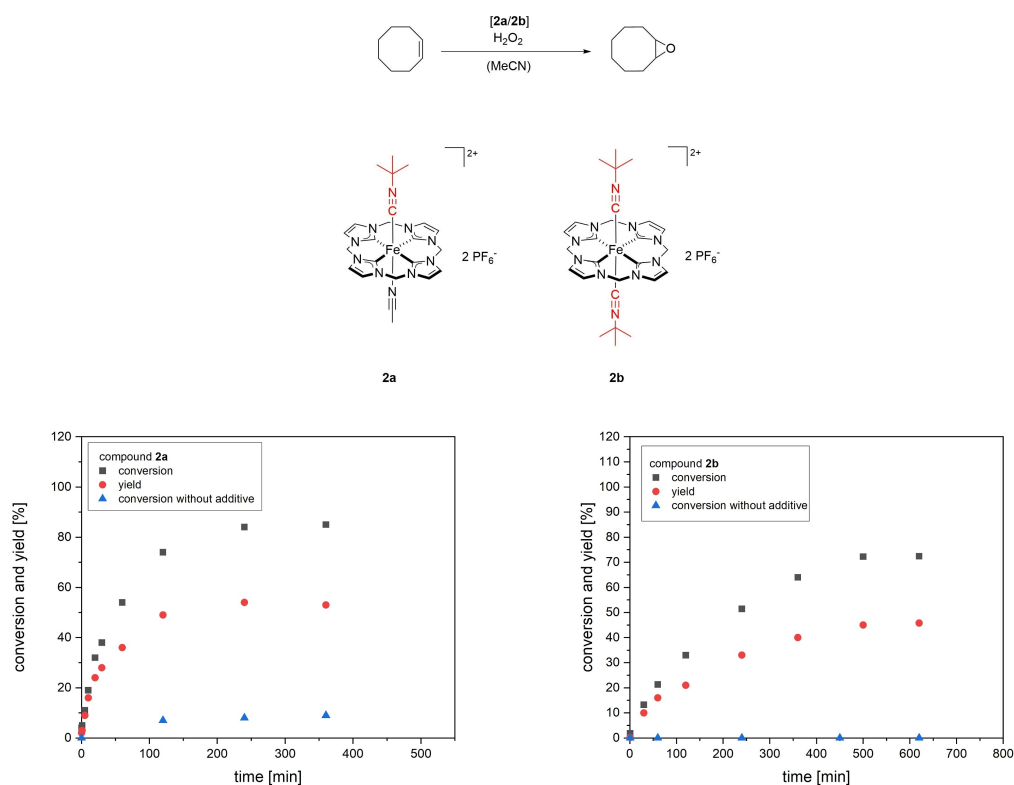


Figure 3. Conversions and yields (*cis*-cyclooctene oxide) applying catalysts (1.0 mol%) **2a** at 20 °C (left) and **2b** at 20 °C (right) in olefin epoxidation of *cis*-cyclooctene in absence and presence of Sc(OTf)₃.

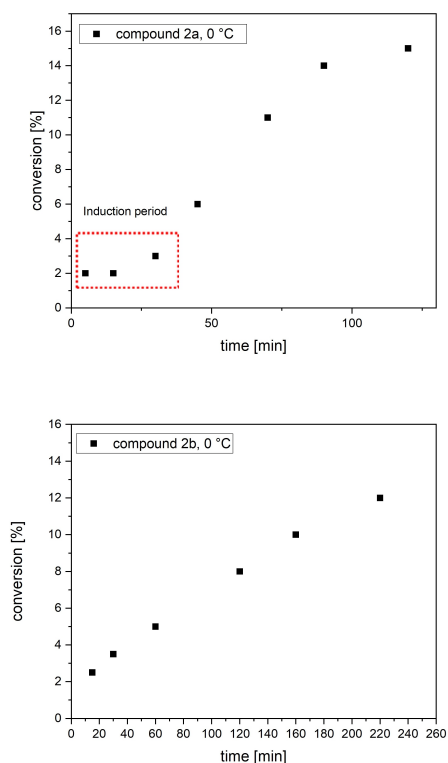


Figure 4. Conversions of cyclooctene applying catalysts (1.0 mol%) **2a** (above) and **2b** (below) at 0 °C in olefin epoxidation of *cis*-cyclooctene in presence of Sc(OTf)₃ in order to determine the existence of an induction period. The approximate length of the induction period is marked in red.

While the curve shape for complex **2b** shows an almost linear path, a slight induction period for complex **2a** can be observed. The length of the induction period is about 30 min (Figure 4) in spite of the presence of Sc(OTf)₃ and highlights the overall low activity associated with a slow oxidation step from Fe(II) to Fe(III) towards more active catalyst species.^[4,25] The oxidation to the active species in case of complex **2b** seems to be extremely slow so that the key reaction, the epoxidation of *cis*-cyclooctene may outperform the rate-determining step resulting in a curve linearity.

Due to the overall low catalytic performance of both compounds, the reaction temperature is increased from 20 °C to 40 °C and 60 °C with the focus on the development of the catalyst activity (TOF) and catalyst stability (TON) (Figure 5). It is clear that the TOF numbers of each catalyst are rising at elevated temperatures and that the reaction time is highly reduced to a time range of 15 min to max. 120 min for both compounds. Consequently, the reaction is already completed after 15 min for **2a** and after 30 min for **2b** in the fastest case (60 °C) at a catalyst concentration of 1.0 mol% in combination with Sc(OTf)₃.

In order to determine max. TOFs, a catalyst concentration of 0.25 mol% is used for **2a** and **2b** (Table 1). The results achieved at different temperatures show a rapid increase of the TOF from 1,400 h⁻¹ to 25,900 h⁻¹ for complex **2a** and demonstrate its already examined higher catalytic activity. On the other hand, **2b** also shows a rather low increase of activity displayed in its TOF indicating a considerable higher stability towards increas-

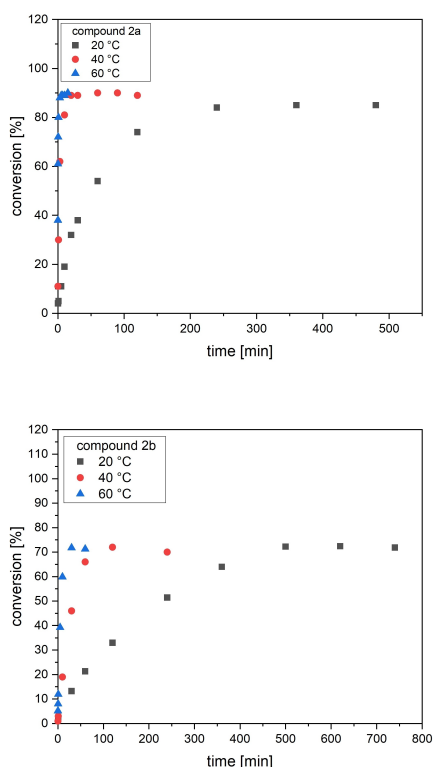


Figure 5. Conversions of cyclooctene applying catalysts (1.0 mol%) **2a** (above) and **2b** (below) at 20 °C, 40 °C and 60 °C in olefin epoxidation of *cis*-cyclooctene in presence of Sc(OTf)₃.

catalyst	T [°C]	conv. [%] ^[a]	yield [%] ^[a]	sel. [%] ^[a]	TOF [h ⁻¹] ^[b]
2a	20	85	54	83	1 400*
2a	40	90	58	71	6 200
2a	60	90	52	59	25 900
2b	20	72	46	75	240
2b	40	72	45	72	2 900
2b	60	72	41	59	4 300
1 ^[c]	20	66	66	> 99	792
2 ^[c]	20	24/59 ^[d]	100	> 99	50.000/ 415.000 ^[d]
3 ^[c]	20	100	96	96	11.000 ^[e]

Reaction conditions: *cis*-cyclooctene (269 μmol, 1.0 eq.), Sc(OTf)₃ (26.9 μmol, 0.1 eq.), H₂O₂ (403 μmol, 1.5 eq.), catalyst (2.69 μmol, 1.0 mol%); [a] all yields (*cis*-cyclooctene oxide) and conversion were determined by GC-FID after the completion of the reaction; [b] Max. TOFs were determined at a catalyst concentration of 0.25 mol% at 20 °C, 40 °C and 60 °C for catalyst **2a** and **2b**. [c] **1** & **3**: catalyst concentration of 1.0 mol%. **2**: 0.05 mol% without additive. [d] with additive Sc(OTf)₃. [e] TOF number of Fe(III) species. * catalyst concentration of 1.0 mol% for **2a** at 20 °C. Blank experiments (reaction mixture **1**) without iron catalysts and with **2**) a simple iron salt) are included.

ing temperatures along with a low level of activity based on its substitution with two weakly dissociating *tert*-butylisocyanide ligands in axial position.

Compared to the first investigated classical cCCCC and NCCN systems,^[4,22] the determined TOFs of **2a** and **2b** do not reach the same level of activity of these previously in literature reported catalysts, even by using an additive (Table 1). How-

ever, catalyst **2a** (1.0 mol%) with a max. TOF of 1,400 h⁻¹ at 20 °C lies in between these two systems, but remains all in all in the lower area of potential achievable TOF numbers.

A particularly conspicuous new aspect among all existing iron epoxidation catalysts is the widely constant TON observed at higher temperatures. The TON in case of **2a** and **2b** remains largely identical within the margin of error from 20 °C to 60 °C (Table 1, Figure 6). These outcomes demonstrate once again the exceptionally high temperature stability of both complexes, in particular of complex **2b**. The temperature consistency and the associated high stability contrast with the low catalyst activity, which may constitute the limiting factor with respect to the average TON values, especially for complex **2b**. Reducing the catalyst concentration (0.1 mol%) leads to max. TONs up to 330 for **2a** and 150 for **2b**. Thus, rising temperatures may have a stronger impact on lower catalyst concentrations, major fluctuations can be seen at a catalyst concentration of 0.1 mol% compared to 1.0 mol% (Figure 6).

Simultaneously, a general decline of yield and selectivity for compound **2a** and **2b** (Table 1) can be explained by the fact that another reaction type, competing with the epoxidation takes place as no further *cis*-diol formation can be noticed in comparison to catalytic reactions at 20 °C, attributable to the growing activity and remaining stability at higher temperatures. Conceivable would be, that these features may orient the catalyst selectivity to more challenging substrates as for example in the C–H oxidation. Analogous to derivative **3**

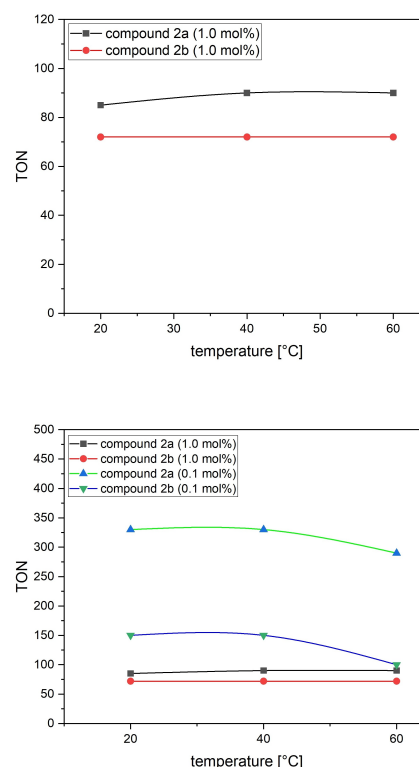


Figure 6. Comparison of TONs of catalysts (1.0 mol%) **2a** and **2b** at various elevated temperatures in presence of Sc(OTf)₃ (above). All TONs were determined at catalyst concentrations of 1.0 mol% and 0.1 mol% for maximum achievable values (below).

(Figure 1), bearing a characteristic tetradentate macrocyclic benzimidazolylidene ligand, catalysts **2a** and **2b** show high stability combined with a high temperature tolerance (up to 60 °C), but an overall lower activity in contrast to the most active non-heme iron epoxidation catalyst to date (**2**) due to the electronic-finetuning at the iron center or the modified scaffold in case of **3**.^[25] Interestingly, the initial oxidation step of catalyst **3** from Fe(II) to Fe(III) is slowed down by the withdrawing properties of the modified scaffold, coinciding with the significantly higher half-cell potential ($E_{1/2}=0.44$ V).^[25] This fact can be transferred to the more active mono-(*tert*-butylisocyanide) substituted compound **2a** having a nearly related half-cell potential ($E_{1/2}=0.35$ V), resulting in a long-lasting induction period even in the presence of $\text{Sc}(\text{OTf})_3$.^[25]

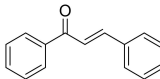
Moreover, the better catalyst performance of **3** compared to **2a** and **2b**^[25] is a good indication of the exact location for the selective modification at the classical iron NHC complex with two axial acetonitrile ligands. Direct modifications on the base frame or the iron center obviously evoke widely divergent features with regard to the catalytic activity.

For a broad understanding concerning the catalytic potential of **2a** and **2b**, supplementary epoxidation reactions with various cyclic, acyclic, terminal and functionalized olefin substrates are conducted via ¹H-NMR spectroscopy (SI, Figures 1–17). All experiments are realized using 1.0 mol% of the respective Fe(II)-catalyst and 0.1 eq. $\text{Sc}(\text{OTf})_3$ at 20 °C with a reaction time of approximately 24 h. Due to the overall low activity of both catalysts and the crucial necessity of $\text{Sc}(\text{OTf})_3$ as additive, a comparatively long reaction time is chosen for maximal achievable conversions and yields (Table 2). For better

control of the reaction progression over a longer time period, the setting of higher temperatures is avoided. To obtain suitable NMR spectra, the overall concentration is doubled. By means of the ¹H-NMR experiments, it becomes visible, that catalysts **2a** and **2b** are capable to reach conversions up to 73% for more challenging double bond systems except for the substrate allyl chloride (entry 6). As the formed active species in epoxidation catalysis possesses an electrophilic oxygen,^[11c] the electron density of the double bond plays a decisive role in the reactivity of the relevant substrate. The chloride substituent at entry 6 exerts a negative inductive effect and leads to a lower electron density, which finally impedes the desired electrophilic attack of the active species.

If the chloride substituent is replaced by an electron-donating hydroxyl group (entry 5), conversions up to 42% are feasible due to the increased electrophilic character of the double bond. The highest conversion is obtained for hex-2-ene (entry 3) as another acyclic system with 73% followed by allylic alcohol (entry 5) and styrene (entry 7) as an aromatic system with 38%. Hex-2-ene (entry 3) has an increased reactivity based on the fact, that the internal double bond is affected by neighboring alkyl groups as opposed to 1-hexene (entry 2) and 1-octene (entry 4) with less reactive terminal double bonds. Styrene (entry 7) contains an aromatic system, which can apparently better stabilize the formed epoxide product, whereas *trans*-chalcone (entry 8) bears additionally an electron-withdrawing carbonyl group close to the double bond, provoking a reduced electron density. As observed in the catalytic epoxidation of *cis*-cyclooctene, the more active catalyst **2a** reaches higher conversion and selectivity in comparison to **2b**. With respect to the resulting conversions, the epoxide yields of all investigated substrates, leading to maximal selectivities of 23% are negligible, which again supports the assumption, that another reaction type potentially interferes. Concerning this matter, a divergent behavior pattern of **2a** and **2b** referring to other cyclic substrates like cyclohexene (entry 1) is basically recognizable when compared to other non-heme catalysts.^[4,24–25] Usually, cyclic olefins are considered as favored substrates in epoxidation reactions as the electron donating effect of the neighboring CH_2 -groups. Contrary to the assumptions, the oxidation products of the catalyzed cyclohexene are not just limited to the formation of *cis*-diol, but also arise from oxidation of existing C–H bonds and can be assigned by NMR spectroscopy to several ketone (2-cyclohexen-1-one) and alcohol (2-cyclohexen-1-ol) species nearby located to the double bond. Apart from the new findings, *cis*-diol appears in nearly all cases as one of the main side products and emphasize the unfavored epoxide formation, probably inhibited by the present $\text{Sc}(\text{OTf})_3$, which is able to open epoxides to *cis*-diols in presence of water unlike coordinating Brønsted acids.^[18b] However, due to the high amounts of existing co-products, the signal assignment remains mainly an assumption. The appearance of new functional groups as ketones, alcohols and aldehydes like acrolein for entry 5 and benzaldehyde in the case of entries 7 and 8 clearly underlines the expected significant low selectivity towards more challenging substrates in olefin epoxidation. The NMR experiments are also conducted for the standard substrate

Table 2. Catalytic epoxidation of various olefins by catalyst **2a** and **2b**.

entry	substrate	2a conv. [%]	2a sel. [%] ^[a]	2b conv. [%]	2b sel. [%] ^[a]
1		19	5 ^[b]	19	5 ^[b]
2		30	23	23	17
3		73	8	58	5
4		14	14	14	14
5		42	– ^[c]	42	– ^[c]
6		–	–	–	–
7		38	3 ^[c]	35	3 ^[c]
8		12	– ^[c]	12	– ^[c]

Reaction conditions: substrate (135 μmol, 1.0 eq.), $\text{Sc}(\text{OTf})_3$ (13.5 μmol, 0.1 eq.), H_2O_2 (aq. 50%, 202 μmol, 1.5 eq.), **2a** & **2b** (1.0 mol%), solvent MeCN-d_3 , $t_r=24$ h, $T_r=20$ °C; conversions and selectivities are identified by ¹H-NMR spectroscopy applying benzol (entry 1–6) and toluene (entry 7, 8) as external standard; [a] *cis*-diol formation and identified high amounts of byproducts with new functional groups as ketones, alcohols and aldehydes (see SI for further information); [b] possible side products of the catalyzed cyclohexene: 2-cyclohexen-1-one and 2-cyclohexen-1-ol; [c] aldehyde formation to acrolein (entry 5) and benzaldehyde (entries 7 & 8).

cis-cyclooctene under the same conditions and showed similarly to cyclohexene, the formation of C–H oxidation products as well. This outcome confirms the former detection of several side products *via* the quite more sensitive gas chromatography (see SI for further information) and may switch the future focus on investigations of C–H-oxidations with the catalysts **2a** and **2b**.

Thermogravimetric Analysis (TGA)

In regards to the unusual high tolerance of catalyst **2a** and **2b** to increased temperatures in epoxidation catalysis, thermogravimetric measurements were conducted for catalyst **2**, **2a** and **2b** in solid state (Figure 7).

The thermal stability of all three compounds is determined through monitoring the weight change by heating the sample at a constant rate of 10 K/min in a temperature range from 25 °C to 300 °C. The heating chamber where the respective catalyst is placed, is purged with nitrogen with a volume flow of 100 ml/min. Initial irregularities arise from small fractions of volatile components. Thus, the samples are examined in solid state, catalytic reaction conditions in solution can not be imitated realistically on account of the respective components (e.g. oxygen, H₂O₂, additives) which influence or rather reduce the actual thermo-stability of the catalysts during the reaction, so that the real decomposition process under catalytic conditions possibly occurs at lower temperatures. Nevertheless, a general trend of the catalyst decomposition in temperature dependency is essential for further interpretation. Catalyst **2** decomposes already at 155 °C, while the decomposition onset of compounds **2a** and **2b** is detected at 185 °C and 225 °C, respectively. This observation supports the catalytic results relating to unvarying turnover numbers coming from a high temperature tolerance, corresponding to following catalytic activity order: **2** > **2a** > **2b**.

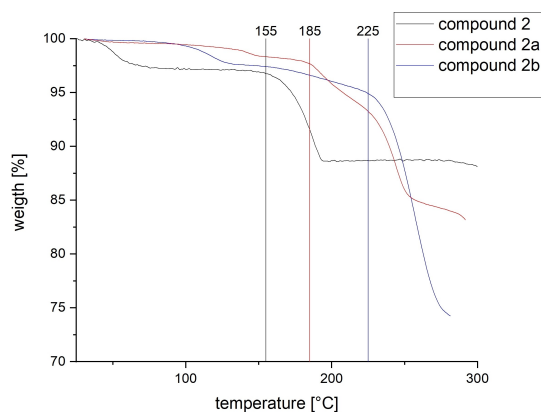


Figure 7. Thermogravimetric analysis of catalyst **2**, **2a** and **2b** and determination of the dissociation temperature in solid

Conclusion

The previous estimation of an overall lower catalyst activity by CV data could be largely confirmed by means of the catalytic epoxidation reaction of *cis*-cyclooctene with *trans* axially substituted mono (**2a**) and bis(*tert*-butylisocyanide) (**2b**) (pre-) catalysts. According to the comparison of half-cell potentials, the catalytic activity of **2a** and **2b** should be between that of the iron(II) complex **2** bearing a macrocyclic tetra-NHC ligand cCCCC and *trans* labile acetonitrile ligands and the iron(II) complex **1** with a tetradentate bis(pyridyl-NHC) ligand NCCN, also bearing *trans* labile acetonitrile ligands. Contrary to expectations, both complexes **2a** and **2b** show comparatively low activities correlating to their electrochemical properties, which are highly influenced by the isocyanide ligands with π -accepting character. This finding is supported by the necessary use of Sc(OTf)₃ as an additive in order to activate the (pre-)catalysts for the epoxidation of olefins. Due to the fact that **2a** possesses one accessible coordination site with a weakly coordinating and hence easily replaceable acetonitrile ligand, an increased activity compared to **2b** with two comparatively weak dissociating isocyanide ligands is found. The stronger electron donating cCCCC scaffold compared to NCCN makes the dissociation of one isocyanide ligand rather difficult, resulting from the reinforced π -backbonding from the iron center and could explain the limited catalyst activity of **2a** towards other non-heme iron(II) catalysts despite the freely accessible coordination site. Rising temperatures effect increased activities, manifested by a significant development of the TOF values from 1,400 h⁻¹ to 25,900 h⁻¹ for **2a** and 240 h⁻¹ to 4,300 h⁻¹ for **2b**. Thereby, a particular new aspect is the consistent TON and consequently high stability of the catalysts at different temperature levels such as (pre-)catalyst **3** with analog electrochemical features, but equatorially placed modifications. High decomposition temperatures, especially for **2b** specified by TGA measurements correlate well with an observed great temperature tolerance during epoxidation reaction. As a whole, the compound is also exceptionally stable in solid state in addition to a high temperature stability under oxidative conditions compared to various other iron NHC catalysts.

An overall higher catalyst performance of **3** evidently makes a difference if new functional groups with unique electron properties are introduced axially or equatorially to the iron center where the initial oxidation step takes place.

Related to selectivities in epoxidation reactions, a clear gap between the conversion and the yield can be observed for both catalysts **2a** and **2b**, pointing out a relatively high amount of unidentifiable side products apart from the minimal formation of *cis*-diol detected by gas chromatography. Finally, the presented catalytic experiments are considered essential for future improvements of catalyst activities (TON) and stabilities (temperature tolerance) based on the modification location and redox potentials. Additional substrate screening with more challenging olefins leads – not unexpectedly – to low yields and selectivities regarding epoxide formation. The unusual formation of C–H oxidation products, particularly in the case of cyclohexene is additionally supporting the assumption of

another competing reaction type. Inspired by NCCN ligand derivatives **1a–1d**, showing improved turnover numbers in the C–H oxidation reaction after replacing one labile acetonitrile ligand through one isocyanide ligand, the same substitution pattern at (pre-)catalyst **2** might have enhanced the potential for activating unreactive alkanes for the challenging C–H oxidation and may be worth further examination.

Experimental Section

General Procedures and Analytical Methods

All reagents and solvents for the catalytic procedures were purchased from commercial suppliers and used without further purification. NMR spectra were recorded on a Bruker AV 400 (¹H-NMR, 400.13 MHz) and chemical shifts are reported relative to the residual signal of the deuterated solvent. UV-Vis spectra were recorded on an Agilent Technologies Cary 60 UV-Vis spectrophotometer at 20 °C. Solutions of **2a** and **2b** with an initial concentration of 10⁻⁴ M in acetonitrile were treated with 10.0 eq. Sc(OTf)₃ and 1.50 eq. H₂O₂.

Catalytic procedures

All reactions were conducted in a cryostat (Julabo FP-50) with a total reaction volume of 4.0 mL. Acetonitrile (HPLC-grade) as solvent was applied for all experiments. The catalyst (1.0 mol%, 2.69 μmol) was added from a preformed stock solution (5.5 mg/mL in acetonitrile) corresponding to the appropriate stoichiometry to a solution of *cis*-cyclooctene (100 mol%, 269 μmol) and, if applied, the respective Brønsted acid (0.1 mol%, 26.9 μmol) in acetonitrile. The reaction was started upon addition of H₂O₂ (150 mol%, 403.5 μmol). The reaction was terminated by adding electrolytically precipitated activated MnO₂ in order to decompose the excess of H₂O₂ in the reaction solution. After filtration over activated neutral alumina (separation of the catalyst), two GC samples were prepared for each experiment using 200 μL filtrate, 500 μL external standard (*p*-xylene, 4.0 mg/mL in *i*-PrOH) and 800 μL *n*-hexane for each chosen time point. Control experiments without catalyst were performed as a reference for all reactions. An additional blank experiment with a simple iron salt, iron(II) chloride in the presence of H₂O₂ was conducted in order to stress the relevance of iron complexes associated with NHCs due to minimal product and unselective side-product formation.

The screening of other substrates beside *cis*-cyclooctene was performed using ¹H-NMR spectroscopy. All reactions were carried out at 20 °C in a total volume of 1.0 mL with a catalyst concentration of 1.0 mol% in doubled absolute concentrations. A catalyst stock solution (5.5 mg/mL in CD₃CN) was added to a prepared solution of the respective substrate (100 mol%, 134.5 μmol) in deuterated acetonitrile and the reaction was started upon addition of H₂O₂ (150 mol%, 201.8 μmol). Then, the reaction was aborted after 24 h by adding electrolytically precipitated activated MnO₂. The suspension was filtered and benzol or toluene was added as an external standard. For each experiment, ¹H-NMR spectra were recorded and the products were quantified by integral ratios of the respective olefin, epoxide and *cis*-diol protons.

Thermogravimetric analysis

TGA measurements were recorded with a TGA/DSC 3+ from Mettler-Toledo. Approximately up to 5.0 mg of the respective

catalyst (**2a**, **2b**) were placed in a sapphire skillet attached to a microbalance. The heating chamber was purged with nitrogen with a volume flow of 100 mL/min. The thermal stability, especially the decomposition temperature of all three compounds was determined through monitoring the weight change by heating the sample at a constant rate of 10 K/min in a temperature range from 25 °C to 300 °C.

Acknowledgements

The authors thank the TUM graduate school of chemistry for financial support. Open Access funding enabled and organized by Projekt DEAL.

Conflict of Interest

The authors declare no conflict of interest.

Keywords: non-heme iron complexes · *N*-heterocyclic carbenes · isocyanide ligands · olefin epoxidation · homogeneous catalysis

- [1] a) A. Blanckenberg, R. Malgas-Enus, *Catal. Rev.* **2019**, *61*, 27–83; b) F. Cavani, J. H. Teles, *ChemSusChem* **2009**, *2*, 508–534; c) S. A. Hauser, M. Cokoja, F. E. Kühn, *Catal. Sci. Technol.* **2013**, *3*, 552–561.
- [2] a) S. Enthaler, K. Junge, M. Beller, *Angew. Chem. Int. Ed.* **2008**, *47*, 3317–3321; *Angew. Chem.* **2008**, *120*, 3363–3367; b) J. W. Kück, R. M. Reich, F. E. Kühn, *Chem. Rec.* **2016**, *16*, 349–364.
- [3] P. P. Chandrachud, D. M. Jenkins, *Tetrahedron Lett.* **2015**, *56*, 2369–2376.
- [4] J. W. Kück, M. R. Anneser, B. Hofmann, A. Pöthig, M. Cokoja, F. E. Kühn, *ChemSusChem* **2015**, *8*, 4056–4063.
- [5] a) K. Chen, M. Costas, J. Kim, A. K. Tipton, L. Que, *J. Am. Chem. Soc.* **2002**, *124*, 3026–3035; b) M. S. Chen, M. C. White, *Science* **2010**, *327*, 566–571.
- [6] L. Que, W. B. Tolman, *Nature* **2008**, *455*, 333–340.
- [7] A. Lindhorst, S. Haslinger, F. E. Kühn, *Chem. Commun.* **2015**, *51*, 17193–17212.
- [8] a) J. Rittle, M. T. Green, *Science* **2010**, *330*, 933–937; b) O. Shoji, Y. Watanabe, *Isr. J. Chem.* **2015**, *55*, 32–39.
- [9] a) I. D. Cunningham, T. N. Danks, J. N. Hay, I. Hamerton, S. Gunathilagan, C. Janczak, *J. Mol. Catal. A* **2002**, *185*, 25–31; b) S. Enthaler, G. Erre, M. K. Tse, K. Junge, M. Beller, *Tetrahedron Lett.* **2006**, *47*, 8095–8099; c) W. Nam, S.-Y. Oh, Y. J. Sun, J. Kim, W.-K. Kim, S. K. Woo, W. Shin, *J. Org. Chem.* **2003**, *68*, 7903–7906; d) W. J. Song, M. S. Seo, S. DeBeer George, T. Ohta, R. Song, M.-J. Kang, T. Tosha, T. Kitagawa, E. I. Solomon, W. Nam, *J. Am. Chem. Soc.* **2007**, *129*, 1268–1277; e) K. Srinivas, A. Kumar, S. S. Chauhan, *Chem. Commun.* **2002**, *20*, 2456–2457.
- [10] a) M. R. Anneser, S. Haslinger, A. Pöthig, M. Cokoja, J.-M. Basset, F. E. Kühn, *Inorg. Chem.* **2015**, *54*, 3797–3804; b) A. Raba, M. Cokoja, S. Ewald, K. Riener, E. Herdtweck, A. Pöthig, W. A. Herrmann, F. E. Kühn, *Organometallics* **2012**, *31*, 2793–2800.
- [11] a) Y. Feng, J. England, L. Que Jr, *ACS Catal.* **2011**, *1*, 1035–1042; b) S. M. Hölzl, P. J. Altmann, J. W. Kück, F. E. Kühn, *Coord. Chem. Rev.* **2017**, *352*, 517–536; c) W. Nam, *Acc. Chem. Res.* **2007**, *40*, 522–531.
- [12] a) R. Noyori, M. Aoki, K. Sato, *Chem. Commun.* **2003**, *16*, 1977–1986; b) N. A. Stephenson, A. T. Bell, *J. Am. Chem. Soc.* **2005**, *127*, 8635–8643.
- [13] a) B. De Poorter, M. Ricci, B. Meunier, *Tetrahedron Lett.* **1985**, *26*, 4459–4462; b) S. E. Denmark, D. C. Forbes, D. S. Hays, J. S. DePue, R. G. Wilde, *J. Org. Chem.* **1995**, *60*, 1391–1407.
- [14] a) D. Y. Kim, Y. J. Choi, H. Y. Park, C. U. Joung, K. O. Koh, J. Y. Mang, K.-Y. Jung, *Synth. Commun.* **2003**, *33*, 435–443; b) B. Meunier, E. Guilmet, M. E. De Carvalho, R. Poilblanc, *J. Am. Chem. Soc.* **1984**, *106*, 6668–6676.
- [15] B. Bahramian, V. Mirkhani, M. Moghadam, S. Tangestaninejad, *Catal. Commun.* **2006**, *7*, 289–296.
- [16] F. G. Gelalcha, *Adv. Synth. Catal.* **2014**, *356*, 261–299.

- [17] R. Mas-Ballesté, M. Costas, T. Van Den Berg, L. Que Jr, *Chem. Eur. J.* **2006**, *12*, 7489–7500.
- [18] a) S. Kal, A. Draksharapu, L. Que Jr, *J. Am. Chem. Soc.* **2018**, *140*, 5798–5804; b) R. Mas-Ballesté, L. Que, *J. Am. Chem. Soc.* **2007**, *129*, 15964–15972.
- [19] a) S. Kal, L. Que Jr, *Angew. Chem.* **2019**, *131*, 8572–8576; *Angew. Chem. Int. Ed.* **2019**, *58*, 8484–8488; b) M. Swart, *Chem. Commun.* **2013**, *49*, 6650–6652.
- [20] F. Dyckhoff, J. F. Schlagintweit, R. M. Reich, F. E. Kühn, *Catal. Sci. Technol.* **2020**, *10*, 3532–3536.
- [21] a) S. Haslinger, A. Lindhorst, J. Kück, M. Cokoja, A. Pöthig, F. Kühn, *RSC Adv.* **2015**, *5*, 85486–85493; b) J. F. Schlagintweit, C. Hintermeier, M. R. Anneser, E. M. H. Esslinger, S. Haslinger, F. E. Kühn, *Chem. Asian J.* **2020**, *15*, 1896–1902.
- [22] J. W. Kück, A. Raba, I. I. Markovits, M. Cokoja, F. E. Kühn, *ChemCatChem* **2014**, *6*, 1882–1886.
- [23] S. Haslinger, A. Raba, M. Cokoja, A. Pöthig, F. E. Kühn, *J. Catal.* **2015**, *331*, 147–153.
- [24] J. F. Schlagintweit, F. Dyckhoff, L. Nguyen, C. H. G. Jakob, R. M. Reich, F. E. Kühn, *J. Catal.* **2020**, *383*, 144–152.
- [25] M. A. Bernd, F. Dyckhoff, B. J. Hofmann, A. D. Böth, J. F. Schlagintweit, J. Oberkofler, R. M. Reich, F. E. Kühn, *J. Catal.* **2020**, *391*, 548–561.

Manuscript received: August 4, 2021

Accepted manuscript online: August 16, 2021

Version of record online: September 2, 2021

Cite this: *Catal. Sci. Technol.*, 2022,
12, 4940

Organometallic 3d transition metal NHC complexes in oxidation catalysis

Greta G. Zámbo,  Jonas F. Schlagintweit, 
Robert M. Reich and Fritz E. Kühn *

The development of processes for the selective oxidation of hydrocarbons is a major focus in catalysis research. Making this process simultaneously environmentally friendly is still challenging. 3d transition metals are highly promising candidates to replace expensive and/or toxic heavier metals in their applications as oxidation catalysts. Optimizing such catalytic systems is closely connected to the improvement of stabilizing ligands. In this context, *N*-heterocyclic carbenes (NHCs) have attracted particular attention. Their strong σ -donor properties, compared to nitrogen or oxygen-donor ligands, allow the stabilisation of transition metals in high oxidation states, known to be key intermediates in oxidation catalysis. This review provides an overview of recent applications of 3d transition metal NHC complexes in oxidation catalysis, by summarising the advances towards the catalytic oxidation of the most important substrates namely alkenes, alkanes, aromatics, alcohols and amines until the end of 2021. Additionally the activation of molecular oxygen, representing a green and abundantly available oxidant, is described with first row transition metal NHC complexes.

Received 19th January 2022,
Accepted 17th February 2022

DOI: 10.1039/d2cy00127f

rsc.li/catalysis

Introduction

Selective oxidation of hydrocarbons is a fundamental topic in academia and industry, requiring the design of efficient and inexpensive catalytic systems.^{1,2} The unique properties of 3d metals Sc, Ti, V, Cr, Mn, Fe, Co, Ni, Cu and Zn have found a wide range of applications in modern synthetic chemistry, biology and material science.^{3,4} Their high-oxidation state complexes are key intermediates in valuable biological and catalytic conversions of organic compounds.^{5,6} Some metalloenzymes, such as cytochrome C, possess active sites exhibiting these metals, reflecting their high reactivity potential.^{7,8} Commonly applied active catalytic systems often depend on expensive and/or toxic noble metals, *e.g.* rhenium or ruthenium.^{9–11} Since first row transition metals are abundant in earth's crust and may feature a non-toxic character (depending on the oxidation state and applied ligand systems), they are considered to be economical and sustainable alternatives as organometallic catalysts.³

Substantial factors for a catalyst are, *inter alia*, selectivity, activity, indicated by the turnover frequency (TOF), and stability, indicated by the turnover number (TON).¹² A good catalyst features both a high to very high TOF and TON, associated with

high selectivity.¹⁰ Development of effective, non-toxic abundant-metal-based catalysts regularly involves synthesis and modification of metal stabilizing ligands. The introduction of metal supporting *N*-heterocyclic carbenes (NHCs) has become a multifunctional tool in homogeneous catalysis, opening an enormous field of applications for transition metal complexes, *e.g.* in oxidation catalysis.^{13–16} NHCs are electron-rich heterocyclic compounds, allowing easy tuning of their electronic and steric properties, by insertion of *N*-substituents or backbone modification.^{17,18} Over the past three decades, numerous NHC scaffolds have been synthesized, derived from imidazole, imidazoline, pyrazole, triazole or tetrazole, varying in ring size, the number and type of heteroatoms, the nature of their substituents and the resulting stabilization.^{17,19} By far the most applied building units are based on imidazole.^{20,21} The remarkable stability of the carbene centre C² in NHCs originates from the favourable electronic properties and the easy introduction of steric constraints of this compound class. When coordinated to a metal, NHCs are able to vary both in their metal-carbon interaction and in electron donating as well as accepting properties. The σ -donor capability and kinetic stability are significantly higher in NHCs, compared to previously reported nitrogen, phosphine or oxygen-donor ligands, usually preventing rapid dissociation and association processes.^{20,22} These features render NHCs suitable candidates for stabilizing high valent metal intermediates, which are proven to be the active species in several catalytic oxidation reactions.²³

Molecular Catalysis, Department of Chemistry and Catalysis Research Center, Technische Universität München, Lichtenbergstr. 4, 85748 Garching bei München, Germany. E-mail: fritz.kuehn@ch.tum.de

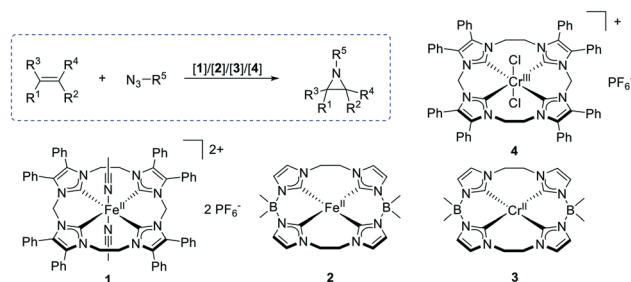
The literature on the stabilization of 3d transition metals with NHC moieties already exists;⁵ however there is, to the best of our knowledge, so far no concise summary of the application of 3d transition metal NHC complexes available in the context of oxidation catalysis of hydrocarbons. Additionally, a quite recently published review of Liang and Song in 2020 is restricted to the application of exclusively iron NHC complexes.²⁴ With this work, a comprehensive overview on first row transition metal NHC catalysts for alkene oxidation, C–H activation of unreactive alkanes and aromatics, alcohol as well as amine oxidation, and activation of molecular oxygen is provided. Although there are publications about the application of *in situ* generated metal NHC complexes of metal precursors combined with separate addition of stabilizing NHC salts for catalytic oxidation reactions,^{25,26} only isolated and/or well characterized metal NHC systems are described in the present review.

Oxidation of alkenes

Aziridination

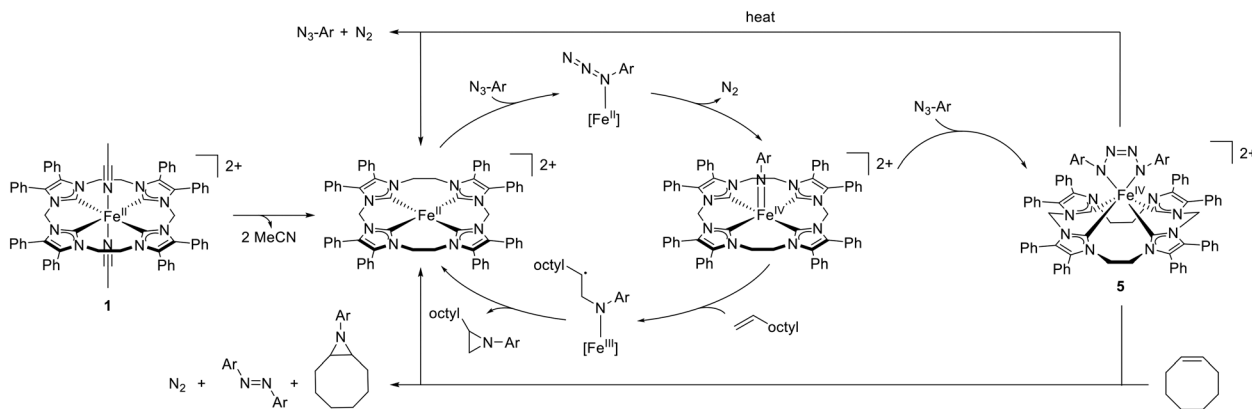
Aziridination of alkenes is one of the most valuable transformations in organic synthesis.^{27–29} The nitrogenous analogues of epoxidations are important C–N bond forming reactions, since the resulting products are useful building blocks for a variety of nitrogen containing compounds.³⁰ Aziridines are three membered heterocycles with high reactivity due to their cyclic strain and the reactivity of the integrated nitrogen atom.³¹ Ring openings take place with excellent regio- and stereoselectivity and yield a variety of stable and ring-open or -expanded chiral amines and more complex molecule precursors.^{28,29} Their physical nature and biological activity render these heterocycles a target of interest, not only in organic synthesis, but also in biology and medicinal chemistry, mainly as antitumor agents.³² The common synthetic approach is to combine an alkene with a nitrene fragment such as $\text{PhI}=\text{NTs}$ (Ts = tosylate) or chloramine-T with the disadvantage of the necessary tosyl group removal before the desired final substituent is transferred.^{33,34} A promising alternative is the catalytic conversion of alkenes with organic azides exhibiting high functional group tolerance and further improving the atom economy of these reactions.³⁵ In recent decades, various aziridination catalysts have been developed, usually containing rather toxic metals whose applicability is limited to a narrow range of substrates.^{27,36–38}

The group of Jenkins studied the use of chromium and iron complexes supported by NHC ligands as catalysts in aziridination reactions of alkenes (*e.g.* 1-decene, 9-decenol, 4-pentenol or *N*-allylaniline) with organic azides (*e.g.* *p*-tolyl azide, 3-azidophenol or 1-azidooctane).^{39–43} In 2011, the group developed an equatorial plane forming macrocyclic tetracarbene ligand supporting an iron(II) centre for the aziridination of electron-donating and -withdrawing aryl azides and substituted aliphatic alkenes (Scheme 1, **1**).³⁹ Due to the insolubility of the catalyst in the reaction mixture at



Scheme 1 Aziridination of alkenes with organic azides catalysed by iron and chromium NHC complexes.

room temperature, the complex can be easily recovered and reused up to three additional times without a significant loss in its catalytic performance. As indicated by the presence of weakly coordinating axial acetonitrile ligands, which can be easily exchanged in CD_3CN solution, the diamagnetic octahedral complex **1** exhibits accessible coordination sites, necessary for catalytic reactions. The X-ray crystal structure of **1** shows an average Fe–C bond distance of 201 pm. At a catalyst loading from 0.1 to 1 mol%, yields between 20 and 97% are achieved at 70–90 °C within 18–160 h, depending on the inserted alkene.³⁹ The best catalytic results are obtained in the conversion of *cis*-cyclooctene with an excess of *p*-tolyl azide. Based on previous studies⁴⁴ on the mechanism of catalytic aziridinations, the potentially active species is assumed to be an iron(IV) imide intermediate (Scheme 2). Although the isolation of this particular iron imido species was unsuccessful, its formation during the aziridination reaction of 1-azido-4-(trifluoromethyl)-benzene is indicated by electrospray ionization mass spectrometry (ESI-MS) data.³⁹ Insights into the mechanism of **1** as a catalyst has been provided by a subsequent publication in 2014 by Jenkins *et al.* highlighting the synthesis and characterization of the corresponding iron(IV) tetrazene complex.⁴³ Reacting two equivalents of organic azide with **1** results in the formation of iron tetrazene **5** (Scheme 2). Single crystal X-ray crystallography (SC-XRD) data show the complex in an unusual trigonal prismatic geometry with binding of the tetrazene in a dianionic mode. The Fe–C bond length in **5** of 198 pm (error range of 0.3 pm) is slightly shorter than that in **1**. However, the axial coordination site is accessible due to the NHC ligand occupying the *cis* position. Reaction with *cis*-cyclooctene leads to the formation of the initial iron NHC complex **1**, by releasing the corresponding aziridine. Thermal decomposition also yields compound **1**.⁴³ Combining density-functional theory (DFT) calculations with experimental results identifies iron imide intermediate formation as the first catalytic key step. This step proceeds *via* an α -bound azide with subsequent direct loss of N_2 (Scheme 2).⁴⁵ Formation of the aziridine from the iron imide is the second key step. The addition of alkene to imide is considered to be the rate determining step *via* an open chain radical pathway causing loss in stereochemical information, which would explain the generation of both *syn*- and



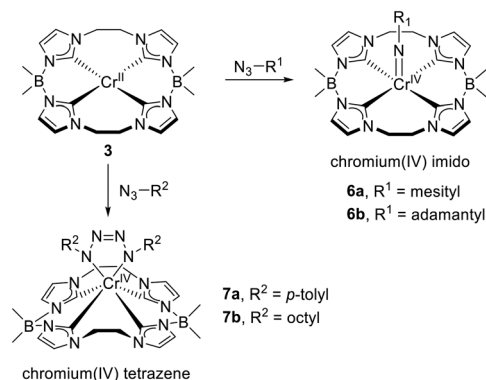
Scheme 2 Proposed catalytic pathway for the aziridination of alkenes on iron(II) NHC complex **1** with formation of the active iron(IV) imido and iron(IV) tetrazene species.

anti-aziridines of *cis*- and *trans*-isomers.⁴⁵ Tetrazene and aziridine formation are in direct competition. Increasing the steric bulk of the organic azide causes a reversal of the relative stability of the product aziridine and metal tetrazene, which strongly favours the formation of aziridine, explaining why no tetrazene is formed with mesityl azide and no alkene excess is necessary.⁴⁵

In 2013 the group of Jenkins designed a comparable macrocycle with an increase in its σ -donor strength by additional inserted borate bridges between the imidazoles.⁴⁶ The corresponding iron(II) complex **2** (Scheme 1) is capable of catalysing inter- and intramolecular alkene aziridination, achieving higher yields with defined stereoselectivity compared to previously reported catalysts.^{42,47} The complex is tolerant towards a variety of functional groups on both alkenes and azides, resulting in a broad range of linear and cyclic aziridination products with yields between 30 and 95% and low catalyst loading (0.1–10%) at 90 °C within 18 h.⁴² Expecting an octahedral structure, common for tetracarbene iron(II) complexes,^{48–52} X-ray crystallography of **2** shows an unusual square planar geometry with an Fe–C bond distance of 199 pm, equal to the average Fe–C distance of iron–NHC complexes in the Cambridge Structural Database.⁵³ Due to paramagnetism, even in polar solvents, suggesting the retention of the square-planar mode, associated with an electron-deficient complex, **2** has easily accessible sites to bind apical ligands. The fact that weaker nitrene sources, such as alkyl azides, undergo aziridination and higher yields are obtained with aryl azides with **2** as a catalyst is consistent with the proposed catalytic cycle (Scheme 2). The energy required for the first step, the formation of iron(IV) imide, is probably lowered by the increased electron density caused by the borate based macrocycle.⁴² In the solid state, complex **1** is air stable,³⁹ whereas **2** is very air and moisture sensitive.⁴²

On the basis of the same NHC ligand system as in compound **2**, Jenkins *et al.*⁴⁰ and Lu *et al.*⁵⁴ studied the catalytic capability of the corresponding chromium(II) tetra(NHC) complex **3** (Scheme 1). The paramagnetic complex exhibits a square planar structure and is extremely sensitive

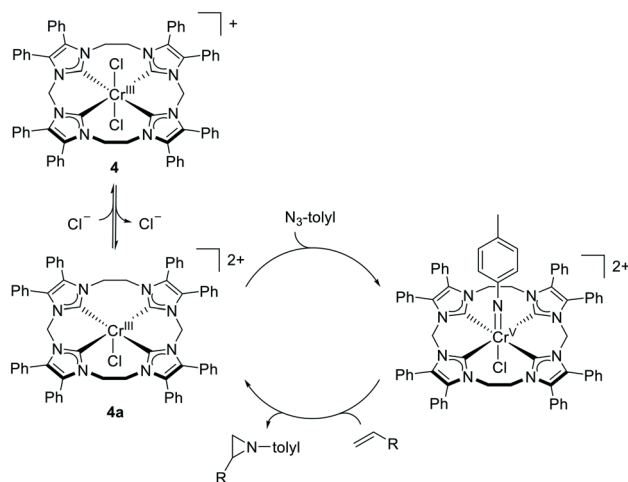
towards oxygen and traces of water.⁴⁰ The high electronic unsaturation and the low valent state of **3** lead to a high activity towards oxidative group transfer reactions. In contrast to previously discussed iron complexes, conversion with mesityl azide or adamantyl azide yields stable and isolable bent square pyramidal chromium(IV) imido species **6a** and **6b** (Scheme 3). The paramagnetic complex **6a** is active in the nitrene group transfer with 1-decene and exhibits with 170 pm an exceptional long Cr(IV)–imido bond. 1-Mesityl-2-octylaziridine is generated at 75 °C within 18 h in 86% yield. Experiments on direct catalytic aziridination with **3** investigated at 75 °C were however unsuccessful. Unfortunately, the initial complex is susceptible to thermal degeneration. The reaction with less sterically bulky azides like tolyl azide gives dianionic chromium(IV) tetrazene **7a** in which the NHC ligand is in a slightly distorted trigonal prismatic fashion (Scheme 3). In contrast to the situation observed for iron(IV) tetrazene **5**, the ethylene bridges are in the same plane as the metal center. Investigations on the challenging alkyl azide activation lead to the formation of metallotetrazene **7b**, an analogue of compound **7a**, but with a



Scheme 3 Reaction of the chromium(II) tetracarbene complex with stereo chemical bulky azides to form chromium(IV) imido species and with less sterically bulky azides to form chromium(IV) tetrazene species.

slightly higher distortion in the ligand geometry (Scheme 3). Due to the potential metal accessibility and the comparability to iron, analogous chromium(IV) tetrazene complexes are promising candidates for oxidative nitrene transfer reactions with alkenes.⁴⁰

In 2018 the first group six metal aziridination catalyst has been described to be a tetracarbene chromium(III) complex.⁴¹ Pioneered by the catalytic activity of iron NHC compound **1**, an octahedral chromium(III) complex was designed based on the same imidazole macrocycle with additional chloride ligands in axial positions (Scheme 1, **4**).⁵⁵ In contrast to the initial iron catalyst, **4** is effective for aziridination at low alkene loadings. At 2 mol% catalyst loading, the reaction of decene and *p*-tolyl azide in a 1:1 ratio gives the aziridine in 26% yield. An excess of alkene to a 3:1 ratio increases the product yield to 67%, whereas the use of iron catalyst **1** under the same conditions is ineffective. In comparison to the behaviour in polar solvents, **4** shows no catalytic activity in non-polar solvents.⁴¹ As a variety of aziridine containing natural products include protic functional groups⁵⁶ and the initial iron complex is unable to catalyse such substrates, **4** was further evaluated. Chromium(III) tetracarbene is capable of inducing aziridination with protic functional groups such as alcohols or amines on both the alkene and the azide. However, conversions with short chain alcohols lead to alkene amination, either caused by nucleophilic intramolecular ring opening through the hydroxyl group and subsequent proton shift with **4**, or by forming a carboradical intermediate from the aziridine *via* an attack of the alcohol. Short chain alkenes with a terminal aryl alcohol give either an aziridine or an amine, depending on the hydroxyl position. *Para* arrangement yields the aziridine, while the *ortho* position leads to the amine. With carboxylic acids (*e.g.* 9-decenoic) the reaction was not possible. Mechanistic insights into the catalytic cycle of **4** are based on additional DFT calculations (Scheme 4).⁴¹ While iron complex **1** is able to exchange its labile acetonitrile ligands rapidly,³⁹ chromium(III) catalyst **4** needs to release a chloride to generate an open site, which apparently occurs in polar

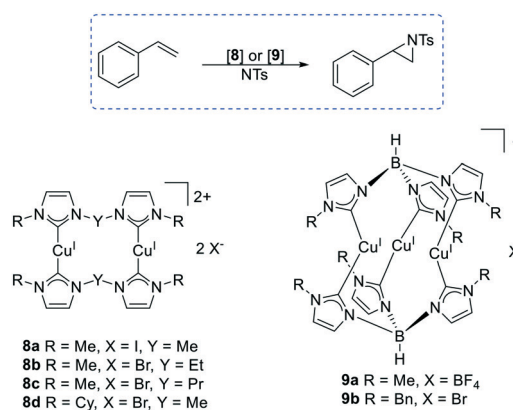


Scheme 4 Proposed mechanistic insights in aziridination of alkenes with tolyl azide catalysed by tetracarbene chromium(III) complex **4**.

solvents. The subsequent reaction with an azide to chromium(V) imido intermediate in which only one chloride is removed is highly favourable. According to DFT calculations and in agreement with experimental observations, a reaction with a second azide to form a metallotetrazene is disfavoured by the *trans* chloride ligand on **4a** solely. Consequently, direct formation of the aziridine from chromium(V) imido with alkene is more favourable. These theoretical results would explain why **4** is active at low azide loading. Probably the increased activity is due to two features. On the one hand, the tetra NHC ligand system is a strong σ -donor; on the other hand, ligands in the *trans* position to the imido promote the reactivity with alkenes. Furthermore, **4** is considered to be the most effective catalyst for aliphatic alkenes at low loading up to date.⁴¹

Di- and tri-nuclear copper(I) complexes **8** and **9**, bearing bis- or tris-NHC moieties, have been applied in catalytic nitrene transfer reactions from $\text{PhI}=\text{NTs}$ with styrene (Scheme 5). Under optimal reaction conditions (2 mol% catalyst, 50 °C, styrene:nitrene = 30:1) yields up to 95% aziridine in acetonitrile with molecular sieve are obtained after 17 h. Di-nuclear copper complexes are more active than tri-nuclear Cu(I) NHCs. **8b** was found to be active for a series of substituted styrene substrates, however with moderate to low yields. Changing to room temperature, or replacing $\text{PhI}=\text{NTs}$ with chloramine T led to a decrease in the aziridination yield. The presence of water was found to be highly detrimental in this case, as the reaction yield improved strongly upon the addition of molecular sieves.⁵⁷

In summary, the iron, chromium and copper NHC catalysts described above are active in the aziridination of alkenes with good to excellent yields and low catalyst loadings. Stabilization of the metal centre with macrocyclic tetra NHCs allows the aziridination of a variety of substituted aliphatic alkenes with diverse aromatic and aliphatic azide sources with and without functional groups at high temperatures. Di- and tri-nuclear copper NHC complexes require alkene aziridination with a tosyl containing nitrene fragment, which has to be removed for further processing of the product. However, the Cu(I) complexes are active even at moderate temperatures.



Scheme 5 Styrene aziridination catalysed by copper(I) NHC complexes (NTs = nitrene tosylate).

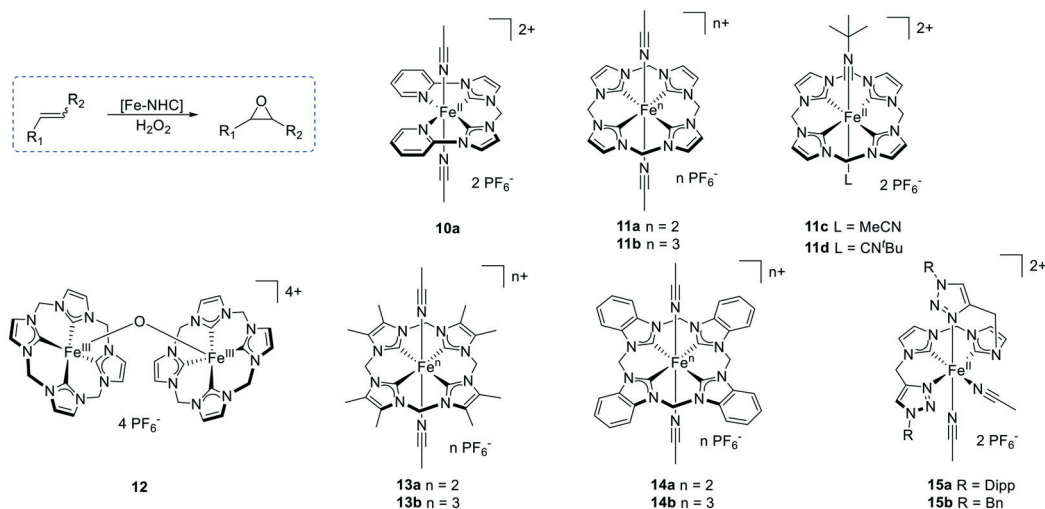
Epoxidation

Catalytic alkene epoxidation has evoked great interest in the chemical industry and academia since epoxides are of high importance for the production of bulk and fine chemicals.^{58,59}

Ethylene oxide and propylene oxide are key intermediates and therefore among the most produced chemicals in industry as they are in high demand especially for polymer synthesis.⁶⁰ Epoxidation reactions have been investigated in academia for decades without using a catalyst, with peroxocarbonic acids being applied as stoichiometric epoxidation agents with the disadvantage of being rather unselective and quite “aggressive” reagents.^{61,62} Heterogeneous epoxidation catalysts are industrially used for the conversion of simple bulk alkenes, particularly silver based systems for the epoxidation of ethylene. Such systems are generally very substrate specific and have little or no tolerance to functional groups.⁶³ Homogeneous catalysts are often employed to overcome such challenges for speciality chemicals, by offering both high selectivity and activity.^{64–66} However, most homogeneous epoxidation catalysts rely on scarce (*i.e.* expensive) and/or toxic transition metals such as rhenium, tungsten and molybdenum (the latter metal being for example applied in the Arco–Halcon process for propene epoxidation).¹⁰ Consequently, considerable efforts have been made to develop suitable catalysts based on cheaper, more abundant and non-toxic metals for selective epoxidations. In particular iron as the most abundant transition metal in earth's crust proved to be a promising candidate for several catalytic applications, among them alkene epoxidation.^{10,58,67} Inspired by biological systems, such catalysts have been designed with a variety of iron stabilizing ligands.^{23,68} Predominantly octahedral iron(II) complexes bearing tetradentate N-donors, like amines, pyridines and pyrroles, were developed, where two labile ligands coordinated to the metal centre are orientated *cis* or *trans* to each other, mimicking the active site of oxidation catalysing enzymes.^{23,69–71} Hypochlorides,⁷² periodates,⁷³ molecular oxygen⁷⁴ and peroxides^{10,23,67} are applied as oxidants for these

reactions. Hydrogen peroxide is most commonly used, due to its atom efficiency and the fact that water is formed as the sole by-product in the oxidation process.^{23,75} *Cis*-Cyclooctene is most widely applied as a model substrate for epoxidations in the scientific literature.

Inspired by their structural heme analogy, iron NHC complexes are utilized by applying these compounds in catalytic alkene epoxidation reactions (Scheme 6).^{67,76–78} Displaying particularly high activity, some iron NHC catalysts exceed the activity of the organometallic “standard” oxidation catalyst methyltrioxorhenium (MTO) significantly.^{67,79} This latter compound has been very well examined as an epoxidation catalyst since the late 1980s and is sometimes considered as the “benchmark catalyst” for alkene epoxidations in academia with TOFs up to 40 000 h⁻¹.⁸⁰ Even the most active molybdenum complexes (usually employing organo hydroperoxides as oxidants, however) with TOFs up to 53 000 h⁻¹ are clearly outperformed by several more recently described iron based catalysts, which are described in detail in the following paragraphs.⁸¹ The first iron NHC complex to be examined in an epoxidation reaction coordinates an acyclic tetradentate di(*o*-imidazol-2-ylidenepyridine)methane ligand *via* its two carbene carbon atoms and two pyridine N-donors (Scheme 6, **10a**).^{76,82} The NHC system exhibits an equatorial plane geometry around the metal centre by leaving the remaining axial positions as accessible coordination sites. Although iron–carbon bonds are thermodynamically labile compared to iron–oxo bonds, complex **10a** is nevertheless stable towards air and water due to the chelating and stabilising iron–NHC bonds. **10a** shows remarkable selectivity (>99%) towards cyclooctene epoxide with hydrogen peroxide as the oxidant in high yields with the benchmark substrate *cis*-cyclooctene. A conversion of 92% within a reaction time of only 5 min at 2 mol% catalyst loading without the need for additives underlines its high activity. TOFs up to *ca.* 2600 h⁻¹ are achieved with a high selectivity for a broad range of alkenes. However, catalyst deactivation occurs under oxidative conditions. Higher concentrations of the

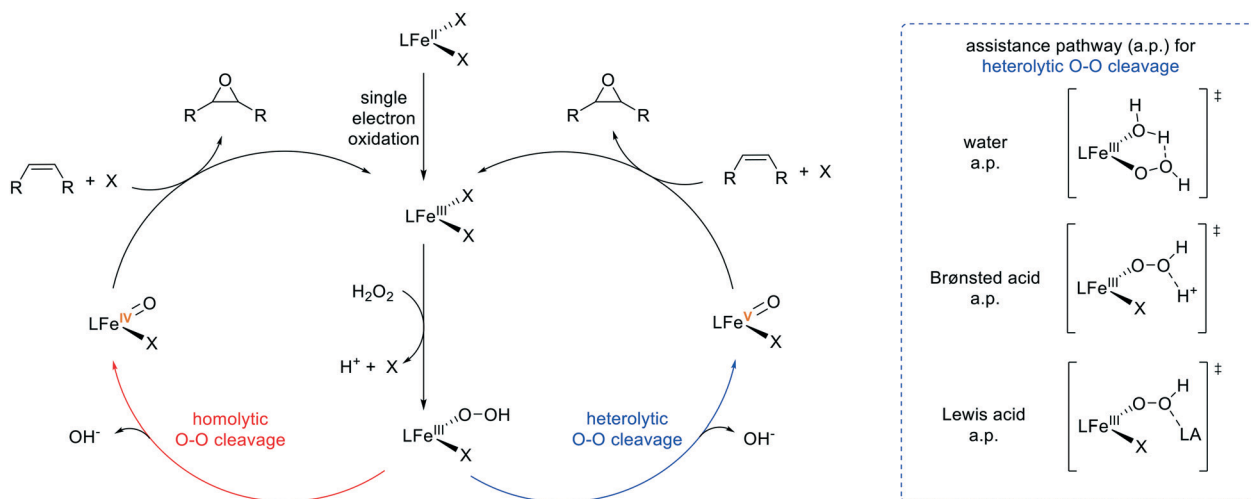


Scheme 6 Epoxidation of alkenes with hydrogen peroxide catalysed by open chain and macrocyclic tetradentate iron NHC complexes.

oxidizing agent lead to a decrease in the alkene conversion, suggesting a partial catalyst deactivation. Two competing influences were found to be present. The reaction rate decreases with decreasing reaction temperature, while the catalyst becomes significantly more stable at reduced temperatures.⁷⁶

Finding the active species of nonheme iron complexes has been a major target of investigations in the past decades by several groups. Two possible catalytic pathways in the oxidation pathway with synthetically generated iron catalysts, bearing tetradentate nitrogen donors, are discussed in the literature. It has to be emphasized that mechanistic studies have – so far – not been executed with complexes containing iron carbene bonds. Mechanisms *via* high valent iron oxo compounds²³ are in competition with the undesired radical based Fenton-type^{83,84} pathway. The hypothesis of adverse non-selective Fenton-type mechanisms occurring *via* long-lived radicals has to be seen in this context. The decomposition of hydrogen peroxide at iron(II) or (III) leads to highly reactive hydroxyl radicals, which immediately undergo several radical-based reactions in the presence of organic substrates. Additional auto-oxidative reactions of the radicals with dioxygen generate equal amounts of alcohols and ketones.⁸⁴ The second (and desired) pathway is proposed to be similar to the catalytic cycle for the active site of cytochrome P450 oxidase.⁸⁵ Despite comprehensive studies, the mechanism of non-heme iron complexes is still not examined in all necessary detail. Nevertheless, Scheme 7 presents pathways that are currently accepted by the scientific community working on organometallic iron oxidation catalysis. To generate the active species, the initial formation of an iron(III) hydroperoxo intermediate with oxidants like hydrogen peroxide appears to be necessary, after single electron oxidation of the iron(II) catalyst precursor.^{23,71} An *in situ* generated Fe(III)-OOH intermediate undergoes homolytic or heterolytic O–O bond cleavage, which is regarded as the rate determining step

(r.d.s.) for the formation of the active species, which is either an iron(IV) or (V) oxo intermediate. This step has been verified by Que *et al.* by a SC-XRD characterization of $[\text{Fe}(\text{IV})(\text{O})(\text{TMC})(\text{NCCH}_3)]^{2+}$ (TMC = 1,4,8,11-tetramethyl-1,4,8,11-tetraazacyclotetradecane).⁸⁶ Heterolytic cleavage can be accelerated by water, Brønsted acids or Lewis acids. The transition state in the water assisted pathway (w.a.p.) affords complexes with *cis* labile coordination sites due to the coordination of water proximally to the hydroperoxo intermediate,⁷⁰ whereas the latter two assistance pathways (Brønsted and Lewis acid a.p.) also allow for labile coordination sites in the *trans* position.⁸⁷ Binding water forms *cis*-Fe^{III}(OOH)(OH₂) as a five membered cyclic transition state. Electrophilic attack on alkenes by the resulting high valent *cis*-iron(V) oxo compound leads to epoxide formation. Here, the oxygen is derived either from the bound water molecule or from the initial hydrogen peroxide, possibly by the rapid oxo-hydroxo tautomerization of the intermediate.^{23,71,75} Alternatively, *cis* orientated labile ligands cause the formation of *cis*-diols. *Cis*-Dihydroxylation of the alkene occurs when the iron(V) hydroxo ligand coordinates to the substrate, resulting in the creation of an intermediate in which the oxygen of the hydroxo group additionally coordinates to the alkene.^{23,69,70} Dihydroxylation is not observed with *trans* labile ligands on tetradentate iron complexes.⁸ In general, the formation of iron(III) hydroperoxo intermediates can be detected using UV/Vis spectroscopy, due to their characteristic absorption band corresponding to an intensive purple colour.²³ Variable-temperature mass spectroscopy supports the existence of the proposed iron(V) species.⁸⁸ In this context, Mössbauer spectroscopy can be applied to determine the oxidation states of iron intermediates in the catalytic mechanism, based on recoilless emission and resonant absorption of gamma radiation by atomic nuclei.⁸⁹



Scheme 7 Catalytic mechanism for epoxidation of alkenes by iron(II) complexes with tetradentate ligands (L) affording *cis* labile coordination sites *via* iron(IV) oxo species by homolytic O–O bond cleavage (left circle) or *via* iron(V) oxo species by heterolytic O–O bond cleavage (right circle) and transition states for assistance pathways (X = labile ligand). Acceleration of the r.d.s. heterolytic O–O bond cleavage is possible by water, Brønsted acid or Lewis acid (LA) assistance. Catalysts with *trans* labile coordination sites follow the same pathway without the possibility of water assistance.

A remarkable increase of the reactivity toward epoxidation on complexes with labile ligands in a *cis* fashion can be achieved by the addition of acetic acid. The acid binds to Fe^{III}-OOH in the same way as water and generates the catalytically active Fe^V(O)(OAc) intermediate, which is highly electrophilic and epoxide selective.⁹⁰ However, hydrogen peroxide decomposition *via* the Fenton-type mechanism always occurs parallel to the mechanism *via* high valent iron oxo intermediates. Moreover, homolytic O–O bond cleavage produces hydroxyl radicals, which can also enter a radical chain reaction, lowering the selectivity.⁸⁴ Consequently, the key is to prevent such decomposition processes by optimizing the electronic structure of iron precursors with the design of the ligand system and additionally balancing the reaction conditions for the catalytic conversion.⁶⁷

Significantly higher epoxide yields are obtained by replacing the stabilizing ligand system of **10a** with a macrocyclic tetra NHC.⁶⁷ Comparable to **10a** iron(II) complex **11a** exhibits an octahedral coordination geometry with two acetonitrile ligands in axial positions (Scheme 6).⁹¹ Under standard conditions applied for catalytic investigations with **10a** (2 mol% catalyst, 5 min, 25 °C) in the case of **11a** epoxide yields of 100% with a high selectivity (>99%) are achieved using hydrogen peroxide and *cis*-cyclooctene. The TOF for complex **11a** (*ca.* 50 000 h⁻¹) demonstrates its high reactivity.⁶⁷ Since iron(III) hydroperoxo species are considered intermediates in the formation of the oxidation catalytically active species, an iron(III) analogue to complex **11a** was synthesized *via* a one electron oxidation of **11a**. Regarding the catalytic behaviour of macrocyclic tetracarbene iron(III) complex **11b** (Scheme 6), some unique differences emerge. The TOF almost quadruples to a value of 184 000 h⁻¹. The difference in catalytic performance supports the thesis of high valent oxo intermediates as active species. The required *in situ* formation of an iron(III) intermediate from the initial iron(II) complex **11a** by one electron oxidation in the catalytic cycle may lead to the formation of radicals *via* a Fenton type mechanism, thus lowering the selectivity. In the case of complex **11b** as a starting material, direct conversion to a high valent, active oxo intermediate without a primary oxidation step in an induction period is possible during catalytic conversion. The remarkable activity of **11b** allows the epoxidation of various cyclic and acyclic alkyl and aryl alkenes with yields between 36 and 93% with high selectivities.⁶⁷

The addition of strong Lewis acids considerably improves the catalytic performance of **11a**. By using Sc(OTf)₃, Ce(OTf)₄ or the even more beneficial Fe(ClO₄)₃·H₂O as a supporting additive, the TOFs again more than double to reach 410 000 h⁻¹. Such high values are achieved due to the facilitated heterolytic O–O bond cleavage of the initially formed iron(III) hydroperoxo species.⁷⁹ Furthermore, possible reactivation of μ₂-oxodiiron(III) Fe^{III}–O–Fe^{III} species, which are considered as “dead-end” compounds discussed in relation to iron catalyst deactivation pathways under oxidative conditions, is proven, increasing also the TON by a factor of 2.5 from 480 to 1200

(0.05 mol% catalyst loading, 20 °C).^{79,92–94} UV-vis experiments show that isolable complex **12** (Scheme 6) and **11a** form the same active catalyst **11b**, using scandium triflate as an additive. Employing Sc(OTf)₃ in the catalytic epoxidation reaction with **11b** does not lead to a rise in activity or stability. Corresponding UV-vis experiments show no significant changes. Depending on these observations, the *in situ* oxidation of iron(II) complexes to the active iron(III) analogue must proceed instantaneously upon the start of the reaction.⁷⁹

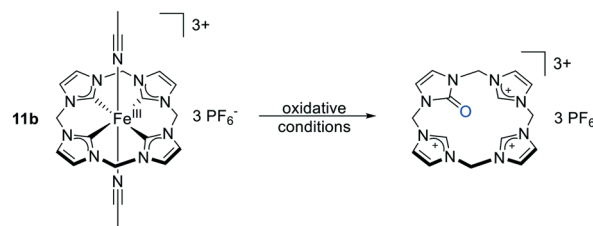
By tuning the electronic properties of **11**, two macrocyclic ligand motifs are introduced varying in their NHC backbone modification. The corresponding iron(II) or (III) complexes **13** with methyl substituted imidazole backbones and **14** with benzimidazolylidenes (Scheme 6) are employed due to their catalytic alkene epoxidation activity. Hereby, complex **14b** shows remarkable stability for an iron complex under oxidative conditions with a TON of 1000 at 20 °C and high tolerance towards functionalized alkenes and temperatures (up to 80 °C). In comparison to **11**, the ligand in **14** exhibits lower electron-donating properties due to its aromatic ring system, whereas the ligand system in **13** exhibits higher electron-donating properties due to the +I effect of the methyl groups. Even if complex **14** is more stable than the benchmark system **11**, the activity with a TOF of 11 000 h⁻¹ is comparatively low, requiring the application of Sc(OTf)₃. However, contrary to expectations, **13a** and **13b** display a significant decrease of catalytic performance due to an inherently low stability, even at low temperatures. In contrast to the non-substituted ligand scaffold, the ligands in **13** and **14** additionally exhibit strong π-back bonding capabilities. Even if the methyl groups in **13** seem to induce stronger σ-donor properties than **11** and especially **14**, this +I effect probably competes with additional π-back bonding. This aspect correlates to the lower catalytic activity of **13b**.⁷⁸

Besides the modification of the NHC system in **11**, axial MeCN ligands of highly active catalyst **11a** and **11b** can be substituted with ligands bearing less activated C–H bonds, such as ^tBuCN and PhCN. The obtained complexes exhibit significantly more stable axial ligands against C–H oxidation, as demonstrated by UV/vis kinetics, by depicting similar electrochemical properties. These complexes may have the potential to be more robust against oxidative degeneration during the catalytic reaction, by enhancing the stability against oxidation of the axial ligand, which is in competition with substrate oxidation.⁹⁵ In this context, the catalytic performance of iron(II) complexes **11c** and **11d** substituted by *trans* axially mono- and bis-CN^tBu ligands has been investigated (Scheme 6).⁹⁶ The catalytic activity was expected to be between that of Fe(II) NCCN complex **10a** and Fe(II) macrocyclic NHC complex **11a** with labile MeCN ligands.^{97,98} However, both complexes exhibit comparatively low epoxidation activities due to the π-accepting character of ^t-BuCN. The strongly electron-donating NHC framework makes dissociation of an isocyanide ligand difficult, which is in correlation with the catalytic results. The use of Sc(OTf)₃ is

essential to activate the compounds. **11c** possesses one accessible coordination site, while both *trans* positions in **11d** are occupied. Consequently, **11c** is a more efficient catalyst precursor than **11d**. Increasing the temperature to 40 and 60 °C increases the catalyst activity. **11c** reaches TOFs up to *ca.* 26 000 h⁻¹ and **11d** *ca.* 4000 h⁻¹, while TONs stay low, but largely temperature independent (330 for **11c** and 150 for **11d**), proving high temperature tolerance.⁹⁶ Additional modifications of the NHC scaffold may be required to achieve higher activities with comparable stability.

In 2020 the first iron(II) NHC complexes (**15a** and **15b**) with only *cis* labile coordination sites were reported and applied in alkene epoxidation (Scheme 6). These compounds bear acyclic mixed tetradentate NHC/1,2,3-triazole ligands. In acetonitrile, an equilibrium of the sawhorse-type coordination with *cis*- α arranged acetonitrile ligands and a C₂-symmetric species with *cis*- β orientated labile acetonitrile ligands can be observed by ¹H- and ¹³C-NMR spectroscopy. An equatorial geometry of the ligand system could not be verified, probably due to the steric bulk of the substituents (Dipp or Bn) on the triazoles, acting as N-donors.⁷⁷ As mentioned before, catalytic systems affording *cis* labile coordination sites are more active in oxidation catalysis due to the water or Brønsted acid assistance in the catalytic cycle.⁹⁹ Initial assignments of the catalytic performance of **15a** and **15b** reveals only low activity by the catalysts themselves. Meanwhile the introduction of acidic additives such as HOAc (1.0 eq., 20 °C) leads to high selectivity (97%) and activity and TOFs up to 76 000 h⁻¹ (0.1 mol% catalyst loading), which is the highest value reported so far for an acyclic iron(II) catalyst precursor.⁷⁷ Applying HOAc in the catalytic performance of **11a** and **11b** affording *trans* labile coordination sites does not improve their activity, which supports the proposed catalytic pathway.⁷⁹ In contrast to iron(II/III) macrocyclic and N_{py}CCN_{py} complexes, **15a** and **15b** reveal functional group tolerance (Cl, OH) with high selectivity. Since complex **15b** displays a comparable TON of 200, the stability still has to be improved significantly to be applicable not only in academia.⁷⁷

In conclusion iron(II/III) macrocyclic tetra NHC complex **11** with *trans* labile MeCN ligands is currently the most active non-heme iron epoxidation catalyst. The reaction setup allows mild conditions with H₂O₂ being the oxidant. However, the catalyst stability is low and has to be improved considerably in order to obtain a compound of industrial interest or value. Different degeneration pathways are described in the published literature for non-heme iron catalysts supported by N-donating ligand motifs. Besides the formation of a μ_2 -oxo bridged Fe^{III}-O-Fe^{III} dimer, methylene bridge C-H oxidation is described.^{100,101} For NHC supported iron catalysts, irreversible ligand protonation at the carbene C-donors with subsequent dissociation and/or oxidation of the ligand could be possible.¹⁰⁰ As mentioned before, degeneration over the Fe^{III}-O-Fe^{III} dimer can be excluded due to the regeneration with Lewis acids. Methylene bridged oxidation can also be ruled out by ESI-MS analysis and



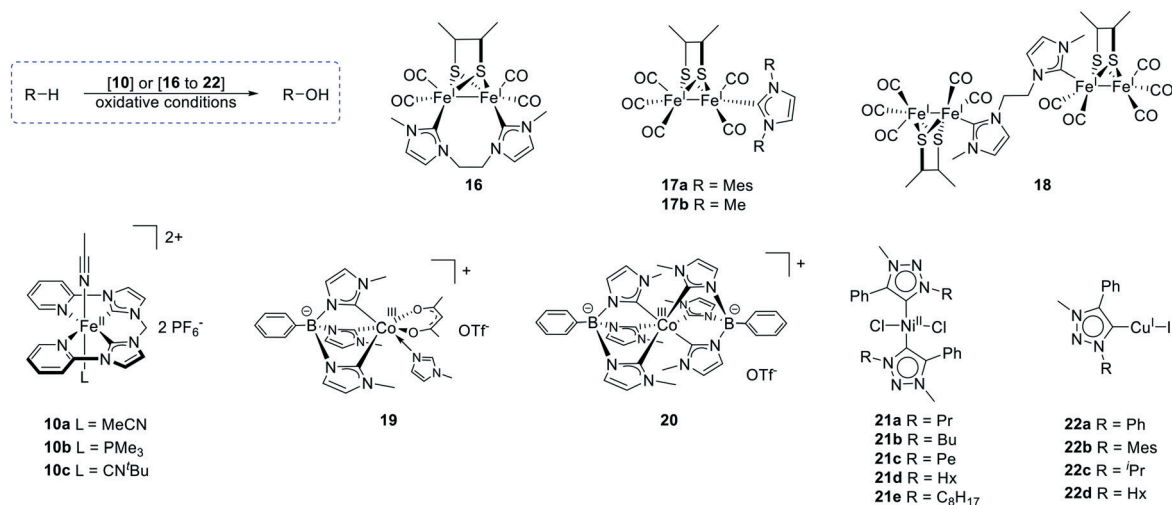
Scheme 8 Decomposition pathway of iron NHC catalyst **11b** under oxidative conditions.

comparative catalytic epoxidation experiments by employing an analogue of **11b** with deuterated methylene bridges, where no distinct differences in performance are observed. Furthermore, ESI-MS and experimental results exclude complete ligand protonation with and without subsequent oxidation at any of the imidazolium C-H positions. The addition of an H⁺ scavenging base to a catalytic epoxidation reaction to **11b** resulted in no improvement in the stability of the catalyst. Detailed HR-ESI-MS and ¹H-NMR spectroscopy studies have demonstrated that direct oxidation of a carbene C-position followed by dissociation of the ligand from the Fe centre, which induces protonation of the other NHC moieties, proves to be the most important route of catalyst degradation (Scheme 8). By HR-ESI-MS, an intermediate degradation species consisting of a mono-oxidized ligand still coordinating to an Fe(III) centre was found and correlates with DFT calculations.¹⁰¹

Oxidation of alkanes and aromatics

Hydroxylation

The selective oxidation of inert C-H bonds of aliphatic and aromatic hydrocarbons is among the most challenging reactions in current catalysis.^{102,103} The direct formation of C-H bonds plays a crucial role in the eco-friendly production of fine chemicals and pharmaceuticals.¹⁰⁴ Energy-intensive cracking and thermal hydrogenation are the major processes in industry for the direct conversion of alkanes into more valuable products. Natural gas with methane as the main component is one of the most important primary energy sources in the world. The synthetic access of methanol from methane, which allows the synthesis of a broad range of organic intermediates including formic acid and acetic acid *via* steam reforming, is well established, but requires a multistep process with temperatures above 230 °C. A more efficient conversion would lead to an enormous energy consumption reduction.^{105,106} Unfortunately, the cleavage of C-H bonds requires drastic conditions, due to the high C-H bond dissociation energy, lowering the selectivity or necessitating highly active catalyst systems.^{105,106} In the case of aromatic compounds, the bond strength is even higher and phenolic products are commonly more reactive resulting in over-oxidation. Even phenol, being among the simplest hydroxyl-arenes with a million-ton scale production per year, is currently synthesized *via* a multi-step process with acetone

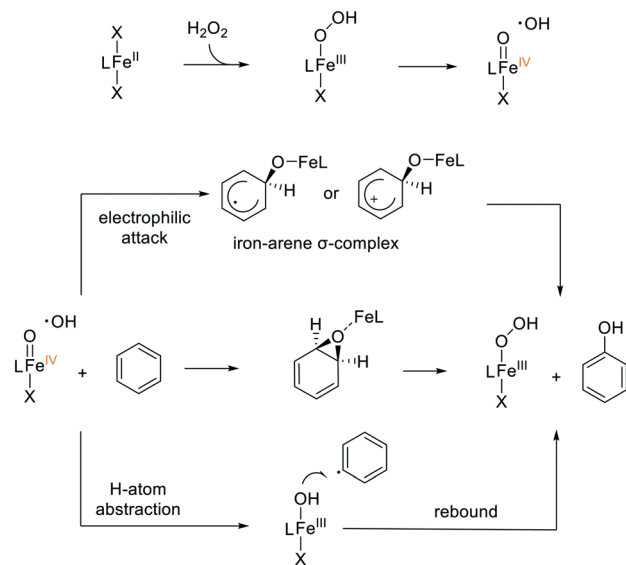


Scheme 9 Hydroxylation of alkanes and aromatics with hydrogen peroxide catalysed by iron, copper, cobalt and nickel NHC complexes.

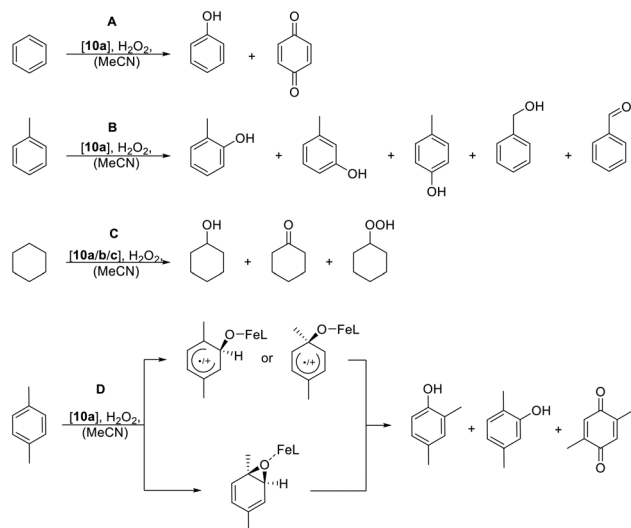
as an equimolar by-product.¹⁰⁷ The transformation under mild conditions is still one of the “dream reactions” in the chemical industry. In this context, homogeneous catalysts are beacons of hope as their active sites can be tuned comparably easily.¹⁰⁸ Introducing NHC transition metal complexes might help to overcome these challenges and offer high selectivity. Herrmann *et al.* applied a palladium(II) bis-NHC complex, which shows catalytic activity in the oxidation of methane, and Sarkar *et al.* described the catalytic activity of abnormal iridium 1,2,3-triazol-5-ylidene complexes in C–H oxidation of alkanes.¹⁰⁹

Our group recently reported a tetradentate NHC ligand stabilizing iron(II) as a promising and very active catalyst in the oxidation of arenes and alkanes.^{110–113} The exploitation of this complex **10a** (Scheme 9) described before as active in the oxidation of alkenes was inspired by the oxidative catalytic capability of cytochrome P450.⁸⁵ As described above for the catalytic alkene epoxidation cycle, the C–H bond activation mechanism proceeds *via* high valent iron oxo compounds (Scheme 10).²³ This mechanism, however, is again in competition with undesired Fenton-type pathways. Investigations on the catalytic oxidation of benzene and toluene (Scheme 11A and B) with **10a** gave insights into the mechanism.^{110,113} Three possible reaction pathways had been considered, either an electrophilic attack on a tetrahedral iron–arene σ -complex intermediate, an aromatic oxidation process *via* an arene oxide species or a H-atom abstraction followed by hydroxyl group transfer (rebound) (Scheme 10).^{110,113} Which pathway dominates depends on several factors, the oxidation state of iron, which defines the character of the active species, the spin state and the first coordination sphere depending on the ligand environment.^{114,115} Theoretical and experimental investigations favour an electrophilic attack of the active iron oxo species on the π -system of the arene. To elucidate the reaction pathway, the kinetic isotope effect (KIE) was taken into account. A low intramolecular KIE of 0.9 through competition experiments between perdeuterated and protic benzene is in

accordance with an electrophilic attack. High KIE values would indicate an H-atom abstraction due to the different bond energies of deuterated or protic educts.⁷⁶ The presence of radical scavengers does not significantly affect the reaction outcome, suggesting that a Fenton-type reaction does not occur. Additionally, a hydrogen abstraction pathway for the catalytic oxidation of benzene to phenol and 1,4-benzoquinone by **10**/H₂O₂ can be ruled out, which is also supported by additional KIE measurements at 20 °C (inverse KIE of 0.8).⁷⁹ Intramolecular migration reactions with 1,3,5-[D₃]benzene as the test substrate were examined to investigate if a migration of substituents (so-called “NIH-shift reaction”) takes place, which was reported for iron containing enzymes as well as iron (non-)heme complexes. The fact that not exclusively 2,6-[D₂]-



Scheme 10 Mechanistic insights into the oxidative hydroxylation of benzene by iron NHC complexes with axial labile ligands (X), with L being the supporting ligand.



Scheme 11 Oxidative hydroxylation of different model substrates (A: benzene, B: toluene, C: cyclohexane, D: *p*-xylene) with iron NHC complex **10a** and its derivatives **10b** and **10c**.

1,4-benzoquinone is formed strongly suggests an NIH shift.⁷⁹ DFT calculations⁷⁹ and experiments with toluene as the substrate¹¹⁰ support the hypothesis of a high valent Fe^{IV}=O intermediate as the active species and assume a pathway most likely *via* the iron-arene σ -complex intermediate (Scheme 10). The high selectivity of 78% towards ring oxidation clearly indicates an electrophilic mechanism, while aliphatic oxidation with a selectivity of 17% is less likely, as would be the case for H-atom abstraction or radical reaction by Fenton type reactions.¹¹⁰

Complex **10a** oxidizes benzene and toluene to phenols and cresols with high *ortho/para* selectivity. A catalyst loading of 1 mol% in acetonitrile at 25 °C with hydrogen peroxide as the oxidant has been used.¹¹⁰ Under these conditions, a conversion of 7.4% for benzene with a selectivity toward phenol formation of 94% can be achieved, which is in the range of the best catalytic systems in the homogeneous phase.^{110,116–118} Furthermore, complex **10a** is the most efficient homogeneous catalyst for aromatic hydroxylation of toluene at the time. High catalyst concentration increases the conversion and *vice versa*, indicating a catalyst deactivation over time. As oxidation of the substrate becomes less likely at lower concentrations, the decay of a potentially short-lived intermediate may cause catalyst deactivation. High excess of H₂O₂ decreases the selectivity substantially. High selectivities are obtained at low temperatures down to 0 °C.¹¹⁰

Complex **10a** and its modifications were also applied in the C–H oxidation of cyclohexane (Scheme 11C),¹¹¹ which is well established as a model substrate in homogeneous catalysed oxidation of light hydrocarbons^{93,119,120} due to its comparable bond strength¹²¹ to methane.¹²² To overcome the disadvantages of high ketone formation, described by the alcohol to ketone ratio (A/K) and a low catalyst stability – indicated by the turnover number – **10a** is additionally modified in its axial ligands. In complexes **10b** and **10c**, one

acetonitrile ligand is replaced by trimethylphosphine⁸⁸ and *tert*-butyl isocyanide,¹¹¹ respectively (Scheme 9). PMe₃, as a strong σ -donor as well as CN^{*t*}Bu as a strong π -acceptor exhibits a much stronger interaction with the iron centre than acetonitrile. In acetonitrile solution, therefore, no exchange with MeCN can be observed once the phosphine or the cyanide is coordinated.^{111,123,124} All three complexes are capable of oxidizing cyclohexane under ambient conditions with high alcohol selectivity (A/K ratios up to 26) and good stabilities (TON up to 43). Cyclohexanol, cyclohexanone and cyclohexyl hydroperoxide are the main oxidation products,^{111,120,125} whereby the latter can be converted quantitatively to cyclohexanol by reduction with triphenylphosphine.^{111,126,127} The experimental data support a metal centred mechanism with rather low Fenton reactivity. The amount of H₂O₂, which is used as the oxidant, clearly influences the catalytic reaction. The best stabilities are obtained with 2 eq. for **10a** and **10b** and 3 eq. for **10c**. Using 2 eq. H₂O₂ leads to the highest A/K ratios. Irreversible substitution and the nature of one of the axial ligands lead to a higher stability of the catalyst towards hydrogen peroxide. The axial isonitrile ligand slightly improves the TON (from 32 turnovers for **10a** and 39 turnovers for **10b** to 43 turnovers for **10c**).¹¹¹ The groups of Que (A/K = 19)¹²⁸ and Costas (A/K = 12)¹²⁹ gave examples of catalysts with good selectivity and Di Stefano¹³⁰ and Costas¹²⁹ provided comparatively stable catalysts (TON = 64). However, selectivity and stability could not be optimized at the same time. Selectivity increases consistently with lower relative catalyst concentration. Turnover frequencies decrease from 47 h⁻¹ for **10a** to 8 h⁻¹ for **10b** and to 4 h⁻¹ for **10c**. In contrast to its derivatives, the mono(iso-cyanide) complex shows an induction period of approximately 1 h, due to the π -acceptor properties of CN^{*t*}Bu, which disfavours the dissociation of the acetonitrile ligand in the *trans* position. This effect can be overcome by higher temperatures up to 50 °C due to the dissociation of the acetonitrile ligand. In addition to cyclohexane, other substrates were selectively oxidized (H-atom abstraction product anthracene and the secondary alcohol oxidation product from 2,3-DMB), attesting to the broad applicability of the catalyst system as a C–H oxidation catalyst.¹¹¹

The oxidation of non-active arene substrates poses a formidable challenge in reaction design. Complex **10a** has been proven to be a versatile catalyst for the oxidation of *p*-xylene and pseudocumene with hydrogen peroxide and high selectivity for aromatic C–H bonds in comparison to benzylic C–H bonds (Scheme 11D). Remarkably low oxidation agent amounts and catalyst loadings are required. The methyl shift (NIH shift) reaction, which had been reported for the first time for Fe–NHCs in this context, plays a major role in the catalytic mechanism. Two different mechanistic pathways are considered, including the formation of an iron-arene σ -intermediate or the formation of an arene oxide with a subsequent isomerization (Scheme 11D). 2,5-Dimethylbenzoquinone is formed during the reaction as a secondary product and 2,5-dimethylphenol is identified as an

intermediate. Lowering the reaction temperature to $-10\text{ }^{\circ}\text{C}$ further increases both the selectivity and catalyst lifetime. Additionally, catalyst deactivation, caused by side reactions and H_2O_2 decomposition, is reduced. However, substrate conversion and selectivity cannot be simultaneously optimized. The best catalytic performance for the hydroxylation of *p*-xylene (13% conversion and 85% selectivity) is obtained at $-10\text{ }^{\circ}\text{C}$, 1 mol% catalyst loading, 0.5 M substrate concentration, and low oxidant concentration (0.25 eq.). The introduction of additives like acids and bases does not affect the reaction outcome positively.¹¹²

Sheng *et al.* described the catalytic activity of diiron complexes for the direct hydroxylation of benzene to phenol with hydrogen peroxide in correlation to the redox potential of the catalysts. NHC supported diiron complexes bearing 2,3-butanthiol and terminal carbonyl ligands were investigated as catalysts (Scheme 9, **16**–**18**). X-ray crystallographic analysis identifies the Fe_2S_2 skeleton exhibiting a butterfly conformation where each iron centre adopts a distorted square-pyramidal coordination geometry. The ethane-bridged bis-NHC di-iron complex **16** adopts a symmetrically chelated cisoidal basal/basal coordination pattern, resulting in a distorted square pyramid geometry. CV measurements show that **16** with a reduction potential of -2.57 V displays the most negative potential among the examined diiron complexes, caused by its bis-NHC ligand, suggesting a strong influence on the catalytic activity. The redox potential increases from complex **16** to **17a** and **17b** to **18**. However, due to the similarity of the electron density of complexes **17a**, **17b**, and **18**, the reduction potentials are very similar under the applied CV conditions. Consequently, insertion of the bidentate NHC ligand bridged with two Fe atoms exerts a stronger influence on the redox potentials of the diiron complexes *versus* the introduction of a monodentate carbene. These findings are consistent with the catalytic activity being the highest for **16** and the lowest for **18**. Under optimised experimental conditions (0.01 mmol catalyst loading, 0.1 mL benzene, 2.0 mL MeCN, 6.0 mmol H_2O_2 , $60\text{ }^{\circ}\text{C}$ and 3 h) phenol yields up to 27% are obtained.¹³¹ Mechanistic insights from previous experimental and theoretical data suggest that an active $\text{Fe}^{\text{II}}-(\mu\text{-O})-\text{Fe}^{\text{II}}$ intermediate is formed from an electrophilic addition during the oxidation process with hydrogen peroxide, capable of transferring an oxygen atom to the substrate after a H-atom shift.¹³²

Besides iron, cobalt is a 3d transition metal with high potential of being active in catalytic oxidation reactions. Cobalt(III) tris(1-methylimidazol-2-ylidene)phenylborate ($[\text{PhB}(\text{MeIm})_3]^-$) complexes **19** and **20** (Scheme 9) are capable of oxidizing inert alkane C–H bonds.¹³³ The tris(NHC)borates in the compounds are unique chelating ligands offering *cis*-orientated vacant sites for binding reactants. Besides the NHC stabilization, negatively charged borate creates intramolecular charge separation which is capable of stabilizing high valent metals.⁵ **19** possesses a hexa-coordinated heteroleptic structure with a less hindered κ^3 -capping $[\text{PhB}(\text{MeIm})_3]^-$ ligand and a bidentate acac ligand, as revealed by X-ray crystallography. The sixth coordination site is occupied by a 1-methylimidazole N-donor. **20** is a hexa-coordinated

homoleptic pseudo-octahedral cobalt(III) complex supported by two κ^3 - $[\text{PhB}(\text{MeIm})_3]$ ligands in a C_3 symmetric arrangement of the tris(NHC)borates. The catalytic performance of both complexes in the oxidation of cyclohexane was examined with *m*CPBA as the oxidant due to previous studies with comparable NHC free cobalt catalysts.^{133–135} Compared to the NHC free cobalt catalysts $\text{Co}^{\text{II}}(\text{acac})_2$, complex **19** exhibits enhanced selectivities towards alcohols at $25\text{ }^{\circ}\text{C}$ (A/K = 8.7 and a TON of 540). **19** achieves an increased TOF of 1050 h^{-1} at $35\text{ }^{\circ}\text{C}$. The highest conversion (53%) is obtained after a short reaction time of 30 min. At $25\text{ }^{\circ}\text{C}$, complex **20** is almost inactive (TOF = 20 h^{-1}), probably caused by the occupied coordination site from a second $[\text{PhB}(\text{MeIm})_3]^-$ ligand. Raising the reaction temperature to $35\text{ }^{\circ}\text{C}$ increases the activity (A/K = 4.2, TON = 530), which nevertheless is 50% lower than that of **19**. UV-vis spectra under catalytic conditions show a stable intermediate for **20**, which is formed at $25\text{ }^{\circ}\text{C}$ and changes to another species when rising the temperature up to $35\text{ }^{\circ}\text{C}$, supporting a difference in the catalytic pathway of **19** and **20**.¹³³

Bala *et al.* introduced nickel(II) NHC complexes (Scheme 9, **21a–e**), bearing straight chain alkyl wingtip substituents, in the oxidative hydrogenation of cyclohexane and *n*-octane applying *tert*-butyl hydroperoxide (TBHP) as the oxidant. The nickel centre is symmetrically aligned within a square planar coordination of *trans*-halides and *trans*-1,2,3-triazol-5-ylidenes, as revealed by single crystal XRD. The difference in the hydrophobic alkyl chain wingtip groups influences the catalytic performance towards the product selectivity. As the length of the substituent increases, the alcohol formation is enhanced. CV measurements show that an increase in the length of the alkyl substituents has a negligible influence on the values of the oxidation, suggesting that any different behaviour in catalysis is due to structural and geometric changes rather than in electronic properties. Oxidation of *n*-octane with catalysts **21a–e** results in a substrate conversion of up to 19% to a mixture of isomeric alcohols and ketones.¹³⁶ The maximal conversion of the oxidation of cyclohexane is 15% with a TON of 150 and high selectivity towards the ketone, demonstrating higher activity, but lower or the same TON as previously used nickel(II) catalysts without stabilizing NHC ligands.^{136–138} Mechanistic considerations suggest a mechanism *via* a Fenton-like pathway involving the reactive Ni(II) species¹³⁶ due to a reported Ni(II) alkylperoxo complex generated in the presence of $t\text{BuOOH}$ for the oxidation of cyclohexane.¹³⁹ Addition of a radical scavenger to the reaction increases the yield significantly.¹³⁶ These considerations would also be in accord with the high ketone selectivity caused by the over oxidation of the alcohol by radical involving reactions.

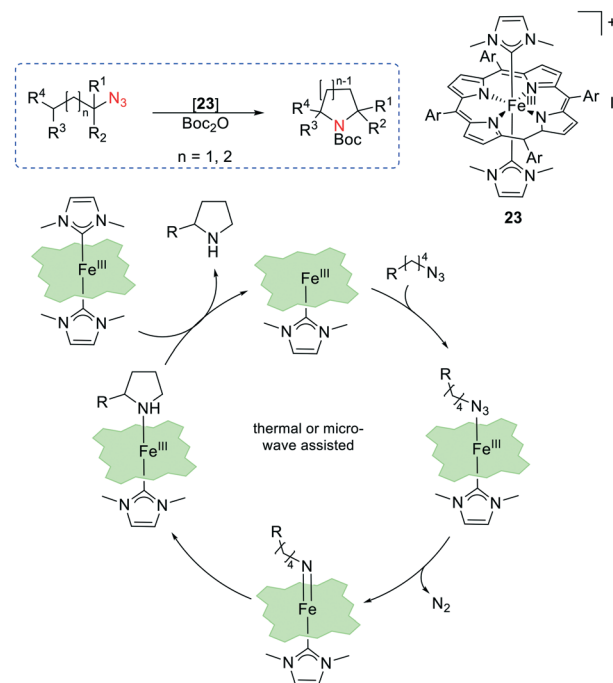
Copper(I) complexes bearing 1,2,3-triazol-5-ylidene ligands (Scheme 9, **22a–d**) were evaluated as *in situ* generated catalysts for homogeneous oxidation of cyclohexane, toluene and *n*-octane with H_2O_2 . Due to the poor stability of these complexes in solution, even under inert gas atmosphere (complete decomposition after 24 h), the *in situ* technique was adopted, by adding the NHC precursor and Cu_2O

separately to the reaction mixture. Aliphatic *N*-substituents show higher catalytic activities than bulky aromatic wingtip *N*-substituents in the oxidation of cyclohexane as a substrate. Conversions of up to 39% with a A/K ratio of 1.7 are achieved. The addition of acids is problematic, causing catalyst decomposition. Radical scavengers suppress the catalytic activity suggesting a radical (Fenton-type) mechanistic pathway.¹⁴⁰ A proposed mechanism involves the oxidation of Cu(I)-NHC to Cu(II)-NHC with H₂O₂ by generating a hydroxyl radical, which subsequently activates the substrate alkane *via* proton abstraction. The so-formed highly activated alkyl radical further reacts with molecular oxygen by forming an alkyl peroxy radical, which may undergo dismutation or reduction into alkyl hydroperoxide yielding the alcohol and ketone, for the latter through decomposition.^{140,141} Oxidation of toluene with **22c** yielded a mixture of benzaldehyde and benzyl alcohol as the main products.¹⁴⁰

Amination

Functionalization of inert C–H alkane bonds by insertion of nitrogen is an important and challenging area in the pharmaceutical industry. For instance, alicyclic amines are ubiquitous in natural and pharmaceutical molecules.¹⁴² Examples for these medicinally important alkanoids are nornicotine,¹⁴³ tropane, the basic framework for a variety of medications,¹⁴⁴ *cis*-octahydroindole, a potent inhibitor of the blood coagulation cascade¹⁴⁵ and leelamine, a potent anti-melanoma agent.¹⁴⁶ Transition metal catalysed direct amination of alkanes *via* C–H activation is receiving attention for being able to overcome certain challenges such as substrate limitation and undesired product regioselectivity.¹⁴⁷

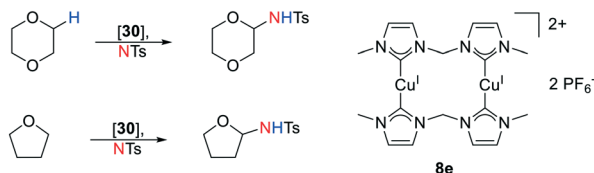
In this context and inspired by the catalytic efficiency of noble metal based ruthenium(II) porphyrins,¹⁴⁸ an iron(III) porphyrin complex, bearing axial imidazole ligands, is introduced (Scheme 12, **23**). Compound **23** provides catalytic access to a wide range of alicyclic amines *via* an intramolecular C(sp³)-H-amination of alkyl azides (Scheme 12). Selective product formation of tertiary, benzylic, allylic, secondary, and primary C–H bonds with yields up to 95% is afforded. Treatment of the substrates with 10 mol% catalyst loading and 1 eq. Boc₂O at 115 °C under inert atmosphere results in conversions above 99% with good to excellent product yields together with a remarkable selectivity. Changing the conditions to microwave-assistance at 140 °C and 50 W results in high tolerance towards oxygen and moisture with comparable performance but ten times faster reaction time and improved product yield. Additionally, the recycling of the catalyst is possible up to three times without a significant loss in its performance. Furthermore, compound **23** is able to catalyse the synthesis of the Boc protected precursors of tropane, *cis*-octahydroindole and leelamine. Deprotection with TFA leads to the desired products in good yields. Paramagnetic low spin Fe(III) complex **23** is stable towards air and moisture for several



Scheme 12 Amination of alkanes catalysed by an iron NHC complex and the proposed mechanistic pathway (Ar = 2,6-Cl₂C₆H₃).

weeks due to the NHC occupation of the axial positions. To gain insight into the reaction mechanism and the role of the axial NHC ligands, the same complex was investigated, bearing no axial ligands. Under such conditions, the product yield decreases significantly from 95 to 8%. DFT calculations for the complex with unoccupied axial positions show that the coordination of Fe³⁺ with alkyl azide appears to be required by the abolition of heme coplanarity, with the iron lying outside the porphyrin plane. Ligation with NHC already breaks the conformation, minimizing the required displacement upon adduct formation with alkyl azide. Subsequently, the iron(III)-alkylazide adduct tends to undergo decomposition and cyclization. Mechanistic proposals suggest a thermally driven initial dissociation of one NHC ligand to give access to the metal centre (Scheme 12). [Fe^{III}(porphyrin)(NHC)]⁺, which has been detected by ESI-MS analysis, binds an alkyl azide to give [Fe^{III}(porphyrin)(NHC)(N₃R)]⁺ followed by azide decomposition and cyclization to afford the cyclic amine. These findings reveal the vital role of the NHC in the mechanism of C–H amination.¹⁴⁹

Nitrene insertion into C–H bonds is a highly attractive synthetic strategy for the introduction of amino groups into organic molecules. With this C–H bond amination method, an amino group can ideally be incorporated into an organic skeleton in one single step, avoiding lengthy multi-step functional group conversions.¹⁵⁰ Originating from previously described molecular skeleton **8** in the aziridination of alkenes (Scheme 5), the dinuclear copper(I) complex **8e** supported by bis-NHCs has also been applied in tosylamidation of alkanes (Scheme 13). Caused by the solubility of **8e**, 1,4-dioxane and tetrahydrofuran were used as suitable substrates. At 70 °C



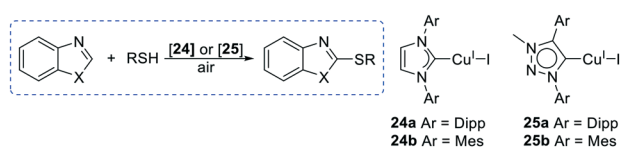
Scheme 13 Nitrene insertion catalysed by a dinuclear copper NHC complex.

and in acetonitrile, the bis-Cu(I) NHC complex promotes the formal insertion of a NTs group from chloramine T into the α -C–H bond of cyclic ethers.⁵⁷

Thiolation

The C–S bond formation of aromatic hydrocarbons is a key step in pharmaceutical and biological synthesis, as well as in the formation of functional materials.^{151,152} The direct C–H thiolation is a promising alternative to cross-coupling reactions, requiring the presence of functional groups.¹⁵³ Transition metal catalysts have been developed for this reaction based on expensive noble metals.¹⁵⁴ Recently copper has attracted attention in this research field showing good catalytic activity.^{154,155}

In this context copper(I) complexes **24** and **25** supported by imidazole or triazole moieties have been applied in the oxidative C–H bond functionalization of benzothiazoles and benzoxazoles with aryl and alkyl thiols (Scheme 14). In the presence of air and base (K_2CO_3), all Cu(I) NHC complexes are capable of forming the desired thioethers at elevated temperatures (140 °C) with moderate to good yields (22–95%). Imidazole supported complexes show better performances compared to abnormal triazole NHC complexes with **24a** being the most active one. At a high catalyst loading of 20 mol%, yields up to 95% are achieved within 3 h, which is much faster compared to NHC free copper catalysts. Ligand-free Cu(I) is also capable of catalysing the reaction but slower when using **24a**. In the absence of air, the yield dropped to 10% indicating an oxidative process. Furthermore, the use of inexpensive Cu catalysts and O_2 as the stoichiometric oxidant is a significant advantage. Application of various substituted benzothiazoles in catalyst screening showed that the position of the substituent hardly affects the reaction. Applying electron-donating substituents in 4- and 6-positions results in lower yields. In the case of the thiolation of benzoxazole electron-donating substituents on the alkyl- and arylthio substrates, the corresponding thioethers are obtained.¹⁵⁶

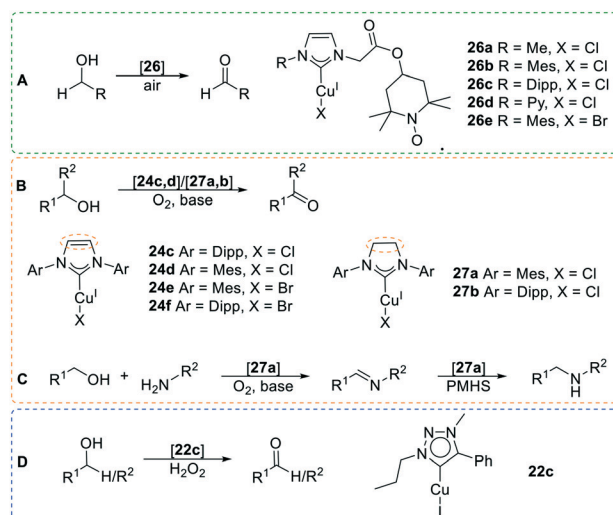


Scheme 14 Oxidative direct C–H thiolation of benzothiazoles (X = S) and -oxazoles (X = O) catalysed by copper(I) NHC complexes.

Oxidation of alcohols and amines

Carbonyl compounds play an important role in the total synthesis of natural products and fine chemicals. Consequently, the selective oxidation of alcohols to their corresponding carbonyl products is one of the most fundamental organic transformations.¹⁵⁷ Much attention has been devoted to the development of methods for catalytic aerobic alcohol oxidation. While most common traditional methods usually require the application of toxic oxidants under harsh reaction conditions, the stoichiometric use of molecular oxygen or air combined with transition metal catalysts has emerged as a very powerful alternative for this reaction.^{158,159} Numerous palladium or ruthenium containing systems have been developed in aerobic alcohol oxidation with the disadvantage of their noble character.^{160–162} As a result, researchers now focus on the catalytic applicability of cheaper and more environmentally friendly transition metals.

In situ generated Cu(I)–NHC–TEMPO complexes **26a–e** have been introduced as efficient catalysts for aerobic and selective oxidation of primary alcohols into aldehydes with excellent yields (Scheme 15A). Outstanding activity properties are obtained by functionalizing the catalytic system with TEMPO, a potent oxidant. Cu–NHC–TEMPO complexes were analysed by ESI-MS and EPR spectra, showing the expected complex mass and the characteristic nitrosyl radical mass, respectively. All complexes give access to the desired aldehyde. Under optimized conditions (80 °C, 15 h, 10 mol% catalyst loading) **26e** exhibits the highest activity in the oxidation of decan-1-ol with yields up to 95%. Regarding the effect of solvents, the oxidation proceeds more efficiently in chlorobenzene (than in MeCN, toluene, THF and DMF). Examinations under molecular oxygen showed no significant improvement compared to the results driving the reaction in



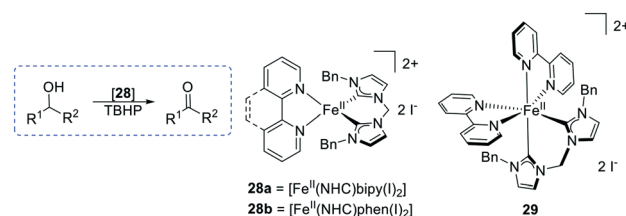
Scheme 15 Oxidation of primary and secondary alcohols by copper(I) NHC complexes (A, B and D) and catalytic one-pot oxidation of benzylic primary alcohols and -amines affording imines and secondary amines *via* subsequent catalytic reduction with **22c** (C).

air. Bases mostly favour the oxidation reaction of alcohols in reported Cu–ligand–TEMPO systems. Addition of KO^tBu or Et₃N, however, resulted in negative effects on the catalytic system. Under the same conditions, comparable Cu(I)–NHCs **24d–f** (Scheme 15), bearing two mesityl or diisopropyl phenyl N-wingtips without the functionalization of TEMPO, are completely inactive, indicating the need for TEMPO anchorage to ensure a facile intramolecular proton abstraction. **26e** proved to be active for a variety of other benzylic, allylic, propargylic, and heterocyclic-substituted primary alcohols with yields up to 99% within 15 h.¹⁶³

Jiang *et al.* examined the catalytic activity of complexes **24c,d** and additionally **27a,b**, where the copper(I) centre is supported by an imidazoline ligand instead of an imidazole (Scheme 15B). In the presence of a base and O₂, various primary and secondary alcohols are oxidized to ketones in high yields (up to 99%) after 12 h at room temperature and 2 mol% catalyst loading. The saturated NHC–Cu(I) complexes are less active than their unsaturated analogues presumably due to the slightly reduced electron donating properties. Changing the pure oxygen atmosphere to air or to argon decreases the yield or even no product could be detected for the latter. Furthermore, **27a** shows versatile tolerance towards an aerobic one-pot oxidation of benzylic primary alcohols and amines, affording imines and secondary amines *via* subsequent catalytic reduction (Scheme 15, C). Desired products are obtained in high yields (75–94%) and under mild reaction conditions (r.t., 2 mol% catalyst loading, base). PMHS and additional catalyst (2 mol%) were added to the mixture after consumption of the alcohol to reduce the imine to secondary amine.¹⁶⁴ Amines are important compounds mainly found in bioactive molecules and natural products and are frequently used in agrochemicals, chemical industry and pharmaceuticals. Currently applied methods are prone to over-alkylation.^{165,166} Consequently, the insertion of a catalyst is a promising opportunity.

The catalytic copper(I) system **22c**, bearing a 1,2,3-triazol-5-ylidene moiety (Scheme 15D), which is described in the hydroxylation of alkanes and aromatics, is used for the further oxidation of (the received) alcohols to the corresponding ketones with H₂O₂ as an oxidizing agent. High conversions (up to 91%) are achieved with phenolic and benzylic alcohols compared to aliphatic variants, due to the C–OH bond activation capacity. Here secondary alcohols are more reactive than primary ones.¹⁴⁰

Chelating bis-NHC complexes of iron(II) containing bipyridyl ligands are applied as catalyst precursors for oxidation of a series of aromatic and aliphatic secondary alcohols to the corresponding ketones in excellent yields (Scheme 16). Complexes **28a** and **28b** are soluble in polar, but insoluble in non-polar solvents. Additionally, these compounds are air and moisture stable for several weeks in the solid state. In catalytic studies, TBHP functions as an oxidant. The replacement of TBHP with H₂O₂ leads to the inactivity of the bipyridyl complex **28a**. Under neat conditions or in the presence of a polar solvent (MeCN or water) above 99% acetophenone from 1-phenylethanol is formed within 4.5 h at 80 °C with 2 mol%

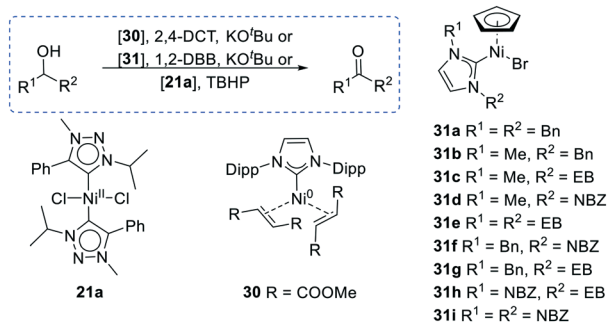


Scheme 16 Oxidation of secondary alcohols by iron(II) NHC complexes.

loading of **28a/b** and a TON of 1500 for **28a**. The reaction profile shows conversions at early reaction times (5 min), indicating a rapid formation of the active species upon addition of the oxidant. The active reaction mixture with **28a** can be reused upon six consecutive additions of the substrate and oxidant with quantitative ketone conversions. ¹H- and ¹³C-NMR analyses during stability explorations with **28a** in CD₃CN show significant resonances associated with a mixture of complex **29** (Scheme 16) and [Fe(bipy)₃]²⁺, along with small quantities of bis-imidazolium salt after stirring for 16 h. The colour of the solution changed from the initial deep purple to purplish red. The identity of **29** was confirmed by single crystal XRD. The molecular structure displays a slightly distorted octahedral geometry with one bipyridyl in the equatorial plane. Axial positions are occupied by a moiety of the second bipyridyl and one NHC moiety. Because of these findings, the catalytic activity of acetonitrile solutions of **28a** after incubation for 16 h was further explored. Under identical reaction conditions, acetophenone is formed in 40% yield, suggesting that **28a** is a pre-catalyst in the catalytic oxidation reaction. Additional spin trap experiments give information about the mechanistic pathway. Since the presence of an oxygen-radical reduces the yield significantly and a carbon-radical trap does not affect the catalytic reaction, the oxidation reaction proceeding *via* a radical mechanism involving oxygen-centred radicals is expected.¹⁶⁷

Nickel as an abundant and comparatively cheap metal was used in recent NHC supported catalytically active systems for oxidation processes.^{168,169} Navarro *et al.* presented highly active, anaerobic Ni(0)–NHC catalytic systems for the selective oxidation of secondary alcohols with addition of KO^tBu (Scheme 17, **30**).¹⁶⁸ 2,4-Dichlorotoluene acts as both an oxidant and solvent. Air-stable bis-dimethyl fumarate Ni(0)–NHC complex **30** enables the reaction at room temperature. Elevating the temperature to 40 °C and 60 °C strongly decreases the reaction time from 12 h to 2.5 h and 1 h, respectively, with high yields of up to 98%, even for 40 °C at a catalyst loading of 5 mol%. Different to aryl–alkyl or aryl–aryl alcohols, alkyl–alkyl substrates require 60 °C to reach completion in short reaction times.^{168,170}

A series of nickel(II) NHC complexes of the type [CpNiBr(NHC)] effectively catalyse the aerobic oxidation of a range of secondary alcohols using KO^tBu as a mild base and 1,2-dibromobenzene as an oxidant. The NHC moieties either contain a symmetric or asymmetric imidazole (Scheme 17, **31**). X-ray crystallographic analysis of **31e, f** and **h** displays a



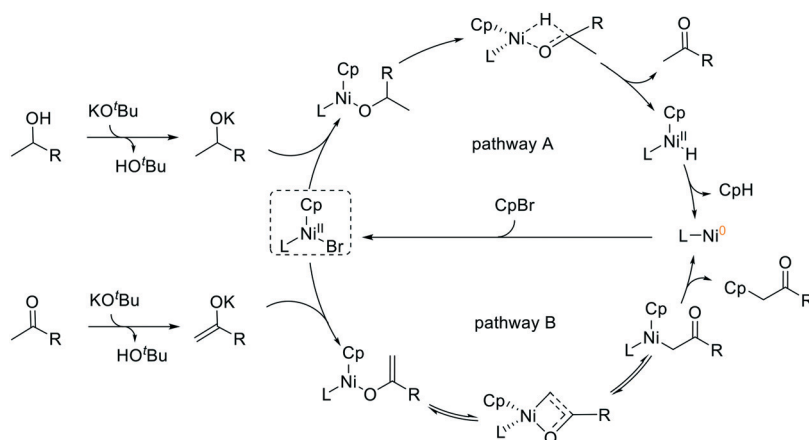
Scheme 17 Oxidation of primary and secondary alcohols by nickel(0) and (II) NHC complexes.

half-sandwich geometry around the metal centre. Under optimized conditions (3 mol% catalyst, 110 °C or microwave assisted and 2.6 eq. base) high conversions up to 98% and excellent yields are obtained within 2 h. Microwave assistance decreases the necessary reaction time to 30 min. Electronic and steric differences in the *N*-substitutions of the coordinated NHC ligands affect the performance and efficiency of the catalyst. Complexes **31a**, **b** and **e** are the most active ones due to their strong electron donating character. This electron donation in conjunction with bulky substituents leads to more stable and active nickel species. Due to the high flexibility of the substituents, unhindered substrate coordination to the metal is nevertheless ensured and enhances reductive elimination steps in the catalytic cycle. Insertion of nitrobenzene substituents, having an electron-withdrawing effect, decreases the catalytic activity. Mechanistic studies with DFT calculations give more insight into the favoured reaction. Two different mechanistic pathways are considered (Scheme 18).¹⁷¹ Besides the ketone formation over the anaerobic alcohol oxidation (path A) subsequent domino α -ketone arylation (path B) is proposed to be possible as well.^{171,172} In path A, the secondary alcohol is dehydrogenated by the base to form an active alcoholate salt, dehalogenating the catalyst by releasing of KBr. The ketone is generated by β -hydride elimination and subsequent

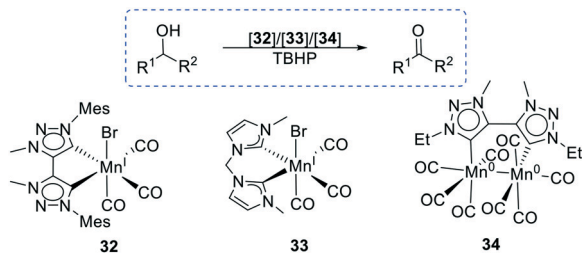
elimination of the nickel centre. The nickel(II)-hydride species undergoes elimination of the aryl group (Cp) leading to the nickel(0) intermediate, regenerating the initial complex after addition of another aryl halide molecule. In path B, ethoxide, being formed by the reaction of the desired ketone with KO^tBu, may react with the catalyst. The Ni(0) intermediate is generated *via* a tautomeric shift and reductive elimination steps yielding 1-arylethanone as an organic side product. DFT calculations reject the possible mechanism *via* path B due to the highly exergonic character of path A compared to its endergonic character. Additionally, intermediates in path A are more stable, favouring the ketone product formation.¹⁷¹

Previously described catalytic system **21a** is also efficient for the oxidation of linear primary and secondary alcohols to the corresponding ketones with TBHP as an oxidant. Conversions of up to 72% are achieved at 80 °C after 12 h. Substrates with an alcohol moiety in the C2 position were found to be the most reactive linear alkanes, since the conversions with substrates where the hydroxyl group is located at C3 or C4 are lower and the activity is lowest for primary alcohols.¹³⁶

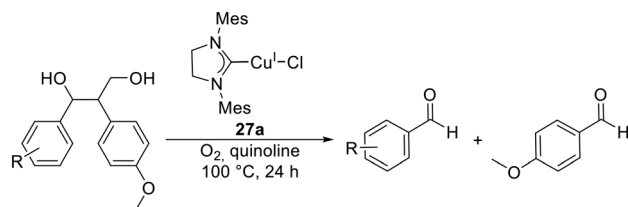
Non-toxic manganese, as the third most abundant transition metal in earth's crust, offers facile access to multiple oxidation states with great potential in catalytic activity to a variety of reactions. Additionally, manganese can accommodate up to seven ligands in its first coordination sphere.¹⁷³ Albrecht and Royo *et al.* were the first to describe the capability of a manganese NHC complex in the catalytic oxidation of secondary alcohols and benzyl alcohols. Monometallic Mn(I) complexes containing bis-1,2,3-triazol-5-ylidene or bis-imidazol-2-ylidene ligands are compared with a bimetallic Mn(0) bis-1,2,3-triazol-5-ylidene complex (Scheme 19). X-ray crystallographic analysis display the molecular structure of highly symmetric **34** with two formally zero-valent Mn centres in a slightly distorted octahedral geometry. Complexes **32–34** are air and moisture stable and therefore easy to handle. Under optimized conditions (40 °C, MeCN, 1 mol% catalyst) all three complexes are active with TBHP being the oxidizing agent. Bimetallic complex **34**



Scheme 18 Mechanistic insights into the oxidation of secondary alcohols by nickel(II) NHC complexes.



Scheme 19 Oxidation of secondary alcohols with TBHP catalysed by manganese NHC complexes.



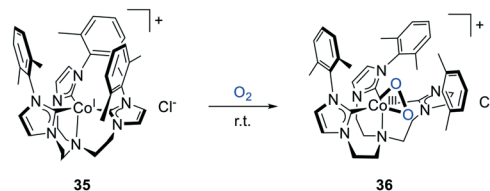
Scheme 20 Oxidative cleavage of lignin with copper(I) NHC complex **27b**.

turned out to exhibit the best performance with excellent yields ($\geq 99\%$) after 2 h and TOFs up to 72 h^{-1} . It can be reused up to six times without any loss in its performance. Replacing TBHP with H_2O_2 decreases the yield to 27% after 24 h, indicating a critical role of the oxidant in the mechanism, or water sensitivity of the catalyst. However, primary aliphatic alcohols do not undergo oxidation under these conditions.¹⁷⁴

Lignins are bio-renewable biopolymers, incorporated into the plant cell wall. These phenolic macromolecules are hoped to replace rare fossil resources, by synthetic depolymerisation to sustainable aromatic compounds with high added value. However, the cleavage of such systems requires the development of efficient catalysts. In this context Li *et al.* presented the catalytic selectivity of copper(I) NHC **27a** in the aerobic cleavage of β_1 lignin (Scheme 20). Over 99% conversion and good to excellent yields (up to 90%) of the corresponding aldehydes are achieved after 24 h (20 mol% catalyst, 3 eq. quinolone, 100 °C), using dioxane as a solvent. The $\text{C}_\alpha\text{-C}_\beta$ bond cleavage reaction is suggested to proceed *via* a retro-aldol reaction after the selective oxidation of the primary alcohol. No ketone formation was observed. Modification of the NHC system by backbone variation (imidazole *vs.* imidazoline, insertion of phenyl or cyclohexane) or *N*-substituent variation (Mes *vs.* Dipp *vs.* anisole) decreases the efficiency significantly.¹⁷⁵

Molecular oxygen activation

The activation of molecular oxygen by metalloproteins containing iron or copper plays a vital role in biology.^{176–178} The coordination of O_2 to a protein metal centre is a primary step in aerobic respiration and enzymatic oxidation reactions.¹⁷⁹ For environmentally friendly and sustainable chemistry, molecular oxygen is considered as an ideal and

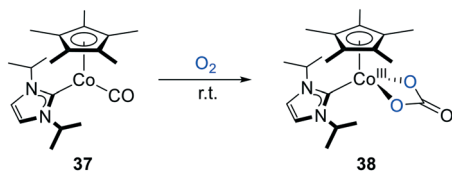


Scheme 21 Activation of dioxygen by a tris-NHC cobalt(I) complex, forming a side-on peroxy complex.

cost-effective oxidant.¹⁸⁰ Unfortunately, it cannot oxidize most organic substances under ambient conditions because the reactions are spin forbidden.¹⁸¹ Reactive oxygen species including superoxo, (hydro)peroxo and oxo moieties as active intermediates are remarkably efficient and led to the development of bioinspired transition metal complexes with the ability to activate dioxygen.^{182–184} Dioxygen activation at transition metal centres is a fundamentally important process due to its postulated role in molecular catalysis.

Meyer *et al.*,¹⁸⁵ Radius *et al.*¹⁸⁶ and our group¹⁸⁷ worked on the selective activation of dioxygen from air utilizing cobalt NHC complexes and their potential use as artificial oxygen carriers. Ligands that enforce a tripodal topology on coordinated metal ions are known to provide powerful platforms for small molecule activation and functionalization. A low-valent cobalt(I) tris NHC complex was found to react with O_2 from air at ambient temperature to form a rare cobalt side-on (η^2) peroxy species (Scheme 21), as proven by IR spectra (O-O stretching frequency of 890 cm^{-1}) and SC-XRD. Under an inert gas atmosphere, **35** is stable in the solid state but oxidizes in solution to its cobalt(II) counterpart with one chloride counter ion being in the axial position. SC-XRD shows that in this counterpart of **35** the ligand is only bound by the three carbenes without N-donation. Complex **36** exhibits a pseudo-octahedral coordination sphere with two carbene carbon pendant arms in an axial position and the dioxygen coordinates side-on. The three xylene substituents on the highly flexible tris-NHC ligand flank the activated dioxygen ligand, effectively blocking the frequently observed bimolecular decomposition pathway to form μ -peroxy dimers. DFT calculation and reactivity studies with triphenylphosphineoxide and the extremely electron-deficient alkene tetracyanoethylene verify the nucleophilic character of the coordinated dioxygen ligand. The peroxy complex reacts with strong electrophiles and allows the transfer of the O_2 fragment.¹⁸⁵

NHC-stabilized cobalt carbonyl half-sandwich complex **37** reacts in the solid state and in solution with O_2 at room temperature by yielding cobalt(III) carbonato complex **38** (Scheme 22). UV/vis spectroscopy combined with stopped-flow techniques suggests the formation of an intermediate. Additional DFT calculations assume a mechanism *via* superoxo and peroxy intermediates, in which a peroxy acyl complex is proposed as the key intermediate in this process. Exchanging pentamethylcyclopentadiene with cyclopentadienyl leads to the formation of a compound which



Scheme 22 Activation of dioxygen by an cobalt NHC complex, forming a cobalt(III) carbonato complex.

subsequently decomposes under air exposure and does not form a comparable carbonato complex.¹⁸⁶

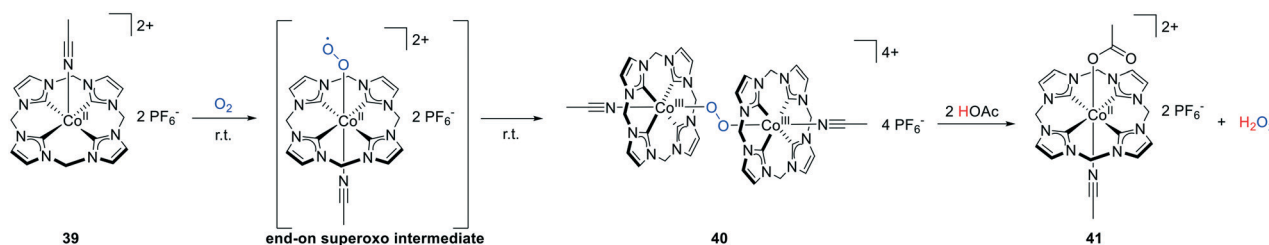
Recently a bioinspired cobalt(II) complex **39** supported by a macrocyclic tetra NHC ligand, being the same as that applied in the iron based epoxidation catalyst **11** (Scheme 6), was reported to activate dioxygen from air at ambient temperatures (Scheme 23). As proven by SC-XRD, **39** displays a slightly distorted square pyramidal structure, comparable to that of its iron analogue. When exposing a solution of **39** in MeCN to air, an immediate colour change from yellow to green is observed. Subsequent addition of Et₂O yields a green precipitate. SC-XRD identified a μ₂-peroxo dicobalt(III) complex, with two Co-centres, bridged *via* a *trans* μ₂-peroxo ligand in a distorted octahedral fashion. Formation of this 18-valence-electron complex **40** is thermodynamically favoured and a consequence of a redox-reaction oxidizing two Co(II) centres to Co(III) and reducing O₂ (Scheme 23). Related μ₂-peroxo (di)cobalt complexes, bearing nitrogen donor ligands, are often only achieved and/or stable at extremely low temperatures, while the first isolable macrocyclic μ₂-peroxo (di)cobalt NHC complex **40** is stable at room temperature. The reaction of such compounds usually proceeds *via* superoxo intermediates. *In situ* EPR spectroscopy analysis during the reaction of **39** with O₂ detected an end-on superoxo species, which could be supported by DFT calculations. The nucleophilic nature of the peroxo moiety is also suggested by DFT analyses. Upon addition of acetic acid, the formed peroxo moiety can be cleaved, yielding a Co(II) acetate complex **41**, by simultaneously releasing H₂O₂ (Scheme 23).¹⁸⁷

As described before, oxoiron(IV) or (V) species are considered to be key intermediates in the catalytic cycle of numerous (non)-heme iron enzymes and complexes allowing for the insertion of an oxygen atom into unreactive C–H bonds. F. Meyer *et al.* were able to isolate and crystallize such an iron(IV) oxo complex

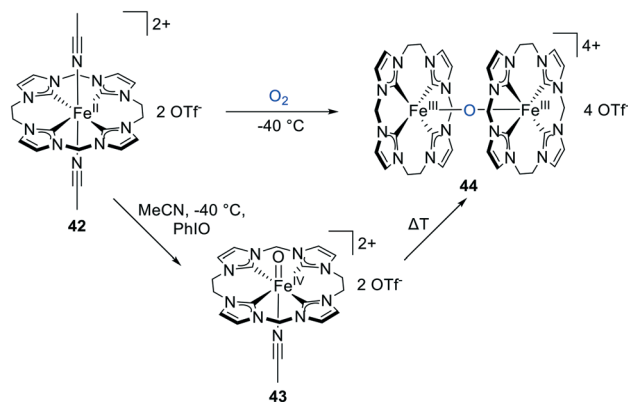
supported by an NHC unit. Treatment of a macrocyclic NHC iron(II) compound **42** with a PhIO derivate in MeCN at –40 °C results in the formation of oxoiron(IV) complex **43** in an planar tetradentate carbene coordination with *trans* axial oxygen and a solvent ligand, as confirmed by ESI-MS, UV/vis spectroscopy and SC-XRD (Scheme 24). Warming a MeCN solution of **43** results in a reduction to binuclear μ-oxo dimeric complex **44**, identified by ESI-MS and UV/vis data. Treating the initial compound **42** with aerial O₂ in MeCN at –40 °C directly gives access to the diiron species (Scheme 24), detected *via* SC-XRD. Mössbauer spectra reveal the cyclic tetra-NHC as an extremely strong equatorial σ-donor with high stabilizing capacity towards high valent metals.⁵¹

As described previously in the catalytic epoxidation section (*vide supra*) of alkenes, macrocyclic tetra-NHC iron(II) complex **11a** forms a μ₂-oxo diiron(III) compound **12** when exposed to air (Scheme 22). Interestingly, reaction of **11a** with oxygen in MeCN yields the oxidized iron(III) complex **11b** (Scheme 6) instead of **12**. Changing the solvent to acetone (benzonitrile or pivalonitrile) at –40 °C, the formation of a side-on superoxidic iron(III) intermediate **45** is detectable and analysed by UV/vis experiments, DFT calculations, EPR and NMR spectroscopy. Subsequent heating to room temperature results in complex **12** (Scheme 25). The molecular structure shows a slightly distorted square pyramidal geometry with the tetradentate cyclic ligand coordinated in a saddle distorted fashion, as analysed by SC-XRD. The reactivity test of **12** showed that PPh₃ could be oxidized stoichiometrically to OPPh₃ *via* simultaneous reduction of the bimetallic complex to the initial compound **11a**. Reducing agents such as Zn powder lead also to the reduction of **12** to **11a**.¹⁸⁸ Recently, a one electron oxidation of Fe^{III}–O–Fe^{III} species **12** with ThPF₆ to diiron(III,IV)-μ₂-oxo tetracarbene complex **46** has been reported (Scheme 25). Complex **46** is characterized by SC-XRD, UV/vis, EPR, Evans' NMR and elemental analysis. The Fe–O–Fe angle significantly changes during the oxidation, resulting in a nearly linear arrangement of the central diiron(III,IV)-μ₂-oxo motif with stabilizing acetonitrile ligands. CV measurement, UV/vis kinetic and NMR experiments demonstrate a feasible consecutive second oxidation of **46** by forming a highly stable diiron(IV)-μ₂-oxo complex **47**.¹⁸⁹

Molecular oxygen activation by nickel NHC complexes also attracts increasing attention.^{190–194} Sigman *et al.*,^{191,192,194} Whittlesey *et al.*¹⁹³ and Mandal *et al.*¹⁹⁰ reported NHC stabilized Ni(I) and Ni(II) complexes that form μ-hydroxo-bridged dimeric



Scheme 23 Activation of dioxygen by an macrocyclic NHC cobalt(II) complex *via* an superoxo intermediate forming a bimetallic μ₂-peroxo complex **46**. Reaction of **46** with HOAc results in the formation of H₂O₂ and an cobalt(III) acetate complex.

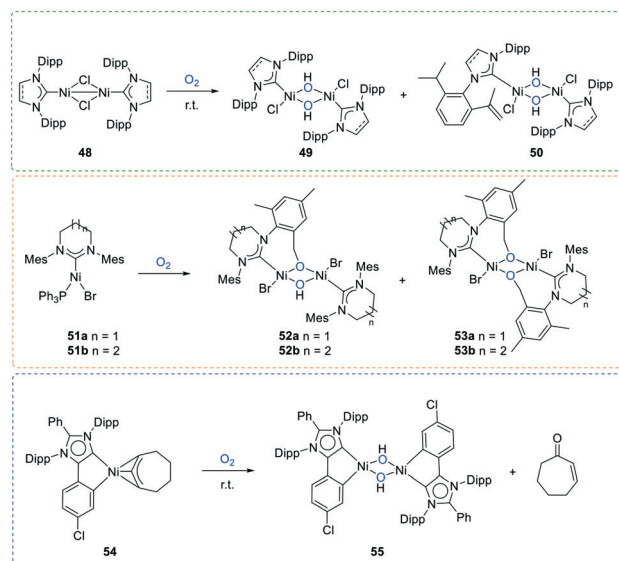


Scheme 24 Activation of dioxygen by a macrocyclic NHC iron(II) complex forming a binuclear μ -oxo diferric complex **44**. Reaction of **42** with a PhIO forms a oxoiron(IV) complex **43**. Subsequent heating gives bimetallic compound **44**.

Ni(II) complexes by O_2 activation either by oxidation of the coordinated allyl ligand or ligand dehydrogenation (Scheme 26). The complexes differ in their NHC moieties. Each metal in binuclear compound **48** possesses an imidazole ligand, while mononuclear nickel complex **54** displays an abnormal bounded imidazole unit. Meanwhile compound **51** has a ring expanded NHC, which is six (**51a**) and seven (**51b**) membered, respectively. Complex **48** undergoes facile aerobic oxidation *via* a fast colour change to purple, caused by the formation of bis- μ -hydroxo nickel(II) dimer **50** with concomitant ligand dehydrogenation of a single isopropyl group from one Dipp *N*-substituent.¹⁹⁴ Activation of O_2 by the three-coordinate Ni(I) compounds **51a** and **51b** yields dimeric Ni(II) complexes containing oxidized *ortho*-mesityl groups from one of the carbene ligands to afford dinuclear species with bridging aryloxy and hydroxyl ligands.¹⁹³ Treatment of the NHC based Ni(II) η^3 -allyl complex **54** with oxygen leads to a dimeric Ni(II)-hydroxo complex, as well as to the cleavage of cyclooctene to form η^3 -cyclooctenyl, which is detected with GC-MS analysis. Dimer **55** is only generated when the reaction is performed under dry O_2 atmosphere.¹⁹⁰

Conclusions

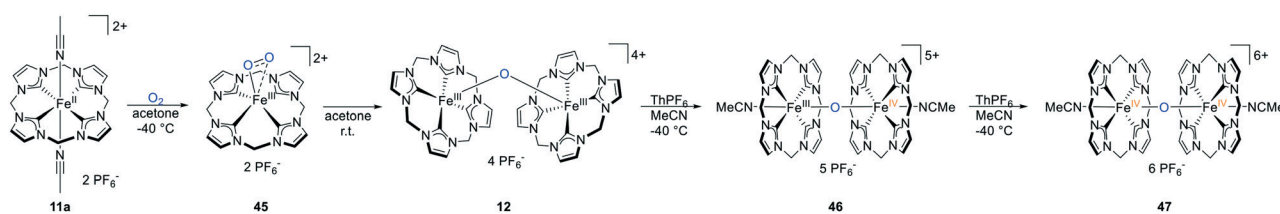
3d transition metal–NHC complexes are versatile catalysts for the oxidation of alkenes, aliphatic and aromatic hydrocarbons, alcohols, and amines. The application of these abundant, inexpensive, and likely less toxic first row



Scheme 26 Activation of dioxygen by nickel NHC complexes.

transition metals in oxidative catalysis has recently received a significant impetus. NHC systems are comparatively easy to synthesize and modify ligands for the stabilization of catalytically active metal complexes and therefore an important tool to regulate activity and selectivity in catalysis. NHC motifs have been shown to support catalytically highly active chromium, manganese, iron, cobalt, nickel, and copper complexes in oxidation catalysis, even in high oxidation states. The catalyst activity is comparable to, or in most cases, exceeds that of expensive and/or toxic metal complexes. Moreover, some 3d transition metal–NHC complexes even enable the activation of molecular oxygen.

However, challenges still remain to be overcome in oxidative reactions with these 3d transition metal–NHC complexes. The catalyst activity is limited to certain substrates and does not always have a high tolerance towards functional groups, thus limiting their application. The recycling of the catalyst is still a major issue in many of the described reactions. In the oxidation reactions discussed here, the recycling was either non-existent or is restricted to a few cycles, mostly caused by the short lifetime of the catalysts under oxidative conditions. The promising high TOFs *versus* comparable complexes without NHC support are overshadowed by significantly lower TONs. Consequently, the



Scheme 25 Activation of dioxygen by a macrocyclic NHC iron(II) complex forming a superoxide iron(III) intermediate **51**. Subsequent heating gives μ_2 -oxo diiron(III) complex **12**. Further oxidation of **12** leads to high valent diiron(III,IV)- μ_2 -oxo and diiron(IV,IV)- μ_2 -oxo NHC complexes **46** and **47**.

catalyst stability has to be significantly improved, ideally enabling a proper recycling of the catalyst as well. The general mechanisms of catalytic oxidation reactions are not yet fully understood and need to be further investigated to gain additional knowledge to design active, selective and particularly more stable catalysts. Even if 3d metals are considered as an environmentally friendly alternative to noble metals, the toxicity is certainly significantly influenced by the applied ligand system. This has to be taken into account when designing a suitable ligand system. Moreover, the more complex the syntheses of the applied ligand motifs are, the more expensive these systems eventually become, offsetting the advantage of the inexpensive metals.

Author contributions

GGZ thanks TUM Graduate School for financial support.

Conflicts of interest

There are no conflicts to declare.

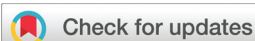
References

- H. Arakawa, M. Aresta, J. N. Armor, M. A. Barteau, E. J. Beckman, A. T. Bell, J. E. Bercaw, C. Creutz, E. Dinjus and D. A. Dixon, *Chem. Rev.*, 2001, **101**, 953–996.
- T. Punniyamurthy, S. Velusamy and J. Iqbal, *Chem. Rev.*, 2005, **105**, 2329–2364.
- N. N. Greenwood and A. Earnshaw, *Chemistry of the Elements*, Elsevier, 2012.
- J. I. van der Vlugt, *Eur. J. Inorg. Chem.*, 2012, **2012**, 363–375.
- J. Cheng, L. Wang, P. Wang and L. Deng, *Chem. Rev.*, 2018, **118**, 9930–9987.
- M. W. Kanan and D. G. Nocera, *Science*, 2008, **321**, 1072–1075.
- K. P. Bryliakov and E. P. Talsi, *Coord. Chem. Rev.*, 2014, **276**, 73–96.
- W. Nam, *Acc. Chem. Res.*, 2007, **40**, 522–531.
- D. A. Hey, R. M. Reich, W. Baratta and F. E. Kühn, *Coord. Chem. Rev.*, 2018, **374**, 114–132.
- J. W. Kück, R. M. Reich and F. E. Kühn, *Chem. Rec.*, 2016, **16**, 349–364.
- E. I. Solomon, T. C. Brunold, M. I. Davis, J. N. Kemsley, S.-K. Lee, N. Lehnert, F. Neese, A. J. Skulan, Y.-S. Yang and J. Zhou, *Chem. Rev.*, 2000, **100**, 235–350.
- A. Behr and P. Neubert, *Applied homogeneous catalysis*, John Wiley & Sons, 2012.
- L. A. Schaper, S. J. Hock, W. A. Herrmann and F. E. Kühn, *Angew. Chem., Int. Ed.*, 2013, **52**, 270–289.
- J. A. Mata, M. Poyatos and E. Peris, *Coord. Chem. Rev.*, 2007, **251**, 841–859.
- B. Ramasamy and P. Ghosh, *Eur. J. Inorg. Chem.*, 2016, **2016**, 1448–1465.
- M. Koy, P. Bellotti, M. Das and F. Glorius, *Nat. Catal.*, 2021, **4**, 352–363.
- P. Bellotti, M. Koy, M. N. Hopkinson and F. Glorius, *Nat. Rev. Chem.*, 2021, 1–15.
- A. Kumar and P. Ghosh, *Eur. J. Inorg. Chem.*, 2012, **2012**, 3955–3969.
- M. N. Hopkinson, C. Richter, M. Schedler and F. Glorius, *Nature*, 2014, **510**, 485–496.
- W. A. Herrmann, *Angew. Chem., Int. Ed.*, 2002, **41**, 1290–1309.
- B. Gómez, V. Francisco, F. Fernández-Nieto, L. Garcia-Rio, M. Martín-Pastor, M. R. Paleo and F. J. Sardina, *Chem. – Eur. J.*, 2014, **20**, 12123–12132.
- H. Jacobsen, A. Correa, A. Poater, C. Costabile and L. Cavallo, *Coord. Chem. Rev.*, 2009, **253**, 2784–2784.
- S. M. Hölzl, P. J. Altmann, J. W. Kück and F. E. Kühn, *Coord. Chem. Rev.*, 2017, **352**, 517–536.
- Q. Liang and D. Song, *Chem. Soc. Rev.*, 2020, **49**, 1209–1232.
- C. Berini and O. Navarro, *Chem. Commun.*, 2012, **48**, 1538–1540.
- C. Berini, D. F. Brayton, C. Mocka and O. Navarro, *Org. Lett.*, 2009, **11**, 4244–4247.
- M. Nakanishi, A. F. Salit and C. Bolm, *Adv. Synth. Catal.*, 2008, **350**, 1835–1840.
- W. McCoull and F. A. Davis, *Synthesis*, 2000, **2000**, 1347–1365.
- P. Müller and C. Fruit, *Chem. Rev.*, 2003, **103**, 2905–2920.
- G. S. Singh, *Adv. Heterocycl. Chem.*, 2019, **129**, 245–335.
- J. B. Sweeney, *Chem. Soc. Rev.*, 2002, **31**, 247–258.
- L. Degennaro, P. Trinchera and R. Luisi, *Chem. Rev.*, 2014, **114**, 7881–7929.
- A. K. Yudin, *Aziridines and epoxides in organic synthesis*, John Wiley & Sons, 2006.
- I. Aviv and Z. Gross, *Chem. Commun.*, 2007, 1987–1999.
- Y. Li, L. X. Gao and F. S. Han, *Chem. – Eur. J.*, 2010, **16**, 7969–7972.
- Z. Li and C. He, *Eur. J. Org. Chem.*, 2006, **2006**, 4313–4322.
- Z. Li, X. Ding and C. He, *J. Org. Chem.*, 2006, **71**, 5876–5880.
- G. F. Keaney and J. L. Wood, *Tetrahedron Lett.*, 2005, **46**, 4031–4034.
- S. A. Cramer and D. M. Jenkins, *J. Am. Chem. Soc.*, 2011, **133**, 19342–19345.
- G. R. Elpitiya, B. J. Malbrecht and D. M. Jenkins, *Inorg. Chem.*, 2017, **56**, 14101–14110.
- C. L. Keller, J. L. Kern, B. D. Terry, S. Roy and D. M. Jenkins, *Chem. Commun.*, 2018, **54**, 1429–1432.
- P. P. Chandrachud, H. M. Bass and D. M. Jenkins, *Organometallics*, 2016, **35**, 1652–1657.
- S. A. Cramer, R. H. Sánchez, D. F. Brakhage and D. M. Jenkins, *Chem. Commun.*, 2014, **50**, 13967–13970.
- S. Fantauzzi, A. Caselli and E. Gallo, *Dalton Trans.*, 2009, 5434–5443.
- S. B. Isbill, P. P. Chandrachud, J. L. Kern, D. M. Jenkins and S. Roy, *ACS Catal.*, 2019, **9**, 6223–6233.
- H. M. Bass, S. A. Cramer, A. S. McCullough, K. J. Bernstein, C. R. Murdock and D. M. Jenkins, *Organometallics*, 2013, **32**, 2160–2167.
- C. Li, H. Zhang, D. Jiang and Q. Yang, *Chem. Commun.*, 2007, 547–558.
- K. Riener, S. Haslinger, A. Raba, M. P. Högerl, M. Cokoja, W. A. Herrmann and F. E. Kühn, *Chem. Rev.*, 2014, **114**, 5215–5272.

- 49 S. Meyer, C. M. Orben, S. Demeshko, S. Dechert and F. Meyer, *Organometallics*, 2011, **30**, 6692–6702.
- 50 Y. Liu, T. Harlang, S. E. Canton, P. Chábera, K. Suárez-Alcántara, A. Fleckhaus, D. A. Vithanage, E. Göransson, A. Corani and R. Lomoth, *Chem. Commun.*, 2013, **49**, 6412–6414.
- 51 S. Meyer, I. Klawitter, S. Demeshko, E. Bill and F. Meyer, *Am. Ethnol.*, 2013, **125**, 935–939.
- 52 C. Kupper, A. Schober, S. Demeshko, M. Bergner and F. Meyer, *Inorg. Chem.*, 2015, **54**, 3096–3098.
- 53 F. Allen, *Acta Crystallogr., Sect. B: Struct. Sci.*, 2002, **58**, 380–388.
- 54 N. Lu, X. Lan, C. Miao and P. Qian, *Int. J. Quantum Chem.*, 2020, **120**, e26340.
- 55 Z. Lu, S. A. Cramer and D. M. Jenkins, *Chem. Sci.*, 2012, **3**, 3081–3087.
- 56 R. S. Coleman and J.-S. Kong, *J. Am. Chem. Soc.*, 1998, **120**, 3538–3539.
- 57 C. Tubaro, A. Biffis, R. Gava, E. Scattolin, A. Volpe, M. Basato, M. M. Díaz-Requejo and P. J. Perez, *Eur. J. Org. Chem.*, 2012, **2012**, 1367–1372.
- 58 F. Cavani and J. H. Teles, *ChemSusChem*, 2009, **2**, 508–534.
- 59 S. A. Hauser, M. Cokoja and F. E. Kühn, *Catal. Sci. Technol.*, 2013, **3**, 552–561.
- 60 V. Russo, R. Tesser, E. Santacesaria and M. Di Serio, *Ind. Eng. Chem. Res.*, 2013, **52**, 1168–1178.
- 61 K. A. Jørgensen, *Chem. Rev.*, 1989, **89**, 431–458.
- 62 D. I. Metelitsa, *Russ. Chem. Rev.*, 1972, **41**, 807.
- 63 T. A. Nijhuis, M. Makkee, J. A. Moulijn and B. M. Weckhuysen, *Ind. Eng. Chem. Res.*, 2006, **45**, 3447–3459.
- 64 Q.-H. Xia, H.-Q. Ge, C.-P. Ye, Z.-M. Liu and K.-X. Su, *Chem. Rev.*, 2005, **105**, 1603–1662.
- 65 G. Parshall, *J. Mol. Catal.*, 1978, **4**, 243–270.
- 66 B. Cornils, W. A. Herrmann, J.-H. Xu and H.-W. Zanthoff, *Catalysis from A to Z: a concise encyclopedia*, John Wiley & Sons, 2020.
- 67 J. W. Kück, M. R. Anneser, B. Hofmann, A. Pöthig, M. Cokoja and F. E. Kühn, *ChemSusChem*, 2015, **8**, 4056–4063.
- 68 L. Que and W. B. Tolman, *Nature*, 2008, **455**, 333–340.
- 69 Y. Feng, J. England and L. Que Jr, *ACS Catal.*, 2011, **1**, 1035–1042.
- 70 K. Chen, M. Costas, J. Kim, A. K. Tipton and L. Que, *J. Am. Chem. Soc.*, 2002, **124**, 3026–3035.
- 71 A. R. McDonald and L. Que Jr, *Coord. Chem. Rev.*, 2013, **257**, 414–428.
- 72 D. Y. Kim, Y. J. Choi, H. Y. Park, C. U. Joung, K. O. Koh, J. Y. Mang and K.-Y. Jung, *Synth. Commun.*, 2003, **33**, 435–443.
- 73 B. Bahramian, V. Mirkhani, M. Moghadam and S. Tangestaninejad, *Catal. Commun.*, 2006, **7**, 289–296.
- 74 L. Hadian-Dehkordi and H. Hosseini-Monfared, *Green Chem.*, 2016, **18**, 497–507.
- 75 A. Lindhorst, S. Haslinger and F. E. Kühn, *Chem. Commun.*, 2015, **51**, 17193–17212.
- 76 J. W. Kück, A. Raba, I. I. Markovits, M. Cokoja and F. E. Kühn, *ChemCatChem*, 2014, **6**, 1882–1886.
- 77 J. F. Schlagintweit, F. Dyckhoff, L. Nguyen, C. H. Jakob, R. M. Reich and F. E. Kühn, *J. Catal.*, 2020, **383**, 144–152.
- 78 M. A. Bernd, F. Dyckhoff, B. J. Hofmann, A. D. Böth, J. F. Schlagintweit, J. Oberkofler, R. M. Reich and F. E. Kühn, *J. Catal.*, 2020, **391**, 548–561.
- 79 F. Dyckhoff, J. F. Schlagintweit, R. M. Reich and F. E. Kühn, *Catal. Sci. Technol.*, 2020, **10**, 3532–3536.
- 80 P. Altmann, M. Cokoja and F. E. Kühn, *Eur. J. Inorg. Chem.*, 2012, **2012**, 3235–3239.
- 81 A. Schmidt, N. Grover, T. K. Zimmermann, L. Graser, M. Cokoja, A. Pöthig and F. E. Kühn, *J. Catal.*, 2014, **319**, 119–126.
- 82 A. Raba, M. Cokoja, S. Ewald, K. Riener, E. Herdtweck, A. Pöthig, W. A. Herrmann and F. E. Kühn, *Organometallics*, 2012, **31**, 2793–2800.
- 83 C. Walling and R. A. Johnson, *J. Am. Chem. Soc.*, 1975, **97**, 363–367.
- 84 F. Haber and J. Weiss, *Proc. R. Soc. London, Ser. A*, 1934, **147**, 332–351.
- 85 B. Meunier, S. P. De Visser and S. Shaik, *Chem. Rev.*, 2004, **104**, 3947–3980.
- 86 J.-U. Rohde, J.-H. In, M. H. Lim, W. W. Brennessel, M. R. Bukowski, A. Stubna, E. Münck, W. Nam and L. Que, *Science*, 2003, **299**, 1037–1039.
- 87 W. N. Oloo, A. J. Fielding and L. Que Jr, *J. Am. Chem. Soc.*, 2013, **135**, 6438–6441.
- 88 I. Prat, J. S. Mathieson, M. Güell, X. Ribas, J. M. Luis, L. Cronin and M. Costas, *Nat. Chem.*, 2011, **3**, 788.
- 89 Y. Yoshida and G. Langouche, *Mössbauer spectroscopy*, Springer, Berlin Heidelberg, 2013.
- 90 S. R. Iyer, M. M. Javadi, Y. Feng, M. Y. Hyun, W. N. Oloo, C. Kim and L. Que, *Chem. Commun.*, 2014, **50**, 13777–13780.
- 91 M. R. Anneser, S. Haslinger, A. Pöthig, M. Cokoja, J.-M. Basset and F. E. Kühn, *Inorg. Chem.*, 2015, **54**, 3797–3804.
- 92 C. Cordes, M. Morganti, I. Klawitter, C. Schremmer, S. Dechert and F. Meyer, *Angew. Chem., Int. Ed.*, 2019, **58**, 10855–10858.
- 93 L. Gómez, I. Garcia-Bosch, A. Company, J. Benet-Buchholz, A. Polo, X. Sala, X. Ribas and M. Costas, *Angew. Chem., Int. Ed.*, 2009, **48**, 5720–5723.
- 94 N. A. Vermeulen, M. S. Chen and M. C. White, *Tetrahedron*, 2009, **65**, 3078–3084.
- 95 T. P. Schlachta, J. F. Schlagintweit, M. R. Anneser, E.-M. H. Esslinger, M. Muhr, S. Haslinger and F. E. Kühn, *Inorg. Chim. Acta*, 2021, **518**, 120228.
- 96 E.-M. H. J. Esslinger, J. F. Schlagintweit, G. G. Zámbo, A. M. Imhof, R. M. Reich and F. E. Kühn, *Asian J. Org. Chem.*, 2021, **10**, 2654–2662.
- 97 S. Haslinger, A. Lindhorst, J. Kück, M. Cokoja, A. Pöthig and F. Kühn, *RSC Adv.*, 2015, **5**, 85486–85493.
- 98 J. F. Schlagintweit, C. Hintermeier, M. R. Anneser, E. M. H. Esslinger, S. Haslinger and F. E. Kühn, *Chem. – Asian J.*, 2020, **15**, 1896–1902.
- 99 R. Mas-Ballesté, M. Costas, T. Van Den Berg and L. Que Jr, *Chem. – Eur. J.*, 2006, **12**, 7489–7500.
- 100 Y. Zhang, B. Liu, H. Wu and W. Chen, *Chin. Sci. Bull.*, 2012, **57**, 2368–2376.

- 101 F. Dyckhoff, J. F. Schlagintweit, M. A. Bernd, C. H. Jakob, T. P. Schlachta, B. J. Hofmann, R. M. Reich and F. E. Kühn, *Catal. Sci. Technol.*, 2021, **11**, 795–799.
- 102 D. A. Alonso, C. Nájera, I. M. Pastor and M. Yus, *Chem. – Eur. J.*, 2010, **16**, 5274–5284.
- 103 Y. Qin, L. Zhu and S. Luo, *Chem. Rev.*, 2017, **117**, 9433–9520.
- 104 J. Wencel-Delord and F. Glorius, *Nat. Chem.*, 2013, **5**, 369.
- 105 C. Hammond, S. Conrad and I. Hermans, *ChemSusChem*, 2012, **5**, 1668–1686.
- 106 M. Sun, J. Zhang, P. Putaj, V. Caps, F. D. R. Lefebvre, J. Pelletier and J.-M. Basset, *Chem. Rev.*, 2014, **114**, 981–1019.
- 107 R. J. Schmidt, *Appl. Catal., A*, 2005, **280**, 89–103.
- 108 S. S. Stahl, J. A. Labinger and J. E. Bercaw, *Angew. Chem., Int. Ed.*, 1998, **37**, 2180–2192.
- 109 S. Hohloch, S. Kaiser, F. L. Duecker, A. Bolje, R. Maity, J. Košmrlj and B. Sarkar, *Dalton Trans.*, 2015, **44**, 686–693.
- 110 A. Raba, M. Cokoja, W. A. Herrmann and F. E. Kühn, *Chem. Commun.*, 2014, **50**, 11454–11457.
- 111 S. Haslinger, A. Raba, M. Cokoja, A. Pöthig and F. E. Kühn, *J. Catal.*, 2015, **331**, 147–153.
- 112 A. C. Lindhorst, J. Schütz, T. Netscher, W. Bonrath and F. E. Kühn, *Catal. Sci. Technol.*, 2017, **7**, 1902–1911.
- 113 A. C. Lindhorst, M. Drees, W. Bonrath, J. Schütz, T. Netscher and F. E. Kühn, *J. Catal.*, 2017, **352**, 599–605.
- 114 S. Sahu, L. R. Widger, M. G. Quesne, S. P. De Visser, H. Matsumura, P. Moëne-Loccoz, M. A. Siegler and D. P. Goldberg, *J. Am. Chem. Soc.*, 2013, **135**, 10590–10593.
- 115 A. Ansari, A. Kaushik and G. Rajaraman, *J. Am. Chem. Soc.*, 2013, **135**, 4235–4249.
- 116 A. Thibon, V. Jollet, C. Ribal, K. Sénéchal-David, L. Billon, A. B. Sorokin and F. Banse, *Chem. – Eur. J.*, 2012, **18**, 2715–2724.
- 117 O. V. Makhlynets and E. V. Rybak-Akimova, *Chem. – Eur. J.*, 2010, **16**, 13995–14006.
- 118 A. Thibon, J.-F. Bartoli, R. Guillot, J. Sainton, M. Martinho, D. Mansuy and F. Banse, *J. Mol. Catal. A: Chem.*, 2008, **287**, 115–120.
- 119 M. S. Chen and M. C. White, *Science*, 2007, **318**, 783–787.
- 120 E. P. Talsi and K. P. Bryliakov, *Coord. Chem. Rev.*, 2012, **256**, 1418–1434.
- 121 J. Kaizer, E. J. Klinker, N. Y. Oh, J.-U. Rohde, W. J. Song, A. Stubna, J. Kim, E. Münck, W. Nam and L. Que, *J. Am. Chem. Soc.*, 2004, **126**, 472–473.
- 122 S. J. Blanksby and G. B. Ellison, *Acc. Chem. Res.*, 2003, **36**, 255–263.
- 123 S. Haslinger, J. W. Kück, E. M. Hahn, M. Cokoja, A. Pöthig, J.-M. Basset and F. E. Kühn, *Inorg. Chem.*, 2014, **53**, 11573–11583.
- 124 K. Haav, J. Saame, A. Kütt and I. Leito, *Eur. J. Org. Chem.*, 2012, **2012**, 2167–2172.
- 125 G. B. Shulpin, D. Attanasio and L. Súber, *J. Catal.*, 1993, **142**, 147–152.
- 126 A. E. Shilov and G. B. Shul'pin, *Chem. Rev.*, 1997, **97**, 2879–2932.
- 127 G. B. Shul'pin, *J. Mol. Catal. A: Chem.*, 2002, **189**, 39–66.
- 128 K. Chen and L. Que, *J. Am. Chem. Soc.*, 2001, **123**, 6327–6337.
- 129 A. Company, L. Gómez, X. Fontrodona, X. Ribas and M. Costas, *Chem. – Eur. J.*, 2008, **14**, 5727–5731.
- 130 G. Olivo, O. Lanzalunga, L. Mandolini and S. Di Stefano, *J. Org. Chem.*, 2013, **78**, 11508–11512.
- 131 Y. Wang, T. Zhang, B. Li, S. Jiang and L. Sheng, *RSC Adv.*, 2015, **5**, 29022–29031.
- 132 X. Wang, T. Zhang, Q. Yang, S. Jiang and B. Li, *Eur. J. Inorg. Chem.*, 2015, **2015**, 817–825.
- 133 T. Nishiura, A. Takabatake, M. Okutsu, J. Nakazawa and S. Hikichi, *Dalton Trans.*, 2019, **48**, 2564–2568.
- 134 T. Nishiura, T. Uramoto, Y. Takiyama, J. Nakazawa and S. Hikichi, *Molecules*, 2018, **23**, 1466.
- 135 J. Nakazawa, Y. Doi and S. Hikichi, *Mol. Catal.*, 2017, **443**, 14–24.
- 136 S. G. Mncube and M. D. Bala, *Polyhedron*, 2019, **157**, 467–473.
- 137 T. Nagataki, Y. Tachi and S. Itoh, *Chem. Commun.*, 2006, 4016–4018.
- 138 T. Nagataki, K. Ishii, Y. Tachi and S. Itoh, *Dalton Trans.*, 2007, 1120–1128.
- 139 S. Hikichi, H. Okuda, Y. Ohzu and M. Akita, *Angew. Chem., Int. Ed.*, 2009, **48**, 188–191.
- 140 S. G. Mncube and M. D. Bala, *Transition Met. Chem.*, 2019, **44**, 145–151.
- 141 I. Garcia-Bosch and M. A. Siegler, *Angew. Chem., Int. Ed.*, 2016, **55**, 12873–12876.
- 142 J. L. Jeffrey and R. Sarpong, *Chem. Sci.*, 2013, **4**, 4092–4106.
- 143 B. Siminszky, L. Gavilano, S. W. Bowen and R. E. Dewey, *Proc. Natl. Acad. Sci. U. S. A.*, 2005, **102**, 14919–14924.
- 144 M. Lounasmaa and T. Tamminen, in *The Alkaloids: Chemistry and Pharmacology*, ed. G. A. Cordell, Academic Press, 1993, vol. 44, pp. 1–114.
- 145 A. R. Carroll, G. K. Pierens, G. Fechner, P. de Almeida Leone, A. Ngo, M. Simpson, E. Hyde, J. N. Hooper, S.-L. Boström and D. Musil, *J. Am. Chem. Soc.*, 2002, **124**, 13340–13341.
- 146 R. Gowda, S. V. Madhunapantula, O. F. Kuzu, A. Sharma and G. P. Robertson, *Mol. Cancer Ther.*, 2014, **13**, 1679–1689.
- 147 M.-L. Louillat and F. W. Patureau, *Chem. Soc. Rev.*, 2014, **43**, 901–910.
- 148 K. H. Chan, X. Guan, V. K. Y. Lo and C. M. Che, *Angew. Chem.*, 2014, **126**, 3026–3031.
- 149 K. P. Shing, Y. Liu, B. Cao, X. Y. Chang, T. You and C. M. Che, *Angew. Chem., Int. Ed.*, 2018, **57**, 11947–11951.
- 150 A. Ricci, *Amino group chemistry: from synthesis to the life sciences*, John Wiley & Sons, 2008.
- 151 J. F. Hartwig, *Acc. Chem. Res.*, 2008, **41**, 1534–1544.
- 152 M. A. Fernández-Rodríguez, Q. Shen and J. F. Hartwig, *Chem. – Eur. J.*, 2006, **12**, 7782–7796.
- 153 R. N. Baig and R. S. Varma, *Chem. Commun.*, 2012, **48**, 2582–2584.
- 154 X. Chen, X.-S. Hao, C. E. Goodhue and J.-Q. Yu, *J. Am. Chem. Soc.*, 2006, **128**, 6790–6791.

- 155 S.-I. Fukuzawa, E. Shimizu, Y. Atsuumi, M. Haga and K. Ogata, *Tetrahedron Lett.*, 2009, **50**, 2374–2376.
- 156 H. Inomata, A. Toh, T. Mitsui and S.-I. Fukuzawa, *Tetrahedron Lett.*, 2013, **54**, 4729–4731.
- 157 G. Tojo and M. I. Fernandez, *Oxidation of alcohols to aldehydes and ketones: a guide to current common practice*, Springer Science & Business Media, 2006.
- 158 R. A. Sheldon, I. W. Arends, G.-J. Ten Brink and A. Dijkstra, *Acc. Chem. Res.*, 2002, **35**, 774–781.
- 159 B.-Z. Zhan and A. Thompson, *Tetrahedron*, 2004, **13**, 2917–2935.
- 160 T. F. Blackburn and J. Schwartz, *J. Chem. Soc., Chem. Commun.*, 1977, 157–158.
- 161 J. Muzart, *Tetrahedron*, 2003, **59**, 5789–5816.
- 162 B.-Z. Zhan, M. A. White, T.-K. Sham, J. A. Pincock, R. J. Doucet, K. R. Rao, K. N. Robertson and T. S. Cameron, *J. Am. Chem. Soc.*, 2003, **125**, 2195–2199.
- 163 X. Liu, Q. Xia, Y. Zhang, C. Chen and W. Chen, *J. Org. Chem.*, 2013, **78**, 8531–8536.
- 164 L.-W. Zhan, L. Han, P. Xing and B. Jiang, *Org. Lett.*, 2015, **17**, 5990–5993.
- 165 P. D. Pham, P. Bertus and S. Legoupy, *Chem. Commun.*, 2009, 6207–6209.
- 166 J.-Q. Li and P. G. Andersson, *Chem. Commun.*, 2013, **49**, 6131–6133.
- 167 M. F. Pinto, B. D. P. Cardoso, S. Barroso, A. M. Martins and B. Royo, *Dalton Trans.*, 2016, **45**, 13541–13546.
- 168 C. Berini, O. H. Winkelmann, J. Otten, D. A. Vicic and O. Navarro, *Chem. – Eur. J.*, 2010, **16**, 6857–6860.
- 169 A. Prakasham and P. Ghosh, *Inorg. Chim. Acta*, 2015, **431**, 61–100.
- 170 V. Ritleng, M. Henrion and M. J. Chetcuti, *ACS Catal.*, 2016, **6**, 890–906.
- 171 F. P. Malan, E. Singleton, B. W. Bulling, I. Cukrowski, P. H. van Rooyen and M. Landman, *Mol. Catal.*, 2017, **432**, 47–56.
- 172 B. Landers, C. Berini, C. Wang and O. Navarro, *J. Org. Chem.*, 2011, **76**, 1390–1397.
- 173 E. M. McGarrigle and D. G. Gilheany, *Chem. Rev.*, 2005, **105**, 1563–1602.
- 174 M. F. Pinto, M. Olivares, Á. Vivancos, G. Guisado-Barríos, M. Albrecht and B. Royo, *Catal. Sci. Technol.*, 2019, **9**, 2421–2425.
- 175 Z.-Z. Zhou, M. Liu and C.-J. Li, *ACS Catal.*, 2017, **7**, 3344–3348.
- 176 M. Costas, M. P. Mehn, M. P. Jensen and L. Que, *Chem. Rev.*, 2004, **104**, 939–986.
- 177 H. Chen, M. Ikeda-Saito and S. Shaik, *J. Am. Chem. Soc.*, 2008, **130**, 14778–14790.
- 178 E. I. Solomon, D. E. Heppner, E. M. Johnston, J. W. Ginsbach, J. Cirera, M. Qayyum, M. T. Kieber-Emmons, C. H. Kjaergaard, R. G. Hadt and L. Tian, *Chem. Rev.*, 2014, **114**, 3659–3853.
- 179 L. Pauling and C. D. Coryell, *Proc. Natl. Acad. Sci. U. S. A.*, 1936, **22**, 210–216.
- 180 Z. Shi, C. Zhang, C. Tang and N. Jiao, *Chem. Soc. Rev.*, 2012, **41**, 3381–3430.
- 181 M. Metz and E. I. Solomon, *J. Am. Chem. Soc.*, 2001, **123**, 4938–4950.
- 182 S. Kal, S. Xu and L. Que Jr, *Angew. Chem., Int. Ed.*, 2020, **59**, 7332–7349.
- 183 W. N. Oloo, R. Banerjee, J. D. Lipscomb and L. Que Jr, *J. Am. Chem. Soc.*, 2017, **139**, 17313–17326.
- 184 A. L. Linsebigler, G. Lu and J. T. Yates Jr, *Chem. Rev.*, 1995, **95**, 735–758.
- 185 X. Hu, I. Castro-Rodriguez and K. Meyer, *J. Am. Chem. Soc.*, 2004, **126**, 13464–13473.
- 186 S. Dürr, B. Zarzycki, D. Ertler, I. Ivanović-Burmazović and U. Radius, *Organometallics*, 2012, **31**, 1730–1742.
- 187 J. F. Schlagintweit, P. J. Altmann, A. D. Böth, B. J. Hofmann, C. Jandl, C. Kaußler, L. Nguyen, R. M. Reich, A. Pöthig and F. E. Kühn, *Chem. – Eur. J.*, 2021, **27**, 1311–1315.
- 188 M. R. Anneser, S. Haslinger, A. Pöthig, M. Cokoja, V. D'Elia, M. P. Högerl, J.-M. Basset and F. E. Kühn, *Dalton Trans.*, 2016, **45**, 6449–6455.
- 189 T. P. Schlachta, M. R. Anneser, J. F. Schlagintweit, C. H. Jakob, C. Hintermeier, A. D. Böth, S. Haslinger, R. M. Reich and F. E. Kühn, *Chem. Commun.*, 2021, **57**, 6644–6647.
- 190 S. K. Mandal, A. Das and S. Chakraborty, *Chem. – Asian J.*, 2021, **16**(16), 2257–2260.
- 191 B. R. Dible and M. S. Sigman, *J. Am. Chem. Soc.*, 2003, **125**, 872–873.
- 192 B. R. Dible and M. S. Sigman, *Inorg. Chem.*, 2006, **45**, 8430–8441.
- 193 R. C. Poulten, I. López, A. Llobet, M. F. Mahon and M. K. Whittlesey, *Inorg. Chem.*, 2014, **53**, 7160–7169.
- 194 B. R. Dible, M. S. Sigman and A. M. Arif, *Inorg. Chem.*, 2005, **44**, 3774–3776.



Cite this: *Dalton Trans.*, 2022, **51**, 13591

Received 5th August 2022,
Accepted 23rd August 2022

DOI: 10.1039/d2dt02561b

rsc.li/dalton

The first macrocyclic abnormally coordinating tetra-1,2,3-triazole-5-ylidene iron complex: a promising candidate for olefin epoxidation†

Greta G. Zámbo,  Johannes Mayr, Michael J. Sauer, Tim P. Schlachta, 
Robert M. Reich  and Fritz E. Kühn *

The first macrocyclic and abnormally coordinating, mesoionic *N*-heterocyclic carbene iron complex has been synthesised and characterised via ESI-MS, EA, SC-XRD, CV, NMR and UV/Vis spectroscopy. ¹³C-NMR spectroscopy and CV measurements indicate a strong σ -donor ability of the carbene moieties, suggesting an efficient catalytic activity of the iron complex in oxidation reactions. Initial tests in the epoxidation of *cis*-cyclooctene as a model substrate confirm this assumption.

Inspired by the activity of iron metalloenzymes,¹ several non-heme macrocyclic tetradentate iron complexes have been designed over the last decade,^{2,3} mimicking, *inter alia*, their capability of oxidation of hydrocarbons as well as for oxygen transport.^{2–4} In this context, metal supporting *N*-heterocyclic carbenes (NHC) have received attention as ligands stabilising high oxidation state transition metals.⁵ Accordingly, iron tetra (NHC) complexes have been successfully applied in oxidation catalysis,^{2–4,6} including aziridination, epoxidation and C–H activation. Based on the extensive work of Que *et al.*^{1,7–9} and Costas *et al.*^{7,10} high valent iron intermediates are considered to be the active species in these reactions. A remarkable activity in the catalytic oxidation of olefins is displayed by an imidazole based cyclic tetra(NHC) iron complex with turnover frequencies (TOFs) up to 410 000 h^{–1} (Fig. 1, middle). However, limited catalyst stability (TON = 1200) overshadows its high activity.¹¹ Tuning of its electronic properties by insertion of substituents varying the NHC backbone affects not only catalyst stability but also its activity, emphasising once more the role of ligand design.¹² Pioneering work on bio-inspired non-heme macrocyclic iron tetra(NHCs) has been done by

Jenkins *et al.*^{13–18}, Meyer *et al.*^{19–21} and our group.^{12,22–26} During these studies several bridged tetra(imidazole-2-ylidene) iron complexes have been prepared and characterised (Fig. 1, left).

Abnormally coordinating NHC moieties (aNHCs) are considered to be stronger σ -donors and post-modification of the ligand macrocycle is possible.^{27–29} However, all macrocyclic tetra(NHC) iron complexes reported so far are based on normally coordinating imidazole-2-ylidenes, where the ligand modification occurs in the very first synthetic step. On the other hand, application of aNHCs as ligands in transition metal catalysis proved to be a powerful tool for tuning the electronic nature of the central metal and improving the catalytic performance.^{29,30} In this context, 1,2,3-triazol-5-ylidenes (trz) come into mind, representing a promising subclass of aNHCs with easy synthetic access *via* click chemistry.^{27,31} To date, only a rather limited number of trz-iron complexes is known. Besides a homoleptic C,O-chelating trz-iron complex,³² three different general complex scaffolds have been described so far, where the ligands have an open chain shape: (a) cyclopentadienyl iron half sandwich complexes bearing one trz ligand,^{33–35} (b) hetero- and homoleptic iron complexes bearing two or three bis(trz) in octahedral fashion^{36–38} and (c) a class that contains one or two pincer-type bis(trz) entities, bridged *via* pyridine, that latter acting as additional *N*-donor.^{39,40}

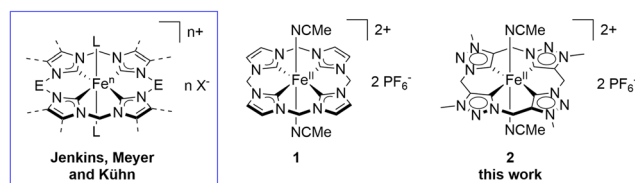


Fig. 1 General framework of macrocyclic tetra(NHC) iron complexes reported by Jenkins, Meyer and Kühn (left) with E = CH₂, C₂H₄ or BMe₂, L = ligand, n = 2 or 3, X = PF₆ or OTf and this work (**2**, right), and the chemical structure of the most active (pre-)catalyst Fe^{II}[cCCCC]_{im} **1** in the epoxidation of *cis*-cyclooctene with H₂O₂ (middle).

Molecular Catalysis, Department of Chemistry and Catalysis Research Centre, Technische Universität München, Lichtenbergstr. 4, 85784 Garching bei München, Germany. E-mail: fritz.kuehn@ch.tum.de

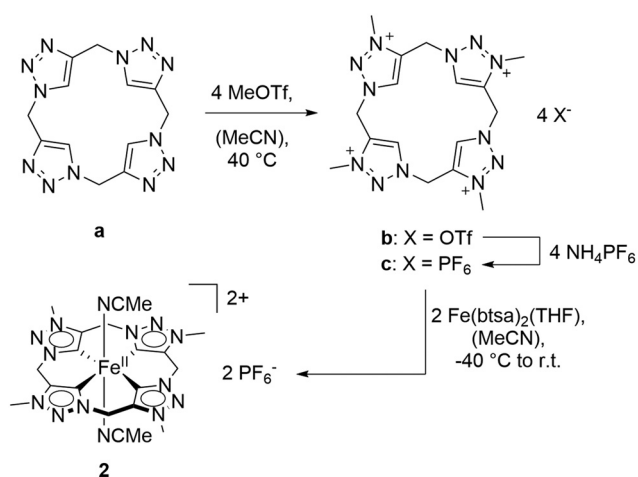
† Electronic supplementary information (ESI) available: Experimental details, analytical methods, crystallographic data, ORTEP-style structure of **1**, ¹H-, ¹³C-, ³¹P-, ¹⁹F-NMR-spectra and catalytic procedure. CCDC 2184662 and 2184663. For ESI and crystallographic data in CIF or other electronic format see DOI: <https://doi.org/10.1039/d2dt02561b>

In this work, the synthesis and characterisation of the – to the best of our knowledge – first macrocyclic aNHC iron complex is reported (Fig. 1, right). A synthetic strategy, differing from the literature known calix[4]1,2,3-triazole,⁴¹ proceeding *via* repeated click reactions and azidations, is described. Subsequent alkylation with MeOTf results in the formation of the cyclic tetra(trz) ligand precursor. *In situ* deprotonation and complexation yields the methyl bridged tetra(aNHC) iron complex $\text{Fe}^{\text{II}}[\text{cCCCC}]_{\text{trz}}$ **2**. Application of **2** for initial catalytic investigations demonstrates its activity in the epoxidation of *cis*-cyclooctene with hydrogen peroxide.

The modified synthesis of methylene bridged calix[4]1,2,3-triazole is based on the copper(i) catalysed click reaction of a terminal alkyne with an azide, introduced by Sharpless *et al.*⁴² and Meldal *et al.*⁴³ to form 1,4-substituted 1,2,3-triazoles.³¹ Starting from propargyl bromide the ligand synthesis includes eleven steps (ESI, Scheme S1[†]). First, the terminal alkyne has to be protected with a triisopropylsilyl (TIPS) group to avoid an undesired second click reaction in the following steps. Afterwards, the bromide is replaced by an azide group. Then, a click reaction with propargyl alcohol occurs initially, followed by an Appel reaction⁴⁴ of the alcohol with PPh_3 and CBr_4 and an *in situ* azidation with NaN_3 . These steps are subsequently repeated for two more times until three triazole moieties are formed within the chain. The cyclisation occurs *via* an *in situ* deprotection and an intramolecular click reaction. Post modification of the macrocycle by alkylation of the N3 positions with an excess of methyl triflate yields calix[4]3-methyl-1,2,3-triazolium triflate **b** (72% isolated yield, Scheme 1, for SC-XRD data see ESI[†]). Methylation with significant less reactive methyl iodide in DMF, which has been applied in previous synthetic approaches for the alkylation of 1,2,3-triazoles^{34,45} does not result in any product formation, even at temperatures of up to 70 °C. Subsequently, salt metathesis of **b** with NH_4PF_6 quantitatively yields the hexafluorophosphate salt trz precursor **c** (Scheme 1). Recently, a second salt analogue of **b** and **c** with

BF_6^- -anion was described and synthesised *via* grinding with a vibration ball mill of **a** with the corresponding *Meerwein* salt.⁴⁶

Iron bis(trimethylsilyl)amide (btsa, $\text{N}(\text{SiMe}_3)_2$) THF adduct $\text{Fe}(\text{btsa})_2(\text{THF})$ proved to be a viable agent to form iron(II) complexes.^{19,22} Deprotonation of 1.00 eq. alkylated calix[4]1,2,3-triazole salt **c** by the internal base of 2.00 eq. $\text{Fe}(\text{btsa})_2(\text{THF})$ under formation of the free carbene in immediate metal vicinity gives $\text{Fe}^{\text{II}}[\text{cCCCC}]_{\text{trz}}$ complex **2** in 78% yield (Scheme 1). During the synthesis of **1**, $[\text{Fe}(\text{MeCN})_6](\text{PF}_6)_2$ is formed as a by-product, due to the excess of $\text{Fe}(\text{btsa})_2(\text{THF})$ in MeCN.²² Under optimal conditions, complex **2** precipitates directly as orange solid, which makes further purification *via e.g.* column chromatography or fractional precipitation unnecessary. ^{13}C -NMR spectroscopy shows the coordinating carbene carbon signals at $\delta(^{13}\text{C}) = 190$ ppm (ESI, Fig. S32[†]). The carbene carbon signal is significantly high field shifted, compared to imidazole-2-ylidene iron complexes ($\delta(^{13}\text{C})_{\text{NHC}} = 205\text{--}194$ ppm)^{12,13,15,20,22,47} and especially its imidazole counterpart **1** $\text{Fe}[\text{cCCCC}]_{\text{im}}$, where the carbene signals appear at $\delta(^{13}\text{C}) = 205$ ppm.²² The observed ^{13}C shifts indicates a high electron density environment at the iron centre, as expected for a strong σ -donation. Single crystals of **2** suitable for SC-XRD were obtained by the slow diffusion of diethyl ether into a solution of **2** in acetonitrile. The complex exhibits a distorted octahedral coordination sphere around the iron (Fig. 2). The aNHC ligand is ideal square-planar, differing from the previously characterised macrocyclic tetra(NHC) iron complexes, which are showing a saddle-distorted conformation for the NHC ligand (ESI, Fig. S3[†]). Axial positions are occupied by two acetonitrile ligands. The $\text{Fe}\text{--}\text{C}_{\text{NHC}}$ distances of **2** with 1.925(2) and 1.931(2) Å are slightly longer than observed for the saddle-distorted NHC iron complexes. Selected bond length and angles of complexes **1** and **2** are compared in Table S3 (ESI[†]).



Scheme 1 Synthesis of the calix[4]1,2,3-triazolium salts **b** and **c** and subsequent iron complexation to complex **2**.

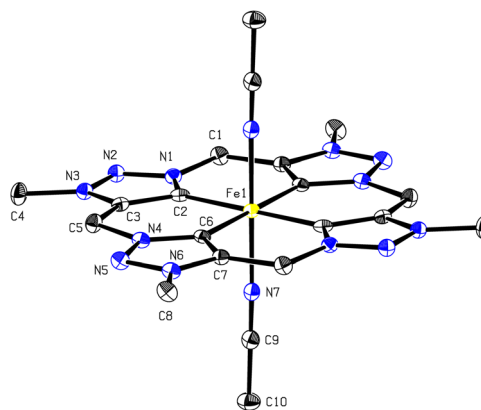


Fig. 2 ORTEP-style representation of the cationic fragment of compound **2**. Hydrogen atoms and PF_6^- -anions, as well as a co-crystallised MeCN molecule are omitted for clarity and thermal ellipsoids are shown at a 50% probability level. Due to the inversion centre only half of the atoms are labelled. Selected bond lengths (Å) and angles (°): $\text{Fe1}\text{--}\text{C2}$ 1.925(2), $\text{Fe1}\text{--}\text{C6}$ 1.931(2), $\text{Fe1}\text{--}\text{N7}$ 1.9247(17), $\text{N7}\text{--}\text{Fe1}\text{--}\text{N7}^*$ 180.00(0), $\text{C2}\text{--}\text{Fe1}\text{--}\text{C2}^*$ 180.00(0), $\text{C6}\text{--}\text{Fe1}\text{--}\text{C6}^*$ 180.00(0), $\text{C2}\text{--}\text{Fe1}\text{--}\text{C6}$ 90.15(8), $\text{C2}\text{--}\text{Fe1}\text{--}\text{C6}^*$ 89.85(8). Symmetry code: $-x + 1, -y + 2, -z + 1$.

To get further insights of the electronic structure of $\text{Fe}[\text{cCCCC}]_{\text{trz}}$ complex **2**, cyclic voltammetry (CV) measurements were performed in acetonitrile solution with $[\text{N}(n\text{-Bu})_4]\text{PF}_6$ as the supporting electrolyte. The cyclic voltammogram shows a fully reversible one-electron redox process, assigned to the $\text{Fe}^{\text{II}}/\text{Fe}^{\text{III}}$ redox couple (ESI, Fig. S4†). The half-cell potential is $E_{1/2} = -0.34$ V ($\text{Fe}^{\text{II}}/\text{Fe}^{\text{III}}$) and oxidation/reduction potentials are determined to be $E_{\text{ox}} = -0.31$ V and $E_{\text{red}} = -0.38$ V. The insertion of the aNHC ligand significantly decreases the half-cell potential compared to similar macrocyclic imidazol-2-ylidene iron complexes with $E_{1/2} = 0.00\text{--}0.44$ V vs. Fc/Fc^+ (ref. 12, 15, 17, 28 and 47) (e.g. $E_{1/2} = 0.15$ V vs. Fc/Fc^+ for **1**),²³ indicating an easier oxidation of Fe^{II} to Fe^{III} . As defined by the *Lever's Electronic Parameter* (LEP),⁴⁸ the stronger the donor capability of a ligand, the lower the resulting $E_{1/2}$ values,⁴⁹ due to the high electron density at the iron centre induced by the strong σ -donor properties of the aNHC. These results suggest the applicability of **2** as suitable pre-catalyst for oxidation reactions, as recent investigation on the catalytic mechanism of iron complexes in oxidation catalysis, such as epoxidation and C–H activation, indicate an one electron oxidation of Fe^{II} to Fe^{III} as prerequisite to form the active catalyst.^{11,50} UV/Vis spectrometry of complex **2** was performed in acetonitrile at 20 °C. Two absorption bands are visible at 405 nm and 480 nm (Fig. 3). In order to gain information about the formation of iron(III), one equivalent of thianthrenyl hexafluorophosphate (ThPF_6) was added to the solution of complex **2** in acetonitrile under inert conditions. ThPF_6 as one-electron oxidising agent has been successfully used for the selective oxidation of iron(II) to iron(III) complexes.^{23,51,52} The measured UV/Vis spectrum shows the disappearance of the two absorption bands by generating a new band around 431 nm, indicating the occurrence of an oxidation process (Fig. 3).

Building on the characteristic findings and electronic properties, complex **2** is examined as pre-catalyst in the epoxidation of *cis*-cyclooctene, being widely applied as model substrate using H_2O_2 as oxidising agent. First time-dependant catalytic studies using standard conditions (269 μmol *cis*-

cyclooctene, 403 μmol H_2O_2) and 0.50 mol% of **2** have been performed at variable temperatures in MeCN (Fig. 4, left). No side product formation occurs with an epoxide selectivity of >99%. At 20 °C, maximal conversion of 37% is reached after 30 s. Lowering the temperature enhances the catalyst stability, as a consequence of a longer catalyst lifetime.²³ After 10 min the conversion increases from 49% for 10 °C over 72% for 0 °C to 89% for –10 °C. In previous catalytic studies strong Lewis acids like $\text{Sc}(\text{OTf})_3$ are utilised in the oxidation process with $\text{Fe}^{\text{II}}[\text{cCCCC}]_{\text{im}}$ complex **1** as catalyst, resulting in a significantly improved performance.¹¹ Sc^{3+} initiates the *in situ* oxidation of Fe^{II} complex to the active Fe^{III} catalyst.¹¹ Although an epoxidation mechanism with iron carbenes as catalyst precursors is not yet established beyond any doubt, it can be assumed, based on observations of related catalysts, that heterolytic O–O bond cleavage of a $\text{Fe}^{\text{III}}\text{--OOH}$ species, which is initially formed upon reaction of the Fe^{III} catalyst with H_2O_2 , is facilitated by $\text{Sc}(\text{OTf})_3$, resulting in the formation of an active iron(v) oxo species.^{1,7–10} Furthermore, the addition of Lewis acids to the catalytic reaction proved to reactivate μ_2 -oxodiiron(III) $\text{Fe}^{\text{III}}\text{--O--Fe}^{\text{III}}$ species, which has been identified as important deactivation product.^{11,47} With the addition of 0.10 eq. $\text{Sc}(\text{OTf})_3$ to the reaction under standard conditions at 20 °C and 0.50 mol% of **2**, the reaction is completed after 30 min and a 97% conversion is reached with a cyclooctene oxide yield of 93% (Fig. 4). After 5 min the formation of side products starts, including 1,2-cyclooctandiol, decreasing the selectivity from initial >99% to 96%. The 1,2-cyclooctandiol yield remains at 2%. The TOF has been determined after 10 s to be 41 000 h^{-1} , which is lower than that of its imidazole counterpart **1**, but in the range of the homogeneous laboratory benchmark catalyst methyltrioxorhenium(vII) (TOF < 40 000 h^{-1})⁵³ and the area of magnitude of some of the most active molybdenum based epoxidation complexes (TOF ca. 41 000 h^{-1}).⁵⁴

In summary, the first macrocyclic, aNHC iron complex $\text{Fe}^{\text{II}}[\text{cCCCC}]_{\text{trz}}$ was successfully synthesised. SC-XRD shows an octahedral geometry with the tetradentate ligand in an ideal square-planar coordination. As indicated by the carbene shifts in the ¹³C-spectra, as well as by its half-cell potential the complex displays a remarkably electron-rich iron centre, corre-

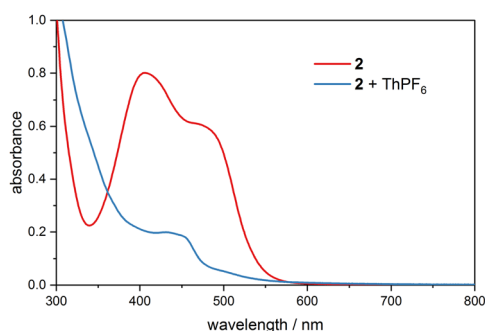


Fig. 3 UV/Vis spectrum of **2** (red); $c = 0.20$ mM, $T = 20$ °C in MeCN. Two absorption bands appear at 405 nm and 480 nm. Addition of 1.00 eq. ThPF_6 to the light orange solution results in a light yellow solution. The two absorption bands of **2** disappear and a new band around 431 nm occurs ($c = 0.2$ mM, $T = 20$ °C in MeCN).

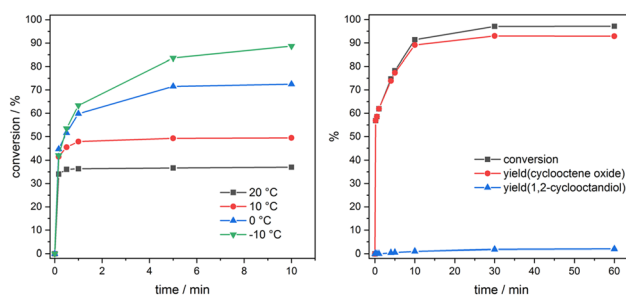


Fig. 4 Time-dependant epoxidation of *cis*-cyclooctene (403 μmol , 1.50 eq.), in MeCN using **2** as catalyst (1.35 μmol , 0.005 eq.), and H_2O_2 (403 μmol , 1.50 eq.) as oxidising agent at variable temperatures (left) and at 20 °C using $\text{Sc}(\text{OTf})_3$ (26.9 μmol , 0.10 eq.) as additive (right). Yields and conversions are determined by GC-FID.

lating to a high σ -donor strength of the aNHCs. CV measurements and UV/Vis experiments suggest the possible oxidation to the Fe^{III} derivative, which is crucial for the catalytic activity in oxidation reactions, including epoxidation and C–H activation. First epoxidation reactions applying **2** as catalyst show a substrate conversion up to 97% (TOF = 41 000 h⁻¹). As simple modification inserting different N3 substituents on the ligand after cyclisation is expected to be possible, this already highly suitable ligand can be modified to further tune its electronic and steric environment. The application of 1,2,3-triazol-5-ylidenes as ligands offers two major advantages over imidazole-2-ylidene iron complexes: (a) a significantly higher σ -donation of the NHC moieties and (b) post modification of the ligand, which is not possible for imidazole-2-ylidene ligand precursors, where the NHC moieties are defined within the very first synthetic step. This new ligand system opens great opportunities for the design of selective and stable (immobilisation) Fe^{II/III} metal complexes (e.g. for the (ep)oxidation of olefins). Further catalytic in-depth studies, as well as the synthetic modification of the macrocycle are currently ongoing in our laboratories.

Conflicts of interest

There are no conflicts to declare.

Acknowledgements

G. G. Z., M. J. S., and T. P. S. gratefully acknowledge support from TUM Graduate School.

References

- 1 A. J. Jasniewski and L. Que Jr., *Chem. Rev.*, 2018, **118**, 2554–2592.
- 2 S. M. Hölzl, P. J. Altmann, J. W. Kück and F. E. Kühn, *Coord. Chem. Rev.*, 2017, **352**, 517–536.
- 3 G. G. Zámbo, J. F. Schlagintweit, R. M. Reich and F. E. Kühn, *Catal. Sci. Technol.*, 2022, **12**, 4949–4961.
- 4 K. Riener, S. Haslinger, A. Raba, M. P. Högerl, M. Cokoja, W. A. Herrmann and F. E. Kühn, *Chem. Rev.*, 2014, **114**, 5215–5272.
- 5 M. N. Hopkinson, C. Richter, M. Schedler and F. Glorius, *Nature*, 2014, **510**, 485–496.
- 6 J. W. Kück, R. M. Reich and F. E. Kühn, *Chem. Rec.*, 2016, **16**, 349–364.
- 7 M. Borrell, E. Andris, R. Navrátil, J. Roithová and M. Costas, *Nat. Commun.*, 2019, **10**, 1–9.
- 8 X. Lu, X.-X. Li, Y.-M. Lee, Y. Jang, M. S. Seo, S. Hong, K.-B. Cho, S. Fukuzumi and W. Nam, *J. Am. Chem. Soc.*, 2020, **142**, 3891–3904.
- 9 S. Kal and L. Que Jr., *Angew. Chem., Int. Ed.*, 2019, **58**, 8484–8488.
- 10 K. Chen, M. Costas, J. Kim, A. K. Tipton and L. Que, *J. Am. Chem. Soc.*, 2002, **124**, 3026–3035.
- 11 F. Dyckhoff, J. F. Schlagintweit, R. M. Reich and F. E. Kühn, *Catal. Sci. Technol.*, 2020, **10**, 3532–3536.
- 12 M. A. Bernd, F. Dyckhoff, B. J. Hofmann, A. D. Böth, J. F. Schlagintweit, J. Oberkofler, R. M. Reich and F. E. Kühn, *J. Catal.*, 2020, **391**, 548–561.
- 13 M. R. Anneser, G. R. Elpitiya, X. B. Powers and D. M. Jenkins, *Organometallics*, 2019, **38**, 981–987.
- 14 J. F. DeJesus and D. M. Jenkins, *Chem. – Eur. J.*, 2020, **26**, 1429–1435.
- 15 S. A. Cramer and D. M. Jenkins, *J. Am. Chem. Soc.*, 2011, **133**, 19342–19345.
- 16 P. P. Chandrachud, H. M. Bass and D. M. Jenkins, *Organometallics*, 2016, **35**, 1652–1657.
- 17 K. M. Blatchford, C. J. Mize, S. Roy and D. M. Jenkins, *Dalton Trans.*, 2022, **51**, 6153–6156.
- 18 M. R. Anneser, G. R. Elpitiya, J. Townsend, E. J. Johnson, X. B. Powers, J. F. DeJesus, K. D. Vogiatzis and D. M. Jenkins, *Angew. Chem.*, 2019, **131**, 8199–8202.
- 19 S. Meyer, I. Klawitter, S. Demeshko, E. Bill and F. Meyer, *Angew. Chem.*, 2013, **125**, 935–939.
- 20 C. Schremmer, C. Cordes, I. Klawitter, M. Bergner, C. E. Schiewer, S. Dechert, S. Demeshko, M. John and F. Meyer, *Chem. – Eur. J.*, 2019, **25**, 3918–3929.
- 21 A. A. Massie, C. Schremmer, I. Ruter, S. Dechert, I. Siewert and F. Meyer, *ACS Catal.*, 2021, **11**, 3257–3267.
- 22 M. R. Anneser, S. Haslinger, A. Pöthig, M. Cokoja, J.-M. Basset and F. E. Kühn, *Inorg. Chem.*, 2015, **54**, 3797–3804.
- 23 J. W. Kück, M. R. Anneser, B. Hofmann, A. Pöthig, M. Cokoja and F. E. Kühn, *ChemSusChem*, 2015, **8**, 4056–4063.
- 24 T. P. Schlachta, J. F. Schlagintweit, M. R. Anneser, E.-M. H. Esslinger, M. Muhr, S. Haslinger and F. E. Kühn, *Inorg. Chim. Acta*, 2021, **518**, 120228.
- 25 J. F. Schlagintweit, C. Hintermeier, M. R. Anneser, E. M. H. Esslinger, S. Haslinger and F. E. Kühn, *Chem. – Asian J.*, 2020, **15**, 1896–1902.
- 26 M. R. Anneser, S. Haslinger, A. Pöthig, M. Cokoja, V. D'Elia, M. P. Högerl, J.-M. Basset and F. E. Kühn, *Dalton Trans.*, 2016, **45**, 6449–6455.
- 27 D. Schweinfurth, L. Hettmanczyk, L. Suntrup and B. Sarkar, *Z. Anorg. Allg. Chem.*, 2017, **643**, 554–584.
- 28 J. D. Crowley, A.-L. Lee and K. J. Kilpin, *Aust. J. Chem.*, 2011, **64**, 1118–1132.
- 29 O. Schuster, L. Yang, H. G. Raubenheimer and M. Albrecht, *Chem. Rev.*, 2009, **109**, 3445–3478.
- 30 R. H. Crabtree, *Coord. Chem. Rev.*, 2013, **257**, 755–766.
- 31 L. Liang and D. Astruc, *Coord. Chem. Rev.*, 2011, **255**, 2933–2945.
- 32 W. Stroek, M. Keilwerth, D. M. Pividori, K. Meyer and M. Albrecht, *J. Am. Chem. Soc.*, 2021, **143**, 20157–20165.
- 33 Q. Liang, K. Hayashi, K. Rabeda, J. L. Jimenez-Santiago and D. Song, *Organometallics*, 2020, **39**, 2320–2326.

- 34 P. V. Nylund, N. C. Ségaud and M. Albrecht, *Organometallics*, 2021, **40**, 1538–1550.
- 35 C. Johnson and M. Albrecht, *Organometallics*, 2017, **36**, 2902–2913.
- 36 Y. Liu, K. S. Kjær, L. A. Fredin, P. Chábera, T. Harlang, S. E. Canton, S. Lidin, J. Zhang, R. Lomoth and K. E. Bergquist, *Chem. – Eur. J.*, 2015, **21**, 3628–3639.
- 37 P. Chábera, K. S. Kjaer, O. Prakash, A. Honarfar, Y. Liu, L. A. Fredin, T. C. Harlang, S. Lidin, J. Uhlig and V. Sundström, *J. Phys. Chem. Lett.*, 2018, **9**, 459–463.
- 38 P. Chábera, Y. Liu, O. Prakash, E. Thyraug, A. E. Nahhas, A. Honarfar, S. Essén, L. A. Fredin, T. C. Harlang and K. S. Kjær, *Nature*, 2017, **543**, 695–699.
- 39 Y. Liu, P. Persson, V. Sundström and K. Wärnmark, *Acc. Chem. Res.*, 2016, **49**, 1477–1485.
- 40 H. Iwasaki, Y. Teshima, Y. Yamada, R. Ishikawa, Y. Koga and K. Matsubara, *Dalton Trans.*, 2016, **45**, 5713–5719.
- 41 I. Kim, K. C. Ko, W. R. Lee, J. Cho, J. H. Moon, D. Moon, A. Sharma, J. Y. Lee, J. S. Kim and S. Kim, *Org. Lett.*, 2017, **19**, 5509–5512.
- 42 V. V. Rostovtsev, L. G. Green, V. V. Fokin and K. B. Sharpless, *Angew. Chem.*, 2002, **114**, 2708–2711.
- 43 C. W. Tornøe, C. Christensen and M. Meldal, *J. Org. Chem.*, 2002, **67**, 3057–3064.
- 44 R. Appel, *Angew. Chem., Int. Ed. Engl.*, 1975, **14**, 801–811.
- 45 J. F. Schlagintweit, C. H. Jakob, N. L. Wilke, M. Ahrweiler, C. Frias, J. Frias, M. König, E.-M. H. Esslinger, F. Marques and J. F. Machado, *J. Med. Chem.*, 2021, **64**, 15747–15757.
- 46 J. Cho, J. Shin, M. Kang, P. Verwilt, C. Lim, H. Yoo, J. G. Kim, X. Zhang, C. S. Hong and J. S. Kim, *Chem. Commun.*, 2021, **57**, 12139–12142.
- 47 F. Dyckhoff, J. F. Schlagintweit, M. A. Bernd, C. H. Jakob, T. P. Schlachta, B. J. Hofmann, R. M. Reich and F. E. Kühn, *Catal. Sci. Technol.*, 2021, **11**, 795–799.
- 48 A. Lever, *Inorg. Chem.*, 1990, **29**, 1271–1285.
- 49 V. N. Nemykin, D. E. Nevonon, W. R. Osterloh, L. S. Ferch, L. A. Harrison, B. S. Marx and K. M. Kadish, *Inorg. Chem.*, 2021, **60**, 16626–16644.
- 50 S. Kal, S. Xu and L. Que Jr., *Angew. Chem., Int. Ed.*, 2020, **59**, 7332–7349.
- 51 J. M. Smith and J. R. Long, *Inorg. Chem.*, 2010, **49**, 11223–11230.
- 52 T. P. Schlachta, M. R. Anneser, J. F. Schlagintweit, C. H. Jakob, C. Hintermeier, A. D. Böth, S. Haslinger, R. M. Reich and F. E. Kühn, *Chem. Commun.*, 2021, **57**, 6644–6647.
- 53 P. Altmann, M. Cokoja and F. E. Kühn, *J. Organomet. Chem.*, 2012, **701**, 51–55.
- 54 A. Schmidt, N. Grover, T. K. Zimmermann, L. Graser, M. Cokoja, A. Pöthig and F. E. Kühn, *J. Catal.*, 2014, **319**, 119–126.



Tailoring activity and stability: Effects of electronic variations on iron-NHC epoxidation catalysts

Tim P. Schlachta^a, Greta G. Zámbo^a, Michael J. Sauer^a, Isabelle Rüter^b, Carla A. Hofer^a, Serhiy Demeshko^b, Franc Meyer^b, Fritz E. Kühn^{a,*}

^a Technical University of Munich, School of Natural Sciences, Department of Chemistry and Catalysis Research Center, Molecular Catalysis, Lichtenbergstraße 4, 85748 Garching, Germany

^b Georg-August-Universität Göttingen, Institut für Anorganische Chemie, Tammannstraße 4, 37077 Göttingen, Germany

ARTICLE INFO

Keywords:

Non-heme iron complexes
N-heterocyclic carbene
Epoxidation catalysis
Lewis acids
Electronic properties
Iron NHC complexes
Electronic fine-tuning of catalyst
Catalytic optimization
Tailoring catalytic properties

ABSTRACT

A comparative study of three iron(II) NHC epoxidation catalysts with different electronic properties is performed to gain more profound insight into the influence of electronic variations on catalytic performance. One iron complex contains a pyridyl-NHC ligand, the other two are prepared with a modified ligand counterpart. The complexes are comprehensively characterized by various methods including Mössbauer, SQUID and DFT. While a lower electron density at the iron atom can be associated with a decline in epoxidation activity, a more electron rich iron center does not necessarily correspond with higher activity, due to reduced catalyst stability. Addition of Lewis acids increases both activity and stability significantly and is more effective than temperature variations. All three epoxidation catalysts achieve high selectivity, with a maximum TOF of 24 500 h⁻¹ and TON of >700 for the unmodified complex. More nucleophilic alkenes promote higher activity and conversion.

1. Introduction

In nature, iron containing enzymes like cytochrome P450, facilitate the oxidation of various substrates under mild conditions with high activity and selectivity [1]. Aspired to mimic their reactivity, iron based complexes have been intensively studied in oxidation reactions. The relatively low price of iron in comparison to noble metals, as it is one of the most abundant elements in the Earth's crust, make iron complexes interesting candidates for applications in industrial catalysis, although the cost of the ligands may be considerable [2]. A potentially lower toxicity of iron is often also mentioned as another advantage of iron complexes. However, even though iron is an essential trace element, toxicity of catalysts depends on several factors, e.g. ligands and oxidation state, and cannot be assessed as generally as it is often attempted, particularly by laypersons or in popular science [2–4].

Previous research on bio-inspired iron catalysts featured N-donor ligands, like porphyrins or other non-heme ligands [5–12]. In catalytic epoxidations, the use of N-heterocyclic carbene (NHC) ligands has been shown to be superior to N-donor ligands [13–17], especially in terms of activity given in turnover frequency (TOF). A variety of NHC ligated Fe systems outperform one of the most active N-ligated iron catalysts (25

200 h⁻¹) [18] as well as other organometallic transition metal benchmark catalysts, e.g. based on Re (up to ca. 40 000 h⁻¹) [13] or Mo (up to > 50 000 h⁻¹) [19]. A TOF of > 400 000 h⁻¹ and a turnover number (TON) of ca. 1200 were reached at room temperature in the presence of Lewis acid Sc(OTf)₃ as additive by the current benchmark system for homogeneous olefin epoxidation, an iron(II) tetracarbene complex (**a**, and its iron(III) homologue **b**, Fig. 1), published by our group [15]. Nevertheless, for a potential application in industry, particularly the stability has to be significantly increased, while maintaining high activity. Therefore, we have investigated various methods described in the following to improve the catalytic performance of our benchmark catalyst (**a/b**) or to synthesize a next-generation iron epoxidation catalyst. Application of Lewis acids like Sc(OTf)₃ already more than doubled the average number of catalytic cycles possible with one active center derived from **a** from ca. 500 to ca. 1200 by, among other reasons, suppressing a deactivation pathway, the formation of a diiron(III)-μ₂-oxo species [14–15,20–21]. The impact of modification of the NHC backbone with electron donating (**c**, **d**) and accepting moieties (**e**, **f**, Fig. 1) on the catalytic performance was investigated next by our group. Complexes **c** and **d** are more active than **e** and **f**, but they all lack behind in activity compared to **a** and **b** [22]. The stability could also not be

* Corresponding author.

E-mail address: fritz.kuehn@ch.tum.de (F.E. Kühn).

<https://doi.org/10.1016/j.jcat.2023.07.018>

Received 22 May 2023; Received in revised form 16 July 2023; Accepted 20 July 2023

Available online 22 July 2023

0021-9517/© 2023 Elsevier Inc. All rights reserved.

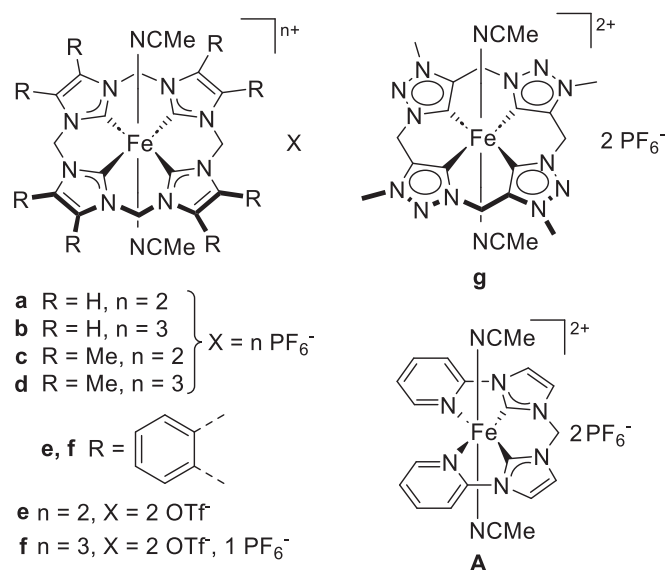


Fig. 1. (Pre-)Catalysts.

enhanced: while **f** has a similar TON of 1000, the catalytic performance of **c** and **d** is hampered by their low stability. A different strategy is the electronic fine-tuning of the iron center through axial ligand substitution, with which we could for example increase the stability of iron-NHC catalysts in C–H hydroxylation by up to 34% [23]. However, in epoxidation catalysis this method even decreased the catalytic performance [24–26]. The rate determining step in epoxidation catalysis is assumed to be the formation of an electrophilic iron(IV) or iron(V)-oxo intermediate and a more electron rich iron(III) center is presumed to facilitate its formation [22,27–28]. Hence, an iron(II) tetracarbenes (**g**, Fig. 1) containing the theoretically strongest electron donating ligand in this series and thus most electron rich iron center has been investigated by us. However, preliminary experiments did not indicate a beneficial effect as a comparably low TOF of 41 000 h⁻¹ is reached in presence of Sc(OTf)₃ [16].

In order to deepen the understanding of the influence of electronic changes on the catalytic performance, a different catalytic system from our group is used in this work (**A**, Fig. 1). The pyridine-NHC-based system [29], although less active, is structurally similar to the “flagship” iron tetracarbenes scaffold, while being sufficiently different and, most importantly, easy to modify to make it a suitable candidate. Iron(II) complex **A** specifically has been extensively studied in C–H hydroxylation [23,30–33] and a preliminary study on the epoxidation of olefins has been conducted by us [34]. The latter was largely done using ¹H NMR spectroscopy. In this work, the results are reevaluated using GC analysis as a more precise method and compared to two novel iron(II)

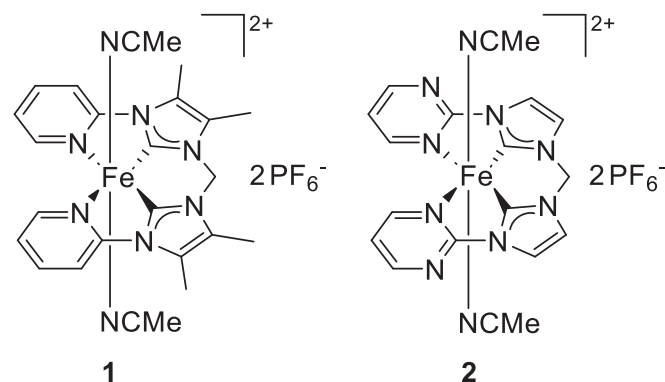


Fig. 2. Novel complexes.

complexes, **1** and **2** (Fig. 2), in the epoxidation of *cis*-cyclooctene as model substrate. In addition, a series of more challenging olefin substrates is screened with all three complexes and the impact of Lewis acidic additives is investigated. **1** and **2** are designed to have a more electron rich (**1**) and less electron rich iron center (**2**) than **A**, by having a ligand with supposedly donating (**1**) or accepting properties (**2**), respectively. The impact of these modifications of the catalytic system on its catalytic performance allows to gain valuable information for the epoxidation reaction in general, such as whether these effects are universal or limited to the tetracarbenes framework, in order to advance research related to the benchmark catalytic system. Furthermore, the synthesis of the two novel complexes **1**, bearing two methyl groups at the 4 and 5 position of the imidazole backbone, and **2**, having the pyridine moiety formally substituted by pyrimidine, is reported. The new compounds **1** and **2**, and if applicable, **A**, are elaborately characterized using NMR spectroscopy, electrospray mass spectrometry (ESI-MS), single crystal X-ray diffraction (SC-XRD), UV/Vis spectroscopy, cyclic voltammetry (CV), Mössbauer spectroscopy, buried volume and steric map calculations, SQUID magnetometry (for **A**), DTF calculations, and elemental analysis.

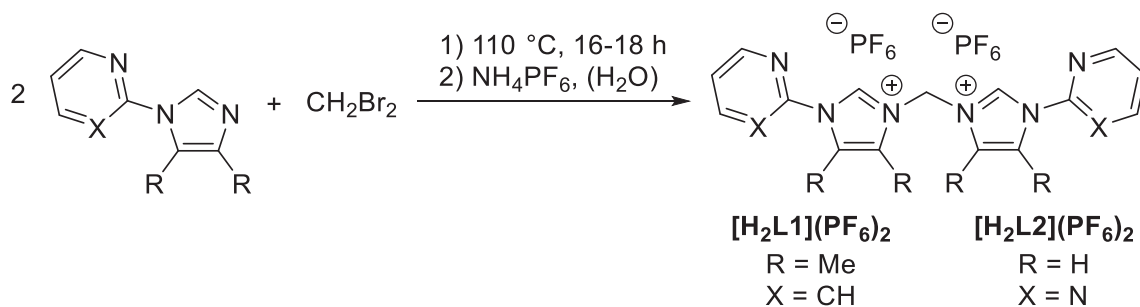
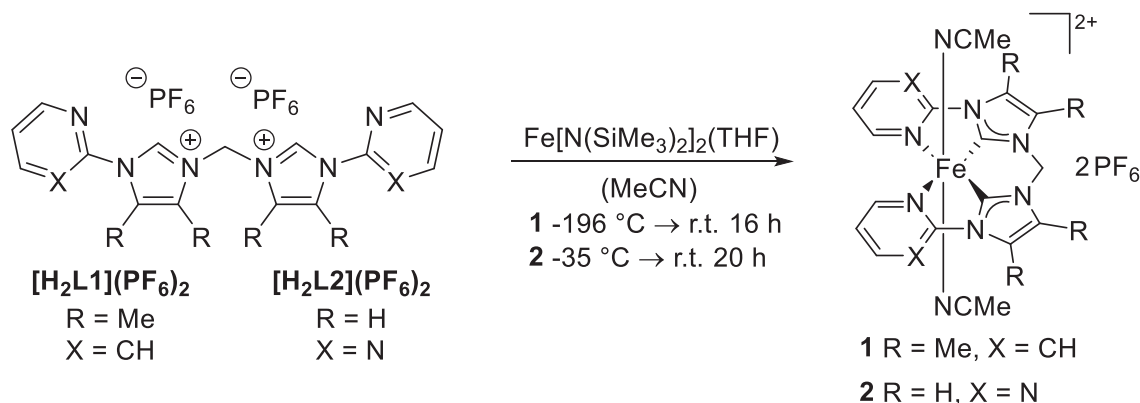
2. Results and discussion

2.1. Synthesis and characterization of the iron(II) complexes **1** and **2**

The synthesis of the ligand precursor of **1** starts with the coupling of two 2-(4,5-dimethyl-1*H*-imidazol-1-yl)pyridine [35] moieties with excess dibromomethane without additional solvent to give the dibromide salt [H₂L1](Br)₂. In a next step, the bromide anions are exchanged with weakly coordinating hexafluorophosphate anions in order to increase the solubility towards organic solvents and as additional purification step [28], to obtain [H₂L1](PF₆)₂ (Scheme 1). The synthesis of the ligand precursor of **2**, [H₂L2](PF₆)₂, follows the same pathway with 2-(1*H*-imidazol-1-yl)pyrimidine [35–36] as starting material (Scheme 1).

Direct metalation of the ligand precursors with the iron(II) precursor and internal base Fe[N(SiMe₃)₂]₂(THF) affords the complexes **1** and **2** (Scheme 2) [28,37]. The amide as strong, non-nucleophilic base is often used for the synthesis of iron(II) NHC complexes. It deprotonates the imidazolium salts and iron immediately coordinates to the *in-situ* generated carbenes. The thereby formed amine HN(SiMe₃)₂ is readily removed under vacuum [28].

Similar to **A**, both **1** and **2** are diamagnetic low-spin iron(II) (*S* = 0) complexes, as indicated in ¹H NMR and as evidenced in the following. Successful complexation is confirmed by the absence of the C2 imidazolium proton resonance signals in the ¹H NMR spectra. The two labile axial MeCN ligands are quickly exchanged in solution with deuterated MeCN, resulting in two equivalents of free MeCN being visible in the ¹H NMR spectrum. The signals of the methylene bridges are singlets, verifying the equatorial coordination of the ligand, like in complex **A**. The carbene signals in ¹³C NMR are sensitive to the electronic properties of the metal center and allow evaluation of the σ-donor strength of the NHC ligand [28,38]. The NHC moieties of **1** should be stronger σ-donors than the unmodified imidazolylidenes of **A** due to the +1 effect of the methyl groups at the backbone. This expectation is supported by Tolman electronic parameters [39]. The ¹³C_{NHC} signal of **1** (215.49 ppm) is shifted upfield 0.66 ppm compared to **A** (216.15 ppm [29]), confirming the stronger electron donation in **1**. This change appears to be rather small but any difference exceeding 0.4 ppm in NMR is significant by means of statistic uncertainty [28,38]. The upfield shift can be explained by an increased diamagnetic shielding term of the carbene carbon atom in **1** due to its higher electron density donated by the methyl groups. For **2**, the ¹³C_{NHC} signal (216.24 ppm) does not show any significant shift change compared to **A** because both NHC units have the same chemical structure. Nevertheless, the electron density of the iron center in **2** should be lower than in **A**, mainly because of pyrimidine being a weaker

Scheme 1. Synthesis of ligand precursors $[\text{H}_2\text{L1}](\text{PF}_6)_2$ and $[\text{H}_2\text{L2}](\text{PF}_6)_2$.Scheme 2. Synthesis of iron(II) complexes **1** and **2**.

σ -donor than pyridine due to the -I effect of adding a second nitrogen atom to the aromatic ring, while the amount of π -backdonation is expected to stay the same [40]. The successful synthesis of **1** and **2** is further shown with ESI-MS where three characteristic fragments are detected of the iron center with equatorial ligand and without, with one, or with both axial MeCN ligands, demonstrating again the lability of the axial ligands. The chemical composition of the new complexes is confirmed by elemental analysis. Like **A**, **1** and **2** can be stored as solid under ambient conditions for a few weeks without degradation. Furthermore, all three complexes are stable in solution in untreated HPLC-grade MeCN (*i.e.* not dried or degassed) under ambient conditions for at least one day.

The redox potential of a complex can provide further insight into the electronic properties of its metal center, which is influenced by the surrounding ligands. Actually, for the iron tetracarbene system of **a-f**, a linear correlation between chemical shift of the $^{13}\text{C}_{\text{NHC}}$ signal and redox potential has been found, allowing to predict one parameter once the respective other parameter is known [28]. Similarly, for a series of complexes derived by axial ligand substitution of **A**, a linear relationship could be established between the redox potentials and the highest occupied molecular orbital (HOMO) energy determined by DFT [41]. The redox potential of **1** is $E_{1/2} = 0.337 \text{ V}$ (see SI), which is 86 mV lower than that of **A** ($E_{1/2} = 0.423 \text{ V}$) [29,41–43], indicating a more electron rich iron center in **1**, as had been intended. In contrast, **2** has a 136 mV more positive half-cell potential of $E_{1/2} = 0.559 \text{ V}$ compared to **A**, implying a lower electron density at the iron center due to a weaker equatorial σ -donor [28]. While **1** shows a reversible redox process ($\Delta E = 106 \text{ mV}$), complex **2** has a quasi-reversible redox process ($\Delta E = 259 \text{ mV}$). Possible explanations of the latter could be a conformational change upon oxidation to iron(III), like a 180° ring-flip of one pyrimidine unit or the coordination of a third MeCN molecule, leading to decoordination of one pyrimidine from the iron atom. Such a behavior has been observed with similar complexes [42–44].

The UV/Vis spectrum of **1** shows similar absorption characteristics

like **A**, but slightly red-shifted (see SI). The bathochromic effect of around 8 nm can be explained by a higher electron donation in **1** due to the methyl substituents, decreasing the energy of the HOMO/LUMO gap [45–47]. The characteristic two absorption maxima around 340 nm and 400 nm (**A**: 329 and 400 nm, **1**: 340 and 408 nm, **2**: 355 and 403 nm) can be assigned to charge-transfer bands based on similar complexes [41].

Solid material of all three Fe(II) complexes was studied using ^{57}Fe Mössbauer spectroscopy at 80 K to gain further information about their electronic properties. They all exhibit isomer shifts in the range of octahedral iron(II) low-spin species [28,48] (**A**: $\delta = 0.26 \text{ mm s}^{-1}$; **1**: $\delta = 0.23 \text{ mm s}^{-1}$; **2**: $\delta = 0.24 \text{ mm s}^{-1}$) but are more positive compared to **a** ($\delta = 0.08 \text{ mm s}^{-1}$) [28,49], attributed to the weaker σ -donation of the equatorial ligand compared to the tetracarbene ligand. However, they are on the same scale as the 18-membered iron tetracarbene Fe(II) complexes ($\delta = 0.23 \text{ mm s}^{-1}$) [28,50–51]. A small influence of the donating properties of the methyl substitution in the backbone of **1** is visible, moving the isomer shift as expected to smaller values for a more electron rich iron center. The length of the Fe–ligand bonds can have a considerable impact on the isomer shift through compression of the *s*-orbitals resulting in a higher electron density [48]. However, all three complexes show similar bond lengths (Table 1) resulting in similar δ values. The quadrupole splittings are rather large for iron(II) low-spin

Table 1
Comparison of selected structural parameters of **A** [29], **1** and **2**.

Bond lengths (Å)	Fe–C _{NHC}	Fe–N	Fe–NCMe
A	1.837(2)	2.096(2)	1.915(2)
1	1.8429(18)	2.0801(16)	1.9283(18)
2	1.8359(14)	2.1028(12)	1.9146(12)
Bond angles (°)	C _{NHC} –Fe–C _{NHC}	C _{NHC} –Fe–N'	MeCN–Fe–NCMe
A	85.85(9)	165.12(6)	172.23(7)
1	86.59(11)	165.84(7)	167.99(8)
2	86.01(9)	165.12(6)	170.73(7)

complexes. No valence contribution is expected for them, but the results are in line with a heteroleptic ligand coordination sphere (different equatorial donor atoms and axial ligands) and strongly anisotropic covalent bonds (*vide infra*) as already seen in the case of the 18-membered tetracarbenes complexes [28,50–53]. Especially the strong σ -donation of the NHC moieties in an equatorial plane deforms the charge distribution surrounding the iron nucleus leading to the observed high quadrupole splitting. The quadrupole splitting increases in the order **2** ($\Delta E_Q = 1.80 \text{ mm s}^{-1}$) < **A** ($\Delta E_Q = 2.07 \text{ mm s}^{-1}$) < **1** ($\Delta E_Q = 2.22 \text{ mm s}^{-1}$) due to the increasing electron donor strength of the equatorial ligands and the resulting higher amount of deformation of the electric field (Fig. 3).

All three complexes **A**, **1** and **2** are low-spin diamagnetic complexes at 293 K. The magnetic susceptibility of complex **A** was analyzed exemplarily using a SQUID magnetometer from 2 K up to 400 K (see SI). No thermally induced spin crossover [54] from low-spin to high-spin is observed at elevated temperatures. **A** is diamagnetic up to 400 K reflecting the strong ligand field induced by the NHC ligand.

Single crystals suitable for SC-XRD were obtained by slow evaporation of a solution of **1** in MeCN and by slow vapor diffusion of 1,4-dioxane into a solution of **2** in MeCN (see SI). Both **1** (Fig. 4) and **2** (Fig. 5) show a distorted-octahedral geometry around the Fe center, as had been observed for **A**. The tetradentate ligand is coordinating equatorial and the labile MeCN ligands axial to the iron(II) center. In all three complexes, the Fe–C_{NHC} bond (~1.839 Å) is significantly shorter than the Fe–N bond (~2.101 Å, see Table 1). In **1**, the Fe–N bond is significantly shorter and the Fe–NCMe bond significantly longer in terms of statistic uncertainty (*i.e.* three times the weighted standard deviation) [28] compared to the other two complexes. Apart from that, the structures are similar. The vertical axis passing through the two axial MeCN ligands and the iron center is more curved compared to iron tetracarbenes complexes [28], probably because of the steric influence of the open NCCN ligand.

The ligand modifications should only change one variable, the electronic properties of the complexes, to ensure a good comparability of the catalytic experiments. The catalytic pocket is intended to remain constant. This is proposed to be the case, as derived by the structural parameters shown in Table 1 of the iron(II) pre-catalysts, and confirmed by calculations regarding the percentage of buried volume %V_{Bur} of the iron center, being around 86%V_{Bur} for all three (see SI). The topographic steric maps of the buried volume of **A** are exemplarily shown in Fig. 6 (for **1** and **2** see SI).

Finally, DTF calculations were performed to gain more insights of the electronic properties of **A**, **1** and **2**. In the case of **c/d**, the worse catalytic performance compared to **a/b** was explained by computational methods, which indicated – contrary to the experimental methods – that the σ -donation of the methyl groups in fact is counterbalanced with an increased π -backbonding character [22]. This results in a less electron rich iron center compared to **a/b**, and, as a more electron-rich iron(III) center is expected to be beneficial for catalysis (*vide supra*), worse catalytic performance. The electronic influence of the ligand in **A**, **1** and **2** is investigated by calculation of the electronic charge of the respective low-spin iron(III) center. Löwdin population analysis [55] was applied for that reason. The iron(III) Löwdin charge is most negative for **1**, followed by **A** and **2** (Table 2). This trend is in accordance to the experimentally determined electronic properties of the three complexes, with **1** having the most electron rich iron center, **A** in between and **2** with the lowest electron density at the nucleus. Contrary to **c/d** [22], the methyl groups in **1** appear to only increase the σ -donation towards the iron atom without enhanced π -backbonding character.

The strong equatorial electron donation of the tetracarbenes ligand in iron tetracarbenes like **a/b** (Fig. 1) rises the 3d_{x²-y²} above the 3d_{z²} orbital, opposite to most *N*-ligated iron complexes, leading to exclusive triplet reactivity in epoxidation catalysis [28]. This is also the case for **A** [41], **1** and **2**, based on the calculation of the LUMO and LUMO + 1 orbitals (see SI). Despite having only two NHCs, the x²-y² orbital is also elevated above the z² orbital (see SI), justifying again the suitability of

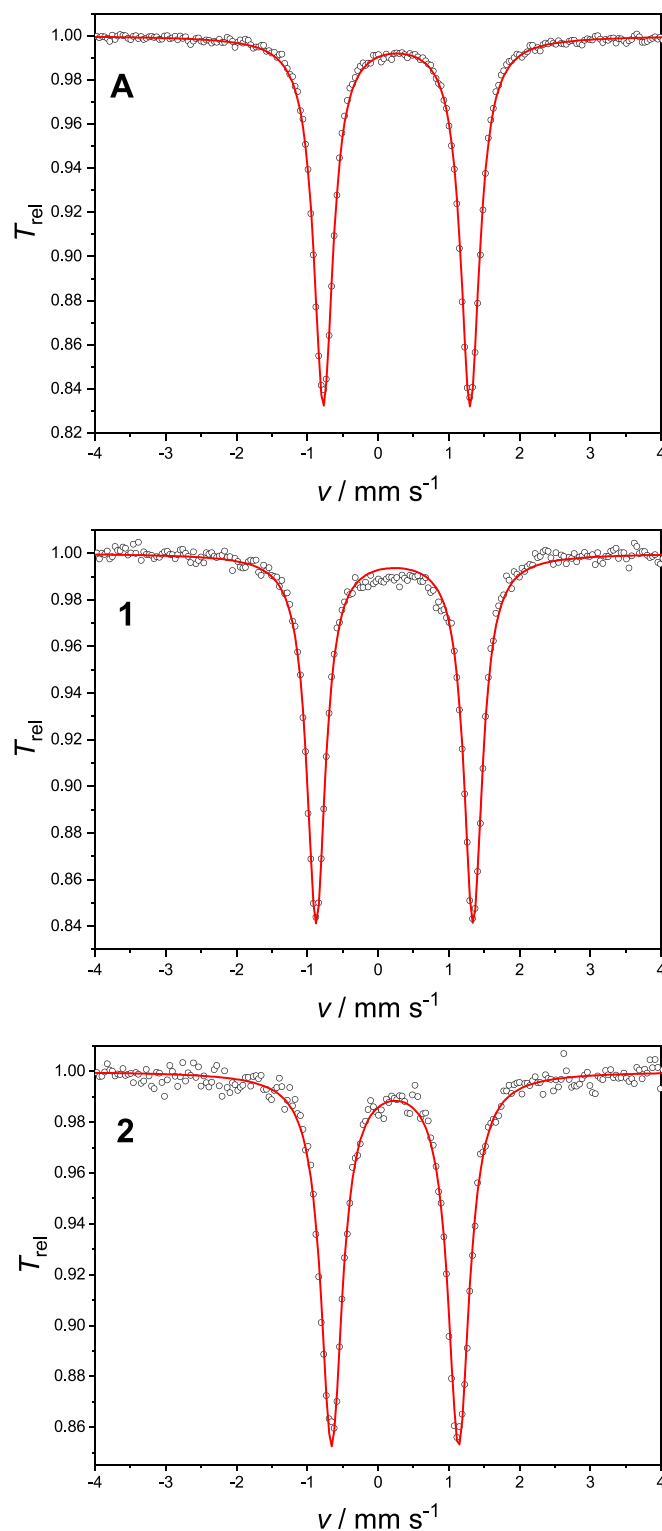


Fig. 3. Zero-field ^{57}Fe Mössbauer spectrum of solid **A**, **1** and **2** at 80 K. The red line represents a simulation with $\delta = 0.26 \text{ mm s}^{-1}$ and $\Delta E_Q = 2.07 \text{ mm s}^{-1}$ (**A**, top); $\delta = 0.23 \text{ mm s}^{-1}$ and $\Delta E_Q = 2.22 \text{ mm s}^{-1}$ (**1**, middle); $\delta = 0.24 \text{ mm s}^{-1}$ and $\Delta E_Q = 1.80 \text{ mm s}^{-1}$ (**2**, bottom).

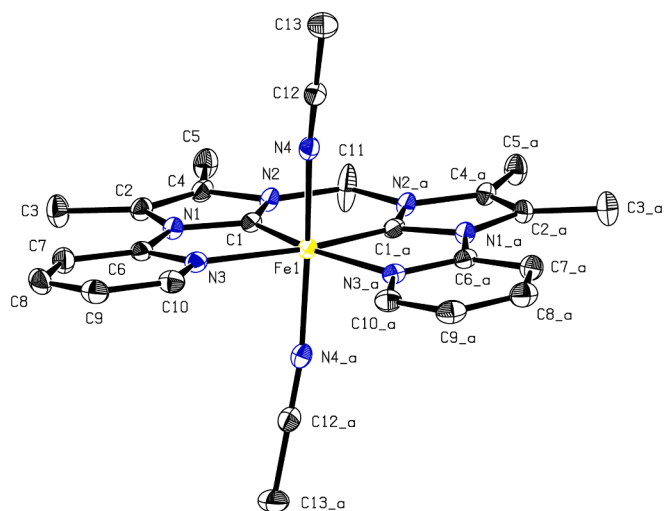


Fig. 4. ORTEP-style representation of the cationic fragment of complex **1**. Hydrogen atoms and hexafluorophosphate anions are omitted for clarity. Thermal ellipsoids are shown at a 50% probability level.

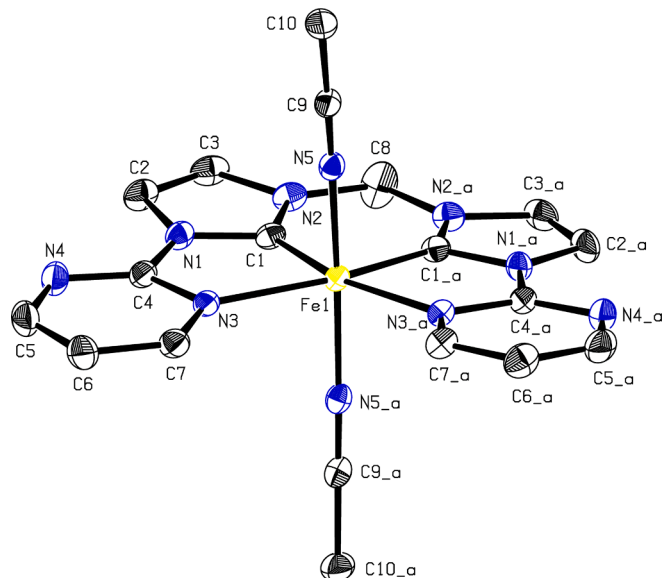


Fig. 5. ORTEP-style representation of the cationic fragment of complex **2**. Hydrogen atoms and hexafluorophosphate anions are omitted for clarity. Thermal ellipsoids are shown at a 50% probability level.

the catalytic system of **A**/**1**/**2** for comparison with **a**/**b** in epoxidation catalysis in the following, due to an expected similar reactivity.

2.2. Catalytic olefin epoxidation reactions

The impact of the ligand modifications of **1** and **2** on the catalytic performance is investigated in the following. All three complexes **A**, **1** and **2** are employed as catalysts in olefin epoxidation reactions. Standard conditions are defined as 20 °C using H₂O₂ (1.50 eq.) as oxidant, MeCN as solvent, *cis*-cyclooctene (1.00 eq.) as model substrate in the presence of one of the three complexes as catalyst (0.02 eq.). Hydrogen peroxide was used as oxidant, as it has been found to be superior in comparison to other common peroxides such as *tert*-butyl hydroperoxide or the urea hydrogen peroxide adduct in iron-NHC epoxidation catalysis [14,34]. In addition, being atom-efficient and environmentally friendly are two further advantages [56–57]. Excess of H₂O₂ was used for best results based on previous optimizing studies with different loadings

[14,34]. For the quantification of the formed epoxide, GC-FID and ¹H NMR spectroscopy were applied.

In a first experiment, all three complexes have been employed in the olefin epoxidation of *cis*-cyclooctene under standard conditions for 60 min (Fig. 7). Complex **A** achieves a conversion of 84% after 10 min that afterwards only marginally increases to 87% at 60 min. Surprisingly, **1** shows a slightly lower activity than **A**, reaching 16% conversion after 30 s versus 20% for **A**. In contrast to **A**, however, **1** only reaches a conversion of 20% after 1 min (**A**: 32%), which does not increase during the remaining time. This indicates a relatively short lifetime of the catalyst. Possible degradation (*vide infra*) might involve the dissociation of the NCCN ligand, C–C bond formation resulting in a highly-strained annulated 2,2'-biimidazole and subsequent cleavage of the methylene bridge, as observed under oxidative conditions for **A** [44,58]. **2** in turn shows a remarkably longer lifetime albeit being the least active catalyst, as expected, and stays active for 4 h, reaching a conversion of 45% (see SI). As demonstrated by its higher redox potential, the initial required pre-oxidation from Fe^{II} to Fe^{III} might be slower in the case of **2**, restraining the activity. These different catalytic performances are mainly attributed to the different electronic properties of the complexes due to the equatorial ligand modifications. All complexes achieve a selectivity of > 99% under the applied conditions, placing them among the most selective Fe-NHC catalytic systems, on par with **a**/**b** [28].

A stable diiron(III)- μ_2 -oxo complex is formed in iron tetracarbene epoxidation catalysis of **a** and **b**, possessing a low activity [15,20–21]. This dead-end species can be reactivated through the addition of Lewis acids like Sc(OTf)₃. Interestingly, in the presence of Lewis acids, **a**, **b** and the diiron(III)- μ_2 -oxo complex all show the same activity (TOF of ~410 000 h⁻¹), which can be explained by the suppression of this deactivation pathway, the formation of the bridged oxo-species [15,24]. In addition, the observed activity (TOF) is several times higher compared to systems without additive (**a**: 50 000 h⁻¹; **b**: 183 000 h⁻¹) and the stability is significantly enhanced (TON: 1200 vs. without additive **a**: 390; **b**: 740) [15,28].

Although no μ_2 -oxo bridged complex of **A** has been reported, the analogy of these two catalytic systems suggests similar mechanisms. The impact of Lewis acids on **A** has not been studied yet. Therefore, in a next experiment, the olefin epoxidation of *cis*-cyclooctene under standard conditions for 60 min is repeated but in the presence of Sc(OTf)₃, the most efficient Lewis acid found for **a**/**b** [15]. Under these conditions, all three catalysts achieve relatively high conversions (**A**: 100%; **1**: 92%; **2**: 97%, Fig. 8), implying a similar deactivation pathway being present in the first experiment in Fig. 7, which is now suppressed. Furthermore, both stability (measured as TON, e.g. 10 vs. 46 for **1**, entry 14 and 15) and activity (determined as TOF, e.g. 1 700 h⁻¹ vs. 18 000 h⁻¹ for **A**, entry 2 and 3) are significantly enhanced (Table 3). Another reason for the beneficial effect of Lewis acids on the catalytic activity is their ability to facilitate crucial proposed mechanistic steps like the initial oxidation of Fe^{II} to Fe^{III}, and the OH^{•/•-} cleavage of the Fe^{III}-OOH intermediate shifting the rate determining step towards olefin oxidation [15,28,59]. Selectivity is not influenced by the Lewis acid and remains unchanged high (Table 3). In fact, for **a**, the selectivity is even improved from 94% to 99% upon addition of Sc(OTf)₃ [14–15].

Different catalyst concentrations have been screened in the epoxidation of *cis*-cyclooctene under standard conditions using the three complexes with and without Sc(OTf)₃ as additive. They all show a nearly linear relationship between catalyst loading and conversion (Table 3, visualized in the SI). **A** reaches an initial TOF of up to 3 400 h⁻¹ (entry 7) and TON of up to 65 (entry 9) without any additive. In the presence of Sc(OTf)₃, **A** achieves a highest TOF of 24 500 h⁻¹ (entry 10), which albeit being an order of magnitude lower than the benchmark iron tetracarbene system **a**/**b** (~410 000 h⁻¹), still is on par with the most active *N*-donor based iron catalysts (25 200 h⁻¹). This emphasizes once more the beneficial effect of employing NHC ligands in epoxidation catalysis [28]. Most *N*-ligated iron complexes have TONs of less than 100 [9], and one of the highest reported TONs are 180 [18], 715 [60] and 252 [61],

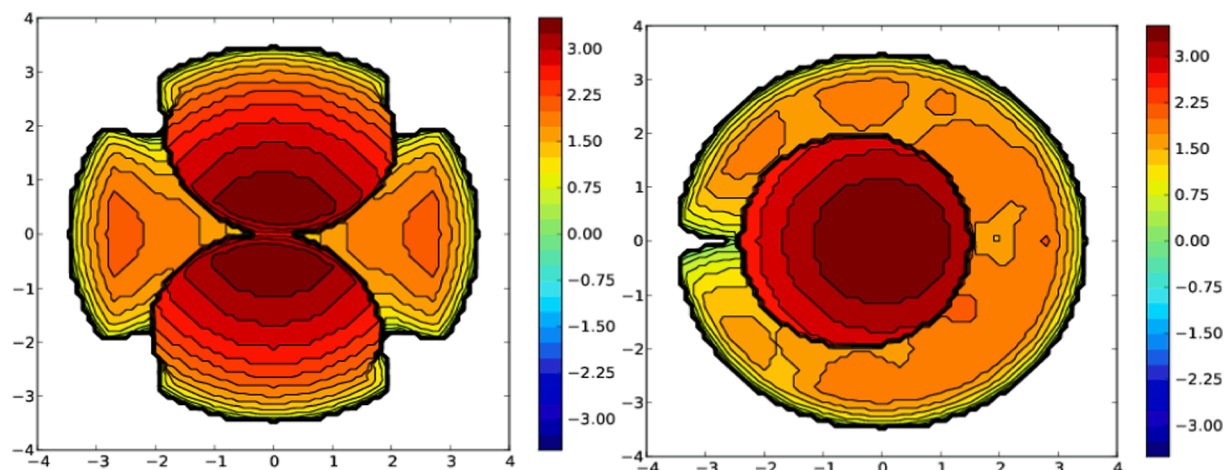


Fig. 6. Topographic steric maps of the buried volume of **A**. The red and blue colors show the more- and less-hindered zones in the catalytic center, respectively. Left: View towards the opening of the NCCN ligand of **A** with the axial ligands horizontal and the NCCN ligand vertical. Right: View on top of **A**, with the red circle marking the axial ligands and the broader orange area representing the NCCN ligand underneath with its opening to the left.

Table 2

Calculated charges at the iron(III) center of **A**, **1** and **2** using the Löwdin charge model. Values are given in atomic units and were rounded to the third decimal digit.

Complex	A	1	2
Löwdin	-1.249	-1.263	-1.236

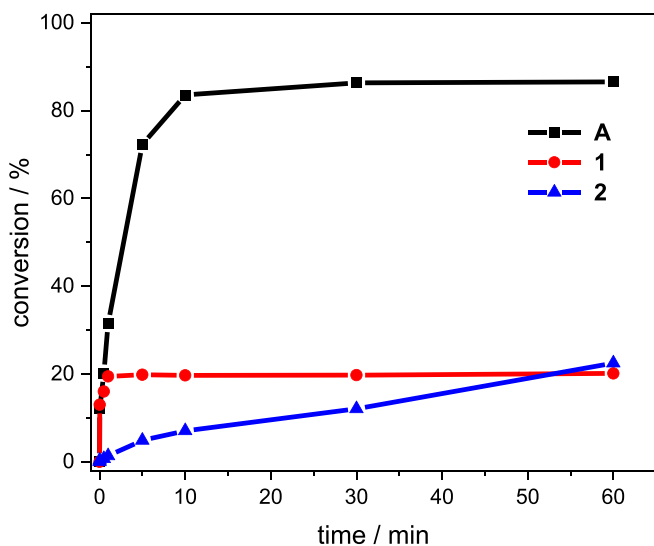


Fig. 7. Time-dependent epoxidation of *cis*-cyclooctene (67.3 $\mu\text{mol/mL}$, 1.00 eq.) in MeCN using **A**, **1** or **2** (1.35 $\mu\text{mol/mL}$, 0.02 eq.) as catalyst, and H_2O_2 (50% aq., 101 $\mu\text{mol/mL}$, 1.50 eq.) as oxidizing agent at 20 °C. Conversions are determined by GC-FID.

but the latter with low selectivity towards the epoxide. Using 0.1 mol% of **A**, a remarkable TON of 711 is attained at 20 °C, which is, to the best of our knowledge, the second highest reported one for a Fe-NHC catalytic system, with the highest TON of 1200 at 20 °C for **a/b** [28]. **1** with the supposedly more electron rich center has at least the second highest TOF of the three complexes with 7 600 h^{-1} , and a TON of 46 in the presence of $\text{Sc}(\text{OTf})_3$ (entry 15). **2** has no measurable TOF after 10 s due to its slow nature without additive, but a TON of 23 can be determined after 4 h and complete reaction (entry 19). However, despite having the least electron rich center, **2** achieves nearly full conversion after 10 min

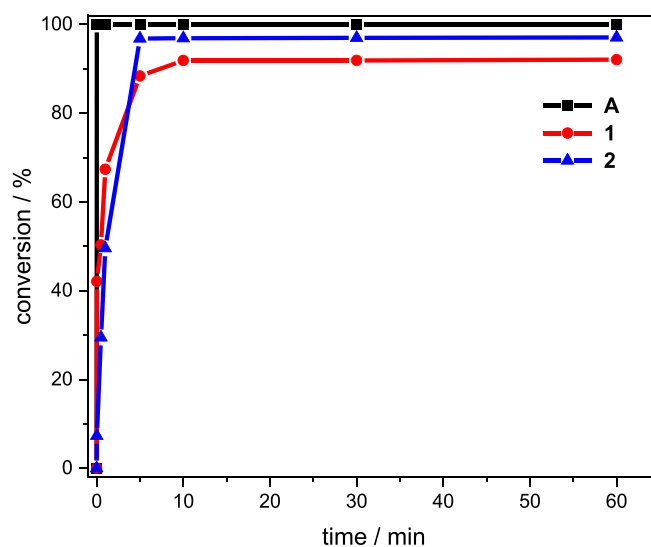


Fig. 8. Time-dependent epoxidation of *cis*-cyclooctene (67.3 $\mu\text{mol/mL}$, 1.00 eq.) in MeCN using **A**, **1** or **2** (1.35 $\mu\text{mol/mL}$, 0.02 eq.) as catalyst, $\text{Sc}(\text{OTf})_3$ (6.73 $\mu\text{mol/mL}$, 0.10 eq.), and H_2O_2 (50% aq., 101 $\mu\text{mol/mL}$, 1.50 eq.) as oxidizing agent at 20 °C. Conversions are determined by GC-FID.

with $\text{Sc}(\text{OTf})_3$, a maximum TOF of 1 300 h^{-1} and a TON of 49 (entry 20). The TON is even slightly higher than **1** and as high as for **A** (50, entry 3).

Variable temperature studies of all three complexes were performed next (Table 3, Fig. 9). Decreasing the temperature below 20 °C has been shown to be beneficial for the stability of Fe-NHC catalysts and thus leading to an enhanced catalyst lifetime [14,17,34]. On the other side, **e/f** (Fig. 1) with an electron pulling tetracarbene ligand similar to **2** have been found to be remarkable temperature-tolerant, albeit also requiring these higher temperatures for an enhanced activity [22]. **A** has a lower activity at 0 °C (400 h^{-1} , entry 1) but achieves an effectively full conversion (98%) in 60 min reaction time in comparison to the 20 °C run (87%), which is attributable to the 14% higher stability with a TON of 49 vs. 43 at 20 °C (entry 2). Based on the slope, a lower catalyst loading would still have been sufficient for complete conversion with a longer reaction time. Increasing the temperature to 40 °C enhances the activity and an initial TOF of 2 200 h^{-1} is determined (entry 4). However, deactivation of **A** also occurs faster, reducing the total conversion to 42% at a TON of 21. For **2**, a rise of the temperature to 40 °C also is beneficial for the activity (200 h^{-1} , entry 21) and at 60 °C the highest

Table 3Epoxidation of *cis*-cyclooctene by A, 1 and 2 at different catalyst concentrations, temperature, and with or without additive.

entry	catalyst	T [°C]	loading [mol%]	additive	X [%] ^[a] (10 min)	S [%]	TOF [h ⁻¹] ^[b]	TON (60 min)
1	A	0	2	–	33	> 99	400	49
2	A	20	2	–	80	> 99	1 700	43
3	A	20	2	Sc(OTf) ₃	100	99	18 000	50
4	A	40	2	–	38	> 99	2 200	21
5	A	20	1	–	43	> 99	2 700	43
6	A	20	1	Sc(OTf) ₃	100	99	20 800	100
7	A	20	0.5	–	24	> 99	3 400	48
8	A	20	0.5	Sc(OTf) ₃	96	99	22 600	194
9	A	20	0.1	–	7	> 99	2 900	65
10	A	20	0.1	Sc(OTf) ₃	26	99	24 500	711
11	1	-10	2	–	2	> 99	0	4
12	1	0	2	–	27	> 99	1 000	19
13	1	0	2	Sc(OTf) ₃	74	> 99	6 500	44
14	1	20	2	–	19	> 99	900	10
15	1	20	2	Sc(OTf) ₃	91	99	7 600	46
16	1	20	1	–	10	> 99	900	11
17	1	20	0.5	–	5	> 99	1 400	12
18	1	20	0.1	–	1	> 99	1 300	12
19	2	20	2	–	6	> 99	0	23
20	2	20	2	Sc(OTf) ₃	97	99	1 300	49
21	2	40	2	–	22	> 99	200	15
22	2	60	2	–	20	> 99	700	13
23	2	20	1	–	3	> 99	0	3
24	2	20	0.5	–	1	> 99	0	2
25	2	20	0.1	–	0	–	0	0

Reaction conditions: *cis*-cyclooctene (67.3 μmol/mL, 1.00 eq.) in MeCN, Fe-catalyst, if stated Sc(OTf)₃ (6.73 μmol/mL, 0.10 eq.), and H₂O₂ (50% aq., 101 μmol/mL, 1.50 eq.). Selectivity is related to the epoxide. [a] Conversions are determined by GC-FID. [b] TOFs are determined after 10 s. [c] TON determined after 10 min. [d] TON determined after 240 min. T = temperature. X = conversion. S = selectivity.

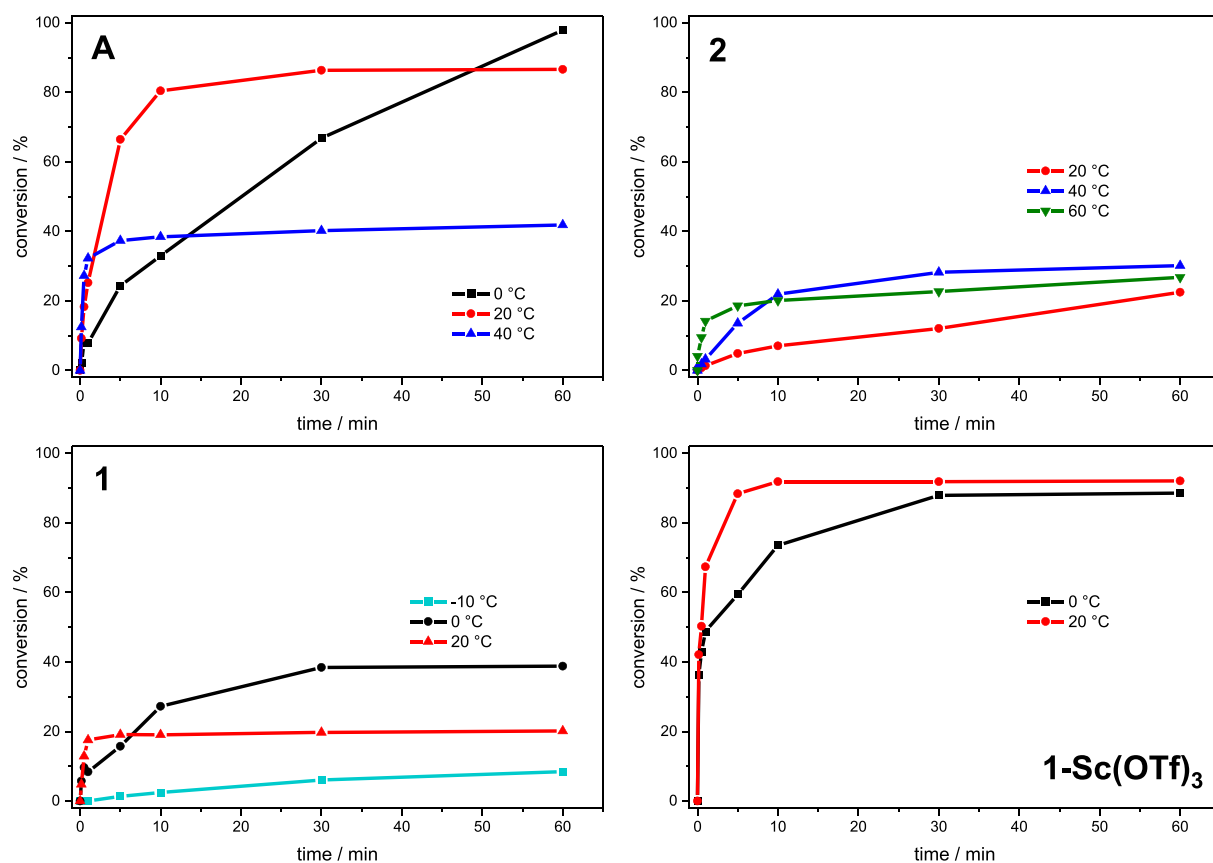


Fig. 9. Time-dependent epoxidation of *cis*-cyclooctene (67.3 μmol/mL, 1.00 eq.) in MeCN, Fe-catalyst (1.35 μmol/mL, 0.02 eq.), and H₂O₂ (50% aq., 101 μmol/mL, 1.50 eq.) as oxidizing agent at different temperatures. Conversions are determined by GC-FID. Top left: A as catalyst. Top right: 2 as catalyst. Bottom left: 1 as catalyst. Bottom right: 1 as catalyst with Sc(OTf)₃ (6.73 μmol/mL, 0.10 eq.).

initial TOF of 700 h⁻¹ (entry 22) without additive is attained. But even at higher temperatures, **2** still requires longer reaction times for a complete reaction. On the other side, this is evidence of the high temperature-tolerance of **2**. Based on the rather low stability of **1** in comparison to **A** and **2** (Fig. 7) the temperature was lowered for **1**. At 0 °C a significant increase of the stability can be observed for **1**, as the TON is almost doubled (0 °C: 19 vs. 20 °C: 10, entries 12 and 14). Hence, the total conversion is also twice as high (39% vs. 20%, Fig. 9) and the activity is even slightly higher (1000 h⁻¹ vs. 900 h⁻¹). Lowering the temperature to -10 °C does not benefit the stability further, as the activity is reduced drastically giving a total conversion of only 8% after 60 min with a TON of 4. In all cases, and in contrast to other Fe-NHC catalysts [17,22], the high selectivity of >99% remains constant even at elevated temperatures.

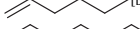
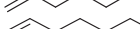
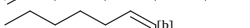
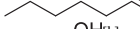
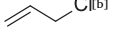
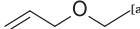
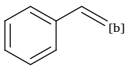
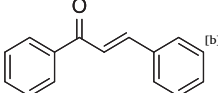
Reducing the temperature to 0 °C could enhance the stability for **A** and **1**, which can be explained by potentially decelerated catalyst deactivation, e.g. slower formation of an assumed μ_2 -oxo species or NCCN ligand dissociation (*vide supra*). However, lowering the temperature to 0 °C in the presence of Sc(OTf)₃ does not further increase the stability for **1** (entry 13, Fig. 9) but in this case reduces the activity (entry 13 vs 15). Therefore, using a Lewis acid as additive is superior to varying the temperature in the present case and achieves the best catalytic performance. Furthermore, the significant beneficial effect for the stability by addition of Sc(OTf)₃ gives the following indications: a) The formation of a deactivation species without Lewis acid as dead-end in the catalytic cycle. However, this species can either be reactivated or its formation suppressed by Lewis acids such as Sc(OTf)₃. It is likely, that this species is a diiron- μ_2 -oxo complex, as it was demonstrated for the tetracarbene system **a/b**, and both **a/b** and **A/1/2** are structurally similar and show analog reactivity in epoxidation catalysis. For **a/b**, this diiron(III)- μ_2 -oxo complex could be reactivated with Lewis acids and had the same activity like **a/b**. b) The presence of an additional degradation pathway. If the formation of a diiron- μ_2 -oxo complex was the only decomposition mechanism, addition of Sc(OTf)₃ should give complete conversions for all three complexes. This is, however, not the case. In contrast to the formation of the deactivation species, this degradation

is terminal and results in a permanently decomposed catalyst. As mentioned above, possible degradation might involve the dissociation of the NCCN ligand, C–C bond formation resulting in a highly-strained annulated 2,2'-biimidazole and subsequent cleavage of the methylene bridge, as observed under oxidative conditions for **A** [44,58]. But also carbene oxidation, as observed for **a/b**, methylene bridge oxidation or carbene protonation are plausible [24]. c) The formation of the deactivated species is faster than the terminal degradation. In the case of faster permanent decomposition, the addition of Lewis acids would not have a significant effect on the stability and lifetime of the catalyst.

Epoxides do not only act as final products in industry, but are also building blocks in synthetic organic chemistry [62–65]. In the following, various relevant olefin substrates are screened with **A**, **1** and **2** in the epoxidation catalysis for 5 min with Sc(OTf)₃, as their epoxides are valuable intermediates in industry (Table 4). Here, the functional group tolerance is tested as well. The respective epoxides are for example used as monomers in polymerization (entry 27) [66], as stabilizers for halogen hydrocarbons or oil-soluble bases in cosmetics (entries 28–32) [67], epoxy resins (entry 34) and reactive diluent for epoxy resins (entry 36) [63].

The overall best catalytic performance is achieved by **A**, followed by **2** while **1** has the lowest substrate adaptability. **A** converts the smaller ring *cis*-cyclohexene completely with high selectivity (>99%, entry 27), whereas **1** and **2** show rather low reactivity to this substrate with 27% and 22% conversion, respectively, albeit retaining the high selectivity of >99%. The terminal alkenes (entries 28–30) are again completely converted by **A** (selectivity > 90%) but for **1** and **2** the conversion drops with a longer hydrocarbon chain from 71% to 28% for **1** and 92% to 54% for **2**. **1** shows the lowest selectivity for 1-hexene (68%) and 1-octene (71%), and it drastically drops to 20% for 1-decene, in contrast to the other catalysts (**A**: 90%; **2**: 82%), because of diol formation. Interestingly, **2** reaches a new maximum TOF of 6 400 h⁻¹ in the epoxidation of 1-decene. The iron(III) tetracarbene **b** favors the *cis*-2-octene over the *trans* isomer, a behavior also common for other iron epoxidation catalysts [14,68]. **A** follows this trend with an epoxide yield of 86% (*cis*) against 80% (*trans*). However, especially for **1**, this trend is reversed

Table 4
Epoxidation of various olefin substrates using **A**, **1** and **2** as catalyst with 5 min reaction time and Sc(OTf)₃.

Entry	Substrate	A			1			2		
		X [%]	S [%]	TOF [h ⁻¹] [c]	X [%]	S [%]	TOF [h ⁻¹] [c]	X [%]	S [%]	TOF [h ⁻¹] [c]
26		100	> 99	18 000	88	> 99	7 600	97	99	1 300
27		100	> 99	18 000	27	> 99	4 900	22	> 99	0
28		100	93	–	71	68	–	92	87	–
29		100	95	17 400	34	71	3 800	61	82	1 500
30		100	90	17 500	28	20	2 800	54	82	6 400
31		100	86	–	53	76	–	70	84	–
32		100	80	–	64	87	–	66	93	–
33		100	37	–	41	0	–	78	33	–
34		76	> 99	–	11	78	–	38	> 99	–
35		100	> 99	18 000	100	> 99	18 000	47	> 99	1 200
36		34	0	–	15	0	–	18	0	–
37		85	86	–	22	76	–	17	67	–

Reaction conditions: substrate (67.3 $\mu\text{mol/mL}$, 1.00 eq.) in MeCN, Fe-catalyst (1.35 $\mu\text{mol/mL}$, 0.02 eq.), Sc(OTf)₃ (6.73 $\mu\text{mol/mL}$, 0.10 eq.) and H₂O₂ (50% aq., 101 $\mu\text{mol/mL}$, 1.50 eq.), 20 °C, 5 min. Selectivity is related to the epoxide. [a] Conversions are determined by GC-FID. [b] Conversions are determined by ¹H NMR spectroscopy, applying benzene as external standard. [c] TOFs are determined after 10 s. X = conversion. S = selectivity.

with an epoxide yield of 40% for *cis*-2-octene compared to 56% for the *trans* isomer. **2** effectively has the same epoxide yields for both isomers (*cis*: 58% vs. *trans*: 61%). Allyl alcohol (entry 33) and allyl chloride (entry 34) are more challenging to epoxidize resulting in either a low selectivity for the former due to diol and aldehyde formation or low conversion for the latter. Interestingly, in the epoxidation of the allyl ethyl ether (entry 35) **1** is on par with **A**, reaching the highest TOF of 18 000 h⁻¹ for **1** in this study at complete conversion and >99% selectivity. In this case, **2** is left behind and achieves only 47% conversion. No epoxide formation is observed for all catalysts using styrene as substrate, opposite to **A** without Sc(OTf)₃ and **a** with or **b** without Sc(OTf)₃ [14–15,34]; instead formation of a variety of side products is observed (see SI). Chalcone is also rather difficult to epoxidize, especially by **1** and **2**. In general, a more nucleophilic character of the alkene through inductive effects results in a higher reactivity towards the epoxide, which is in line with an electrophilic active species [14,60]. For example, a highly substituted alkene is more reactive compared to its terminal alkene due to the +I effect of the substituents and the –M effect of the carbonyl in chalcone reduces the reactivity of the alkene.

3. Conclusions and outlook

Two novel complexes **1** and **2** were synthesized, characterized and, together with **A**, applied as catalysts in the epoxidation of olefins. The methyl backbone modifications in **1** result in a more electron rich iron center than in **A**. A less electron rich iron center is achieved by substitution of pyridine with pyrimidine in **2**. The impact of the different electronic properties of the complexes on the catalysis has been investigated. Surprisingly, the activity is the highest for **A**, followed by **1** and, as expected, lowest for **2**. Although **2** is the least active, it has the longest lifetime. Hence, **2** eventually achieves a higher conversion than **1**. The catalysts enable an overall high selectivity, placing them among the most selective Fe-NHC catalytic systems, on par with **a/b**. Addition of Sc(OTf)₃ as Lewis acid increases the activity and stability of all catalysts significantly, while their selectivity remains high, in contrast to the benchmark system **a/b**. The enhancement of the activity and stability with Sc(OTf)₃ indicates the presence of two degradation pathways; one can be suppressed by Sc(OTf)₃, while the slower pathway is terminal. In the epoxidation of *cis*-cyclooctene with Sc(OTf)₃ as additive, a TOF of 24 500 h⁻¹ is achieved for **A**, followed by 7 600 h⁻¹ for **1** and 1 300 h⁻¹ for **2**. **A** reaches a remarkable TON of 711, **1** a TON of 46 and **2** a TON of 49. Lower temperatures can increase the stability for **A** and **1**, and higher temperatures lead to enhanced activity for **2**. Various other substrates have been screened in the epoxidation reaction. **A** has the best overall catalytic performance, followed by **2** and **1**. In general, more nucleophilic alkenes lead to a higher activity and conversion toward the epoxide.

This work demonstrates ligand modification as easy and effective tool to steer the electronic properties of transition metal catalysts and how they can influence the catalytic performance. The impact of electronic variations on the epoxidation catalysis was studied on the iron NHC catalytic system **A/1/2** as potential tool for optimization of the benchmark system **a/b**. **A/1/2** was chosen as candidate due to its structural and electronic similarities to **a/b**. Electronic changes of **A/1/2** result in the same catalytic trends as for **a/b** in epoxidation. This confirms the universal underlying mechanistic functionality for both systems. Further evidence for that is the similar effect of Lewis additives on catalysis and the inferred presumed alike degradation of the catalysts.

Interestingly, the overall lower activity of the **A/1/2** system compared to the flagship iron tetracarbene system **a/b** is likely a result of the lower electron density at the iron center of the first compared to the latter with its significantly stronger electron donating tetracarbene ligand. Furthermore, decreasing the electron density at the iron atom in **2** is again reducing the activity vs. **A** – however, this is not true for the opposite: increasing the electron density in **1** does not lead to a higher activity vs. **A**. In other words, modifications within the catalytic system

of **A** towards a more electron rich iron center in **1** are not accompanied by improved activity, analog to the tetracarbene system (**c/d** vs. **a/b**). While the σ -donation of the dimethylimidazole is counterbalanced with enhanced π -backbonding in **c/d** [22] – which has been proposed as explanation for the missing catalytic benefit of the tetracarbene modification in **c/d** vs. **a/b** – this is not the case for **1**, which contains the same ligand modification like **c/d**, namely two methyl groups at the 4 and 5 position of the imidazole backbone. Here, all analytical methods support the higher electron density in **1** compared to **A**. In theory, a higher electron density is expected to increase the activity due to acceleration of the formation of the Fe^{IV/V} = O active species as the rate determining step [22,28], but a ligand modification might have a larger impact on other factors, which in turn suppress the activity gain, such as catalyst stability. Indeed, complex **1** has a reduced stability compared to **A**. Based on the overall best catalytic performance out of all three complexes, **A** seems to have the most balanced set of properties like electron density and ligand/catalyst stability, analog to the unmodified benchmark system **a/b**. In the case of the tetracarbene system **a/b**, the increase of electron density, like in **c/d** or more pronounced in **g**, also does not result in an improved activity in epoxidation of *cis*-cyclooctene vs. **a/b**. While more catalytic experiments of **g** are necessary for a comprehensive discussion, this raises doubts to the simple relation of the electron density at the iron atom and catalytic activity. A crucial factor to be considered is the stability of a new or modified ligand under oxidative conditions. Other parameters might be the ligand rigidity or overall geometry. In any case, more knowledge about the catalytic mechanism and structure activity relationships in epoxidation catalysis are required in order to tailor the next generation of catalysts with the desired features.

4. Experimental

4.1. General procedures and analytical methods

The syntheses of complexes **1** and **2** were performed under argon atmosphere using standard Schlenk and glovebox techniques as well as dry and degassed solvents. 4,5-Dimethyl-1*H*-imidazole [22], 2-(4,5-dimethyl-1*H*-imidazol-1-yl)pyridine [35], 2-(1*H*-imidazol-1-yl)pyrimidine (ACE pressure tube under Ar atmosphere) [35–36] were synthesized according to literature procedures. Fe[N(SiMe₃)₂]₂(THF) has been synthesized according to a modified literature procedure (see SI) [69–73]. Solvents were purified, dried and degassed using standard methods [74] or received from a solvent purification system by M. Braun. All other chemicals were obtained from commercial suppliers and were used without further purification. NMR spectra were recorded on a Bruker Advanced Ultrashield AV400 (¹H NMR, 400.13 MHz; ¹³C NMR, 100.53 MHz). The chemical shifts are given in δ values in ppm (parts per million) relative to TMS (tetramethylsilane) and are reported relative to the residual deuterated solvent signal [75]. Elemental analyses (C/H/N/S) were obtained by the microanalytical laboratory at Technical University Munich. Electrospray ionization mass spectrometry (ESI-MS) data were measured on a Thermo Fisher Ultimate 3000. Electrochemical measurements were carried out using an EmStat3 + potentiostat using a three-electrode cell equipped with glassy carbon electrodes as counter and working electrodes and Ag/AgNO₃ (0.1 mM) as the reference electrode. Potentials are measured with a scan rate of 100 mV/s and reported with reference to an internal standard of ferrocenium/ferrocene (Fc^{+/0}). Tetrabutylammonium hexafluorophosphate (100 mM in MeCN) was used as electrolyte. The concentration of the complexes was about 2 mM. UV/Vis spectra were recorded on an Agilent Cary 60 UV-Vis spectrophotometer with a concentration of 0.2 mM complex in acetonitrile. Solid material of all Fe(II) complexes (30 to 40 mg) was studied using ⁵⁷Fe Mössbauer spectroscopy at 80 K. ⁵⁷Fe Mössbauer spectra were measured using a ⁵⁷Co source in a Rh matrix using an alternating constant acceleration Wissel Mössbauer spectrometer equipped with a Janis closed-cycle helium cryostat.

Transmission data were collected, and isomer shifts are reported relative to iron metal at ambient temperature. Experimental data were simulated with *mf2.SL* software.[76] A temperature-dependent magnetic susceptibility measurement of **A** (19.4 mg) was carried out with a *Quantum-Design* MPMS3 SQUID magnetometer equipped with a 7 Tesla magnet in the range from 400 to 2.0 K at a magnetic field of 0.5 T. The powdered sample was contained in a polycarbonate capsule (29.4 mg) and fixed in a non-magnetic sample holder. Each raw data file for the measured magnetic moment was corrected for the diamagnetic contribution of the sample holder and the polycarbonate capsule. The molar susceptibility data was corrected for the diamagnetic contribution. Temperature-independent paramagnetism ($TIP = 1980 \cdot 10^{-6} \text{ cm}^3 \text{ mol}^{-1}$) and paramagnetic impurities ($PI = 1.3\%$ with $S = 5/2$) were included according to $\chi_{\text{calc}} = (1 - PI) \cdot \chi + PI \cdot \chi_{\text{mono}} + TIP$. Simulation of the experimental magnetic data was performed with the *julX* program.[77].

4.2. Catalytic procedures

Experimental remarks. GC analysis was performed with an Agilent Technologies 7890B GC-FID system with a 7693A Automatic Liquid Sampler for 150 samples with G4513A Autoinjector using a HP-5 column (30 m \times 320 μm \times 0.25 μm). NMR spectra were recorded on a Bruker Advanced Ultrashield AV400 (400 MHz) or AV500 (500 MHz) spectrometer at a temperature of 297 K. Chemical shifts (δ) are reported in ppm and referenced to the residual signal of the deuterated solvent [75].

Catalytic procedure. All catalytic reactions were conducted in a cryostat (JulaboFP-50). Acetonitrile (HPLC-grade) as solvent was applied for all experiments, which are screened *via* GC (substrates: *cis*-cyclooctene, *cis*-cyclohexene, 1-octene, 1-decene and allyl ethyl ether). The screening of other substrates (*cis*-cyclohexene, 1-hexene, allyl alcohol, allyl chloride, styrene, chalcone, *cis*-2-octene and *trans*-2-octene) was performed using ^1H NMR spectroscopy and deuterated acetonitrile as solvent. The catalyst was added from a preformed stock solution in acetonitrile corresponding to the appropriate stoichiometry to a solution of the respective substrate (1.00 eq., 67.3 $\mu\text{mol/mL}$). Hydrogen peroxide (50% aq., 1.50 eq., 101 $\mu\text{mol/mL}$) was used as oxidizing agent and, if required, $\text{Sc}(\text{OTf})_3$ as additive (0.10 eq., 8.41 $\mu\text{mol/mL}$). The reaction was started upon addition of the catalyst stock solution, by adding the catalyst solution all at once. The reaction was terminated by adding electrolytically precipitated activated MnO_2 in order to decompose the excess of H_2O_2 in the reaction solution. After filtration over activated neutral alumina (separation of the catalyst), GC samples were prepared for each experiment and time point using 200 μL filtrate, diluted with 1300 μL MeCN, in which *p*-xylene (0.9 $\mu\text{L/mL}$) is dissolved as an external standard. For the screening *via* ^1H NMR spectroscopy, 500 μL filtrate was added to 1 μL benzene as external standard. Control experiments without catalyst were performed for all reactions and did not show catalytic activity. An additional blank experiment with a simple iron salt, iron(II) chloride, in the presence of H_2O_2 was conducted to highlight the importance of iron complexes associated with NHCs due to minimal product and unselective side-product formation. Analogous, the additive $\text{Sc}(\text{OTf})_3$ itself shows minimal unselective catalytic activity [15].

4.3. Synthetic procedures

[**H₂L1**](Br)₂

The synthesis follows a similar procedure with regard to literature methods [78]. 2-(4,5-Dimethyl-1*H*-imidazol-1-yl)pyridine (0.49 g, 2.83 mmol, 2.00 eq.) is dissolved in excess dibromomethane (4.00 mL, 57.3 mmol, 40.5 eq.) and heated to 110 °C for 16 h while stirring. The brown oil is dried *in vacuo*, leaving a brown solid, which is washed with MeCN (~27 mL) to yield a white precipitate. The brown supernatant is removed, the white solid is washed with cold MeCN and dried *in vacuo* to obtain [**H₂L1**](Br)₂ as white powder (0.35 g, 0.74 mmol, 48%).

^1H NMR (400.13 MHz, CDCl_3): δ 10.92 (s, 2H, NCHN), 8.59 (dd, $^3J = 4.8$, $^4J = 1.8$ Hz, 2H, H_{py}), 8.24 (d, $^3J = 7.9$ Hz, 2H, H_{py}), 8.04 (td, $^3J = 7.9$, $^4J = 1.8$ Hz, 2H, H_{py}), 7.74 (s, 2H, CH_2), 7.52 (dd, $^3J = 7.6$, $^3J = 4.8$ Hz, 2H, H_{py}), 2.67 (s, 6H, CH_3), 2.41 (s, 6H, CH_3).

MS-ESI (m/z): [**H₂L1** - H⁺]⁺ calcd., 359.20; found, 359 (100); [**H₂L1** + H⁺ - CH_2ImPy]⁺ calcd., 174.10; found, 174 (35).

[**H₂L1**](PF₆)₂

The synthesis follows a similar procedure with regard to literature methods [78]. [**H₂L1**](Br)₂ (202 mg, 388 μmol , 1.00 eq.) is dissolved in 2 mL H_2O and slowly added to a vigorously stirred solution of NH_4PF_6 (316 mg, 1.94 mmol, 5.00 eq.) in 25 mL H_2O . After stirring for 45 min, the white precipitate is filtered off and washed with cold H_2O . The white solid is redissolved in 1.5 mL acetone and precipitated by adding 7 mL Et_2O . The precipitate is filtered, washed with Et_2O and dried under vacuum to obtain [**H₂L1**](PF₆)₂ as white powder (118 mg, 181 μmol , 47%). The product is dried overnight at 60 °C at 10^{-3} mbar and stored under argon.

^1H NMR (400.13 MHz, CD_3CN): δ 9.01 (s, 2H, NCHN), 8.68 (ddd, $^3J = 4.8$ Hz, $^4J = 1.9$ Hz, $^4J = 0.9$ Hz, 2H, H_{py}), 8.14 (td, $^3J = 7.9$ Hz, $^4J = 1.9$ Hz, 2H, H_{py}), 7.68 (ddd, $^3J = 7.6$ Hz, $^3J = 4.8$ Hz, $^4J = 0.9$ Hz, 2H, H_{py}), 7.63 (dd, $^3J = 8.0$, $^4J = 0.9$ Hz, 2H, H_{py}), 6.45 (s, 2H, CH_2), 2.40 (s, 6H, CH_3), 2.34 (s, 6H, CH_3).

^{13}C NMR (100.53 MHz, CD_3CN): δ 151.06 (2C, CH), 147.31 (2C, CH), 141.36 (2C, CH), 136.36 (2C, CH), 130.01 (2C, CH), 129.36 (2C, CH), 127.34 (2C, CH), 120.74 (2C, CH), 57.33 (1C, CH_2), 9.86 (2C, CH_3), 8.96 (2C, CH_3).

MS-ESI (m/z): [**H₂L1**](PF₆)₂⁺ calcd., 505.17; found, 505 (10); [**H₂L1** - H⁺]⁺ calcd., 359.20; found, 359 (100); [**H₂L1** + H⁺ - CH_2ImPy]⁺ calcd., 174.10; found, 174 (12).

Anal. calcd. for $\text{C}_{21}\text{H}_{24}\text{F}_{12}\text{N}_6\text{P}_2$: C 38.78; H 3.72; N 12.92. Found: C 38.87; H 3.56; N 12.71.

[**FeL1**(MeCN)₂](PF₆)₂ (1)

The synthesis follows a similar procedure with regard to literature methods [78]. $\text{Fe}[\text{N}(\text{SiMe}_3)_2](\text{THF})$ (302 mg, 673 μmol , 1.00 eq.) is dissolved in ~5 mL MeCN giving a green solution, which becomes yellow and light brown after 15 min and is frozen in liquid N_2 . A solution of [**H₂L1**](PF₆)₂ (492 mg, 756 μmol , 1.12 eq.) in 10 mL MeCN is added over 1 min to the frozen solution, which changes its color to red and is slowly warmed to r.t. while stirring overnight. The following red suspension is dried *in vacuo* and suspended in 20 mL MeCN. The solvent is removed under vacuum and the red solid is suspended in 20 mL MeCN again. This is repeated once more to remove residual amine. The red suspension (in 20 mL MeCN) is filtrated, and the yellow residue is washed twice with 20 mL MeCN in order to dissolve all solid. The three filtrates are collected in one batch (60 mL MeCN) and 60 mL Et_2O are added to precipitate an orange solid. The orange solid is filtered off, washed with Et_2O (3 \times 4 mL), dried at 60 °C at 10^{-3} mbar overnight to yield 370 mg of the iron complex. The orange filtrate (60 mL MeCN + 60 mL Et_2O) is concentrated under vacuum until ~10 mL of dark-red solution are remaining. 40 mL of Et_2O are added to give an orange precipitate, which is filtrated, washed with Et_2O (3 \times 5 mL), dried at 60 °C at 10^{-3} mbar overnight to yield additional 15 mg of iron complex. [**FeL1**(MeCN)₂](PF₆)₂ can be obtained as orange powder in total yield of 73% (385 mg, 490 μmol). Single crystals suitable for X-ray diffraction were obtained by slow evaporation of a solution of [**FeL1**(MeCN)₂](PF₆)₂ in MeCN over 3 weeks at r.t. under ambient conditions (see SI for details).

^1H NMR (400.13 MHz, CD_3CN): δ 9.60 (ddd, $^3J = 5.4$ Hz, $^4J = 1.7$ Hz, $^4J = 0.9$ Hz, 2H, H_{py}), 8.29 (ddd, $^3J = 8.5$ Hz, $^3J = 7.5$ Hz, $^4J = 1.7$ Hz,

^2H , H_{py} , 8.17 (dt, $^3J = 8.5$ Hz, $^4J = 0.9$ Hz, 2H, H_{py}), 7.72 (ddd, $^3J = 7.5$ Hz, $^3J = 5.4$ Hz, $^4J = 0.9$ Hz, 2H, H_{py}), 6.77 (s, 2H, CH_2), 2.77 (d, $^5J = 1.2$ Hz, 6H, CH_3), 2.50 (d, $^5J = 1.2$ Hz, 6H, CH_3), 1.96 (s, 6H, CH_3CN).

^{13}C NMR (100.53 MHz, CD_3CN): δ 215.49 (2C, C_{carbene}), 156.93 (2C, CH), 153.56 (2C, CH), 141.95 (2C, CH), 131.08 (2C, CH), 127.51 (2C, CH), 123.71 (2C, CH), 114.03 (2C, CH), 62.30 (1C, CH_2), 11.70 (2C, CH_3), 9.00 (2C, CH_3).

MS-ESI (m/z): $[\text{FeL1} + \text{HCOO}]^+$ calcd., 459.12; found, 458.89 (69); $[\text{FeL1}(\text{MeCN})_2]^{2+}$ calcd., 248.09; found, 247.63 (50); $[\text{FeL1}(\text{MeCN})]^{2+}$ calcd., 227.57; found, 227.26 (82); $[\text{FeL1}]^{2+}$ calcd., 207.06; found, 207.21 (100).

Anal. calcd. for $\text{C}_{25}\text{H}_{28}\text{F}_{12}\text{FeN}_8\text{P}_2$: C 38.19; H 3.59; N 14.25. Found: C 38.41; H 3.68; N 14.23.

$[\text{H}_2\text{L2}](\text{Br})_2$

The synthesis follows a similar procedure with regard to literature methods [78]. 2-(1H-imidazol-1-yl)pyrimidine (323 mg, 1.65 mmol, 2.00 eq.) is dissolved in excess dibromomethane (25 mL, 358 mmol, 433 eq.) and heated to 110 °C for 16 h while stirring. The brown suspension is dried *in vacuo*. The crude product is dissolved in MeOH (~20 mL), precipitated with approximately 30 mL of EtOAc, filtered and washed with EtOAc to yield $[\text{H}_2\text{L2}](\text{Br})_2$ as off-white powder (291 mg). To increase the yield, the yellow filtrate was dried *in vacuo*. The brown solid was suspended in little MeOH, Et_2O was added and the resulting light-brown precipitate was filtered, washed with MeCN and Et_2O to give additional $[\text{H}_2\text{L2}](\text{Br})_2$ as off-white powder (55 mg). 74% yield in total (346 mg, 0.61 mmol).

^1H NMR (400.13 MHz, $\text{DMSO}-d_6$): δ 10.59 (ps. t, $^4J = 1.7$ Hz, 2H, NCHN), 9.11 (d, $^3J = 4.9$ Hz, 4H, H_{pym}), 8.59 (ps. t, $^4J = 2.0$ Hz, 2H, CH_{im}), 8.39 (ps. t, $^4J = 2.0$ Hz, 2H, CH_{im}), 7.84 (t, $^3J = 4.9$ Hz, 2H, H_{pym}), 6.99 (s, 2H, CH_2).

MS-ESI (m/z): $[\text{H}_2\text{L2} - \text{H}^+]^+$ calcd., 305.13; found, 305.10 (43); $[\text{H}_2\text{L2}]^{2+}$ calcd., 153.06; found, 153.10 (100); $[\text{H}_2\text{L2} + \text{H}^+ - \text{CH}_2\text{ImC}_4\text{H}_3\text{N}_2]^+$ calcd., 147.07; found, 147.03 (72).

$[\text{H}_2\text{L2}](\text{PF}_6)_2$

The synthesis follows a similar procedure with regard to literature methods [78]. $[\text{H}_2\text{L2}](\text{Br})_2$ (614 mg, 1.32 mmol, 1.00 eq.) is dissolved in around 14 mL H_2O and slowly added to a vigorously stirred solution of NH_4PF_6 (1.02 g, 6.25 mmol, 5.00 eq.) in 25 mL H_2O . After stirring for 15 min, the off-white precipitate is filtered off, washed with H_2O and Et_2O . The product is dried at 60 °C at 10^{-3} mbar and stored under argon. $[\text{H}_2\text{L2}](\text{PF}_6)_2$ is obtained as off-white solid in 69% yield (542 mg, 909 μmol).

^1H NMR (400.13 MHz, $\text{DMSO}-d_6$): δ 10.51 (ps. t, $^4J = 1.4$ Hz, 2H, NCHN), 9.11 (d, $^3J = 4.9$ Hz, 4H, H_{pym}), 8.59 (ps. t, $^4J = 1.9$ Hz, 2H, CH_{im}), 8.25 (ps. t, $^4J = 1.9$ Hz, 2H, CH_{im}), 7.83 (t, $^3J = 4.9$ Hz, 2H, H_{pym}), 6.86 (s, 2H, CH_2).

^1H NMR (400.13 MHz, CD_3CN): δ 9.89 (m, 2H, NCHN), 8.95 (d, $^3J = 4.9$ Hz, 4H, H_{pym}), 8.38 (m, 2H, CH_{im}), 7.88 (m, 2H, CH_{im}), 7.70 (t, $^3J = 4.9$ Hz, 2H, H_{pym}), 6.68 (s, 2H, CH_2).

^{13}C NMR (100.53 MHz, $\text{DMSO}-d_6$): δ 160.32 (4C, CH), 151.81 (2C, CH), 138.38 (2C, CH), 123.56 (2C, CH), 122.97 (2C, CH), 119.66 (2C, CH), 59.30 (1C, CH_2).

^{13}C NMR (100.53 MHz, CD_3CN): δ 161.13 (4C, CH), 152.86 (2C, CH), 137.77 (2C, CH), 124.51 (2C, CH), 124.17 (2C, CH), 121.43 (2C, CH), 60.89 (1C, CH_2).

MS-ESI (m/z): $[\text{H}_2\text{L2} + \text{PF}_6]^+$ calcd., 451.10; found, 450.77 (77); $[\text{H}_2\text{L2} - \text{H}^+]^+$ calcd., 305.13; found, 305.11 (37); $[\text{H}_2\text{L2}]^{2+}$ calcd., 153.06; found, 153.09 (100).

Anal. calcd. for $\text{C}_{15}\text{H}_{14}\text{F}_{12}\text{N}_8\text{P}_2$: C 30.22; H 2.37; N 18.79. Found: C 30.19; H 2.14; N 18.56.

$[\text{FeL2}(\text{MeCN})_2](\text{PF}_6)_2$ (2)

The synthesis follows a similar procedure with regard to literature methods [78]. A -35 °C cold solution of $\text{Fe}[\text{N}(\text{SiMe}_3)_2](\text{THF})$ (178 mg, 396 μmol , 1.05 eq.) in 5 mL MeCN is added to a -35 °C cold solution of $[\text{H}_2\text{L2}](\text{PF}_6)_2$ (225 mg, 377 μmol , 1.00 eq.) in 5 mL MeCN. The red solution becomes a red suspension after 10 min and is stirred at r.t. for 20 h. The formed dark brown solution is dried *in vacuo* and suspended in 10 mL MeCN. 10 mL Et_2O are added to precipitate an orange solid. The brown supernatant is removed and the solid washed twice with 3 mL Et_2O , once dropwise with around 0.5 to 1 mL MeCN and finally 3 mL Et_2O again. $[\text{FeL2}(\text{MeCN})_2](\text{PF}_6)_2$ can be obtained as orange solid in 68% yield (189 mg, 258 μmol). Single crystals suitable for X-ray diffraction were obtained by slow vapor diffusion of 1,4-dioxane into a solution of $[\text{FeL2}(\text{MeCN})_2](\text{PF}_6)_2$ in MeCN after 1 to 2 weeks (see SI for details).

^1H NMR (400.13 MHz, CD_3CN): δ 9.77 (dd, $^3J = 5.4$, $^4J = 2.2$ Hz, 2H, H_{pym}), 9.13 (dd, $^3J = 4.9$, $^4J = 2.2$ Hz, 2H, H_{pym}), 8.33 (d, $^4J = 2.3$ Hz, 2H, CH_{im}), 7.87 (d, $^4J = 2.4$ Hz, 2H, CH_{im}), 7.79 (ps. t, $^3J = 5.2$ Hz, 2H, H_{pym}), 7.02 (s, 2H, CH_2), 1.96 (s, 6H, CH_3CN).

^{13}C NMR (100.53 MHz, CD_3CN): δ 216.24 (2C, C_{carbene}), 164.28 (2C, CH), 161.34 (2C, CH), 160.68 (2C, CH), 126.69 (2C, CH), 120.99 (2C, CH), 120.55 (2C, CH), 64.86 (1C, CH_2).

MS-ESI (m/z): $[\text{FeL2} + \text{HCOO}]^+$ calcd., 405.05; found, 404.91 (96); $[\text{FeL2}(\text{MeCN})_2]^{2+}$ calcd., 221.05; found, 220.61 (67); $[\text{FeL2}(\text{MeCN})]^{2+}$ calcd., 200.54; found, 200.27 (94); $[\text{FeL2}]^{2+}$ calcd., 180.02; found, 180.03 (100).

Anal. calcd. for $\text{C}_{19}\text{H}_{18}\text{F}_{12}\text{FeN}_{10}\text{P}_2$: C 31.17; H 2.48; N 19.13. Found: C 31.20; H 2.29; N 18.84.

Declaration of Competing Interest

The authors declare that they have no known competing financial interests or personal relationships that could have appeared to influence the work reported in this paper.

Data availability

No data was used for the research described in the article.

Acknowledgements

Dr. Irina Znakovskaya is thanked for preliminary SQUID measurements. I.R. acknowledges support from the Fonds der Chemischen Industrie (Kekulé fellowship). Part of this work has been supported by the Deutsche Forschungsgemeinschaft (DFG), project no. 445916766 (to F.M.), in the framework of the Research Unit “Bioinspired Oxidation Catalysis with Iron Complexes” (FOR 5215).

Appendix A. Supplementary material

Supplementary data to this article can be found online at <https://doi.org/10.1016/j.jcat.2023.07.018>.

References

- [1] O. Shoji, Y. Watanabe, in: Fifty Years of Cytochrome P450 Research (Ed.: H. Yamazaki), Springer Japan: Tokyo, 2014, pp. 107–124, DOI: 10.1007/978-4-431-54992-5_6.
- [2] K.S. Smith, H.L.O. Huyck, G.S. Plumlee, M.J. Logsdon, L.F. Filipek, in: The Environmental Geochemistry of Mineral Deposits: Part A: Processes, Techniques,

- and Health Issues Part B: Case Studies and Research Topics, Vol. 6, Society of Economic Geologists, 1997, pp. 29–70, DOI: 10.5382/Rev.06.02.
- [3] K.S. Egorova, V.P. Ananikov, *Organometallics* 36 (2017) 4071–4090, <https://doi.org/10.1021/acs.organomet.7b00605>.
- [4] K.S. Egorova, V.P. Ananikov, *Angew. Chem. Int. Ed.* 55 (2016) 12150–12162, <https://doi.org/10.1002/anie.201603777>.
- [5] D. Dolphin, T.G. Traylor, L.Y. Xie, *Acc. Chem. Res.* 30 (1997) 251–259, <https://doi.org/10.1021/ar960126u>.
- [6] I.D. Cunningham, T.N. Danks, J.N. Hay, I. Hamerton, S. Gunathilagan, C. Janczak, *J. Mol. Catal. A: Chem.* 185 (2002) 25–31, [https://doi.org/10.1016/S1381-1169\(02\)00057-2](https://doi.org/10.1016/S1381-1169(02)00057-2).
- [7] M.A. Sainna, S. Kumar, D. Kumar, S. Fornarini, M.E. Crestoni, S.P. de Visser, *Chem. Sci.* 6 (2015) 1516–1529, <https://doi.org/10.1039/C4SC02717E>.
- [8] K.P. Bryliakov, E.P. Talsi, *Coord. Chem. Rev.* 276 (2014) 73–96, <https://doi.org/10.1016/j.ccr.2014.06.009>.
- [9] S.M. Hözl, P.J. Altmann, J.W. Kück, F.E. Kühn, *Coord. Chem. Rev.* 352 (2017) 517–536, <https://doi.org/10.1016/j.ccr.2017.09.015>.
- [10] C.-L. Sun, B.-J. Li, Z.-J. Shi, *Chem. Rev.* 111 (2011) 1293–1314, <https://doi.org/10.1021/cr100198w>.
- [11] W.N. Oloo, L. Que, *Acc. Chem. Res.* 48 (2015) 2612–2621, <https://doi.org/10.1021/acs.accounts.5b00053>.
- [12] L. Que, W.B. Tolman, *Nature* 455 (2008) 333–340, <https://doi.org/10.1038/nature07371>.
- [13] S.A. Hauser, M. Cokoja, F.E. Kühn, *Catal. Sci. Technol.* 3 (2013) 552–561, <https://doi.org/10.1039/C2CY20595E>.
- [14] J.W. Kück, M.R. Anneser, B. Hofmann, A. Pöthig, M. Cokoja, F.E. Kühn, *ChemSusChem* 8 (2015) 4056–4063, <https://doi.org/10.1002/cssc.201500930>.
- [15] F. Dyckhoff, J.F. Schlagintweit, R.M. Reich, F.E. Kühn, *Catal. Sci. Technol.* 10 (2020) 3532–3536, <https://doi.org/10.1039/D0CY00631A>.
- [16] G.G. Zámbo, J. Mayr, M.J. Sauer, T.P. Schlachta, R.M. Reich, F.E. Kühn, *Dalton Trans.* 51 (2022) 13591–13595, <https://doi.org/10.1039/D2DT02561B>.
- [17] J.F. Schlagintweit, F. Dyckhoff, L. Nguyen, C.H.G. Jakob, R.M. Reich, F.E. Kühn, *J. Catal.* 383 (2020) 144–152, <https://doi.org/10.1016/j.jcat.2020.01.011>.
- [18] R. Mas-Ballesté, L. Que, *J. Am. Chem. Soc.* 129 (2007) 15964–15972, <https://doi.org/10.1021/ja075115i>.
- [19] A. Schmidt, N. Grover, T.K. Zimmermann, L. Graser, M. Cokoja, A. Pöthig, F.E. Kühn, *J. Catal.* 319 (2014) 119–126, <https://doi.org/10.1016/j.jcat.2014.08.013>.
- [20] M.R. Anneser, S. Haslinger, A. Pöthig, M. Cokoja, V. D'Elia, M.P. Högerl, J.-M. Basset, F.E. Kühn, *Dalton Trans.* 45 (2016) 6449–6455, <https://doi.org/10.1039/C6DT00538A>.
- [21] T.P. Schlachta, M.R. Anneser, J.F. Schlagintweit, C.H.G. Jakob, C. Hintermeier, A. D. Böth, S. Haslinger, R.M. Reich, F.E. Kühn, *Chem. Commun.* 57 (2021) 6644–6647, <https://doi.org/10.1039/D1CC02027G>.
- [22] M.A. Bernd, F. Dyckhoff, B.J. Hofmann, A.D. Böth, J.F. Schlagintweit, J. Oberkofler, R.M. Reich, F.E. Kühn, *J. Catal.* 391 (2020) 548–561, <https://doi.org/10.1016/j.jcat.2020.08.037>.
- [23] S. Haslinger, A. Raba, M. Cokoja, A. Pöthig, F.E. Kühn, *J. Catal.* 331 (2015) 147–153, <https://doi.org/10.1016/j.jcat.2015.08.026>.
- [24] F. Dyckhoff, J.F. Schlagintweit, M.A. Bernd, C.H.G. Jakob, T.P. Schlachta, B. J. Hofmann, R.M. Reich, F.E. Kühn, *Catal. Sci. Technol.* 11 (2021) 795–799, <https://doi.org/10.1039/D0CY02433C>.
- [25] E.-M.-H.-J. Esslinger, J.F. Schlagintweit, G.G. Zámbo, A.M. Imhof, R.M. Reich, F.E. Kühn, *Asian J. Org. Chem.* 10 (2021) 2654–2662, <https://doi.org/10.1002/ajoc.202100487>.
- [26] T.P. Schlachta, J.F. Schlagintweit, M.R. Anneser, E.-M.-H.-J. Esslinger, M. Muhr, S. Haslinger, F.E. Kühn, *Inorg. Chim. Acta* 518 (2021), 120228, <https://doi.org/10.1016/j.ica.2020.120228>.
- [27] M. Guo, Y.-M. Lee, S. Fukuzumi, W. Nam, *Coord. Chem. Rev.* 435 (2021), 213807, <https://doi.org/10.1016/j.ccr.2021.213807>.
- [28] T.P. Schlachta, F.E. Kühn, *Chem. Soc. Rev.* 52 (2023) 2238–2277, <https://doi.org/10.1039/D2CS01064J>.
- [29] A. Raba, M. Cokoja, S. Ewald, K. Riener, E. Herdtweck, A. Pöthig, W.A. Herrmann, F.E. Kühn, *Organometallics* 31 (2012) 2793–2800, <https://doi.org/10.1021/om2010673>.
- [30] A.C. Lindhorst, J. Schütz, T. Netscher, W. Bonrath, F.E. Kühn, *Catal. Sci. Technol.* 7 (2017) 1902–1911, <https://doi.org/10.1039/C7CY00557A>.
- [31] A. Raba, M. Cokoja, W.A. Herrmann, F.E. Kühn, *Chem. Commun.* 50 (2014) 11454–11457, <https://doi.org/10.1039/C4CC02178A>.
- [32] A.C. Lindhorst, M. Drees, W. Bonrath, J. Schütz, T. Netscher, F.E. Kühn, *J. Catal.* 352 (2017) 599–605, <https://doi.org/10.1016/j.jcat.2017.06.018>.
- [33] G.G. Zámbo, J.F. Schlagintweit, R.M. Reich, F.E. Kühn, *Catal. Sci. Technol.* 12 (2022) 4940–4961, <https://doi.org/10.1039/D2CY00127F>.
- [34] J.W. Kück, A. Raba, I.I.E. Markovits, M. Cokoja, F.E. Kühn, *ChemCatChem* 6 (2014) 1882–1886, <https://doi.org/10.1002/cctc.201402063>.
- [35] A. Raba, M.R. Anneser, D. Jantke, M. Cokoja, W.A. Herrmann, F.E. Kühn, *Tetrahedron Lett.* 54 (2013) 3384–3387, <https://doi.org/10.1016/j.tetlet.2013.04.060>.
- [36] L. Zhu, L. Cheng, Y. Zhang, R. Xie, J. You, *J. Org. Chem.* 72 (2007) 2737–2743, <https://doi.org/10.1021/jo062059f>.
- [37] A.A. Danopoulos, N. Tsoureas, J.A. Wright, M.E. Light, *Organometallics* 23 (2004) 166–168, <https://doi.org/10.1021/om0341911>.
- [38] H.V. Huynh, Y. Han, R. Jothibasu, J.A. Yang, *Organometallics* 28 (2009) 5395–5404, <https://doi.org/10.1021/om900667d>.
- [39] D.G. Gusev, *Organometallics* 28 (2009) 6458–6461, <https://doi.org/10.1021/om900654g>.
- [40] W. Yao, K. Kavallieratos, S. de Gala, R.H. Crabtree, *Inorg. Chim. Acta* 311 (2000) 45–49, [https://doi.org/10.1016/S0020-1693\(00\)00308-X](https://doi.org/10.1016/S0020-1693(00)00308-X).
- [41] S. Haslinger, J.W. Kück, E.M. Hahn, M. Cokoja, A. Pöthig, J.-M. Basset, F.E. Kühn, *Inorg. Chem.* 53 (2014) 11573–11583, <https://doi.org/10.1021/ic501613a>.
- [42] S. Haslinger, A.C. Lindhorst, J.W. Kück, M. Cokoja, A. Pöthig, F.E. Kühn, *RSC Adv.* 5 (2015) 85486–85493, <https://doi.org/10.1039/C5RA18270K>.
- [43] D.T. Weiss, M.R. Anneser, S. Haslinger, A. Pöthig, M. Cokoja, J.-M. Basset, F.E. Kühn, *Organometallics* 34 (2015) 5155–5166, <https://doi.org/10.1021/acs.organomet.5b00732>.
- [44] S. Haslinger, J.W. Kück, M.R. Anneser, M. Cokoja, A. Pöthig, F.E. Kühn, *Chem. Eur. J.* 21 (2015) 17860–17869, <https://doi.org/10.1002/chem.201503282>.
- [45] D.A. Kurtz, K.R. Brereton, K.P. Ruoff, H.M. Tang, G.A.N. Felton, A.J.M. Miller, J. L. Dempsey, *Inorg. Chem.* 57 (2018) 5389–5399, <https://doi.org/10.1021/acs.inorgchem.8b00360>.
- [46] C. Kupper, J.A. Rees, S. Dechert, S. DeBeer, F. Meyer, *J. Am. Chem. Soc.* 138 (2016) 7888–7898, <https://doi.org/10.1021/jacs.6b00584>.
- [47] E.U. Mughal, M. Mirzaei, A. Sadiq, S. Fatima, A. Naseem, N. Naem, N. Fatima, S. Kausar, A.A. Altaf, M.N. Zafar, B.A. Khan, *Royal Society Open Science* 7 (2020), 201208, <https://doi.org/10.1098/rsos.201208>.
- [48] P. Gütllich, E. Bill, A. X. Trautwein, *Mössbauer Spectroscopy and Transition Metal Chemistry: Fundamentals and Applications*, Springer Berlin Heidelberg: Berlin, Heidelberg, 2011, DOI: 10.1007/978-3-540-88428-6.
- [49] J. Donat, P. Dubourdeaux, M. Clémancey, J. Rendon, C. Gervasoni, M. Barbier, J. Barilone, J. Pécaut, S. Gambarelli, P. Maldivi, J.-M. Latour, *Chem. Eur. J.* 28 (2022) e202201875.
- [50] S. Meyer, I. Klawitter, S. Demeshko, E. Bill, F. Meyer, *Angew. Chem. Int. Ed.* 52 (2013) 901–905, <https://doi.org/10.1002/anie.201208044>.
- [51] C. Schremmer, C. Cordes, I. Klawitter, M. Bergner, C.E. Schiewer, S. Dechert, S. Demeshko, M. John, F. Meyer, *Chem. Eur. J.* 25 (2019) 3918–3929, <https://doi.org/10.1002/chem.201805855>.
- [52] P. Gütllich, *Chem. unserer Zeit* 4 (1970) 133–144, <https://doi.org/10.1002/ciuz.19700040502>.
- [53] P. Gütllich, *Chem. unserer Zeit* 5 (1971) 131–141, <https://doi.org/10.1002/ciuz.19710050502>.
- [54] P. Gütllich, *Eur. J. Inorg. Chem.* 2013 (2013) 581–591, <https://doi.org/10.1002/ejic.201300092>.
- [55] P.O. Löwdin, *J. Chem. Phys.* 18 (1950) 365–375, <https://doi.org/10.1063/1.1747632>.
- [56] C.L. Hill, *Nature* 401 (1999) 436–437, <https://doi.org/10.1038/46704>.
- [57] R. Noyori, M. Aoki, K. Sato, *Chem. Commun.* (2003) 1977–1986, <https://doi.org/10.1039/B303160H>.
- [58] S. Haslinger, A. Pöthig, M. Cokoja, F.E. Kühn, *Acta Cryst. C* 71 (2015) 1096–1099, <https://doi.org/10.1107/S2053229615021968>.
- [59] F.G. Cantú Reinhard, S.P. de Visser, *Chem. Eur. J.* 23 (2017) 2935–2944, <https://doi.org/10.1002/chem.201605505>.
- [60] E.A. Mikhalyova, O.V. Makhlynets, T.D. Palluccio, A.S. Filatov, E.V. Rybak-Akimova, *Chem. Commun.* 48 (2012) 687–689, <https://doi.org/10.1039/C1CC15935F>.
- [61] A. Company, L. Gómez, X. Fontrodona, X. Ribas, M. Costas, *Chem. Eur. J.* 14 (2008) 5727–5731, <https://doi.org/10.1002/chem.200800724>.
- [62] H.C. Kolb, M.G. Finn, K.B. Sharpless, *Angew. Chem. Int. Ed.* 40 (2001) 2004–2021, [https://doi.org/10.1002/1521-3773\(20010601\)40:11<2004::AID-ANIE2004>3.0.CO;2-5](https://doi.org/10.1002/1521-3773(20010601)40:11<2004::AID-ANIE2004>3.0.CO;2-5).
- [63] S.T. Oyama, in: *Mechanisms in Homogeneous and Heterogeneous Epoxidation Catalysis* (Ed.: S. T. Oyama), Elsevier: Amsterdam, 2008, pp. 3–99, DOI: 10.1016/B978-0-444-53188-9.00001-8.
- [64] H.H. Szmant, *Organic Building Blocks of the Chemical Industry*, Wiley, New York, 1989.
- [65] C. Anaya de Parrodi, E. Juaristi, *Synlett* 2006 (2006) 2699–2715, <https://doi.org/10.1055/s-2006-950259>.
- [66] I. Kim, S.M. Kim, C.-S. Ha, D.-W. Park, *Macromol. Rapid Commun.* 25 (2004) 888–893, <https://doi.org/10.1002/marc.200300287>.
- [67] A. Ansmann, R. Kawa, M. Neuss, *Patent* US7083780B2, 2006.
- [68] R. Mas-Ballesté, M. Costas, T. van den Berg, L. Que Jr., *Chem. Eur. J.* 12 (2006) 7489–7500, <https://doi.org/10.1002/chem.200600453>.
- [69] M.M. Olmstead, P.P. Power, S.C. Shoner, *Inorg. Chem.* 30 (1991) 2547–2551, <https://doi.org/10.1021/ic00011a017>.
- [70] R.A. Andersen, K. Faegri Jr., J.C. Green, A. Haaland, M.F. Lappert, W.P. Leung, K. Rypdal, *Inorg. Chem.* 27 (1988) 1782–1786, <https://doi.org/10.1021/ic00283a022>.
- [71] D.L.J. Broere, I. Čorić, A. Brosnahan, P.L. Holland, *Inorg. Chem.* 56 (2017) 3140–3143, <https://doi.org/10.1021/acs.inorgchem.7b00056>.
- [72] A. Fedulin, A.J. von Wangelin, in: *Encyclopedia of Reagents for Organic Synthesis*, pp. 1–4, DOI: 10.1002/047084289X.rm02274.
- [73] A. Eichhöfer, Y. Lan, V. Mereacre, T. Bodenstern, F. Weigend, *Inorg. Chem.* 53 (2014) 1962–1974, <https://doi.org/10.1021/ic401677j>.
- [74] W. L. Armarego, *Purification of laboratory chemicals*, Butterworth-Heinemann: 2017, <https://www.sciencedirect.com/book/9780128054574/purification-of-laboratory-chemicals#book-description>.
- [75] G.R. Fulmer, A.J.M. Miller, N.H. Sherden, H.E. Gottlieb, A. Nudelman, B.M. Stoltz, J.E. Bercaw, K.I. Goldberg, *Organometallics* 29 (2010) 2176–2179, <https://doi.org/10.1021/om100106e>.

- [76] E. Bill, mf2.SL, Max-Planck Institute for Chemical Energy Conversion: Mülheim/Ruhr, Germany, 2021.
- [77] E. Bill, julX, Max-Planck Institute for Chemical Energy Conversion: Mülheim/Ruhr, Germany, 2008.
- [78] A. D. Raba, Synthesis of Iron N-Heterocyclic Carbene Complexes and Their Application in the Oxidation Catalysis of Hydrocarbons, PhD thesis, Verlag Dr.Hut: München, 2014, <https://www.dr.hut-verlag.de/978-3-8439-1788-9.html>.



Communication

Unraveling the potential of backbone modifications in iron(II) NHC complexes for olefin aziridination and imination

Carla A. Hoefler¹, Nicole K. Dietl¹, Greta G. Zámbo, Tim P. Schlachta, Robert M. Reich, Fritz E. Kühn*

Technical University of Munich, School of Natural Sciences, Department of Chemistry and Catalysis Research Center, Molecular Catalysis, Lichtenbergstraße 4, 85748 Garching, Germany



ARTICLE INFO

Keywords:

Aziridination
Iron *N*-Heterocyclic Carbene (NHC) Complex
Catalytic Optimization
Density Functional Theory (DFT) Calculation
Isomeric Distribution
Backbone Modification

ABSTRACT

A model catalysis reaction for a $C_2 + N_1$ type aziridination and imination of *p*-tolyl azide with *cis*-cyclooctene in toluene is reported. Applying 10 equivalents related to the azide, *cis*-cyclooctene is consumed within 24 h. A reaction temperature of 90 °C is chosen for solubility and activity reasons. A variety of Fe(II) *N*-heterocyclic carbene (NHC) complexes (1–5) are tested as additives. All show promising formation of aziridine and its imine isomer in the benchmark reaction. However, similar activities are also achieved by a metal-free control reaction together with a similar product distribution of **A** (aziridine), **B** (imine) and **C** (aziridine). The metal compounds cannot be considered as catalysts, but they do indeed influence the isomeric distribution of the reaction. To contextualize the conceivable product isomers, density functional theory calculations were performed (B3LYP/6–31G(d,p)) to determine the minimum ground state energies. As expected, these are nearly identical. However, the backbone modification of the open-chain NHC ligated iron(II) complex (5) allows switching of the predominant reaction, favoring imine (**B**) as main product.

1. Introduction

Ethylenimines or aziridines are the nitrogenous analogues of epoxides and therefore the smallest saturated *N*-heterocycles [1]. The azaheterocycle was presumably first synthesized by Gabriel in 1888 by base initiated ring closure of bromoethylamine [2]. Starting from ethanolamine, Wenker prepared aziridine in a two-step procedure by esterification with sulfuric acid and subsequent intramolecular cyclization mediated by NaOH in 1935 [3].

The high ring strain energy infers a highly reactive structure, facilitating an easy cleavage of the C–N bond, consequently leading to rapid participation in nucleophilic ring opening, expanding or rearrangement reactions [4,5]. Apart from acting as building blocks for a multitude of complex nitrogen containing molecules or as monomers for polymer synthesis, their chiral derivatives are useful for the stereoselective construction of a variety of compounds [5–7].

Solely organic strategies are one option for the syntheses of aziridines as well as recently reported electrochemical approaches *via* alkene transformation to a metastable dicationic intermediate and subsequent

basic coupling with a primary amine [8]. Mitigating the conditions in comparison to classic synthesis strategies, transition metal catalyzed methods have been developed to improve selectivity and yield. Similar to historic procedures, base or Lewis acid mediated ring closures are possible. Another infrequently applied method are $C_1N_1 + C_1$ reactions, where a carbene fragment is transferred to an imine [1,4]. Despite efficient performance especially for enantioselective aziridinations, the deficiency of stable imines limits the implementation of such transformations. Prevalent reactions are of the $C_2 + N_1$ type. It involves the addition of a nitrene source that necessitates catalytic activation to ubiquitous olefin substrates. With chiral catalysts, stereochemically pure aziridines can be obtained [4]. The abundance of stable nitrene precursors for aziridination comprise peculiarities like *N*-tosyloxycarbamates, chloramine-T and bromamine-T as well as hypervalent iminoiodinane species such as $PhI=NTs$ [4]. Whereas the latter imply easy activation, their challenging synthesis and poor solubility are disadvantageous. Additionally, the amount of substrate required in excess for this reaction causes low yields and selectivities, as well as the formation of amination and stoichiometric aryl iodide side products. In

* Corresponding author.

E-mail address: fritz.kuehn@ch.tum.de (F.E. Kühn).¹ These authors contributed equally to this work.

contrast, the usage of azides as nitrene reagents generates N_2 as the only side product [4]. Organic azides are of particular interest as they enhance atom economy and functional group tolerance. Aryl and alkyl azides can be easily prepared from amines and sodium azide in a one-step procedure [9,10]. Moreover, they simultaneously allow the direct insertion of a vast number of residues [4].

Microwave-assisted aziridination is performed using catalysts containing Cu, Ni, Co, Fe, Mg, Mn, Sr, Cu, and Rh as metals. With bromamine-T as nitrogen source and styrene as substrate, yields in the range from 40 to 88% are reported. The tested catalysts were nearly exclusive metal halides [11]. More sophisticated catalysts based on porphyrin scaffolds incorporating Ru as metal catalyzed the olefin aziridination by aryl azides leading to conversions up to 100% [12,13].

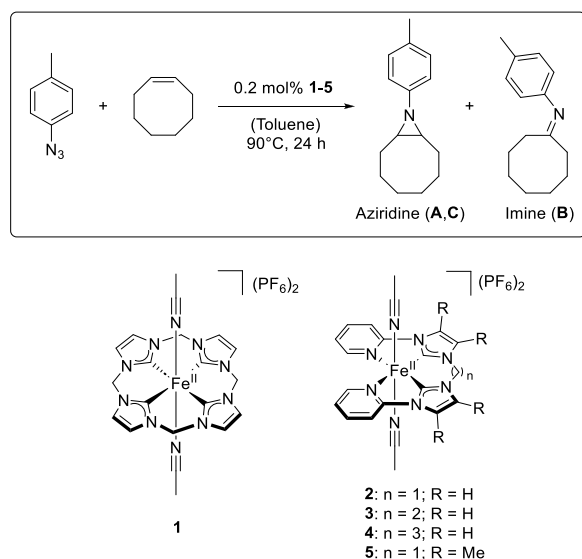
The group of Jenkins applied tetracarbene iron(II) catalysts in olefin aziridination [14,15]. In addition, other studies showed that the structurally similar complex **1** also results in good conversions in the aziridination of a variety of substrates with $PhI=NTs$ as nitrene source [16]. This struck the interest of testing complex **1** amongst other complexes published by our group with regard to their catalytic activity with organic azides [14,15,17–21]. A first indication is given by the good activities of complexes **1–5** in olefin epoxidation [22–25].

The aim of this work was to develop a catalysis method to monitor the reaction of the Fe(II) NHC complexes (**1–5**) in olefin aziridination, by performing preliminary kinetic studies. Analysis was performed *via* GC and GC–MS. In addition, the catalytic impact of **1–5** especially in terms of selectivity was investigated and compared to the metal-free transformation (Scheme 1).

2. Experimental Section

The olefin aziridination reactions reported in this work were performed according to the following procedure:

A Schlenk tube was equipped with a magnetic stir bar, sealed with a septum and put under inert gas atmosphere. The solid Fe(II) complex (**1–5**, 4.20 μ mol, 0.20 mol%, 0.002 equiv.) was added followed by syringe injections of *cis*-cyclooctene (2.75 mL, 21.1 mmol, 10.0 equiv.) and toluene (2.25 mL). In case the complexes were not soluble in this mixture at r.t. (**2–5**) the respective tubes were put in an ultrasonic bath to form homogenous suspensions. Subsequent to tempering the reaction mixture at 90 °C for 15 min, *p*-tolyl azide (281 mg, 2.11 mmol, 1.00 equiv.) was injected as the starting point of the reaction. During the entire reaction time, the mixture was kept at constant 90 °C and stirred with 300 rpm.



Scheme 1. Reaction scheme for the model reaction of *p*-tolyl azide and *cis*-cyclooctene with the different additives (**1–5**) tested.

Samples (0.30 mL) were taken with syringes after 5 min, 0.5 h, 1 h, 2 h, 3 h, 4 h, 5 h, 6 h, 7 h, 8 h and 24 h and cooled to room temperature for 5 min maintaining inert gas atmosphere. The crude samples were filtrated over a miniature silica column to remove the metal species and flushed with MeCN (1.5 mL). Two GC samples were prepared for each chosen data point combining 120 μ L filtrate and 500 μ L standard (*p*-xylene in MeCN 8.00 mg mL⁻¹) which were diluted in 880 μ L MeCN. Analytics are supplied in the Supporting Information.

3. Results and Discussion

The substrates *cis*-cyclooctene and *p*-tolyl azide were chosen for this model reaction as they exhibit good conversions in previous reported aziridination reactions [14,19]. The model reaction was optimized for the additives (“catalysts”) **1–5**. Most reported aziridination reactions employing organic azides only use neat *cis*-cyclooctene as both substrate and solvent [14,19]. Since complexes **2–5** show low solubility at room temperature (r.t. = 25 °C), a mixture of *cis*-cyclooctene and toluene has been used in this work, also significantly reducing the required substrate amount. The optimum amount of *cis*-cyclooctene was set to 10 equiv. for maximum activity in the period of 24 h (see Fig. SI. 26). To further overcome solubility issues and to ensure sufficient product formation, a reaction temperature of 90 °C was chosen, similar to literature conditions [14,15]. To substantiate the elevated temperature, the aziridination reaction was conducted at r.t. in the presence of readily soluble complex **1** and metal-free as control reaction. Product formation was observed to be negligible in both reactions (see Fig. SI.27 + SI.28).

Since organic azides are prone to eliminate N_2 [12], they are not directly detectable *via* GC. However, under the chosen conditions the fragments dimerize to 1,2-di-*p*-tolyl diazene. This was validated by a single peak with corresponding diazene mass in both GC and GC–MS analysis of pure *p*-tolyl azide. This diazene species was also reported as side product in mechanistic studies by Isbill [15]. The GC data show that during the reactions the diazene, respectively azide, is consumed as expected for an undersupplied substrate (see Fig. SI.26). This evidences against the formation of diazene as off-cycle product, hence corroborating the correlation of azide consumption by diazene decrease to reaction progress. With all examined complexes (**1–5**) similar formation levels to the corresponding aziridine (9-(*p*-tolyl)-9-azabicyclo[6.1.0]nonane) and imine (*N*-(*p*-tolyl)cyclooctanimine) are observed.

The optimized catalytic conditions were also tested in the absence of an iron complex as control reaction to justify the addition of an iron complex. Interestingly, this experiment (**metal-free**) results in similar activity, which is implying that the high temperature facilitating the dissolving of the complexes in the reaction mixture is also sufficient to yield product without the presence of an additional metal species. This has recently been reported also for other aryl aziridines [26].

Computational and experimental studies of the catalytic mechanism of $C_2 + N_1$ aziridination by a tetracarbene iron(II) complex have been reported in literature [15]. These examinations confirmed the formation *via* a radical open-chain mechanism instead of an azametallacyclobutane intermediate in the aziridination of *p*-tolyl azide and *cis*-/*trans*-2-octene. A low rotational barrier of the open-chain intermediate allows the formation of diastereomers. For the model reaction reported herein three stereoisomers are conceivable as well as the imine compound featuring the same molecular mass (See Fig. 1).

In the considerations of the possible products aziridines (*S,R*), (*R,R*), (*S,S*) and the respective imine were extended by the imine tautomer, further referred to as enamine.

For all of them, density functional theory (DFT) calculations were performed on a B3LYP/6–31G(d,p) level of theory, as benchmarked for *cis*-cyclooctene systems (see Table 1, Fig. 2) [29]. Multiple local minima were determined for all conceivable products by conformational analysis and global minima were identified (see Table SI.7–SI.9). Coordinates of the (*R,R*) isomer were derived from its (*S,S*) enantiomer by mirroring. Their similar ground state energies (*E*) imply likewise

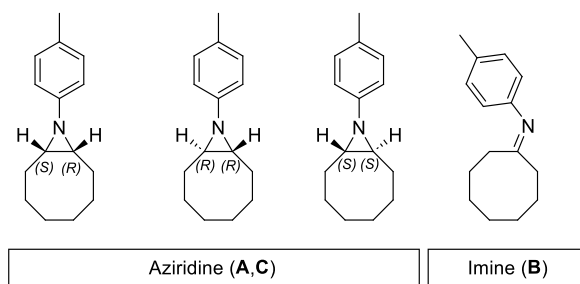


Fig. 1. Structures of the different stereoisomers from the resulting aziridine (A, C) and imine (B).

Table 1

Ground state energies (charge 0, multiplicity 1) of the stereoisomers calculated by Gaussian [27]. Further calculations of the different energies can be found in the supporting information.

	E [kcal mol ⁻¹]	ΔG [kcal mol ⁻¹]
Aziridine (S,R)	-396,093.93	-51.01
Aziridine (R,R)	-396,089.21	-46.67
Aziridine (S,S)	-396,089.21	-46.67
Imine	-396,105.41	-63.84

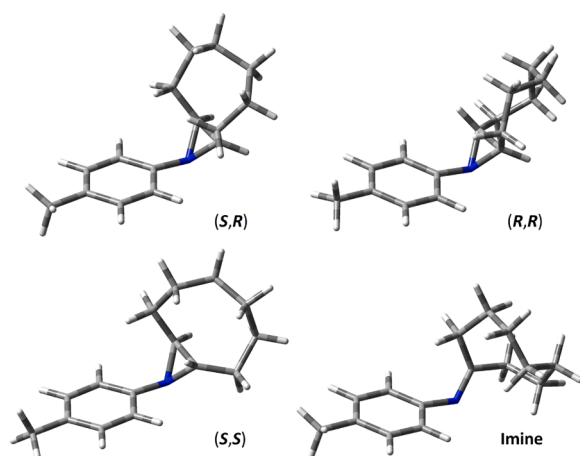


Fig. 2. Tube representation of the different products visualized in Gauss-View [28].

chemical and physical properties of the molecules. As expected, the enamine tautomer is energetically disfavored in comparison to the imine isomer and hence not included in further considerations. In the mechanistic studies by Jenkins *et al.* the intramolecular rotational barrier determining stereochemistry is 10.5 kcal mol⁻¹ for a similar Fe(II) tetracarbene additive [15]. With the presented metal containing systems this is expected to be slightly higher due to the torsional strain of the cyclic substrate, also supported by conformational analysis of *cis*-cyclooctene [29]. However, it indicates, that the reaction temperature of 90 °C is sufficient to overcome the rotational barrier, enabling the formation of all depicted products.

Indeed, three signals were found by GC and GC-MS analysis of the aziridination reaction mixtures. As (R,R) and (S,S) are enantiomers, their signals are expected to coincide on the non-chiral GC column. All products were further analyzed by GC-MS featuring the same mass (215.2 g mol⁻¹).

The splitting of these products results in very similar retention times on the GC comparable to GC-MS (see Table SI.1). All reported reactions result in all three signals without exception, even in the metal-free reaction. This correlates with the findings of Jenkins *et al.* who also

reported formation of the *syn*- respectively *anti*-2-methyl-3-pentyl-1-(*p*-tolyl) aziridine [15,19].

The distributions of all products are presented in Table 2. In the metal-free reaction as well as with the complexes 1–4, the major product A is an aziridine species. This was confirmed *via* separation and identification by ¹H and ¹³C NMR and ESI-MS analysis. The analytical data is in accordance to literature values [14]. Experimental FT-IR characterization was corroborated by comparison with DFT calculated spectra.

The second isomer B does not possess the aziridine functionality but in fact is an imine isomer. Targeted synthesis of the imine *via* an adapted established organic route [30] substantiated isomer B as imine due to the same retention time on GC and GC-MS. While peaks are superimposed with residual reactants in the ¹H NMR spectrum, ¹³C NMR analysis corroborated the characteristics of the imine as well as ESI-MS and IR studies (see Fig. SI.25) [31,32]. The experimental FT-IR spectra revealed a characteristic imine signal shoulder at 1644 cm⁻¹. Transition metal catalyzed (Co, Cu) imination from hydrocarbons is known in literature [33,34]. Here it was also found that the amount of imine can also be influenced by the substrate amount. Imine formation was also reported for reactions targeting aziridine as product [35].

Compound C is only obtained as minor isomer in small amounts compared to A and B in all experiments, solely detectable by GC and GC-MS. The imine does not induce stereoisomers, only tautomerism is conceivable. However, this is energetically disfavored according to the DFT calculations (see Table SI.7-SI.9). A rearrangement equilibrium of the tautomers was not observed by performed analytical characterizations. Hence, product C is presumed to be another aziridine stereoisomeric species, all of which are depicted in Fig. 1 and 2. This is supported by three possible stereoisomers, while the two enantiomers are coinciding on the non-chiral columns of GC and GC-MS. Due to their challenging separation and identification, the assignment of the aziridine stereoisomers to the corresponding peaks in the GC spectra was not further examined in this work. This certainly challenging task is kept for ongoing studies including more relevant or even chiral substrates.

Complexes 1, 3 and 4 do not show considerable influence on the selectivity compared to the metal-free reaction. Together with complex 2, the following distribution was found: A (aziridine) > B (imine) > C (aziridine). However, 2 already pushes the distribution in favor of the imine.

Considering complex 5, the distribution of the isomers is switched to imine B as the major product and assists the formation of isomer C, which is formed in much lower amounts in the presence of any other metal complex. 5 leads to the order B (imine) > A (aziridine) > C (aziridine). Since complexes 2–5 are based on the same ligand system, it is presumed that the backbone modification of the NHC moiety is able to alter the type of preferred reaction. Interestingly, the open chain complex 2 with a methyl bridge (*n* = 1) shows also an influence on the distribution of the main products. Here, the common order of amounts formed, A (aziridine) > B (imine) > C (aziridine), is observed, but instead of nearly 80% of A less than 60% are formed and 36% for B instead of < 20%. Even though the structures of complexes 1, 3 and 4 vary more (tetracarbene vs. open-chain), they do not exhibit a comparable effect. Catalytic experiments using pure aziridine A instead of azide as substrate in combination with complex 5 under the same conditions confirmed a competitive formation pathway of aziridine and

Table 2

Product distribution in percent after 24 h.

	A Aziridine	B Imine	C Aziridine
metal-free	84	15	1
1	85	14	1
2	58	36	6
3	82	16	2
4	79	19	2
5	35	51	14

imine, excluding isomerization.

However, as the complexes show these remarkable selectivity effects even with such simple substrates, an enhanced influence of the iron complexes is certainly of interest with more sophisticated and particularly with chiral substrates inducing stereocontrol. Introducing chiral groups in the NHC backbone is also expected to improve selectivity. A larger variation of complexes with functional modifications will be screened.

This preliminary work shows that the synthesis of isomeric products with important nitrogen functionalities can be targeted from the same (simple) reactants by choice of a specifically designed additive. The influence of steric and electronic properties is part of ongoing research as well as mechanistic studies to target specific applications.

4. Conclusion and Outlook

The formation of *p*-tolyl azide and *cis*-cyclooctene in toluene to the corresponding aziridines and imines at 90 °C is almost unaffected by the presence of the iron(II) NHC species (1–5), when compared to the metal-free reaction. Although not enhancing the activity of the reaction complex 5 is able to tune the selectivity between the different isomers.

Since the selectivity of the benchmark system is tunable with the metal containing systems, an enhanced influence regarding selectivity is very likely on more sophisticated substrate systems. Continuation studies are currently ongoing to determine the influence of extended variations in the ligand framework of these Fe(II) complexes. This forms the foundation for developing customized designed additives for specific applications.

CRedit authorship contribution statement

Carla A. Hoefler: Conceptualization, Data curation, Formal analysis, Investigation, Methodology, Validation, Visualization, Writing – original draft, Writing – review & editing. **Nicole K. Dietl:** Data curation, Methodology, Validation, Writing – original draft, Writing – review & editing. **Greta G. Zámbo:** Conceptualization, Project administration, Supervision, Writing – review & editing, Formal analysis. **Tim P. Schlachta:** Writing – review & editing. **Robert M. Reich:** Conceptualization, Project administration, Supervision. **Fritz E. Kühn:** Resources, Supervision.

Declaration of competing interest

The authors declare that they have no known competing financial interests or personal relationships that could have appeared to influence the work reported in this paper.

Acknowledgements

C. A. Hoefler, N. K. Dietl., G. G. Zámbo. and T. P. Schlachta gratefully acknowledge support by the Graduate School. C. A. Hoefler. and N. K. Dietl. thank B. Smolka and L. F. Richter for experimental support.

Supplementary Materials

Supplementary material associated with this article can be found, in the online version, at [doi:10.1016/j.jorganchem.2024.123018](https://doi.org/10.1016/j.jorganchem.2024.123018).

References

- J.B. Sweeney, Aziridines: epoxides' ugly cousins? *Chem. Soc. Rev.* 31 (5) (2002) 247–258, <https://doi.org/10.1039/B006015L>.
- S. Gabriel, J. Weiner, Ueber einige abkömmlinge des propylamins, *Ber. Dtsch. Chem. Ges.* 21 (2) (1888) 2669–2679, <https://doi.org/10.1002/cher.18880210288>.
- H. Wenker, The preparation of ethylene imine from monoethanolamine, *J. Am. Chem. Soc.* 57 (11) (1935) 2328, <https://doi.org/10.1021/ja01314a504>.
- P.P. Chandrachud, D.M. Jenkins, Transition metal aziridination catalysts. *Encyclopedia of Inorganic and Bioinorganic Chemistry*, 2011, pp. 1–11, <https://doi.org/10.1002/9781119951438.eibc2516>.
- H. Pellissier, Recent developments in asymmetric aziridination, *Adv. Synth. Catal.* 356 (9) (2014) 1899–1935, <https://doi.org/10.1002/adsc.201400312>.
- Y. Zhu, Q. Wang, R.G. Cornwall, Y. Shi, Organocatalytic asymmetric epoxidation and aziridination of olefins and their synthetic applications, *Chem. Rev.* 114 (16) (2014) 8199–8256, <https://doi.org/10.1021/cr500064w>.
- G.S. Singh, M. D'hooghe, N. De Kimpe, Synthesis and reactivity of C-heteroatom-substituted aziridines, *Chem. Rev.* 107 (5) (2007) 2080–2135, <https://doi.org/10.1021/cr0680033>.
- D.E. Holst, D.J. Wang, M.J. Kim, I.A. Guzei, Z.K. Wickens, Aziridine synthesis by coupling amines and alkenes via an electrogenerated dication, *Nature* 596 (7870) (2021) 74–79, <https://doi.org/10.1038/s41586-021-03717-7>.
- S. Zhou, H. Liao, M. Liu, G. Feng, B. Fu, R. Li, M. Cheng, Y. Zhao, P. Gong, Discovery and biological evaluation of novel 6, 7-disubstituted-4-(2-fluorophenoxy) quinoline derivatives possessing 1, 2, 3-triazole-4-carboxamide moiety as c-Met kinase inhibitors, *Biorg. Med. Chem.* 22 (22) (2014) 6438–6452, <https://doi.org/10.1016/j.bmc.2014.09.037>.
- S.-Y. Baek, Y.-W. Kim, S.-H. Yoo, K. Chung, N.-K. Kim, J.-S. Kim, Synthesis and redox preventing properties of dodecyl succinate derivatives containing triazole groups, *Ind. Eng. Chem. Res.* 51 (28) (2012) 9669–9678, <https://doi.org/10.1021/ie300316f>.
- B.M. Chanda, R. Vyas, A.V. Bedekar, Investigations in the transition metal catalyzed aziridination of olefins, amination, and other insertion reactions with Bromamine-T as the source of nitrene, *J. Org. Chem.* 66 (1) (2001) 30–34, <https://doi.org/10.1021/jo000013v>.
- J. Zardi, A. Pozzoli, F. Ferretti, G. Manca, C. Mealli, E. Gallo, A mechanistic investigation of the ruthenium porphyrin catalyzed aziridination of olefins by aryl azides, *Dalton Trans* 44 (22) (2015) 10479–10489, <https://doi.org/10.1039/C5DT00951K>.
- S. Fantauzzi, E. Gallo, A. Caselli, C. Piangiolino, F. Ragaini, S. Cenini, The (Porphyrin) ruthenium-catalyzed aziridination of olefins using aryl azides as nitrogen sources, *Eur. J. Org. Chem.* (2007), <https://doi.org/10.1002/ejoc.200700678>.
- S.A. Cramer, D.M. Jenkins, Synthesis of aziridines from alkenes and aryl azides with a reusable macrocyclic tetracarbene iron catalyst, *J. Am. Chem. Soc.* 133 (48) (2011) 19342–19345, <https://doi.org/10.1021/ja2090965>.
- S.B. Isbill, P.P. Chandrachud, J.L. Kern, D.M. Jenkins, S. Roy, Elucidation of the reaction mechanism of C2 + N1 aziridination from tetracarbene iron catalysts, *ACS Catal.* 9 (7) (2019) 6223–6233, <https://doi.org/10.1021/acscatal.9b01306>.
- J. Donat, P. Dubourdeaux, M. Clémancey, J. Rendon, C. Gervasoni, M. Barbier, J. Barilone, J. Pécaut, S. Gambarelli, P. Maldivi, Catalytic nitrene transfer by an FeIV-imido complex generated by a comproportionation process, *Chem. Eur. J.* 28 (70) (2022) e202201875, <https://doi.org/10.1002/chem.202201875>.
- M.R. Anneser, S. Haslinger, A. Pöthig, M. Cokoja, J.-M. Basset, F.E. Kühn, Synthesis and characterization of an iron complex bearing a cyclic tetra-N-heterocyclic carbene ligand: an artificial heme analogue? *Inorg. Chem.* 54 (8) (2015) 3797–3804, <https://doi.org/10.1021/acs.503043h>.
- G.G. Zámbo, J. Mayr, M.J. Sauer, T.P. Schlachta, R.M. Reich, F.E. Kühn, The first macrocyclic abnormally coordinating tetra-1, 2, 3-triazole-5-ylidene iron complex: a promising candidate for olefin epoxidation, *Dalton Trans.* 51 (36) (2022) 13591–13595, <https://doi.org/10.1039/D2DT02561B>.
- T.P. Schlachta, F.E. Kühn, Cyclic iron tetra N-heterocyclic carbenes: synthesis, properties, reactivity, and catalysis, *Chem. Soc. Rev.* 52 (6) (2023) 2238–2277, <https://doi.org/10.1039/D2CS01064J>.
- A. Raba, M. Cokoja, S. Ewald, K. Riener, E. Herdtweck, A. Pöthig, W.A. Herrmann, F.E. Kühn, Synthesis and characterization of novel iron (II) complexes with tetradentate bis (N-heterocyclic carbene)-bis (pyridine)(NCCN) ligands, *Organometallics* 31 (7) (2012) 2793–2800, <https://doi.org/10.1021/om2010673>.
- M.A. Bernd, F. Dyckhoff, B.J. Hofmann, A.D. Böth, J.F. Schlagintweit, J. Oberkofler, R.M. Reich, F.E. Kühn, Tuning the electronic properties of tetradentate iron-NHC complexes: towards stable and selective epoxidation catalysts, *J. Catal.* 391 (2020) 548–561, <https://doi.org/10.1016/j.jcat.2020.08.037>.
- J.W. Kück, A. Raba, I.I. Markovits, M. Cokoja, F.E. Kühn, Epoxidation of olefins catalyzed by a molecular iron N-heterocyclic carbene complex: influence of reaction parameters on the catalytic activity, *ChemCatChem* 6 (7) (2014) 1882–1886, <https://doi.org/10.1002/cctc.201402063>.
- J.F. Schlagintweit, F. Dyckhoff, L. Nguyen, C.H. Jakob, R.M. Reich, F.E. Kühn, Mixed tetradentate NHC/1, 2, 3-triazole iron complexes bearing cis labile coordination sites as highly active catalysts in Lewis and Bronsted acid mediated olefin epoxidation, *J. Catal.* 383 (2020) 144–152, <https://doi.org/10.1016/j.jcat.2020.01.011>.
- F. Dyckhoff, J.F. Schlagintweit, R.M. Reich, F.E. Kühn, Pushing the limits of activity and stability: the effects of Lewis acids on non-heme iron–NHC epoxidation catalysts, *Catal. Sci. Technol.* 10 (11) (2020) 3532–3536, <https://doi.org/10.1039/D0CY00631A>.
- T.P. Schlachta, G.G. Zámbo, M.J. Sauer, I. Rüter, C.A. Hoefler, S. Demeshko, F. Meyer, F.E. Kühn, Tailoring activity and stability: effects of electronic variations on iron-NHC epoxidation catalysts, *J. Catal.* 426 (2023) 234–246, <https://doi.org/10.1016/j.jcat.2023.07.018>.
- F. Sebest, L. Rattanajiravong, S. Kaukver, A.J. White, S. Díez-González, Expedient metal-free preparation of aryl aziridines via thermal cycloaddition reactions, *Chem. Commun.* 58 (22) (2022) 3681–3684, <https://doi.org/10.1039/D1CC07213G>.

- [27] M.J. Frisch, G.W. Trucks, H.B. Schlegel, G.E. Scuseria, M.A. Robb, J.R. Cheeseman, G. Scalmani, V. Barone, G.A. Petersson, H. Nakatsuji, X. Li, M. Caricato, A. V. Marenich, J. Bloino, B.G. Janesko, R. Gomperts, B. Mennucci, H.P. Hratchian, J. V. Ortiz, A.F. Izmaylov, J.L. Sonnenberg, D. Williams-Young, F. Ding, F. Lipparini, F. Egidi, J. Goings, B. Peng, A. Petrone, T. Henderson, D. Ranasinghe, V. G. Zakrzewski, J. Gao, N. Rega, G. Zheng, W. Liang, M. Hada, M. Ehara, K. Toyota, R. Fukuda, J. Hasegawa, M. Ishida, T. Nakajima, Y. Honda, O. Kitao, H. Nakai, T. Vreven, K. Throssell, J.A. Montgomery Jr., J.E. Peralta, F. Ogliaro, M. J. Bearpark, J.J. Heyd, E.N. Brothers, K.N. Kudin, V.N. Staroverov, T.A. Keith, R. Kobayashi, J. Normand, K. Raghavachari, A.P. Rendell, J.C. Burant, S.S. Iyengar, J. Tomasi, M. Cossi, J.M. Millam, M. Klene, C. Adamo, R. Cammi, J.W. Ochterski, R.L. Martin, K. Morokuma, O. Farkas, J.B. Foresman, D.J. Fox, *Gaussian 16 Rev. C.01*, Gaussian, Inc., Wallingford, CT, 2019.
- [28] R. Dennington, T.A. Keith, J.M. Millam. *GaussView Version 6.0.16*, Semicem Inc., Shawnee Missions, KS, 2016.
- [29] U. Neuenschwander, I. Hermans, The conformations of cyclooctene: consequences for epoxidation chemistry, *J. Org. Chem.* 76 (24) (2011) 10236–10240, <https://doi.org/10.1021/jo202176j>.
- [30] M. Tokunaga, M. Eckert, Y. Wakatsuki, Ruthenium-catalyzed intermolecular hydroamination of terminal alkynes with anilines: a practical synthesis of aromatic ketimines, *Angw. Chem. Int. Ed.* 38 (21) (1999) 3222–3225, [https://doi.org/10.1002/\(SICI\)1521-3773\(19991102\)38:21.<3222::AID-ANIE3222>3.0.CO;2-7](https://doi.org/10.1002/(SICI)1521-3773(19991102)38:21.<3222::AID-ANIE3222>3.0.CO;2-7).
- [31] J.E. Lynch, S.M. Riseman, W.L. Laswell, D.M. Tschäen, R.P. Volante, G.B. Smith, I. Shinkai, Mechanism of an acid chloride-imine reaction by low-temperature FT-IR: β -lactam formation occurs exclusively through a ketene intermediate, *J. Org. Chem.* 54 (16) (1989) 3792–3796, <https://doi.org/10.1021/jo00277a011>.
- [32] H.L. Spell, Infrared spectra of N-substituted aziridine compounds, *Anal. Chem.* 39 (2) (1967) 185–193, <https://doi.org/10.1021/ac60246a009>.
- [33] F. Ragaini, A. Penoni, E. Gallo, S. Tollari, C.Li Gotti, M. Lapadula, E. Mangioni, S. Cenini, Amination of benzylic C-H bonds by arylazides catalyzed by Co II-porphyrin complexes: a synthetic and mechanistic study, *Chem. Eur. J.* 9 (1) (2003) 249–259, <https://doi.org/10.1002/chem.200390018>.
- [34] S. Cenini, E. Gallo, A. Penoni, F. Ragaini, S. Tollari, Amination of benzylic C-H bonds by aryl azides catalysed by CoII (porphyrin) complexes. A new reaction leading to secondary amines and imines, *Chem. Commun.* (22) (2000) 2265–2266, <https://doi.org/10.1039/B006136K>.
- [35] S. Cenini, E. Gallo, A. Caselli, F. Ragaini, S. Fantauzzi, C. Piangiolino, Coordination chemistry of organic azides and amination reactions catalyzed by transition metal complexes, *Coord. Chem. Rev.* 250 (11–12) (2006) 1234–1253, <https://doi.org/10.1016/j.ccr.2005.10.002>.



Homobimetallic *bis*-NHC(Ptdvtms)₂ Complexes for the Hydrosilylation of Alkenes

Michael J. Sauer^a, Jeff Offorjindu^{a,b}, Greta G. Zábó^a, Robert M. Reich^a, Fritz E. Kühn^{a,*}

^a Molecular Catalysis, Department of Chemistry and Catalysis Research Center, TUM School of Natural Sciences, Technical University Munich, Lichtenbergstr. 4, D-85748, Garching bei München, Germany

^b Ausbildungszentrum der Technischen Universität München, Lichtenbergstr. 4, D-85748, Garching bei München, Germany

ARTICLE INFO

Keywords:

Bimetallic
Induction period
Mercury poisoning
N-heterocyclic carbenes
Platinum
Silanes

ABSTRACT

A series of six bimetallic *bis*-NHC(Ptdvtms)₂ complexes **1–6** (dvtms = 1,1,3,3-tetramethyl-1,3-divinyldisiloxane) has been designed by expansion of the monometallic Markó-type system in anticipation of synergistic bimetallic cooperation. The new compounds are easily accessible using Karstedt's catalyst [Pt₂(dvtms)₃] as platinum(0) precursor and the respective *bis*-(imidazolium) salts (**L1–6**), deprotonated by potassium *tert*-butoxide. Characterization via NMR spectroscopy (¹H, ¹³C, ²⁹Si, ¹⁹⁵Pt) and SC-XRD reveals a strong similarity of this new complex class to the parent monometallic complexes. The hydrosilylation reactions of oct-1-ene or 1,1,1,3,3-pentamethyl-3-vinyldisiloxane (MM^{Vi}) with 1,1,3,5,5-heptamethyltrisiloxane (MD^{HM}), respectively, are efficiently and selectively catalyzed with turn-over frequencies (TOF) of up to 78,000 h⁻¹ after a significantly shortened induction period compared to their monometallic relatives. Mercury poisoning experiments demonstrate the superiority of bimetallic compared to monometallic systems in terms of stability when exposed to silanes.

1. Introduction

Metalloproteins are essential in living organisms to perform countless reactions efficiently and, first and foremost, selectively to sustain vital biological functions. Frequently, bimetallic sites are capable of overcoming reaction barriers under physiological conditions that pose problems in artificial non-protein systems [1–4]. A range of biomimetic studies has been inspired by these proteins, indicating the larger protein structure has to be considered in many cases in addition to the first coordination sphere [5–12]. Synergistic or cooperative effects between metals in close proximity have been recognized to promote activity and selectivity [13–17] and led to studies of a plethora of bimetallic complexes in catalysis [18–26]. This also holds true for the hydrosilylation reaction [27–35], where platinum catalysts dominate in industrial applications [36–38]. However, the Pt-Ir heterobimetallic complexes of Ishii *et al.* are the only platinum-containing bimetallic complexes that have been subjected to hydrosilylation so far [39]. The introduction of N-heterocyclic carbenes (NHCs) as spectator ligands by Markó *et al.* for monometallic platinum (NHC)Pt(dvtms) complexes proved beneficial in terms of selectivity and stability, reducing colloidal platinum formation under catalytic conditions [40–43]. They do, however, suffer from a pronounced initiation process, which is why they are frequently referred

to as “slow-release” precursors.

In this work the class of Markó-type complexes is extended to homobimetallic systems with the anticipation of cooperative effects and the synthesis and characterization of six *bis*-NHC(Ptdvtms)₂ complexes **1–6** (Fig. 1) is reported. The basic scaffold consists of two methylene-bridged imidazole-2-ylidene-Pt(dvtms) moieties that enable variable distances of the platinum atoms by conformational dynamics. The outer wingtips of the NHCs are altered in terms of steric bulk and contain, *inter alia*, dangling pyridine (**3**) or triazole (**6**) groups as presumed N-donors, virtually duplicating monometallic complexes [40,42,44,45]. These compounds are evaluated as catalytic precursors in the hydrosilylation of alkenes and compared to Im^{Mes}Pt(dvtms) (**7**) [41,42,46] as monometallic catalytic reference. A comparison of monometallic and bimetallic complexes is presented, especially in the presence of silanes.

2. Experimental

2.1. Methods and materials

All reactions were carried out under oxygen-free, dry conditions in an argon atmosphere using standard Schlenk and glovebox techniques unless specifically stated otherwise. The solvents were purified,

* Corresponding author.

E-mail address: fritz.kuehn@ch.tum.de (F.E. Kühn).

<https://doi.org/10.1016/j.jorgchem.2024.123030>

Received 22 December 2023; Received in revised form 12 January 2024; Accepted 18 January 2024

Available online 24 January 2024

0022-328X/© 2024 The Author(s). Published by Elsevier B.V. This is an open access article under the CC BY-NC-ND license (<http://creativecommons.org/licenses/by-nc-nd/4.0/>).

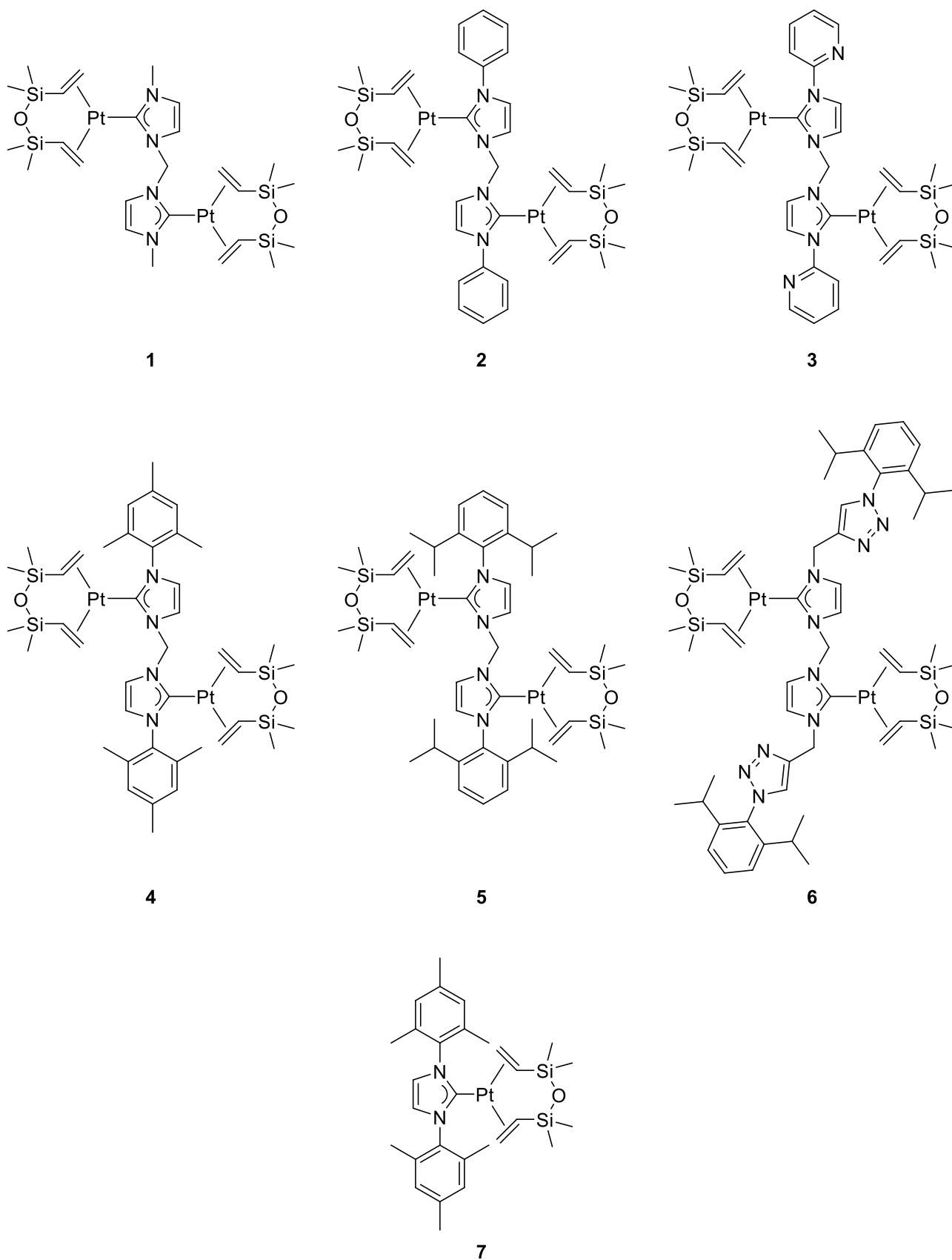


Fig. 1. Structure of NHC(Ptdvtms)_x (x = 1,2) complexes used in this study. Compound 7 is literature known and used as catalytic reference [42].

degassed, and dried according to standard purification techniques or obtained from an MBraun solvent purification system (SPS). The ligand precursor salts *bis*-Im^{Me}·(PF₆)₂ (**L1**) [47], *bis*-Im^{Ph}·(Br)₂ (**L2**) [48], *bis*-Im^{Py}·(PF₆)₂ (**L3**) [49], *bis*-Im^{Mes}·(Br)₂ (**L4**) [48], *bis*-Im^{Dipp}·(PF₆)₂ (**L5**) [48], *bis*-Im^{MeTrzDipp}·(PF₆)₂ (**L6**) [50] and Im^{Mes}·BF₄ (**L7**) [51] were prepared according to literature procedures. Where necessary, the ligand precursor salts were further purified by an anion exchange with 5 eq. NH₄PF₆. All further chemicals were purchased from Sigma-Aldrich, VWR, or abcr and used as received. NMR spectra were recorded on a Bruker Avance Ultrashield 400 MHz and a Bruker DPX 400 MHz spectrometer. All ¹H, ¹³C, and ²⁹Si chemical shifts are reported in parts per million (ppm) relative to TMS, with the residual solvent peak serving as an internal reference. ¹⁹⁵Pt chemical shifts are externally referenced to K₂PtCl₄ in H₂O ($\delta = -1628$ ppm). ²⁹Si NMR spectra were recorded via the INEPT technique. Abbreviations for NMR multiplicities are singlet (s), broad singlet (bs), doublet (d), triplet (t), and multiplet (m). Coupling constants are given in Hz. Catalytic experiments were conducted under atmospheric conditions and GC-grade *p*-xylene and *n*-hexane were employed therein. GC analysis was performed with an Agilent Technologies 7890B GC system using an HP-5 column (30 m × 320 μ m × 0.25 μ m). The injection volume was 1 μ L at an oven temperature of 50 °C and with a split ratio of 30:1. A flow of 0.9 mL·min⁻¹ of nitrogen as carrier gas was applied and the system was equipped with an FID detector, that was kept at 50 °C. After injection of the sample at 50 °C the oven temperature was held for 9 min and subsequently ramped to 80 °C at a rate of 6 °C·min⁻¹. Afterward, the ramp was increased to 15 °C·min⁻¹ until 205 °C was reached and the final temperature of 250 °C was reached by heating at 30 °C·min⁻¹ and then keeping the temperature for 3 min. Elemental analyses were performed at the microanalytical laboratory of the Catalysis Research Center, Technical University Munich. Single crystals were measured in the SC-XRD laboratory of the Catalysis Research Center at Technical University Munich, Germany.

2.2. Synthesis and characterization

2.2.1. General protocol for the synthesis of *bis*-NHC(Ptdvtms)₂ complexes (**1**–**6**)

Under argon, the respective *bis*-(imidazolium) salt (**L1**–**L6**, 1.00 eq.), Karstedt's catalyst (2.00 eq. Pt), potassium *tert*-butoxide (3.00 eq.; 2.05 eq. for **6**) and toluene are combined. The resulting suspension is stirred overnight in the dark. Under air, *n*-pentane is added to the reaction mixture and stirred before filtration over Celite. Elution with *n*-pentane and removal of all volatiles *in vacuo* gives crude product. The target compound is obtained by washing with propan-2-ol and *n*-pentane and subsequent drying. A more detailed account is presented in the ESI.

2.2.2. *bis*-Im^{Me}(Ptdvtms)₂ (**1**)

Yield: 53%. ¹H NMR (400 MHz, CDCl₃, 298 K): δ [ppm] = 7.12 (s, 2H, H_{im}), 6.93 (s, 2H, H_{im}), 5.99 (s, 2H, NCH₂N), 3.51 (s, 6H, CH₃), 2.20 (bs, 4H, CH₂CHSi), 2.06–1.82 (m, 8H, CH₂CHSi), 0.34 (s, 12H, SiCH_{3,eq}), -0.27 (s, 12H, SiCH_{3,ax}). ¹³C{¹H} NMR (101 MHz, CDCl₃, 298 K): δ [ppm] = 185.8 (Pt–C_{car}), 122.8 (C_{im}), 120.4 (C_{im}), 61.6 (NCH₂N), 41.4 (CH₂CHSi, ¹J_{Pt,C} = 160.6 Hz), 37.1 (CH₃), 35.5 (CH₂CHSi), 1.6 (SiCH_{3,eq}), -1.6 (SiCH_{3,ax}). ²⁹Si{¹H} NMR (79 MHz, CDCl₃, 298 K): δ [ppm] = 3.11 (s, ²J_{Pt,Si} = 41.1 Hz, 4 Si). ¹⁹⁵Pt NMR (85 MHz, CDCl₃, 298 K): δ [ppm] = -5390 (s, Pt, rotamer), -5395 (s, Pt, rotamer), -5399 (s, Pt, rotamer). Elemental analysis calcd (%) for C₂₅H₄₈N₄O₂Pt₂Si₄: C 31.97; H 5.15; N 5.97; found: C 31.62; H 5.12; N 5.83.

2.2.3. *bis*-Im^{Ph}(Ptdvtms)₂ (**2**)

Yield: 89%. ¹H NMR (400 MHz, CDCl₃, 298 K): δ [ppm] = 7.49–7.35 (m, 6H, H_{ar}), 7.34–7.27 (m, 6H, H_{ar}), 7.17 (s, 2H, H_{ar}), 6.23 (s, 2H, NCH₂N), 2.35–2.08 (m, 4H, CH₂CHSi), 2.03–1.69 (m, 8H, CH₂CHSi), 0.30 (s, 12H, SiCH_{3,eq}), -0.54 (s, 12H, SiCH_{3,ax}). ¹³C{¹H} NMR (101 MHz, CDCl₃, 298 K): δ [ppm] = 186.5 (Pt–C_{car}), 140.4 (C_{ar}), 129.0 (C_{ar}), 128.2 (C_{ar}), 124.6 (C_{ar}), 122.4 (C_{im}), 121.2 (C_{im}), 62.3 (NCH₂N), 42.6

(CH₂CHSi, ¹J_{Pt,C} = 161.6 Hz), 35.3 (CH₂CHSi), 1.6 (SiCH_{3,eq}), -2.5 (SiCH_{3,ax}). ²⁹Si{¹H} NMR (79 MHz, CDCl₃, 298 K): δ [ppm] = 2.98 (s, ²J_{Pt,Si} = 40.1 Hz, 4 Si). ¹⁹⁵Pt NMR (85 MHz, CDCl₃, 298 K): δ [ppm] = -5339 (s, Pt, rotamer), -5356 (s, Pt, rotamer), -5363 (s, Pt, rotamer). Elemental analysis calcd (%) for C₃₅H₅₂N₄O₂Pt₂Si₄: C 39.53; H 4.93; N 5.27; found: C 39.53; H 4.91; N 5.17.

2.2.4. *bis*-Im^{Py}(Ptdvtms)₂ (**3**)

Yield: 16%. ¹H NMR (400 MHz, CDCl₃, 298 K): δ [ppm] = 8.54–8.40 (m, 2H, H_{ar}), 8.40–8.19 (m, 2H, H_{ar}), 8.19–7.91 (m, 2H, H_{ar}), 7.64–7.47 (m, 2H, H_{ar}), 7.43–7.24 (m, 2H, H_{ar}), 7.24–7.17 (m, 2H, H_{ar}), 6.38 (s, 2H, NCH₂N, rotamer), 6.17 (s, 2H, NCH₂N, rotamer), 2.44–2.17 (m, 4H, CH₂CHSi), 2.15–1.74 (m, 8H, CH₂CHSi), 0.35 (s, 12H, SiCH_{3,eq}), -0.31 (s, 12H, SiCH_{3,ax}). ¹³C{¹H} NMR (101 MHz, CDCl₃, 298 K): δ [ppm] = 187.6 (Pt–C_{car}), 151.6 (C_{ar}), 148.1 (C_{ar}), 137.7 (C_{ar}), 122.7 (C_{ar}), 121.1 (C_{ar}), 120.5 (C_{ar}), 116.0 (C_{ar}), 63.0 (NCH₂N), 43.1 (CH₂CHSi, ¹J_{Pt,C} = 161.6 Hz), 36.1 (CH₂CHSi), 1.6 (SiCH_{3,eq}), -1.8 (SiCH_{3,ax}, rotamer), -2.5 (SiCH_{3,ax}, rotamer). ²⁹Si{¹H} NMR (79 MHz, CDCl₃, 298 K): δ [ppm] = 3.11 (s, ²J_{Pt,Si} = 41.1 Hz, 4 Si). ¹⁹⁵Pt NMR (85 MHz, CDCl₃, 298 K): δ [ppm] = -5343 (s, rotamer), -5347 (s, rotamer), -5353 (s, rotamer). Elemental analysis calcd (%) for C₃₅H₅₀N₆O₂Pt₂Si₄: C 37.21; H 4.73; N 7.89; found: C 37.10; H 4.66; N 7.79.

2.2.5. *bis*-Im^{Mes}(Ptdvtms)₂ (**4**)

Yield: 79%. ¹H NMR (400 MHz, CDCl₃, 298 K): δ [ppm] = 7.41 (d, ³J_{H,H} = 2.0 Hz, 2H, H_{im}), 6.86 (d, ³J_{H,H} = 2.0 Hz, 2H, H_{im}), 6.83 (s, 4H, H_{ar}), 6.28 (s, 2H, NCH₂N), 2.31–1.67 (m, 12H, CH₂CHSi), 2.22 (s, 6H, *p*-CH₃), 2.00 (s, 12H, *o*-CH₃), 0.26 (s, 12H, SiCH_{3,eq}), -0.69 (s, 12H, SiCH_{3,ax}). ¹³C{¹H} NMR (101 MHz, CDCl₃, 298 K): δ [ppm] = 187.0 (Pt–C_{car}, ¹J_{Pt,C} = 1381.7 Hz), 139.1 (C_{ar}), 136.3 (C_{ar}), 135.1 (C_{ar}), 129.0 (C_{ar}), 123.2 (C_{ar}), 120.6 (C_{ar}), 62.1 (NCH₂N), 42.3 (CH₂CHSi, ¹J_{Pt,C} = 164.6 Hz), 35.9 (CH₂CHSi, ¹J_{Pt,C} = 119.2 Hz), 21.1 (*p*-CH₃), 18.0 (*o*-CH₃), 1.6 (SiCH_{3,eq}), -2.3 (SiCH_{3,ax}). ²⁹Si{¹H} NMR (79 MHz, CDCl₃, 298 K): δ [ppm] = 3.78 (s, ²J_{Pt,Si} = 40.3 Hz, 4 Si). ¹⁹⁵Pt NMR (85 MHz, CDCl₃, 298 K): δ [ppm] = -5390 (s, Pt). Elemental analysis calcd (%) for C₄₁H₆₄N₄O₂Pt₂Si₄: C 42.92; H 5.62; N 4.88; found: C 43.14; H 5.61; N 4.71.

2.2.6. *bis*-Im^{Dipp}(Ptdvtms)₂ (**5**)

Yield: 55%. ¹H NMR (400 MHz, CDCl₃, 298 K): δ [ppm] = 7.43 (d, ³J_{H,H} = 2.0 Hz, 2H, H_{im}), 7.34 (t, ³J_{H,H} = 7.8 Hz, 2H, H_{ar}), 7.15 (d, ³J_{H,H} = 7.8 Hz, 4H, H_{ar}), 6.96 (d, ³J_{H,H} = 2.0 Hz, 2H, H_{im}), 6.37 (s, 2H, NCH₂N), 2.81–2.52 (m, 4H, CH(CH₃)₂), 2.23–1.95 (m, 4H, CH₂CHSi), 1.92–1.68 (m, 8H, CH₂CHSi), 1.21 (bs, 12H, CH(CH₃)₂), 1.05 (d, ³J_{H,H} = 6.8 Hz, 12H, CH(CH₃)₂), 0.28 (s, 12H, SiCH_{3,eq}), -0.42 (bs, 12H, SiCH_{3,ax}). ¹³C{¹H} NMR (101 MHz, CDCl₃, 298 K): δ [ppm] = 187.5 (Pt–C_{car}), 145.9 (C_{ar}), 135.9 (C_{ar}), 129.8 (C_{ar}), 125.5 (C_{im}), 123.7 (C_{ar}), 119.4 (C_{im}), 62.2 (NCH₂N), 42.5 (CH₂CHSi, ¹J_{Pt,C} = 165.6 Hz), 36.3 (CH₂CHSi, ¹J_{Pt,C} = 120.2 Hz), 28.4 (CH(CH₃)₂), 26.3 (CH(CH₃)₂), 22.4 (CH(CH₃)₂), 1.7 (SiCH_{3,eq}), -1.7 (SiCH_{3,ax}). ²⁹Si{¹H} NMR (79 MHz, CDCl₃, 298 K): δ [ppm] = 3.41 (s, ²J_{Pt,Si} = 41.1 Hz, 4 Si). ¹⁹⁵Pt NMR (85 MHz, CDCl₃, 298 K): δ [ppm] = -5382 (s, Pt). Elemental analysis calcd (%) for C₄₇H₇₆N₄O₂Pt₂Si₄: C 45.83; H 6.22; N 4.55; found: C 45.97; H 6.50; N 4.39.

2.2.7. *bis*-Im^{MeTrzDipp}(Ptdvtms)₂ (**6**)

Yield: 50%. ¹H NMR (400 MHz, CDCl₃, 298 K): δ [ppm] = 7.50 (t, ³J_{H,H} = 7.8 Hz, 2H, H_{ar}), 7.44–7.11 (m, 6H, H_{ar}), 7.29 (d, ³J_{H,H} = 7.7 Hz, 4H, H_{ar}), 6.09 (s, 2H, NCH₂N, rotamer), 5.99 (s, 2H, NCH₂N, rotamer), 5.35 (s, 4H, NCH₂C, rotamer), 5.40 (s, 4H, NCH₂C, rotamer), 2.37–1.80 (m, 4H, CH₂CHSi, 4H, CH(CH₃)₂, 4H, CH₂CHSi), 1.14 (d, ³J_{H,H} = 6.8 Hz, 12H, CH(CH₃)₂), 1.09 (d, ³J_{H,H} = 6.8 Hz, 12H, CH(CH₃)₂), 0.34 (s, 12H, SiCH_{3,eq}), -0.28 (s, 12H, SiCH_{3,ax}). ¹³C{¹H} NMR (101 MHz, CDCl₃, 298 K): δ [ppm] = 186.5 (Pt–C_{car}), 146.0 (C_{ar}), 143.1 (C_{ar}), 142.8 (C_{ar}), 132.9 (C_{ar}), 131.1 (C_{ar}), 124.9 (C_{ar}), 124.0 (C_{ar}), 121.9 (C_{ar}), 120.9 (C_{ar}), 61.8 (NCH₂N), 45.3 (NCH₂C), 42.2 (CH₂CHSi, ¹J_{Pt,C} = 158.6 Hz), 36.3

(CH₂CHSi, rotamer), 35.9 (CH₂CHSi, rotamer), 28.5 (CH(CH₃)₂), 24.2 (CH(CH₃)₂), 24.1 (CH(CH₃)₂), 1.5 (SiCH_{3,eq}), -1.6 (SiCH_{3,ax}). ²⁹Si{¹H} NMR (79 MHz, CDCl₃, 298 K): δ [ppm] = 3.11 (s, 4 Si). ¹⁹⁵Pt NMR (85 MHz, CDCl₃, 298 K): δ [ppm] = -5386 (s, Pt, rotamer), -5391 (s, Pt, rotamer), -5396 (s, Pt, rotamer). Elemental analysis calcd (%) for C₅₃H₈₂N₁₀O₂Pt₂Si₄: C 45.67; H 5.93; N 10.05; found: C 45.62; H 6.00; N 9.88.

2.2.8. Platinum hydride test – reaction of 1 with MD^HM

Under atmospheric conditions 1 (20.0 mg, 21.3 μmol, 1.0 eq.), MD^HM (40.5 μL, 149 μmol, 7.0 eq.) and toluene-*d*₈ (0.3 mL) are reacted for 7 min at 72 °C. Analysis by ¹H NMR reveals four major hydride resonances at δ = -4.25 (¹J_{Pt,H} = 640 Hz), -5.16, -7.18 (¹J_{Pt,H} = 632 Hz) and -9.46 ppm (¹J_{Pt,H} = 652 Hz) with ¹⁹⁵Pt satellites.

2.3. Single crystal X-ray structure determination

Single crystals of 1 were obtained by slow evaporation of a concentrated solution in CDCl₃. The same procedure was successfully applied for a *n*-pentane solution of 3. The layering of a solution of either 2 or 4 in DCM with *n*-pentane gave suitable crystals of the respective compounds. Complex 5 was carefully recrystallized from *n*-hexane at 80 °C. Finally, crystals of 6 were obtained by layering a solution thereof in CDCl₃ with *n*-pentane. X-ray crystallographic data was collected on a Bruker D8 Venture single crystal X-ray diffractometer, equipped either with a CMOS detector (κ-CMOS) and a TXS rotating anode or a CMOS detector (Bruker Photon-100) and an IMS micro source, both in conjunction with a Helios optic as setup using the APEX4 software package [52]. The measurement used MoK_α radiation (λ = 0.71073 Å) and was performed on single crystals coated with perfluorinated ether. The crystals were fixed on top of a micromount sample holder and frozen under a stream of cold nitrogen at 100 K. A matrix scan was used to determine the initial lattice parameters. Reflections were corrected for Lorentz and polarization effects, scan speed, and background using SAINT [53]. Absorption corrections, including odd and even ordered spherical harmonics were performed using SADABS [54]. Space group assignment was based upon systematic absences, E statistics, and successful refinement of the structure. The structure was solved by direct methods (SHELXT) with the aid of successive difference Fourier maps and was refined against all data using SHELXL-2015 in conjunction with SHELXLE [55–57]. Hydrogen atoms were calculated in ideal positions as follows: Methyl hydrogen atoms were refined as part of rigid rotating groups, with a C–H distance of 0.98 Å and U_{iso}(H) = 1.5·U_{eq}(C). Other H atoms were placed in calculated positions and refined using a riding model, with methylene, aromatic, and other C–H distances of 0.99 Å, 0.95 Å, and 1.00 Å, respectively, and U_{iso}(H) = 1.2·U_{eq}(C). Non-hydrogen atoms were refined with anisotropic displacement parameters. Full-matrix least-squares refinements were carried out by minimizing Σw(F_o² - F_c²)² with the SHELXL weighting scheme [55]. Neutral atom scattering factors for all atoms and anomalous dispersion corrections for the non-hydrogen atoms were taken from *International Tables for Crystallography* [58]. The images of the crystal structures were generated with PLATON [59]. CCDC 2321225–2321230 contain the supplementary crystallographic data for this paper. This data can be obtained free of charge via www.ccdc.cam.ac.uk/data_request/cif, by emailing data_request@ccdc.cam.ac.uk, or by contacting The Cambridge Crystallographic Data centre, 12 Union Road, Cambridge CB2 1EZ, UK; fax: +44 1223 336033.

3. Results and discussion

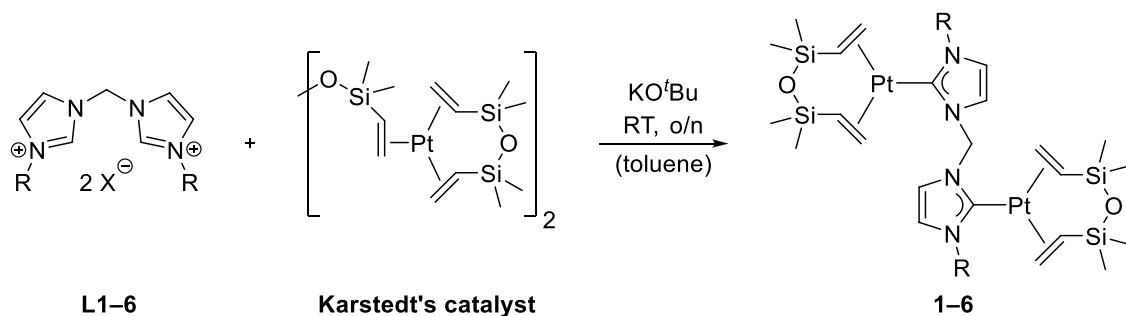
3.1. Synthesis and characterization of bis-NHC(Ptdvtms)₂ complexes (1–6)

The homobimetallic bis-NHC(Ptdvtms)₂ complexes 1–6 are easily accessible by reaction of the respective bis-(imidazolium) salt (L1–L6,

1.00 eq.) with potassium *tert*-butoxide (3.00 eq.) in the presence of Karstedt's catalyst (2.00 eq. Pt) [37,60,61], based on the synthetic procedure of Markó et al. (Scheme 1) [42]. Solely in the synthesis of 6, the amount of potassium *tert*-butoxide was reduced to 2.05 equivalents in accordance with the synthesis of a monometallic congener [45] to avoid unintended deprotonation of the triazoles [62,63]. The target compounds, bis-Im^{Me}(Ptdvtms)₂ (1, 53%), bis-Im^{Ph}(Ptdvtms)₂ (2, 89%), bis-Im^{Py}(Ptdvtms)₂ (3, 16%), bis-Im^{Mes}(Ptdvtms)₂ (4, 79%), bis-Im^{Dipp}(Ptdvtms)₂ (5, 55%) and bis-Im^{MeTrzDipp}(Ptdvtms)₂ (6, 50%) were isolated as off-white or colorless, air- and moisture stable compounds. The comparatively low yield of 3 is caused by the low solubility of the desired complex during the filtration step, which was however found to be necessary on top of the washing process to obtain pure product. Improving the yields might be facilitated by the weak base approach in acetone as solvent [64,65], recrystallization [43], precipitation [66,67], or column chromatography [41,68] which have been applied in the purification of related complexes. A potential yield optimization achieved by screening alternative synthetic routes, however, was not the goal of this work.

The chemical composition of 1–6 was confirmed by comprehensive NMR spectroscopy (¹H, ¹³C, ²⁹Si, ¹⁹⁵Pt), SC-XRD, and elemental analysis. Complex formation is indicated by vanishing of the carbenoid proton resonances in the ¹H NMR, upfield shifting of the dvtms vinyl protons from δ = 6.17–5.70 ppm for the free molecule to δ = 2.44–1.68 ppm and splitting of the SiMe₂ singlet into two resonances at approximately δ = 0.3 and -0.4 ppm, for equatorial and axial methyl groups, respectively. The ¹³C carbene signal is observed in the narrow range of δ = 187.6–185.8 ppm (Table 1), approving the similar Pt–C bond in the investigated complexes. In addition, a singlet at δ = 3.78–2.98 ppm in the ²⁹Si NMR with ²J_{Pt,Si} = 40.1–41.1 Hz platinum satellites reinforces the claim of (NHC)Pt(dvtms) complex formation. ¹⁹⁵Pt satellites are also observed for the ¹³C resonances at ¹J_{Pt,C,terminal} = 158.6–165.6 Hz and ¹J_{Pt,C,internal} = 119.2–120.2 Hz. These results match with the monometallic Markó-type complexes, for instance 7, with δ = 184.4 ppm for the carbene signal, ¹J_{Pt,C,terminal} = 165.6 Hz, ¹J_{Pt,C,internal} = 118.2 Hz and for the ²⁹Si resonance δ = 3.57 ppm, with a coupling constant of ²J_{Pt,Si} = 40.3 Hz. This demonstrates a very similar chemical environment for the monometallic and bimetallic systems, which is the prerequisite for a meaningful comparison in catalysis in terms of structure.

The electronic environment of the catalytically active platinum atom is directly probed by highly sensitive ¹⁹⁵Pt NMR, where σ-donor properties of ligands lead to an increase in electron density and π*-acceptor properties of ligands induce the opposite [42,69,70]. The observed resonances range from δ = -5339 for 2 with phenyl wings to -5399 ppm for 1 with methyl wings for the bimetallic complexes and are characteristic for Pt(0) complexes [70]. The ¹⁹⁵Pt shifts of 1 and 6 with aliphatic wingtips at the NHC, although slightly more shielded, resemble their monometallic congeners [45]. Complexes 2–5 with terminal aromatic wingtips at the NHC are significantly upfield shifted by Δδ = 22 for 4 and 76 ppm for 3 compared to their monometallic counterparts. This is attributed to the internal methylene bridge that renders these compounds mixed aromatic/aliphatic substituted NHCs and partly introduces a characteristic of Im^{Me}Pt(dvtms) (Im^{Me} = 1,3-dimethylimidazolyl) that exhibits an upfield shifted ¹⁹⁵Pt of δ = -5392 ppm [45]. The most striking feature however is, that for 1–3 and 6 three slightly chemically different platinum atoms are observed at room temperature. This behavior was previously reported for asymmetric monometallic (tetrylene)Pt(dvtms) compounds (tetrylene = carbene or silylene) and is induced by a hindered rotation along the Pt–C axis which might result in *syn* and *anti*-conformational isomers [44,46,67,68,71,72]. Our group [46] and Iwamoto et al. [72] investigated the issue for their compounds by variable temperature ¹H NMR from 183 to 363 K and from 203 to 343 K, respectively but no coalescence point was reported. The group of Iwamoto pushed even further and calculated the preference of the *syn* conformation (≠ rotational barrier) by 4.3 kJ·mol⁻¹. Expansion of this concept to incorporate two hindered rotational Pt–C axes is necessary to



Scheme 1. Syntheses of bimetallic complexes 1–6 from Karstedt's catalyst [37,60,61]. **1:** R = Me, X[−] = PF₆[−]; **2:** R = Ph, X[−] = Br[−]; **3:** R = 2-Py, X[−] = PF₆[−]; **4:** R = 2,4,6-trimethylphenyl (Mes), X[−] = Br[−]; **5:** R = 2,6-diisopropylphenyl (Dipp), X[−] = PF₆[−]; **6:** R = 4-methylene-1-(2,6-diisopropylphenyl)-1H-1,2,3-triazole (MeTrzDipp), X[−] = PF₆[−]. Stoichiometry: 1.00 eq. L1–6, 2.00 eq. Pt, 3.00 eq. KO^tBu (2.05 eq. for 6).

Table 1

Chemical shifts of complexes 1–7 as observed by NMR spectroscopy. Main species are highlighted.

Complex	1	2	3	4	5	6	7
Chemical shifts δ [ppm]							
¹³ C _{carbene}	185.8	186.5	187.6	187.0	187.5	186.5	184.4
¹⁹⁵ Pt	−5390	−5339	−5343			−5386	
	−5395	−5356	−5347	−5390	−5382	−5391	−5368 ^a
	−5399	−5363	−5353			−5396	

^a Differs by 29 ppm from the previously reported shift of −5339 ppm [42].

properly describe *bis*-NHC(Pt(dvtms))₂ complexes 1–6 (Fig. 2). This requires three permutations with *syn/syn* as the energetically most favorable according to the SC-XRD results (*vide infra*). Evaluation of the ratio of rotamers is not presented due to improper resolution of the NMR signals. Variable temperature ¹H NMR studies were performed from 233 K to 363 K in steps of 10 K for 5 and 6 to elucidate conformational dynamics (ESI). Complex 5 was selected as it exhibits a clean singlet in the ¹⁹⁵Pt NMR and is sterically more hindered than 4, where also a singlet is observed. It is expected that an increased steric bulk should enhance conformational effects, making them easier to monitor. In contrast, 6 was selected as distinct rotamers are present at room temperature, and, on top of the internal methylene bridge, the external methylene bridges that connect the triazoles to the central scaffold also serve as a probe for conformational dynamics. Analysis of the VT NMR data of 5 reveals the splitting of the NCH₂N bridge into two individual singlets at δ = 5.90 and 5.53 ppm at 233 K. Also, the axial methyl groups of the dtvms moiety separate into singlets at δ = 0.13 and −0.24 ppm at 233 K. Both signal groups coalesce at about 268 K with $\Delta\nu$ = 148 Hz, calculating ΔG^\ddagger = 52.5 kJmol^{−1} for both barriers using a derivation of the Eyring equation [73,74]. This indicates that these dynamics are linked to one another. Values of similar magnitude were reported for rotation along a metal–NHC bond [75–77]. Lastly, the equatorial methyl groups of dtvms start to separate at 233 K into peaks at δ = 0.77 and 0.69 ppm. The axial methyl groups of dtvms are generally further split as they point towards the NHC ligand and hence their separation is more easily detected, while

the equatorial methyl groups, that point away from the complex, are not that well unraveled [44,72]. The VT NMR data of 6 reveals a more complex behavior, where both the equatorial and axial methyl groups of dtvms split into three, narrowly parted signals each at 233 K at δ = 0.83, 0.81, 0.80 and 0.10, 0.08 and 0.07 ppm, respectively. This contradicts the previously stated findings and is attributed to the introduction of additional degrees of freedom in the form of the methylene bridge on the outer wingtip of the complex scaffold. Coalescence of both peak sets into two singlets is observed at roughly 298 K. At 363 K two singlets at δ = 6.10 and 5.31 ppm in the ratio of 2:4 indicate chemically equivalent protons in each case of the internal and external methylene bridge(s), respectively. The internal methylene bridge exhibits a T_c = 343 K and disintegrates into three peaks at low temperatures, which might be explained by the conformational isomers of Fig. 2. For the outer methylene bridges two consecutive coalescence points are observed at T_c = 333 and 308 K, splitting each peak into two successors repeatedly. Contrary to expectations, the sterically more hindered specimens 4 and 5 don't impose a barrier on the Pt–C rotation at room temperature, while 1–3 are divided into rotamers. This hints at an additional factor that – so far – remains unaccounted for.

Structure elucidation of 1–6 by single crystal XRD reveals coordination of the platinum atoms in characteristic [45,46,66,68,78–80], distorted trigonal planar fashion by the carbene and vinyl groups of the dtvms moiety (Fig. 3). The dtvms groups invariably crystallize in strict *syn/syn* orientation, pointing away from each other, thereby reducing

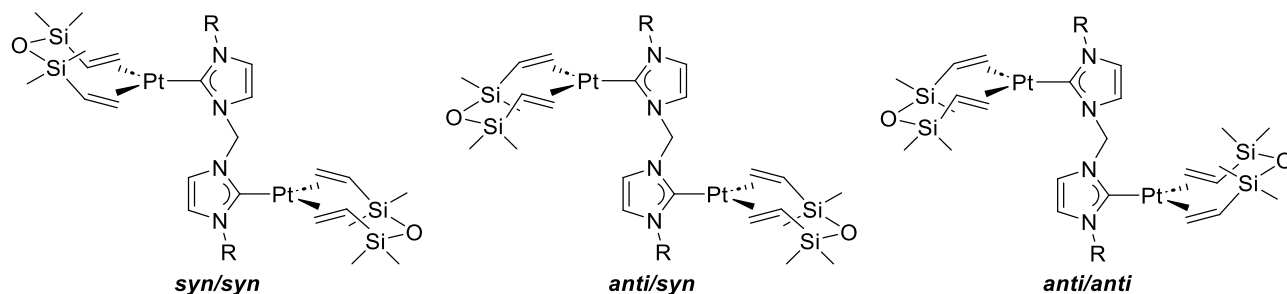


Fig. 2. Conformational isomers produced by hindered rotation along Pt–C_{carbene} axes. *Syn*: the dtvms moiety is pointing towards the NHC wingtip R. *Anti*: the dtvms moiety is pointing away from the NHC wingtip R.

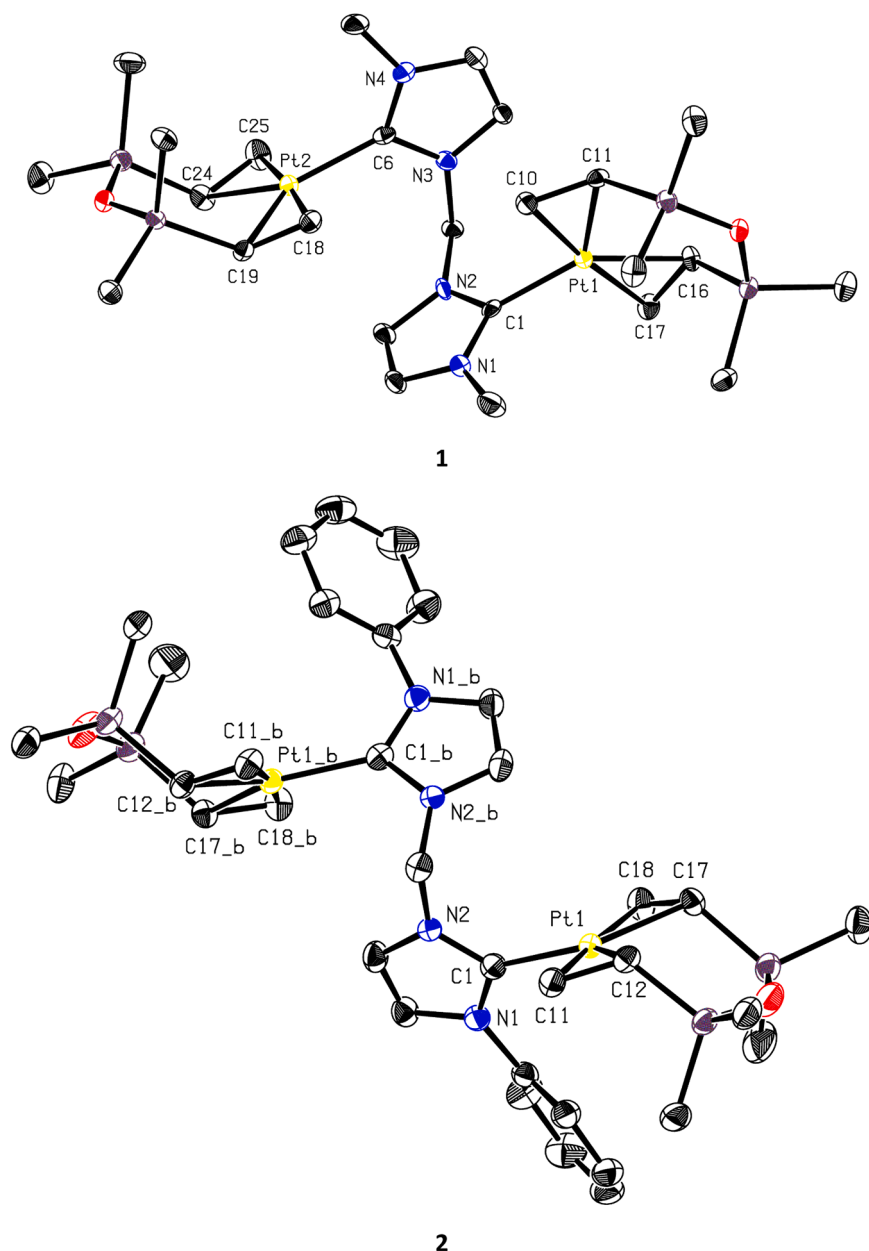
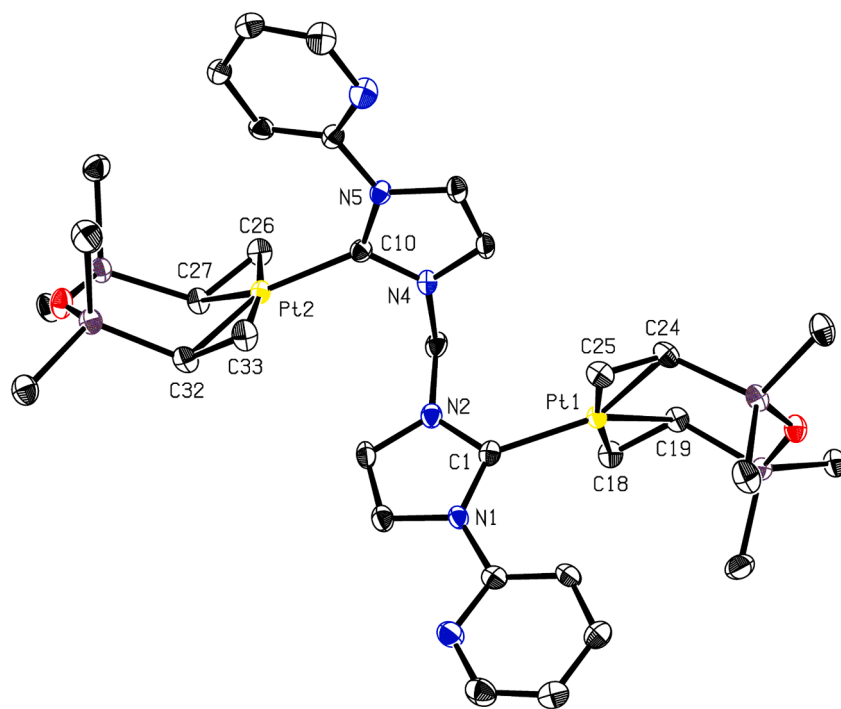


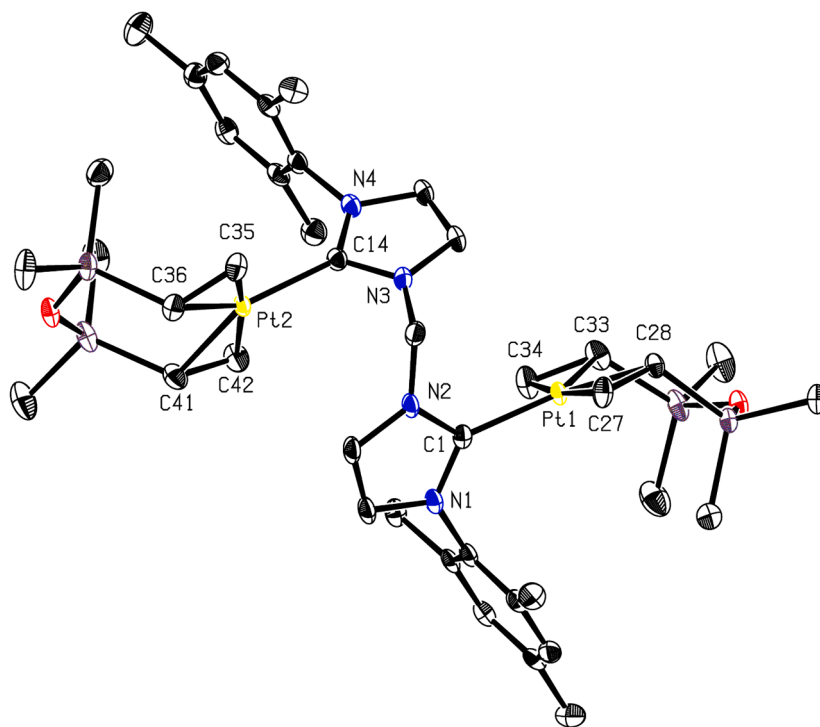
Fig. 3. ORTEP style molecular structure representation of complexes 1–6. Thermal ellipsoids are given at a 50% probability level. Hydrogen atoms are omitted for clarity. One molecule of co-crystallized dichloromethane per unit cell is omitted for 2. Only the mainly occupied site is depicted for the disordered *iso*-propyl group in 5.

steric strain. Therefore, only the most energetically favorable conformation is observed in the crystalline state, which may also be due to packing, while other rotamers may prove viable in solution. The supposedly hemilabile *N*-donors in 3 and 6 are oriented in the opposite direction to the platinum centers, which rules out an intramolecular interaction between the two groups in the solid state. This is consistent with monometallic Markó-type complexes that also contain pyridine or triazole wingtips at the NHC, where no Pt–N interaction was observed either [45]. The main geometric parameters of the bimetallic complexes are summarized in Table 2 and compared to 7 as representative of monometallic complexes. The Pt–C_{carbene} bond lengths lie in the narrow range of 2.022 Å for the sterically least hindered 1 to 2.054 Å for 6 with bulky, though admittedly flexible NHC wingtips. The geometric parameters of the trifold ligated platinum centers are consistent with their monometallic relatives, which further emphasizes the similarity of the

bimetallic and monometallic complexes. However, torsion of the dtvms vinyl groups is generally more pronounced in the bimetallic system, culminating at $-14.7(4)^\circ$ for 5 in this study. This value has so far only been exceeded once in a report by Pietraszuk *et al.* where an extremely bulky ligand forces a distortion of $17.2(6)^\circ$ [79]. Although bound to the identical main scaffold, the Pt–Pt distances vary in the range of 5.787 Å in 1 to 7.004 Å in 6. For complexes 2–5, which contain aromatic NHC wingtips, the Pt–Pt distance correlates with the Pt–C_{carbene} bond length, indicating that both parameters are affected by steric strain in the same way. Thus, the ideal metal–metal distance for bimetallic catalysis of 3.5–6 Å [19] is partially exceeded but could be realized after the loss of the dtvms moieties and due to conformational dynamics in solution. Interaction of the substrate with both platinum atoms or binding of two reactants in close proximity might still prove beneficial, even if there is no direct interaction between the platinum atoms.



3



4

Fig. 3. (continued).

3.2. Catalytic hydrosilylation of alkenes

3.2.1. Catalytic reaction of oct-1-ene with MD^HM

The performance of the bimetallic catalyst precursors 1–6 was evaluated and compared to 7 as a reference system for monometallic Markó-type complexes in the catalytic hydrosilylation reaction of oct-1-

ene and MD^HM at 72 °C. The bulky MD^HM mimics a PMHS (poly-methylhydrosiloxane) in this by Markó *et al.* established benchmark reaction (\equiv A, Table 3) [40,41], which finds widespread application in research [45,46,66,81]. The target compound M₂D-oct is formed at very good to excellent yields of up to 98% with respect to the alkene. Linked byproducts are observed at total yields < 1% and are therefore neglected

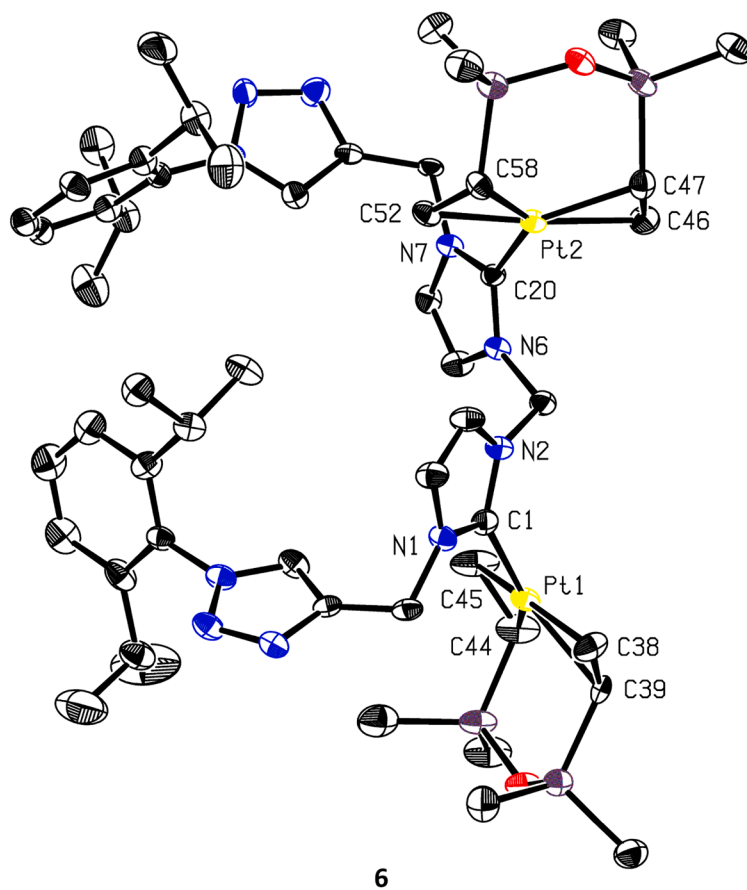
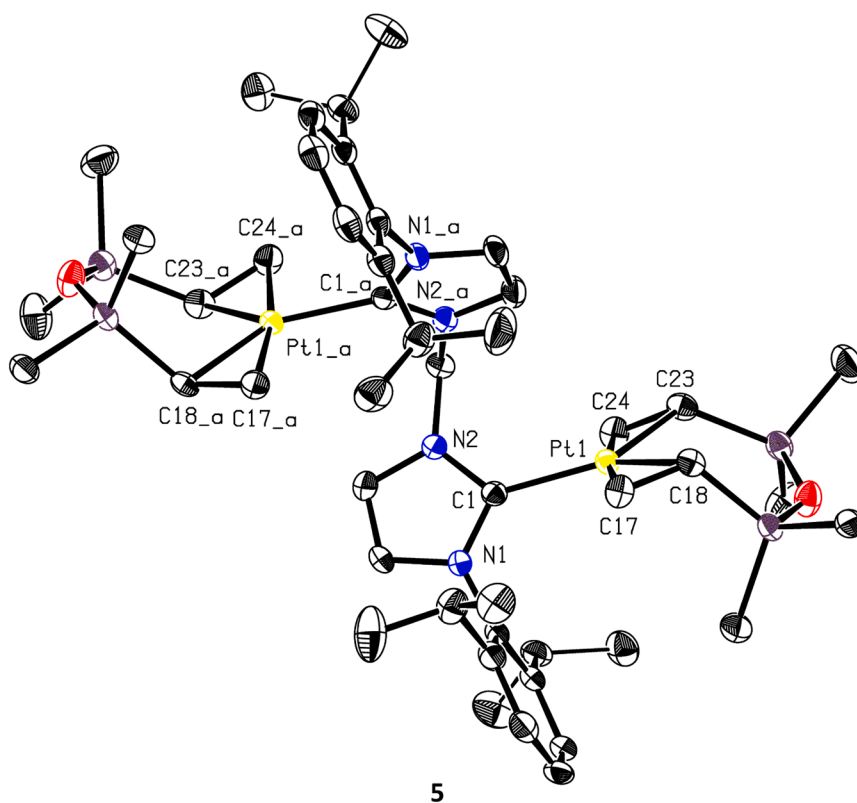


Fig. 3. (continued).

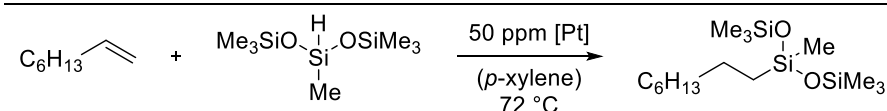
Table 2

Selected crystallographic data of bimetallic complexes (1–6) in comparison to literature known complex 7 [42].

Complex	1	2	3	4	5	6	7 ^b
Bond lengths (Å)							
Pt–C _{carbene}	2.027(5)	2.050(4)	2.050(3)	2.044(3)	2.044(4)	2.054(7)	2.046(4)
	2.022(5)		2.042(4)	2.039(3)		2.039(6)	
Pt–C _{C=C} ^c	2.124(4)	2.133(4)	2.120(4)	2.114(3)	2.124(4)	2.147(6)	2.141(5)
	2.110(4)	2.123(4)	2.133(4)	2.129(3)	2.106(4)	2.116(7)	2.138(5)
	2.127(5)		2.138(4)	2.122(3)		2.123(7)	
	2.120(6)		2.137(5)	2.130(3)		2.103(7)	
Pt–C _{C=C} ^d	2.143(5)	2.141(4)	2.140(4)	2.141(3)	2.134(4)	2.151(7)	2.146(4)
	2.121(5)	2.143(4)	2.137(4)	2.142(3)	2.139(4)	2.141(6)	2.148(5)
	2.142(5)		2.140(4)	2.133(3)		2.151(7)	
	2.139(5)		2.147(4)	2.148(3)		2.145(7)	
C _{C=C} –C _{C=C} ^e	1.420(7)	1.436(6)	1.426(5)	1.428(4)	1.429(6)	1.428(9)	1.437(7)
	1.447(7)	1.429(6)	1.427(6)	1.426(4)	1.425(6)	1.432(11)	1.419(7)
	1.438(7)		1.435(5)	1.433(4)		1.439(9)	
	1.442(8)		1.435(5)	1.427(5)		1.426(9)	
Pt–Pt	5.7874(4)	6.7208(8)	6.5177(6)	6.2245(5)	6.396(1)	7.0041(8)	n.a.
Angles (°)							
N _{im} –CH ₂ –N _{im}	113.4(4)	113.0(4)	114.2(4)	113.8(2)	112.9(4)	112.5(5)	n.a.
tilt angle θ	84.12	70.81	83.32	69.42	61.21	66.11	64.67
NHC–Pt(dvtms)	82.05		78.03	72.80		74.82	
Torsion (°)							
C _{C=C} –C _{C=C} –C _{C=C} –C _{C=C}	5.9(5)	0.0(4)	8.2(4)	–3.8(3)	–14.7(4)	–1.1(7)	4.3(5)
	4.3(5)		–3.4(4)	–4.0(3)		–6.6(7)	

^b Data was extracted from CCDC 275,306 [42].^c Denotes the distance to the terminal carbon.^d Denotes the distance to the internal carbon.^e Denotes the distance between the two olefinic carbons of dvtms.

Table 3

Model reaction A: Catalytic formation of product (M₂D-oct) by hydrosilylation of oct-1-ene (1.0 eq., 2.024 mmol, 0.5 M) with MD^HM (1.0 eq., 2.024 mmol, 0.5 M) in *p*-xylene at 72 °C with 50 ppm [Pt] and *n*-decane (1.518 mmol) as internal standard. Analysis by GC-FID.

Catalyst	Y(M ₂ D-oct) [%]	X(oct-1-ene) [%]	X(MD ^H M) [%]	S [%] ^f	Y(isomerization) [%] ^g	TOF [h ⁻¹] ^h
1	36	43	37	85	2	5000 ⁱ
2	90	92	88	98	3	48,000
3	22	27	23	80	1	12,000 ⁱ
4	90	94	90	96	3	38,000
5	95	99	93	96	3	43,000
6	52	56	51	92	2	5000 ⁱ
7	91	98	90	92	4	17,000

Y = yield. X = conversion. S = selectivity.

^f Selectivity regarding oct-1-ene at t = 6 h; Selectivity regarding MD^HM ≥ 97%.^g Sum of C₈ isomers at t = 6 h. *n*-Octane is included herein.^h TOF of oct-1-ene calculated at the steepest slope.ⁱ Yield used for calculation.

(S_{MDHM} ≥ 97%). However, the catalysts compete for the minimization of C₈ byproducts that are formed by isomerization and reduction of oct-1-ene.

Equimolar amounts of oct-1-ene and MD^HM are reacted under air at 72 °C in the presence of 50 ppm [Pt]. In the case of the bimetallic compounds 1–6, this entails loading the respective complexes at 25 ppm to account for both platinum atoms in them. For 7 on the other hand, loading is fixed at 50 ppm complex, which equals the platinum concentration due to the monometallic nature. This allows comparison of catalytic performance in relation to the amount of platinum sites independent of the catalyst precursor. The reactions were monitored by GC-FID using *n*-decane as an internal standard. The observed time-yield kinetics (Fig. 4) exhibit sigmoidal behavior due to an initiation period in which the active catalyst is formed by hydrosilylation of the dvtms ligand, which is the rate-determining step [42].

This characteristic is most pronounced for 7 and results in < 1%

product formation after 20 min. Classical, monometallic Markó-type (NHC)Pt(dvtms) complexes are therefore described as “slow-release” precursors of catalytically active platinum species [42], a drawback that limits the performance of these complexes and is surpassed by bimetallic complexes 1–6. For instance, a yield of 37% M₂D-oct is obtained for 4 after 20 min, both compounds being related and containing mesityl wingtips at the NHC(s). However, the overall catalytic performance also depends on the inherent activity and stability of the active species. The latter appears to be poor for 1, 3, and 6, as is indicated by flattening of the kinetic curves at yields < 10% in a logarithmic form. Previously, pyridine and triazole wingtips at the NHC moiety proved detrimental in monometallic (NHC)Pt(dvtms) complexes and was attributed to the stabilization of a Pt(II) species [45]. However, these *N*-donor-containing ligands prevent catalysis for bimetallic systems at a different magnitude. An inflection point, caused by increasing activity, around the 1 h mark for 1 and 6 implies another transformation. Investigation and discussion

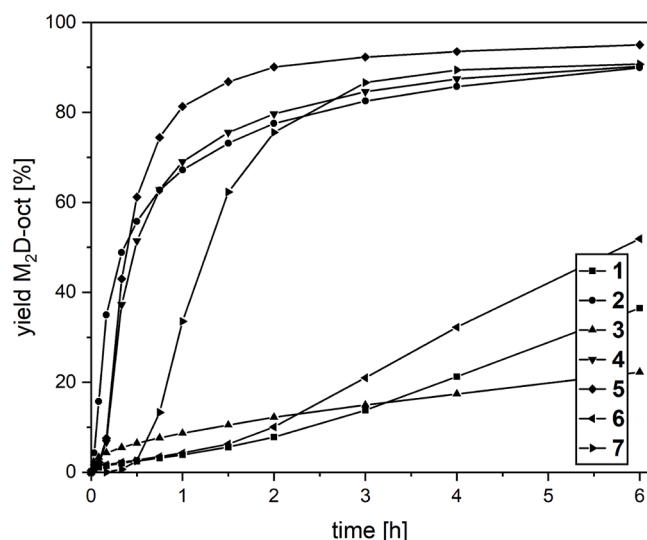
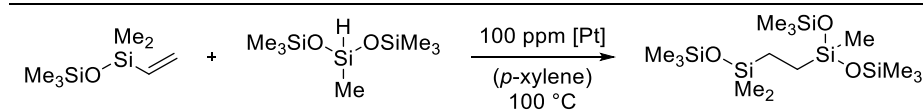


Fig. 4. Time dependent catalytic formation of product ($M_2D\text{-oct}$) by hydrosilylation of oct-1-ene (1.0 eq., 2.024 mmol, 0.5 M) with MD^{HM} (1.0 eq., 2.024 mmol, 0.5 M) in *p*-xylene at 72 °C with 50 ppm [Pt] and *n*-decane (1.518 mmol) as internal standard. Analysis by GC-FID.

of the deactivation and transformation reactions are presented below. At this point a discrepancy of calculated selectivity ($S = Y \cdot X^{-1}$) and observed byproduct formation for 1, 3, and 6, which yield the least desired product is worth mentioning. This finding was however confirmed by a fourfold determination for each complex. The cause of this might be the minimal evaporation of oct-1-ene, which has the lowest boiling point in the catalysis mixture, and the resulting error propagation since no additional byproduct was identified by GC-FID. Addressing the difference of 4 and 7 again, not only does initiation occur faster for 4, but also the turnover frequency (TOF) of 38,000 h^{-1} more than doubles the TOF of 17,000 h^{-1} for 7. The highest TOF in this study is observed for 2 at 48,000 h^{-1} with no distinct induction period, just as for the monometallic $Im^{Me}Pt(dvtms)$, where a TOF of 31,000 h^{-1} was achieved [45]. The monometallic relative of 2, $Im^{Ph}Pt(dvtms)$, falls short at a TOF of 39,000 h^{-1} and a selectivity of 96% compared to 98% for 2, but forms more $M_2D\text{-oct}$ at a yield of 94% (2: $Y = 90\%$) [45]. Contradicting our expectations, 4 and 5 exhibit virtually the same induction period, while in the case of the monometallic relatives $Im^{Me}Pt(dvtms)$ and $Im^{Dipp}Pt(dvtms)$, the steric bulk of the later prolongs the induction period by 1/3 [41]. With the highest yield of 95% and a TOF of 43,000 h^{-1} at $S = 96\%$, 5 emerges with the best performance in the investigated series.

Table 4

Model reaction B: Catalytic formation of product ($MM(C_2H_4)DM_2$) by hydrosilylation of MM^{Vi} (1.0 eq., 2.024 mmol, 0.5 M) with MD^{HM} (1.0 eq., 2.024 mmol, 0.5 M) in *p*-xylene at 100 °C with 100 ppm [Pt] and *n*-decane (1.518 mmol) as internal standard. Analysis by GC-FID. Evaluation of selected byproducts is included in the ESI.



Catalyst	Y($MM(C_2H_4)DM_2$) [%]	X(MM^{Vi}) [%]	X(MD^{HM}) [%]	S(MM^{Vi}) [%]	S(MD^{HM}) [%]	TOF [h^{-1}] ^j
1	75	97	97	77	77	51,000
2	71	97	98	72	72	78,000
3	72	92	91	79	80	34,000
4	71	98	99	73	72	46,000
5	73	97	99	75	73	52,000
6	72	91	89	80	82	51,000
7	68	94	94	72	72	9000

Y = yield. X = conversion. S = selectivity. All data given at $t = 6$ h.

^j TOF of MM^{Vi} calculated at the steepest slope.

3.2.2. Catalytic reaction of vinylsiloxane MM^{Vi} with MD^{HM}

The hydrosilylation of MM^{Vi} with MD^{HM} is selected to simulate industrial-relevant three-dimensional silicone network formation by addition-cure crosslinking using a platinum catalyst ($\equiv B$) [82,83]. Experiments were carried out at 100 °C with a loading of 100 ppm [Pt] for direct comparison to the performance of the monometallic relatives of 1–6 [45]. The results are summarized in Table 4, showing excellent performance of the bimetallic complexes (reaction kinetics are provided in the ESI).

The highest yield of the target product $MM(C_2H_4)DM_2$ is achieved by 1, namely 75%, contradicting the results in A (*vide supra*), where poor performance was realized, due to deactivation. This is attributed to the raised reaction temperature of 100 °C compared to 72 °C in A, which supports the presumed transformation in A that is accompanied by an increase in activity. A TOF of 51,000 h^{-1} is calculated for 1, slightly exceeding 50,000 h^{-1} of $Im^{Me}Pt(dvtms)$ under equal conditions, which signals that the reaction is not limited by diffusion, even though two platinum atoms are linked in close proximity. Complex 2 is by far the most active with a TOF of 78,000 h^{-1} , outperforming the monometallic relatives by over 50%. Substitution of the phenyl wingtips in 2 with pyridine in 3 impairs catalytic performance significantly to a TOF of 34,000 h^{-1} . This detrimental effect of *N*-donors was previously reported for monometallic Markó-type (NHC)Pt(*dvtms*) complexes and is attributed to excessive stabilization of the Pt(II) state as mentioned above [45]. Lowering the catalyst loading and the temperature might prove beneficial in more clearly distinguishing the kinetics of 1–6 but was not pursued in the work presented here.

3.2.3. Comparison of a monometallic (7) and bimetallic (4) complex

In the following, a detailed comparison of the homobimetallic platinum system with the classical monometallic system is presented, with the mesityl-containing complexes 4 and 7 serving as representatives of their respective classes and A as benchmark reaction (Table 5). The temperature is fixed at $T = 72$ °C, while the [Pt] loading is set to 100, 50, 25, and 10 ppm and even as low as 5 ppm for 7. At a loading of 100 ppm, 4 yields 91% of the main product with a TOF of 42,000 h^{-1} which is calculated based on the recorded reaction kinetics (see ESI). Lowering the catalyst concentration to 50 and subsequently to 25 ppm yields 90 and 89% product while maintaining catalyst activity at TOFs of 38,000 and 42,000 h^{-1} , respectively. The difference in TOFs is negligible in terms of uncertainty and indicates that catalytic activity is decoupled from the catalyst loading. This is however contradicting experiments at 10 ppm of 4, where the TOF is reduced to half to 20,000 h^{-1} . Complex 7 on the other hand increases activity while catalyst loading is reduced. At 100 ppm a TOF of 11,000 h^{-1} is calculated that continuously improves and peaks at 33,000 h^{-1} at the lowest investigated loading of 5 ppm. This finding is attributed to catalytic overloading at higher catalyst

Table 5

Catalytic hydrosilylation of oct-1-ene with MD^HM at varying temperature and catalyst loading. The corresponding reaction kinetics are included in the ESI.

Catalyst	T [°C]	Catalyst loading [ppm] ^k	Y(MM(C ₂ H ₄)DM ₂) [%]	TOF [h ⁻¹] ^l
4	72	100	91	42,000
4	72	50	90	38,000
4	72	25	89	42,000
4	72	10	59	20,000
4	62	50	86	29,000
4	52	50	84	12,000
7	72	100	94	11,000
7	72	50	91	17,000
7	72	25	91	26,000
7	72	10	82	31,000
7	72	5	62	33,000
7	62	50	78	6000
7	52	50	45	3000

Yields (Y) after 6 h.

^k denotes the loading of platinum.

^l TOF of oct-1-ene calculated at the steepest slope.

concentrations and emphasizes the inherently different nature of the investigated systems. To examine the thermal dependence of the catalysts, the temperature is lowered in steps of 10 K to 62 and 52 °C, while the platinum loading is fixed at 50 ppm. The bimetallic complex **4** achieves yields of 86 and 84% at TOFs of 29,000 and 12,000 h⁻¹ at 62 and 52 °C, respectively. This preserves 76 and 35% of the activity at standard conditions as the temperature is lowered. This retained activity to original activity ratio is significantly lower for **7**, where TOFs of 6000 and 3000 h⁻¹ reveal that merely 32 and 18% of the activity at standard conditions are preserved. This is rationalized in terms of the initiation process, which was determined as the rate-determining step for monometallic Markó-type complexes [42]. The induction period of **7** is considerably longer compared to **4** (Fig. 4) and is consequently more strongly affected as temperature is decreased. To summarize, the performance of **7** exceeds **4** at low catalyst loadings, while **4** is superior at low temperatures.

3.2.4. Addition of fresh reactants

The initiation behavior is further investigated by the addition of fresh reactants (equimolar ratio of oct-1-ene and MD^HM) after completion of a standard experiment (see ESI for kinetics and detailed experimental). Conversion of the second batch of reactants starts immediately without an induction period, demonstrating that **4** and **7** are still catalytically active. TOFs of 20,000 and 14,000 h⁻¹ are calculated (3 to 10 min) for **4** and **7**, respectively. The decrease in activity is – at least in part – attributable to the dilution of educts from 0.5 to 0.4 M due to their repeated addition. However, **4** only retains 53% activity, while **7** performs at 82%. This may be due to the continuous activation of **7** upon the addition of fresh reactants, due to the inherently slow initiation behavior of the monometallic complex. Previously, Im^{Cy}Pt(dvtms) was repeatedly subjected to fresh reactants under similar conditions [84]. The absence of the initiation period in follow-up runs was here also observed, but the TOF increased ninefold, while a third addition raised the activity 16 times compared to the first experiment. The disagreement with the herein presented results might be attributable to the different characteristics of the catalysts and applied methods.

3.2.5. Pre-catalytic reaction of complexes and MD^HM

Since it is assumed that the initiation process of Markó-type complexes proceeds by partial dissociation of the dvtms chelate and subsequent hydrosilylation of the latter by two SiH entities [42], model reaction A was modified with the objective of comparing “true” TOFs of **4** and **7**. The respective complex is reacted with MD^HM for defined durations t_{SiH} in the presence of solvent (*p*-xylene) and internal standard (*n*-decane) prior to the addition of oct-1-ene that launches catalysis (≡

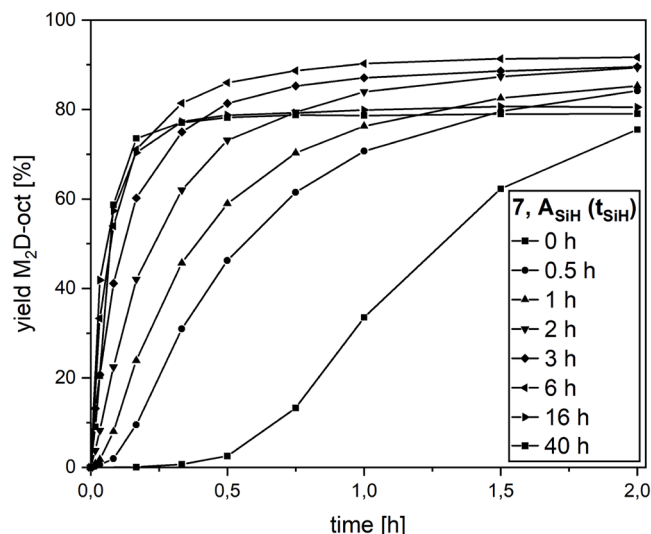


Fig. 5. A_{SiH} – Preceding reaction of **7** with MD^HM for defined durations t_{SiH} . Catalysis is launched upon addition of oct-1-ene. Reaction conditions: oct-1-ene (1.0 eq., 2.024 mmol, 0.5 M) and MD^HM (1.0 eq., 2.024 mmol, 0.5 M) in *p*-xylene at 72 °C with 50 ppm [Pt] and *n*-decane (1.518 mmol) as internal standard. Analysis by GC-FID.

A_{SiH}). As expected, the induction period is significantly shortened after exposing **7** to MD^HM for 0.5 h (Fig. 5), but disappears completely at $t_{\text{SiH}} = 3$ h, transforming the sigmoidal shape to a logarithmic curve. Activity accumulates to a TOF = 220,000 h⁻¹ at $t_{\text{SiH}} = 6$ h, a 13 times increase compared to the performance of **7** in A (Table 6). The selectivity and yield remain virtually unchanged at 91 and 92%, respectively, compared to 92 and 91% in A. At $t_{\text{SiH}} = 16$ and 40 h a notable decrease in yield to 81 and 79%, respectively, can be observed, accompanied by S = 82 and 81%. This indicates a transformation of the catalytically active species and is supported by TOFs of 296,000 h⁻¹ and a decline to 174,000 h⁻¹ after exposure of **7** to MD^HM for 16 and 40 h, respectively. The drop in activity at $t_{\text{SiH}} = 40$ h also transforms the kinetic curve back into a sigmoidal shape, reintroducing an initiation phase. Potential loss of the NHC moiety and platinum agglomeration might form colloids where reactivation due to the “oxygen effect” occurs [85,86]. This is further investigated by mercury poisoning experiments that are presented below.

Contrary to our expectations **4** shows inverse behavior to **7** in A_{SiH} (Fig. 6). Exposure of **4** to MD^HM before catalysis results in a prolonged induction period and activity loss, which is most pronounced at $t_{\text{SiH}} = 6$ h. The selectivity is slightly reduced to 92% and activity is cut down to 7000 h⁻¹, compared to 96% and 38,000 h⁻¹ in A, respectively. This indicates deactivation by transformation into another species. However, at longer t_{SiH} higher activities are observed again with TOFs of 25,000 and 79,000 h⁻¹ after 16 and 40 h, respectively, which is only a fraction of the activity of **7**. Interestingly, the selectivity remains at 92% and is even slightly enhanced to 95% at $t_{\text{SiH}} = 40$ h, which matches – within the

Table 6

Preceding reaction of **4** and **7** with MD^HM for defined durations t_{SiH} in A_{SiH}.

Catalyst	t_{SiH} [h]	Y(M ₂ D-oct) [%]	S [%] ^m	TOF [h ⁻¹] ⁿ
7	6	92	91	220,000
7	16	81	82	296,000
7	40	79	81	174,000
4	6	48	92	7000
4	16	85	92	25,000
4	40	90	95	79,000

Y = yield. S = selectivity.

^m Selectivity regarding oct-1-ene at $t = 2$ h.

ⁿ TOF of oct-1-ene calculated at the steepest slope.

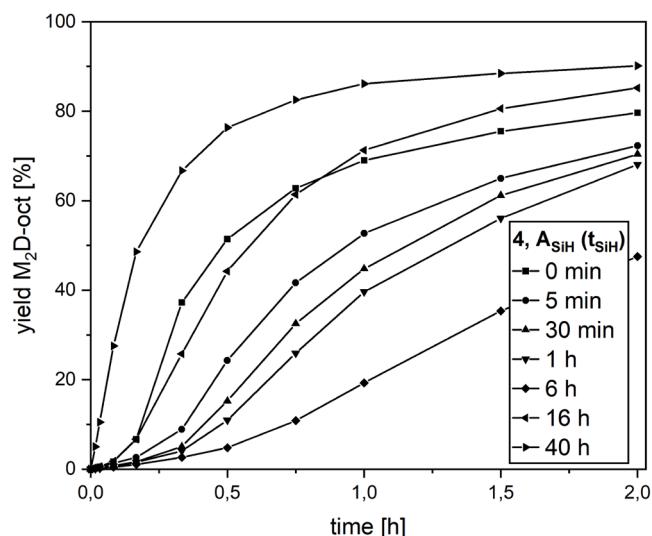


Fig. 6. A_{SiH} – Preceding reaction of **4** with MD^{HM} for defined durations t_{SiH} . Catalysis is launched upon addition of oct-1-ene. Reaction conditions: oct-1-ene (1.0 eq., 2.024 mmol, 0.5 M) and MD^{HM} (1.0 eq., 2.024 mmol, 0.5 M) in *p*-xylene at 72 °C with 50 ppm [Pt] and *n*-decane (1.518 mmol) as internal standard. Analysis by GC-FID.

margin of error – $S = 96\%$ under standard conditions. This indicates, that the Pt–C bond remains undamaged and an interim species is formed upon exposure of **4** to MD^{HM} . In this context, di- μ -hydrido platinum dimers **D** and **E** (Fig. 7) were reported to form in the presence of silanes [84,87]. The structures of both species were unequivocally resolved by SC-XRD. Catalytic evaluation of **D** revealed a longer initiation period and lower activity compared to $Im^{Cy}Pt(dvtms)$, which matches the behavior of **4** in the A_{SiH} method. To investigate this issue, **1** (1.0 eq.) is reacted with MD^{HM} (7.0 eq.) at 72 °C for 7 min. Analysis by 1H NMR reveals four major hydride resonances with ^{195}Pt satellites at $\delta = -4.25$ ($^1J_{Pt,H} = 640$ Hz), -5.16 , -7.18 ($^1J_{Pt,H} = 632$ Hz) and -9.46 ppm ($^1J_{Pt,H} = 652$ Hz). Chemical shifts and coupling constants are consistent with platinum hydride complexes, among them μ -hydrido platinum dimers [88–96]. Attempts to isolate or crystallize the formed species remained unsuccessful. Based on this, di- μ -hydrido-bridged species **C** is postulated, whose formation is favored due to the proximity of two platinum atoms in the bimetallic complex. This also serves as an explanation of the inferior performance of **1** in **A**, which indicates that the sterically least occupying methyl wingtips at the NHCs cannot prevent the formation of **C** even under standard catalytic conditions. In this context and also relevant for **7** in A_{SiH} , the di- μ -hydrido-bridged $Im^{Cy}Pt$ species of Markó *et al.* was obtained under relatively mild conditions with five equivalents silane at 80 °C for 10 h. Harsher conditions of 20 equivalents silane and

100 °C for 15 h however facilitate conversion of $Im^{Dipp}Pt(dvtms)$ into tricoordinate bis-(silyl)platinum(II)-NHC complex **F** that remains stable in the presence of excess silane even under ambient conditions [97]. Especially in the hydrosilylation of alkynes, **F** proves significantly more active and selective than the parent $Im^{Dipp}Pt(dvtms)$ complex [98]. Following this model, further conversion of **C** into a silyl species appears reasonable and explains the increase in activity [99,100]. In addition, the initial activation of *dvtms* is of particular interest as it was reported that the catalyst activation pathway for mono- and bimetallic complexes might be fundamentally different. Investigation of monometallic (NHC) $Rh(COD)$ and bimetallic bis-NHC($RhCOD$)₂ complexes revealed hydrogen transfer from one to another COD moiety that forms cycloocta-1,3,5-triene and opens up a free coordination site at the site with reduced cyclooctene [34]. This pathway is significantly faster than the dissociation of COD for the monometallic complex and increases catalytic performance. Work is currently in progress to unveil the origin of the synergistic effect and to elucidate the transformations of bimetallic bis-NHC($Ptdvtms$)₂ complexes, especially their induction period.

3.2.6. Mercury(0) poisoning experiments

The pre-catalytic reaction of **7** with MD^{HM} (*vide supra*) raised the question of (NHC)Pt stability and clearly demanded a more in-depth examination, as colloid formation for similar complexes has been assumed in previous reports [81,101]. The catalyst poisoning experiment with elemental mercury is commonly used to distinguish homogeneous molecular catalysis from heterogeneous catalysis [102,103] and is applied to the monometallic (**7**) and bimetallic (**4**) systems. The method is based on the assumption that Hg(0) will amalgamate Pt(0) clusters/colloids and nanoparticles and render them inactive. However, wrong conclusions might be drawn as it was shown that there are molecular complexes that are reactive to Hg(0) and a proper methodology is crucial to obtain meaningful results [102–106]. To overcome these issues 1500 equivalents of Hg(0) with regards to platinum are used and intimate contact of Hg(0) with the reaction mixture is ensured by raising the stirring frequency from 500 to 1400 rpm. Also, mercury is only added to the reactor, after educt conversion is higher than 10%, which results in a bending of the kinetic curve if Hg(0) influences the catalyst. On top of this, the mercury poisoning experiment is conducted under standard conditions (**A**) and after 40 h of pre-reaction of **4** and **7** with MD^{HM} . In this study, no visual discoloration of the reaction mixtures was observed, which would indicate the formation of colloidal platinum

Table 7

Results of mercury poisoning experiments (1500 eq. Hg/Pt) and observed final yields in parentheses.

Catalyst	A	A_{SiH} (40 h)
4	Negative (90%)	Negative (88%)
7	Negative (94%)	Positive (56%)

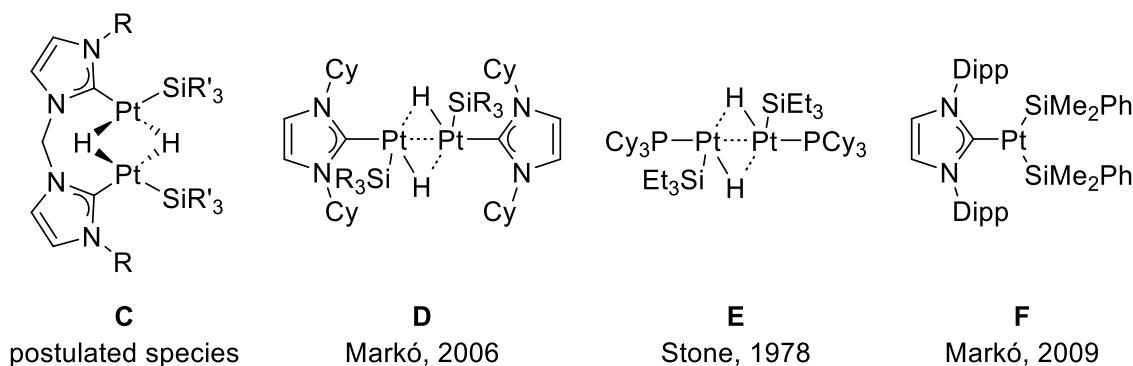


Fig. 7. Postulated di- μ -hydrido complex **C**. Platinum dimer **D** of Markó *et al.* with $SiR_3 = MDM$ [84]. Platinum dimer **E** of Stone *et al.* [87]. Bis-(silyl)platinum(II)-NHC complex **F** of Markó *et al.* [97].

species but does not necessarily rule out their existence. There is no abnormality in the kinetics of the mercury test of **4** in either **A** or A_{SiH} (40 h) as is expected from the maintained selectivities (Table 7, kinetics in ESI). While no poisoning is observed for **7** under standard conditions (**A**), Hg(0) completely deactivates the catalyst in A_{SiH} (40 h). This matches with the behavior of **7** in A_{SiH} (40 h), without mercury addition, where a decrease in selectivity and activity was recorded, which even leads to the formation of an induction period. These independent results indicate the formation of colloidal platinum from **7** in the presence of $MD^H M$ after 40 h, while **4** is intermediately stabilized as di- μ -hydrido complex.

4. Conclusion

A series of six homobimetallic *bis*-NHC(Ptdvtms)₂ complexes **1–6** was prepared with the anticipation of cooperative effects. Characterization by NMR spectroscopy (¹H, ¹³C, ²⁹Si, and ¹⁹⁵Pt) and SC-XRD revealed the strong similarity of this new complex class to the parent monometallic Markó-type (NHC)Pt(dvtms) complexes. Hindered rotation of the Pt–C bond generates conformational isomers for **1–3** and **6** at room temperature. ¹H VT-NMR experiments with **5** disclose coalescence at 233 K, which gives $\Delta G^\ddagger = 52.5 kJmol^{-1}$ as a rotational barrier, using the Eyring equation. The bimetallic complexes prove to be potent catalyst precursors for the hydrosilylation of alkenes and are characterized by minuscule initiation periods compared to $Im^{Mes}Pt(dvtms)$ (**7**) which is used as a reference to Markó-type complexes. Inverse behavior was observed for **4** and **7** in the pre-catalytic reaction of the complexes with $MD^H M$. Activation of **7** results in a TOF of 296,000 h⁻¹, with selectivity decreasing under harsh conditions, while **4** is first deactivated and then reactivated under harsh conditions, with selectivity being maintained. These findings are explained by the decomposition of **7** to platinum colloids after extended exposure to $MD^H M$ as revealed by mercury poisoning experiments and intermediate stabilization of **4** as the postulated di- μ -hydrido complex **C** under the same conditions. Relevant for the application is the performance of **7** at low catalyst loadings, while **4** is superior at low temperatures due to easier activation.

CRediT authorship contribution statement

Michael J. Sauer: Writing – review & editing, Writing – original draft, Visualization, Validation, Methodology, Investigation, Formal analysis, Conceptualization. **Jeff Offorjindu:** Methodology, Investigation. **Greta G. Zámbo:** Methodology, Investigation. **Robert M. Reich:** Supervision, Project administration. **Fritz E. Kühn:** Supervision, Project administration.

Declaration of competing interest

The authors declare that they have no known competing financial interests or personal relationships that could have appeared to influence the work reported in this paper.

Data availability

Data will be made available on request.

Acknowledgments

M.J.S. and G.G.Z. thank the TUM Graduate School and WACKER Chemie AG for financial support. J.O. gratefully acknowledges the support of AuTUM (Ausbildungszentrum der Technischen Universität München) and all authors thank AuTUM for the cooperation during J. O.'s apprenticeship.

Supplementary materials

Supplementary material associated with this article can be found, in the online version, at doi:10.1016/j.jorganchem.2024.123030.

References

- [1] R.H. Holm, P. Kennepohl, E.I. Solomon, Structural and functional aspects of metal sites in biology, Chem. Rev. 96 (1996) 2239–2314, <https://doi.org/10.1021/cr9500390>.
- [2] R.E. Stenkamp, Dioxygen and hemerythrin, Chem. Rev. 94 (1994) 715–726, <https://doi.org/10.1021/cr00027a008>.
- [3] E.I. Solomon, D.E. Heppner, E.M. Johnston, J.W. Ginsbach, J. Cirera, M. Qayyum, M.T. Kieber-Emmons, C.H. Kjaergaard, R.G. Hadt, L. Tian, Copper active sites in biology, Chem. Rev. 114 (2014) 3659–3853, <https://doi.org/10.1021/cr400327t>.
- [4] T. Guchhait, S. Sasmal, F.S.T. Khan, S.P. Rath, Oxo- and hydroxo-bridged diiron (III) porphyrin dimers: inorganic and bio-inorganic perspectives and effects of intermacrocylic interactions, Coord. Chem. Rev. 337 (2017) 112–144, <https://doi.org/10.1016/j.ccr.2017.02.008>.
- [5] A.L. Gavrilova, B. Bosnich, Principles of mononucleating and binucleating ligand design, Chem. Rev. 104 (2004) 349–384, <https://doi.org/10.1021/cr020604g>.
- [6] R. Boulatov, Understanding the reaction that powers this world: biomimetic studies of respiratory O₂ reduction by cytochrome oxidase, Pure Appl. Chem. 76 (2004) 303–319, <https://doi.org/10.1351/pac200476020303>.
- [7] E.Y. Tshuva, S.J. Lippard, Synthetic models for non-heme carboxylate-bridged diiron metalloproteins: strategies and tactics, Chem. Rev. 104 (2004) 987–1012, <https://doi.org/10.1021/cr020622y>.
- [8] J. Weston, Mode of action of Bi- and trinuclear zinc hydrolases and their synthetic analogues, Chem. Rev. 105 (2005) 2151–2174, <https://doi.org/10.1021/cr020057z>.
- [9] A. Magnuson, M. Anderlund, O. Johansson, P. Lindblad, R. Lomoth, T. Polivka, S. Ott, K. Stensjö, S. Styring, V. Sundström, L. Hammarström, Biomimetic and microbial approaches to solar fuel generation, Acc. Chem. Res. 42 (2009) 1899–1909, <https://doi.org/10.1021/ar900127h>.
- [10] S. Friedle, E. Reisner, S.J. Lippard, Current challenges of modeling diiron enzyme active sites for dioxygen activation by biomimetic synthetic complexes, Chem. Soc. Rev. 39 (2010) 2768–2779, <https://doi.org/10.1039/C003079C>.
- [11] M.M. Najafpour, G. Renger, M. Holyńska, A.N. Moghaddam, E.M. Aro, R. Carpentier, H. Nishihara, J.J. Eaton-Rye, J.R. Shen, S.I. Allakhverdiev, Manganese compounds as water-oxidizing catalysts: from the natural water-oxidizing complex to nanosized manganese oxide structures, Chem. Rev. 116 (2016) 2886–2936, <https://doi.org/10.1021/acs.chemrev.5b00340>.
- [12] V.C.C. Wang, S. Maji, P.P.Y. Chen, H.K. Lee, S.S.F. Yu, S.I. Chan, Alkane oxidation: methane monooxygenases, related enzymes, and their biomimetics, Chem. Rev. 117 (2017) 8574–8621, <https://doi.org/10.1021/acs.chemrev.6b00624>.
- [13] P. Buchwalter, J. Rosé, P. Braunstein, Multimetallic catalysis based on heterometallic complexes and clusters, Chem. Rev. 115 (2015) 28–126, <https://doi.org/10.1021/cr500208k>.
- [14] N.P. Mankad, Selectivity effects in bimetallic catalysis, Chem. Eur. J. 22 (2016) 5822–5829, <https://doi.org/10.1002/chem.201505002>.
- [15] J. Campos, Bimetallic cooperation across the periodic table, Nat. Rev. Chem. 4 (2020) 696–702, <https://doi.org/10.1038/s41570-020-00226-5>.
- [16] B. Chatterjee, W.C. Chang, S. Jena, C. Werlé, Implementation of cooperative designs in polarized transition metal systems—significance for bond activation and catalysis, ACS Catal. 10 (2020) 14024–14055, <https://doi.org/10.1021/acscatal.0c03794>.
- [17] R. Maity, B.S. Birenheide, F. Breher, B. Sarkar, Cooperative effects in multimetallic complexes applied in catalysis, ChemCatChem 13 (2021) 2337–2370, <https://doi.org/10.1002/cctc.202001951>.
- [18] A. Dey, Bimetallic cooperativity and hydrogen bonding allow efficient reduction of CO₂, Angew. Chem. Int. Ed. 62 (2023) e202301760, <https://doi.org/10.1002/anie.202301760>.
- [19] E.K. van den Beuken, B.L. Feringa, Bimetallic catalysis by late transition metal complexes, Tetrahedron 54 (1998) 12985–13011, [https://doi.org/10.1016/S0040-4020\(98\)00319-6](https://doi.org/10.1016/S0040-4020(98)00319-6).
- [20] J.M. Gil-Negrete, E. Hevia, Main group bimetallic partnerships for cooperative catalysis, Chem. Sci. 12 (2021) 1982–1992, <https://doi.org/10.1039/D0SC05116K>.
- [21] J. Park, S. Hong, Cooperative bimetallic catalysis in asymmetric transformations, Chem. Soc. Rev. 41 (2012) 6931–6943, <https://doi.org/10.1039/C2CS35129C>.
- [22] D.R. Pye, N.P. Mankad, Bimetallic catalysis for C–C and C–X coupling reactions, Chem. Sci. 8 (2017) 1705–1718, <https://doi.org/10.1039/C6SC05556G>.
- [23] K.J. Evans, S.M. Mansell, Functionalised N-Heterocyclic carbene ligands in bimetallic architectures, Chem. Eur. J. 26 (2020) 5927–5941, <https://doi.org/10.1002/chem.201905510>.
- [24] S. Klaus, M.W. Lehenmeier, C.E. Anderson, B. Rieger, Recent advances in CO₂/epoxide copolymerization—new strategies and cooperative mechanisms, Coord. Chem. Rev. 255 (2011) 1460–1479, <https://doi.org/10.1016/j.ccr.2010.12.002>.
- [25] J.I. van der Vlugt, Cooperative catalysis with first-row late transition metals, Eur. J. Inorg. Chem. (2012) 363–375, <https://doi.org/10.1002/ejic.201100752>, 2012.

- [26] N. Xiong, G. Zhang, X. Sun, R. Zeng, Metal-metal cooperation in dinucleating complexes involving late transition metals directed towards organic catalysis, *Chin. J. Chem* 38 (2020) 185–201, <https://doi.org/10.1002/cjoc.201900371>.
- [27] C. Adams, P. Riviere, M. Riviere-Baudet, C. Morales-Verdejo, M. Dahrouch, V. Morales, A. Castel, F. Delpech, J.M. Manriquez, I. Chavez, Catalytic study of heterobimetallic rhodium complexes derived from partially alkylated *s*-indacene in dehydrogenative silylation of olefins, *J. Organomet. Chem.* 749 (2014) 266–274, <https://doi.org/10.1016/j.jorganchem.2013.10.017>.
- [28] V. Comte, P. Le Gendre, P. Richard, C. Moise, [TIPHOS(Rh)]⁺: a fortuitous coordination mode and an effective Hydrosilylation bimetallic catalyst, *Organometallics* 24 (2005) 1439–1444, <https://doi.org/10.1021/om040058c>.
- [29] A.J. Huckaba, T.K. Hollis, T.O. Howell, H.U. Valle, Y. Wu, Synthesis and characterization of a 1,3-Phenylene-Bridged *N*-Alkyl Bis(benzimidazole) CCC-NHC pincer ligand precursor: homobimetallic silver and rhodium complexes and the catalytic Hydrosilylation of Phenylacetylene, *Organometallics* 32 (2013) 63–69, <https://doi.org/10.1021/om3008037>.
- [30] V. Diachenko, M.J. Page, M.R.D. Gatus, M. Bhadbhade, B.A. Messerle, Bimetallic *N*-Heterocyclic Carbene Rh(I) complexes: probing the cooperative effect for the Catalyzed Hydroelementation of Alkynes, *Organometallics* 34 (2015) 4543–4552, <https://doi.org/10.1021/acs.organomet.5b00594>.
- [31] M.R.D. Gatus, I. Pernik, J.A. Tompsett, S.C. Binding, M.B. Peterson, B.A. Messerle, Simple and reactive Ir(I) *N*-heterocyclic carbene complexes for alkyne activation, *Dalton Trans* 48 (2019) 4333–4340, <https://doi.org/10.1039/C9DT00313D>.
- [32] S. Leelasubcharoen, P.A. Zhizhko, L.G. Kuzmina, A.V. Churakov, J.A.K. Howard, G.I. Nikonov, Niobium/Rhodium Bimetallic complexes: synthesis, structure, and catalytic hydrosilylation of acetophenone and benzaldehyde, *Organometallics* 28 (2009) 4500–4506, <https://doi.org/10.1021/om900363r>.
- [33] A.E. Findlay, S. Leelasubcharoen, L.G. Kuzmina, J.A.K. Howard, G.I. Nikonov, Phosphido-bridged Ta/Rh bimetallic complex: synthesis, structure, and catalytic hydrosilylation of acetophenone, *Dalton Trans* 39 (2010) 9264–9269, <https://doi.org/10.1039/C0DT00141D>.
- [34] R.H. Lam, S.T. Keaveney, B.A. Messerle, I. Pernik, Bimetallic rhodium complexes: precatalyst activation-triggered bimetallic enhancement for the hydrosilylation transformation, *ACS Catal* 13 (2023) 1999–2010, <https://doi.org/10.1021/acscatal.2c04388>.
- [35] W. Zhou, S.L. Marquard, M.W. Bezpalko, B.M. Foxman, C.M. Thomas, Catalytic hydrosilylation of ketones using a Co/Zr heterobimetallic complex: evidence for an unusual mechanism involving Ketyl Radicals, *Organometallics* 32 (2013) 1766–1772, <https://doi.org/10.1021/om301194g>.
- [36] J.L. Speier, D.E. Hook, Process for the Production of Organosilicon Compounds, 1958 US2823218, February 11.
- [37] B.D. Karstedt, Platinum Complexes of Unsaturated Siloxanes and Platinum Containing Organopolysiloxanes, 1973 US3775452, November 27.
- [38] D. Troegel, J. Stohrer, Recent advances and actual challenges in late transition metal catalyzed hydrosilylation of olefins from an industrial point of view, *Coord. Chem. Rev.* 255 (2011) 1440–1459, <https://doi.org/10.1016/j.ccr.2010.12.025>.
- [39] N. Nakata, M. Sakashita, C. Komatsubara, A. Ishii, Synthesis, structure, and catalytic activity of bimetallic Pt(II)–Ir(III) complexes Bridged by Cyclooctane-1,2-dithiolato ligands, *Eur. J. Inorg. Chem.* (2010) 447–453, <https://doi.org/10.1002/ejic.200900958>, 2010.
- [40] I.E. Markó, S. Stérin, O. Buisine, G. Mignani, P. Branlard, B. Tinant, J.P. Declercq, Selective and efficient Platinum(0)-Carbene complexes as hydrosilylation catalysts, *Science* 298 (2002) 204–206, <https://doi.org/10.1126/science.1073338>.
- [41] I.E. Markó, S. Stérin, O. Buisine, G. Berthon, G. Michaud, B. Tinant, J.P. Declercq, Highly active and selective Platinum(0)-Carbene complexes. Efficient, catalytic hydrosilylation of functionalised olefins, *Adv. Synth. Catal.* 346 (2004) 1429–1434, <https://doi.org/10.1002/adsc.200404048>.
- [42] G. Berthon-Gelloz, O. Buisine, J.F. Brière, G. Michaud, S. Stérin, G. Mignani, B. Tinant, J.P. Declercq, D. Chapon, I.E. Markó, Synthetic and structural studies of NHC–Pt(dvtms) complexes and their application as alkene hydrosilylation catalysts (NHC = *N*-heterocyclic carbene, dvtms = divinyltetramethylsiloxane), *J. Organomet. Chem.* 690 (2005) 6156–6168, <https://doi.org/10.1016/j.jorganchem.2005.08.020>.
- [43] O. Buisine, G. Berthon-Gelloz, J.F. Brière, S. Stérin, G. Mignani, P. Branlard, B. Tinant, J.P. Declercq, I.E. Markó, Second generation *N*-heterocyclic carbene–Pt(0) complexes as efficient catalysts for the hydrosilylation of alkenes, *Chem. Commun.* (2005) 3856–3858, <https://doi.org/10.1039/B506369H>.
- [44] D. Brissy, M. Skander, P. Retailleau, G. Frison, A. Marinetti, Platinum(II) complexes featuring chiral diphosphines and *N*-heterocyclic carbene ligands: synthesis and evaluation as cycloisomerization catalysts, *Organometallics* 28 (2009) 140–151, <https://doi.org/10.1021/om800743r>.
- [45] M.J. Sauer, L.F. Richter, J. Offorjindu, R.M. Reich, F.E. Kühn, Synthesis and characterization of Markó-type (NHC)Pt(dvtms) complexes and their evaluation in the hydrosilylation reaction of alkenes, *J. Organomet. Chem.* 1005 (2024) 122995–123005, <https://doi.org/10.1016/j.jorganchem.2023.122995>.
- [46] T.K. Meister, J.W. Kück, K. Riener, A. Pöthig, W.A. Herrmann, F.E. Kühn, Decoding catalytic activity of platinum carbene hydrosilylation catalysts, *J. Catal.* 337 (2016) 157–166, <https://doi.org/10.1016/j.jcat.2016.01.032>.
- [47] T. Strassner, M. Muehlhofer, A. Zeller, E. Herdtweck, W.A. Herrmann, The counterion influence on the CH-activation of methane by palladium(II) biscarbene complexes – structures, reactivity and DFT calculations, *J. Organomet. Chem.* 689 (2004) 1418–1424, <https://doi.org/10.1016/j.jorganchem.2004.02.013>.
- [48] M. Micksch, T. Strassner, Palladium(II) Complexes with chelating biscarbene ligands in the catalytic suzuki–miyaura cross-coupling reaction, *Eur. J. Inorg. Chem.* (2012) 5872–5880, <https://doi.org/10.1002/ejic.201200940>, 2012.
- [49] T. Wagner, A. Pöthig, H.M.S. Augenstein, T.D. Schmidt, M. Kaposi, E. Herdtweck, W. Brütting, W.A. Herrmann, F.E. Kühn, From simple ligands to complex structures: structural diversity of Silver(I) complexes bearing Tetradentate (alkylenebimpy) NHC ligands, *Organometallics* 34 (2015) 1522–1529, <https://doi.org/10.1021/om5013067>.
- [50] J.F. Schlagintweit, L. Nguyen, F. Dyckhoff, F. Kaiser, R.M. Reich, F.E. Kühn, Exploring different coordination modes of the first tetradentate NHC/1,2,3-triazole hybrid ligand for group 10 complexes, in: *Dalton Trans.*, 48, 2019, pp. 14820–14828, <https://doi.org/10.1039/C9DT03430G>.
- [51] H. Richter, H. Schwertfeger, P.R. Schreiner, R. Fröhlich, F. Glorius, Thieme chemistry journal awardees - where are they now? synthesis of diamantane-Derived *N*-heterocyclic carbenes and applications in catalysis, *Synlett* (2009) 193–197, <https://doi.org/10.1055/s-0028-1087676>, 2009.
- [52] APEX Suite of Crystallographic Software (Version APEX4), Bruker AXS Inc., 2021.
- [53] SAINT (Version 8.38A), Bruker AXS Inc., 2017.
- [54] SADABS (Version 2016/2), Bruker AXS Inc., 2016.
- [55] C.B. Hübschle, G.M. Sheldrick, B. Dittrich, ShelXle: a Qt graphical user interface for SHELXL, *J. Appl. Crystallogr.* 44 (2011) 1281–1284, <https://doi.org/10.1107/S002188911043202>.
- [56] G.M. Sheldrick, Crystal structure refinement with SHELXL, *Acta Crystallogr. Sect. C* 71 (2015) 3–8, <https://doi.org/10.1107/S2053229614024218>.
- [57] G.M. Sheldrick, SHELXT - Integrated space-group and crystal-structure determination, *Acta Crystallogr. Sect. A* 71 (2015) 3–8, <https://doi.org/10.1107/S2053273314026370>.
- [58] A.J. Wilson, *International Tables for Crystallography*, Kluwer Academic Publishers, Dordrecht, 1992.
- [59] A. Spek, Structure validation in chemical crystallography, *Acta Crystallogr. Sect. D* 65 (2009) 148–155, <https://doi.org/10.1107/S090744490804362X>.
- [60] G. Chandra, P.Y. Lo, P.B. Hitchcock, M.F. Lappert, A Convenient and Novel Route to Bis(η -alkyne)platinum(0) and other Platinum(0) Complexes from Speier's Hydrosilylation Catalyst H₂[PtCl₆]-xH₂O. X-ray Structure of [Pt{(η -CH₂=CHSiMe₂)₂O}(P-*t*-Bu₃)], *Organometallics* 6 (1987) 191–192, <https://doi.org/10.1021/om00144a036>.
- [61] P.B. Hitchcock, M.F. Lappert, N.J.W. Warhurst, Synthesis and structure of a rac-Tris(divinyl)disiloxane)diplatinum(0) complex and its reaction with maleic anhydride, *Angew. Chem. Int. Ed.* 30 (1991) 438–440, <https://doi.org/10.1002/anie.199104381>.
- [62] B. Schulze, U.S. Schubert, Beyond click chemistry – supramolecular interactions of 1,2,3-triazoles, *Chem. Soc. Rev.* 43 (2014) 2522–2571, <https://doi.org/10.1039/C3CS60386E>.
- [63] S. Sinn, B. Schulze, C. Friebe, D.G. Brown, M. Jäger, E. Altuntaş, J. Kübel, O. Guntner, C.P. Berlinguette, B. Dietzek, U.S. Schubert, Physicochemical analysis of Ruthenium(II) sensitizers of 1,2,3-Triazole-derived mesoionic carbene and cyclometalating ligands, *Inorg. Chem.* 53 (2014) 2083–2095, <https://doi.org/10.1021/ic402702z>.
- [64] B.P. Maliszewski, N.V. Tzouras, S.G. Guillet, M. Saab, M. Beliš, K. Van Hecke, F. Nagra, S.P. Nolan, A general protocol for the synthesis of Pt-NHC (NHC = *N*-heterocyclic carbene) hydrosilylation catalysts, *Dalton Trans.* 49 (2020) 14673–14679, <https://doi.org/10.1039/D0DT03480K>.
- [65] B.P. Maliszewski, I. Ritacco, M. Beliš, I.I. Hashim, N.V. Tzouras, L. Caporaso, L. Cavallo, K. Van Hecke, F. Nagra, C.S.J. Cazin, S.P. Nolan, A green route to platinum *N*-heterocyclic carbene complexes: mechanism and expanded scope, *Dalton Trans* 51 (2022) 6204–6211, <https://doi.org/10.1039/D2DT00504B>.
- [66] J.J. Dunsford, K.J. Cavell, B. Kariuki, Expanded ring *N*-heterocyclic carbene complexes of zero valent platinum dvtms (divinyltetramethylsiloxane): highly efficient hydrosilylation catalysts, *J. Organomet. Chem.* 696 (2011) 188–194, <https://doi.org/10.1016/j.jorganchem.2010.08.045>.
- [67] A.M. Ruiz-Varilla, E.A. Baquero, G.F. Silbestri, C. Gonzalez-Arellano, E. de Jesús, J.C. Flores, Synthesis and behavior of novel sulfonated water-soluble *N*-heterocyclic carbene (η^4 -diene) platinum(0) complexes, *Dalton Trans.* 44 (2015) 18360–18369, <https://doi.org/10.1039/C5DT02622A>.
- [68] N. Schneider, S. Bellemin-Laponnaz, H. Wadeppohl, L.H. Gade, A new class of modular Oxazoline-NHC ligands and their coordination chemistry with platinum metals, *Eur. J. Inorg. Chem.* (2008) 5587–5598, <https://doi.org/10.1002/ejic.200800908>, 2008.
- [69] J.R.L. Priqueler, I.S. Butler, F.D. Rochon, An overview of ¹⁹⁵Pt nuclear magnetic resonance spectroscopy, *Appl. Spectrosc. Rev.* 41 (2006) 185–226, <https://doi.org/10.1080/05704920600620311>.
- [70] B.M. Still, P.G.A. Kumar, J.R. Aldrich-Wright, W.S. Price, ¹⁹⁵Pt NMR—theory and application, *Chem. Soc. Rev.* 36 (2007) 665–686, <https://doi.org/10.1039/B606190G>.
- [71] T. Troadec, A. Prades, R. Rodriguez, R. Mirgalet, A. Baceiredo, N. Saffon-Merceron, V. Branchadell, T. Kato, Silacyclopropylideneplatinum(0) Complex as a robust and efficient hydrosilylation catalyst, *Inorg. Chem.* 55 (2016) 8234–8240, <https://doi.org/10.1021/acs.inorgchem.6b01505>.
- [72] T. Iimura, N. Akasaka, T. Kosai, T. Iwamoto, A Pt(0) complex with cyclic (alkyl) (amino)silylene and 1,3-divinyl-1,1,3,3-tetramethylsiloxane ligands: synthesis, molecular structure, and catalytic hydrosilylation activity, *Dalton Trans.* 46 (2017) 8868–8874, <https://doi.org/10.1039/C7DT01113J>.
- [73] H. Gunther, The influence of dynamic effects on ¹H nuclear magnetic resonance spectra, in: H. Gunther (Ed.), *NMR Spectroscopy*, Wiley, New York, 1995, pp. 335–390.

- [74] M.T. Huggins, T. Kesharwani, J. Buttrick, C. Nicholson, Variable temperature NMR experiment studying restricted bond rotation, *J. Chem. Educ.* 97 (2020) 1425–1429, <https://doi.org/10.1021/acs.jchemed.0c00057>.
- [75] L.N. Appelhans, C.D. Incarvito, R.H. Crabtree, Synthesis of monodentate bis(*N*-heterocyclic carbene) complexes of iridium: mixed complexes of abnormal NHCs, normal NHCs, and triazole NHCs, *J. Organomet. Chem.* 693 (2008) 2761–2766, <https://doi.org/10.1016/j.jorganchem.2008.05.024>.
- [76] M. Dangelov, M. Stoyanova, P. Petrov, M. Putala, N.G. Vassilev, Fluxional Pd(II) NHC complexes – synthesis, structure elucidation and catalytic studies, *J. Organomet. Chem.* 817 (2016) 1–14, <https://doi.org/10.1016/j.jorganchem.2016.05.002>.
- [77] C.P. Newman, R.J. Deeth, G.J. Clarkson, J.P. Rourke, Synthesis of mixed NHC/L Platinum(II) complexes: restricted rotation of the NHC group, *Organometallics* 26 (2007) 6225–6233, <https://doi.org/10.1021/om700671y>.
- [78] P. Žak, M. Boit, B. Dudzic, M. Kubicki, Synthesis of (E)-1,4-disilsequioxylsubstituted but-1-en-3-yne via platinum-catalyzed dimerization of ethynylsiloxylsilsequioxanes, *Dalton Trans* 48 (2019) 2657–2663, <https://doi.org/10.1039/C8DT05142A>.
- [79] P. Žak, M. Boit, M. Kubicki, M. Kubicki, C. Pietraszuk, Platinum complexes bearing Bulky *N*-Heterocyclic carbene ligands as efficient catalysts for the fully selective dimerization of terminal alkynes, *ChemCatChem* 9 (2017) 3627–3631, <https://doi.org/10.1002/cctc.201700580>.
- [80] S.A. Rzhavskiy, M.A. Topchiy, K.A. Lyssenko, A.N. Philippova, M.A. Belaya, A.A. Agheshina, M.V. Bermeshev, M.S. Nechaev, A.F. Asachenko, New expanded-ring NHC platinum(0) complexes: synthesis, structure and highly efficient dimerization of terminal alkenes, *J. Organomet. Chem.* 912 (2020) 121140–121162, <https://doi.org/10.1016/j.jorganchem.2020.121140>.
- [81] P. Žak, M. Boit, M. Kubicki, C. Pietraszuk, Highly selective hydrosilylation of olefins and acetylenes by platinum(0) complexes bearing bulky *N*-heterocyclic carbene ligands, *Dalton Trans* 47 (2018) 1903–1910, <https://doi.org/10.1039/C7DT04392A>.
- [82] R.J. Hofmann, M. Vlatković, F. Wiesbrock, Fifty years of Hydrosilylation in polymer science: a review of current trends of low-cost transition-metal and metal-free catalysts, non-thermally triggered hydrosilylation reactions, and industrial applications, *Polymers (Basel)* 9 (2017) 534–570, <https://doi.org/10.3390/polym9100534>.
- [83] J.M. Lambert, The nature of platinum in silicones for biomedical and healthcare use, *J. Biomed. Mater. Res. Part B Appl. Biomater.* 78B (2006) 167–180, <https://doi.org/10.1002/jbm.b.30471>.
- [84] G. Berthon-Gelloz, I.E. Markó, Efficient and selective Hydrosilylation of Alkenes and Alkynes Catalyzed by Novel *N*-Heterocyclic Carbene Pt(0) Complexes, *N-Heterocyclic Carbenes in Synthesis*, WILEY-VCH, Weinheim, 2006, pp. 119–161.
- [85] J. Stein, L.N. Lewis, Y. Gao, R.A. Scott, *In Situ* determination of the active catalyst in hydrosilylation reactions using highly reactive Pt(0) catalyst precursors, *J. Am. Chem. Soc.* 121 (1999) 3693–3703, <https://doi.org/10.1021/ja9825377>.
- [86] L.N. Lewis, On the mechanism of metal colloid catalyzed hydrosilylation: proposed explanations for electronic effects and oxygen cocatalysis, *J. Am. Chem. Soc.* 112 (1990) 5998–6004, <https://doi.org/10.1021/ja00172a014>.
- [87] M. Ciriano, M. Green, J.A.K. Howard, J. Proud, J.L. Spencer, F.G.A. Stone, C. A. Tsipis, Synthesis of *trans*-di- μ -hydrido(*bis*(silyl)*bis*(trialkylphosphine)diplatinum) complexes: crystal and molecular structure of di- μ -hydrido-*bis*(tricyclohexylphosphine)*bis*(triethylsilyl)diplatinum, *J. Chem. Soc., Dalton Trans.* (1978) 801–808, <https://doi.org/10.1039/DT9780000801>.
- [88] S. Ouis, D.A. Rouag, L. Bendjedou, C. Bailly, Crystal structure of homodinuclear platinum complex containing a metal-metal bond bridged by hydride and phosphide ligands, *Acta Crystallogr. Sect. E* 74 (2018) 977–980, <https://doi.org/10.1107/S205698901800868X>.
- [89] J. Chang, F. Fang, J. Zhang, X. Chen, Hydrosilylation of aldehydes and ketones catalyzed by Bis(phosphinite) pincer platinum hydride complexes, *Adv. Synth. Catal.* 362 (2020) 2709–2715, <https://doi.org/10.1002/adsc.202000166>.
- [90] H.C. Clark, M.J.H. Smith, Chemistry of platinum hydrides: a platinum(II) *cis*-dihydride or a platinum(0) η^2 -dihydrogen complex? *J. Am. Chem. Soc.* 108 (1986) 3829–3830, <https://doi.org/10.1021/ja00273a047>.
- [91] S.P. Millar, M. Jang, R.J. Lachicotte, R. Eisenberg, Hydride complexes of platinum (II) containing unsymmetrical di(phosphine) ligands: synthesis, characterization and evidence for pairwise addition of hydrogen based on parahydrogen induced polarization, *Inorg. Chim. Acta* 270 (1998) 363–375, [https://doi.org/10.1016/S0020-1693\(97\)05870-2](https://doi.org/10.1016/S0020-1693(97)05870-2).
- [92] M. Brendel, R. Engelke, V.G. Desai, F. Rominger, P. Hofmann, Synthesis and reactivity of Platinum(II) *cis*-Dialkyl, *cis*-Alkyl Chloro, and *cis*-Alkyl Hydrido *Bis-N*-heterocyclic Carbene Chelate Complexes, *Organometallics* 34 (2015) 2870–2878, <https://doi.org/10.1021/acs.organomet.5b00204>.
- [93] J. Real, E. Prat-Gil, M. Pagès-Bareny, A. Polo, J.F. Piniella, Á. Álvarez-Larena, Platinum phosphinothiolato hydride complexes: synthesis, structure and evaluation as tin-free hydroformylation catalysts, *Dalton Trans.* 45 (2016) 3964–3973, <https://doi.org/10.1039/C5DT04107D>.
- [94] M.P. Brown, R.J. Puddephatt, M. Rashidi, K.R. Seddon, Some binuclear hydrides of platinum, *J. Chem. Soc., Dalton Trans.* (1978) 516–522, <https://doi.org/10.1039/DT9780000516>.
- [95] N. Hidalgo, F. de la Cruz-Martínez, M.T. Martín, M.C. Nicasio, J. Campos, A highly constrained *cis*-dihydride platinum complex trapped by cooperative gold/platinum dihydrogen activation, *Chem. Commun.* 58 (2022) 9144–9147, <https://doi.org/10.1039/D2CC03089F>.
- [96] A.L. Bandini, G. Banditelli, G. Minghetti, Binuclear hydrido platinum(II) complexes: syntheses of $[\{Pt(P-P)\}_2(\mu-CHCH_2R)(\mu-H)] [BF_4]$ ($R=C_6H_5$, H) and easy cleavage of a P-C bond in a chelating 1,4-*bis*(diphenyl)phosphinobutane (P-P), *J. Organomet. Chem.* 595 (2000) 224–231, [https://doi.org/10.1016/S0022-328X\(99\)00628-2](https://doi.org/10.1016/S0022-328X(99)00628-2).
- [97] G. Berthon-Gelloz, B. deBruin, B. Tinant, I.E. Markó, Structure and reactivity of a unique Y-Shaped Tricoordinate *Bis*(silyl)platinum(II)-NHC complex, *Angew. Chem. Int. Ed.* 48 (2009) 3161–3164, <https://doi.org/10.1002/anie.200900435>.
- [98] S. Dierick, E. Vercreyus, G. Berthon-Gelloz, I.E. Markó, User-friendly platinum catalysts for the highly stereoselective hydrosilylation of alkynes and alkenes, *Chem. Eur. J.* 21 (2015) 17073–17078, <https://doi.org/10.1002/chem.201502643>.
- [99] M.J. Michalczyk, J.C. Calabrese, C.A. Recatto, M.J. Fink, Reaction of disilanes with a *cis*-platinum dihydride: novel platinum complexes with terminal disilanyl groups and bridging disilene ligands, *J. Am. Chem. Soc.* 114 (1992) 7955–7957, <https://doi.org/10.1021/ja00046a077>.
- [100] A.K. Roy, R.B. Taylor, The First Alkene–platinum–silyl complexes: lifting the hydrosilylation mechanism shroud with long-lived precatalytic intermediates and true Pt catalysts, *J. Am. Chem. Soc.* 124 (2002) 9510–9524, <https://doi.org/10.1021/ja0127335>.
- [101] B.P. Maliszewski, T.A.C.A. Bayrakdar, P. Lambert, L. Hamdouna, X. Trivelli, L. Cavallo, A. Poater, M. Belli, O. Lafon, K. Van Hecke, D. Ormerod, C.S.J. Cazin, F. Nihara, S.P. Nolan, Pt(II)-*N*-heterocyclic carbene complexes in solvent-free Alkene Hydrosilylation, *Chem. Eur. J.* 29 (2023) e202301259, <https://doi.org/10.1002/chem.202301259>.
- [102] V.M. Chernyshev, A.V. Astakhov, I.E. Chikunov, R.V. Tyurin, D.B. Eremin, G. S. Ranny, V.N. Khrustalev, V.P. Ananikov, Pd and Pt catalyst poisoning in the study of reaction mechanisms: what does the mercury test mean for catalysis? *ACS Catal.* 9 (2019) 2984–2995, <https://doi.org/10.1021/acscatal.8b03683>.
- [103] O.N. Gorunova, I.M. Novitskiy, Y.K. Grishin, I.P. Glorizov, V.A. Roznyatovsky, V. N. Khrustalev, K.A. Kochetkov, V.V. Dunina, When applying the mercury poisoning test to palladacycle-catalyzed reactions, one should not consider the common misconception of Mercury(0) selectivity, *Organometallics* 37 (2018) 2842–2858, <https://doi.org/10.1021/acs.organomet.8b00363>.
- [104] J.A. Widegren, R.G. Finke, A review of the problem of distinguishing true homogeneous catalysis from soluble or other metal-particle heterogeneous catalysis under reducing conditions, *J. Mol. Catal. A: Chem.* 198 (2003) 317–341, [https://doi.org/10.1016/S1381-1169\(02\)00728-8](https://doi.org/10.1016/S1381-1169(02)00728-8).
- [105] J.A. Widegren, M.A. Bennett, R.G. Finke, Is it homogeneous or heterogeneous catalysis? Identification of bulk ruthenium metal as the true catalyst in benzene hydrogenations starting with the monometallic precursor, $Ru(II)(\eta^6-C_6Me_6)(OAc)_2$, plus kinetic characterization of the heterogeneous nucleation, then autocatalytic surface-growth mechanism of metal film formation, *J. Am. Chem. Soc.* 125 (2003) 10301–10310, <https://doi.org/10.1021/ja021436c>.
- [106] G.M. Whitesides, M. Hackett, R.L. Brainard, J.P.P.M. Lavalleye, A.F. Sowinski, A. N. Izumi, S.S. Moore, D.W. Brown, E.M. Staudt, Suppression of unwanted heterogeneous platinum(0)-catalyzed reactions by poisoning with mercury(0) in systems involving competing homogeneous reactions of soluble organoplatinum compounds: thermal decomposition of *bis*(triethylphosphine)-3,3,4,4-tetramethylplatinacyclopentane, *Organometallics* 4 (1985) 1819–1830, <https://doi.org/10.1021/om00129a023>.



Cite this: DOI: 10.1039/d4cy00992d

Exploring the impact of abnormal coordination in macrocyclic *N*-heterocyclic carbene ligands on bio-inspired iron epoxidation catalysis†

Greta G. Zámbo, ^a Carla A. Esslinger, ^a Michael J. Sauer,^a Isabelle Rüter,^b Robert M. Reich, ^a Serhiy Demeshko,^b Franc Meyer ^b and Fritz E. Kühn ^{*a}

The first macrocyclic abnormal *N*-heterocyclic carbene (aNHC) Fe^{III} complex, featuring a calix[4]3-methyl-1,2,3-triazole-5-ylidene ligand system is synthesised and characterised *inter alia* via EA, SC-XRD, NMR and UV/vis spectroscopy. Including Mössbauer spectroscopy, SQUID and DFT calculations, the impact of the aNHC on the Fe^{III} complex and its corresponding Fe^{II} derivative is investigated. A comprehensive study of the aNHC Fe complexes in their performance in homogenous epoxidation reactions is reported and compared to the established benchmark catalysts. The complexes demonstrate efficient and selective catalytic activity in the epoxidation of *cis*-cyclooctene with H₂O₂, with TOFs up to almost 60 000 h⁻¹. Additionally, the epoxidation of more challenging olefinic substrates is possible. The reactivity under oxidative conditions of both complexes is investigated. NMR measurements reveal the formation of a mono-oxidised triazole ligand as degradation product. HR-ESI-MS measurements, supported by DFT calculations indicate the formation of an oxoiron species.

Received 14th August 2024,
Accepted 11th September 2024

DOI: 10.1039/d4cy00992d

rsc.li/catalysis

Introduction

Inspired by nature, organometallic iron *N*-heterocyclic carbene (NHC) systems have gained attention as attractive alternatives to established catalyst systems due to their activity in oxidation reactions.^{1–4} Following the model of cytochrome P450, various non-heme iron complexes have been designed to mimic its ability to undergo fundamental chemical transformations such as the oxidation of hydrocarbons and oxygen transport.¹ This includes the epoxidation of olefins, which represents an essential approach for the modification of organic intermediates in the production of various fine and bulk chemicals.⁵ In this context, the investigation of the activity of macrocyclic tetradentate iron complexes in the epoxidation of alkenes has evoked interest.⁶ Previously, focus was laid primarily on examining the mechanisms of corresponding porphyrin-like systems featuring exclusively N-donor ligands.

High valent iron intermediates of oxidation state IV or V are considered to be the active species in these reactions.^{1,7–12} However, most catalytic reactions are starting from iron(II) pre-catalysts, which requires a pre-oxidation to form an active iron(III) hydroperoxo species, usually involving an undesired Fenton-type radical step.^{2,13–16} The radical formation can affect catalyst activity, represented by the turnover frequency (TOF) and stability, represented by the turnover number (TON).¹⁷ Even if the results on mechanistic studies of iron NHC complexes in epoxidation catalysis are limited,² NHC ligands are expected to be superior due to their favourable electronic properties as strong σ -donors possessing high kinetic stability.^{4,18,19} The current benchmark catalyst for homogenous olefin epoxidation is an iron(II) tetracarbene complex with a ligand system consisting of four imidazole-2-ylidene units connected *via* methylene bridges and two labile acetonitrile ligands in *trans* positions to each other (Fig. 1, A).^{20,21} Complex A reaches a TOF of *ca.* 50 000 h⁻¹ with a TON of 480. The unfavourable Fenton-type reactivity in the oxidation reaction could be suppressed applying its iron(III) homologue B (Fig. 1) as catalyst by increasing the TOF to > 180 000 h⁻¹.²² Adding Lewis acids like Sc(OTf)₃ to the catalytic reaction increases activity and stability of the catalyst significantly (TOF > 400 000 h⁻¹, TON \approx 1200).²⁰ These results outperform previous established epoxidation catalysts based on rhenium (TOFs up to *ca.* 40 000 h⁻¹)⁵ or molybdenum (TOFs up to *ca.* 50 000 h⁻¹).²³ However, for application of iron NHC complexes in industrial catalysis, the stability has to be considerably enhanced without

^a School of Natural Sciences, Department of Chemistry and Catalysis Research Centre, Molecular Catalysis, Technical University of Munich, Lichtenbergstraße 4, 85748 Garching bei München, Germany. E-mail: fritz.kuehn@ch.tum.de

^b Georg-August-Universität Göttingen, Institut für Anorganische Chemie, Tammannstraße 4, 37077 Göttingen, Germany

† Electronic supplementary information (ESI) available: ¹H-NMR-spectra, crystallographic data, analytical methods, buried volume and topographic steric map calculations, thermochromism, magnetic susceptibility, HR-ESI-MS spectra, DFT calculations. CCDC 2362784. For ESI and crystallographic data in CIF or other electronic format see DOI: <https://doi.org/10.1039/d4cy00992d>



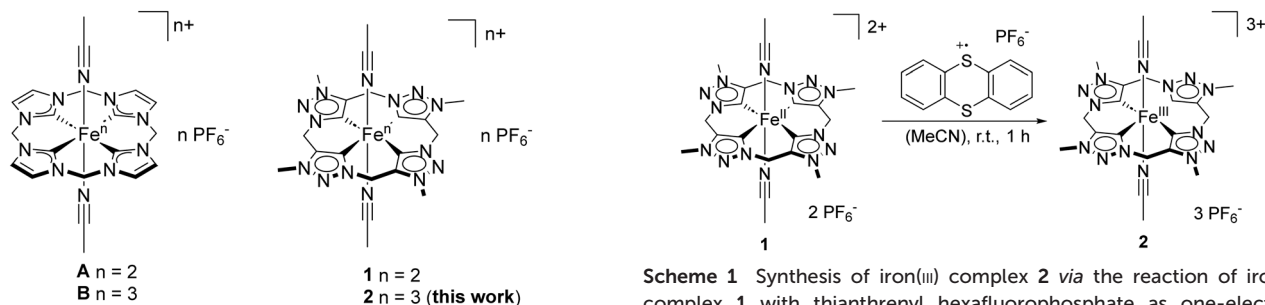


Fig. 1 Chemical structure of the precursor of the most active catalyst $\text{Fe}^{\text{II}}[\text{cCCCC}]_{\text{im}}$ **A** in the epoxidation of *cis*-cyclooctene with H_2O_2 and its $\text{Fe}^{\text{III}}[\text{cCCCC}]_{\text{im}}$ derivative **B** and the structure of the abnormal coordinating iron NHC complexes $\text{Fe}^{\text{II}}[\text{cCCCC}]_{\text{trz}}$ **1** and $\text{Fe}^{\text{III}}[\text{cCCCC}]_{\text{trz}}$ **2** (this work).

compromising the remarkable activity. The electronic properties of **A** and **B** can be adjusted by introducing substituents into the NHC backbone, impacting both their respective TON and TOF, with a lag in activity compared to **A** and **B**.²⁴

Abnormal NHCs (aNHCs) are considered to be stronger σ -donors than normal coordinating imidazole-2-ylidene units as in complexes **A** and **B**.^{25,26} Introducing aNHCs as ligands in transition metal catalysis has proven to be effective in adjusting the electronic characteristics of the central metal and enhancing its catalytic performance. Among these, 1,2,3-triazol-5-ylidenes turned out as a promising aNHC subclass due to their straightforward synthesis *via* click chemistry.^{26–29} In order to deepen the understanding of the influence of the NHC σ -donor strength on the iron catalyst performance in oxidation reactions, our group recently designed a ligand which is geometrically similar to the calix[4]imidazol in complex **A** and **B**. However, the designed ligand differs in its NHC units and mode of coordination with the metal, changing from a normal NHC to an aNHC.³⁰ To date only one macrocyclic abnormal coordinating iron NHC complex is reported in literature (Fig. 1, **1**).³⁰ Complex **1** represents a promising candidate for olefin epoxidation³⁰ due the high donor abilities of its tetra NHC ligand consisting of 1,2,3-triazole-5-ylidene moieties.^{26–29} First epoxidation reactions of *cis*-cyclooctene with H_2O_2 applying **1** as pre-catalyst reach conversions up to 97% with a TOF of $41\,000\text{ h}^{-1}$ and a TON of 200.³⁰

In this work, on the one hand, the synthesis and characterisation of the iron(III) homologue **2** (Fig. 1) of the first macrocyclic aNHC iron complex **1** is reported. The new compound **2** and if applicable, **1**, are characterised using NMR spectroscopy, high-resolution electrospray ionisation mass spectroscopy (HR-ESI-MS), single crystal X-ray diffraction (SC-XRD), UV/VIS spectroscopy, Mössbauer spectroscopy, elemental analysis (EA) and multiple DFT calculations. On the other hand, catalytic in-depth studies using complex **1** and **2** in the epoxidation of olefins and the comparison to the so far most active catalyst allow to gain valuable information for effective ligand design. Additional DFT calculations regarding the modification of the triazole ligand backbone provide further

Scheme 1 Synthesis of iron(III) complex **2** via the reaction of iron(II) complex **1** with thianthrenyl hexafluorophosphate as one-electron oxidant.

information about the theoretical influence of the aNHC electrons on the iron centre.

Results and discussion

Synthesis and characterisation of aNHC Fe^{II} and Fe^{III} complexes **1** and **2**

Thianthrenyl hexafluorophosphate proved to be an efficient one-electron oxidant to oxidise iron(II) complexes to their iron(III) derivatives selectively and in high yields.^{22,24,31} Complex **2** is synthesised by an outer-sphere one-electron oxidation of 1.00 eq. of the previously reported aNHC iron complex **1** with 1.00 eq. thianthrenyl hexafluorophosphate (Scheme 1). **2** can be isolated in 96% yield as yellow solid.

The paramagnetism of complex **2** poses challenges for the NMR spectroscopy analysis and complicates the comparison with **1**. The ^1H -NMR spectrum shows a significant low field shift of the methylene bridge protons from 6.12 ppm for **1** to 44.33 ppm for **2**, confirming its paramagnetism (see ESI † Fig. S1). Whereas the signal for the methyl substituent protons with 4.31 ppm is barely shifted (*vs.* 4.21 ppm for **1**).

Single crystals of **2** suitable for SC-XRD were obtained by the slow diffusion of diethyl ether into a solution of **2** in acetonitrile under an argon atmosphere. In general, the crystal structure of **2** differs only marginally from that of complex **1**.³⁰ Similar to its iron(II) counterpart, complex **2** displays a distorted octahedral coordination sphere around the iron centre (Fig. 2). Axial positions are occupied by two acetonitrile ligands, while the tetradentate ligand is coordinating equatorially. The bond angles around the iron centre in **1** and **2** are very close to the ideal octahedral angle with a mean deviation of 0.50° for **1** and 0.29° for **2**. Varying from the geometry of previous characterised macrocyclic tetracarbene iron complexes with imidazole moieties in a saddle-distorted conformation,³ the aNHC ligand exhibits an ideal square-planar geometry. Selected structural parameters of complexes **A**, **B**, **1** and **2** are summarised in Table 1. The $\text{Fe}-\text{C}_{\text{NHC}}$ distances of **2** with 1.950(2) and 1.943(3) Å are slightly longer than measured for **1** with 1.925(2) and 1.931(2) Å.³⁰ In contrast to the comparison of $\text{Fe}^{\text{II}}[\text{cCCCC}]_{\text{im}}$ complex **A** (ref. 21) with $\text{Fe}^{\text{II}}[\text{cCCCC}]_{\text{trz}}$ complex **1**,³⁰ **2** and **B** (ref. 22) show similar bond $\text{Fe}-\text{C}_{\text{NHC}}$ length. The geometric parameters are in conformity with DFT calculated values in gas phase and solution of both structures **1** and **2** (see ESI †



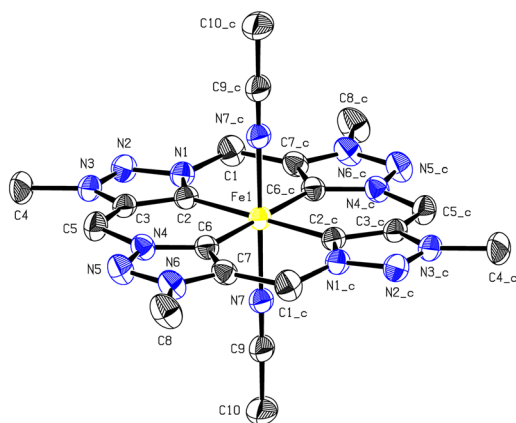


Fig. 2 ORTEP-style representation of the cationic fragment of iron(III) calix[4]3-methyl-1,2,3-triazole-5-ylidene hexafluorophosphate **2**. Hydrogen atoms and PF_6^- anions are omitted for clarity and thermal ellipsoids are shown at 30% probability level.

Table S7). Removing one molecule of acetonitrile as labile ligand does not affect the geometry of the structure to a greater extent.

The electronic influence of the ligand in **1** and **2** is investigated *via* DFT by calculation of the electronic charge. Löwdin population analysis³² was applied for that reason. Although theoretically calculated charge values are not realistic charge distribution representations, relative trends can be examined for the comparison of similar molecules.³³ Löwdin population analysis revealed a more negative value for the Fe^{II} centre **1** due to the lower oxidation state, however with only a difference of 0.32 atomic units compared to **2** (Table 2). Hence the additional positive charge of **2** is not solely located at the iron atom but compensated by the ligand system. This is also corroborated by the electrostatic potential (ESP) mapped total density plots (see ESI,† Fig. S26). As expected, the iron(II) complex features overall a more negative charge. The removal of one MeCN molecule increases the Löwdin charge to 0.33 and 0.39 less negative values for iron(II) and iron(III), respectively. This shows that not only the equatorial ligand scaffold influences the electronic characteristics, but also the axial labile ligands. Their substitution was reported to influence the catalytic activity of olefin epoxidation not only statistically by vacating and blocking a catalytic site but also from an electron density point of view.³⁴

To gain further information about the electronic properties of **1** and **2**, solid material of the complexes was studied using ^{57}Fe Mössbauer spectroscopy at 80 K. The respective spectra show a quadrupole doublet with a small isomer shift and a large quadrupole splitting (Fig. 3). The integer iron(II) spin system feature a sharp line in its quadrupole doublet. In contrast, a broadened asymmetric doublet was observed for iron(III) complex **2**, which is in accordance with Mössbauer spectra of half-spin systems and can be ascribed to slow relaxation processes.³⁵ The isomer shifts of both compounds with $\delta = 0.13 \text{ mm s}^{-1}$ for **1** and $\delta = -0.01 \text{ mm s}^{-1}$ for **2** are in the range of octahedral iron(II) ($\delta = -0.18\text{--}0.50 \text{ mm s}^{-1}$, $S = 0$) respectively iron(III) low spin species ($\delta = -0.18\text{--}0.25 \text{ mm s}^{-1}$, $S = 1/2$).^{3,36–38} Nevertheless, the isomer shift of **1** is slightly more positive than for **A** (ref. 39) (Table 3).

The Fe–ligand bond lengths can have a considerable influence on the isomer shift through compression of the s-orbitals resulting in a higher electron density.³⁷ In both cases, oxidising the iron(II) complex to iron(III) moves the isomer shift to lower values, although the length of the Fe–carbene bond increases. This can be ascribed to the decreased number of d-electrons, so that less shielding of the core electron density is observed for the iron(III) species. The quadrupole splitting with $|\Delta E_Q| = 3.34 \text{ mm s}^{-1}$ for **1** and $|\Delta E_Q| = 2.12 \text{ mm s}^{-1}$ for **2** are rather large for low-spin complexes, but in line with iron tetra NHC complexes^{3,36,37} with a heteroleptic ligand coordination sphere (different equatorial donor atoms and axial ligands) and an axial elongated octahedral ligand field.⁴⁰

The magnetic susceptibility of complexes **1** and **2** were analysed using a SQUID magnetometer (see ESI,† Fig. S14 and S15), confirming the diamagnetic ($S = 0$) ground state of **1** and the absence of any SCO in the temperature range from 2–400 K. This is in line with a strong ligand field induced by the aNHC ligand and with observations for all related six-coordinate tetra(NHC) ligated complexes including **A**.³ The SQUID measurement for **2** validate its $S = 1/2$ low-spin state with the absence of any SCO in the measured temperature area.

In view of occupancy, the molecular frontier orbitals of DFT calculated structures **1** and **2** were analysed (see ESI,† Fig. S27 and S28). The vacating of one catalytic site by MeCN dissociation does not notably affect the occupied orbitals of **1** (HOMO – 1 and HOMO, see ESI,† S29). Regarding the six-coordinate complex **1**, the LUMO does not exhibit iron(II) participation, while the LUMO + 1 is of e_g symmetry. This order of the unoccupied orbitals is reversed for the five-

Table 1 Comparison of selected structural parameters of **A**,²¹ **B**,²² **1**,³⁰ and **2**

	Bond lengths [Å]		Bond angles [°]		
	Fe–C _{NHC} ^a	Fe–NCMe ^b	MeCN–Fe–NCMe	C _{NHC} –Fe–C _{NHC} ^c	C _{NHC} –Fe–NCMe ^d
A	1.907(3)	1.932(2)	177.09(10)	178.93(67)	90.00(66)
B	1.941(2)	1.922(8)	179.04(9)	179.09(8)	90.00(23)
1	1.928(2)	1.9247(17)	180.00	180.00	90.00(8)
2	1.947(3)	1.926(2)	180.00	180.00	90.00(10)

^a Average distance between iron centre and carbene carbon atom. ^b Average distance between iron centre and axial ligands. ^c Average angle between carbene and the carbene in *trans* position. ^d Average angle between carbene, iron centre and axial ligand.



Table 2 Calculated charges at the iron center of **1** and **2** and the MeCN dissociated species using the Löwdin charge model

Complex	1	2	1-MeCN	2-MeCN
Löwdin	-1.793	-1.475	-1.399	-1.142

Values are given in atomic units and were rounded to the third decimal digit.

coordinate iron(II) species. A strong electronic influence also from the axial ligands is inferred.

The generation of an electrophilic oxygen species for catalytic epoxidation is expected to proceed *via* overlap of the HOMO of the incoming oxo species with the five-coordinate iron complex LUMO. The comparison of 1-MeCN and 2-MeCN show a fairly similar LUMO, asymmetrically distorted along the z-axis and with slightly more carbene participation in case of the iron(III) centre, attributed to the stabilisation of the additional positive charge. A direct comparison of the α -HOMOs of **2** with **B** show similar symmetry, taking into account the inherent asymmetry of the triazole rings in comparison to imidazole rings.

Reactivity of aNHC Fe^{II} and Fe^{III} complexes **1** and **2** with H₂O₂

UV/Vis spectroscopy of complex **1** (ref. 30) and **2** was performed in dry and degassed acetonitrile at 20 °C under an

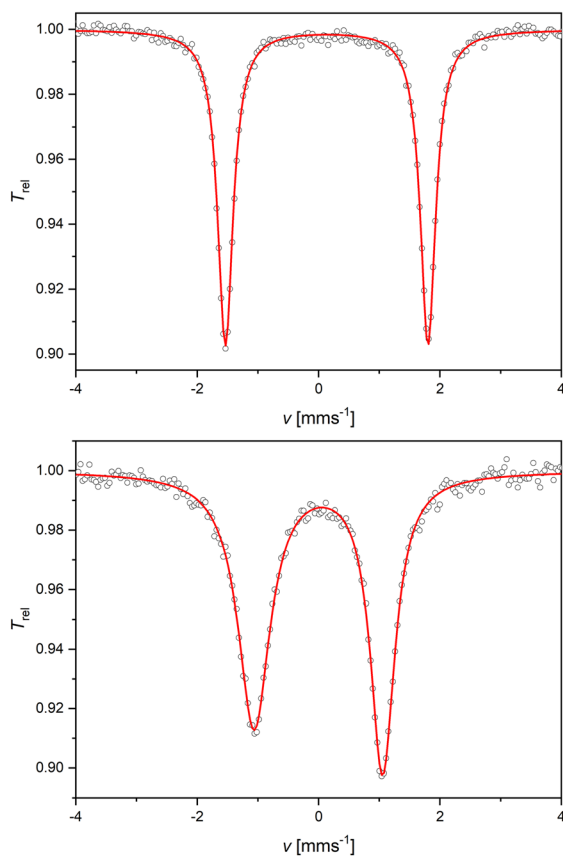


Fig. 3 Zero-field ⁵⁷Fe Mössbauer spectrum of solid **1** and **2** at 80 K. The red line represents a simulation with $\delta = 0.13 \text{ mm s}^{-1}$ and $\Delta E_Q = 3.34 \text{ mm s}^{-1}$ (**1**, top) and $\delta = -0.01 \text{ mm s}^{-1}$ and $\Delta E_Q = 2.12 \text{ mm s}^{-1}$ (**2**, bottom).

Table 3 Selected spectroscopic parameters of **A**,^{21,39} **B**,^{22,39} **1**,³⁰ and **2**

	$\delta_{\text{C}_{\text{NHC}}}$ ^a	$E_{1/2}$ [V] vs. F_c/F_c^{+b}	δ [mm s ⁻¹] ^c	$ \Delta E_Q $ [mm s ⁻¹] ^d
A	205.05	0.15	0.08	3.45
B	—	—	0.01	3.73
1	190.35	-0.34	0.13	3.34
2	—	—	-0.01	2.12

^a ¹³C-NMR carbene signal. ^b Half-cell potential in MeCN. ^c Isomer shift. ^d Quadrupole splitting.

argon atmosphere to maintain anhydrous and oxygen-free conditions. Handling the measurements under these inert conditions is necessary due to the sensitivity of both the catalyst precursor and the active catalyst to atmospheric moisture and oxygen. Two absorption bands and an absorption shoulder around 337 nm are visible for complex **2** (Fig. 4). The major band seems to be consisting of two bands in close proximity, appearing at a wavelength of 441 nm. The second band is observed at 302 nm. In order to gain information about the formation of the high valent active catalytic species in the oxidative catalysis with Fe^{III}[cCCCC]_{trz}, 1.50 eq. of the oxidising agent H₂O₂ was added to the solution of **2**. The UV/vis spectrum shows the disappearance of the two absorption bands by generating a shoulder around 378 nm and a second one around 450 nm.

Decomposition studies of the iron epoxidation catalyst **A**, respectively **B** identify the Fe-NHC bond as weak spot. Direct oxidation of one of the carbenes results in metal de-coordination, which induces protonation of the remaining NHC moieties.⁴¹ The addition of 10.0 eq. H₂O₂ (50% aq.) to a solution of iron(III) complex **2** in dry and degassed acetonitrile under argon is investigated further with ¹H-NMR spectroscopy. After 21 h, selective formation of another species, is detectable. In addition to the paramagnetic complex broad singlet at 4.34 ppm, three singlets occur at 8.85, 8.69 and 8.42 ppm, each with an integral of 1, which are assigned to protons in carbene positions of the diamagnetic ligand (see ESI,† Fig. S2). Additionally, four

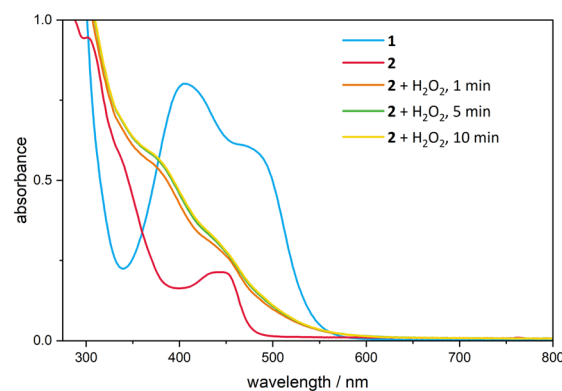


Fig. 4 UV/Vis spectrum of **1** (blue) and **2** (red); $c = 0.20 \text{ mM}$, $T = 20 \text{ °C}$ in MeCN with the addition of 1.50 eq. H₂O₂ to **2** with a reaction time of 1 min (orange), 5 min (green) and 10 min (yellow) in the absence of substrate.



singlets occur at 6.12, 6.09, 5.75 and 5.49 ppm, each with an integral of 2, which are attributed to the protons of the ligand bridges. The singlet of the methyl substituents splits into four singlets at 4.31, 4.28, 4.25 and 3.92 ppm caused by asymmetric effects of the resulting species. This is in accordance with the disappearance of the two absorption bands in the UV/Vis experiment, indicating a direct oxidation of the complex ligand by H₂O₂, resulting in the formation of a mono-oxidised and three-fold protonated ligand, which is consistent with the observations regarding the degradation of **B** under oxidative conditions.⁴¹

Decomposition studies of catalyst **1** *via* HR-ESI-MS reveal the formation of a mono-deprotonated Fe^{III} complex ($m/z = 217.56$) and an oxidised iron compound ($m/z = 225.56$) after adding 10 eq. H₂O₂ to a solution of complex **1** in dry, degassed acetonitrile (see ESI,† Fig. S16). Even under ambient conditions without adding an oxidant, an oxidised iron compound ($m/z = 226.06$) was detected, in addition to the main signal for unreacted complex **1** ($m/z = 218.06$; see ESI,† Fig. S17). According to mechanistic studies regarding iron epoxidation catalysts with *trans* labile coordinating sites by Que *et al.*,⁴² the reaction between the Fe complex and H₂O₂ initiates with the formation of a Fe^{III}-OOH intermediate by a simple ligand exchange process after a crucial single electron transfer (Fenton reaction). Mechanistic studies indicate that this can lead to either a high-valent iron(v) oxo compound or an iron(iv) oxo species with an oxyl radical, depending on whether the cleavage pathway is homolytic or heterolytic. The heterolytic pathway is less favourable, as electron-deficient oxidants such as H₂O₂ cannot stabilise the resulting radical so that it cannot attack the oxygen source and the catalyst.^{11,42} The corresponding oxoiron species with the aNHC scaffold (aNHC-Fe^{IV}=O and aNHC-Fe^V=O) are validated *via* DFT calculations (see ESI†). The HOMOs of both proposed species include the Fe=O bond of π^* symmetry, making them capable of π -donation into the alkene π^* -LUMO in order to break the double bond for the epoxide formation. In contrast, the LUMO of the oxoiron(iv) compound is entirely ligand centered while the iron(v) species exhibits a metal centered LUMO, rotated by 90° in comparison to the HOMO (see ESI,† S31 and S32).

Catalytic olefin epoxidation reactions

Complexes **1** and **2** were investigated with regard to their suitability as catalysts for the epoxidation of olefins, with a comparison to the most active non-heme iron complexes **A**, respectively **B** reported in literature.²⁰ Established standard conditions for oxidation reactions with iron NHC catalysts comprise 20 °C, the use of H₂O₂ (101 $\mu\text{mol mL}^{-1}$, 1.50 eq.) as oxidising agent, MeCN as solvent and *cis*-cyclooctene (67.3 $\mu\text{mol mL}^{-1}$, 1.00 eq.), widely applied as model substrate.² Hydrogen peroxide was chosen as the oxidising agent due to its superiority over other common peroxides such as *tert*-butyl hydroperoxide (TBHP) or the urea-hydrogen peroxide adduct in iron-NHC epoxidation catalysis.^{22,43}

Previous optimising studies revealed that the best results were achieved with an excess of 1.50 eq. of H₂O₂.^{22,43} Product quantification was performed using GC-FID for the model substrate (*cis*-cyclooctene) and ¹H NMR spectroscopy for the screening of various other olefinic substrates.

Initial evaluation employing the abnormally coordinated Fe^{II} macrocycle **1** demonstrate the remarkable difference in activity and stability of this complex class in comparison to the iron catalyst **A** with normal NHC coordination.^{22,30} At 20 °C different catalyst concentrations of Fe^{II} pre-catalyst **1** are screened (Fig. 5a). A nearly linear relationship between catalyst loading and conversion is expected if no degradation products^{22,41,44} prevent catalytic activity. Nevertheless, this trend remains imperceptible in this case (Table 4, entry 1–4). At 0.1 mol% a maximal conversion of 6% (TON = 60) and at 0.5 mol% of 37% (TON = 74) has been detected. However, if the catalyst loading is doubled to 1 mol%, the maximal conversion only increases to 49% (TON = 49). At a concentration of 2 mol% of **1** a conversion of 84% (TON = 42) is reached after 5 min. These results indicate a fast degeneration, possibly promoted by higher catalyst concentrations. A common method to increase the catalyst lifetime is to reduce the reaction temperature.^{22,30,45} Hence, at a catalyst loading of 1 mol% of **1** the conversion and catalyst stability increases from 84% (TON = 80) for 10 °C over 92% (TON = 92) for 0 °C to full conversion (TON = 100) for –10 °C after 10 min with raising the stability respectively (Fig. 5b and Table 4, entry 2, 5–7). Remarkably, unlike the constantly increasing TON, the TOF does not necessarily decrease with lower temperature and can be pushed up to 32 100 h^{–1} at 0 °C (Table 4, entry 9). As stability is one of the biggest challenges of iron catalysts,^{22,34,43,46} including complexes with Fe–carbene bonds^{4,47,48} and many iron complexes decompose rather quickly after the addition of aqueous H₂O₂, influenced by the unavoidable presence of water,^{17,22,49} TBHP (101 $\mu\text{mol mL}^{-1}$, 1.50 eq.) in *n*-decane solution is used in a single reaction with **1** (Fig. 5c). However, at standard conditions and a catalyst loading of 1 mol% a significantly smaller amount of epoxide is formed after 10 min with a TON of 22 (Table 4, entry 12), which is less than half as much when TBHP is substituted with aqueous H₂O₂. All reactions are carried out at atmospheric conditions by starting the reaction with the addition of the catalyst from a preformed stock solution in dry and degassed acetonitrile, which was handled under argon. All experiments achieve a selectivity of >99% towards the product epoxide.

Regarding mechanistic studies towards non-heme iron epoxidation catalysts with *trans* labile coordinating sites (*vide supra*) the impact of atmospheric conditions on the catalysis can significantly affect the reaction outcome. The presence of oxygen under aerobic conditions enhances the formation of epoxide products *via* radical pathways, by suppressing diol product formation, as oxygen traps the radical intermediates. Under argon, the reaction is slower and yields less epoxides, demonstrating the catalysts sensitivity to oxygen.^{11,42} To investigate the influence of atmospheric conditions on **1** a



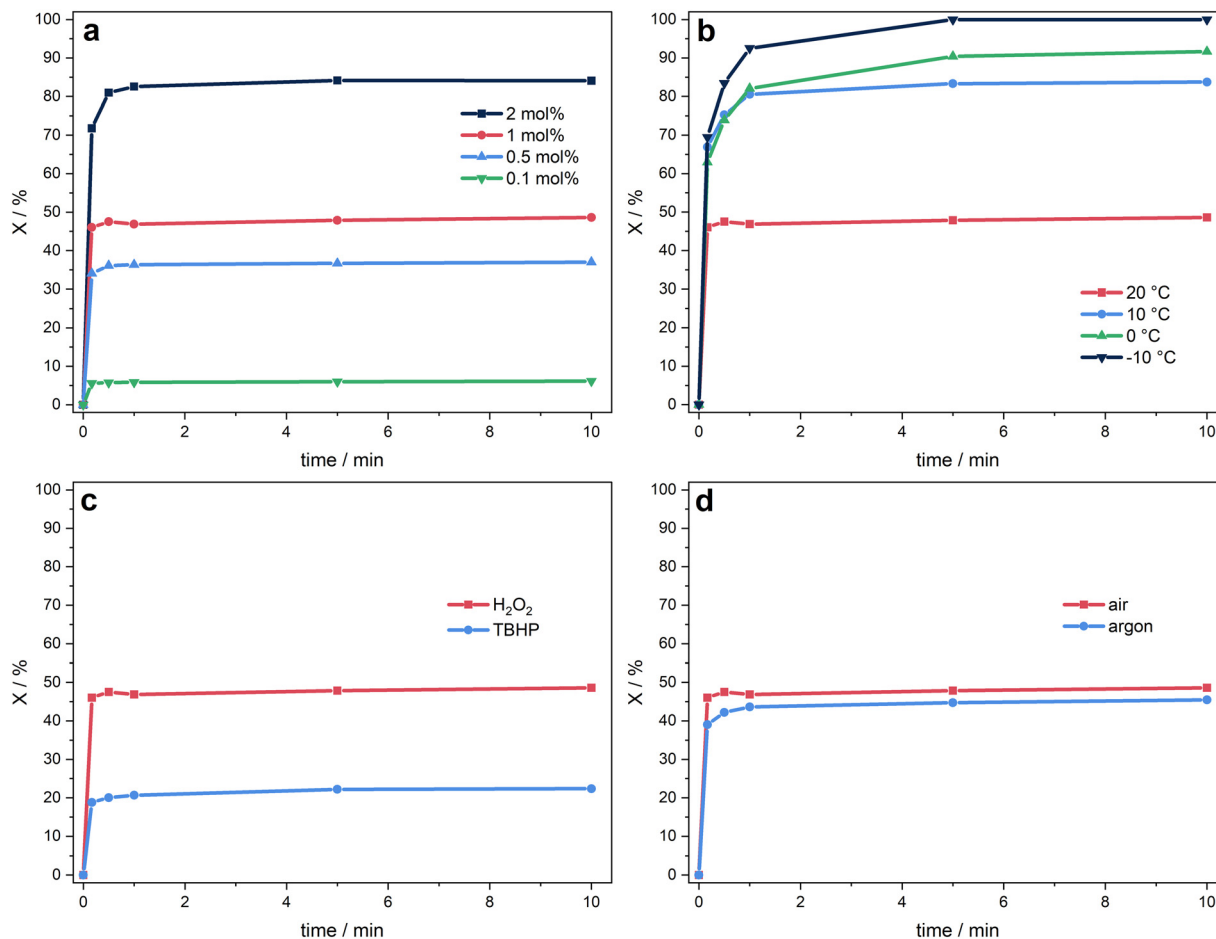


Fig. 5 Time-dependent epoxidation of *cis*-cyclooctene (67.3 $\mu\text{mol mL}^{-1}$, 1.00 eq.) in MeCN using **1** as catalyst and H_2O_2 or TBHP (101 $\mu\text{mol mL}^{-1}$, 1.50 eq.) as oxidant, (a) at different catalyst loadings (20 $^\circ\text{C}$, H_2O_2 , air), (b) at various reaction temperatures (1 mol% of **1**, H_2O_2 , air), (c) with different oxidising agents (1 mol% of **1**, 20 $^\circ\text{C}$, air) and (d) at different ambient conditions (1 mol% of **1**, 20 $^\circ\text{C}$, H_2O_2). Conversions are determined by GC-FID.

catalytic reaction was handled completely under an argon atmosphere with a catalyst loading of 1 mol% (Fig. 5d). The TON with 46 vs. 49 and the maximal conversion is comparable to the reaction under atmospheric conditions with a high selectivity ($S > 99\%$) for both reactions (Table 4, entry 2 and 12). The comparable performance under both conditions suggests a mechanism less dependent on radical intermediates and a higher iron stabilisation due to the macrocyclic aNHC ligand system.

The formation of an iron(III) hydroperoxo intermediate with oxidising agents such as hydrogen peroxide after the one-electron oxidation of the iron(II) catalyst precursor appears to be essential for the formation of the active species.^{2,11,42,50} Applying the abnormally coordinated Fe^{III} macrocycle **2** (0.34 $\mu\text{mol mL}^{-1}$, 0.005 eq.) as catalyst precursor in the epoxidation of *cis*-cyclooctene with H_2O_2 under standard conditions achieves a significant higher conversion within 10 min compared to **1** (Fig. 6a). The maximal conversion of 71% is reached after 5 min. An initial TOF of 44 000 h^{-1} and TON of 142 is achieved (Table 4, entry 16).

Previous catalytic studies have employed strong Lewis acids such as $\text{Sc}(\text{OTf})_3$ in the oxidation process, utilising the normally

coordinated Fe^{II} and Fe^{III} NHC macrocycle **A** and **B** as catalysts, which provides notably enhanced performance.²⁰ Although an epoxidation mechanism involving iron carbenes as catalyst precursors remains uncertain, it can be inferred, that Sc^{3+} triggers the *in situ* oxidation of the Fe^{II} complex to the active Fe^{III} catalyst, based on observations of related complexes.²⁰ Furthermore, it might be assumed that heterolytic cleavage of the O–O bond in a $\text{Fe}^{\text{III}}\text{-OOH}$ species, initially formed upon reaction of the Fe^{III} catalyst with H_2O_2 , is facilitated by $\text{Sc}(\text{OTf})_3$, resulting in the generation of an active oxoiron(IV) or (V) species.^{6–10} Additionally, the application of Lewis acids in the catalytic reaction demonstrated to reactivate μ_2 -oxodiiron(III) $\text{Fe}^{\text{III}}\text{-O-Fe}^{\text{III}}$ species, which has been identified as a crucial deactivation product.^{20,41,44} The addition of 0.10 eq. $\text{Sc}(\text{OTf})_3$ to the reaction with 0.05 mol% of Fe^{II} complex **1** under standard conditions results in an extended lifetime of the catalyst (TON = 194 vs. 74). The reaction is completed after 30 min with an enhanced conversion of 97% (vs. 37%) with a TOF of 40 900 h^{-1} (Table 4, entry 14).³⁰ However, applying Fe^{III} complex **2** as catalyst under the same conditions the reaction is completed after 10 min with a maximum conversion of 99% (vs. 70% without additive) and a TON of 197 (vs. 142), which is



Table 4 Epoxidation of *cis*-cyclooctene by **1** and **2** at different catalyst concentrations, temperatures, atmospheres, oxidising agents and with or without additive

Entry	Catalyst	<i>T</i> [°C]	Loading [mol%]	Additive	<i>X</i> [%]	<i>S</i> [%]	TOF [h ⁻¹]	TON	Oxidant	Atmosphere
1	1	20	2	—	84	>99	13 000	42	H ₂ O ₂	Air
2	1	20	1	—	49	>99	16 600	49	H ₂ O ₂	Air
3 (ref. 30)	1	20	0.5	—	37	>99	24 500	74	H ₂ O ₂	Air
4	1	20	0.1	—	6	>99	20 100	60	H ₂ O ₂	Air
5	1	10	1	—	84	>99	26 500	80	H ₂ O ₂	Air
6	1	0	1	—	92	>99	22 700	92	H ₂ O ₂	Air
7	1	-10	1	—	100	>99	25 000	100	H ₂ O ₂	Air
8 (ref. 30)	1	10	0.5	—	49	>99	29 900	99	H ₂ O ₂	Air
9 (ref. 30)	1	0	0.5	—	72	>99	32 100	145	H ₂ O ₂	Air
10 (ref. 30)	1	-10	0.5	—	89	>99	30 200	177	H ₂ O ₂	Air
11	1	-10	0.1	—	20	>99	40 800	202	H ₂ O ₂	Air
12	1	20	1	—	22	>99	6800	22	TBHP	Air
13	1	20	1	—	46	>99	14 000	46	H ₂ O ₂	Argon
14 (ref. 30)	1	20	0.5	Sc(OTf) ₃	97	96	40 900	194	H ₂ O ₂	Air
15	1	20	0.1	Sc(OTf) ₃	25	97	59 200	248	H ₂ O ₂	Air
16	2	20	0.5	—	70	>99	44 000	142	H ₂ O ₂	Air
17	2	20	0.5	Sc(OTf) ₃	99	97	51 800	197	H ₂ O ₂	Air

Reaction conditions: acetonitrile as solvent, *cis*-cyclooctene (67.3 μmol mL⁻¹, 1.00 eq.), H₂O₂ or TBHP (101 μmol mL⁻¹, 1.50 eq.), if stated Sc(OTf)₃ (6.73 μmol mL⁻¹, 0.10 eq.). Selectivity is related to the epoxide. Conversions are determined by GC-FID. TOFs are determined after 10 s. TONs are determined when maximal conversion is reached. *T* = temperature. *X* = conversion. *S* = selectivity, selectivity = yield(epoxide)/conversion(substrate).

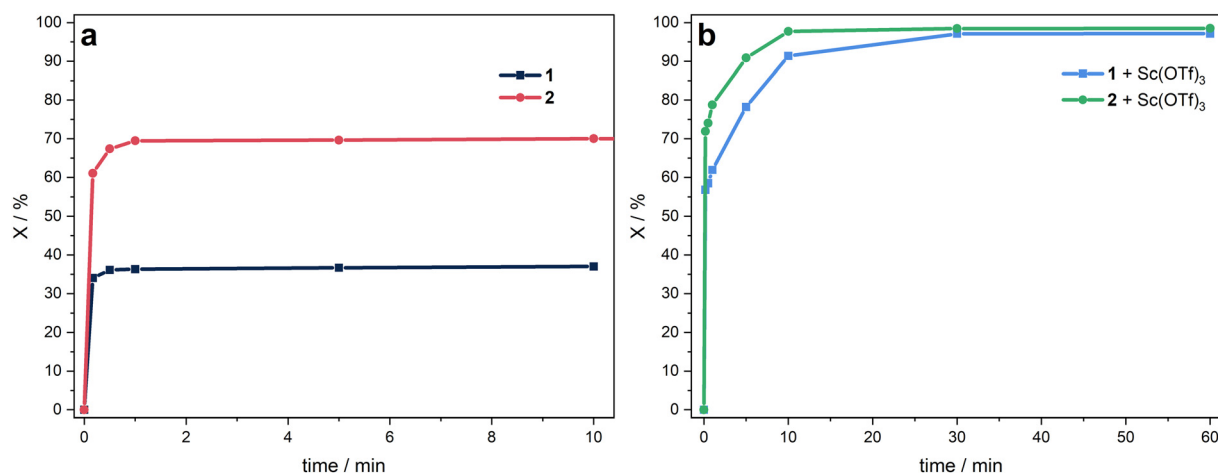


Fig. 6 Time-dependent epoxidation of *cis*-cyclooctene (67.3 μmol mL⁻¹, 1.00 eq.) in MeCN at 20 °C using **1** or **2** (0.34 μmol mL⁻¹, 0.005 eq.) as catalyst and H₂O₂ (101 μmol mL⁻¹, 1.50 eq.) as oxidant, (a) without additive and (b) with the addition of Sc(OTf)₃ (6.73 μmol mL⁻¹, 0.10 eq.). Conversions are determined by GC-FID.

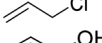
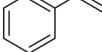
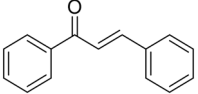
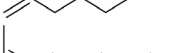
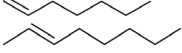
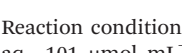
comparable to the results with **1** (Fig. 6b). In contrast to the respective experiments with **A** and **B** (ref. 20), the TOF is pushed to 51 800 h⁻¹ with an increased conversion in the first minutes of the reaction (Table 4, entry 17), which indicates a slower *in situ* single oxidation of **1** to **2** versus the instantaneous *in situ* single oxidation of **A** to **B**. The observed enhancement in activity and stability upon the introduction of Lewis acids to the reaction involving compounds **1** and **2** suggests the potential regeneration of degraded species, analogous to the mechanism observed in systems **A** and **B**.^{20,44} Otherwise, the time-dependent conversion of *cis*-cyclooctene is anticipated to be nearly identical for complex **2** with and without the additive. Unfortunately, the addition of Sc(OTf)₃ to the catalytic reaction

with **1** or **2** decreases the product selectivity slightly to 96 and 97%, respectively. No byproduct formation other than 1,2-cyclooctanediol was observed.

Epoxides not only serve as final products in industrial applications but also function as crucial building blocks in synthetic organic chemistry.^{51–54} In this context, a screening of a variety of olefin substrates is conducted using complex **1** for epoxidation catalysis, as the resulting epoxides are of great value as intermediates in various industrial processes. Additionally, the catalyst tolerance of different functional groups is assessed. The resulting epoxides find wide application as monomers in polymerisation processes,⁵⁵ stabilisers for halogenated hydrocarbons or oil-soluble bases



Table 5 Epoxidation of various substrates using complex 1 as catalyst

	$X_{10\text{ s}}$ [%] (S)	$X_{1\text{ h}}$ [%] (S)	TOF [h^{-1}]	TON	$X_{5\text{ min}}$ [%] (S) ^b
	57 (>99) ^a	97 (96)	40 900	194	37 (>99)
	33 (>99)	39 (38)	23 800	78	25 (>99)
	0 (-)	6 (>99)	—	13	0 (-)
	21 (0)	34 (11)	15 100	67	9 (8)
	19 (24)	27 (0)	13 300	54	24 (89)
	4 (92)	13 (5)	3000	26	2 (83)
	6 (>99)	29 (49)	4100	58	9 (>99)
	40 (64)	51 (45)	28 600	91	27 (96)
	6 (>99)	57 (74)	4500	114	11 (>99)

Reaction conditions: acetonitrile as solvent, substrate, (67.3 $\mu\text{mol mL}^{-1}$, 1.00 eq.), Fe^{II} complex 1 (1.35 $\mu\text{mol mL}^{-1}$, 0.005 eq.), and H₂O₂ (50% aq., 101 $\mu\text{mol mL}^{-1}$, 1.50 eq.), using Sc(OTf)₃ (6.73 $\mu\text{mol mL}^{-1}$, 0.10 eq.) as additive, 20 °C. X = conversion; S = selectivity, related to the epoxide. TOFs are determined after 10 s. TONs are determined after 1 h. Conversions are determined by ¹H-NMR spectroscopy, applying benzene as external standard. ^a Conversions are determined by GC-FID. ^b Without the addition of Sc(OTf).

in cosmetic formulations,^{51–54} as well as constituents in epoxy resins and as reactive diluents for such resins.^{52,56}

All experiments concerning the epoxidation of various olefin substrates are performed using 0.5 mol% of Fe^{II} catalyst 1 and 0.10 eq. Sc(OTf)₃ at standard conditions and are analysed *via* ¹H-NMR spectroscopy. Samples were taken after 10 s and 1 h (Table 5). Catalyst 1 demonstrates the ability to transform all employed substrates. Highest conversion is obtained for the benchmark substrate *cis*-cyclooctene. The smaller ring *cis*-cyclohexene is converted to 33% after 10 s ($S > 99\%$), with a TOF of 23 800 h⁻¹ and to 39% after 1 h with a significant decrease in selectivity (38%). The electron density of the double bond plays a decisive role in the reactivity of the respective substrate.³⁴ After 1 h, lowest conversion of 6% is achieved for allyl chloride, but with a high selectivity of >99%. Replacing the chloride substituent, which possesses an -I effect towards the double bond, by an electron donating hydroxyl group, a conversion of 34% is obtained, with a TOF of 15 100 h⁻¹. However, the increased electrophilic character of the double bond likely leads to a reduced selectivity of 11%. Styrene, as aromatic system is transformed to 27% after 1 h with no selectivity towards the epoxide due to overoxidation. Catalyst 1 shows rather low reactivity to the more challenging olefinic systems *trans*-chalcone, which bears additionally an electron-withdrawing carbonyl group in proximity to the double bond, provoking a reduced electron density. Acyclic 1-hexene with its terminal double bond is converted to 29% after 1 h. Complex 1 exhibits relatively high activity and stability towards *cis*- and *trans*-oct-2-ene (conv. = 57 and 51%, 1 h) attributed to the enhanced reactivity of the internal double bond influenced by neighbouring alkyl groups. Notably the TOFs differ significantly with 28 600 h⁻¹ for *cis*-oct-2-ene and 4500 h⁻¹ for *trans*-oct-2-ene.

This preference for *cis* conversion over *trans* is also a commonly observed for other iron epoxidation catalysts.^{22,49,56} In order to determine whether the respective substrates are also converted without additives, the experiments were carried out under same conditions without the addition of Sc(OTf)₃ with a reaction time of 5 min (Table 5, right column). With the exception of allyl chloride and allyl alcohol, all substrates were successfully transformed with high selectivity. In general, an increased nucleophilic nature of the alkene, induced by inductive effects, correlates with enhanced reactivity towards the epoxide, consistent with an electrophilic active species.^{22,57} A highly substituted alkene has a higher reactivity than its terminal counterpart due to the +I effect of the substituents. In addition, the -M effect of the carbonyl in chalcone reduces the reactivity of the alkene.⁵⁶

Conclusions

In summary, the first macrocyclic aNHC iron(III) complex 2 was successfully synthesised. ¹H-NMR spectroscopy confirms the paramagnetism of 2. Characterisation *via* SC-XRD analysis reveals an octahedral geometry with the tetradentate ligand arranged in an ideal square-planar coordination, as in its iron(II) counterpart 1. Mössbauer measurements as well as SQUID data allow to identify both complexes as low spin species (1: $S = 0$ and 2: $S = \frac{1}{2}$). Epoxidation reactions applying aNHC iron(II) and (III) complexes 1 and 2 and screening of optimal conditions show efficient substrate conversion. However, the performance of the so far most active macrocyclic iron catalyst with classical NHC coordination could not be exceeded or even reached. These findings suggest that a more electron rich iron centre is not necessarily associated with higher activity, due to reduced



catalyst stability and *vice versa*. Decomposition studies *via* $^1\text{H-NMR}$ spectroscopy identify the Fe-aNHC bond as weak spot by detecting the mono-oxidised and three-fold protonated ligand after the addition of H_2O_2 . HR-ESI-MS measurements supported by DFT studies imply the possible formation of an oxoiron(IV) or (V) species under oxidative conditions. While these results provide insights into the correlation between ligand design and activity in oxidation catalysis of iron NHC complexes, the exact nature of the active species remains unclear, and further investigation is necessary. Importantly, this study contributes to the limited analytical and experimental data available on iron aNHC complexes, offering valuable information for future research in this area.

Experimental

General considerations

Unless otherwise stated, all manipulations were performed under argon atmosphere using standard Schlenk and glovebox techniques. Dry and degassed solvents were obtained from an MBraun solvent purification system, degassed *via* freeze-pump-thaw (3 cycles) and stored over molecular sieve (3 or 4 Å) prior to use. $\text{Fe}(\text{btsa})_2(\text{THF})$,^{56,58} thianthrenyl hexafluorophosphate⁵⁹ and the iron(II) calix[4]3-methyl-1,2,3-triazole-5-ylidene hexafluorophosphate complex³⁰ **1** were synthesised according to literature procedures. All other reagents were purchased from commercial suppliers and used without further purification. NMR spectra were recorded on a Bruker Advanced Ultrashield AV400 (400 MHz) at a temperature of 297 K. Chemical shifts (δ) are reported in ppm and referenced to the residual signal of the deuterated solvent.⁶⁰ Elemental analyses (C/H/N/S) were performed by the microanalytical laboratory at Technische Universität München. High resolution electrospray ionization mass spectrometry (HR-ESI-MS) data were acquired on a Thermo Fisher Exactive Plus Orbitrap. UV/vis spectra were recorded on an Agilent Technologies Cary 60 UV/vis spectrophotometer with a concentration of 0.20 mM complex in dry and degassed acetonitrile at 20 °C. Solid material of Fe complexes **1** and **2** was studied using ^{57}Fe Mössbauer spectroscopy at 80 K. ^{57}Fe Mössbauer spectra were measured using a ^{57}Co source in a Rh matrix using an alternating constant acceleration Wissel Mössbauer spectrometer equipped with a Janis closed-cycle helium cryostat. Transmission data were collected, and isomer shifts are reported relative to iron metal at ambient temperature. Experimental data were simulated with *mf2.SL* software.⁶¹ GC analysis was performed with an Agilent Technologies 7890B GC-FID system with a 7693A Automatic Liquid Sampler for 150 samples with G4513A Autoinjector using a HP-5 column (30 m \times 320 μm \times 0.25 μm).

Synthesis of iron(II) calix[4]3-methyl-1,2,3-triazole-5-ylidene hexafluorophosphate (**2**)

Under Schlenk-conditions 44.7 mg thianthrenyl hexafluorophosphate (124 μmol , 1.00 eq.) are dissolved in 2 mL dry and degassed acetonitrile resulting in a dark blue solution. 100 mg of $\text{Fe}(\text{II})[\text{C}(\text{CCCC})_{\text{trz}}$ complex **1** (124 μmol , 1.00 eq.) are dissolved in 3

mL dry and degassed acetonitrile resulting in an orange solution and added to the thianthrenyl hexafluorophosphate solution. The dark purple mixture is stirred at r.t. for 1 h. Subsequently, the addition of 5 mL dry and degassed diethyl ether while stirring leads to the precipitation of a yellow solid and turns the solution from dark purple *via* purple into a colourless supernatant. The yellow solid is separated from the solution *via* Whatman-filtration and washed with dry and degassed diethyl ether (3 \times 2 mL). After drying under vacuum, 113 mg of the product (120 μmol , 96%) are obtained as yellow solid. $^1\text{H-NMR}$ (400 MHz, $\text{CD}_3\text{-CN}$): δ [ppm] = 44.49 (s, 8 H, CH_2), 4.38 (s, 12 H, CH_3). Analytical calculation (%) for $\text{C}_{20}\text{H}_{26}\text{F}_{18}\text{FeN}_{14}\text{P}_3$: C 25.20; H 2.75; N 20.57. Found: C 24.91 H 2.63; N 19.52.

Catalytic procedures

All catalytic reactions were conducted in a cryostat (JulaboFP-50) under atmospheric conditions, unless otherwise stated. Acetonitrile (HPLC-grade) as solvent was applied for all experiments, which are screened *via* GC (substrate: *cis*-cyclooctene). The screening of other substrates was performed using $^1\text{H-NMR}$ spectroscopy and deuteride acetonitrile as solvent. The catalyst was added from a preformed stock solution in dry and degassed acetonitrile, which was handled under argon corresponding to the appropriate stoichiometry to a solution of the respective substrate (67.3 $\mu\text{mol mL}^{-1}$, 1.00 eq.). Hydrogen peroxide (50% aq., 101 $\mu\text{mol mL}^{-1}$, 1.50 eq.) was used as oxidising agent and, if required, $\text{Sc}(\text{OTf})_3$ as additive 8.41 $\mu\text{mol mL}^{-1}$, (0.10 eq.). The reaction was started upon addition of the catalyst stock solution, by adding the catalyst solution all at once. The reaction was terminated by adding electrolytically precipitated activated MnO_2 in order to decompose the excess of H_2O_2 in the reaction solution. After filtration over activated neutral alumina (separation of the catalyst), GC samples were prepared for each experiment using 200 μL filtrate, diluted with 1300 μL MeCN and *p*-xylene (0.90 $\mu\text{L mL}^{-1}$) as external standard for each chosen time point. For the screening *via* $^1\text{H-NMR}$ spectroscopy, 500 μL filtrate was added to 1 μL benzene as external standard. Control experiments without catalyst were performed for all reactions. An additional blank experiment with a simple iron salt, iron(II) chloride in the presence of H_2O_2 was conducted to highlight the importance of iron complexes associated with NHCs due to minimal product and unselective side-product formation. All reactions were conducted at least twice. Analogous, the additive $\text{Sc}(\text{OTf})_3$ itself shows minimal unselective catalytic activity.²⁰

Data availability

The data supporting this article have been included as part of the ESI.†

Conflicts of interest

There are no conflicts to declare.



Acknowledgements

All authors thank Patrick Mollik for HR-ESI-MS measurements. G. G. Z., C. A. E. and M. J. S. gratefully acknowledge support from TUM Graduate School. Part of this work has been supported by the Deutsche Forschungsgemeinschaft (DFG) in the framework of the Research Unit 5215 (FOR 5215 "Bioinspired Oxidation Catalysis with Iron Complexes"; project Me1313/18-1/445916766 to F.M.).

References

- L. Que Jr and W. B. Tolman, *Nature*, 2008, **455**, 333–340.
- G. G. Zámbo, J. F. Schlagintweit, R. M. Reich and F. E. Kühn, *Catal. Sci. Technol.*, 2022, **12**, 4949–4961.
- T. P. Schlachta and F. E. Kühn, *Chem. Soc. Rev.*, 2023, **52**, 2238–2277.
- S. Díez-González and S. P. Nolan, *Coord. Chem. Rev.*, 2007, **251**, 874–883.
- S. A. Hauser, M. Cokoja and F. E. Kühn, *Catal. Sci. Technol.*, 2013, **3**, 552–561.
- A. J. Jasniewski and L. Que Jr, *Chem. Rev.*, 2018, **118**, 2554–2592.
- M. Borrell, E. Andris, R. Navrátil, J. Roithová and M. Costas, *Nat. Commun.*, 2019, **10**, 1–9.
- X. Lu, X.-X. Li, Y.-M. Lee, Y. Jang, M. S. Seo, S. Hong, K.-B. Cho, S. Fukuzumi and W. Nam, *J. Am. Chem. Soc.*, 2020, **142**, 3891–3904.
- S. Kal and L. Que Jr, *Angew. Chem., Int. Ed.*, 2019, **58**, 8484–8488.
- K. Chen, M. Costas, J. Kim, A. K. Tipton and L. Que, *J. Am. Chem. Soc.*, 2002, **124**, 3026–3035.
- S. M. Hölzl, P. J. Altmann, J. W. Kück and F. E. Kühn, *Coord. Chem. Rev.*, 2017, **352**, 517–536.
- W. N. Oloo and L. Que Jr, *Acc. Chem. Res.*, 2015, **48**, 2612–2621.
- D. Dolphin, T. G. Traylor and L. Y. Xie, *Acc. Chem. Res.*, 1997, **30**, 251–259.
- R. Mas-Ballesté and L. Que, *J. Am. Chem. Soc.*, 2007, **129**, 15964–15972.
- E. P. Talsi and K. P. Bryliakov, *Coord. Chem. Rev.*, 2012, **256**, 1418–1434.
- H. J. H. Fenton, *J. Chem. Soc., Trans.*, 1894, **65**, 899–910.
- J. W. Kück, R. M. Reich and F. E. Kühn, *Chem. Rec.*, 2016, **16**, 349–364.
- M. N. Hopkinson, C. Richter, M. Schedler and F. Glorius, *Nature*, 2014, **510**, 485–496.
- N. Demirel, J. Haber, S. I. Ivlev and E. Meggers, *Organometallics*, 2022, **41**, 3852–3860.
- F. Dyckhoff, J. F. Schlagintweit, R. M. Reich and F. E. Kühn, *Catal. Sci. Technol.*, 2020, **10**, 3532–3536.
- M. R. Anneser, S. Haslinger, A. Pöthig, M. Cokoja, J.-M. Basset and F. E. Kühn, *Inorg. Chem.*, 2015, **54**, 3797–3804.
- J. W. Kück, M. R. Anneser, B. Hofmann, A. Pöthig, M. Cokoja and F. E. Kühn, *ChemSusChem*, 2015, **8**, 4056–4063.
- A. Schmidt, N. Grover, T. K. Zimmermann, L. Graser, M. Cokoja, A. Pöthig and F. E. Kühn, *J. Catal.*, 2014, **319**, 119–126.
- M. A. Bernd, F. Dyckhoff, B. J. Hofmann, A. D. Böth, J. F. Schlagintweit, J. Oberkofler, R. M. Reich and F. E. Kühn, *J. Catal.*, 2020, **391**, 548–561.
- A. Lever, *Inorg. Chem.*, 1990, **29**, 1271–1285.
- B. Schulze and U. S. Schubert, *Chem. Soc. Rev.*, 2014, **43**, 2522–2571.
- R. Maity and B. Sarkar, *JACS Au*, 2021, **2**, 22–57.
- G. Guisado-Barrios, M. Soleilhavoup and G. Bertrand, *Acc. Chem. Res.*, 2018, **51**, 3236–3244.
- K. O. Marichev, S. A. Patil and A. Bugarin, *Tetrahedron*, 2018, **74**, 2523–2546.
- G. G. Zámbo, J. Mayr, M. J. Sauer, T. P. Schlachta, R. M. Reich and F. E. Kühn, *Dalton Trans.*, 2022, **51**, 13591–13595.
- J. M. Smith and J. R. Long, *Inorg. Chem.*, 2010, **49**, 11223–11230.
- P. O. Löwdin, *J. Chem. Phys.*, 1950, **18**, 365–375.
- K. B. Wiberg and P. R. Rablen, *J. Comput. Chem.*, 1993, **14**, 1504–1518.
- E.-M. H. J. Esslinger, J. F. Schlagintweit, G. G. Zámbo, A. M. Imhof, R. M. Reich and F. E. Kühn, *Asian J. Org. Chem.*, 2021, **10**, 2654–2662.
- M. Blume, *Phys. Rev. Lett.*, 1965, **14**, 96.
- P. Gütllich, E. Bill and A. X. Trautwein, *Mössbauer spectroscopy and transition metal chemistry: fundamentals and applications*, Springer Science & Business Media, 2010.
- E. Bill, in *Practical approaches to biological inorganic chemistry*, Elsevier, 2020, pp. 201–228.
- C. Schremmer, C. Cordes, I. Klawitter, M. Bergner, C. E. Schiewer, S. Dechert, S. Demeshko, M. John and F. Meyer, *Chem. – Eur. J.*, 2019, **25**, 3918–3929.
- J. Donat, P. Dubourdeaux, M. Clémancey, J. Rendon, C. Gervasoni, M. Barbier, J. Barilone, J. Pécaut, S. Gambarelli and P. Maldivi, *Chem. – Eur. J.*, 2022, **28**, e202201875.
- S. C. Chan, P. Gupta, X. Engelmann, Z. Z. Ang, R. Ganguly, E. Bill, K. Ray, S. Ye and J. England, *Angew. Chem., Int. Ed.*, 2018, **57**, 15717–15722.
- F. Dyckhoff, J. F. Schlagintweit, M. A. Bernd, C. H. Jakob, T. P. Schlachta, B. J. Hofmann, R. M. Reich and F. E. Kühn, *Catal. Sci. Technol.*, 2021, **11**, 795–799.
- M. R. Bukowski, P. Comba, A. Lienke, C. Limberg, C. Lopez de Laorden, R. Mas-Ballesté, M. Merz and L. Que Jr, *Angew. Chem., Int. Ed.*, 2006, **45**, 3446–3449.
- J. W. Kück, A. Raba, I. I. Markovits, M. Cokoja and F. E. Kühn, *ChemCatChem*, 2014, **6**, 1882–1886.
- M. R. Anneser, S. Haslinger, A. Pöthig, M. Cokoja, V. D'Elia, M. P. Högerl, J.-M. Basset and F. E. Kühn, *Dalton Trans.*, 2016, **45**, 6449–6455.
- J. F. Schlagintweit, F. Dyckhoff, L. Nguyen, C. H. Jakob, R. M. Reich and F. E. Kühn, *J. Catal.*, 2020, **383**, 144–152.
- W. N. Oloo, A. J. Fielding and L. Que Jr, *J. Am. Chem. Soc.*, 2013, **135**, 6438–6441.
- M. J. Ingleson and R. A. Layfield, *Chem. Commun.*, 2012, **48**, 3579–3589.



- 48 O. Schuster, L. Yang, H. G. Raubenheimer and M. Albrecht, *Chem. Rev.*, 2009, **109**, 3445–3478.
- 49 R. Mas-Ballesté, M. Costas, T. Van Den Berg and L. Que Jr, *Chem. – Eur. J.*, 2006, **12**, 7489–7500.
- 50 A. R. McDonald and L. Que Jr, *Coord. Chem. Rev.*, 2013, **257**, 414–428.
- 51 H. C. Kolb, M. Finn and K. B. Sharpless, *Angew. Chem., Int. Ed.*, 2001, **40**, 2004–2021.
- 52 S. T. Oyama, *Mechanisms in homogeneous and heterogeneous epoxidation catalysis*, Elsevier, 2011.
- 53 H. H. Szmant, *Organic building blocks of the chemical industry*, John Wiley & Sons, 1989.
- 54 C. A. de Parrodi and E. Juaristi, *Synlett*, 2006, **2006**, 2699–2715.
- 55 I. Kim, S. M. Kim, C.-S. Ha and D.-W. Park, *Macromol. Rapid Commun.*, 2004, **25**, 888–893.
- 56 T. P. Schlachta, G. G. Zámbo, M. J. Sauer, I. Rüter, C. A. Hoefer, S. Demeshko, F. Meyer and F. E. Kühn, *J. Catal.*, 2023, **426**, 234–246.
- 57 E. A. Mikhalyova, O. V. Makhlynets, T. D. Palluccio, A. S. Filatov and E. V. Rybak-Akimova, *Chem. Commun.*, 2012, **48**, 687–689.
- 58 M. M. Olmstead, P. P. Power and S. C. Shoner, *Inorg. Chem.*, 1991, **30**, 2547–2551.
- 59 H. J. Shine, B.-J. Zhao, J. N. Marx, T. Ould-Ely and K. H. Whitmire, *J. Org. Chem.*, 2004, **69**, 9255–9261.
- 60 G. R. Fulmer, A. J. Miller, N. H. Sherden, H. E. Gottlieb, A. Nudelman, B. M. Stoltz, J. E. Bercaw and K. I. Goldberg, *Organometallics*, 2010, **29**, 2176–2179.
- 61 *mf2.SL*, Max-Planck Institute for Chemical Energy Conversion, Mülheim/Ruhr, Germany, 2021.



Impact of Ligand Design on an Iron NHC Epoxidation Catalyst

Tim P. Schlachta^{+, [a]}, Greta G. Zámbo^{+, [a]}, Michael J. Sauer,^[a] Isabelle Rüter,^[b] and Fritz E. Kühn^{*[a]}

An open-chain iron pyridine-NHC framework is expanded utilizing a benzimidazole moiety to deepen the understanding of the impact of electronic variations on iron NHC epoxidation catalysts, especially regarding the stability. The thereby newly obtained iron(II) NHC complex is characterized and employed in olefin epoxidation. It is remarkably temperature tolerant and achieves a TOF of ca. 10 000 h⁻¹ and TON of ca. 700 at 60 °C in

the presence of the Lewis acid Sc(OTf)₃, displaying equal stability, but lower activity than the unmodified iron pyridine-NHC (pre-)catalyst. In addition, a synthetic approach towards another ligand containing 2-imidazoline units is described but formylation as well as hydrolysis hamper its successful synthesis.

1. Introduction

Epoxidation of olefins is an important process to produce commodity chemicals, fine chemicals, pharmaceuticals as well as building blocks for synthetic organic chemistry.^[1-4] The majority of homogeneous epoxidation catalysts are transition metal complexes based on, for example, Re, Ru, W, polyoxometalates, Pt or Mo.^[2] In a bio-inspired approach, iron-containing enzymes like cytochrome P450 have been used as models for a number of Fe epoxidation catalysts.^[5] Originally to study the chemistry of these metalloproteins, the ability of the enzymes to oxidize challenging substrates at mild conditions with high activity and selectivity, has made the artificial iron complexes interesting candidates for catalytic application.^[6-7] Similar to the models in nature, first generations of biomimetic Fe catalysts had *N*-donor ligands such as porphyrins or non-heme ligands.^[6,8-14] While the use of iron makes their application financially attractive, their activity given in turnover frequency (TOF, up to 25 200 h⁻¹)^[15] lacks somewhat behind other organometallic benchmark catalysts containing Re (up to ca. 40 000 h⁻¹)^[16] and Mo (up to ca. 50 000 h⁻¹).^[17] In this context, iron *N*-heterocyclic carbene (NHC) complexes have shown to be on par or better to *N*-ligated iron complexes, especially in terms

of activity.^[16,18-21] The two most studied catalytic systems possess a cyclic iron tetracarbene and open-chain iron pyridine-NHC framework (Figure 1).^[22-25] The iron tetracarbene complex **a/b** is the current benchmark system for homogeneous olefin epoxidation with a TOF > 400 000 h⁻¹ and turnover number (TON) of around 1200 at room temperature in combination with the Lewis acid Sc(OTf)₃ as additive.^[19] The open-chain iron NHC complex **h** is still on par with the most active *N*-ligated iron catalyst with a TOF of 24 500 h⁻¹ and a TON of > 700, also in the presence of Sc(OTf)₃ at room temperature.^[23] While the stability (in TON) of both systems is also better compared to *N*-ligated iron catalysts, where most TONs are below 100,^[12,15,23,26-27] it still has to be improved for potential industrial applications. By suppression of a degradation pathway with Lewis acids like Sc(OTf)₃, the formation of a diiron(III)- μ -oxo complex, the TON could already be more than doubled from ca. 500 to ca. 1200 for **a** and similarly for **h**, **i** and **j**.^[18-19,23,28-29] As another strategic option, the modification of the axial ligands has been chosen, as it appeared to be the synthetically simplest approach to modify the system.^[22] Interestingly, it was possible in this way to increase the stability of **h** in C-H hydroxylation by up to 34%.^[30] However, at least one of the labile axial ligands apparently needs to leave the molecule to enable catalysis by creating a free coordination site.^[5,31-32] Accordingly, an exchange of both axial ligands to stronger coordinating ones has a negative effect on the catalytic performance, at least in the case of the well examined olefin epoxidation.^[33-35]

A more electron rich iron center is assumed to facilitate the proposed rate determining step in epoxidation, the formation of an electrophilic iron(IV)-oxo or iron(V)-oxo intermediate.^[22-23,36-37] On the other hand, a more Lewis acidic iron center might increase the reactivity of the electrophilic active species. Thus, equatorial ligand modifications toward a higher (**c/d**, **g**, **i**) and lower (**e/f**, **j**) electron density at the iron center were executed. However, so far, the changes did neither lead to a higher stability nor to higher activity. Both catalytic systems (**a/b** and **h**) remain most active and stable when unmodified; a more electron rich iron center (**c/d**, **g**, **i**) leads to a

[a] T. P. Schlachta,⁺ G. G. Zámbo,⁺ M. J. Sauer, F. E. Kühn
Technical University of Munich, School of Natural Sciences, Department of Chemistry and Catalysis Research Center, Molecular Catalysis,
Lichtenbergstraße 4, 85748 Garching, Germany
Phone (secretary's office): +49 (0)89 289 13477
E-mail: fritz.kuehn@ch.tum.de

[b] I. Rüter
Institut für Anorganische Chemie, Georg-August-Universität Göttingen,
Tammannstraße 4, 37077 Göttingen, Germany

[†] Tim P. Schlachta and Greta G. Zámbo contributed equally

Supporting information for this article is available on the WWW under
<https://doi.org/10.1002/open.202400071>

© 2024 The Authors. ChemistryOpen published by Wiley-VCH GmbH. This is an open access article under the terms of the Creative Commons Attribution License, which permits use, distribution and reproduction in any medium, provided the original work is properly cited.

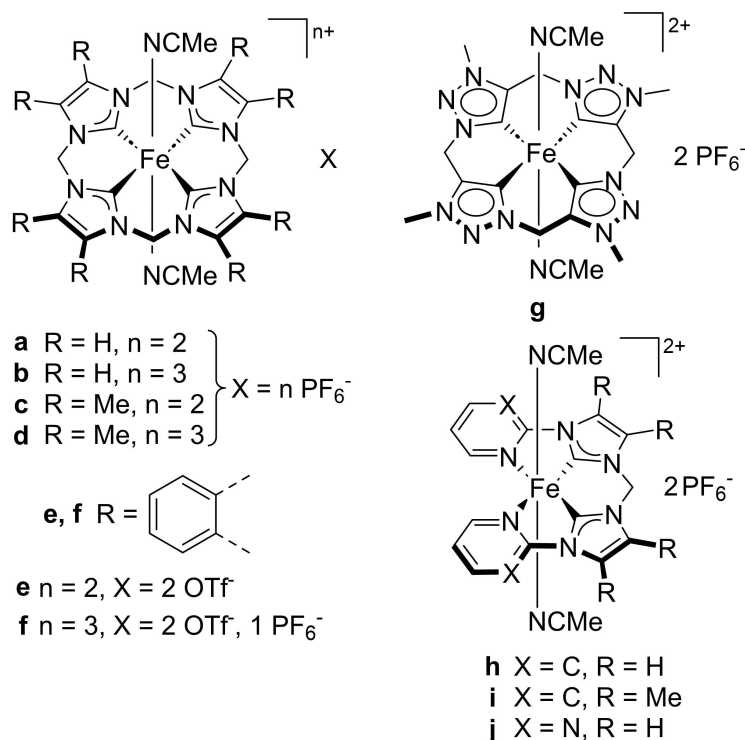


Figure 1. Iron NHC (pre-)catalysts.

lower activity and decreased stability while a less electron donating ligand (e/f, j) results in an even lower activity and additionally to a slightly lower stability, compared to the unmodified complex.^[20,23,37]

In this work, the open-chain iron pyridine-NHC framework is expanded with a benzimidazole moiety (1, Figure 2) and examined in order to deepen the understanding of the impact of electronic variations on iron NHC epoxidation catalysts, especially regarding stability. This modification is analog to e/f, allowing to investigate whether it has a similar effect on the open-chain catalytic system. Furthermore, a synthetic approach toward a ligand precursor containing 2-imidazoline units is described. The previous ligand modifications all had a measurable influence on the catalytic performance. Changing the NHC backbone from unsaturated to saturated might be a

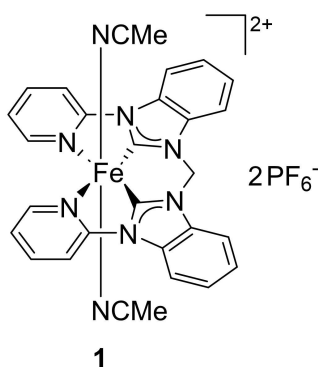


Figure 2. Novel iron(II) NHC complex.

desirable, sufficiently small change with a gentle electron donation toward the iron center. As there is an increasing interest in the application of machine learning models in chemistry, the publication of training data is needed, especially of otherwise neglected unsuccessful reactions.^[38] The successful synthesis and in-depth characterization of the novel iron(II) NHC complex 1 is reported. 1 is employed as (pre-)catalyst in the epoxidation of *cis*-cyclooctene as model substrate. Additionally, more challenging olefin substrates and the effect of Lewis acid Sc(OTf)₃ is investigated. The results are discussed within the framework of the current research state on iron NHC catalyzed olefin epoxidations. The catalytic activity of 1 is assumed to be lower compared to the other complexes. A slower ongoing reaction and degradation would possibly allow the investigation of the epoxidation mechanism of iron NHCs by e.g. trapping intermediates or real-time monitoring at low temperatures. Elucidating the mechanism would also help to find suitable strategies to improve stability.

2. Results and Discussion

2.1. Synthesis and Characterization of the Iron(II) Complex 1

The synthesis of a ligand precursor, analogous to h, but containing a saturated backbone, *i.e.* 2-imidazoline moieties instead of imidazole, was pursued parallel to the synthesis of iron(II) NHC complex 1. However, formylation as well as hydrolysis posed potential problems during the synthesis. The synthetic approaches are described in the SI.

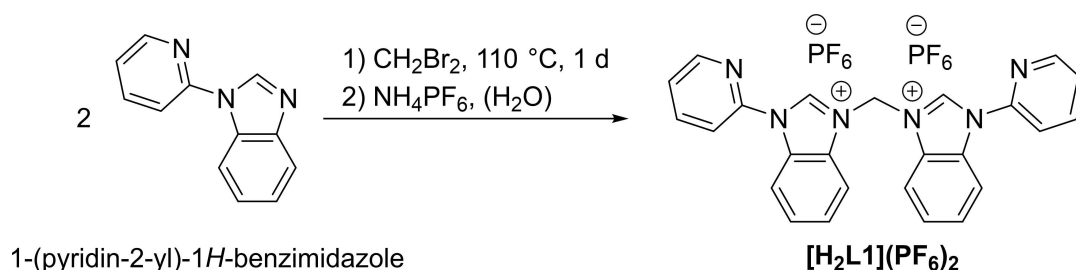
The ligand precursor of iron(II) complex **1** is obtained by a two-step synthesis (Scheme 1). First, 1-(pyridin-2-yl)-1*H*-benzimidazole is reacted with excess CH_2Br_2 to give the bromide salt $[\text{H}_2\text{L1}](\text{Br})_2$. Then, an anion exchange with NH_4PF_6 is performed to increase the solubility of the compound in organic solvents as well as additional purification step to yield $[\text{H}_2\text{L1}](\text{PF}_6)_2$.

The synthesis of iron(II) NHC complex **1** proved to be rather challenging. An established effective way to synthesize Fe NHC complexes is the use of $\text{Fe}[\text{N}(\text{SiMe}_3)_2]_2$ as both internal base and iron precursor and has been used for the similar complexes **h**, **i** and **j**.^[22–23] However, in this case, the conversion remains very low, leaving a large amount of unreacted ligand precursor and an inorganic impurity (see SI). The iron complex and the ligand precursor are difficult to separate, most likely due to very similar polarity, with the iron complex being slightly more polar. While at this point **1** could be isolated analytically pure by precipitation with a specific ratio of Et_2O to MeCN, the yield was very low (3%, method A), and the purification method was poorly reproducible. A more complete reaction would simplify the purification. Thus, efforts were made to increase the conversion of the ligand precursor. Experiments with iron precursor ($\text{FeBr}_2(\text{THF})_2$, $\text{Fe}(\text{OAc})_2$) in combination of a (stronger) external base (NaH , $\text{KN}(\text{SiMe}_3)_2$, *n*-BuLi, LiN^iPr_2) were conducted (see SI), even though the proton at position 2 of the benzimidazole units should be more acidic than for the imidazole ligand precursors of e.g. **h** due to the conjugative effect of the benzene ring.^[39] In addition, the transmetalation route was applied with Ag_2O and $\text{FeBr}_2(\text{THF})_2$.^[40] However, these approaches were not successful. Finally, the best method to obtain **1** (8% yield, method B) proved to be the reaction of $[\text{H}_2\text{L1}](\text{PF}_6)_2$ with $\text{Fe}[\text{N}(\text{SiMe}_3)_2]_2$ (Scheme 2) and removal of

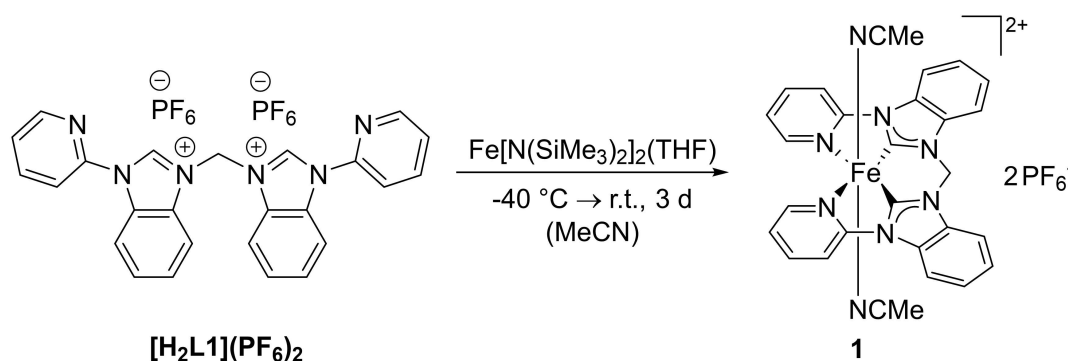
unreacted ligand precursor afterwards by multiple washing steps with a mixture of MeCN/ Et_2O with increasing polarity (see SI). Then, the inorganic impurity derived from unreacted iron precursor can be removed by filtration over neutral Al_2O_3 (see SI).

The successful synthesis of **1** is evidenced in ^1H NMR by the absence of the acidic benzimidazole protons in position 2 and the appearance of the carbene carbon signal in ^{13}C NMR at 230.31 ppm. The $^{13}\text{C}_{\text{NHC}}$ signal of **1** is significantly downfield shifted compared to the other NCCN-ligated complexes (**h**: 216.15, **i**: 215.49, **j**: 216.24 ppm)^[23,41] and the effect is also observed in the iron tetracarbene **e/f**.^[37] This shift can be explained with the lower electron density at the carbene carbon atom compared to the other complexes **h**, **i**, **j** and the followed deshielding noticeable in NMR. The annellation of the benzene ring to the backbone of the NHC results in a transfer of the π -electron density from the carbene carbon into the larger conjugated π system.^[42–43] Other factors may also contribute.^[22] The chemical composition of **1** is further shown by ESI-MS and elemental analysis. Similar to **h**, **i** and **j**, **1** is stable as solid under ambient conditions for at least one month and in MeCN solution (HPLC-grade, not dried or degassed) for at least one day.^[23]

In cyclic voltammetry, the reversible $\text{Fe}^{2+}/\text{Fe}^{3+}$ transition of **1** is located at $E_{1/2} = 0.625$ V ($\Delta E = 91$ mV, V vs. Fc/Fc^+ , see SI) and is the most positive in the series of the NCCN complexes (**h**: 0.423 V, **i**: 0.337 V, **j**: 0.559 V).^[23,41,44–46] The strong downfield shift of the $^{13}\text{C}_{\text{NHC}}$ signal and this positive redox potential reflect the weaker σ electron donation of the benzimidazolylidene ligand to the iron center, supported by Tolman electronic



Scheme 1. Synthesis of ligand precursor $[\text{H}_2\text{L1}](\text{PF}_6)_2$.



Scheme 2. Synthesis of iron(II) complex **1**.

parameters,^[43,47] and implies a lower electron density at the iron atom.^[22]

The UV/Vis spectrum of **1** is similar to the other NCCN-ligated complexes.^[23] It has four local absorption maxima (227 nm, 279 nm, see SI) and the two at 327 nm and 393 nm are assigned to charge-transfer bands.^[45]

A solid sample of **1** was characterized by ⁵⁷Fe Mössbauer spectroscopy to gain more insights on the electronic properties of the complex (Figure 3). As indicated in ¹H NMR, **1** is a diamagnetic iron(II) complex with an isomer shift of $\delta = 0.22 \text{ mm s}^{-1}$ in the range of other octahedral iron(II) low-spin species.^[22–23,48] The isomer shift is close to the other three Fe NCCN complexes ($\Delta\delta$ up to 0.04 mm s^{-1})^[23] as they all exhibit similar Fe-ligand bond lengths (see below) and no significant influence of the benzimidazolylidene ligand is noticeable. For example, a shorter bond length can increase the electron density at the iron atom through compression of the s-orbitals, resulting, among other factors, in a more negative isomer shift.^[48] The quadrupole splitting of **1** is relatively high for an iron(II) low-spin complex with $\Delta E_Q = 2.23 \text{ mm s}^{-1}$, but still in the typical range for NHC-ligated iron(II) low-spin complexes.^[22–23] This is due to the NHC ligand's strong σ -donation in the equatorial plane deforming the charge distribution around the iron nucleus. The quadrupole splitting of the NCCN-ligated complexes could be ranked in the order of increasing ligand electron donor strength, $j < h < i$, resulting in a higher amount of deformation of the electric field.^[23] However, **1** has a quadrupole splitting of $\Delta E_Q = 2.23 \text{ mm s}^{-1}$, effectively the same as **i** ($\Delta E_Q = 2.22 \text{ mm s}^{-1}$), which is counterintuitive at first glance, since **1** exhibits the weakest electron donation from the NHC ligand. The high quadrupole splitting can probably be attributed to the stronger π -accepting properties of the benzimidazolylidene ligand.^[43]

Single crystals suitable for X-ray diffraction were obtained by slow vapor diffusion of Et₂O into a solution of **1** in MeCN (see SI). The molecular structure of **1** is displayed in Figure 4 and it is similar to the other complexes **h**, **i**, **j**.^[23] The NHC ligand

is coordinating in equatorial fashion and the labile MeCN ligands are located at the axial coordination sites of the iron center. The axis intersecting the axial ligands and the iron atom is slightly bent (171.34°) like in **h**, **i**, **j**, while it is usually closer to 180° in iron tetracarbenes.^[22] The other parameters are in the typical range of open-chain iron complexes.^[23] The buried volume of **1** is $86\% V_{\text{Bur}}$ (see SI) and is therefore the same size as **h**, **i**, **j**, ensuring a good comparability in catalysis due to equal steric properties of the iron(II) (pre-)catalysts.

2.2. Catalytic Olefin Epoxidation Reactions

The influence of the backbone modification on the catalytic performance of complex **1** in the epoxidation of olefins is investigated in the following. For a good comparability of the results with **h**, **i** and **j**, identical conditions are applied if not stated otherwise. Hence, standard conditions are defined as 20°C , applying H₂O₂ (1.50 eq.) as oxidant, MeCN as solvent, *cis*-cyclooctene (1.00 eq.) as model substrate and **1** as (pre-)catalyst (0.02 eq.).^[23] Excess hydrogen peroxide was used as it has been found to be best option for iron NHC epoxidation catalysis and is atom-efficient as well as environmentally friendly.^[18,23,49–51] Quantification of the formed epoxide was done with GC-FID and ¹H NMR spectroscopy.

A first experiment was conducted under standard conditions. With the weaker electron donating NHC ligand and the highest redox potential, **1** was expected to show the lowest activity out of **h**, **i** and **j**. However, over the course of 60 min, no conversion was detected at all (Figure 5). A behavior like **j** was anticipated, of course with slightly lower conversion. The performance of **1** is likely a result of a low activity but can also imply a fast degradation within the first seconds. For **h**, decoordination of the NCCN ligand and subsequent reaction to a C–C coupled biimidazole species was found as one degradation pathway under oxidative conditions.^[52–53]

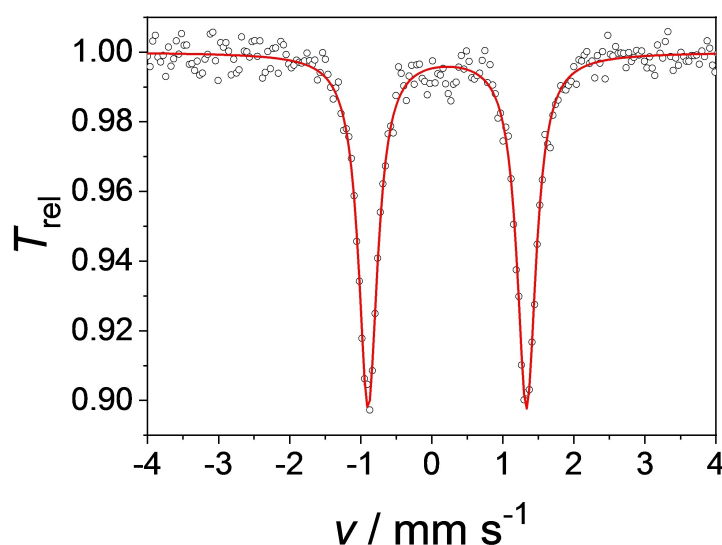


Figure 3. Zero-field ⁵⁷Fe Mössbauer spectrum of solid **1** at 80 K. The red line represents a simulation with $\delta = 0.22 \text{ mm s}^{-1}$ and $\Delta E_Q = 2.23 \text{ mm s}^{-1}$.

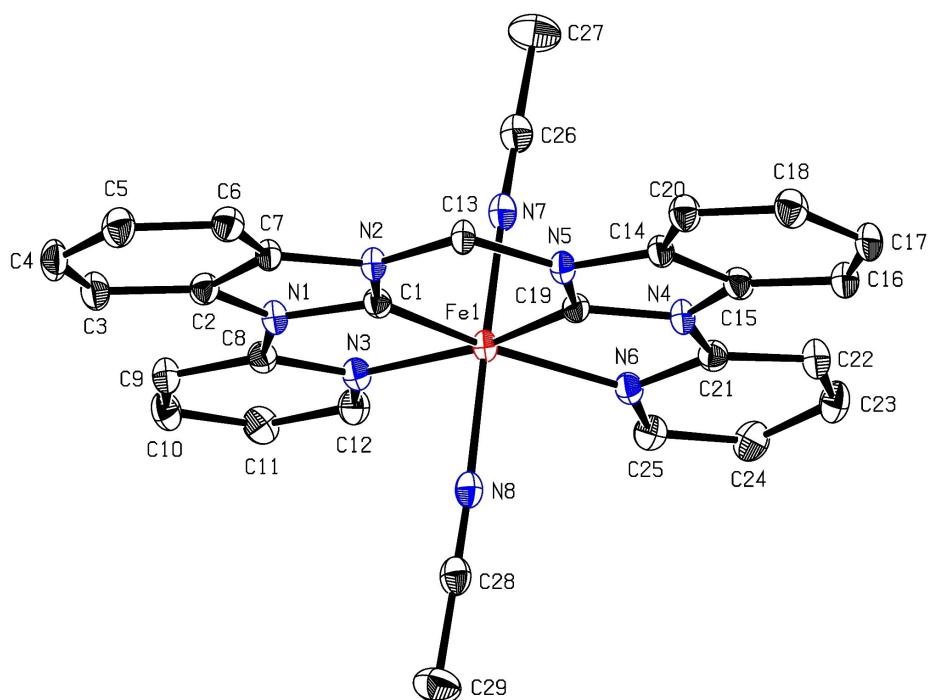


Figure 4. ORTEP-style representation of **1**. Hydrogen atoms and hexafluorophosphate anions are omitted for clarity. Thermal ellipsoids are shown at a 50% probability level. Selected bond lengths (Å) and angles (°): C1–Fe1 1.8314(19); N3–Fe1 2.0721(16); C19–Fe1 1.8293(19); N6–Fe1 2.0852(16); N7–Fe1 1.9136(18); N8–Fe1 1.9253(18); N7–Fe1–N8 171.34(7); C1–Fe1–N3 79.90(7); C1–Fe1–N6 166.66(8); C1–Fe1–N7 95.12(8); C1–Fe1–N8 91.09(8).

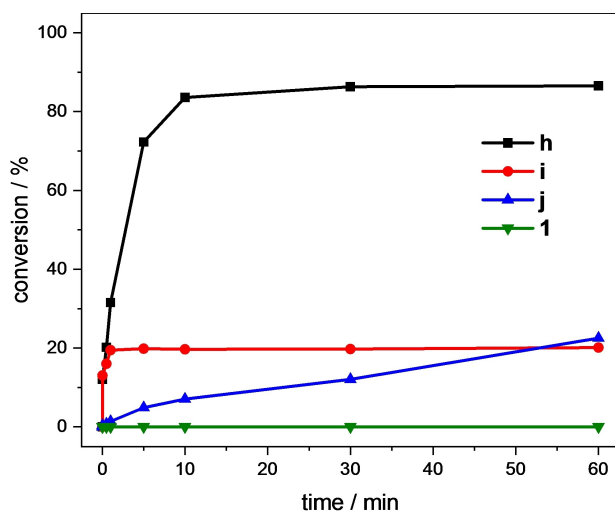


Figure 5. Time-dependent epoxidation of *cis*-cyclooctene (67.3 $\mu\text{mol/mL}$, 1.00 eq.) in MeCN using **h**, **i**, **j**^[23] or **1** (1.35 $\mu\text{mol/mL}$, 0.02 eq.) as catalyst and H_2O_2 (50% aq., 101 $\mu\text{mol/mL}$, 1.50 eq.) as oxidizing agent at 20 °C. Conversions are determined by GC-FID.

The addition of Lewis acids to the reaction has shown to significantly increase the activity and stability of the iron NHC catalyst.^[19,22,33] One reason for this is the reactivation of a potential dead-end species by the Lewis acid, an diiron(III)- μ -oxo complex formed during catalysis of **a/b**.^[19,28–29] Furthermore, the Lewis acid is facilitating the initial oxidation of Fe^{II} to Fe^{III} as well as $\text{OH}^{\bullet}/^-$ cleavage of a proposed $\text{Fe}^{\text{III}}\text{-OOH}$ intermediate transferring the rate determining step to the olefin oxidation.^[19,22–23,54] Hence, the same experiment was repeated

with $\text{Sc}(\text{OTf})_3$ as additive, which has proven to be the most effective Lewis acid for **a/b**.^[19] In its presence **1** reaches a conversion of 89% (Figure 6), which is close to the other complexes (**h**: 100%; **i**: 92%; **j**: 97%)^[23] and indicative for a deactivation pathway which now appears to be suppressed. At these conditions, the selectivity of **1** (99%) is on par with the other NCCN complexes and **a/b**, being among the most selective iron NHC epoxidation catalysts.^[18–19,23] Noticeable is the induction period of **1**, which can be attributed to preoxidation from Fe^{II} to Fe^{III} , aided by $\text{Sc}(\text{OTf})_3$ this time, and is also observed for iron(II) tetracarbenes, e.g. **a** or **e**.^[18,37] This reinforces the proposed mechanism, which continues with the iron(III) complex to form a $\text{Fe}^{\text{III}}\text{-OOH}$ intermediate, followed by the presumably rate-determining step, the homolytic or heterolytic cleavage to generate iron(IV) or iron(V)-oxo species, respectively. Finally, the epoxide is obtained after electrophilic attack of the oxo species on the alkene.^[22] As **1** takes more than 30 min to reach its final conversion, it has the lowest TOF (300 h^{-1} , Table 1 entry 2) of the four NCCN complexes.^[23] However, the TON is on the same level (**1**: 44; **h**: 50; **i**: 46; **j**: 49).^[23]

Both **j** and **e/f** are remarkably temperature tolerant and achieve a higher activity at higher temperatures.^[23,37] Therefore, **1** was screened at different temperatures at otherwise standard conditions (Figure 7). Indeed, in the presence of $\text{Sc}(\text{OTf})_3$ at 40 °C, a final conversion of 90% is already reached after 5 min corresponding to a TOF of over 1000 h^{-1} (entry 4). At 60 °C, most of the conversion is reached even faster after 30 s (83%, Figure 7), equal to a TOF of 5200 h^{-1} (entry 5). The TON effectively does not change at higher temperatures (40 °C: 45;

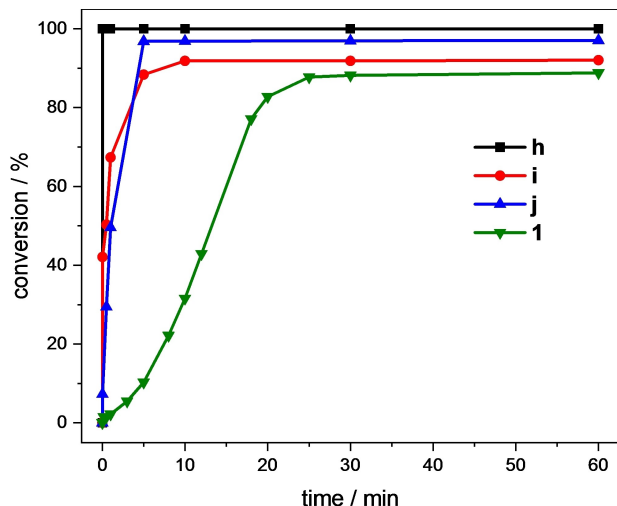


Figure 6. Time-dependent epoxidation of *cis*-cyclooctene (67.3 $\mu\text{mol/mL}$, 1.00 eq.) in MeCN using **h**, **i**, **j**^[23] or **1** (1.35 $\mu\text{mol/mL}$, 0.02 eq.) as catalyst, $\text{Sc}(\text{OTf})_3$ (6.73 $\mu\text{mol/mL}$, 0.10 eq.) and H_2O_2 (50% aq., 101 $\mu\text{mol/mL}$, 1.50 eq.) as oxidizing agent at 20 °C. Conversions are determined by GC-FID.

60 °C: 43), contrary to **j** and **e/f** showing declining TONs but similarly increasing activity like **1**. However, the selectivity is lower in these experiments (40 °C: 91%; 60 °C: 80%). Striking though is that the selectivity is > 99% in the beginning of both runs and gradually decreases over time, while the amount of formed cyclooctane-1,2-diol is increasing (see SI). This strongly suggests catalytic ring-opening of the epoxide by the Lewis acid $\text{Sc}(\text{OTf})_3$ as described in the literature.^[55–59] Another evidence is the high selectivity (> 99%, entry 3) achieved with **1** at 40 °C without $\text{Sc}(\text{OTf})_3$ after even 300 min. This experiment also demonstrates the long lifetime of **1** under oxidative conditions, although only a conversion of 11% is reached in the end (**h**: 42%; **j**: 30%, Figure 7).

At lower catalyst concentrations at 60 °C an induction period can be observed again despite the use of $\text{Sc}(\text{OTf})_3$ (Figure 7). At these seemingly optimal conditions, the highest TOF with 10 200 h^{-1} and TON with 706 are found for **1** (entry 7). Regarding the activity, this places **1** second behind **h**, with the

order **h** (24 500 h^{-1}) > **1** (10 200 h^{-1}) > **i** (7 600 h^{-1}) > **j** (1 300 h^{-1}), while having the most positive redox potential and weakest NHC ligand.^[23] However, at identical conditions, for example 20 °C with $\text{Sc}(\text{OTf})_3$, **1** possesses as expected the lowest activity (**h**: 18 000 h^{-1} > **i**: 7 600 h^{-1} > **j**: 1 300 h^{-1} > **1**: 300 h^{-1}).^[23] The stability of **1** in TON is effectively as high as **h**, resulting in the order **h** (711) \approx **1** (706) > **j** (49) > **i** (46).^[23] While the TOF of **1** is lower than the most active *N*-ligated Fe complex (25 200 h^{-1}),^[15] its TON is like **h** on par with the highest obtained for a *N*-donor Fe complex (715),^[27] which usually have TONs around 200 or below.^[12,15,23,26] The iron tetracarbene **a/b** still has the best reported catalytic performance (TOF > 400 000 h^{-1} ; TON = 1 200 at r. t.).^[19]

A selection of other substrates was examined with **1** at standard conditions in the presence of $\text{Sc}(\text{OTf})_3$ (Table 2). They are important building blocks in industry^[23] and contain functional groups that allow the performance of **1** to be studied for more sophisticated alkenes. The reaction time is set to 30 min based on the achieved full conversion in the case of *cis*-cyclooctene (Figure 6). Although the reaction time was only 5 min for **h**, **i**, **j**,^[23] this should allow to determine the actual performance of **1** for the different substrates while considering its lower activity. Thus, a good comparability amongst the NCCN complexes should be ensured, as the reaction time is standardized relative to the completeness of the reaction with *cis*-cyclooctene.

Overall, **1** exhibits a moderate performance when compared to the other NCCN complexes. While the conversion of cyclohexene is approximately as high as for **i** and **j**,^[23] the selectivity is surprisingly low for **1** (4%, entry 8). The conversion of 1-hexene appears to be challenging for **1** reaching only 22% with a selectivity of 43% (entry 10). Together with **i** and **j**, **1** favors *trans*-2-octene (30% yield) over the *cis* isomer (7% yield), contrary to **h**, **b** and other iron epoxidation catalysts.^[18,23,60] The backbone modifications indicate to have an opposing influence in this regard, possibly because of steric reasons. For all the three linear carbon chains, significant diol formation is measured (1-hexene: 6%; *trans*-2-octene: 16%; *cis*-2-octene: 19% yield). The conversion of allyl alcohol and allyl chloride is lower, but the selectivity is on par or better than for the NCCN

Table 1. Epoxidation of *cis*-cyclooctene by **1** at different catalyst concentrations, temperature, and with or without additive.

entry	catalyst	T [°C]	loading [mol %]	additive	X [%] ^[a] (60 min)	S [%] (60 min)	TOF [h^{-1}] ^[b]	TON (60 min)
1	1	20	2	–	0	0	0	0
2	1	20	2	$\text{Sc}(\text{OTf})_3$	89	99	300	44
3	1	40	2	–	11	> 99	–	5
4	1	40	2	$\text{Sc}(\text{OTf})_3$	90	91	1 000	45
5	1	60	2	$\text{Sc}(\text{OTf})_3$	87	80	5 200	43
6	1	60	0.5	$\text{Sc}(\text{OTf})_3$	82	91	8 500	164
7	1	60	0.1	$\text{Sc}(\text{OTf})_3$	71	92	10 200	706

Reaction conditions: *cis*-cyclooctene (67.3 $\mu\text{mol/mL}$, 1.00 eq.) in MeCN, Fe catalyst, if stated $\text{Sc}(\text{OTf})_3$ (6.73 $\mu\text{mol/mL}$, 0.10 eq.), and H_2O_2 (50% aq., 101 $\mu\text{mol/mL}$, 1.50 eq.). Selectivity is related to the epoxide. [a] Conversions are determined by GC-FID. [b] TOFs are determined at the highest slope of X. [c] X, S and TON determined after 300 min. [d] X, S and TON determined after 10 min. [e] X, S and TON determined after 5 min. T = temperature. X = conversion. S = selectivity.

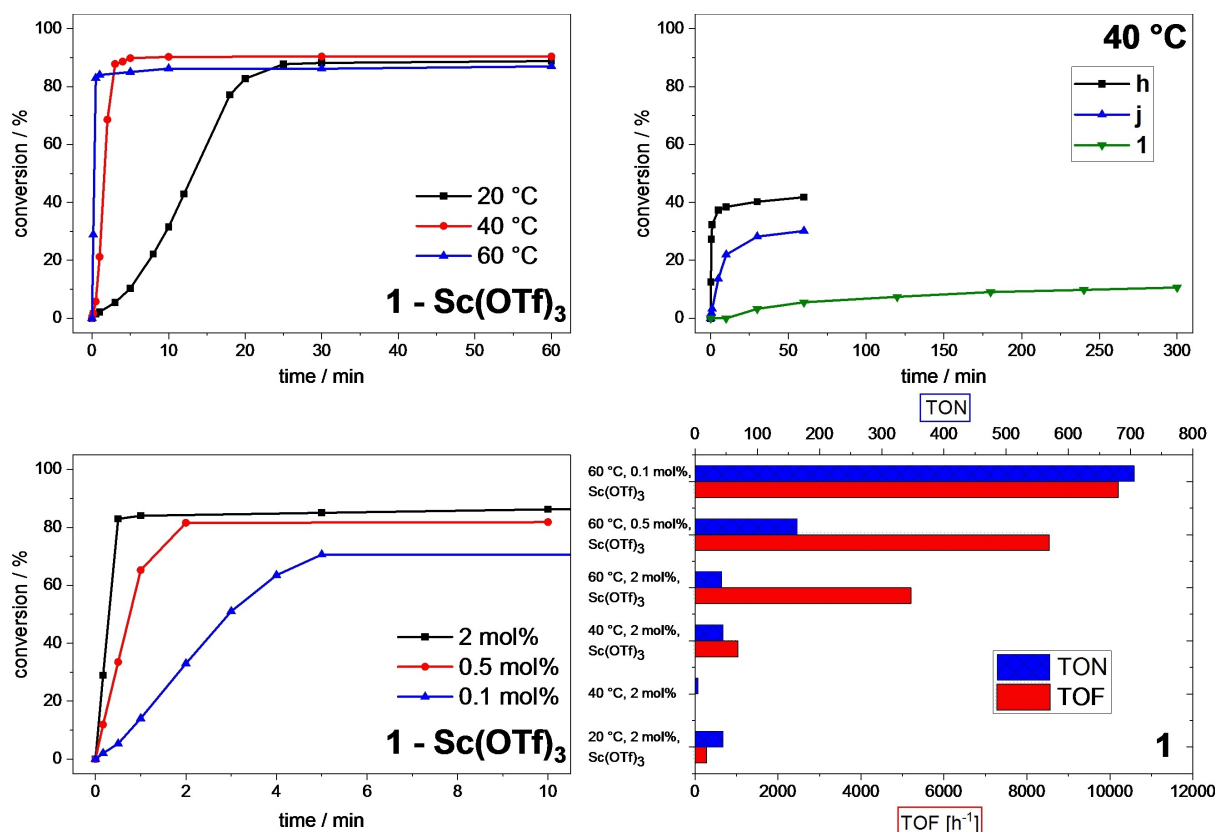


Figure 7. Time-dependent epoxidation of *cis*-cyclooctene (67.3 $\mu\text{mol/mL}$, 1.00 eq.) in MeCN using Fe catalyst and H_2O_2 (50% aq., 101 $\mu\text{mol/mL}$, 1.50 eq.) as oxidizing agent. Conversions are determined by GC-FID. Top left: **1** (1.35 $\mu\text{mol/mL}$, 0.02 eq.) as catalyst and $\text{Sc}(\text{OTf})_3$ (6.73 $\mu\text{mol/mL}$, 0.10 eq.) at 20, 40 and 60 °C. Top right: **h**, **j**^[23] or **1** (1.35 $\mu\text{mol/mL}$, 0.02 eq.) as catalyst at 40 °C. Bottom left: **1** (0.02 eq., 0.005 eq. or 0.001 eq.) as catalyst and $\text{Sc}(\text{OTf})_3$ (6.73 $\mu\text{mol/mL}$, 0.10 eq.) at 60 °C. Bottom right: overview of TON and TOF of **1** at different conditions.

Table 2. Epoxidation of various olefin substrates using 1 as catalyst with 30 min reaction time and $\text{Sc}(\text{OTf})_3$.				
entry	substrate	X [%]	S [%]	
8	<i>cis</i> -cyclooctene	88	> 99	[a]
9	cyclohexene	29	4	
10	1-hexene	22	43	
11	<i>cis</i> -2-octene	37	18	
12	<i>trans</i> -2-octene	54	56	
13	allyl alcohol	36	29	
14	allyl chloride	10	> 99	
15	styrene	16	26	
16	chalcone	8	26	

Reaction conditions: substrate (67.3 $\mu\text{mol/mL}$, 1.00 eq.) in MeCN, **1** (1.35 $\mu\text{mol/mL}$, 0.02 eq.), $\text{Sc}(\text{OTf})_3$ (6.73 $\mu\text{mol/mL}$, 0.10 eq.) and H_2O_2 (50% aq., 101 $\mu\text{mol/mL}$, 1.50 eq.), 20 °C, 30 min. Selectivity is related to the epoxide. Conversions are determined by $^1\text{H-NMR}$ spectroscopy, applying benzene as external standard. [a] Conversion determined by GC-FID. X = conversion. S = selectivity.

complexes. No epoxide formation could be observed with **h**, **i**, **j** for styrene,^[23] but despite severe aldehyde production (12% yield, see SI), 4% yield of product was achieved. In contrast, even though the conversion of chalcone was low for **i** and **j**,^[23]

1 only manages to consume 8% (entry 16). To summarize, for the various substrates, the nucleophilicity of the alkene is decisive for its reactivity, underlining the electrophilic nature of the active species. This is clearly demonstrated for chalcone, for example: The $-\text{M}$ effect of the carbonyl group reduces the nucleophilicity and thereby reactivity of the carbon-carbon double bond, resulting in the observed low conversion.

3. Conclusions and Outlook

A synthetic approach towards a NCCN ligand containing 2-imidazoline units is described. Formylation as well as hydrolysis pose potential problems. A novel iron(II) NHC complex **1** containing a NCCN ligand with benzimidazole moieties has been successfully synthesized by two different methods. **1** contains the most positive redox potential amongst the iron NCCN complexes described so far.^[23] In epoxidation of *cis*-cyclooctene, this results in a noticeable induction phase – oxidation from Fe^{II} to Fe^{III} – even in the presence of $\text{Sc}(\text{OTf})_3$ at 20 °C. Higher temperatures and the Lewis acid $\text{Sc}(\text{OTf})_3$ are beneficial for the catalytic performance of **1** and the catalyst species is – compared to other iron NHC epoxidation catalysts^[22–23] – remarkably temperature tolerant (up to 60 °C). Regardless of its high redox potential induced by the weaker σ -

donation from the NHC ligand, **1** achieves the second highest TOF of 10 200 h⁻¹ amongst the other iron NCCN complexes at 60 °C. Furthermore, a TON of 706 is determined, as high as observed for the unmodified iron NCCN complex **h**. In contrast to the benzimidazole modification in the iron tetracarbene system **e/f**, **1** can keep the stability of its unmodified derivative, **h**. When screening various other substrates, **1** also favors the more nucleophilic alkenes, similar to **h**, **i** and **j**. However, due to its low reactivity at 20 °C, **1** achieves only modest conversions. Based on its slow reaction, the suitability to use **1** for mechanistic studies is demonstrated, particularly low temperatures should ensure controlled conditions.

Experimental

General Procedures and Analytical Methods

The synthesis of complex **1** was performed in argon atmosphere using standard Schlenk and glovebox techniques as well as dry and degassed solvents. N¹-(Pyridin-2-yl)ethane-1,2-diamine,^[61] 1-(pyridin-2-yl)-1*H*-benzimidazole^[62] and Fe[N(SiMe₃)₂](THF)^[23] were synthesized according to literature procedures. The procedures for novel compounds obtained during the synthetic approaches to the saturated ligand precursor, containing 2-imidazoline moieties instead of imidazole, (2-imidazoline, 2-((2-aminoethyl)amino)pyridine 1-oxide, 2-(2-imidazolyl-1-yl)pyridine 1-oxide) are stated in the SI. 1-(Pyridin-2-yl)-1*H*-benzimidazole was purified by column chromatography on silica gel (~30 g silica per gram of crude product) using ethyl acetate as eluent (R_f=0.29) prior to use. Solvents were purified, dried and degassed using standard methods^[63] or received from a solvent purification system by M. Braun. All other chemicals were obtained from commercial suppliers and were used without further purification. NMR spectra were recorded on a Bruker Avance Ultrashield AV400 (¹H NMR, 400.13 MHz; ¹³C NMR, 100.53 MHz). The chemical shifts are given in δ values in ppm (parts per million) relative to TMS (tetramethylsilane) and are reported relative to the residual deuterated solvent signal.^[64] Elemental analyses (C/H/N/S) were obtained by the microanalytical laboratory at Technical University Munich. Electro-spray ionization mass spectrometry (ESI-MS) data were measured on a Thermo Fisher Ultimate 3000. Electrochemical measurements were carried out in a scintillation vial closed with a septum lid under argon atmosphere, equipped with a glassy carbon disc electrode (working electrode), a platinum wire electrode (counter electrode) and a silver wire (pseudo reference electrode) on a Metrohm Autolab PGSTAT302N potentiostat. Potentials are measured with a scan rate of 100 mV/s and are reported with reference to an internal standard of ferrocenium/ferrocene (Fc⁺/0; 0.8 mg). Tetrabutylammonium hexafluorophosphate (100 mM in MeCN) was used as electrolyte. The concentration of the iron complex was about 2 mM. The UV/Vis spectrum was recorded on an Agilent Cary 60 UV-Vis spectrophotometer with a concentration of 0.02 mM complex in acetonitrile. Solid material of **1** (30 to 40 mg) was studied using ⁵⁷Fe Mössbauer spectroscopy at 80 K. The ⁵⁷Fe Mössbauer spectrum was measured using a ⁵⁷Co source in a Rh matrix using an alternating constant acceleration Wissel Mößbauer spectrometer equipped with a Janis closed-cycle helium cryostat. Transmission data were collected, and isomer shifts are reported relative to iron metal at ambient temperature. Experimental data were simulated with *mf2.SL* software.^[65] Deposition Number 2326822 (for **1**) contain the supplementary crystallographic data for this paper. These data are provided free of charge by the joint

Cambridge Crystallographic Data Centre and Fachinformationszentrum Karlsruhe Access Structures service.

Catalytic Procedures

Experimental remarks. GC analysis was performed with an Agilent Technologies 7890B GC-FID system with a 7693A Automatic Liquid Sampler for 150 samples with G4513A Autoinjector using a HP-5 column (30 m×320 μm×0.25 μm). NMR spectra were recorded on a Bruker Avance Ultrashield AV400 (400 MHz) or AV500 (500 MHz) spectrometer at a temperature of 297 K. Chemical shifts (δ) are reported in ppm and referenced to the residual signal of the deuterated solvent.^[64]

Catalytic procedure. All catalytic reactions were conducted in a cryostat (JulaboFP-50). Acetonitrile (HPLC-grade) as solvent was applied for all experiments, which are screened *via* GC (substrate: *cis*-cyclooctene). The screening of other substrates (*cis*-cyclohexene, 1-hexene, allyl alcohol, allyl chloride, styrene, chalcone, *cis*-2-octene and *trans*-2-octene) was performed using ¹H NMR spectroscopy and deuterated acetonitrile as solvent. The catalyst was added from a preformed stock solution in acetonitrile corresponding to the appropriate stoichiometry to a solution of the respective substrate (1.00 eq., 67.3 μmol/mL). Hydrogen peroxide (50% aq., 1.50 eq., 101 μmol/mL) was used as oxidizing agent and, if required, Sc(OTf)₃ as additive (0.10 eq., 8.41 μmol/mL). The reaction was started upon addition of the catalyst stock solution, by adding the catalyst solution all at once. The reaction was terminated by adding electrolytically precipitated activated MnO₂ in order to decompose the excess of H₂O₂ in the reaction solution. After filtration over activated neutral alumina (separation of the catalyst), GC samples were prepared for each experiment and time point using 200 μL filtrate, diluted with 1300 μL MeCN, in which *p*-xylene (0.9 μL/mL) is dissolved as an external standard. For the screening *via* ¹H NMR spectroscopy, 500 μL filtrate was added to 1 μL benzene as external standard. Control experiments without catalyst were performed for all reactions and did not show catalytic activity. An additional blank experiment with a simple iron salt, iron(II) chloride, in the presence of H₂O₂ was conducted to highlight the importance of iron complexes associated with NHCs due to minimal product and unselective side-product formation. Analogous, the additive Sc(OTf)₃ itself shows minimal unselective catalytic activity.^[19,37,55]

Synthetic Procedures

[H₂L1](Br)₂. 1-(Pyridin-2-yl)-1*H*-benzimidazole (266 mg, 1.36 mmol, 2.00 eq.) is dissolved in excess dibromomethane (10 mL, 143 mmol, 105 eq.) and heated to 110 °C for 1 d. The white suspension is cooled to r.t., then 10 mL Et₂O is added. The precipitate is filtered, washed with 5 mL MeCN and 10 mL Et₂O to obtain [H₂L1](Br)₂ as white powder (249 mg, 441 μmol, 65%). ¹H NMR (400.13 MHz, DMSO-*d*₆): δ 11.13 (s, 2H, NCHN), 8.82 (dd, ³J=5.2 Hz, ⁴J=1.7 Hz, 2H, H_{ar}), 8.61 (d, ³J=8.3 Hz, 2H, H_{ar}), 8.48 (d, ³J=8.3 Hz, 2H, H_{ar}), 8.35 (td, ³J=7.8 Hz, ⁴J=1.9 Hz, 2H, H_{ar}), 8.12 (d, ³J=8.3 Hz, 2H, H_{ar}), 7.91 (td, ³J=7.8 Hz, ⁴J=1.1 Hz, 2H, H_{ar}), 7.81 (m, 4H, H_{ar}), 7.67 (s, 2H, CH₂). MS-ESI (m/z): [HL1]⁺ calcd., 403.17; found, 403.18 (6); [L1 - 1-(pyridin-2-yl)-1*H*-benzimidazole + MeOH] calcd., 240.11; found, 240.07 (100); [1-(pyridin-2-yl)-1*H*-benzimidazole + H⁺] calcd., 196.09; found, 196.12 (68).

[H₂L1](PF₆)₂. [H₂L1](Br)₂ (196 mg, 347 μmol, 1.00 eq.) is dissolved in 10 mL H₂O and slowly added to a vigorously stirred solution of NH₄PF₆ (410 mg, 2.52 mmol, 7.24 eq.) in 15 mL H₂O. After stirring for 30 min, the white precipitate is filtered off and washed with H₂O and Et₂O to obtain [H₂L1](PF₆)₂ as somewhat hygroscopic white powder (180 mg, 259 μmol, 75%). The product is immediately

transferred into a Schlenk flask, dried overnight at 70 °C at 10⁻³ mbar and stored under argon. ¹H NMR (400.13 MHz, CD₃CN): δ 9.91 (s, 2H, NCHN), 8.76 (dd, ³J=5.0 Hz, ⁴J=1.8 Hz, 2H, H_{ar}), 8.36 (m, 2H, H_{ar}), 8.22 (td, ³J=7.9 Hz, ⁴J=1.8 Hz, 4H, H_{ar}), 7.88 (m, 6H, H_{ar}), 7.73 (dd, ³J=7.6 Hz, ³J=4.9 Hz, 2H, H_{ar}), 7.28 (s, 2H, CH₂). ¹³C NMR (100.53 MHz, CD₃CN): δ 151.16 (C_{ar}), 147.41 (C_{ar}), 142.90 (C_{ar}), 141.80 (C_{ar}), 132.08 (C_{ar}), 131.26 (C_{ar}), 130.03 (C_{ar}), 129.96 (C_{ar}), 127.31 (C_{ar}), 118.88 (C_{ar}), 117.22 (C_{ar}), 114.54 (C_{ar}), 57.26 (CH₂). MS-ESI (m/z): [L1 + PF₆⁻]⁺ calcd., 549.14; found, 548.65 (20); [HL1]⁺ calcd., 403.17; found, 403.16 (66); [1-(pyridin-2-yl)-1H-benzimidazole + H⁺] calcd., 196.09; found, 196.03 (100). Anal. calcd. for C₂₅H₂₀F₁₂N₆P₂: C 43.24; H 2.90; N 12.10. Found: C 43.26; H 2.94; N 12.06.

[FeL1(MeCN)₂](PF₆)₂ (1). Method A. A -40 °C cold solution of Fe[N(SiMe₃)₂]₂(THF) (108 mg, 241 μmol, 1.05 eq.) in 4 mL MeCN is added to a -40 °C cold solution of [H₂L1](PF₆)₂ (159 mg, 229 μmol, 1.00 eq.) in 4 mL MeCN. The solution becomes red and is stirred at 95 °C for 2 d. The dark red solution is dried under vacuum. The black residue is dissolved in MeCN and dried again under vacuum to remove any remaining free amine HN(SiMe₃)₂. The crude is dissolved in 2 mL MeCN and 5.4 mL Et₂O is added to precipitate a first fraction of a brown precipitate. The supernatant is filtered off and the resulting light brown to yellow solid is dried under vacuum, to obtain the analytically pure iron complex **1** (ca. 6 mg, 7 μmol, 3%). At this point, tiny washing steps with MeCN can be performed (around 0.3 to 0.5 mL MeCN), if necessary.

Method B. A black -40 °C cold solution of Fe[N(SiMe₃)₂]₂(THF) (2.91 g, 6.49 mmol, 1.11 eq.) in 10 mL MeCN is added to a yellow -40 °C cold solution of [H₂L1](PF₆)₂ (4.08 g, 5.87 mmol, 1.00 eq.) in 15 mL MeCN. The solution becomes red at first but turns black upon complete addition and is stirred at r.t. for 3 d. A brown precipitate has formed at the bottom of the black solution. The following work-up is performed under ambient atmosphere without the use of Schlenk technique. The black reaction mixture is dried *in vacuo* resulting in a black residue. A series of washing steps is performed to remove unreacted [H₂L1](PF₆)₂ and other organic impurities from the residue: 12 mL MeCN (obtained from solvent purification system, *i.e.* somewhat dry) is added to the residue in order to completely suspend the solid without any remaining precipitate. 60 mL Et₂O (neither degassed nor dried) is added to the black mixture and the dark yellow supernatant is decanted through a filter in order to catch any solid particles and is discarded. All black solids are combined to be suspended in MeCN again. This process is repeated further 9 times, *i.e.* in total 10 washing steps with the combination of 12 mL MeCN and 60 mL Et₂O. Then, 3 steps with 12 mL MeCN and 55 mL Et₂O are performed, followed by 3 steps with 12 mL MeCN and 50 mL Et₂O. Finally, 9 steps with 14 mL MeCN and 40 mL Et₂O are conducted. As the purification progresses, the mixture becomes lighter resulting in a light brown solid and yellow filtrate in the end. The light brown solid is dissolved in 100 mL MeCN. The resulting black solution is filtrated over a plug of Al₂O₃ (37 g Al₂O₃; pH=7; 7 cm height; column diameter 3 cm; dry Al₂O₃ and not wetted beforehand) to remove inorganic impurities. After filtration of the 100 mL solution, the plug of Al₂O₃ is not washed with additional MeCN as this can re-dissolve the impurities. An intense orange solution is collected and the solvent is removed *in vacuo*. The resulting orange solid is re-dissolved in 18 mL MeCN and 100 mL Et₂O is added to form a yellow precipitate and orange supernatant. The mixture is cooled at -32 °C for 10 min. Afterwards, the suspension is filtrated and the yellow precipitate washed with Et₂O. The precipitate is dried overnight at 60 °C at 10⁻² mbar and stored under argon. [FeL1(MeCN)₂](PF₆)₂ can be obtained as yellow solid in 8% yield (406 mg, 489 μmol). Single crystals suitable for X-ray diffraction were obtained by slow vapor diffusion of Et₂O into a solution of [FeL1(MeCN)₂](PF₆)₂ in MeCN after 1 to 2 weeks at r.t. under

ambient atmosphere (see SI for details). ¹H NMR (400.13 MHz, CD₃CN): δ 9.69 (m, 2H, H_{ar}), 8.50 (m, 4H, H_{ar}), 8.33 (m, 2H, H_{ar}), 8.03 (m, 2H, H_{ar}), 7.86 (td, ³J=5.6 Hz, ⁴J=2.7 Hz, 2H, H_{ar}), 7.69 (m, 4H, H_{ar}), 7.45 (s, 2H, CH₂), 1.96 (s, 6H, CH₃CN). ¹³C NMR (100.53 MHz, CD₃CN): δ 230.31 (C_{carbene}), 155.95 (C_{ar}), 153.47 (C_{ar}), 142.75 (C_{ar}), 138.05 (C_{ar}), 133.95 (C_{ar}), 125.83 (C_{ar}), 125.61 (C_{ar}), 124.07 (C_{ar}), 114.37 (C_{ar}), 112.72 (C_{ar}), 110.80 (C_{ar}), 62.60 (CH₂). MS-ESI (m/z): [FeL1 + HCOO⁻ + HCOONa]⁺ calcd., 571.08; found, 570.92 (19); [FeL1 + HCOO⁻]⁺ calcd., 503.09; found, 502.87 (74); [FeL1(MeCN)]²⁺ calcd., 270.07; found, 269.76 (85); [FeL1(MeCN)]²⁺ calcd., 249.56; found, 249.51 (45); [FeL1]²⁺ calcd., 229.04; found, 229.32 (100). Anal. calcd. for C₂₉H₂₄F₁₂FeN₈P₂: C 41.95; H 2.91; N 13.50. Found: C 41.61; H 2.98; N 13.97.

Acknowledgements

The authors are grateful to Patrick Mollik for technical support with cyclic voltammetry measurements. Part of this work has been supported by the Deutsche Forschungsgemeinschaft (DFG), project no. 445916766 (to I.R.), in the framework of the Research Unit "Bioinspired Oxidation Catalysis with Iron Complexes" (FOR 5215). Open Access funding enabled and organized by Projekt DEAL.

Conflict of Interests

There are no competing interests to declare.

Data Availability Statement

The data that support the findings of this study are available in the supplementary material of this article.

Keywords: Non-heme iron complexes · Carbene ligands · Epoxidation · Iron NHC complexes · Tailoring catalytic properties

- [1] H. C. Kolb, M. G. Finn, K. B. Sharpless, *Angew. Chem. Int. Ed.* **2001**, *40*, 2004–2021, DOI: 10.1002/1521-3773(20010601)40:11 <2004::AID-ANIE2004>3.0.CO;2-5.
- [2] S. T. Oyama, in *Mechanisms in Homogeneous and Heterogeneous Epoxidation Catalysis* (Ed.: S. T. Oyama), Elsevier: Amsterdam, **2008**, pp. 3–99, DOI: 10.1016/B978-0-444-53188-9.00001-8.
- [3] H. H. Szmant, *Organic Building Blocks of the Chemical Industry*, Wiley: New York, **1989**.
- [4] C. Anaya de Parrodi, E. Juaristi, *Synlett* **2006**, *2006*, 2699–2715, DOI: 10.1055/s-2006-950259.
- [5] P. D. Oldenburg, R. Mas-Ballesté, L. Que, in *Mechanisms in Homogeneous and Heterogeneous Epoxidation Catalysis* (Ed.: S. T. Oyama), Elsevier: Amsterdam, **2008**, pp. 451–469, DOI: 10.1016/B978-0-444-53188-9.00018-3.
- [6] L. Que, W. B. Tolman, *Nature* **2008**, *455*, 333–340, DOI: 10.1038/nature07371.
- [7] O. Shoji, Y. Watanabe, in *Fifty Years of Cytochrome P450 Research* (Ed.: H. Yamazaki), Springer Japan: Tokyo, **2014**, pp. 107–124, DOI: 10.1007/978-4-431-54992-5_6.
- [8] D. Dolphin, T. G. Traylor, L. Y. Xie, *Acc. Chem. Res.* **1997**, *30*, 251–259, DOI: 10.1021/ar960126u.

- [9] I. D. Cunningham, T. N. Danks, J. N. Hay, I. Hamerton, S. Gunathilagan, C. Janczak, *J. Mol. Catal. A* **2002**, *185*, 25–31, DOI: 10.1016/S1381-1169(02)-00057-2.
- [10] M. A. Sainna, S. Kumar, D. Kumar, S. Fornarini, M. E. Crestoni, S. P. de Visser, *Chem. Sci.* **2015**, *6*, 1516–1529, DOI: 10.1039/C4SC02717E.
- [11] K. P. Bryliakov, E. P. Talsi, *Coord. Chem. Rev.* **2014**, *276*, 73–96, DOI: 10.1016/j.ccr.2014.06.009.
- [12] S. M. Hölzl, P. J. Altmann, J. W. Kück, F. E. Kühn, *Coord. Chem. Rev.* **2017**, *352*, 517–536, DOI: 10.1016/j.ccr.2017.09.015.
- [13] C.-L. Sun, B.-J. Li, Z.-J. Shi, *Chem. Rev.* **2011**, *111*, 1293–1314, DOI: 10.1021/cr100198w.
- [14] W. N. Oloo, L. Que, *Acc. Chem. Res.* **2015**, *48*, 2612–2621, DOI: 10.1021/acs.accounts.5b00053.
- [15] R. Mas-Ballesté, L. Que, *J. Am. Chem. Soc.* **2007**, *129*, 15964–15972, DOI: 10.1021/ja075115i.
- [16] S. A. Hauser, M. Cokoja, F. E. Kühn, *Catal. Sci. Technol.* **2013**, *3*, 552–561, DOI: 10.1039/C2CY20595E.
- [17] A. Schmidt, N. Grover, T. K. Zimmermann, L. Graser, M. Cokoja, A. Pöthig, F. E. Kühn, *J. Catal.* **2014**, *319*, 119–126, DOI: 10.1016/j.jcat.2014.08.013.
- [18] J. W. Kück, M. R. Anneser, B. Hofmann, A. Pöthig, M. Cokoja, F. E. Kühn, *ChemSusChem* **2015**, *8*, 4056–4063, DOI: 10.1002/cssc.201500930.
- [19] F. Dyckhoff, J. F. Schlagintweit, R. M. Reich, F. E. Kühn, *Catal. Sci. Technol.* **2020**, *10*, 3532–3536, DOI: 10.1039/D0CY00631A.
- [20] G. G. Zámbo, J. Mayr, M. J. Sauer, T. P. Schlachta, R. M. Reich, F. E. Kühn, *Dalton Trans.* **2022**, *51*, 13591–13595, DOI: 10.1039/D2DT02561B.
- [21] J. F. Schlagintweit, F. Dyckhoff, L. Nguyen, C. H. G. Jakob, R. M. Reich, F. E. Kühn, *J. Catal.* **2020**, *383*, 144–152, DOI: 10.1016/j.jcat.2020.01.011.
- [22] T. P. Schlachta, F. E. Kühn, *Chem. Soc. Rev.* **2023**, *52*, 2238–2277, DOI: 10.1039/D2CS01064J.
- [23] T. P. Schlachta, G. G. Zámbo, M. J. Sauer, I. Rüter, C. A. Hoefler, S. Demeshko, F. Meyer, F. E. Kühn, *J. Catal.* **2023**, *426*, 234–246, DOI: 10.1016/j.jcat.2023.07.018.
- [24] C. A. Hoefler, N. K. Dietl, G. G. Zámbo, T. P. Schlachta, R. M. Reich, F. E. Kühn, *J. Organomet. Chem.* **2024**, *1006*, 123018, DOI: 10.1016/j.jorganchem.2024.123018.
- [25] F. E. Kühn, *J. Organomet. Chem.* **2023**, *1000*, 122824, DOI: 10.1016/j.jorganchem.2023.122824.
- [26] A. Company, L. Gómez, X. Fontrodona, X. Ribas, M. Costas, *Chem. Eur. J.* **2008**, *14*, 5727–5731, DOI: 10.1002/chem.200800724.
- [27] E. A. Mikhalyova, O. V. Makhlynets, T. D. Palluccio, A. S. Filatov, E. V. Rybak-Akimova, *Chem. Commun.* **2012**, *48*, 687–689, DOI: 10.1039/C1CC15935F.
- [28] M. R. Anneser, S. Haslinger, A. Pöthig, M. Cokoja, V. D'Elia, M. P. Högerl, J.-M. Basset, F. E. Kühn, *Dalton Trans.* **2016**, *45*, 6449–6455, DOI: 10.1039/C6DT00538A.
- [29] T. P. Schlachta, M. R. Anneser, J. F. Schlagintweit, C. H. G. Jakob, C. Hintermeier, A. D. Böth, S. Haslinger, R. M. Reich, F. E. Kühn, *Chem. Commun.* **2021**, *57*, 6644–6647, DOI: 10.1039/D1CC02027G.
- [30] S. Haslinger, A. Raba, M. Cokoja, A. Pöthig, F. E. Kühn, *J. Catal.* **2015**, *331*, 147–153, DOI: 10.1016/j.jcat.2015.08.026.
- [31] Y. Mekmouche, S. Ménage, J. Pécaut, C. Lebrun, L. Reilly, V. Schuenemann, A. Trautwein, M. Fontecave, *Eur. J. Inorg. Chem.* **2004**, *2004*, 3163–3171, DOI: 10.1002/ejic.200300926.
- [32] S. Taktak, S. V. Kryatov, T. E. Haas, E. V. Rybak-Akimova, *J. Mol. Catal. A* **2006**, *259*, 24–34, DOI: 10.1016/j.molcata.2006.05.071.
- [33] F. Dyckhoff, J. F. Schlagintweit, M. A. Bernd, C. H. G. Jakob, T. P. Schlachta, B. J. Hofmann, R. M. Reich, F. E. Kühn, *Catal. Sci. Technol.* **2021**, *11*, 795–799, DOI: 10.1039/D0CY02433C.
- [34] E.-M. H. J. Esslinger, J. F. Schlagintweit, G. G. Zámbo, A. M. Imhof, R. M. Reich, F. E. Kühn, *Asian J. Org. Chem.* **2021**, *10*, 2654–2662, DOI: 10.1002/ajoc.202100487.
- [35] T. P. Schlachta, J. F. Schlagintweit, M. R. Anneser, E.-M. H. J. Esslinger, M. Muhr, S. Haslinger, F. E. Kühn, *Inorg. Chim. Acta* **2021**, *518*, 120228, DOI: 10.1016/j.ica.2020.120228.
- [36] M. Guo, Y.-M. Lee, S. Fukuzumi, W. Nam, *Coord. Chem. Rev.* **2021**, *435*, 213807, DOI: 10.1016/j.ccr.2021.213807.
- [37] M. A. Bernd, F. Dyckhoff, B. J. Hofmann, A. D. Böth, J. F. Schlagintweit, J. Oberkofler, R. M. Reich, F. E. Kühn, *J. Catal.* **2020**, *391*, 548–561, DOI: 10.1016/j.jcat.2020.08.037.
- [38] Nature editorial, *Nature* **2023**, *617*, 438, DOI: 10.1038/d41586-023-01612-x.
- [39] K. Shen, Y. Fu, J.-N. Li, L. Liu, Q.-X. Guo, *Tetrahedron* **2007**, *63*, 1568–1576, DOI: 10.1016/j.tet.2006.12.032.
- [40] Z. Xi, X. Zhang, W. Chen, S. Fu, D. Wang, *Organometallics* **2007**, *26*, 6636–6642, DOI: 10.1021/om700796g.
- [41] A. Raba, M. Cokoja, S. Ewald, K. Riener, E. Herdtweck, A. Pöthig, W. A. Herrmann, F. E. Kühn, *Organometallics* **2012**, *31*, 2793–2800, DOI: 10.1021/om2010673.
- [42] S. Saravanakumar, A. I. Oprea, M. K. Kindermann, P. G. Jones, J. Heinicke, *Chem. Eur. J.* **2006**, *12*, 3143–3154, DOI: 10.1002/chem.200501183.
- [43] N. U. D. Reshi, J. K. Bera, *Coord. Chem. Rev.* **2020**, *422*, 213334, DOI: 10.1016/j.ccr.2020.213334.
- [44] S. Haslinger, A. C. Lindhorst, J. W. Kück, M. Cokoja, A. Pöthig, F. E. Kühn, *RSC Adv.* **2015**, *5*, 85486–85493, DOI: 10.1039/C5RA18270K.
- [45] S. Haslinger, J. W. Kück, E. M. Hahn, M. Cokoja, A. Pöthig, J.-M. Basset, F. E. Kühn, *Inorg. Chem.* **2014**, *53*, 11573–11583, DOI: 10.1021/ic501613a.
- [46] D. T. Weiss, M. R. Anneser, S. Haslinger, A. Pöthig, M. Cokoja, J.-M. Basset, F. E. Kühn, *Organometallics* **2015**, *34*, 5155–5166, DOI: 10.1021/acs.organomet.5b00732.
- [47] D. G. Gusev, *Organometallics* **2009**, *28*, 6458–6461, DOI: 10.1021/om900654g.
- [48] P. Gütllich, E. Bill, A. X. Trautwein, *Mössbauer Spectroscopy and Transition Metal Chemistry: Fundamentals and Applications*, Springer Berlin Heidelberg: Berlin, Heidelberg, **2011**, DOI: 10.1007/978-3-540-88428-6.
- [49] J. W. Kück, A. Raba, I. I. E. Markovits, M. Cokoja, F. E. Kühn, *ChemCatChem* **2014**, *6*, 1882–1886, DOI: 10.1002/cctc.201402063.
- [50] C. L. Hill, *Nature* **1999**, *401*, 436–437, DOI: 10.1038/46704.
- [51] R. Noyori, M. Aoki, K. Sato, *Chem. Commun.* **2003**, 1977–1986, DOI: 10.1039/B303160H.
- [52] S. Haslinger, J. W. Kück, M. R. Anneser, M. Cokoja, A. Pöthig, F. E. Kühn, *Chem. Eur. J.* **2015**, *21*, 17860–17869, DOI: 10.1002/chem.201503282.
- [53] S. Haslinger, A. Pöthig, M. Cokoja, F. E. Kühn, *Acta Crystallogr. Sect. C* **2015**, *71*, 1096–1099, DOI: 10.1107/S2053229615021968.
- [54] F. G. Cantú Reinhard, S. P. de Visser, *Chem. Eur. J.* **2017**, *23*, 2935–2944, DOI: 10.1002/chem.201605505.
- [55] Z. Chen, L. Yang, C. Choe, Z. Lv, G. Yin, *Chem. Commun.* **2015**, *51*, 1874–1877, DOI: 10.1039/C4CC07981G.
- [56] H. Inaba, S. Kanamaru, F. Arisaka, S. Kitagawa, T. Ueno, *Dalton Trans.* **2012**, *41*, 11424–11427, DOI: 10.1039/C2DT31030A.
- [57] P. Saenz, R. E. Cachau, G. Seoane, M. Kieninger, O. N. Ventura, *J. Phys. Chem. A* **2006**, *110*, 11734–11751, DOI: 10.1021/jp061359y.
- [58] T. Hansen, P. Vermeeren, R. Yoshisada, D. V. Filippov, G. A. van der Marrel, J. D. C. Codée, T. A. Hamlin, *J. Org. Chem.* **2021**, *86*, 3565–3573, DOI: 10.1021/acs.joc.0c02955.
- [59] T. Kitanosono, F. Lu, K. Masuda, Y. Yamashita, S. Kobayashi, *Angew. Chem. Int. Ed.* **2022**, *61*, e202202335, DOI: 10.1002/anie.202202335.
- [60] R. Mas-Ballesté, M. Costas, T. van den Berg, L. Que Jr, *Chem. Eur. J.* **2006**, *12*, 7489–7500, DOI: 10.1002/chem.200600453.
- [61] I. Kumpina, N. Brodyagin, J. A. MacKay, S. D. Kennedy, M. Katkevics, E. Rozners, *J. Org. Chem.* **2019**, *84*, 13276–13298, DOI: 10.1021/acs.joc.9b01133.
- [62] C. J. Stanton, C. W. Machan, J. E. Vandezande, T. Jin, G. F. Majetich, H. F. Schaefer, C. P. Kubiak, G. Li, J. Agarwal, *Inorg. Chem.* **2016**, *55*, 3136–3144, DOI: 10.1021/acs.inorgchem.6b00079.
- [63] W. L. Armarego, *Purification of laboratory chemicals*, Butterworth-Heinemann: **2017**, <https://www.sciencedirect.com/book/9780128054574/purification-of-laboratory-chemicals#book-description>.
- [64] G. R. Fulmer, A. J. M. Miller, N. H. Sherden, H. E. Gottlieb, A. Nudelman, B. M. Stoltz, J. E. Bercaw, K. I. Goldberg, *Organometallics* **2010**, *29*, 2176–2179, DOI: 10.1021/om100106e.
- [65] E. Bill, *mf2.SL*, Max-Planck Institute for Chemical Energy Conversion: Mülheim/Ruhr, Germany, **2021**.

Manuscript received: March 9, 2024
Revised manuscript received: August 4, 2024
Version of record online: September 24, 2024